UNIVERSITY OF NOTTINGHAM
DEPARTMENT OF MECHANICAL ENGINEERING

Void Formation in Resin Transfer Moulding

by

Julian Robert Lowe
BEng

Thesis submitted to the University of Nottingham
for the degree of Doctor of Philosophy
September 1993

Contents

Abstract

Void Formation in Resin Transfer Moulding

by

J.R.Lowe

BEng

In recent years interest has grown in the use of composite components within the automotive industry. Fibre reinforced plastic (FRP) components are of particular interest to the industry, since lower tooling costs and part consolidation can be utilised, whilst lighter, stiffer components can be produced. Several methods are available to produce FRP components at high volumes, including compression moulding (using dough and sheet moulding compounds), reinforced reaction injection moulding (RRIM) and liquid moulding processes (resin transfer moulding (RTM) and structural reaction injection moulding (SRIM)). RTM is a closed mould process, which is widely used to produce components economically in low volumes using matched moulds to produce two good surfaces. The absence of a high volume manufacturing technology, however, has impeded the acceptance and advance of RTM within the automotive industry.

A research programme was established at the University of Nottingham to address the problems associated with the use of RTM for high volume manufacture. This programme has considered the topics of process technology, processing characteristics of polyester resin systems and fibre preforms, fibre wet-out and interfacial bonding, mould design, microwave pre-heating of reactive resin systems and process modelling.

This thesis concerns the research which was undertaken to identify the causes of void formation during the impregnation and polymerisation stages of RTM, and

methods of reducing the final void content within the component. The impregnation phase of the RTM process was identified as being the stage where the majority of voids were formed. A study of oil impregnation (having a similar viscosity to that of resin) into reinforcement was undertaken to determine the reasons for uneven flow and air entrapment. The dry reinforcements were studied to assess the microstructure of the preforms in order to determine reasons for obstruction of the resin flow. Fabric stitching, thermoplastic binder and size deposits were identified as potential causes of flow impediment. Fibre orientation and preform stacking were also assumed to assist in the development of uneven flow, leading to air entrapment. A major factor determining the formation of microvoids within fibre bundles was identified as the transverse impregnation of resin into high Tex fibre bundles.

The major moulding process variables of injection pressure, vent pressure, fibre volume fraction, mould temperature and resin pre-heating have been assessed, to determine their effect on the void content within unidirectional and CFRM reinforced polyester laminates. It was observed that vacuum assistance during impregnation reduced void formation, although higher exotherm pressures and the possibility of monomer boiling arise from its use.

A simple impregnation model was developed to assess the microscopic impregnation rates between fibre bundles, in the capillary between fibres and transversely into fibre bundles. The results from this model were compared with actual moulding histories. The findings of the overall work are discussed and suggestions proposed for the reduction of void content in RTM automotive components.

Acknowledgements

The author would like to thank his supervisors, Professor M.J.Owen and Dr. C.D.Rudd for their guidance and encouragement.

The staff of the Ford Motor Company, Alan Harrison and Stephen Scarborough, are thanked for their financial support and enthusiasm for the project.

The Head of the Department, Professor B.R. Clayton is thanked for the use of department facilities and personnel. Special acknowledgements go to Andrew Kingham and Roger Smith for tireless effort and ingenuity in the laboratory. Brian Foster and John Smalley also deserve thanks for putting other things aside to help.

I must thank the assistance of my fellow researchers, Linda Bulmer, Andrew Long, Kevin Lindsey, Dr. Eddie Rice and Mike Johnson for their assistance and encouragement. Dr. Ken Kendall, Dr. Ian Revill, Pete McGeehin, Dr. John Hill and Patrick Blanchard are also thanked for support within the research group.

Vetrotex St.Gobain are thanked for the supply of reinforcement as are Cray Valley Total Chemie for the supply of polyester resin.

Finally I would like to thank Lynne for her tolerance and understanding and my parents for their continued support and assistance.

Glossary of Terms

Accelerator	A chemical used to increase resin reaction rate.
Anisotropic	Having properties which vary with direction within the material.
Bar	A unit of pressure equal to 10^5 pascals (N/m^2) or 0.987 atmospheres.
Binder	The agent which provides cohesion to the strands in a mat or preform.
CFRM	Continuous Filament Random Mat.
CSM	Chopped Strand Mat.
Catalyst	A chemical that reduces reaction initiation energy, without itself undergoing permanent chemical change.
Coupling Agent	The component of the size system which promotes a chemical bond between the surface of the glass fibre and the matrix.
Cure	Change of resin state from liquid to solid by polymerisation.
Derakane	The trade name of a range of commercially available vinyl ester resins, produced by the Dow chemical company.
Doctor blade	A device for controlling the amount of resin on the surface of the impregnation drum during filament winding.
Drape	The ability of a mat or fabric to conform to a complex geometry.
DSC	Differential Scanning Calorimetry (in this context). A thermal analysis technique used to monitor the heat change during the cure reaction.
E-Glass	The type of glass most commonly used for fibre reinforcement.
Electroforming	A metal forming process in which the metal is electrolytically deposited onto a model of the component for mould manufacture.
Exotherm	Heat liberation during polymerisation.

FD	Finite difference.
Filamentisation	The separation of a fibre bundle into filaments, which is also associated with fibre breakage.
Film former	The component of the size system which provides cohesion between the filaments within a strand.
Filler	An inert substance added to the resin system to improve certain properties or to reduce cost.
FRP	Fibre Reinforced Plastics.
FW	Filament Winding.
GRP	Glass Reinforced Plastics.
Gate	The position at which the resin is injected into the mould.
Gel time	The time measured from the beginning of injection to reach the peak exotherm temperature.
Homogeniser	A pressurised storage cylinder used to deliver resin to the mould (in this context).
Impregnation	The displacement of air and penetration of a fibre preform by liquid resin.
Inhibitor	A chemical used to delay the start of chemical cure in a resin system.
Isotropic	Having properties which do not vary with direction within the material.
LMP	Liquid Moulding Processes.
LPA	Low Profile Additive, a thermoplastic additive mixed into the resin to control surface irregularities by counteracting shrinkage.
Lamina	The basic ply of a composite structure (in this context).
Laminate	A stack of laminae (in this context).
Mandrel	The former onto which a component is wound during filament winding
NCF	Non-Crimp Fabric, a directional reinforcement which is designed to prevent the fibres distorting during shaping. Stitch bonding is used to bind the fabric.
Newtonian fluid	A fluid whose viscosity is independent of the shear rate.

PC	Personal Computer.
Permeability	The property of a porous material which characterises the ease with which a fluid will flow under an applied pressure gradient.
Polymerisation	The chemical reaction in which resin molecules align and cross-link to produce a rigid structure.
Porosity	In the context of reinforcement the volumetric fraction of space between fibres.
Preform	Reinforcement which has been cut and shaped to reproduce the component geometry, which may also include inserts and cores.
Preformer	A machine which produces preforms.
Prepreg	Reinforcement which has been pre-impregnated with resin.
RRIM	Reinforced Reaction Injection Moulding. A process of manufacturing polymeric components by impingement mixing of two or more reactants prior to injection into a mould. Chopped fibre is added to one of the reactants.
RTM	Resin Transfer Moulding, also known as resin injection.
Ra	Roughness average, measured in micrometers (μm).
Rectilinear	Flow advancement in a single plane.
Reinforcement	Fibres used to carry load in composite materials.
Release Agent	A substance used to improve mould release, applied externally to the mould and/or internally within the resin formulation.
Roving or Tow	A collection of relatively fine filaments.
SEM	Scanning Electron Microscope.
Shell Mould	A lightweight mould compromising a thin skin working surface mounted in a backing frame.
Sink	A point to which fluid converges.
Size	An emulsion applied to fibre surfaces for lubrication and protection during processing. The size binds the fibres into strands and provides a coupling agent between the fibre and resin matrix.
Sprue	The material formed in the tapered passage between the thermal break (TBV) valve and the gate.

SRIM	Structural Reaction Injection Moulding. A process for manufacturing polymeric components by impingement mixture of two or more reactive monomers, which impregnate a fibre preform.
Strand	A combination of glass filaments bundled together by means of adhesion (see Roving or Tow).
Styrene	A monomer used as a cross-linking agent in unsaturated polyester and vinyl ester resins.
Synolac	The trade name of a range of commercially available polyester resins produced by Cray Valley (CV).
Synolite	The trade name of a range of commercially available polyester resins produced by Dutch State Mines (DSM).
TBPB	Tertiary Butyl Peroxybenoate, an organic peroxide used as a catalyst for curing resins at elevated temperature.
TBPEH	Tertiary Butyl Peroxy 2-Ethyl Hexanoate, an organic peroxide used as a catalyst for curing resins at elevated temperatures.
TBV	Thermal Break Valve, a resin injection valve which provides a thermal barrier between the hot mould and the colder resin.
Tex	The mass per 1000m of roving (g/Km).
Thermoplastic	A plastic material which is softened by heating and hardened by cooling in a reversible process.
Thermoset	A plastic material which is hardened by an irreversible chemical reaction.
Turbo-Pascal	A high level computer language.
Unifilo	A commercial brand of CFRM, manufactured by Vetrotex.
VARI	Vacuum Assisted Resin Injection, a trade name associated with vacuum assisted RTM, used by Lotus.
Vent	The position from which air and resin are discharged from the mould.
Void	A resin free cavity within the composite (in this context).
Washing	The disturbance of fibres in the preform under the action of resin impregnation.

Wet-out	Complete coating of individual fibres by the matrix resin.
Wet-through	Penetration of resin through a preform, which must take place to permit wet-out (see impregnation).

Nomenclature

Uppercase			Units
A	=	Cross sectional Area	m^2
A_μ	=	Viscosity constant	
B	=	Gelation time and viscosity constant	
C	=	Peripheral contact area	m
C_a	=	Capillary Number	
C_p	=	Specific heat capacity	kJ/kg K
D	=	Diameter	m
E_μ	=	Viscosity constant	
J	=	Heat transfer constant	
K	=	Thermal conductivity	kW/m K
N	=	Number	
N_u	=	Nusselt number	
M	=	Mass fraction	
P	=	Pressure	N/m^2
δP	=	Pressure difference	N/m^2
Q	=	Discharge or volumetric flow rate	m^3/s
R	=	Radius	m
R_e	=	Reynolds Number	
R_R	=	Universal Gas Constant	N m/kg K
T	=	Temperature	K
U_{max}	=	Maximum velocity of the resin in the transverse direction	m/s
V	=	Volume fraction	

Lowercase			
a	=	Constant for transverse heat transfer and viscosity	
b	=	Width of plate	m
e	=	Constant for transverse heat transfer	

d_c	=	Effective hydraulic diameter for the capillary between fibres	m
d	=	Half the fibre spacing	m
g	=	Incremental gelation value	
h	=	Surface heat transfer coefficient or thickness of material	kW/m^2 K : m
k	=	Permeability	m^2
k_r	=	Thermal conductivity for the resin	Kw/m K
l	=	Distance	m
n	=	Heat transfer constant	
m	=	mass : mass flow rate	kg : kg/s
m_a	=	Multiplier for the contact angle	
p	=	Wetted perimeter	m
p_a	=	Power value for the contact angle	
δq	=	Rate of heat transferred	kJ/s
r	=	Distance into the fibre bundle (transverse distance)	m
δr	=	Incremental distance into the fibre bundle	m
r_c	=	Effective radius of the capillary between fibres	m
r_{cc}	=	Radius of curvature of resin meniscus	m
s	=	Position of the centre of the resin meniscus	m
t_g	=	Time for gelation to occur at a specific resin temperature	s
δt	=	Time increment	s
v	=	Velocity	m/s
w	=	Half the effective plate separation	m
w_i	=	Half the plate separation at a body angle ϕ_i	m
x	=	Distance	m
z	=	Distance travelled in the transverse direction	m
δz	=	Distance increment in the transverse direction	m

Greek

α	=	Relative degree of reaction	
β	=	Constant for gelation time	
γ	=	Interfacial tension between the resin and the fibre	N/s^2
θ	=	Contact angle between resin and fibre	Degrees

Λ	=	Constant for gelation time	
μ	=	Viscosity of the resin	Pa s
ν	=	Kinematic viscosity of the resin	m^2/s
π	=	Pi	
ρ	=	density	kg/m^3
ϕ_i	=	Body contact angle of the resin meniscus on the fibre in the transverse direction	Degrees
$\phi_{initial}$	=	Initial contact position of the resin meniscus on the fibre	
ϕ_{last}	=	Final position of the resin meniscus on the fibre before a jump	
ϕ_{ex}	=	Excess body angle to extent channel length	

Subscripts

A	=	Axial direction
b	=	Between fibre bundles (capillary)
bi	=	Binder
c	=	Between fibres (capillary)
ca	=	Axial capillary
co	=	Contact angle
ct	=	Transverse capillary
f	=	Fibre
i	=	Count
it	=	Inhibition time
ip	=	External injection pressure
r	=	Resin
rt	=	Real time
ss	=	Steady state
t	=	Transverse direction
T	=	Temperature
v	=	Void
w	=	Water
x,z	=	Constants for heat transferor constant suffixes
1,2,3	=	Principal laminate axes

Chapter 1

Introduction

1.1 Plastics in the Automotive Industry

The use of fibre reinforced plastics material (FRP) is becoming increasingly extensive in the automotive industry. By 1995 the average European car is expected to contain more than 100kg of plastics[1] (10% of vehicle weight) and the trend is upwards. A forecast is for cars in 2050 to contain 70% plastics[2] (both reinforced and non reinforced), although this will depend upon economics, environmental pressures and market trends.

US car sales average 10 million units per year[3]. This market comprises 600 models, 400 of these being produced by foreign owned manufacturers[4]. In 1991 Japanese and South East Asian car manufacturers controlled over 30% of the US market[3]. Traditionally these producers have updated their product range very frequently, and this increased competition has put pressure on the major American and European automotive producers to re-think their production techniques. There is a requirement to reduce manufacturing costs in three main areas of production[5]: low volume derivatives of basic models, medium volume niche market vehicles and high volume basic products.

The principal alternatives to pressed steel components include thermosetting polymer composites, reinforced thermoplastics and aluminium alloys. Current pressed steel components, although produced at low cost, are heavy, corrode easily and require several sequential operations to produce. Aluminium alloys being technologically more mature than polymers are the leading candidate for short term applications[6,7], since the production processes are known and little risk is incurred. Even with recyclability problems compared to metals the predominant interest in the longer term is aimed at thermosetting composite materials[7].

Eventually material selection will depend upon the component, its physical requirements and total accountable cost, as is the case for all high performance, low weight transport structures.

1.2 The Liquid Moulding Processes (LMP)

Liquid Moulding Processes involve the placement of dry reinforcement or preform, cores and inserts inside a mould cavity which is then impregnated by injection with resin. The resin is polymerised and the component removed from the mould. Preforms must be produced independently of the moulding operation such that the complete production process can be brought under quality control and become automated. These processes provide a clean working environment, with controlled vapour exposure. There are two main LMP's available to the plastics industry, resin transfer moulding (RTM) and structural reaction injection moulding (SRIM).

RTM utilises low injection pressures (generally 0-10 bar), and the resin is usually pre-mixed or statically mixed prior to injection. SRIM uses much higher injection pressures (generally above 20 bar). The resin is mixed as it enters the mould by impingement of the reactants. RTM and SRIM are the only production routes with selective reinforcement and accurate fibre management that lend themselves to automated production. Due to the lower capital costs associated with RTM, it has been identified by the automotive and materials supply industries as possessing the most potential for overcoming the manufacturing difficulties involved in the processing of FRP for medium to high volume production[5].

1.3 The RTM Process

The RTM process shown schematically in Figure 1.1, involves the placement of dry reinforcement into a closed matched mould, into which a liquid thermosetting resin is injected. The resin is polymerised either at room temperature or at elevated temperatures and the component is removed with a smooth surface on both sides. The resin system used will ultimately depend on cost and application. Several types are available to the RTM industry including polyesters, vinyl esters, urethane methacrylates, phenolics and epoxies.

Prior to moulding the reinforcement is normally shaped and cut to produce a fibre preform in a separate process. The preform can consist of different types of fibres such as glass, polyester, aramid or carbon. These fibres may be present in many different material forms, such as woven fabrics, continuous filament random mats or chopped strand mats.

The RTM process has been simplified into five stages (Figure 1.1):

Cutting and stacking reinforcement from roll materials

Heating the dry reinforcement and preforming to shape

Trimming the preformed material

Moulding (preform placement, resin injection, and polymerisation)

Demoulding and deflashing

There are several issues facing the automotive industry before RTM can be accepted as a feasible manufacturing route. These include achieving repeatable quality components, cost effectiveness through automation, acceptable production times, accurate preform fabrication and the waste disposal problems facing composites.

1.4 The RTM Research Programme at the University of Nottingham

Since 1985 there has been an ongoing research programme within the Department of Mechanical Engineering at the University of Nottingham to study the feasibility of producing high volume FRP components using RTM. This programme has been sponsored by the Ford Motor Company Ltd to identify, and where possible solve the problems of manufacturing FRP components at medium to high volumes.

The initial moulding and production work was performed on a plaque mould, measuring 520mm x 540mm, mounted in a 500kN Fox & Offord compression moulding press for mould manipulation and clamping. In 1985 a larger scale moulding facility able to handle a mould measuring up to 2m x 1.5m was designed and built. More recently a complex nickel shell mould has been used in this purpose built facility to produce prototype automotive components using RTM.

The programme has involved several collaborative ventures with industrial moulders for the production of automotive components. These include a tailgate for the P100 Sierra pickup and an undershield for the Sierra Sapphire. Other work carried out within the project includes permeability investigations, process characterisation, interfacial bond formation studies and process modelling. Two associated research programmes are presently underway in the department,"Disposal of Thermosetting Plastics" and "Preforms for Liquid Moulding Processes (PLMP)". As a result of the work carried out in the programme seven successful theses have been submitted along with numerous publications. A list of the supervisory and research staff who have contributed to the RTM programme and their associated research can be found in Appendix 1.

1.5 Theme of this Work

This thesis is concerned with the identification of key quality issues which arise during RTM, especially those which can be related to the impregnation and cure stages of moulding. The objective was to recognise phenomena which result in internal defects, especially voids, and to attempt to define mechanisms which cause these defects and how they may be reduced or eliminated.

The stages of the process that required investigation were identified by examining over two hundred mouldings, both in flat plaque and three-dimensional component form. The defects which arise at each stage were identified. The impregnation phase was selected for further study, concentrating on void formation in multilayered preforms. Mechanisms have been proposed and studied experimentally to determine the causes of these phenomena. The conditions under which these defects occur and the combination of factors which lead to their formation have been recognised. From this study relationships between the processing parameters and defect occurrence have been identified, and the processing windows for the production of high quality products proposed. The work presented has concentrated on the investigation of the internal defects within mouldings. The multitude of issues which arise from surface quality, warpage and dimensional accuracy of composites produced by this manufacturing have not been considered.

Chapter 2 contains a review of the current literature relating to RTM and void formation. The experimental procedures and apparatus used for the work contained in this thesis are described in chapter 3. The types of voids and causes for their formation are introduced in chapter 4. The effect of the major processing conditions used in RTM upon the void content within laminates are then discussed in chapter 5. Following these studies the impregnation phase of RTM is examined in detail in chapter 6. Comparisons between the voidage problem in RTM and filament winding (an alternative composite production route) are made in chapter 7, where similarities are drawn between the impregnation phases of each process. A model to predict the microscopic flow of resin into an ideally spaced unidirectional preform is proposed in chapter 8. Finally chapter 9 contains a discussion of the findings of this thesis and proposals for further work.

List of Figures

Figure 1.1

Resin Transfer Moulding (RTM) Process Schematic

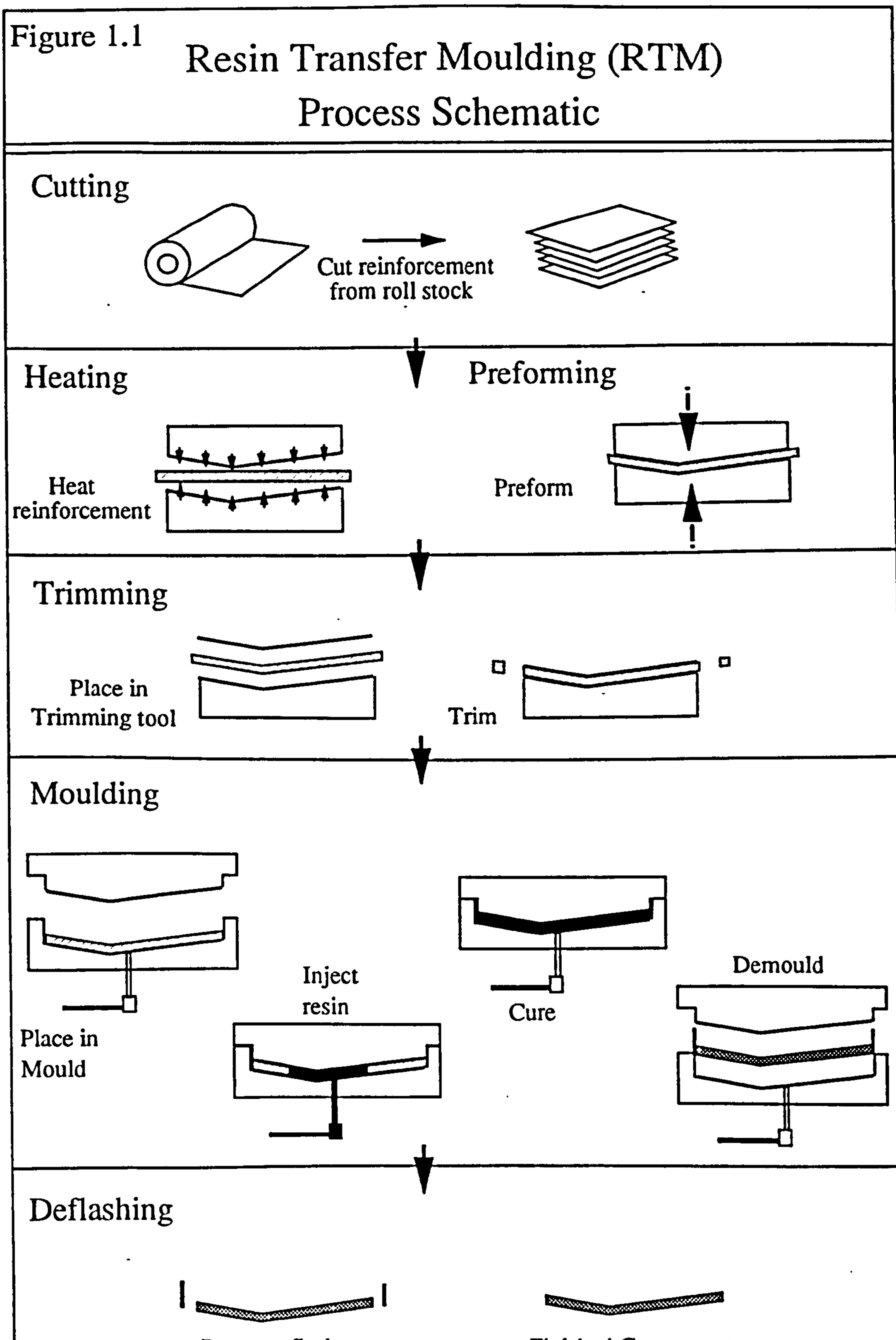

Chapter 2

Literature Survey

2.1 Introduction

Current literature relating to RTM processing for high volume manufacture (over 250,000 units per annum) was studied with special attention to moulding quality and the findings are presented in this chapter. A brief discussion is given of the benefits of using reinforced plastics as an alternative to traditional steel components in terms of manufacturing capability. The RTM process is examined and the potential advantages and disadvantages of the method compared with alternative composite manufacturing routes is considered. Present preforming techniques have been discussed, with particular emphasis on the sizes and binders applied to the reinforcement.

The effect of void content upon the mechanical properties of composite structures has been assessed and techniques for measuring this void content evaluated. Mechanisms suggested for the formation of voids during the injection and curing phases of RTM are discussed, leading to a review of modelling void formation during the impregnation phase. Uneven flow in multilayered preforms during impregnation is believed to influence void formation. In order to assess the permeabilities of multilayered preforms, the measurement techniques used for both in-plane and transverse permeability have been considered.

Filament wound GRP composites are known to contain similar voids to material produced by RTM. Void formation mechanisms during the filament winding process have been reviewed in order to compare the impregnation process with RTM.

2.2 The Use of Fibre Reinforced Plastics

Reinforced plastics materials, although involving higher raw material costs,

exhibit significant benefits over their steel counterparts. Weight reduction using FRP, improvement of mechanical properties, fatigue and corrosion resistance, together with lower thermal conductivity compared with metals, are all very attractive to the automotive industry[8]. The integration of several steel components into a single composite moulding allows greater design flexibility. This component integration leads to less tooling, the costs of which are far lower than tooling for steel components[9].

Several of these advantages are tempered by potential problems including recyclability, the financial risk and the general acceptance of a new materials and processing methods. In particular a solution to the problem of recycling needs to be addressed for composites to become accepted in the volume automotive industry.

Several FRP processing techniques are available to the composites industry, including hand layup, compression moulding, reinforced reaction injection moulding (RRIM), filament winding, pultrusion and RTM[8].

Hand layup is limited to low volume production (less than 5,000 units/year) due to labour intensive manufacture and long production times, eg. the TVR company produce less than 100 hand laid composite vehicles per year[10]. Compression moulded products (DMC & SMC) have limited load bearing ability, due to the use of short fibre reinforcement. Their application has been limited to low strength components such as the Citroen AX tailgate (DMC) (300,000 per annum) and the Citroen BX bonnet (DMC) (300,000 per annum). Compression moulding requires high moulding pressures (50-100 bar) and temperatures in the order of 150°C, thus tooling is costly. RRIM is also limited in its application to low strength components due to the use of short fibre reinforcement. The short fibres are injected within one of the reactants, causing wear and fibre orientation.

Filament winding, Pultrusion and RTM can utilise long fibre reinforcements, which can be aligned during the manufacturing process. Filament winding has only found restricted use in the automotive industry due to the limitations of geometry (eg

driveshafts). Pultrusion has also been limited by the constant cross sections which can be produced.

2.3 The RTM Process

Advantages of the Resin Transfer Moulding Process

RTM is a closed mould process which provides a clean working environment. Low pressures, generally between 0 and 10 bar are used for injection so that low stiffness tooling (lower cost) compared with alternative composite processes is acceptable. The forces needed to clamp the moulds are also low. The preforms can be produced independently of the moulding operation such that the process can be brought under quality control and automation. The mouldings produced by RTM have several advantages over other FRP production processes, which include:

- *The production of complex shapes.*
- *Relatively high fibre volume fractions (40% - 70%) are obtainable.*
- *Selective reinforcement and accurate fibre management can be incorporated into preforms.*
- *Mouldings can be produced with two defined surfaces.*
- *Class 'A' finish can be produced using high quality moulds.*
- *Inserts can be incorporated into the preform before injection.*

One of the major advantages of the closed mould process is the ability to control styrene emissions[11]. The US Occupational Safety and Health Administration (OSHA) have recently imposed a new legislation to reduce the styrene exposure limit from 100ppm to 50ppm[11,12]. Also, air quality regulation bodies in the US are likely to follow the standards on styrene emission regulation acceding California Rule 1162, requiring the use of special low styrene systems or the use of processes which keep emissions below 4% of resin weight[12]. RTM is able to satisfy these requirements.

The length of time required for a new car to evolve from concept to production makes the automotive industry vulnerable to external factors (both political and economic) that are often beyond its control[2]. The possibility of reducing this lead

time would enable increases in competitiveness, product range, diversity and decreased costs. According to a report commissioned by Ford in 1988[13], plastics yield a parts reduction ratio of 5 to 1 (Five steel pressed components can be consolidated into one plastic component). Since each mould for composite component production replaces 2-3 metal stamping sets, the opportunity to cut tooling costs is potentially very large.

Electroformed nickel shell moulds provide an established tooling route which offers potential for the manufacture of composite components by RTM in the volumes required. High quality, high definition components can be produced (eg. the BMW Z1 body parts) and the reduced lead time can result in shorter vehicle development times. Shell tooling can also utilise low investment capital equipment in an automated moulding process. Prototype tooling for a tailgate mould, a joint venture between Ford and Vetrotex in 1987, cost approximately £68,000, which is one third of the lowest comparable pressed steel tooling costs[9].

RTM is an aligned fibre production route which lends itself to automated production. It has been identified by the automotive and materials supply industries as possessing the most potential for overcoming the manufacturing difficulties involved in the processing of FRP for medium to high volume production[5].

Disadvantages of RTM

Despite the significant benefits of the process, several drawbacks limit high volume production and high quality products. The preform production is labour intensive, can be wasteful and the preforms lack strength. Processing of RTM components is generally slow and the control of the moulding cycle is erratic and not fully understood[4].

The RTM marketplace

At present RTM has limited acceptance in the automotive industry. Several case histories can be quoted[10]. The Renault Espace roof, bonnet and sides were produced by Matra in volumes of 35,000 per year. Body components for the BMW Z1 were produced by Seger and Hoffman in volumes of 5000 per year. Lotus have

produced a succession of vehicles by RTM, including the Elan, Esprit and Excel. Ford have used RTM for spoilers for the Escort Cosworth produced by Sotira and the Transit High Roof.

RTM is also an ideal choice for the commercial vehicle market since production volumes for commercial vehicles are low compared to those in mass car production. The market for low emission vehicles is on the verge of expansion. By 1997 at least 2% of all car sales in Los Angeles must be low emission vehicles and by 1998 another 2% must be zero emission vehicles[14]. These low emission vehicles will be electrically powered. Minimising the weight of these electric vehicles will be essential since the batteries account for one third of the vehicle weight. RTM is a major contender to produce the parts for any electrically powered vehicle with predominantly composite material construction[13].

RTM is especially applicable for high cost products requiring structural strength, and good aesthetics. Faced with the imperatives of more aggressive styling, shorter development cycles, greater competition and more limited edition models, designers will have to shift from pressed steel to alternative materials and processes[12].

2.4 Reinforcements and Preforming

The assembly of the reinforcement in the mould before injection is time consuming and labour intensive. Preforming of the reinforcement as a separate process is necessary for high volume production[5]. The fibre reinforcement type and the form in which it is used determines the processing properties of the preform and the mechanical properties of the final component.. E-glass fibres are most commonly used, although carbon, aramid and polyester fibres are also employed[5]. These fibres can be incorporated into a variety of fabrics and mats.

For low to medium stress parts continuous filament random mats (CFRM) are used to produce preforms for RTM. These mats have a thermoplastic binder applied to the rovings to allow thermoforming and to resist fibre washing during the impregnation of resin[15]. The mat can be heated and formed into complex shapes in

a preform tool. The preform usually requires trimming before it is placed in the mould, which generates waste. Reinforcement is also wasted at the initial cutting stage and the overall mat utilisation can be as low as 70%[16]. Volume fractions are limited to 30% since beyond this value fibre damage occurs due to the crushing of fibres during shaping.

Other reinforcements include chopped strand mats, woven fabrics and non-crimp fabrics (NCF). Non-crimp fabrics contain directional fibres which overcome the problems of crimp with woven fabrics[17]. The fibres are set straight within the fabric, and not crimped like woven fabrics, which improves the in-plane properties of the laminate. The stitching used in these fabrics can be varied to produce conformable materials allowing drawing with high fibre volume fractions.

Sizes

During manufacture stage of glass fibres the filaments are coated with an aqueous solution of compounds called size. Size is a polymeric film which covers the individual filaments ensuring cohesion and protection from abrasion. The size contains film former products, antistatic products, plasticisers and coupling agents[18]. The formulations of the sizes used on E-glass fibres remain propriety to the fibre manufacturer. The sizes used on commercial glass fibres contain less than 5% (by mass) of coupling agent, and a mixture of these agents is often used to permit compatibility of the reinforcement with a number of resin types. The plasticisers, lubricants and antistatic compounds constitute 15% of the size with the remaining 80% being film former to bind the individual filaments into strands[19]. Current sizes used in the FRP industry contain water soluble thermoplastic polyester film formers which are also styrene soluble. These are termed soft sizes. Film formers containing thermosetting polymers are termed hard sizes and are insoluble in polyester resin.

Binders

Binder is applied to the fibres during the mat or preform manufacturing stage, to provide cohesion for handling and processing[5]. Thermoplastic or thermosetting polymers in the form of powder or emulsions are also used. The dry thermoplastic

binder on CFRM mats is applied to fibre tows and heated to melt the powder particles onto the fibres[20]. The binder on these mats is a bisphenolic polyester resin[21]. Advanced binders which cure in the presence of ultraviolet radiation have been developed recently[22]. These binders respond to the directed ultraviolet energy applied at wavelengths which are transmitted through the glass fibre reinforcement and the transparent preforming tools.

The binding of fibres can also be accomplished mechanically by stitching with yarn or roving.

2.5 Void Formation in RTM

The effect of voidage upon the mechanical properties of a composite

It is well documented that regardless of resin or fibre types, voidage within the matrix of a composite material is detrimental to the mechanical properties. Judd & Wright[23] concluded that regardless of resin type, fibre type and fibre surface treatment the interlaminar shear strength of a composite material decreases by about 7% for each 1% of void content, up to a total voidage of 4%. Bowles et al[24] found an empirical relationship between void content V_v and interlaminar shear strength (ILSS) of a 0° composite:

$$ILSS=(2.035(1-V_v)(0.486V_f+1.1313))^{4.46} \qquad (2.1)$$

High void content adversely affects the mechanical properties of the composite in other ways, decreasing flexural strength, durability and fatigue resistance, increasing susceptibility to weathering and moisture absorption, and increasing scatter in strength properties[25]. Voids can undermine mechanical properties during service by facilitating moisture absorption and degradation of the fibre-matrix interface. These voids can create pathways for the diffusion of moisture into the system, which can lead to plasticization of the polymer, degradation of polymer chains and weakening of the fibre-matrix interface due to oxidation[25]. The presence of voids at or near the surface of the moulding can be detrimental to the surface finish of the moulding, especially if the moulding requires a hot painting operation, since serious bubbling is likely to occur. It is thus imperative for the mechanisms of void formation to be fully

understood, for the design and integrity of structural RTM components.

Apart from large voids, Hull[26] describes two main types of voids in FRP:

i) Voids between fibres which may be spherical or elongated into ellipsoidal cavities parallel to the fibres. The void diameter will be related to the fibre spacing and is typically in the range 5-20μm.

ii) Voids between laminae and in resin rich pockets.

There are several suggestions for the formation of these voids[26], which occur in all composite processes. Mechanical entrapment of bubbles during the impregnation process results in incomplete wetting out of the fibres by the resin. Entrapment is suggested to occur where the complex micro-flow through the reinforcement in areas of high fibre volume fractions and areas of low volume fractions exist side by side. The second main cause for void formation arises from the presence of volatiles produced during the curing cycle in thermosetting resins. These volatiles may be residual solvents, or may be formed during the reaction between resin and catalyst, or by reactions between catalyst, resin, binder, or sizing of the reinforcement.

The void content within a finished component will be determined by the initial void content in the resin, void formation during the injection, and void growth or shrinkage during cure.

Void Content Analysis

The void content of a composite can be determined using several methods[26]. Voids can be optically detected in polished sections. The volume fraction of the voids can be determined by a quantitative analysis, usually using point counting techniques on micrographs, or by computer aided image analysis techniques. This approach allows a local evaluation of the type and distribution of voids but a large number of sections must be examined to obtain a reliable value. A simpler approach is based on density measurements, where the volume fraction V_v is defined as:

$$V_v = 1 - (V_f + V_r) \qquad (2.2)$$

This method however is inaccurate since V_v is calculated from two relatively large

values and the density measurements are not reliable (resin densities vary between batches, amount of binder on mats vary, etc). Both these methods have difficulty in determining small void fractions (between 0 and 1%).

An ultrasonic scanning technique (C-scan) can also be used for the non-destructive examination of void distribution in composites. The specimen is scanned by an ultrasonic pulse and the attenuation in the material is measured. The information is processed to produce a two-dimensional image of the sample. This method is unable to give an accurate indication of void content (since only 2-D information is provided). The types and locations of voids within the composite structure are unknown.

The results gained from both the section analysis and burn-off techniques may be inaccurate. The section analysis technique can be subjective to a degree, unless the process can be randomised or automated. The burn-off technique allows a much larger volume to be appraised, reducing the effect of human error.

Void formation during injection

Many theories have been suggested for the causes of void formation during injection.

During impregnation, the resin must displace all of the air from the preform before gelation, otherwise voids are formed within the moulding. Parnas and Phelan[27] suggested that as the advancing resin flow front encounters a fibre bundle it flows around it, entrapping a pocket of air as it does so. The bundle is slowly impregnated with fluid, but retains the void. The basis for this assumed entrapment mechanism is that the interstitial space within the fibre bundles is much smaller than the spaces between the bundles which make up the preform. It is expected that the transverse permeability (k_2) of a fibre bundle is much less than the axial permeability (k_1). When the two values are equal the flow front penetrates the fibre bundles at the same rate as it advances through the preform and no air entrapment occurs. Where bundles become successively less permeable and the ratio k_1/k_2 approaches ∞ the rate of fibre

impregnation relative to the motion of the advancing flow front becomes negligible and no voids are formed.

Early impregnation studies were carried out by Williams et al[28], who used a range of liquids to impregnate fibre beds. Liquid was passed through E glass, carbon and nylon fibres, and visual examination showed that some air remained in the bed after the passage of the advancing front. The void volume, determined by weighing was less than 4%, but no dependence on the fluid properties was detectable. Comparison of the results between alcohol and water shows that the effect of entrapped air is dependant on the surface tension, as may be expected. It was postulated that the surface tension of the liquid modifies the flow rate, and alters the distribution of the fibres in the bed. Peterson & Robertson[29] simulated RTM by forcing resin into a glass tube packed with fibres parallel to the tube axis. Flow experiments showed that with low fibre volumes, a few large voids were created, which were elliptical in shape. These voids were fairly mobile and most were washed in the direction of flow. Higher fibre volume fractions (>50%) showed a uniform distribution of voids, which became cylindrical in shape, oriented in the flow direction. These voids were less mobile. The void volume decreased with increasing injection pressure, while the mobility increased. The voids were seen to form primarily at the fibre to resin interface. Voids were found to be trapped where local inhomogenities in the fibre direction constricted the pathway of void movement. In a second paper Peterson & Robertson[30] studied the impregnation of resin into glass fibre filled tubes of variable diameter and with bends. The capillary number,

$$C_a = \frac{\mu v}{\gamma} \tag{2.3}$$

was seen to affect the generation of voids, although this number is linked to the distance from the injection point and the injection pressure. In the bent tube experiments large voids were formed in the bend region. These were explained by the inhomogenities in the resin flow profile, and variations in the local permeability. In variable volume fraction experiments where the section of a straight tube was expanded, the fibre preform was the same, but the expansion of the cavity reduced the

overall fibre volume fraction. This increase in permeability resulted in a large pressure drop and an increase in void content.

Molnar et al[31] showed micrographs of low and high flow rates through a unidirectional (0°) fabric. At low flow rates the liquid front flows faster along the fibres than in the channels between the fibre bundles, which can be explained by a capillary effect. At higher flow rates, the flow is less affected by capillary action and the liquid front flows much slower along the bundles than in the channels. This work supports the air entrapment mechanism proposed by Parnas and Phelan[27].

A similar dual filling action was observed by Wang et al[32]. Liquid was injected into a stack of CFRM and excess resin purged. This bleeding of the resin illustrating two scales of flow in the mat. Large bubbles were believed to be associated with expelling air from gaps between fibre bundles, whereas the flow into the fibre bundles seemed to drive out the smaller bubbles. During the purging stage, both large and small bubbles exited the reinforcement at the fibre flow front, but at a later stage, there was a transition region when all the larger bubbles seem to have been purged and only small bubbles exited the mat. The end of mould bleeding was signified when no more bubbles exited the mat. Wang, Patel and Lee[33] observed this lead-lag phenomenon near the flow front, while impregnating stitched fibre mats. Wang et al[32] also studied the influence of fluid viscosity upon void formation and removal in random fibreglass mats. Lower viscosity liquids (30-100 cp) produced a larger region of bubbles of various sizes, while the higher viscosities produced only small bubbles, which took longer to bleed from the mat. Fibre volume variations showed that higher porosities showed larger bubbles leaving the mat, with the size of the bubbles decreasing as porosity reduced. The work indicated the times taken for all the bubbles to exit the mat but no comment was given on the relative volumes of resin which where required to achieve this.

Dave and Houle[34] used a rectilinear flow mould to observe flow channelling under increasing flow rates. This channelling was explained by the reduction in isolated pore spaces where trapped air bubbles are transported under high shear flow.

Transported air bubbles were either flushed out of the mould or coalesced to form connections between isolated pore spaces. Bubbles were seen to be flushed out of the mould as the flow rate was increased.

Hayward and Harris[35,36,37] studied several factors which affect void content during RTM, and showed that voidage decreases, whilst shear and flexural strength increase when the preform is impregnated with resin with the assistance of a vacuum. Image analysis of mouldings produced using vacuum assistance revealed that there was a substantial reduction in porosity, with mean levels of porosity of 0.15% for vacuum assisted injection and 1.0% without assistance. These improvements did not result from an increased pressure differential between the resin stream and mould cavity. Molnar et al[31] also noticed that by partially evacuating the mould cavity the sizes of the bubbles or voids in the liquid were decreased.

Stabler et al[38] studied the effects of the mould surface, the initial void content of the resin and the vibration of the mould upon the final void content of the composite. Braided carbon fibre preforms were used in the study which were injected with epoxy resin. The mould surface was varied by waxing. Two levels of waxing were applied, heavy and light. A heavy waxed coating permitted more voids to form, probably by providing attachment sites for bubbles on the mould surface or volatilizing partially during polymerisation. The initial void content of the resin was studied by allowing bubbles to form in the feed line which injected resin into the mould. Two levels of initial bubble content were studied. High bubble content caused more voids to form. Studies using a vibrating mould were performed using resin with a high bubble content injected into the mould. A vibration frequency of 10 Hz reduced the void content, but at all other frequencies the void content in the composite was unaffected. The use of vibration to reduce voids during RTM was inconclusive although low frequency vibration has been applied during the processing of pre-preg carbon-epoxy materials[39], where void content was halved.

Modelling void formation during injection

Several attempts have been made to understand and predict void formation

during the resin impregnation phase of RTM[27,29,34]. To model the impregnation phase the permeability of the reinforcement requires characterisation. Several methods of measuring the in-plane permeability of a fabric are available[40,41] (section 2.7). The capillary pressure within a fabric can also be measured, or estimated using simple models[42]. The capillary pressure can also be estimated from a knowledge of the fibre alignment in a fibrous preform, and is expressed as:

$$P_{ca}=\frac{2\gamma\cos\theta}{r_c} \qquad (2.4)$$

Where P_{ca} is the capillary pressure, γ is the surface tension of the wetting fluid, θ is the contact angle between the liquid and the solid and r_c is the equivalent radius of pores in a fibrous form.

Parnas and Phelan[27] have proposed a model using the mechanical entrapment mechanism previously described. The resin first flows around the fibre bundles entrapping air in the bundles. The pressure in the resin surrounding the void will then increase during fill, with the void size consequently becoming smaller. If this pressure then exceeds the vapour pressure in the void, then the entrapped gas should dissolve into the fluid. The extent of dissolution is dependent on what gas is in the void and whether the liquid is already saturated with that gas. This dissolution is a prolonged process dependant on the gases, liquid and pressures involved.

Kardos et al[43] also developed a model to describe the factors affecting void formation in an autoclave process. The model was divided into three phases, void formation and stability at equilibrium, non-equilibrium void growth or dissolution via diffusion, and void transport via resin flow. The void transport during flow is approximated by:

$$\left|\frac{dP}{dx}\right|>\left|\frac{dP}{dx}\right|c=\frac{4\gamma_{LV}\cos\theta}{d_cL_v} \qquad (2.5)$$

where dP/dx is the pressure gradient, γ_{LV} is the resin void surface tension, θ is the apparent contact angle for the void on the solid, d_c is the diameter of the narrowest interstiction in the fibre network perpendicular to the flow, L_v is the void length

projected on the main flow direction. This equation is based upon force balance, for if voids are to be transported by the resin it is necessary for the viscous flow forces to be sufficiently larger than the surface tension forces.

Another approach was used by Chan and Morgan[44] where void formation was presented in a mould filling model utilising multiple injection points. It was assumed that voids were only formed at the flow front and were washed along with it. The model presented a case where as the flow front passed a secondary source the injection from the primary source would cease and injection from the secondary source commence, such that no air could be entrapped in to join line between flow fronts.

Void formation during Cure

Voids may expand or contract due to a pressure variation during the polymerisation stage of the RTM process. A polymer exposed to ambient conditions of temperature and humidity will absorb moisture until a steady state moisture content is achieved within the polymer[25]. This steady state moisture content may be subject to seasonal variations (eg. temperature, humidity), but can be assumed to be uniformly present within a resin. During processing, when the temperature is raised, moisture will evolve from the polymer. The extent of moisture evolution will be governed by the temperature ramp used in the process. The greater the rate of temperature rise the greater the amount of moisture retained within the polymer for a prescribed temperature[25].

Void nucleation during cure is assumed to be due to trapped water vapour, which will expand once its saturation pressure is reached. During the cure the volume of the void changes because, water and other types of molecules are transported across the resin fibre interface and the cure pressure increases the pressure at the location of the void.

Voids formed by monomer boiling (styrene) are briefly mentioned by Hutcheon[4] where vacuum assisted moulding of laminates (using polyester resin and

CFRM reinforcement) was seen to produce voids in the moulding and resin. Apart from this reference no other mention has been found concerning the effects of monomer boil during RTM.

The effects of cure pressures on voids in laminates produced using pre-preg tape were studied by Tang et al[48], with the void content in a composite shown to decrease with an increase in cure pressure. The results are compared to the Loos-Springer model[49] which show reasonable agreement between model and theory.

2.6 Microscopic Impregnation Models

The microscopic flow through the capillaries between fibres has been considered by Bascom et al[45], and more recently Revill[19], where the Hagen-Poiseuille formula was used to predict the rate of flow in small diameter tubes. From the Hagen-Poiseuille formula[53] the discharge through a tube (Q) for laminar, Newtonian, isothermal flow can be obtained by:

$$Q=\frac{\pi d_c^4}{128\mu}\frac{\delta P_A}{l} \qquad (2.6)$$

Revill[19] considered a simple case where resin impregnated a polycorn between four fibres. The impregnation time to fill 0.25m along the section was predicted to take 182 hours, which was thought to be excessive.

Flow transverse to the fibre axis has been considered by Bayramli et al[47]. The fibres were assumed to be packed in a regular hexagonal array and the flow was driven by both impregnation and capillary forces. The cross sectional area available for flow is divided into parallel plates. The capillary pressure is determined from the slopes of the fibre surface and the contact angle between the fibre and the liquid. The two dimensional model assumes steady laminar flow between parallel plates[47]. With the capillary pressure between two parallel plates (δP_{cl}) equal to:

$$\delta P_{cl}=-\frac{\gamma\cos\theta}{r_{cc}} \qquad (2.7)$$

This model was used to compare the effects of the fibre spacing and contact angle

upon impregnation. No realistic material constants were used and no comparison was given with actual liquid impregnation into parallel packed fibres.

2.7 Permeability

The flow of resin through a fibrous reinforcement during the impregnation phase of RTM can be considered the laminar flow of an incompressible fluid through a porous medium. The equation governing the flow process is called Darcy's law, and is defined as[50]:

$$Q = -\frac{kA}{\mu}\frac{\partial p}{\partial x} \qquad (2.8)$$

where k is the permeability of the reinforcement and A is the cross sectional area of the flow regime. The permeability of many reinforcements is anisotropic, varying with the directional nature of the reinforcement. Permeability values for reinforcement structures are at present of great interest to academic and industrial research, where the information is used in a variety of flow modelling applications.

In Plane Permeability measurement

In plane permeability can be measured with the use of a radial mould, as described by Hirt et al[53]. The radial extent of flow is measured over a time period and the two major permeability tensors of the fabric calculated (generally in the X and Y directions).

Transverse permeability measurement

Several British Standards to measure the permeability through the thickness of the material (or transverse permeability) are available, which were originally applicable to the textile industry. BS 4724, Parts 1 (1988)[54] and 2 (1990)[55], describes a method to determine the breakthrough time of a liquid through a fabric, and the permeability of the fabric after breakthrough. BS 5636[56] (1990) relates to the measurement of the permeability of fabrics to air, by measuring the flow rate of air through a fabric with a given pressure drop across that fabric. Both methods were seen to be unsuitable to measure the permeability of RTM reinforcements using

liquids with similar viscosities to resin, since the pressures and flow rates used in these standards were orders of magnitude different to those used in RTM.

Vetrotex have carried out studies[57] to determine the transverse permeability of U750 and U720, two CFRM products. The permeability was measured using 100mm thickness of fabric, located in a pyrex tube, 100mm in diameter. The pressure was measured at either side of this column of reinforcement, using a range of flow rates. Two permeating liquids were used. Firstly water was used for practical reasons and secondly a polyester resin to give an accurate indication of the permeabilities for related liquid injection processes. The results from these trials were given in graphical form as flow rate (cm^3/s) against pressure (bar), no permeability values (k) were calculated for any of the experiments. No comparisons were made of the values gained between the experiments carried out with resin and water.

Adams[58] and Greve et al[59] use a similar pressure differential method with a variation in flow rates. Adams[58] describes the method in detail, but used only single layers of fabric, supported in wire screens to reduce fibre washing or movement. The effect of the screens is eliminated by subtracting the pressure differential due to the screens from the pressure differential for the whole assembly. Water was used with flow rates in the range of 0 to 100 ml/s. The permeability values were repeatable.

A novel method of measuring transverse permeability has been used by Miller et al[60]. The method used a constant volumetric flow rate to displace liquid through a fabric and measured the pressure changes during contact. An Instron testing machine crosshead was used to actuate a piston forcing the liquid through a fabric specimen. A pressure transducer was located below the liquid column. This column height was constant throughout the experiment and only the pressure changes due to the contact with the specimen were measured. This method produced accurate, repeatable measurements of both the wetting phase and steady state flow. Only a small volume of liquid is required for this experiment, which makes it ideal for use with resins and oils of similar viscosities.

For the measurement of transverse permeability the D'Arcy law may be applied[58] as:

$$Q=\frac{k_3 A \Delta P}{\mu h} \tag{2.9}$$

Where Q and ΔP are the volumetric flow rate and the pressure drop across the fabric respectively, A and h are the flow area and the thickness of the fabric, μ is the viscosity of the liquid, and k_3 is the transverse principal perineability.

Multilayer preform assemblies

In many applications multilayer assemblies are used to provide specific mechanical properties, such as stiffness or strength. A number of models are available for flow simulation within a mould cavity[51,52]. These models assume in-plane plug flow in the reinforcement, using either a bulk permeability for the reinforcement stack or assuming that the material is homogeneous.

Several studies and theories have been used to determine the interaction between the in-plane and the transverse flow during the impregnation of multilayer assemblies. Molnar et al[31] performed extensive empirical studies using heterogeneous multilayer assemblies, using a one dimensional rectilinear permeability rig. Adams[58] performed in-plane permeability experiments on multilayer assemblies using a circular permeability rig. Radial filling experiments were carried out on various reinforcement combinations. A hole was cut into the centre of each stack below the injection point, to initiate flow in all layers of the stack. The experiments showed that the transverse flow between the layers had a significant effect on the permeability and reduced the anisotropy of the assembly. In-plane anisotropies could be reduced by the addition of high permeability isotropic layers, whilst the permeability of the stack could be enhanced by the presence of a single high permeability layer. The position of this layer within the stack was also important. By placing the layer in the centre of the assembly the flow was able to divide, filling the preform transversely. Adams[58] suggested that this permeability enhancement was due to the transverse flow mechanism within the multilayered structure and that the transverse permeabilities

were the most important variables in the filling of multilayered assemblies.

2.8 Void Formation in Filament Winding

The filament winding process allows a strand (or strands) of fibres from a reel to be passed through a fibre tensioning system, through a resin impregnation mechanism to be wound onto a rotating mandrel. Several researchers have considered the effects of void formation in the filament winding process. Zisman[61] has pointed out that complete impregnation of a liquid resin into either a fibre mat or a strand of filaments is a complex capillary process and complete impregnation is difficult, especially if the individual filaments are poorly wet by the resin. Voids at the glass resin interface may remain unfilled if the resin is too viscous or if it cannot penetrate all of the accessible surface pores and cracks before polymerising. Zisman[61] also studied the adverse effects of microvoids on the strength and water susceptibility of filament wound composites.

Paul and Thomson[62] studied the types of voids in filament wound structures and their effects on the mechanical properties of the windings produced. They observed that by winding cylinders in a vacuum chamber the void content of the composite could be controlled and reduced. Voids in filament wound components were classified into several categories; macroscopic voids (normally circular holes distributed through the cross section), interstitial voids (microvoids, located between individual filaments, where the resin was unable to penetrate the fibre bundle structure), planar voids (between layers of filaments), and craze voids (usually craze cracks caused by cracking in the composite).

Bascom and Romans[45] during experimental filament winding observed that the liquid in the resin bath became filled with bubbles as the operation progressed. The impregnation of single strands whilst being drawn through a resin bath was observed, and quantitative determinations were made of the effect of resin properties and of different winding conditions upon air entrapment. Microscopic examination of their test rings revealed high void contents. The axial flow in the capillaries between filaments was too slow to make a significant contribution to filling and the strand was

assumed to fill transversely to the fibre axis. They also showed that if the strand tension was allowed to relax and then reapplied, air bubbles reduced their surface area by assuming a more spherical shape. In this condition the bubbles resisted being elongated when the tension was reapplied and were expelled from the strand.

Chandler et al[63] modelled the resin impregnation of fibre tows passing over pins. The pin over which the fibre was passed was divided into four different regions. The entry zone, the impregnation zone, the contact zone and the exit zone. The entry zone is where the fibre tow approaches the pin, at an angle determined by the geometry of the process, as the gap between fibre and pin decreases and a pressure is generated in the resin film between the two. During the impregnation zone the pressure generated in the resin film causes transverse impregnation of the tow, this is considered to be the only zone that affects the impregnation process. The contact zone begins when sufficient resin has been forced through the fibre tow to allow contact between the fibres and the pin. The exit zone is where the tow leaves the pin, at an angle determined by the geometry of the process. Each region was considered in turn and an overall model was used to predict the impregnation of nylon into glass fibre tows .

Kohn et al[64] studied the interaction between void content and interlaminar shear strength in filament wound sections. They used area estimation techniques, on thin sections of the composites studied under a microscope.

Weatherby[65], during experiments to determine the strength of filament wound composites, assessed voidage within the components on a subjective basis. As the number of layers wound increased, so did the number of visible voids. The effect of winding four rovings at once was also seen to increase the voidage. The use of high feed rates resulted in frothing at the guides which contributed to an increased void content.

Revill[19] used a filament winding mechanism to study the dynamic wet-out and air entrapment during rapid flow of resin into reinforcement. By studying a strand

pulled through a resin bath, it was observed that the core of the strand was not wet out until the strand was mechanically worked by passing it over a roller. The amount of air in the strand increased as the speed of impregnation increased. This was thought to be caused by the increased contact angle between fibre and resin, which reduced the wet-out of the strand increasing the entrapment of air.

2.9 Discussion

The literature surveyed in this chapter has considered the state of current research relating to void formation in RTM. Apparently no systematic study has been made to identify voids within RTM components and to postulate their causes.

This review has indicated several factors which influence the presence of voids in RTM components. The viscosity of the resin, reinforcement, porosity, mould surface, mould temperature and injection pressure have all been shown to affect void formation. The effect of mould temperature or injection pressure upon void content is unclear . A low pressure is able to impregnate the fibre bundles better than a higher pressure, when the speed of the flow front is high. It appears that voids trapped in reinforcement can be flushed out with a high injection pressure. The bleeding or purging of the resin flow front has been shown to remove or expel a quantity of air bubbles at the end of resin injection. No attempt has been made to collectively assess all these mechanisms, or to understand their interaction.

The use of vacuum assistance during the injection has shown a reduction in void content, and an increase in the mechanical properties of the composite. Apart from a reference by Hutcheon[4] no mention has been made of the disadvantages of using vacuum assisted moulding. Monomer boil was reported to cause gases in a resin whilst at low pressures, but to what extent this affects void content is unclear.

It has been suggested that during the polymerisation stage voids may decrease in size due to high cure or injection pressures. No effort has been made to link these phenomena to the void content within laminates. Voids may nucleate during the cure stage due to moisture ingress into the resin system. The effect of moisture upon the

void content of the laminate is also unclear.

The addition of size and binders on to glass fibres has been assessed. No publications have been discovered concerning the structure of the size or binder once it has been applied on the strand. The dissolution of these additives into the resin system during the injection phase is not reported. The exact formulations of these additives are unclear and remain the secret of the size and resin manufacturers.

Impregnation studies, usually as a side issue to permeability measurement have been undertaken on a selection of fabrics and mats. Observations were made, but no organised study was undertaken to explain any voids which occurred. The measurement of the permeability of fabrics is now a well accepted practice. Many publications list various methods of gaining permeability data, although no standard method is available. Some work has been published to assess transverse permeability measurements, with attempts to model the interaction between transverse and in plane flow in multilayered preforms. The modelling has been concentrated towards the macroscopic predictions of resin flow through component preforms, and not towards the understanding of air entrapment.

Modelling void formation during the impregnation phase has been attempted by several researchers. Microscopic modelling of flow between ideally packed cylinders has been carried out to study wet out times and to predict flow perpendicular to fibre axes. No attempt has been made however to compare the microscopic flow regimes within a preform, or to understand the impregnation mechanisms which cause air entrapment.

Void formation is not solely limited to the RTM process. In filament winding impregnated tows are wound on to a mandrel and then cured. Several researchers attribute the majority of the voidage in these components to be due to the same impregnation problems associated with completely wetting fibre bundles. The mechanisms which caused these voids have not been studied in the literature.

Chapter 3

Experimental Techniques

3.1 Introduction

This chapter details the experimental apparatus and techniques used within the course of this research. Experiments were performed to study the mechanisms affecting the formation of voids during RTM. Numerous components and plaques were manufactured using the two moulding facilities and materials briefly described in this chapter. For a fuller description of the RTM facility refer to Kendall[16] and for greater detail of the Fox & Offord facility refer to Hutcheon[4].

To study the mechanisms which cause internal defects in mouldings, components have been produced with a selection of process parameters. The manufacture of cylinders by a Pultrex five axis filament winder has also been described. The fibre impregnation mechanism has been considered in detail, and was shown to have many similarities with RTM.

An explanation is given of the various analysis techniques used to examine the specimens taken from the laminates and the dry fibre reinforcements. Finally the methods used to determine values of resin properties for an impregnation model, as considered in chapter 8, are presented.

3.2 RTM Facility

A dedicated RTM facility has been developed over the period 1988-1993, suitable for prototype manufacture of automotive components. The following equipment is sited within this facility:

Preforming and Trimming

A hot air preformer was utilised to enable the reinforcement to be heated

sufficiently to melt the thermoplastic binder for preforming (Figure 3.1). The preformer houses perforated GRP shells supported by a tubular aluminium structure. Both shells are supported on air boxes air was supplied from a centrifugal fan via heaters. Each GRP face was machined with slots to enable the heated air to penetrate the reinforcement. Fibre was laid down on to the lower face of the preformer and thermoplastic binder was applied between the layers of reinforcement if required. The two halves of the preformer are located in a steel framework. The upper framework with the upper preform mould moved relative to the fixed lower half. This framework was actuated by four hydraulic pistons, which were controlled by a flow divider and could close with a pressure of approximately 0.8 bar acting over the preform.

The preform outline was cut to shape using a GRP template. The two halves of this template tool were clamped together and the excess material removed using electrically powered shears.

Moulding

A mould manipulator is shown in Figure 3.2. The mould was placed between two stiffeners. The manipulator is a mechanism actuated by four hydraulic cylinders which raises the upper stiffener and male mould relative to the lower stiffener and female mould. The cylinders were supplied by a hydraulic powerpack operating at a pressure of 50 bar. The pistons have a stroke of 1m and were able to operate at a speed of 0.25m/s, this speed was reduced to 0.05m/s by the use of a flow restriction valve in the last 30mm of the piston stroke during mould closure, in order not to damage or distort the shell mould.

The two stiffeners were locked together with a clamping system which was designed specifically for the undershield mould, although it can be modified for moulds of different depths. Ten clamps were located inboard of the stiffeners, such that the clamps were in close proximity to the mould, and were connected to the stiffeners to reduce deflections to a minimum. The closing force of the system was 65 kN. A reactive force of up to 700 kN was possible, which was approximately 8 bar hydrostatic pressure over the mould surface, once the system had been locked off,

to resist mould opening pressures and pressure activity during the curing phase.

The undershield mould[14] is an electroplated nickel shell, backed with copper and mounted on an aluminium backing frame. The mould was designed to produce components for the Ford Sierra Sapphire RS Cosworth and Escort Cosworth rally sport team vehicles. It is a fully developed component moulding tool. An outer periphery silicone rubber strip sealed the mould cavity. The surface finish was polished to a 0.5 Ra value to be able to produce class 'A' type finish and to aid component release. Each mould half houses sixteen separate heating circuits. The circuits were constructed from copper piping and all connections are brazed. A Mokon 48 Kw oil heater was able to supply the two heating zones at temperatures between 20°C and 140°C. The heater allowed cooling to take place during matrix exotherm, with the oil reservoir maintained at a constant temperature via a 15 Kw chiller unit.

The component was removed from the lower mould half by the use of four stainless steel ejectors, of the poppet valve type. These were pneumatically operated and able to raise the component above the vertical flash gap edge for easy removal.

Two types of instrumentation were housed in the mould faces; thermocouples in the upper mould half and pressure transducers in the lower half. This instrumentation, along with the injection gate which was located at the centre of the lower mould half, were mounted in stainless steel bushes which were inset during the electroforming process. The instrumentation was connected via Burr Brown analogue to digital conversion boards which were interfaced to a PC and the information displayed and processed using software written in a Borland Turbo Pascal programme.

Injection and Venting

The resin injection equipment was a modified commercially available Hypaject system supplied by Plastech UK. The Hypaject consists of a 30 litre pressure vessel termed the homogeniser which was used to store and pressurise pre-mixed resin. This was connected to the lower mould half via an injection line and a thermal break valve (TBV). The system used compressed air (at pressures up to 7 bar) to pressurise the

resin. The TBV provided a thermal barrier between the heated mould and the cooler resin injection line. Following injection, resin could be either left in the line awaiting the next cycle or could be removed and the line cleaned by flushing with acetone. The homogeniser was suspended from a load cell which was connected to the data logging system, and was used to determine the quantity of resin held in the homogeniser, and the amount of resin injected into the mould.

Air and excess resin were vented from the mould cavity from two vent lines. These vent lines were opened or closed by two further TBV's. Acetone was used to flush the venting system, and the residue collected in sealed drainage buckets. The vent lines could be connected to a vacuum pump and the mould partially evacuated for vacuum assisted moulding.

Moulding Sequence

The moulding sequence in the RTM facility is described in Appendix 2 (Figure 1.1):

3.3 Fox & Offord Moulding Facility

The Fox & Offord press is a 500kN upstroking hydraulic press (Figure 3.3a) which houses a flat plaque mould measuring 518mm by 500mm with a cavity thickness of 3.6mm (Figure 3.3b). The plaques produced in this mould were used to evaluate materials and process parameters for the larger undershield mould. The mould was aluminium faced with steel edges and a steel injection gate (Figure 3.3b). Flat preforms were produced by heating the mould to temperatures of 80°C, placing the reinforcement between layers of Melenex and closing the mould for 15-20 minutes to allow the binder to melt.

The injection system was of similar construction to that of the RTM facility. The homogeniser had a 10 litre capacity but no load cell to measure resin qualities. The thermal break valve and vent valves were of similar construction. The injection pressure could be varied between 0 and 5 bar. The mould used an edge injection gate the length of one side of the mould to promote rectilinear flow. The thermal break valve injected resin into a gallery which feeds this gate.

Both mould halves were heated by thermostatically controlled 3.5 Kw platen heaters. The temperature range of these heaters was 20°C to 140°C. Two ejectors were located at the venting end of the mould, these were of a parallel pin type, sealed by 'o' rings. The ejectors were operated manually and were returned by coil springs.

The instrumentation used was similar to that of the undershield mould with 5 thermocouples in the upper mould and 5 pressure transducers in the lower mould. Data was captured in a similar fashion to that previously described for the RTM facility.

Process Variables

The range of fibre volume fractions of unidirectional reinforcement which can be used in the flat plaque mould is influenced by possible fibre washing or incomplete fill. Experimental results determined that the fibre volume fraction range, which could be used for unidirectional reinforcement in this mould, was between 25%-50%. For the purposes of studies in this thesis variations between 25% (4 layers) and 37% (6 layers) were used.

CVP 6345.001 unsaturated polyester resin with 1% TBPEH was used with mould temperatures in the range of 80°C to 120°C. The injection pressure was found to be dependant on fibre washing of the preform. Too small an injection pressure resulted in the resin polymerising prior to the mould filling. If too high an injection pressure was used the preform moved, the compacted preform then exhibited a low permeability and dry patches were created where resin travelled along the edges of the preform. The range of injection pressures (1 to 3 bar) used in this study allowed the preforms to be fully impregnation without washing or premature cure.

Prior to being drawn into the homogeniser the resin can be preheated in a domestic microwave. Pre-heating reduces the viscosity and the gel time of the resin. The resin was only pre-heated to 60°C to allow enough time for it to be drawn into the homogeniser and injected into the mould cavity. The resin loses heat as it is drawn into the cold homogeniser (approximately 3°C).

Whilst impregnating using a positive injection pressure, the mould could also be evacuated using a positive displacement vacuum pump able to create a partial vacuum of 0.02 bar absolute.

3.4 Materials Used in RTM Trials

Resin

Several resins have been used during the course of these investigations. The undershield moulding trials which have used these materials are listed in appendix 3.

i) Cray Valley Total Chemie, Synolac 6345.001 polyester resin. This resin is a medium reactivity orthophalic polyester resin, and has been employed in resin pre-heating trials and mould conditioning work.

ii) Dow, Derakane 8084 vinyl-ester resin. This resin has been used for moulding for rally components, lightweight mouldings and resin preheating trials.

iii) DSM, Synolite 40-7417 low profile polyester resin. This resin has been specifically designed for RTM processing and has been employed in sequential moulding trials, and Class 'A' component work.

Catalyst

Several catalysts have been applied in these resin systems:

i) Interox, TBPEH (t-butyl peroxy 2 ethyl hexanoate) has been used with Derakane vinyl-ester and Synolac polyester resins. This catalyst is used with mould temperatures between 80°C and 110°C.

ii) Interox, TBPB (tertiary butyl perbenzoate) has been used with Synolite low profile polyester resin. It is used with mould temperatures between 70°C and 90°C.

iii) Akzo, Perkadox 16 (bis-peroxy dicarbonate) has been employed with Derakane vinyl-ester and Synolac polyester resin systems. Perkadox is used in temperature ranges between 50°C to 70°C.

Filler

Calcium carbonate, Omya BLR2 has been used with both Synolac low profile and Synolite polyester resins.

Reinforcement

Continuous Filament Random Mat (CFRM)

These are mats of continuous strands, distributed in uniform layers and held together by a binder. The reinforcement is particularly suited to moulding in RTM, since the mats are preformable. The continuous filament random mat utilised in the RTM programme were all Vetrotex products from the Unifilo range.

The binder used on these mats is a thermoplastic unsaturated polyester resin, which has a high solubility in styrene. This is applied to the fibres either during the mat or preform manufacturing stage, to provide cohesion to the fibres during handling and trimming of the preform.

Unifilo U-750

U-750 was designed for preform manufacture. U-750 is held together by 8% (by mass) thermoplastic binder. The strands range between 25-50 Tex.

Unifilo U-720

U-720 was designed for hot press moulding of flat and thick panels. It is preformable, but stiffer than U-750. The thermoplastic content is 10% by mass and the strands are 25 Tex.

Unifilo U-754

This mat is similar to U-750 except that the thermoplastic content has been reduced to 4% (by mass). The strands range between 25-50 Tex.

Non Crimp Fabrics

The non-crimp directional fabrics used in the RTM programme are a selection from the range of the glass fabric manufacturers Tech Textiles. Non-crimp fabrics are directional reinforcements held in place by polyester stitching, creating layers or plies of variable weight or orientation. The fibres are straight within the fabric and not

crimped like woven fabrics, which improves the in-plane properties of the laminate.

E-Lpb 567 0° Glass Fabric

This unidirectional E-glass reinforcement has a surface density of 567 g/m^2. The fabric has a thermoplastic binder content of 1% by mass on one face and a dry thickness of 0.78mm. The rovings used for this fabric are of 2400 Tex.

EBXhd 936 ±45° Glass Fabric

This bi-directional E-glass reinforcement has a surface density of 936 g/m^2 and a dry thickness of 1.08mm. 600 Tex rovings used in this fabric.

Rovings

Several glass rovings available from different glass fibre manufacturers used in the filament winding experiments have been studied. These are Vetrotex Stratifil 2400 tex, PPG Hybon 2400 tex and Slilenka 2400 Tex rovings.

3.5 Filament Winding

Components produced by filament winding exhibit high void volume fractions, as has been discussed in section 2.7. Several windings were produced to explore the impregnation similarities between RTM and filament winding. The impregnation speeds used in both processes are similar (between 10mm and 150mm per second), and the sizes and locations of voids within the composite structure in mouldings from both processes are comparable (as shown in chapter 9).

Experimental Methods

A Pultrex 5 axis NC filament winding machine as described by Weatherby[65] was used to produce simple cylindrical components with fibres placed at ±75° to the axis of rotation of the mandrel. A schematic diagram of the filament winding mechanism is shown in Figure 3.4 and a photograph of a mandrel during winding is shown in Figure 3.5. The mandrel used in the experiments was an aluminium cylinder, 465mm in length and 112mm in diameter.

The materials used for these experiments were standard products. The glass fibre was 2400 tex, 15µm diameter Silenka 084 K28 E-glass, with Scott Bader Crystic 272 polyester resin with 2% of a hot curing catalyst ('Catalyst B', 50% dibenzoyl peroxide dispersed in di-cyclohexyl phthalate) also supplied by Scott Bader.

Prior to winding, the aluminium mandrel was coated with a Wurtz Pat-607/PCM external release agent. Once the cylinder was wound the mandrel was placed on a rotisserie in an oven for 5 hours at 80°C and 2 hours at 120°C. After polymerisation the cylinder was removed from the mandrel by removing the ends of the winding using a diamond edge saw and sliding off the cylindrical section.

The fibre impregnation system on the Pultrex filament winder (Figure 3.6) feeds the strand over a drum which has passed through a resin bath. The amount of resin applied to the drum is controlled by a 'doctor blade' which scrapes excess resin from the drum. This doctor blade can be positioned at a controlled distance from the drum so that the resin film on the face of the drum is at a constant thickness. An overhead roller above the drum works the impregnating resin into the strand, as well as spreading the strand into a tape. After passing over the drum the strand passes through two combs which also remove excess resin from the strand. The strand then passes through a set of guides before being laid on to the mandrel.

After each winding operation a 1m length of impregnated tow was removed from the filament winding mechanism, cured then analysed. This was examined to determine the void content and wet out of the fibres prior to placement on the mandrel.

In this filament winding apparatus the three variables controlling the fibre placement, once the NC program has been set, are:

i) The tension applied to the fibre, which is set by applying an air pressure to a tensioning system..
ii) The position of the doctor blade.

iii) The surface speed of the mandrel, or the speed at which the filament is laid down on to the component.

During these experiments the back pressure controlling the fibre tension remained at 1 bar (applying a force of 7.5N on the fibres) , whilst the position of the doctor blade and the speed of the mandrel were varied.

Vacuum impregnation of the fibre bundles

To reduce voidage during the impregnation stage of filament winding, a different impregnation mechanism was used. The fibre bundles were drawn through a tube at an absolute pressure of 0.05 bar, then passed directly into the resin bath. The apparatus for this vacuum impregnation mechanism is shown schematically in Figure 3.7.

3.6 Volume Fraction Determination

Void volume fractions were measured using two methods. The void volume fraction determination using a burn-off technique is described in Appendix 4. the second technique, using image analysis is described in section 3.8.

3.7 Impregnation Studies

The impregnation studies described in this section all used an oil of high viscosity (0.224 Pa.s) similar to the viscosity of polyester resin (Appendix 6).

Microscopic impregnation

Using a mould as shown in Figure 3.8 several preform impregnation experiments were undertaken. The apparatus uses a low impregnation pressure (gravity fed) and was used to study the flow in the plane of the fabric.

Transverse flow visualisation

In order to visualise the transverse flow effect within a stacked material structure, a flow visualisation rig was constructed (Figure 3.9). The apparatus was manufactured from Perspex, with an aluminium base. The rig was filled with glass

beads of diameters between 2mm and 6mm, to approximate packed beds of different permeabilities, with metal gauze sheet to separate the layers. Glass beads were used because layers of uniform permeability could be produced, in varying thicknesses. These beads were also easy to clean and re-use. The injection and vents were rectilinear gates to approximate 1-D flow through the rig.

In-plane permeability measurement

The measurement of in-plane permeability was carried out by Bulmer[79], and the values given in this thesis are from her work. A circular permeability rig, described by Hirt et al[53] was used to impregnate material and the various flow front positions and times were used to calculate the permeability of the reinforcement, given by equation (2.8). A full explanation of this method is given in Appendix 14.

Transverse permeability measurement

A method of measuring the transverse permeability of fabrics is similar to that proposed by Adams[58]. The rig (shown in Fig 3.10) consists of two 50mm ID tubes connected at two 32mm diameter aluminium flanges. The reinforcement tested was sandwiched between the two flanges into counterbores cut into both flanges. The thickness of each material tested is adjusted by the addition of brass shims in the counterbores. Pressure taps in the flanges were located 2mm upstream and 2mm down stream of the test specimen.

Fluid (water) flow rates were determined on the downstream side of the apparatus with a Rotameter (metric series size 18). The pressure difference between the two pressure tappings was measured with the use of a water manometer.

3.8 Microscopic Examination

Composite sections

The specimens studied were cut from laminates, and then set in a polyester casting resin for the sample to be polished and then studied. The samples were cut from the mouldings using either a hacksaw, or bandsaw. This initial cut damaged the surface of the moulding, breaking fibre ends and pulling fibre bundles from the

composite (Figure 3.11). The cast specimen was ground flat, but the surface although appearing smooth was still damaged (Figure 3.12). Samples were then polished, which consists of refining the surface with a sequence of polishing papers, burnishing with a 6μm diamond grinding paste, then to finish a 1μm paste. Even under these conditions the specimens could still appear either scratched or overpolished.

Specimens which were studied using the scanning electron microscope were gold coated using a Emscope SC500 gold coating unit.

Dry reinforcement

Dry fibres either in fabric or roving form were bonded to an SEM specimen plate. The assembly was then immersed in distilled water and cleaned in an ultrasonic bath. It was then gold coated and electrically conductive silver paint was used to earth the specimen.

Fracture surfaces

Fracture surfaces were prepared for examination using the same method used for dry fibres.

Specimen examination

The samples were studied in the Materials Engineering and Materials Design Department at the University of Nottingham.

Optical Microscopy using a Nikon photomicroscope

Samples were studied under incident light up to a magnification of 200 times. Translucent samples were studied using light transmitted through the composite. By focusing into the section, the initial structure of the composite could be examined to a limited extent.

Scanning Electron Microscopy

The samples were studied and photographed using a Jeol 35C Scanning Electron microscope. X-ray analysis to identify elements present on the surface of the

specimen was carried out on a Jeol JSM-6400 SEM.

Image Analysis

The photographs taken using the SEM were scanned into a PC, using an Epson GT-6500 colour scanner. Once the picture was scanned the package allowed the contrast of the image on the screen to be modified showing only the dark areas of the voids surrounded by a white background. Figure 3.13 shows an original photograph, and Figure 3.14 shows the areas designated as voids by this process. The image was stored as a bit map and a program was written to count the number of pixels in the image and sum the number of coloured pixels (the voids). From this information a percentage of void content of was estimated. An explanation of this method is contained within Appendix 15.

Hardness Testing

Micro-hardness testing was determined using a Leco M-400A micro-hardness tester, which is formulated for Vickers hardness values. Three values were taken for each area studied and the average taken.

3.9 Resin Characterisation

The CVP 6345.001 polyester resin has been characterised for both viscosity and gel time (using a hot curing catalyst) for use in an impregnation model.

Resin Viscosity

The resin viscosity was measured using a Brookfield viscometer. The resin temperature was raised by heating in a oil bath kept at a constant temperature, and the viscosity measured between 20°C and 100°C. The results of these experiments are shown in Appendix 9.

Resin Gelation Time

The resin gelation time with 1% of the catalyst TBPEH was measured according to "The SPI procedure for running polyester resin exotherm curves[66]". The results of these experiments are shown in Appendix 10.

3.10 Discussion

The experimental techniques described in this chapter were used to study the factors affecting void formation in RTM. The moulding apparatus described has been used by previous researchers[16,4]. Modifications to both facilities were undertaken during the course of these investigations. In particular, the installation and development of the undershield mould described in section 3.2 can be attributed to the work of the author. The filament winding apparatus described is a commercially available system, which has been used by previous researchers[65]. The vacuum impregnation system however, was developed during the course of these studies.

Impregnation studies have resulted from the use of a modified microscopic permeability rig utilised by Bulmer[79]. In-plane permeability values were taken from an available source, with transverse permeability measurement carried out on apparatus developed from a method proposed by Adams[58]. Microscopic examinations and analysis were undertaken using facilities available within the Materials Engineering and Materials Design department at the University of Nottingham.

List of Figures

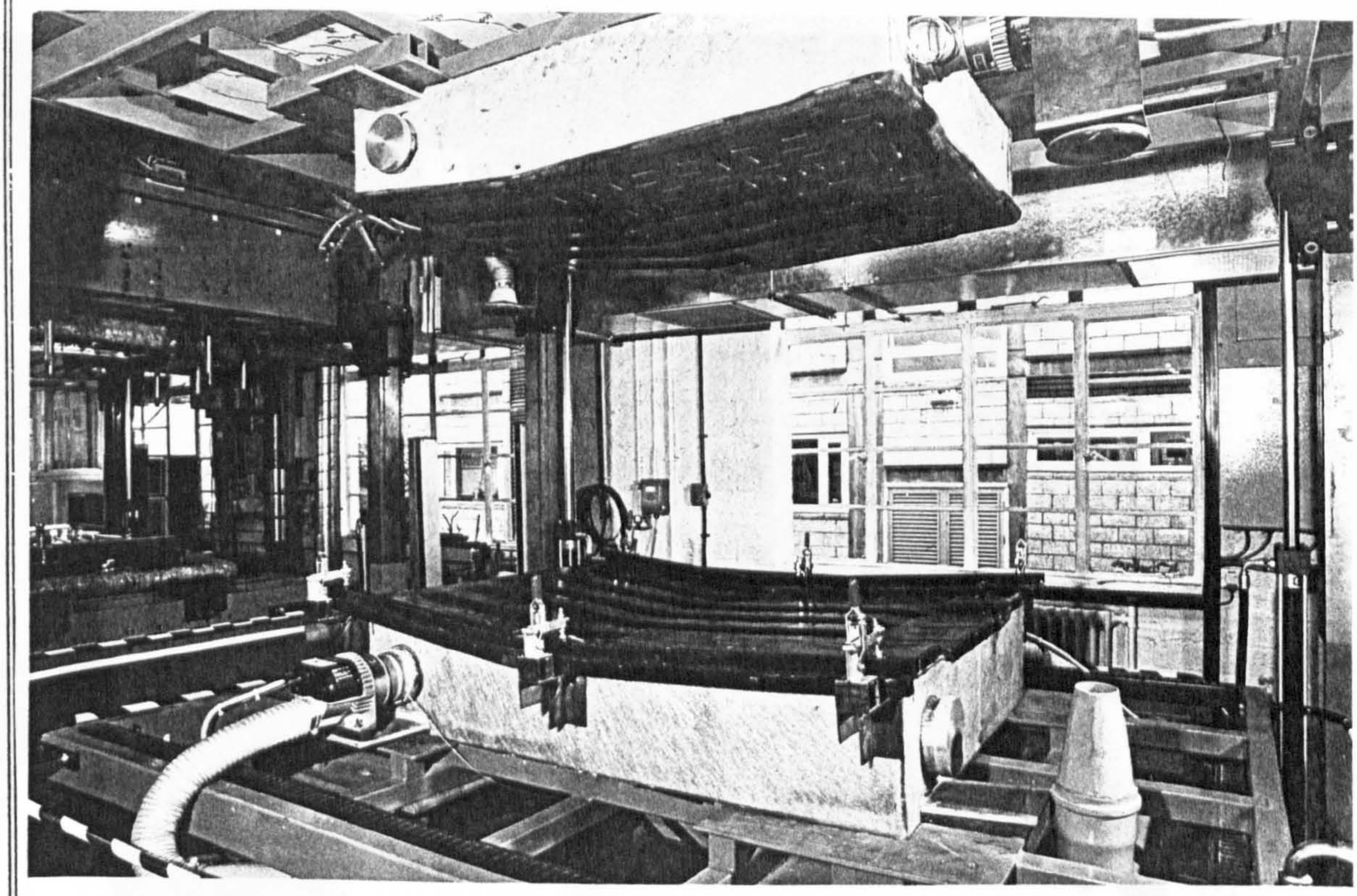

Figure 3.1 The undershield preformer and manipulator.

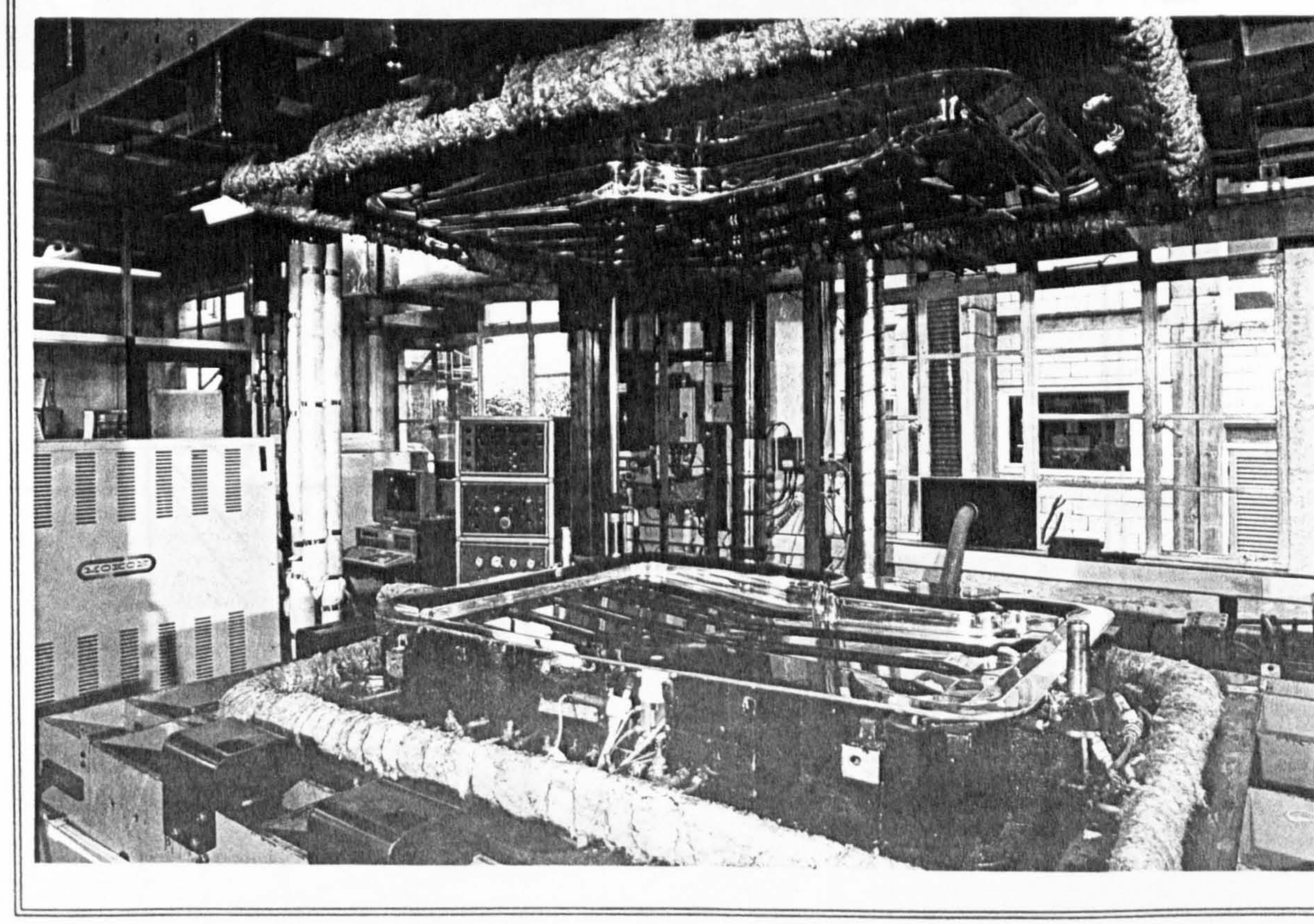

Figure 3.2 The undershield mould and manipulator.

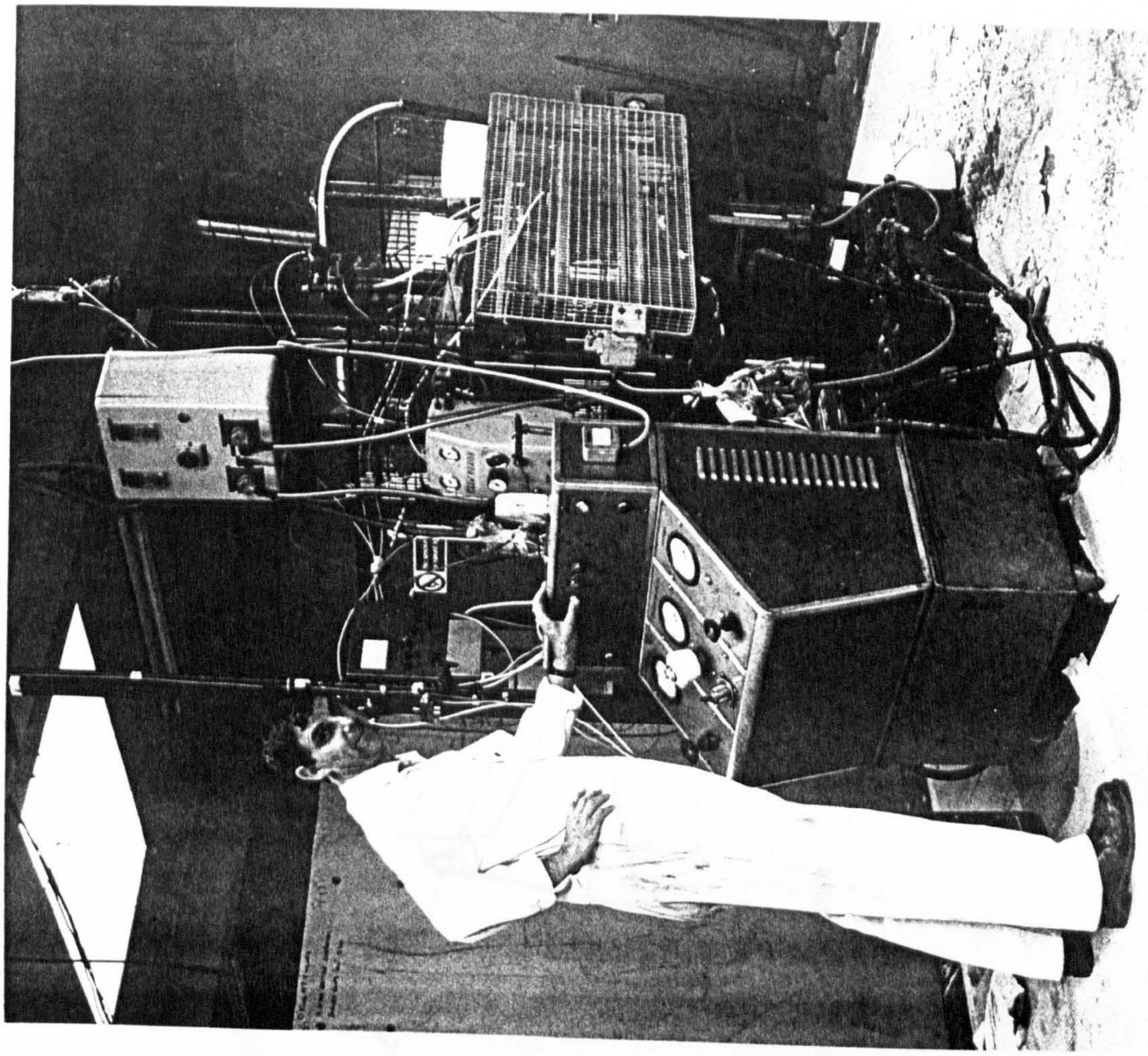

Figure 3.3(a) Fox & Offord Moulding Facility

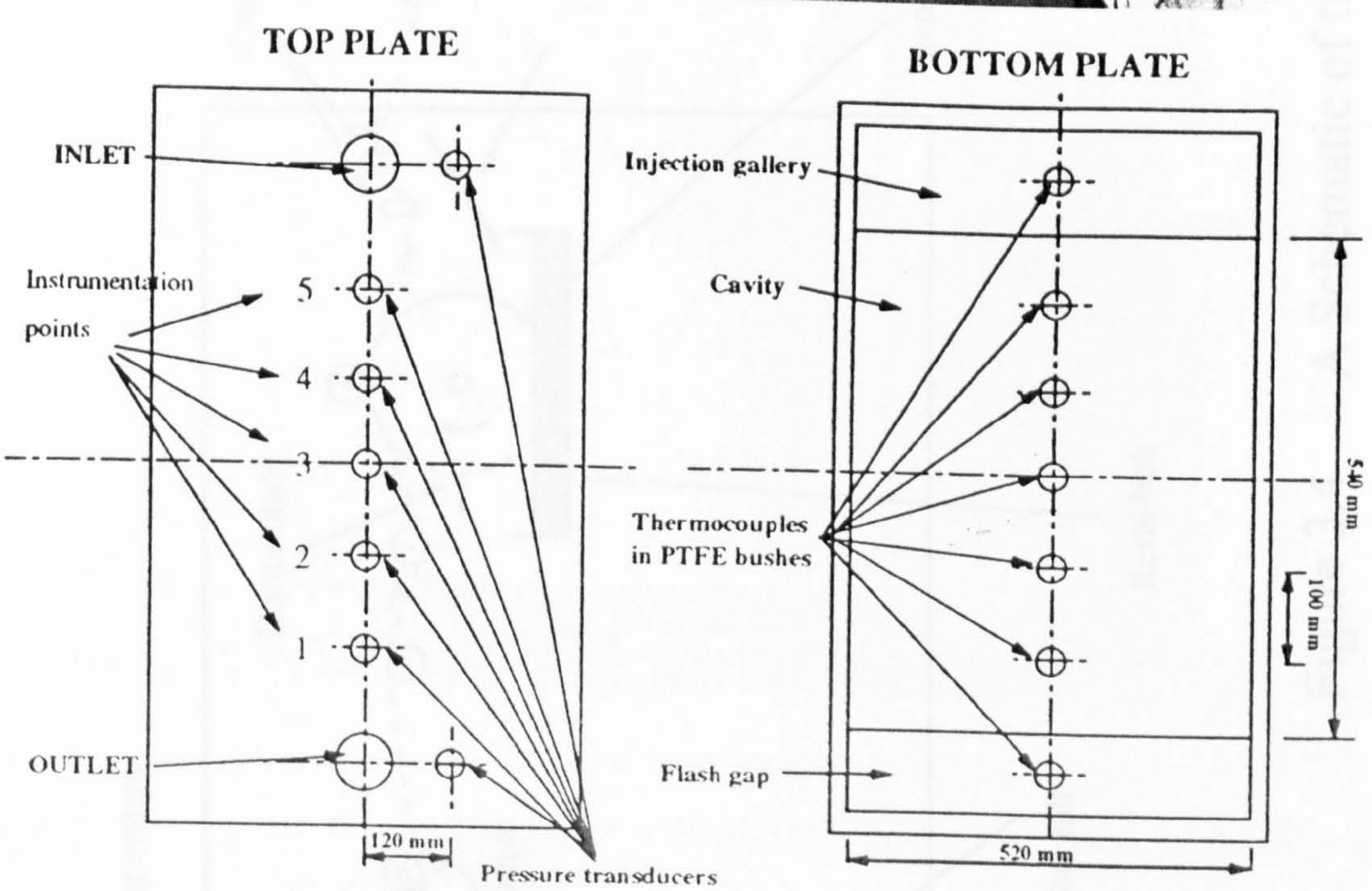

Figure 3.3(b) Flat plaque mould

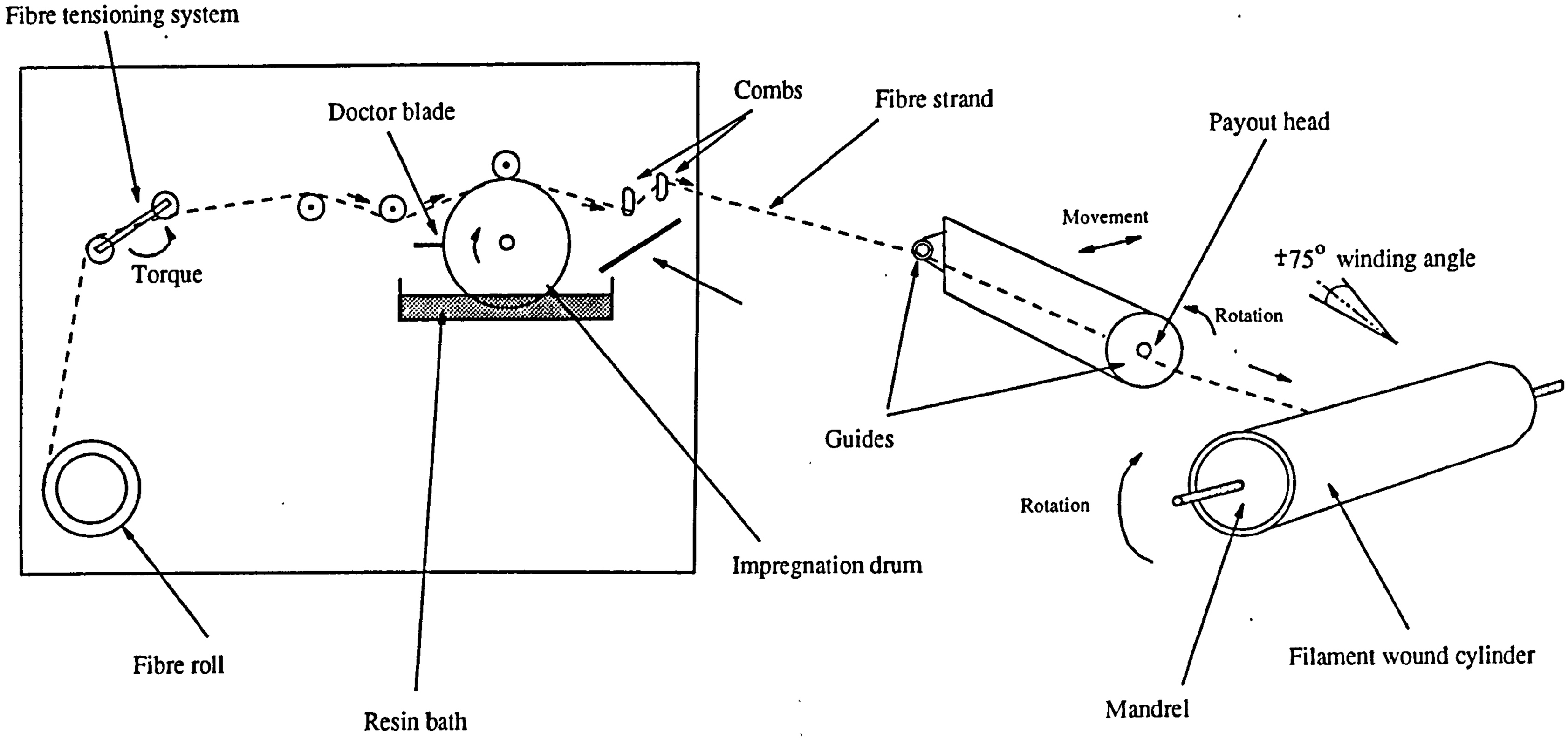

Figure 3.4 A Schematic of the Filament Winding Apparatus

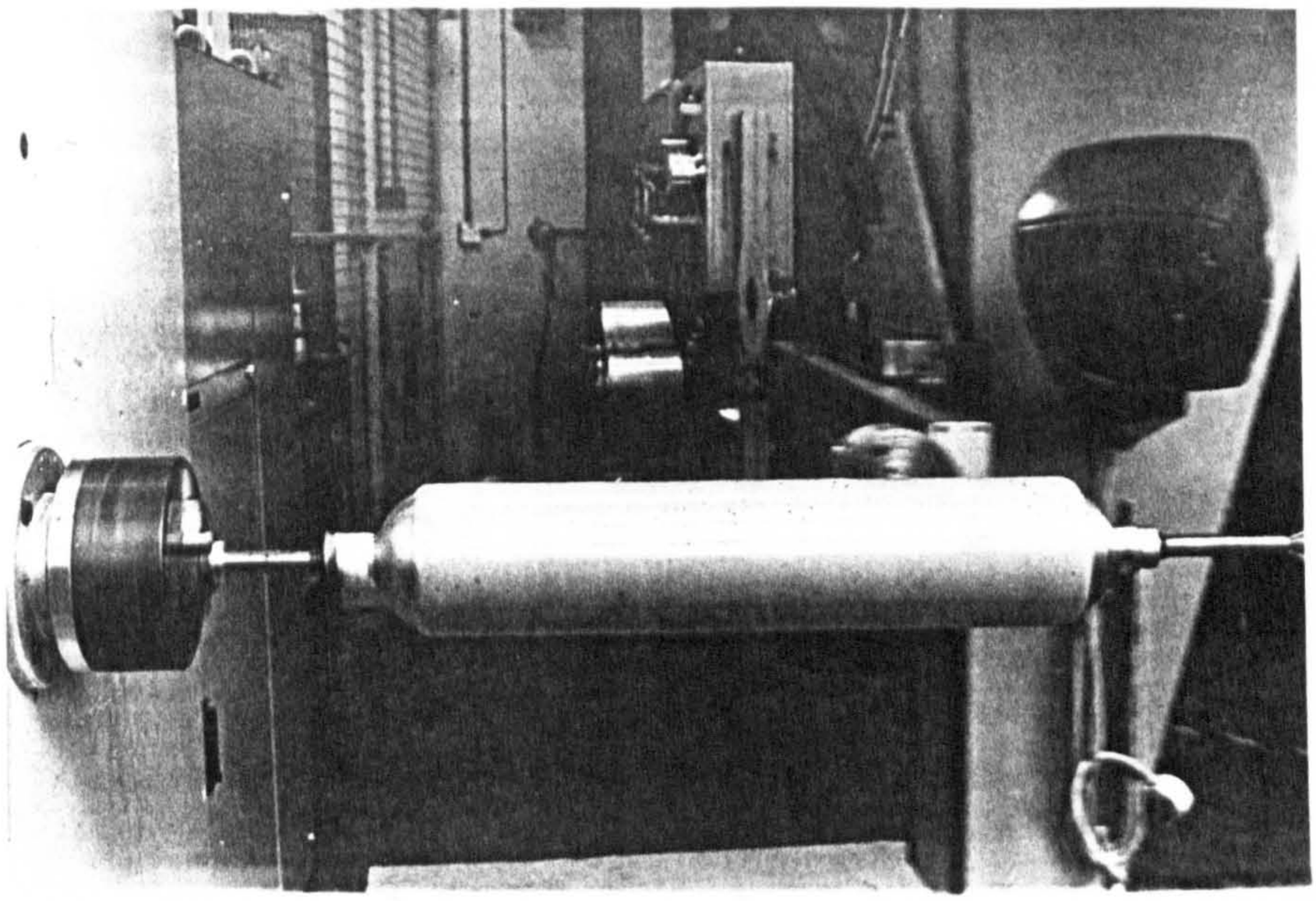

Figure 3.5 The filament winding apparatus with filament tensioning and impregnation mechanism in the background.

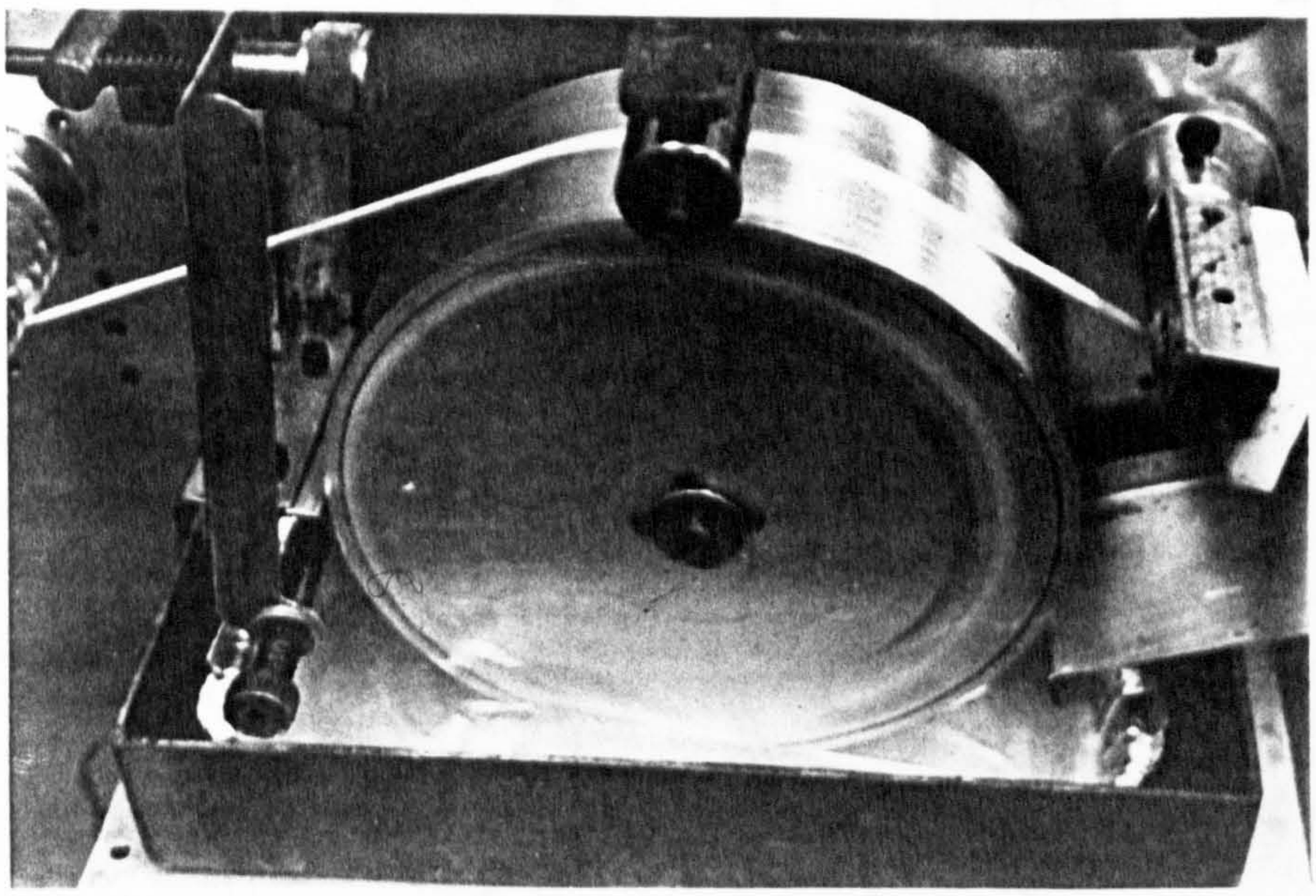

Figure 3.6 The resin impregnation drum, with resin bath used in the filament winding trials.

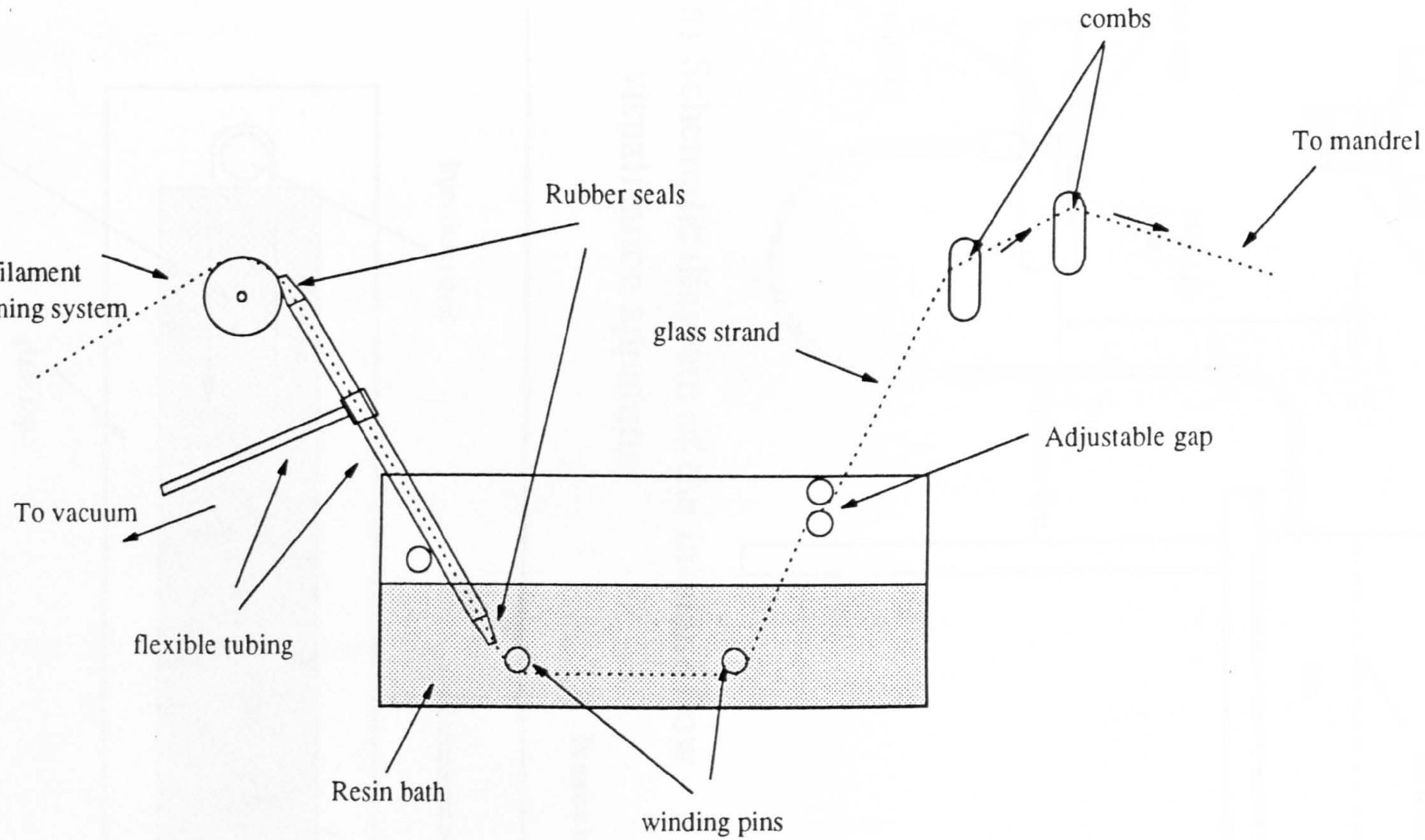

Figure 3.7 Vacuum Impregnation System for Filament Winding

Figure 3.8 In-Plane Flow Visualisation Apparatus

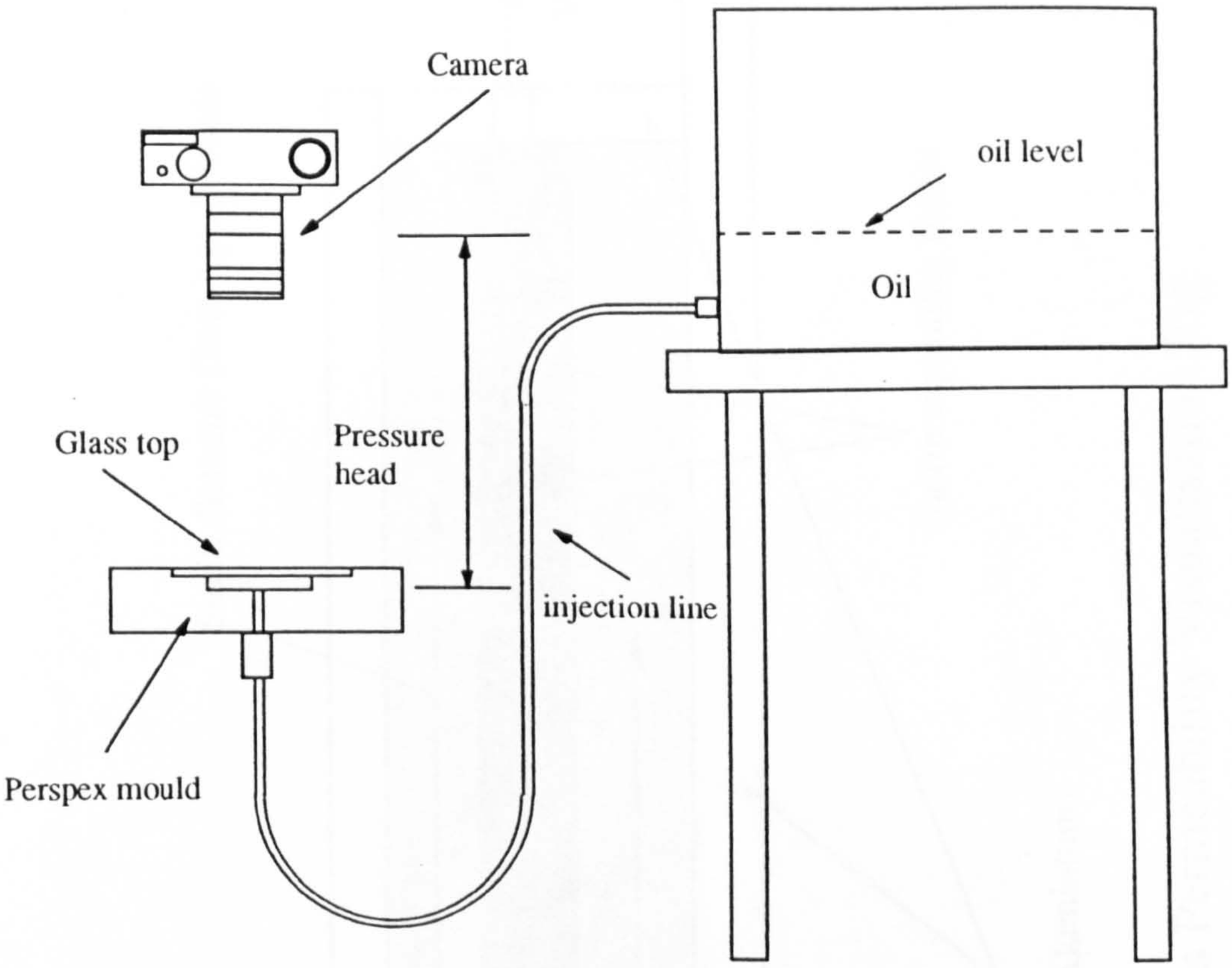

a) Schematic diagram of the in-plane flow visualisation apparatus

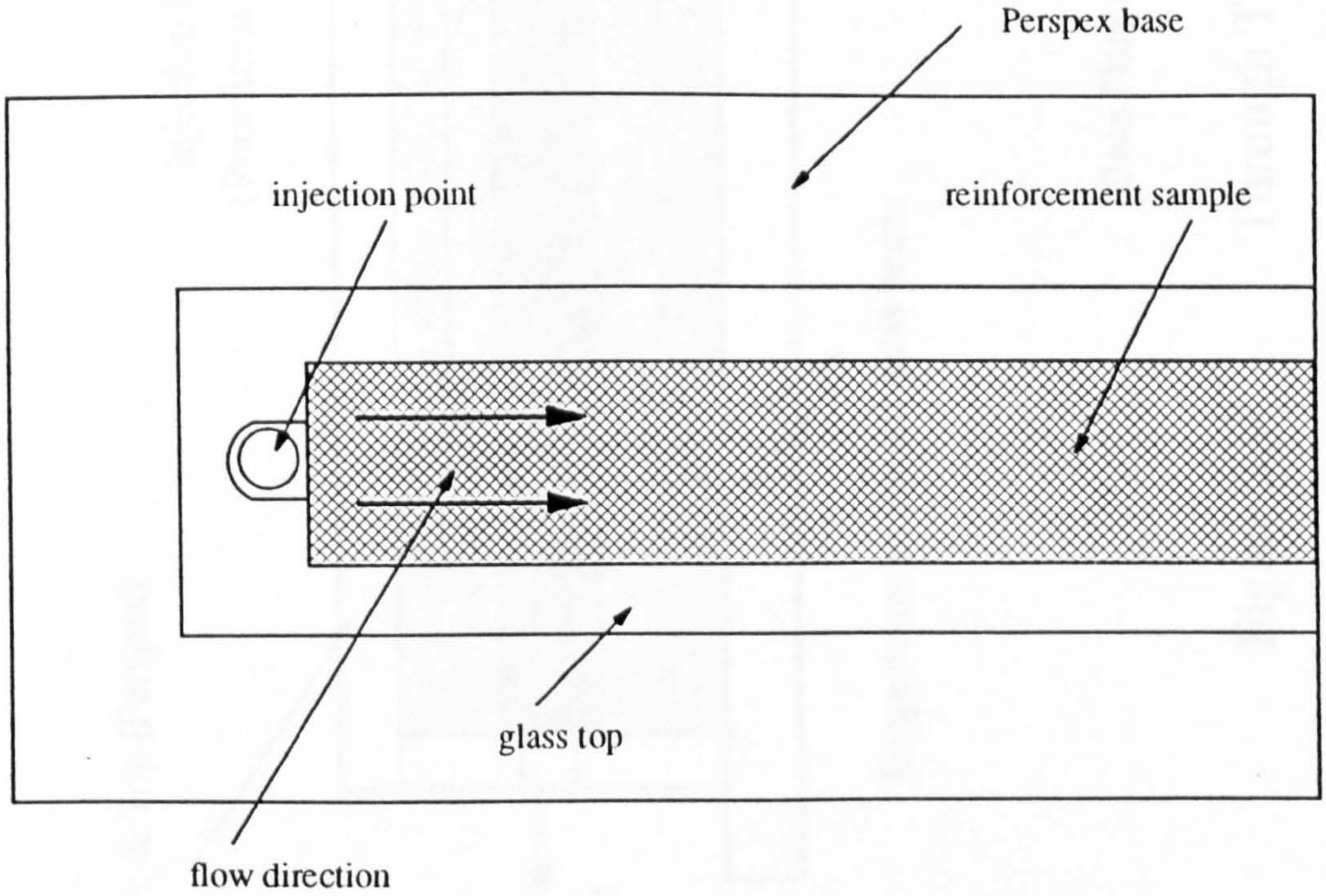

b) Plan view of the flow apparatus

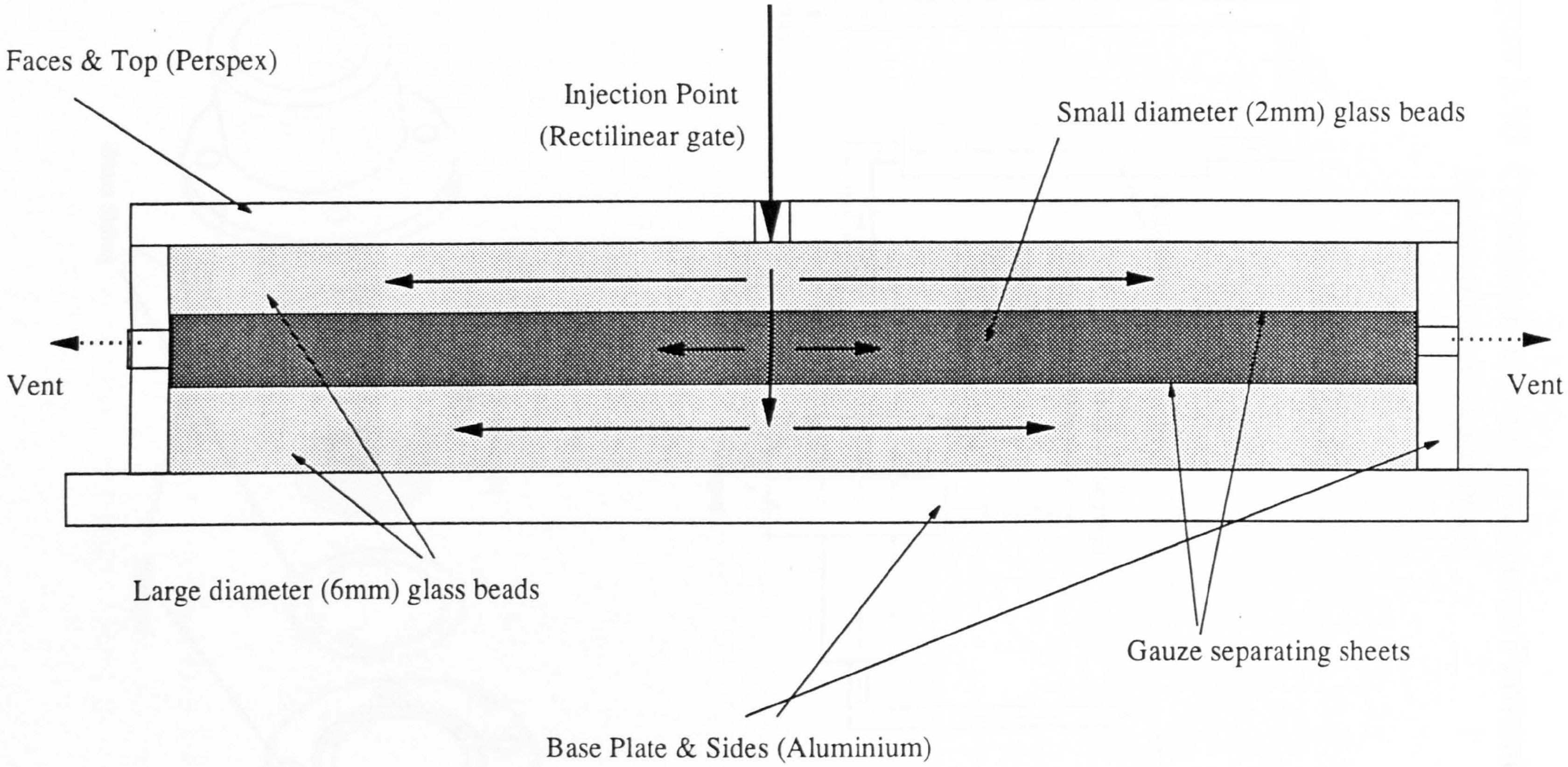

Figure 3.9 Through Thickness Permeability Visualisation Rig

Figure 3.10 Constant Pressure Transverse Permeability Measurement Apparatus

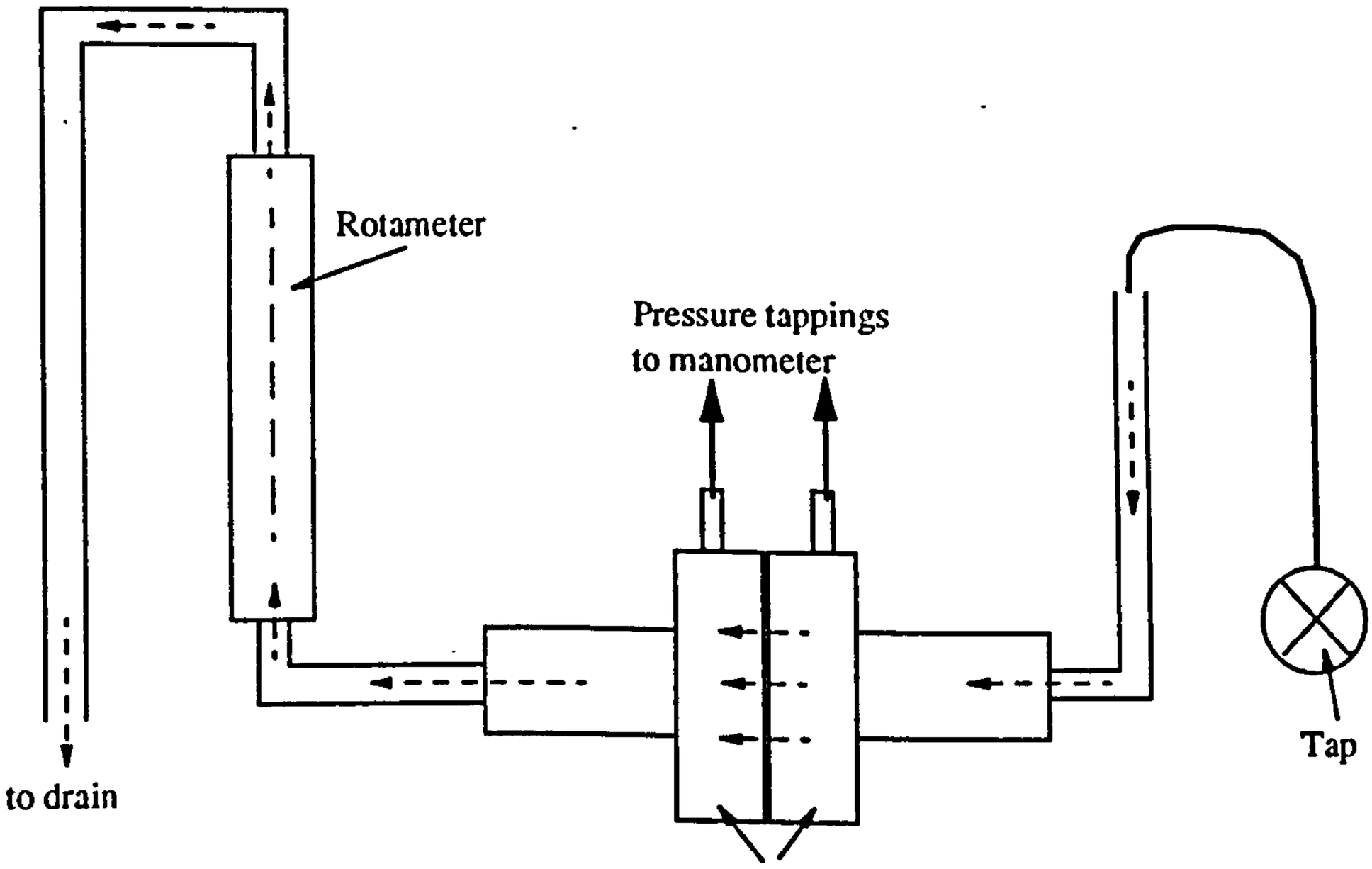

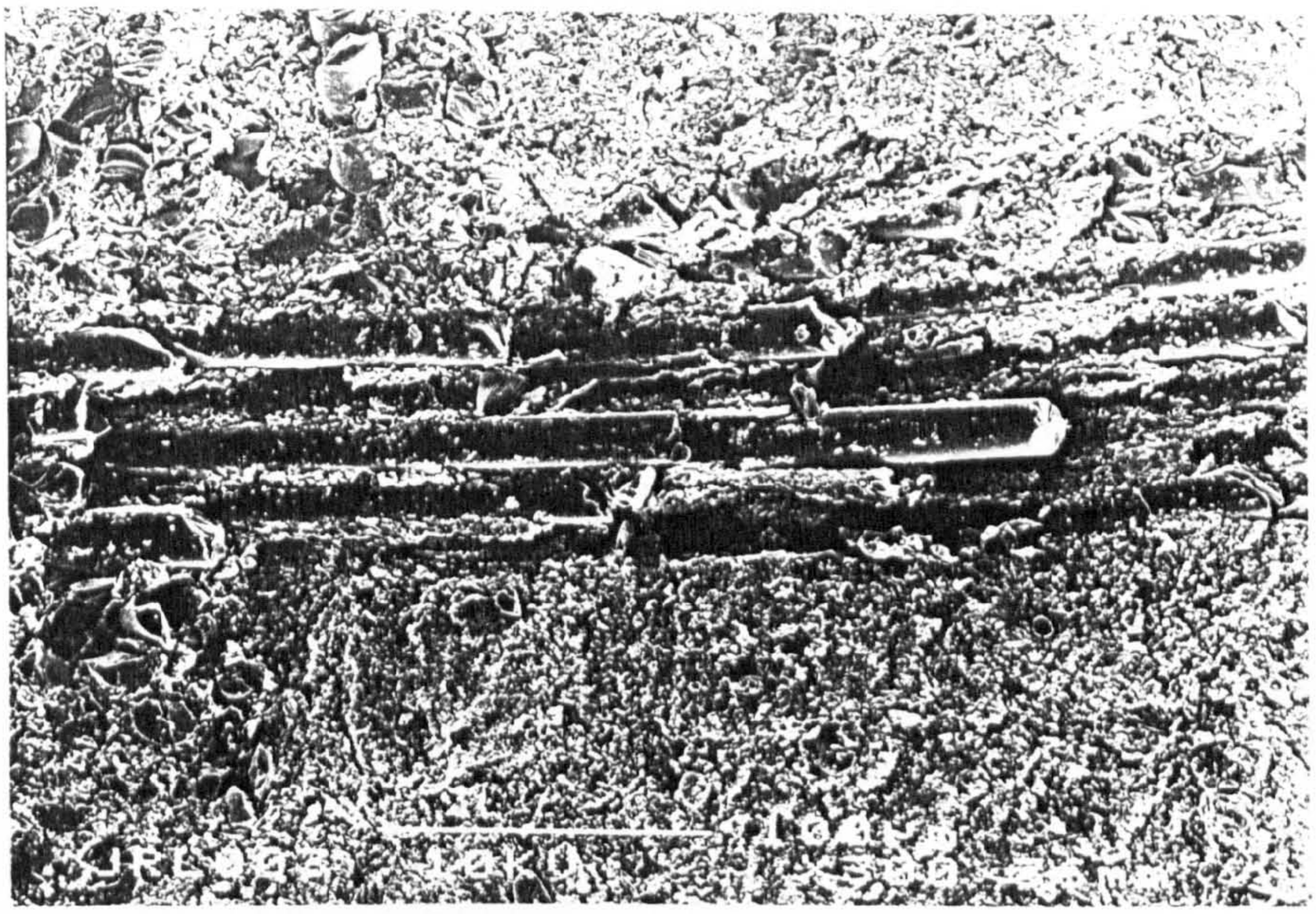

Figure 3.11 The surface of a CFRM reinforced, low profile filled polyester moulding. Sectioning using a bandsaw caused crushed fibre ends and fibre pullout, resulting in an uneven surface.

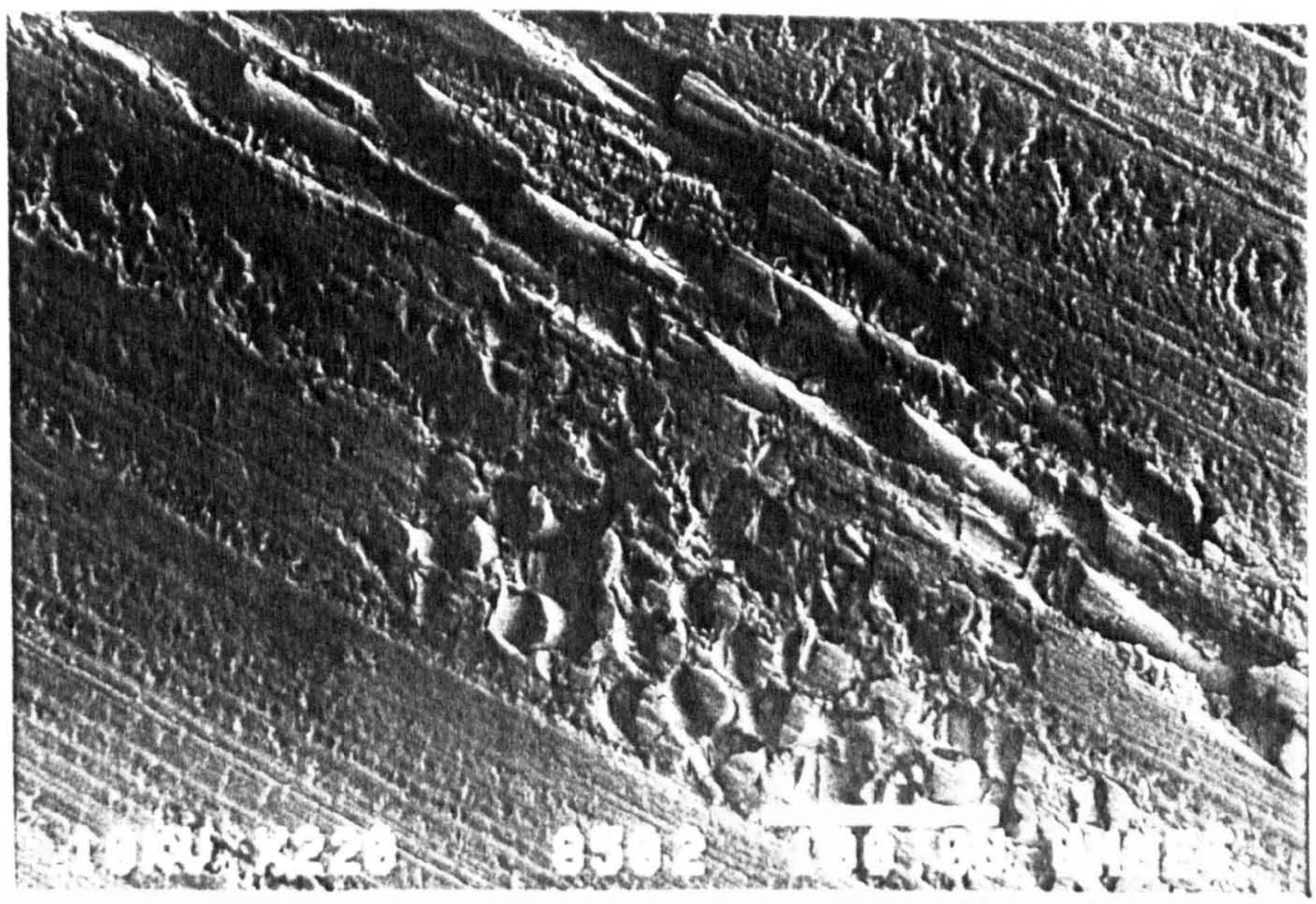

Figure 3.12 The surface of a polyester CFRM reinforced moulding sectioning and polishing using an abrasive surface grinding wheel (grain size 80).

Figure 3.13 A polished hoop section of a filament wound cylinder which has been scanned into a PC using an Epson GT-6500 colour scanner (x25).

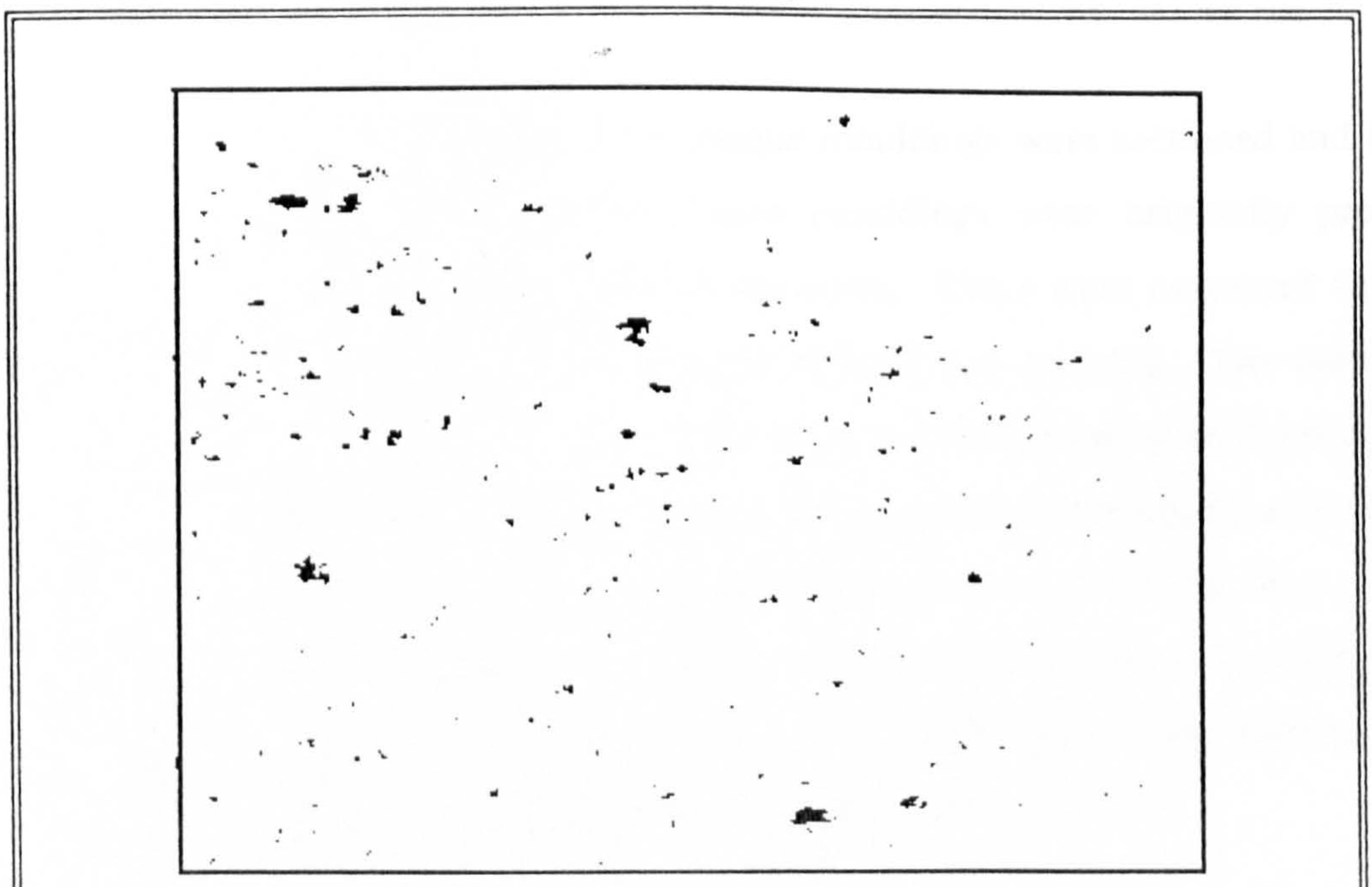

Figure 3.14 A scanned computer image of the dark areas of the photograph corresponding to Figure 3.13 and used to estimate the void content of the section.

Chapter 4

Voidage in RTM

4.1 Introduction

The next step for the automotive RTM industry, away from the mass production of spoilers and other appearance parts, will be the volume manufacture of stressed components such as automotive crossmembers. The presence of voids in structures such as these will be of great concern to the designer since the mechanical and fatigue properties will be affected. This may also influence the choice of manufacturing route and material selection. The purpose of this chapter is to identify the extent of voidage in RTM components and to hypothesise causes for void formation.

Several undershields and flat plaque mouldings were sectioned and the extent of voidage examined. The flat plaque mouldings were originally produced to investigate defect occurrence in RTM laminates. These were examined subjectively and the defects categorised. A range of defects was detected. The majority were concerned with surface finish imperfections caused during the moulding operation, but others including resin richness, fibre washing, preform wrinkling and voids were evident, which could affect the mechanical properties of the component. Following the literature survey described in Chapter 2, the subject of voidage in RTM mouldings was determined to be of academic interest, since preforming issues such as wrinkling and preform fit are under investigation by other researchers[67,68].

The majority of voids were thought to be created by air entrapment in the preform during the injection phase of the moulding process. Some of these bubbles were washed through the moulding during impregnation. However many could be trapped and were left to create voids. After impregnation, pressure and temperature variations due to resin polymerisation were thought to affect void size and shape. The

causes and mechanisms for air entrapment have been suggested by several researchers[29,31,32], but no investigation has been carried out to encompass the overall field of void formation.

4.2 Void Occurrence in RTM Mouldings

Mouldings produced using several material systems and different process conditions (Appendix 2), were sectioned and assessed for the type and frequency of voids in the composite structure. These material systems were:

a) Resin systems

- i) Polyester
- ii) Low profile polyester (with filler)
- iii) Vinyl-ester
- iv) Polyester with filler

b) Reinforcement

- i) Continuous filament random mat
- ii) Non crimp fabrics
- iii) Lightweight core materials

From these mouldings observations were made concerning the types of void, their appearance and the region of the moulding in which they were found.

There were generally two types of void. Firstly, those present on a macroscopic scale may be viewed optically (generally greater than 0.1mm) and have been classified as macrovoids. Secondly, those present on a microscopic scale (generally less than 0.1mm), which have been classified as microvoids. Figure 4.1 shows an electron scanning micrograph of a section through a polyester, CFRM reinforced moulding. A range of voids are exhibited, from macrovoids over 2mm in length to microvoids in the fibre bundles. These voids occur in different regions of the composite.

Macrovoids

Macrovoids generally occur in the matrix of the composite (Figure 4.2). These

may be present due to bubbles washing into the location, having formed elsewhere, or due to the mechanical entrapment of air. Macrovoids may occur in the interphase between fibre and resin (or bundle and resin). These are thought to form where bubbles which have washed through the resin attach themselves onto a fibre, or fibres. Figure 4.3 shows a void encroaching upon a fibre bundle in a polyester reinforced CFRM moulding.

Air which has been entrapped between fibre bundles forms macrovoids, as shown in Figure 4.4. Voids occur at the intersections between fibre bundle and stitching when non crimp fabric, or chopped strand mat with polyester stitching has been used, where an uneven resin flow front can trap air to form macrovoids. Figure 4.5 shows voids in the stitching between 0° fibre bundles. Voids can be formed at the interface between the thermoplastic binder and the resin matrix and are thought to be caused by the resin flow front becoming distorted due to globules of thermoplastic binder, trapping air (Figure 4.6).

The photograph in Figure 4.7 shows voids near the surface of a polyester, CFRM moulding. These macrovoids are large, in the range of 100µm - 500µm and are thought to form due to a distortion of the resin flow front at the surface of the mould. Surface voids may be detrimental to the component, for example if the moulding is to be painted voids close to the surface may erupt causing bubbling due to the heating of the surface, or in stressed conditions a void may act as a crack initiation site.

Microvoids

Microvoids in the fibre bundles were common in the sections observed and appeared as 'straw like' regions, in mouldings where the fibre bundles have not wetted out (Figure 4.8).

4.3 Hypotheses for Void Formation

Voids can be caused by several factors. Air becomes mixed into the resin during the addition of catalysts, accelerators, inhibitors, internal release agents and

especially filler. If the resin is allowed to stand for several minutes the larger bubbles cannot all settle out and the smaller ones tend to be held in the solution. Degassing the resin removes much of this air.

The resin systems when used in conjunction with catalysts such as Perkadox 16 have short pot lives, which require the resin to be injected within minutes of mixing. The air has little time to exit the resin and some bubbles may be injected directly into the moulding.

Voids can be formed during the injection phase by mechanical entrapment and can develop in the following regions:

i) Microvoids can form within the fibre bundles. These are thought to form where the macroscopic resin flow front advances faster than the transverse flow into the fibre bundles. Voids are formed in regions where this uneven flow has left air trapped behind the resin flow front. The resin impregnation between fibres is thought to be restricted by the presence of size bridging the filaments. The surface inside the void shown in Figure 4.8 is rough and resembles size menisci studied in section 6.5. This surface can be compared with that of the macrovoid shown in Figure 4.4, which is smooth. The opacity of the fibres in unfilled mouldings suggested that voids were created within the fibre bundles. When these mouldings were studied microscopically under transmitted light, long cylindrical voids were observed within the fibre bundle structure (Figure 5.8(a)).

ii) Macroscopic voids are evident between fibre bundles and stitching. These are assumed to be formed where air becomes trapped due to uneven resin flow at the interface between fibre and resin.

iii) If thermoplastic binder is present in the preform, air is thought to become trapped at the thermoplastic and fibre interface, where the

globules of thermoplastic are thought to distort the resin flow front.

iv) Macrovoids present at the surface of mouldings, are thought to form where air has been trapped due to uneven flow.

After injection, voids can form due to moisture or effervesce due to a chemical reaction between materials. The monomer within the resin (eg. styrene in polyester and vinyl ester resins) can boil under certain processing conditions (high temperatures or vacuum assistance) and vapour bubbles usually forming macrovoids can be set in the resin. These voids and those caused by air trapped during impregnation will change in size due to pressure and temperature fluctuation due to resin exotherm.

4.4 Voids due to Preform Stacking

Voids are thought to be formed due to different rates of resin impregnation into multilayer preforms. When using reinforcements of substantially different permeabilities, resin is assumed to travel along the higher permeability layer trapping air in the lower permeability layer. Transverse filling of the reinforcement through the layers of the preform allows this to occur. Figure 4.9 shows a flat plaque moulding with a semi-permeable lightweight core, which is sandwiched between layers of CFRM. Resin is thought to have impregnated the outer layers of mat trapping air in the core material. Figure 4.10 shows voids in a multilayered preform consisting of two layers of chopped strand with a central layer of polyester fleece. The voids are thought to form due to the transverse filling of the fibre bundles, from the central layer of polyester fleece, the resin is assumed to fill this lower permeability layer quicker than the higher permeability chopped strand mat. The voids range in size, dependant on where the air has become entrapped.

4.5 Matrix Cracks

A matrix crack can be considered as a type of void, since the crack enables a region of voidage to occur. Cracks are apparent in both CFRM and unidirectional component sections and often can be seen to initiate from voids. Figure 4.11 shows cracking between fibres extending from a void in a 0° laminate.

Matrix cracks occur in resin rich regions. These regions are subject to high local exotherm temperatures during polymerisation, since no reinforcement is available to act as a thermal sink. Cracking is likely to occur due to thermal stress in these regions. This resin shrinkage cracking has also been seen in laminates with low fibre volume fractions[69]. Scott[69] suggested that the cracking was the result of high mould temperature accelerating the cure reaction. Mouldings at increasing mould temperatures (110°C to 125°C) showed an increase in matrix cracking. The addition of a low profile additive and filler, appeared to reduce this cracking.

Cracks or voids within the thermoplastic matrix regions due to binder, occur frequently surrounding fibres. These are widespread in low profile polyester mouldings. They are thought to occur due to the different expansion coefficients of the thermoplastic and thermosetting matrices during the exotherm (ie. polymerisation reduction) of the thermosetting resin. Figure 4.12 shows several of these cracks or voids.

4.6 The Effect of moisture upon voidage

The phenomena of moisture affecting the void content during composite production has been documented by several researchers[25]. The mechanisms for void formation due to moisture are discussed in section 2.5. In order to identify how the moisture content of the resin affects the void content of composite produced by RTM, two mouldings were produced using CVP 6345.001 polyester resin and U750-450 CFRM. The first moulding contained no added water. The second contained 0.5 phr distilled water added to the resin as an emulsion prior to injection. Both void content analysis (shown in Table 4.1) and microscopic examination were carried out. Photographs of the microscopic examination are shown in Figures 4.13 and 4.14.

Figure 4.13 shows a section of a CFRM and polyester moulding. The section is relatively void free. Figure 4.14 shows a section of the moulding with the added moisture. The extent of voidage in this section is more noticeable, with both microvoids and macrovoids in the matrix. The voidage analysis shows an increase in void content from 0.8% to 1.2% (a 50% variation) for the moulding with added water.

The microscopic examinations also indicated that a moisture content of 0.5% gives an increase in voidage within mouldings.

Hutcheon[4] described a method of displacing air from the mould cavity by a vapour (a gas just above its boiling point), instead of displacing air by the use of a vacuum. With a mould at a temperature of 120°C it was possible to use water as the evapourant. Water turns into approximately 2,000 times its own volume of steam when it boils at this temperature. It was calculated that the residual steam would be 0.1% of the resin weight. These studies have shown that any residual moisture present in the mould cavity will affect the void content of the moulding, thus the use of vapour purging to aid resin injection will affect the mechanical properties of the component.

4.7 Discussion

The work contained in this chapter is concerned with observing the phenomenon of voidage in RTM components. Causes for the formation of voids have been hypothesised, such that the mechanisms proposed could be investigated later in this thesis.

The voids found in mouldings produced using RTM have been classified into macrovoids and microvoids, depending on their size. Voids were found in certain locations in the mouldings, such as between fibre bundles, in the matrix, near the surface and between the thermoplastic binder and fibre.

The reasons for the formation of voids during each phase of the moulding cycle has been discussed. Voids may be the result of bubbles present in the resin system washing into the reinforcement. Mechanical entrapment can also occur as the local flow front surrounds and entraps air in the reinforcement, this mechanism creates macrovoids in resin rich areas such as between fibre bundles, stitching and thermoplastic binder. Microvoids are created where air is entrapped within the fibre bundle. Voids may also increase or decrease in size due to the pressure or temperature variation during resin polymerisation.

Matrix cracks have been observed in composite sections. These cracks often appear to emanate from voids in the composite. Cracking or voids has also been observed in the thermoplastic matrix regions in the composite.

The effect of moisture on voidage within the resin system was investigated since previous research[25] has indicated an effect on void formation. Both burn-off determination and section analysis indicated a significant difference in void content between mouldings produced with and without water added into the resin prior to injection. The implications upon void formation of using vapour purging as a form of impregnation assistance has been discussed.

The classification of voids and observations of where they occur within the composite structure has been carried out for other processes such as filament winding[62] and autoclaving[26], but no such survey has been carried out for RTM. The causes postulated indicate that void formation may be influenced by the process conditions used during moulding (eg. injection pressure, mould temperature & vent pressure) which are investigated in Chapter 5. The distortion of the resin flow front during impregnation of the resin, trapping air in the preform is discussed in Chapter 6.

List of Tables

List of Figures

Table 4.1 Void analysis for mouldings with added moisture

Distance from injection gate (mm)	Void content (%) Moulding 4248		Void content (%) Moulding 4249 (with 0.5% water)	
50	0.68		1.43	
100	0.94		1.16	
150	0.87		1.89	
200	1.56		0.94	
250	0.8		1.12	
300	0.98		1.06	
350	0.59		1.24	
400	0.41		0.5	
450	0.4	Average 0.8%	0.7	Average 1.2%

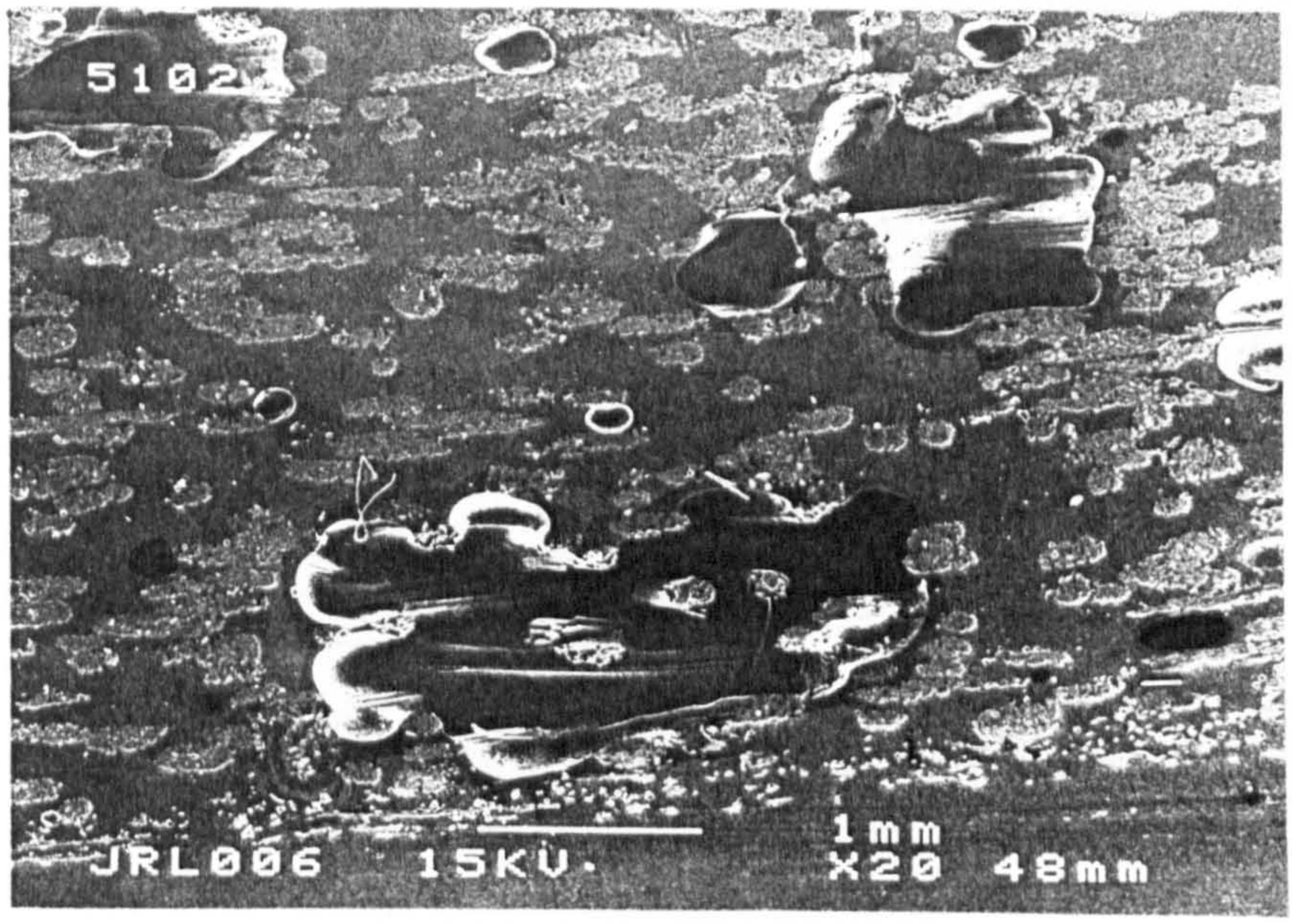

Figure 4.1 A variety of void sizes in a CFRM reinforced polyester laminate. The largest void is over 2mm in length, whilst the smallest voids can only just be discerned within the fibre bundles.

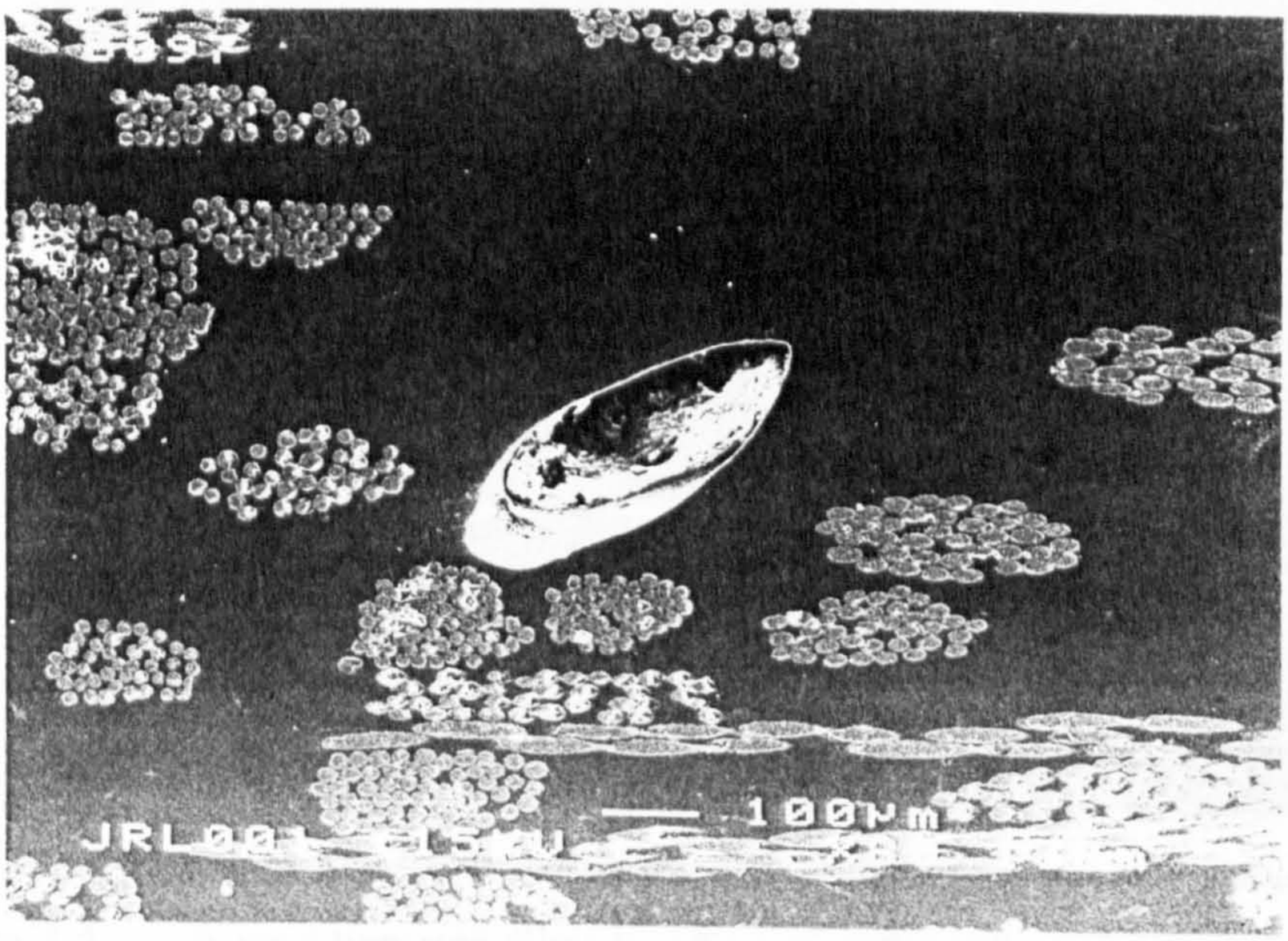

Figure 4.2 A matrix void extending far below the surface of a CFRM reinforced polyester laminate.

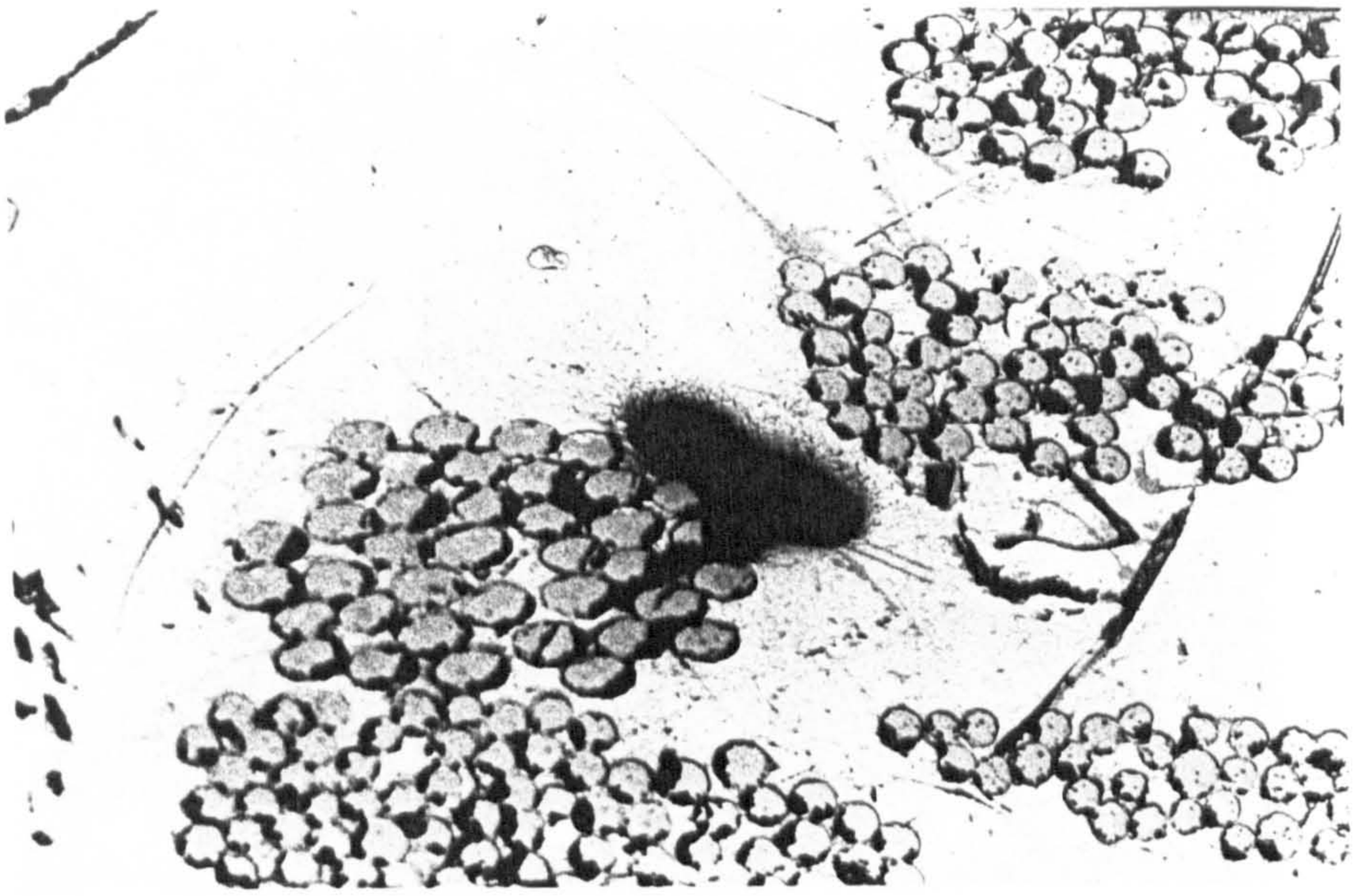

Figure 4.3 A void located adjacent to the fibre bundle in a CFRM reinforced polyester moulding.

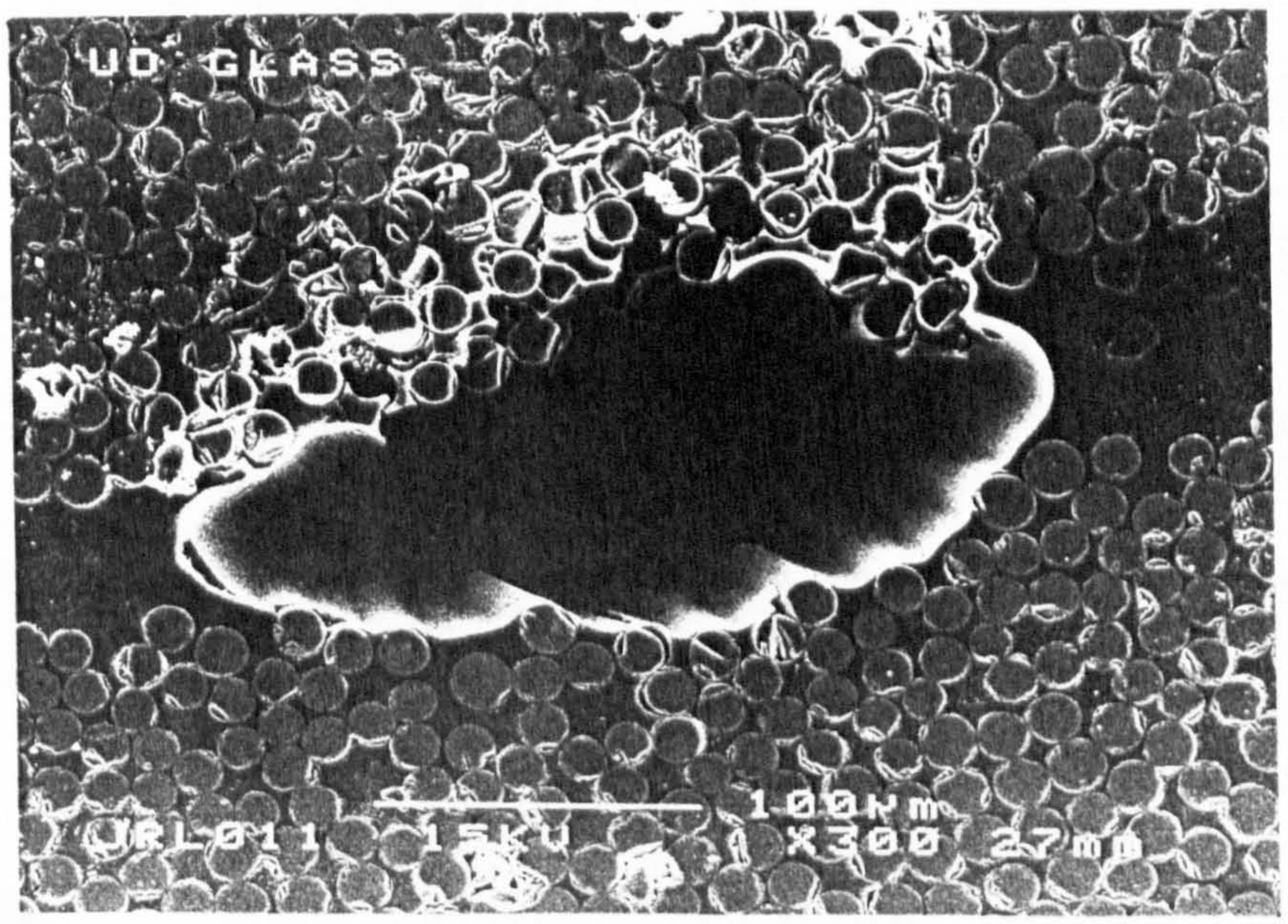

Figure 4.4 A void between fibre bundles of a 0° reinforced polyester laminate. The fibres on the lower side of the picture are well wetted, whilst the fibres on the upper side appear to be poorly wetted and have been damaged during specimen preparation.

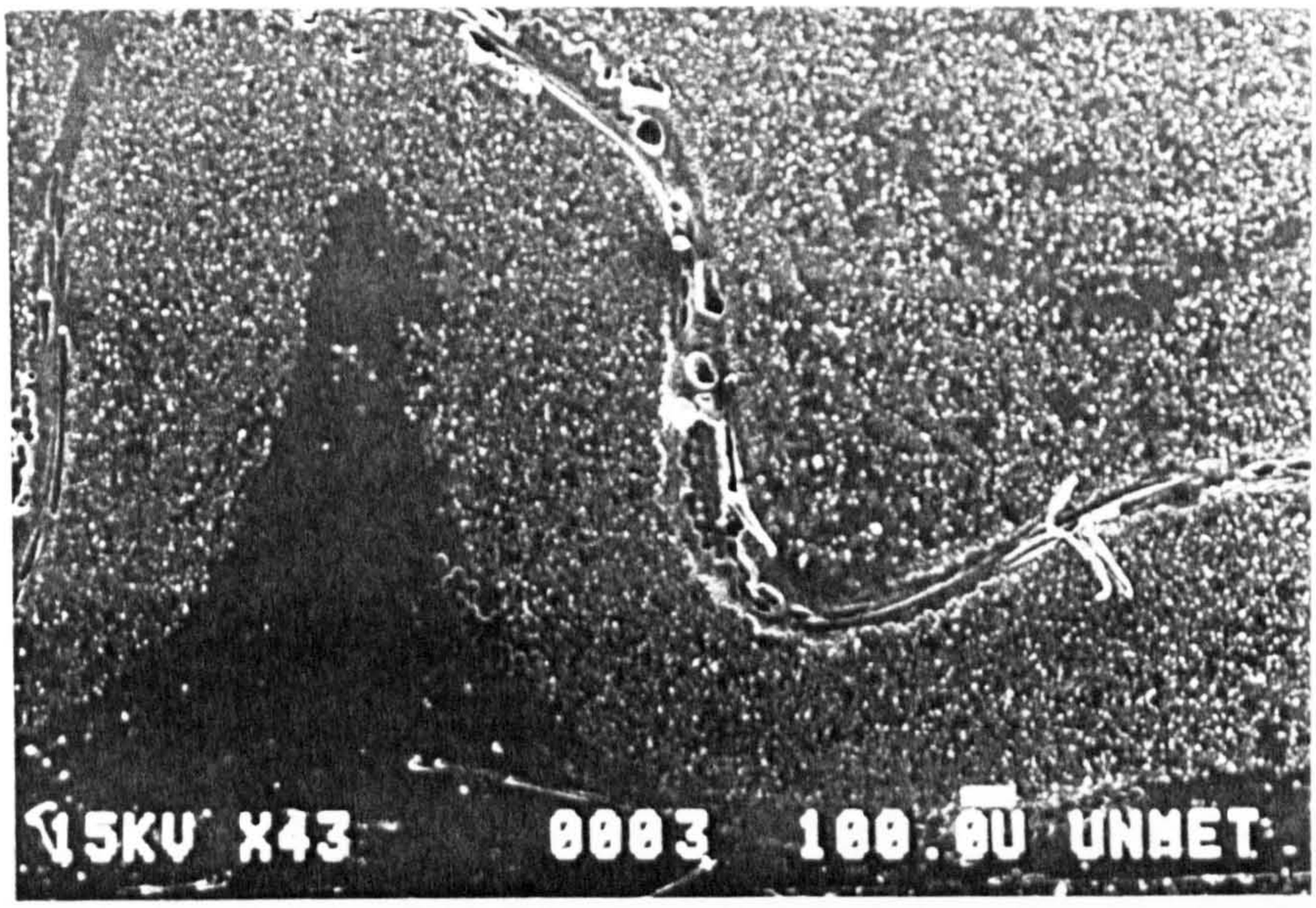

Figure 4.5 Voids along the fibre and stitching interface of a 0° reinforced polyester moulding.

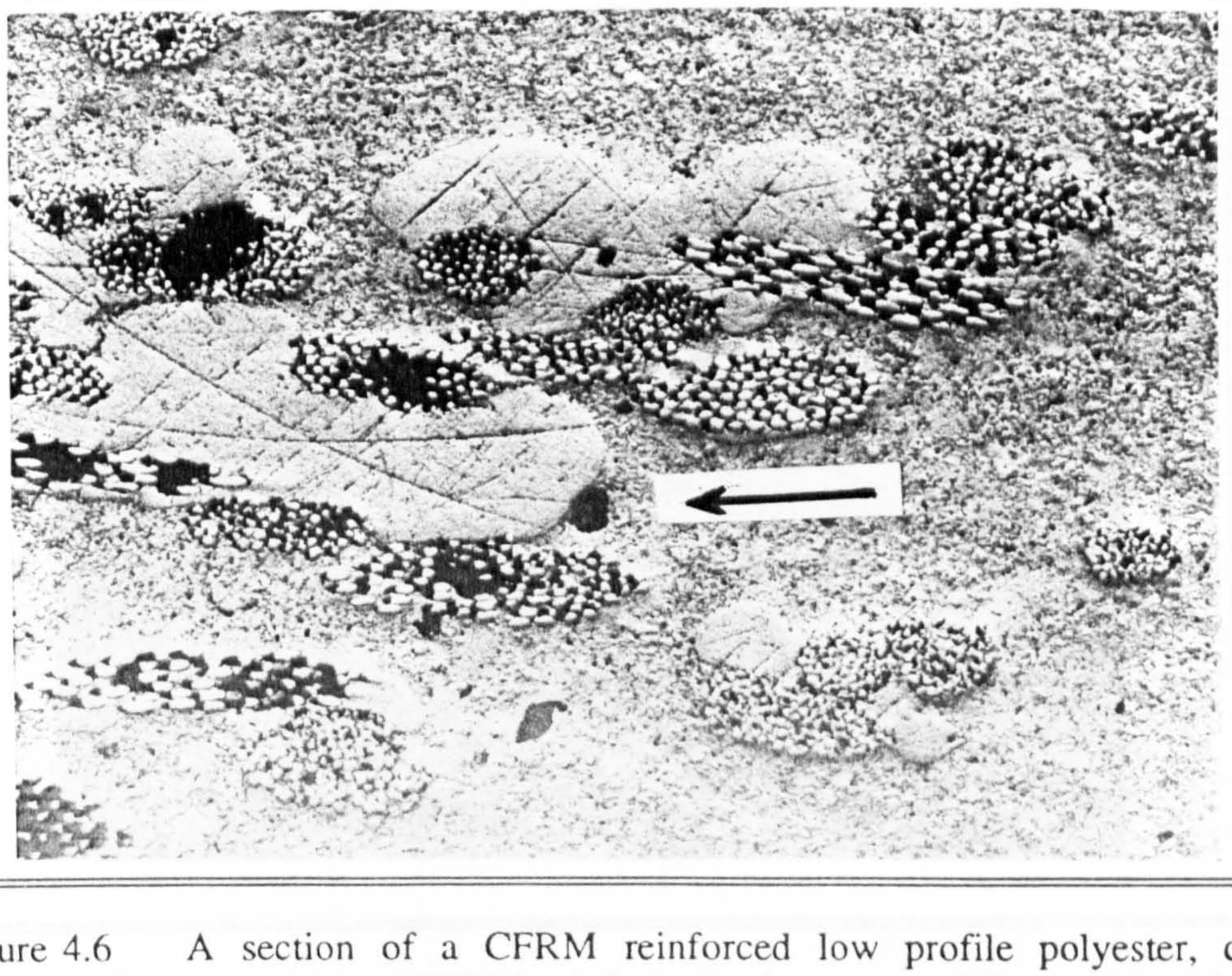

Figure 4.6 A section of a CFRM reinforced low profile polyester, calcium carbonate filled moulding. Two phases of resin can be observed, the darker areas are thermosetting polyester resin, and the lighter ones thermoplastic binder. The arrow indicates a void can in the thermosetting resin, attached to the thermoplastic. (Scale x50)

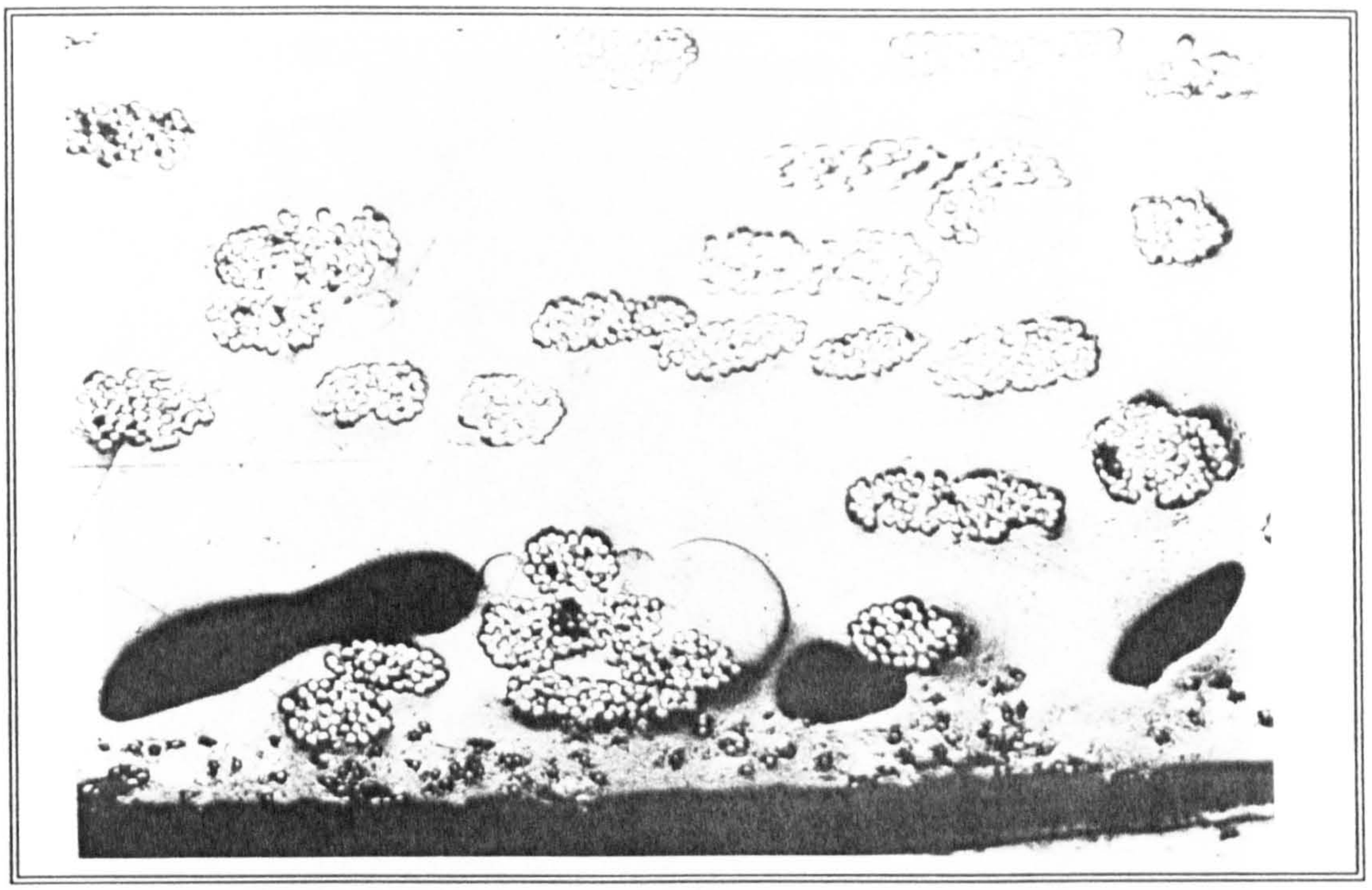

Figure 4.7 Voids in a reflected light photograph, from a CFRM reinforced polyester moulding, formed close to the surface of the moulding. (Scale x50)

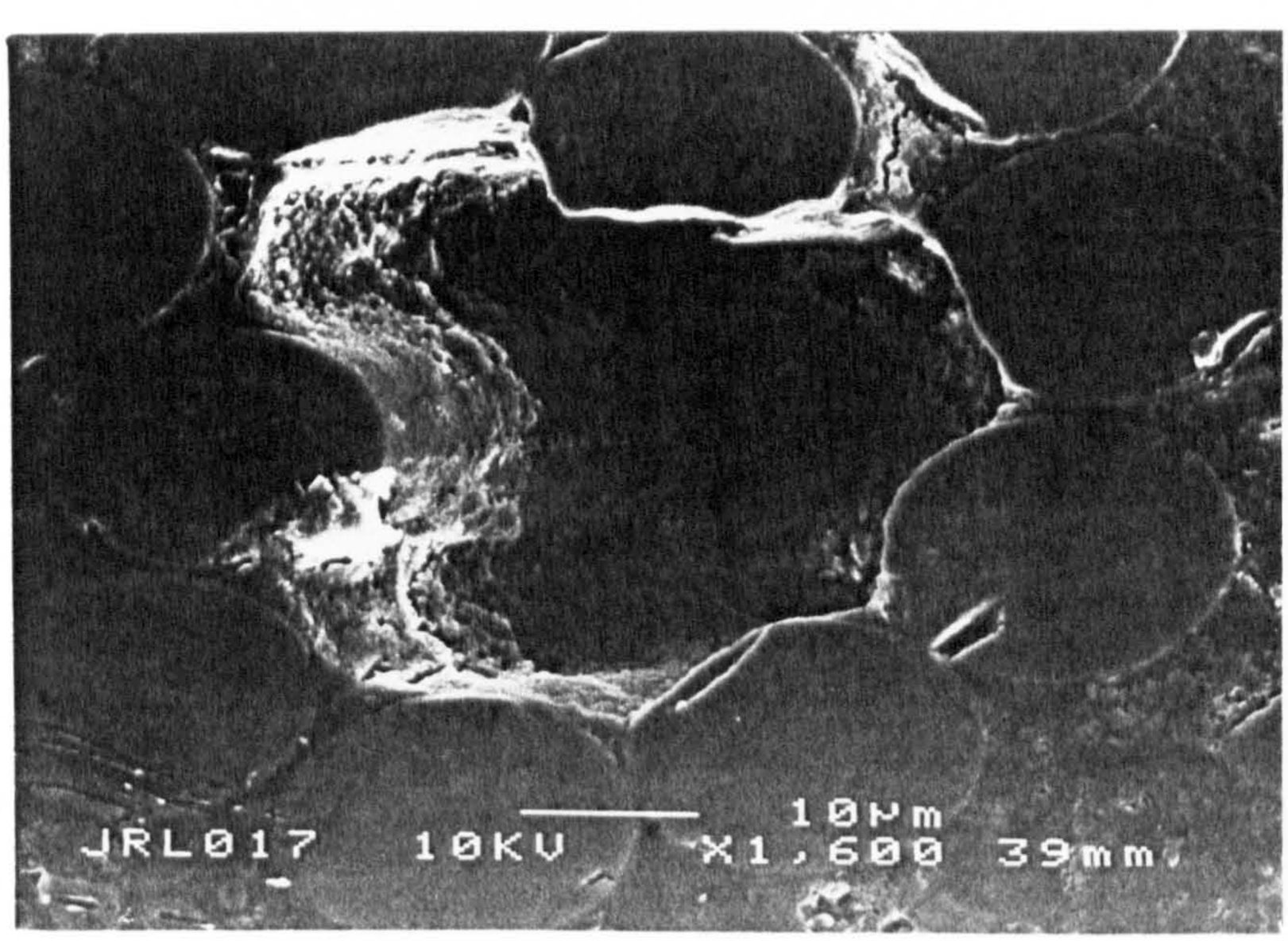

Figure 4.8 A void in a CFRM reinforced polyester moulding within a bundle of low tex fibres, the depth of the void is clearly visible.

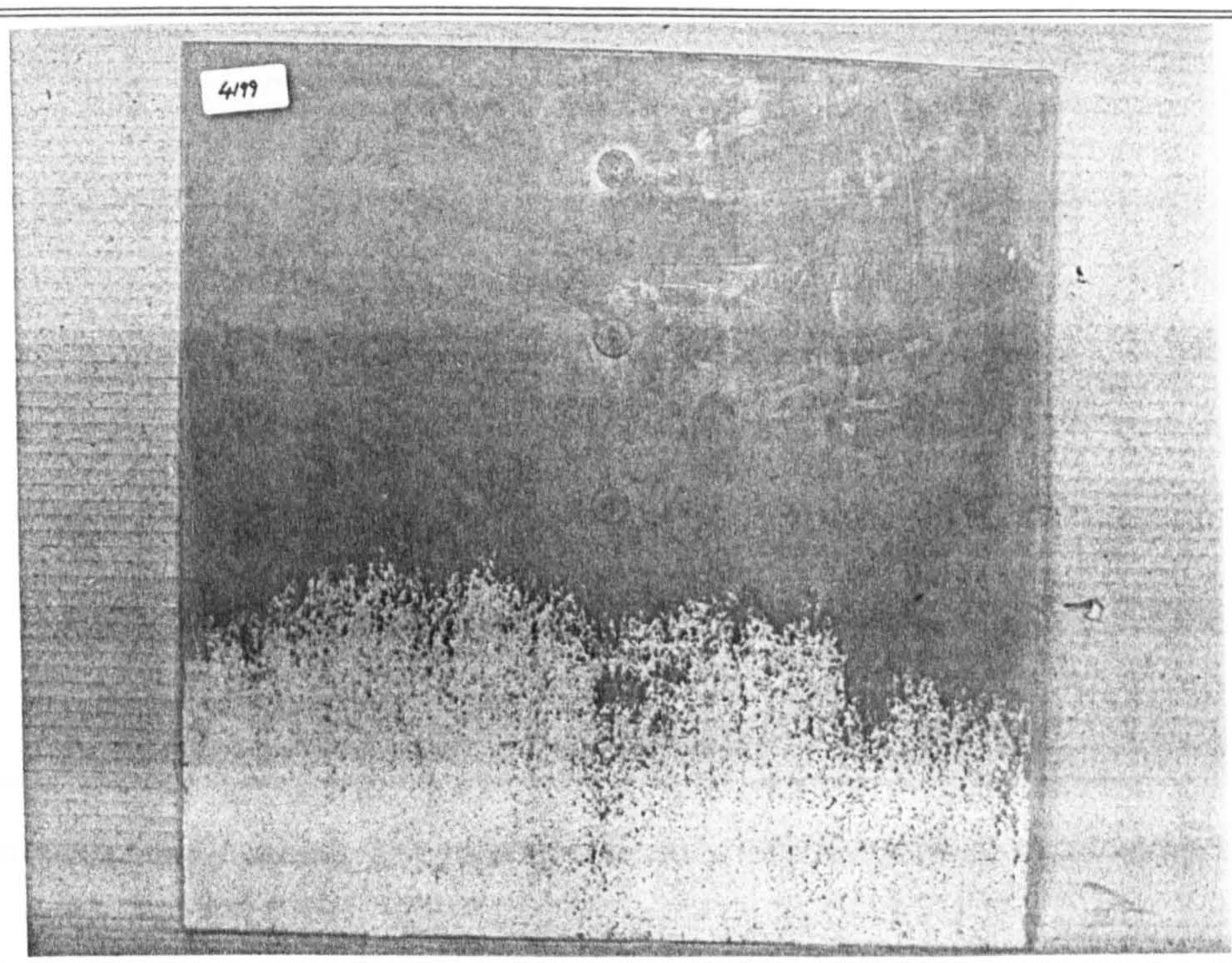

Figure 4.9 A lightweight, high permeability, core material sandwiched between layers of CFRM and impregnated with polyester resin. Resin was seen to impregnate the outer layers whilst entrapping air in the central core.

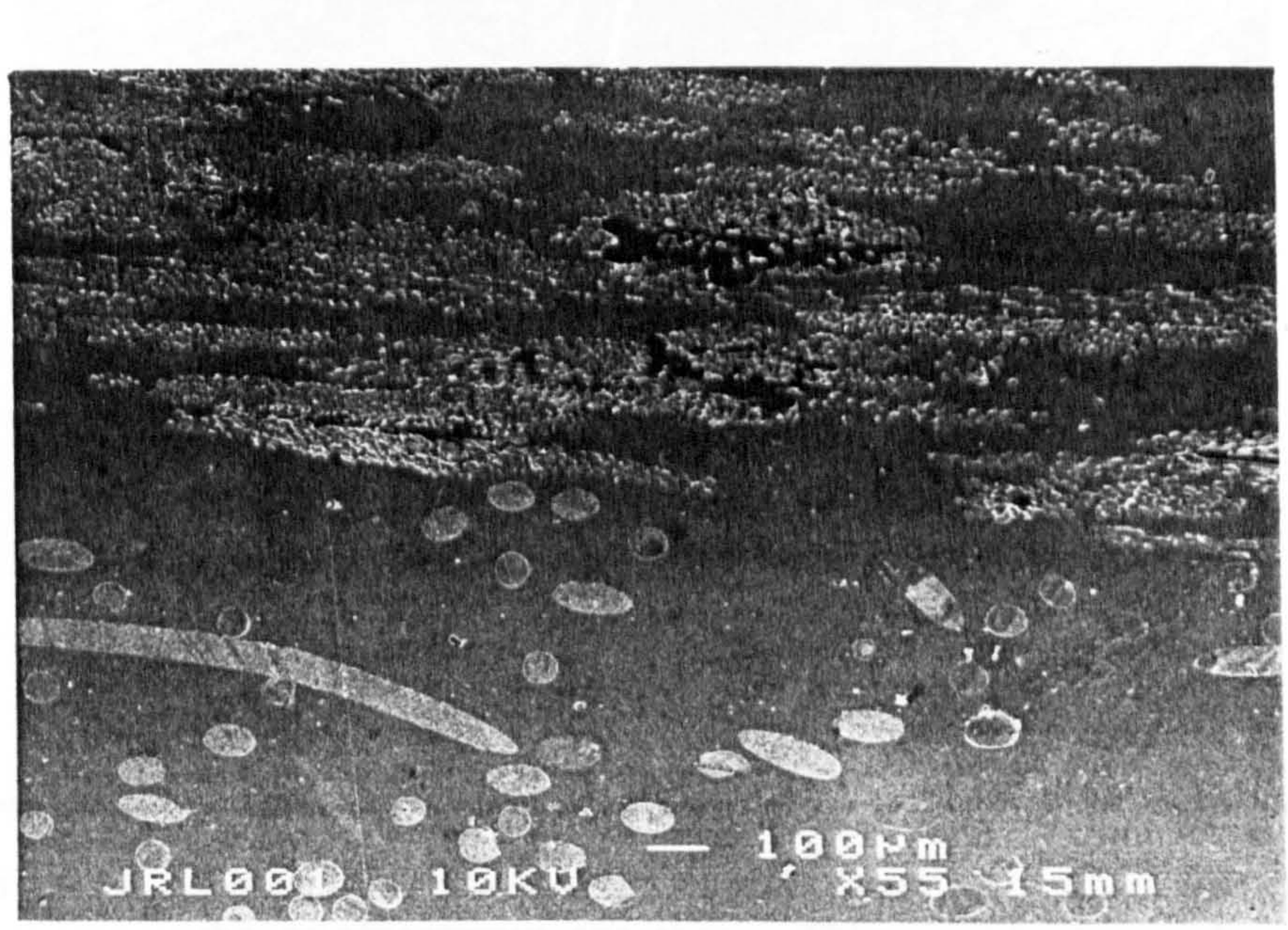

Figure 4.10 A cross section of the two phases of reinforcement, in a chopped strand mat with polyester fleece core reinforced polyester moulding. The void content in the upper layer of mat has a higher void content, due to the transverse filling of the chopped strand mat.

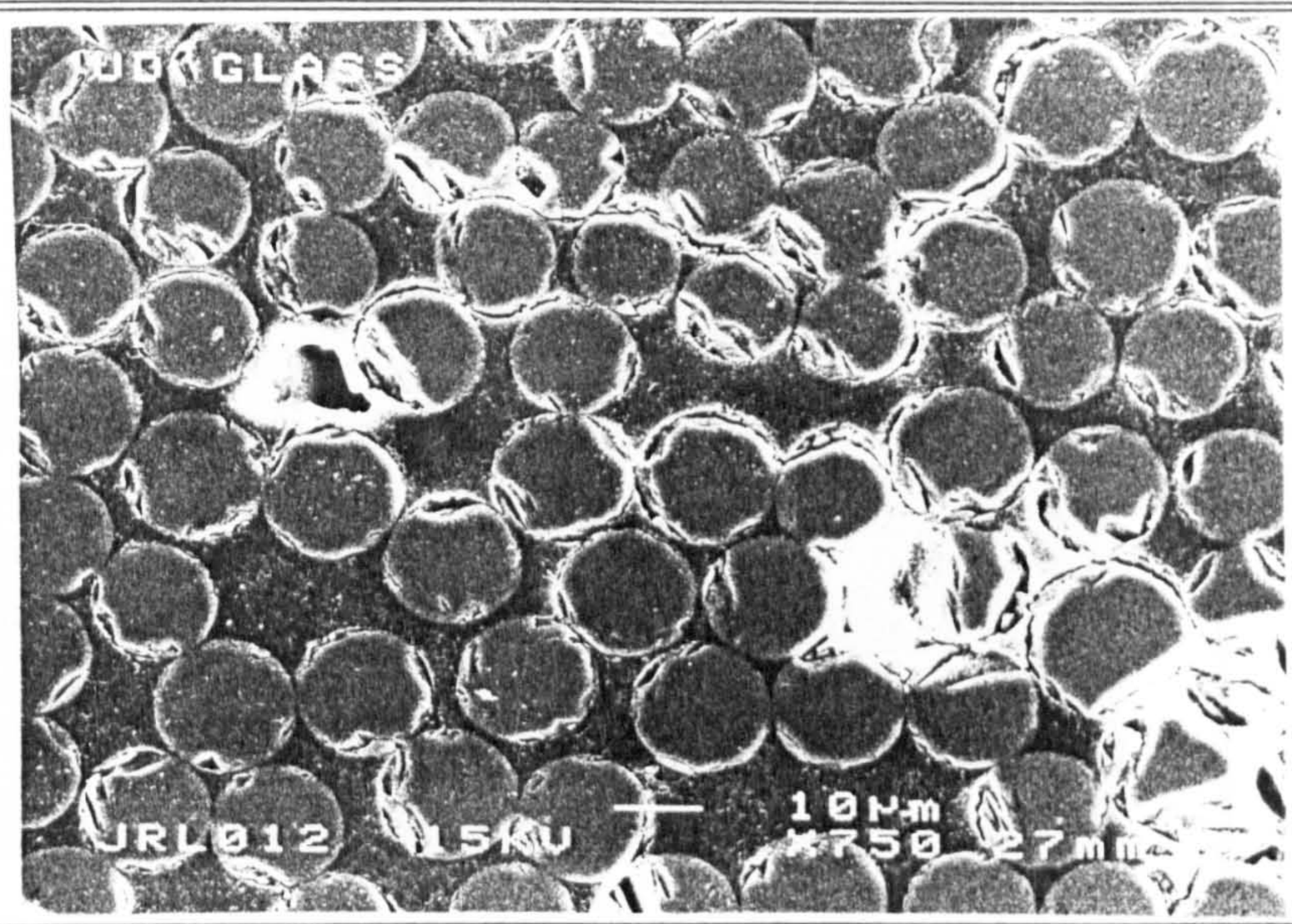

Figure 4.11 Cracking between fibres in a 0° reinforced vinyl ester moulding, extending from a void.

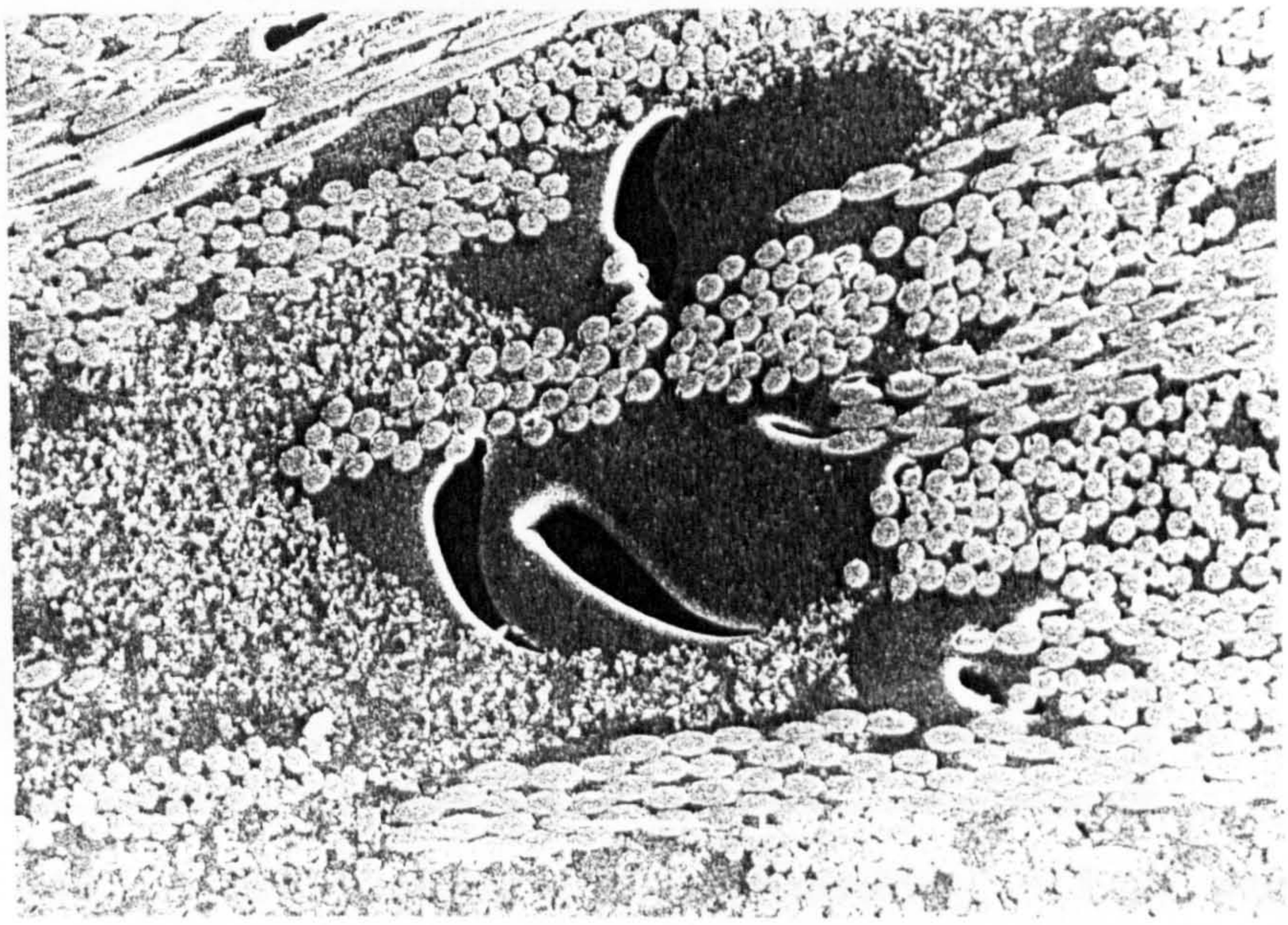

Figure 4.12 Several voids within the thermoplastic resin which was present to bind the reinforcement together. These voids or cracks are especially evident in CFRM reinforced, low profile polyester mouldings, where thermal stress between the two phases is thought to promote cracking.

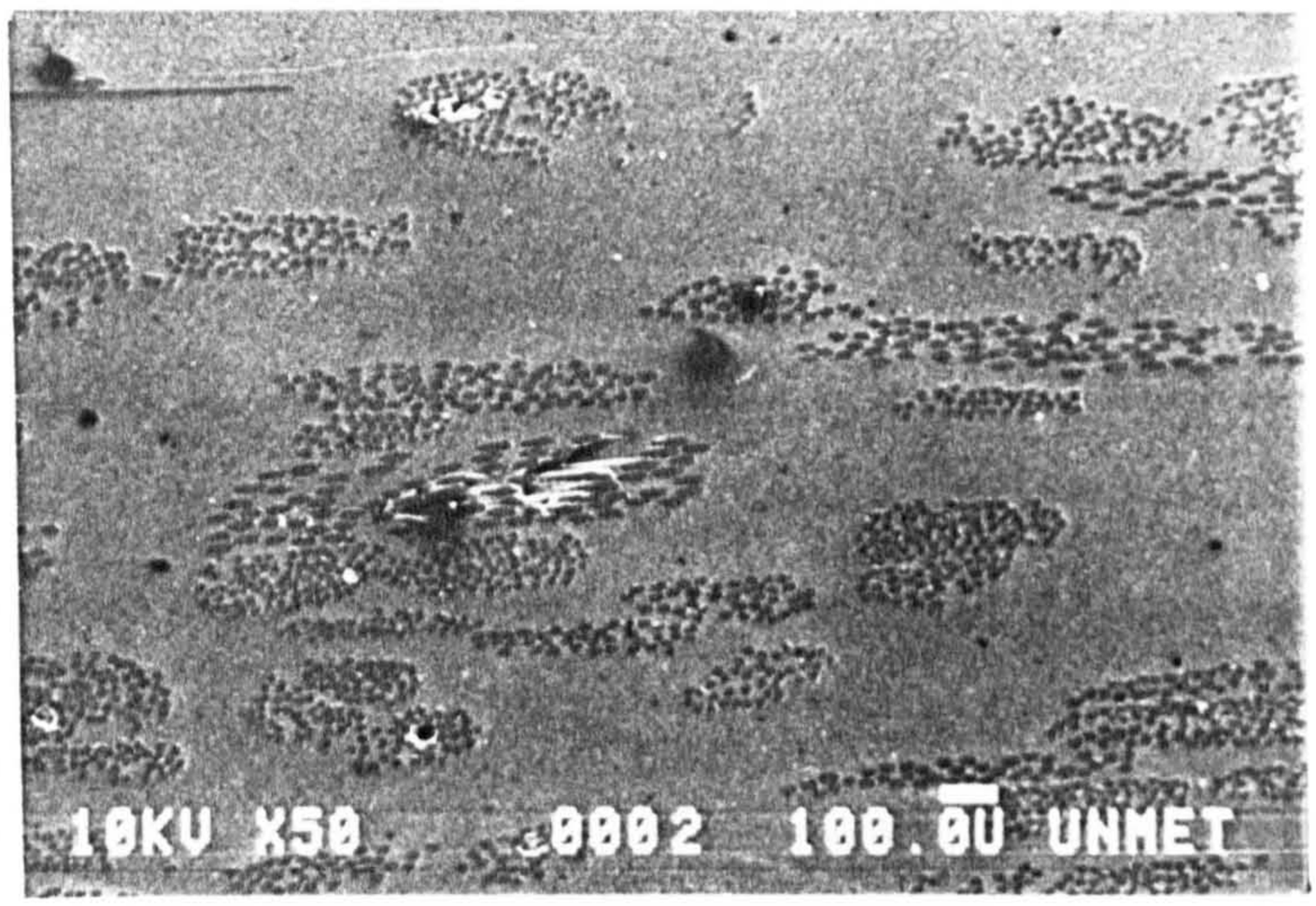

Figure 4.13 A CFRM reinforced polyester moulding (without water added to the resin).

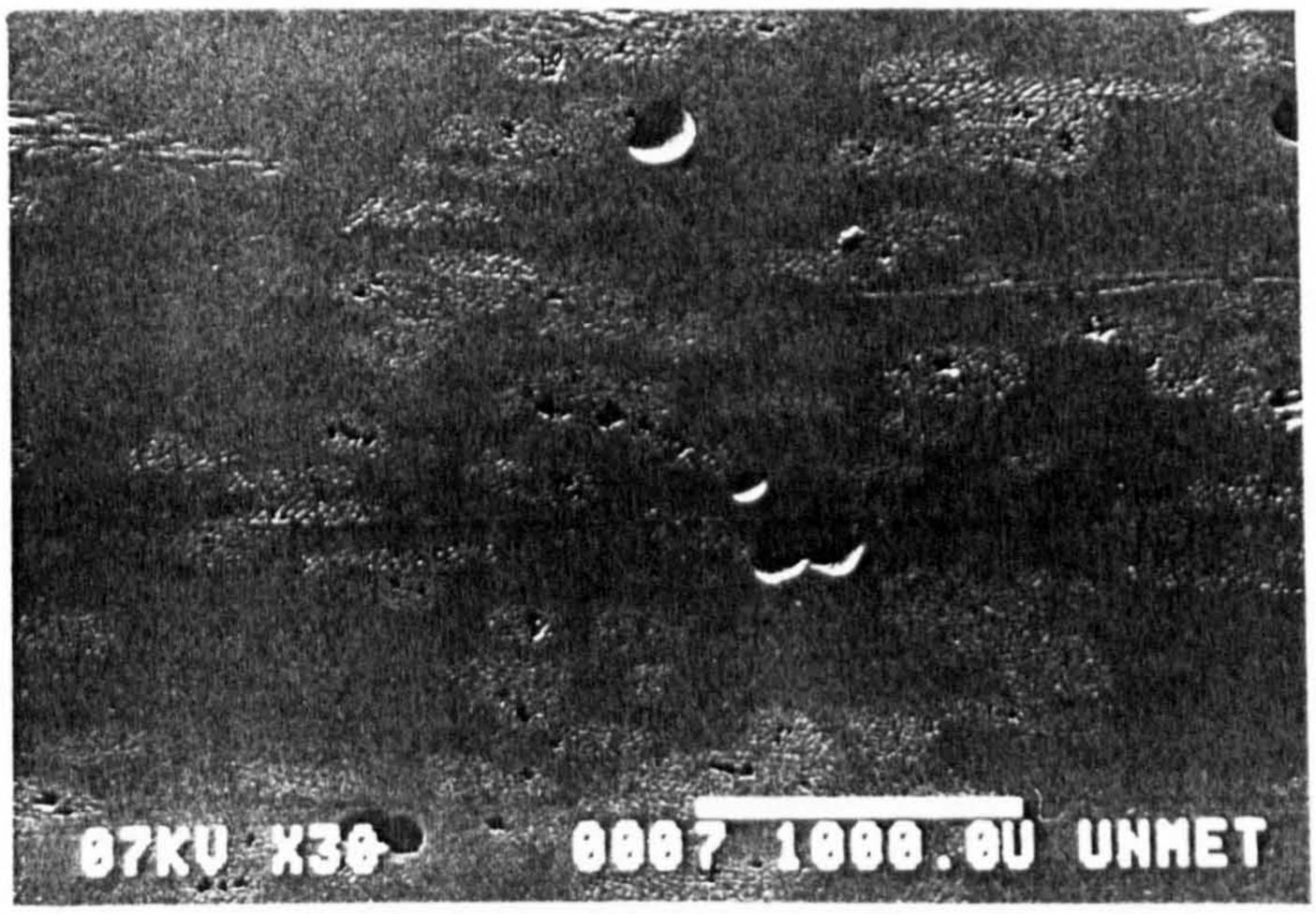

Figure 4.14 A CFRM reinforced polyester moulding. 0.5 phr water was added prior to injection. The void content appears higher than the sections of moulding which were produced without added moisture.

Chapter 5

Effects of Process Conditions upon Void Content in Laminates.

5.1 Introduction

This chapter describes investigations carried out into the effects of the major process conditions upon void content and void position in flat plaque mouldings. Laminates were produced with both unidirectional and CFRM reinforcement, using different process conditions. The parameters available for variation within the flat plaque mould have been previously discussed in Chapter 3. These were the fibre volume fraction, resin pre-heat temperature, injection pressure, vacuum assisted impregnation and mould temperature. Vacuum assisted injection was further investigated to assess the effect of different partial vacuums and the consequence of these on monomer boiling and on the pressure activity in the mould during cure.

The void content of the mouldings was assessed using burn-off and section analysis techniques. The process conditions affecting variations in void contents are discussed and mechanisms proposed for the formation of voids. Flat plaque mouldings using ±45° reinforcement were produced to verify these void formation mechanisms. The resin impregnation speed into the preform, using different resin viscosities to determine the effect on air entrapment, was also investigated.

The relative merits of the methods used for the determination of void content are also discussed.

5.2 Process Variables

The range of process variables within the flat plaque mould were discussed in Chapter 3 and their known effects upon void formation were discussed in Chapter 2.

As has been previously discussed in section 3.3, the process variables available were, fibre volume fractions ranging between 25% and 37% (for unidirectional preforms), injection pressures ranging between 1 and 3 bar, mould temperatures between 80°C and 100°C, resin pre-heating to 60°C and vacuum assistance during impregnation.

The details of the unidirectionally reinforced flat plaque mouldings are shown in Table 5.1.

5.3 Void Content Measurement

The void content of the specimens was determined using the two methods described in Chapter 3. The cutting plan for the specimens taken from the flat plaques for void volume fraction determination by the burn off method and section analysis is shown in Figure 5.1. The burn-off specimens measured 25mm x 70mm x 4mm and the sections for microscopic examination measured 20mm x 4mm. The section analysis results are for the void content estimated among the 0° fibres, analysed perpendicular to the flow front direction. Several sections were also taken parallel to the flow front direction, to examine the void content among the 90° cross fibres. The results from the burn-off experiments are shown graphically in Figure 5.2. The average void contents from the burn-off techniques are shown compared with the results from the section estimations of void content in Table 5.2. Confidence limits for the first nine void content values were calculated and are shown in Figures 5.3(a) to (j). The final void content value at the vent end of the moulding in each case was ignored since all the values were all higher than the average. This trend is discussed later in section 5.5.

5.4 Comparison of Results

Fibre Volume Fraction

Comparison of Figures 5.3(a),(b) and (c) from mouldings using 25%, 33% and 37% fibre volume fractions, show little variation in void content between the 95% confidence limit bands. The average void contents determined by the burn-off technique lie between 2.07% and 2.24%. The section analyses agreed with these

results (Figures 5.5(a),(b) and (c)).

Resin Pre-heating

The moulding which used resin preheated to 60°C, showed a small increase in void content (0.1%) determined by the burn-off method when compared to the non-preheated case (Figures 5.3(c) and (d)). This may have been due to the rapid injection time of 12 seconds (Figure 5.4(b)) compared to the injection time for the non-preheated moulding of 22 seconds (Figure 5.4(a)). Sections of the pre-heated moulding showed extensive voidage in the fibre bundles (Figure 5.5(d)), which was estimated at 2.6%, compared to 2% from the non pre-heated moulding (Figure 5.5(a)). The confidence limits for the pre-heated moulding were ±0.23%, which was low compared to the other mouldings.

The pre-heated resin entered the mould with a viscosity of 0.09 P.as (Appendix 9) and was assumed to travel along the spaces between the fibre bundles, without fully wetting the bundles. The viscosity of the resin as it enters at an ambient temperature of 20°C is 0.64 P.as. The pre-heated resin was able to impregnate the preform in approximately half the time of the non pre-heated case (comparing Figures 5.4(a) and (b)). The injection to cure time was reduced by approximately 10% (40 seconds), compared to the non-preheated case.

The section analyses indicate that the void contents of the mouldings increases with pre-heat, since the fibre bundles are thought not to have time to become impregnated with resin before the resin flow front bypasses them and reaches the vent.

Vacuum Assisted Impregnation

Both mouldings using vacuum assistance during injection showed a decrease in void content compared to unassisted impregnation (Figures 5.3(e) and (f)). The burn off method for the moulding without resin pre-heat gave an average void content of 1.54% whilst the section analysis indicated 0.2%. The void content for the moulding with pre-heat varied between 0.2% (section analysis) and 1.2% (burn-off). The confidence limits for these mouldings were ±0.22% and ±0.1% (Figures 5.3(e)

and (f)), which are low in comparison to the other mouldings. These values indicate that vacuum assisted injection produced laminates of lower void content, which has been previously discussed in section 2.5.

The sections studied (Figures 5.5(e) and 5.5(f)) showed low void contents in the 0° bundles (between 0.18% and 0.24%) suggesting that any voids must be present in another plane if the burn-off results were correct. Sections were taken in the plane parallel to the flow front, but the result was similar with no voids visible in the 90° cross layers (Figure 5.6(b)). The results from burn-off and section analysis vary by over 1% in both cases.

A vacuum of 0.98 bar gauge was drawn on the mould before each moulding. The pressure traces in Figures 5.4(c) and (d) show the pressure reaching -1.5 bar which are due to the thermal shock on the pressure transducers. The pressure activity in these mouldings was higher than in the mouldings without vacuum assistance, with a peak of over 2 bar measured in both cases. The injection times in these mouldings were 8 and 9 seconds indicating that the drop in viscosity for the pre-heated moulding had no effect on the injection time. The overall injection to cure period for the pre-heated moulding with a vacuum was reduced to 330 seconds from 400 seconds for the moulding without vacuum.

The results from this investigation led to further study of vacuum assisted moulding reported in section 5.6.

Injection Pressure

Mouldings produced using increasing injection pressure (1,2 and 3 bar), showed average void contents of 2.95%, 2.07% and 2.71% (Figures 5.3(g),(a) and (h)). The sections of these mouldings (Figures 5.5(g),(a) and (h)) agree with these results.

Comparison of Figures 5.4 (e),(a) and (f) shows the hydrostatic pressure within the mould at the end of injection reaching 0.5 bar, 1.25 bar and 1.6 bar respectively. This increase in pressure during processing does not appear to affect the void content.

Mould Temperature

The void content of the mouldings using different mould temperatures of 80°,90°,100° showed no significant variation (1.75%,2.07%,1.76%). The confidence limits for these mouldings ranged between ±0.3% and ±0.47% (Figures 5.3(i),(c) and (j)), which exhibit the widest band in the set of mouldings.

The low mould temperature of 80°C was associated with a long injection to cure cycle of 1000 seconds (Figure 5.4(g)), which allowed a long wet out period compared to the other moulding cycles. This low mould temperature allowed lower peak exotherm temperatures of between 89°C and 92°C. The injection to cure cycle time for the higher mould temperature of 100°C was 330 seconds, with the peak exotherms measuring between 110°C and 118°C. These mouldings produced with a variation in mould temperature showed that the average void content appears not to be affected by mould temperature or exotherm temperatures. The wide confidence bands suggest that in localised areas, these pressures and temperatures may affect the local void content.

5.5 Void Content Variation with Distance from the Injection Gate

The void contents determined by the burn-off method shown in Figure 5.2 show an increase in void content towards the vent. The sections examined also showed this trend. The diagram in Figure 5.7 shows how the preform is assumed to fill and the possible reason for this increase in void content at the vent end. Air is thought to be entrapped in the preform as the resin reaches the vent gallery. This air is then compressed into voids as the flow front reaches the vent end and the local pressure rises. Some of the voids are washed from the preform but many are held between and within the fibre bundles, remaining in the composite.

The increase in voids near the vent may also be explained by the rate of impregnation into the capillaries between the fibres. The fibre bundles can be impregnated due to two filling mechanisms, either by transverse impregnation into the bundle or axial impregnation along the capillaries between the fibres. If the axial

impregnation into the fibre capillaries lags behind the macroscopic flow front between the fibre bundles the capillaries will fill due to a transverse mechanism. If this occurs voids are likely to be formed in the capillaries if the transverse impregnation is uneven. Other factors which may explain this voidage increase are the air within the voids dissolving into the resin due to residence time[83], or voids forming due to decreasing air displacement during impregnation[29]. The pressure in the resin decreases with distance from the injection gate (shown by Kendall[16]), which may affect void formation and size[29].

5.6 Unidirectional Laminate Observations

To study the structure of the voids within the composite, the unidirectional laminates described in section 5.4 were studied under transmitted light. The mouldings were transparent to some degree, but the amount of transparency is subjective judgement. Figures 5.8(a) and (b) show transmitted light photographs from the mouldings produced using the mid-range conditions and vacuum assistance respectively. In both photographs the darker network of fibres which are easily distinguishable are the polyester stitching which binds the glass fabric. These fibres are visible due to the differences between the refractive indices of fibre and matrix. The darker bands running from the top to the bottom of the photographs are the 90° cross fibres, with the 0° fibres running across the pictures.

Figure 5.8(a) shows long thin dark streaks in the 0° bundles, apart from the obvious larger voids. These streaks are not evident in Figure 5.8(b). The 90° fibres however are more visible than the 0° fibres which are transparent and hardly distinguishable. The two types of fibres have been examined under an SEM and no difference apart from the tex of the fibre bundles was seen. The manufacturers of the reinforcement have stated that the fibres are from the same manufacturer and have the same size coating. The reason for these visible fibres is thought to be due to local higher fibre volume fractions, causing a change locally in the refractive index of the composite, allowing these fibres to become more visible. Figure 5.9 shows a schematic representation of the preforms used in these trials and the sections AA and BB show the maximum and minimum local fibre volume fractions which may be

present in these mouldings. The 90° fibre bundles (Figure 5.6(b)) were expected to contain more voids than the 0° bundles (Figure 5.5(f)) since they were impregnated parallel to the resin flow front and fibre axis. The 90° bundles are 600 Tex however, compared to the 2400 Tex bundles used in the 0° direction, and would have been easier to impregnate.

This examination has indicated that the microvoids within the fibre bundles are long and cylindrical. Further examination of voids within impregnated fibre bundles is carried out in section 7.2.

5.7 ±45° Bidirectional Mouldings

To verify the findings of the unidirectional mouldings in section 5.5 and to examine whether the factors of fibre direction, and process conditions could be optimised to produce a low content moulding in a fast moulding process two bidirectionally reinforced mouldings were produced. The ±45° laminates were produced to assess the effect of fibres lying at 45° to the resin flow front (eg. not transverse or axially). The bidirectional fabric uses 600 Tex fibre bundles, with no thermoplastic binder. The same polyester stitching as the unidirectional fabric was used.

Similar process conditions were used to the unidirectional moulding (4285) which used the mid-range processing conditions, with no resin pre-heat. Vacuum assistance (-0.98 bar gauge) was used during the second moulding. Figure 5.10 shows distance from the injection gate plotted against void content, determined by the burn-off method for these two mouldings. The average void content for the moulding without vacuum assistance was 1.5% and using vacuum assistance 1.25%. These values are low when compared to the unidirectional mouldings discussed in section 5.4, where the mouldings produced under similar conditions exhibited void contents of 2.07% and 1.54% respectively.

These mouldings have shown that the use of fibres oriented at an angle to the flow front, combined with lower tex bundles and lack of thermoplastic binder lowers

the void content when compared to unidirectional mouldings.

5.8 The Effect of a Partial Vacuum within the Mould Cavity upon Void Content

Unidirectional Mouldings Using an End Gate

The investigations described in section 5.4 suggest that the use of a vacuum substantially reduced void content in unidirectional mouldings. Moulding trials were undertaken using a rectilinear flow front and different vacuum pressures (eg. 0.02 bar, 0.25 bar, 0.5 bar, 0.75 bar absolute), to assess the consequences upon void content and cure pressures.

The average void contents for these mouldings are shown in Table 5.3, and the values shown graphically in Figure 5.11. The trend of these results shows that void content reduces with amount of vacuum. The maximum exotherm pressure at each instrumentation position for each moulding has been plotted in Figure 5.12(a). The mouldings produced with increasing amounts of partial vacuum seemed to show an increase in cure pressure.

CFRM Mouldings Using a Central Injection Gate

To study the exotherm pressures in greater detail, further trials were undertaken using a central injection point such that the injection and cure fronts would be radial (assuming uniform heating and an isotropic preform). This radial flow front would offer more meaningful pressure values since the rectilinear cure front pressures were thought to be affected by uneven impregnation and edge effects. The moulding trials were undertaken using CFRM reinforcement since the material is nearly isotropic and would provide an approximately circular flow front in comparison with an elliptical flow front from unidirectional reinforcement. The same moulding conditions were used as in the rectilinear moulding trials.

All the mouldings experienced high exotherm temperatures (approximately 140°C at the injection gate). The mouldings using a full vacuum showed extensive voidage near the injection gate (Figure 5.13). The thermal and pressure histories for

this moulding are shown in Figure 5.14(a). This voidage was thought to be due to styrene boil due to the partial vacuum present in the mould after injection. Moulding 4342 was produced using a lower moulding temperature (60°C) and vacuum assisted injection. Once the moulding was impregnated, the vacuum was removed and a hydrostatic pressure allowed to build up in the moulding (Figure 5.14(b)). This moulding was transparent and showed no signs of styrene boil.

Four mouldings were produced using increasing amounts of vacuum assistance and the mould pressure permitted to reach hydrostatic once the mould had filled. The void contents vs distance from the injection gate for these mouldings are shown graphically in Figure 5.15. The trend of this graph indicates that with increasing evacuation from the mould cavity the void content within the composite will decrease.

The maximum exotherm pressure during the manufacture of these mouldings at the four instrumentation points available in the mould cavity (instrumentation point 3 was used for the central injection gate), are shown in Figure 5.12(b). These pressures show that during the radial cure of the resin in the mould the exotherm pressures increase. This increase may be due to the reduction in void content within the moulding, since the air within the voids would become pressurised prior to polymerisation reducing the pressure exerted onto the mould surface.

Styrene and Polyester Boiling Temperatures

Boiling point values for styrene at a selection of pressures was obtained from "The Handbook of Chemistry and Physics"[82]. No values were available for the polyester resin in question. Using a vacuum chamber and a hot plate the boiling point of CVP 6345.001 polyester resin was determined for a range of pressures between 0 bar (absolute) and atmospheric pressure (1 bar absolute). The values for both styrene and the polyester resin are shown in Figure 5.16. The polyester resin curve can be seen to fit the styrene curve.

Polyester resin will boil at ambient temperature in a full vacuum. This boiling point changes exponentially with pressure. Thus if the resin pressure is allowed to

become lowered the prospect of styrene boiling is high and voids will be present in the final moulding.

5.9 The Effect of Resin Viscosity upon Void Content

The effect of resin viscosity upon void content, in CFRM preforms was investigated to determine whether similar impregnation rates but different resin viscosities would effect void content. Using Equation (2.8), the viscosity information in appendix 6 and the permeability information contained in section 6.5, flow rates into the preform were calculated. To gain the same impregnation rate as resin at 20°C and using an injection pressure of 2 bar, resin pre-heated to a temperature of 60°C required an impregnation pressure of 0.3 bar.

Figure 5.17 shows a graph of distance from the injection gate for the two mouldings, the two mouldings have average void contents, determined by the burn-off method of 2.45% and 2.54% for the 2 bar and 0.3 bar injection pressures respectively. These values indicate that the resin viscosity into preforms influences air entrapment.

5.10 Discussion

The process conditions of injection pressure, mould temperature resin pre-heat, outlet pressure and fibre volume fraction were varied to produce ten mouldings which were analysed for void content. Several samples were taken from each location described in Figure 5.1, to assess the reliability of the results. The factors of injection pressure, and resin pre-heating affected void content, primarily in the fibre bundles (from section examination). The creation of a vacuum in the mould reduced the void content in the mouldings.

Increasing either mould temperature or fibre volume fraction did not appear to affect the void content. Mould temperature increase, reduced the injection to cure times for the mouldings, but did not affect the void content, suggesting that in the time scales presently used for RTM (between 5 and 20 minutes) air cannot dissolve into the liquid resin before polymerisation commences. The mouldings produced using vacuum assistance during injection had low void contents and low confidence

limits. The mouldings produced using increasing mould temperatures indicated high confidence bands, suggesting that in localised areas the temperature or process times may have an effect on the void content.

Both voidage analysis techniques have shown the void content increases with distance from the injection gate. This is especially significant at the vent end of the moulding. This increased voidage has been explained by air becoming entrapped in the preform as resin reaches the vent gallery and by the increase in voids in the fibre bundles as impregnation pressure reduces with distance from the injection gate.

The two void analysis techniques have been compared in this chapter. The burn-off method can be used to analyse a large specimen giving an average void content over a large area. The method is however sensitive to the density values for resin and glass. The fraction of thermoplastic binder and polyester stitching in the moulding was estimated from manufacturers data, such that these values although small could be accounted for. The section analysis technique relies on the contrast between the voids and the composite to estimate the void content in the section. The areas considered (4mm x 20mm) are small.

The values obtained for the two methods have been compared in Figure 5.10. The graph shows burn-off values plotted against section analysis results. The majority (8 out of 10) of the values determined by the burn-off technique are higher than those determined by sectional analysis. The least similar values are those gained from the vacuum assisted impregnation mouldings. The burn-off method gave over 1% void content for both mouldings, which when studied both in 0° and 90° sections appeared to have very a low void content (less than 0.25%).

The banded structure of the mouldings when studied under transmitted light has been explained by the variation in local fibre volume fraction, where the 90° cross fibres have increased the volume fraction. Long thin microvoids were observed with the fibre bundles whilst examining the mouldings under transmitted light.

The ±45° reinforced mouldings were produced to verify the void formation mechanisms hypothesised after the unidirectional moulding trials. The ±45° fabric used lower Tex fibre bundles (600 Tex) compared to the unidirectional fabric (2400 Tex). The fabric had no thermoplastic coating but did incorporate similar polyester stitching to that of the unidirectional fabric.

The moulding trials using increasing amounts of vacuum pressure showed a trend of lower void content. Vacuum assistance during impregnation was also shown to affect styrene boiling and the maximum exotherm pressures in the mould during cure. The styrene boiling effect was reduced by allowing the resin to become pressurised to a hydrostatic pressure once the mould had filled. Whether the styrene had boiled prior to this it is not known. Polyester resin was seen to follow the styrene temperature Vs pressure curve and under room temperature (20°C) in a vacuum (0.98 bar gauge) can boil.

The increase in maximum exotherm pressure during cure due to vacuum assistance during impregnation may be due to the reduction in void content within the composite. The compression of the air within the voids is assumed to reduce the peak exotherm pressures during cure, with lower void contents this pressure will become restricted only by the mould surface. This higher exotherm pressure may have a greater impact during the manufacture of thicker laminates and may influence mould stiffness design if the pressures are large enough to affect mould deflections.

The effect of using different resin viscosities and similar impregnation speeds within CFRM reinforced mouldings was investigated. The two mouldings showed similar void contents, suggesting the air entrapment is influenced by resin viscosity and impregnation speed.

Several of these process conditions including vacuum assistance, pressure and temperature variations upon the quality of RTM laminates have been studied by other researchers[35]. The void content of mouldings were not however studied in detail. No previous research has been undertaken to determine the effect of increasing vacuum

pressure within the mould cavity prior to injection or changing the viscosity to aid impregnation. Pressure and temperature histories for each moulding have been used to discuss the variations in void content, for differing process conditions. The effect of void content increasing with distance from injection sprue has also been discovered.

List of Tables

List of Figures

Table 5.1 **Moulding Summary**

Moulding No.	Layers of reinforcement	Fibre Volume Fraction (%)	Mould Temperature (°C)	Injection Pressure (bar)	Resin pre-heat (temperature)	Vent pressure	Injection Time (seconds)	Injection to cure time (seconds)
4273	4	25	90	2	None	Ambient	18	410
4275	6	37	90	2	None	Ambient	24	420
4285	5	33	90	2	None	Ambient	22.1	400
4286	5	33	90	2	60°C	Ambient	12	360
4287	5	33	90	2	60°C	Vacuum	9	330
4288	5	33	90	2	None	Vacuum	8	440
4289	5	33	90	1	None	Ambient	25	420
4290	5	33	90	3	None	Ambient	14	430
4291	5	33	80	2	None	Ambient	22	1000
4292	5	33	100	2	None	Ambient	20	330

Table 5.2 **Void Contents of the mouldings**

Moulding No.	Average void content by the burn off method	Confidence Limits (± %)	Void content estimation by section analysis
4273	2.24	0.24	1.5
4274	2.14	0.19	1.7
4285	2.07	0.29	2.0
4286	2.18	0.23	2.6
4287	1.54	0.22	0.24
4288	1.18	0.1	0.18
4289	2.95	0.28	1.6
4290	2.71	0.36	1.9
4291	1.75	0.47	1.3
4292	1.76	0.38	2.4

Table 5.3 **Void Contents for Vacuum Assisted Mouldings**

Moulding No.	Reinforcement	Vacuum Pressure (gauge) Bar	Average void content by the burn off method	Confidence Limits (± %)
4285	0°	0	2.07	0.29
4327	0°	-0.98	0.95	0.26
4328	0°	-0.75	1.25	0.11
4329	0°	-0.49	1.17	0.36
4330	0°	-0.26	1.45	0.3
4336	CFRM	0	2.54	0.11
4342	CFRM	-0.98	1.56	0.27
4343	CFRM	-0.75	1.91	0.18
4344	CFRM	-0.5	1.79	0.12
4345	CFRM	-0.25	2.44	0.21

Figure 5.1

Cutting plan for Void fraction Determination

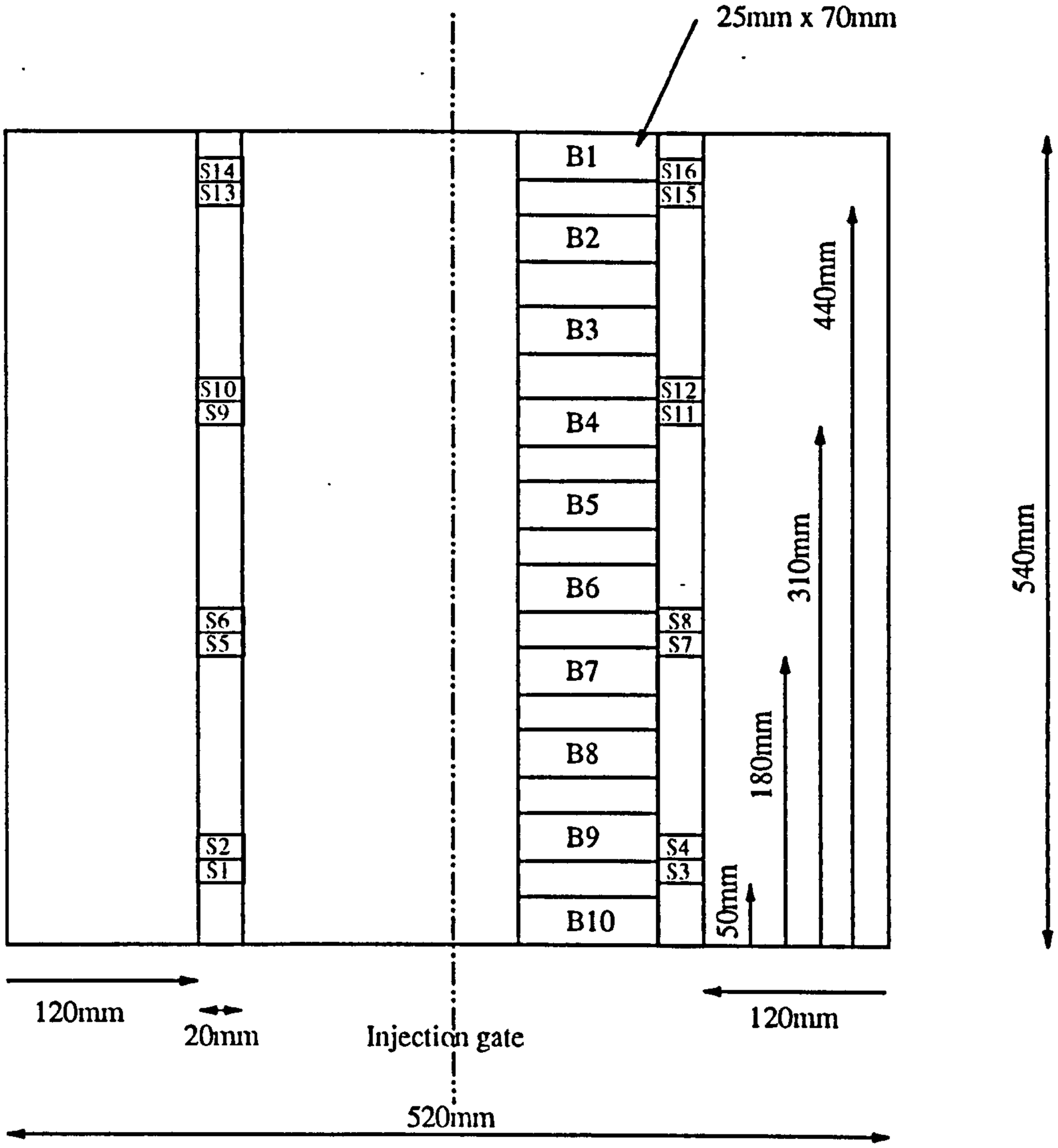

B = Void determination by burn-off specimens

S = Specimens to be sectioned and examined by optical microscopy

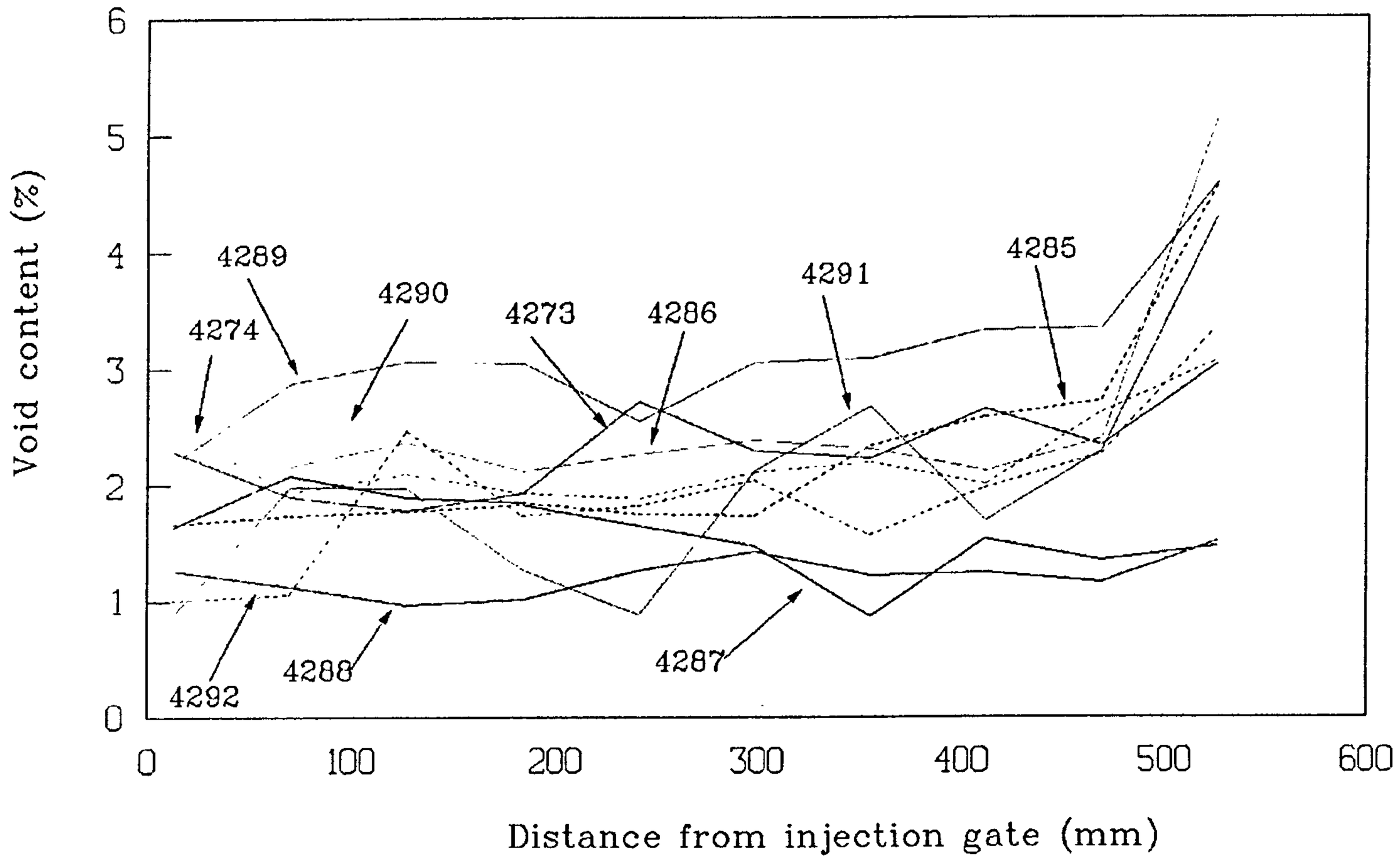

Figure 5.2 Void Content Vs Distance from the Injection Gate for Unidirectional Mouldings

Figure 5.3(a,b,c,d) Void Content (Burn-off Method) Vs Distance from Injection Point

(a) Moulding 4285 (Mid-range process conditions, 2 bar injection pressure 90 C mould temperature and 33% Fibre volume fraction)

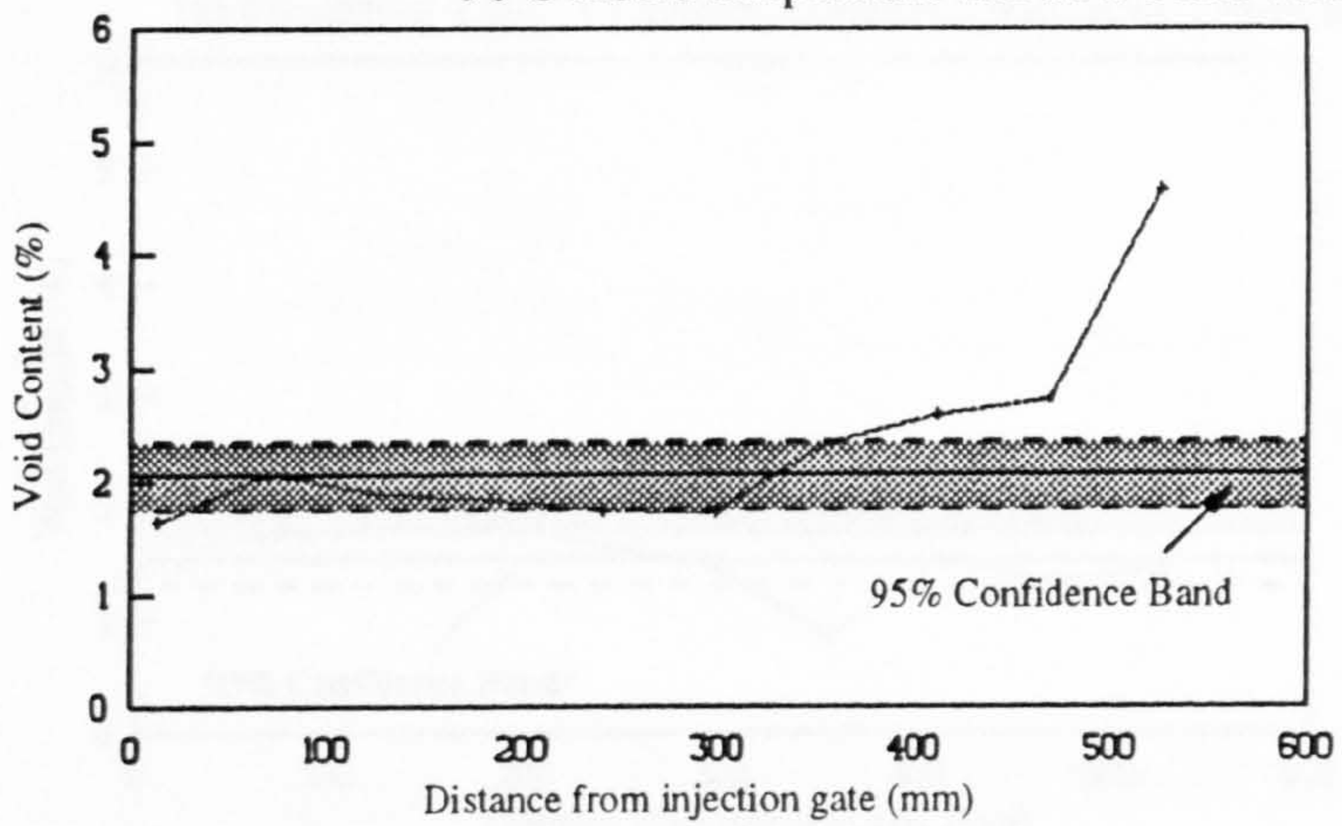

(b) Moulding 4273 (25% fibre volume fraction)

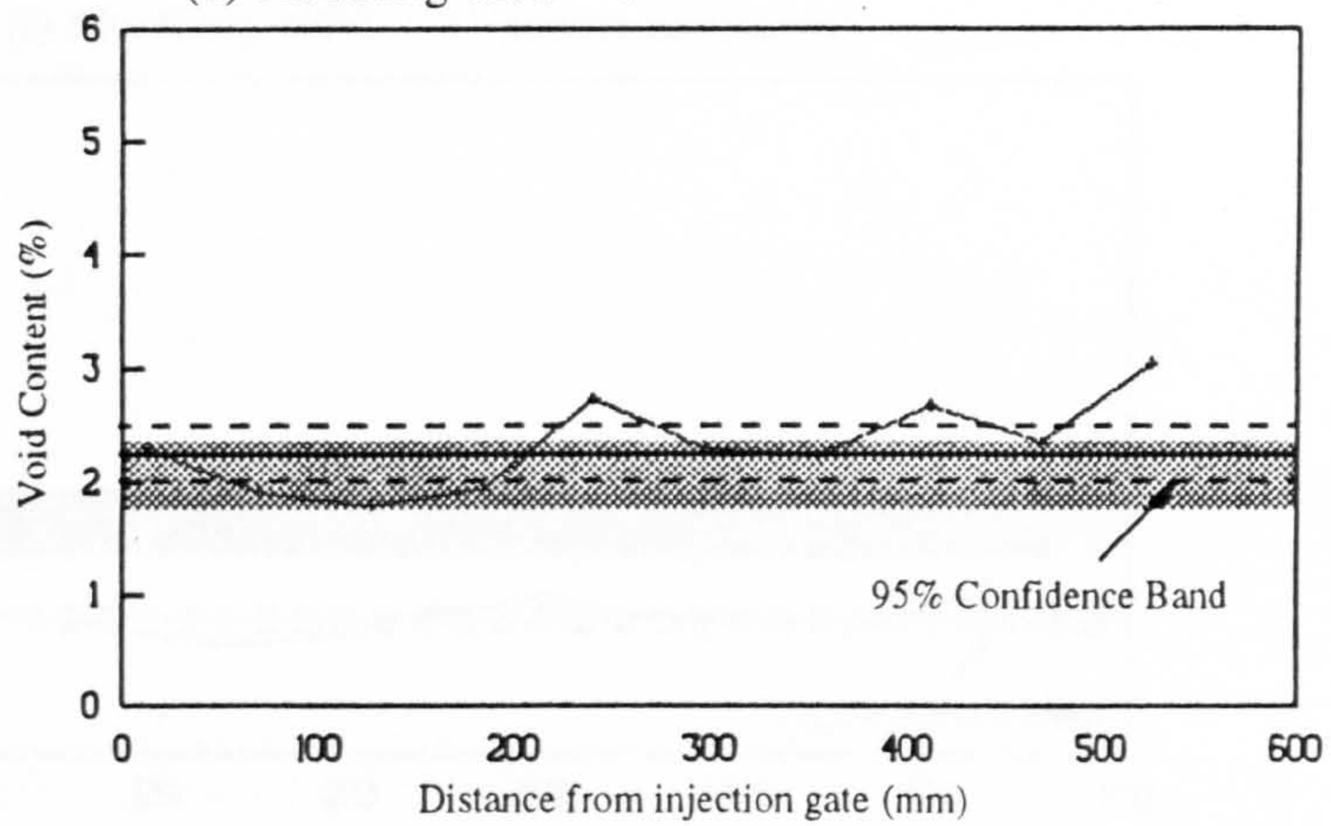

(c) Moulding 4275 (37% fibre voloume fraction)

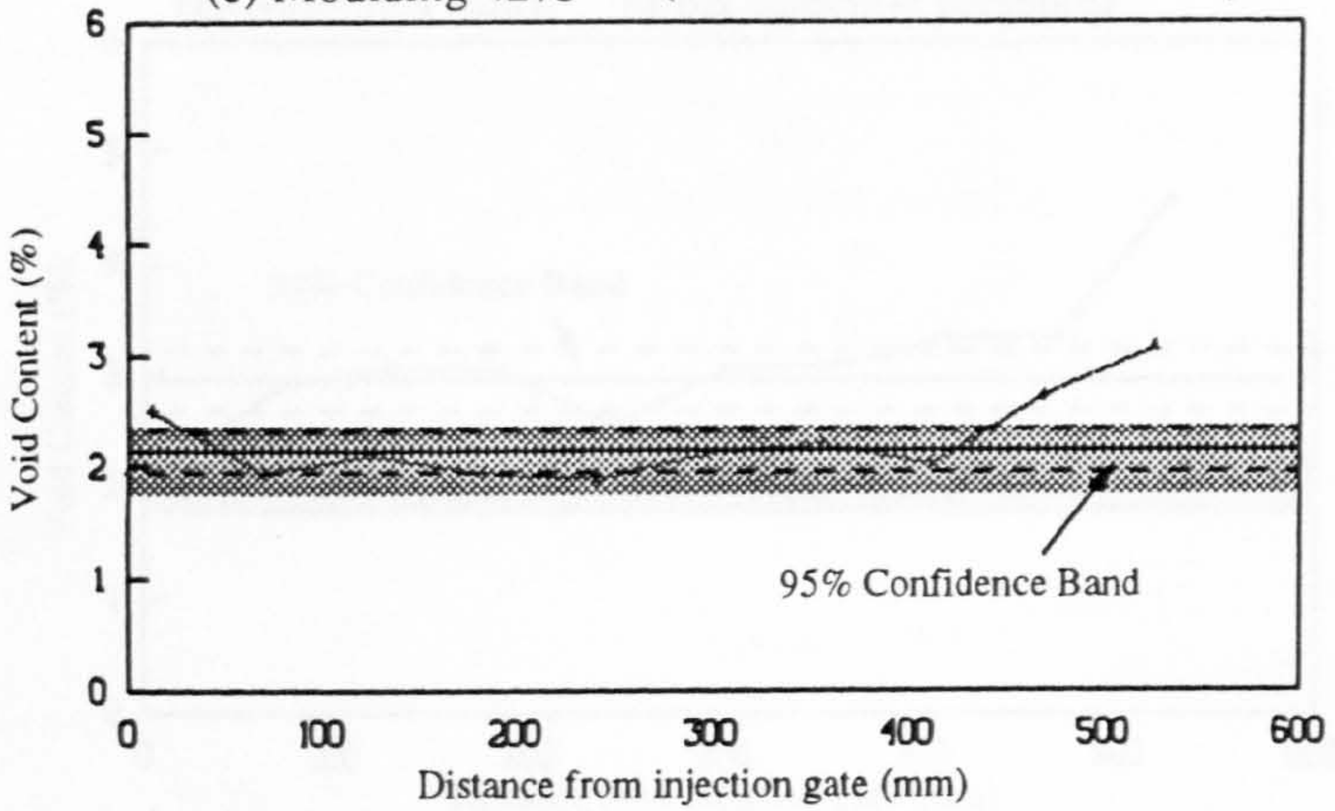

(d) Moulding 4286 (Resin pre-heating)

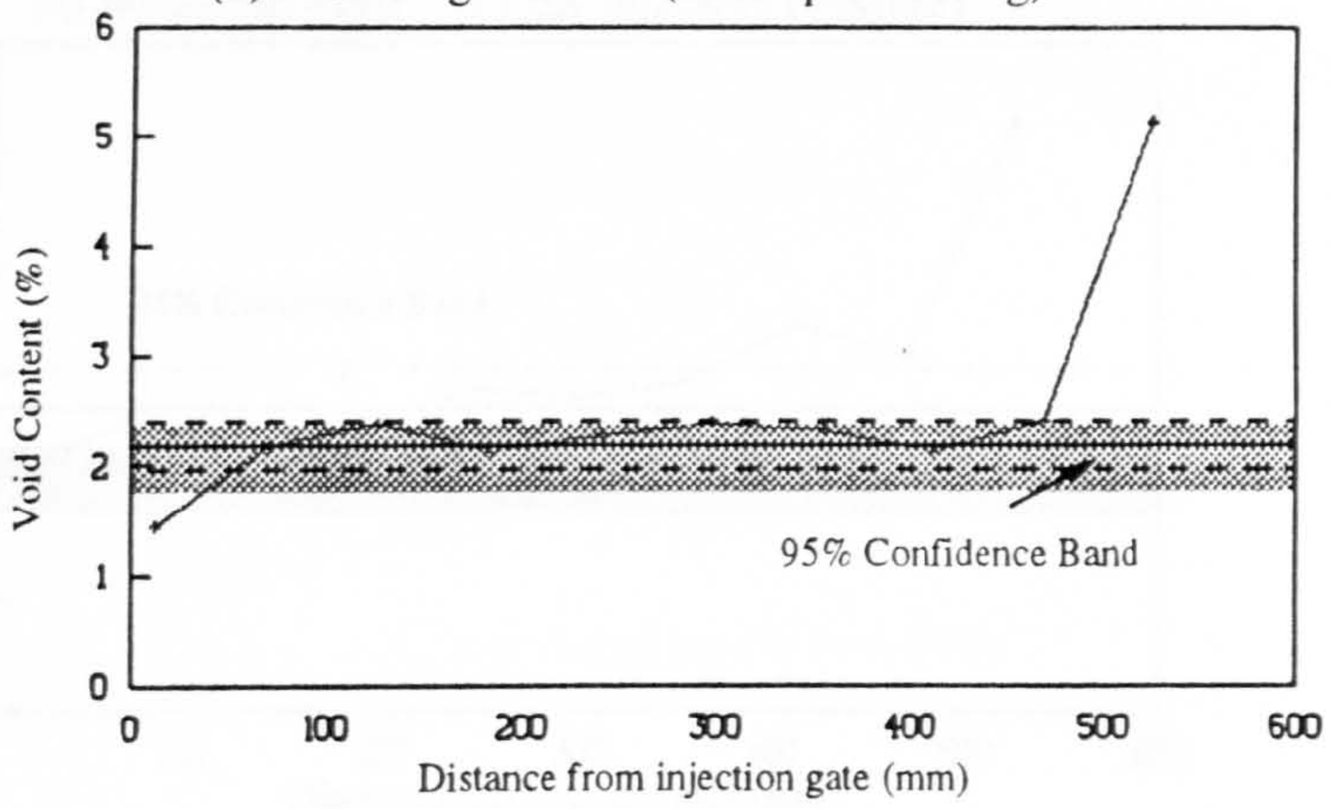

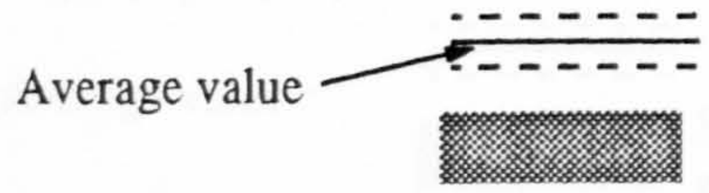

Shaded region shows the 95% confidence bands for the mid-range moulding conditions of 2 bar injection pressure and 90 C mould temperature

Figure 5.3(e,f,g,h) Void Content (Burn-off Method) Vs Distance from Injection Point

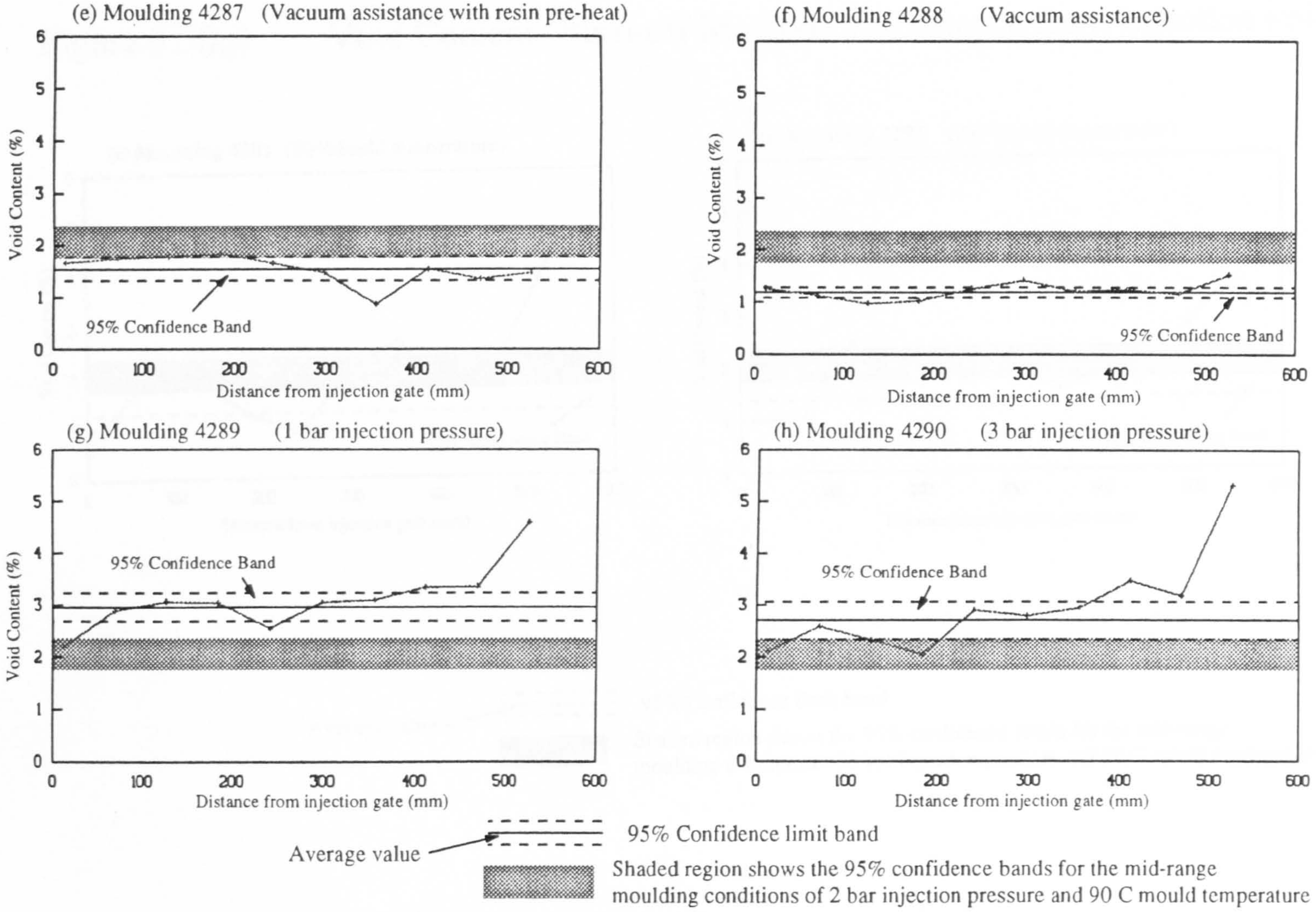

Figure 5.3(i,j) Void Content (Burn-off Method) Vs Distance from Injection Point

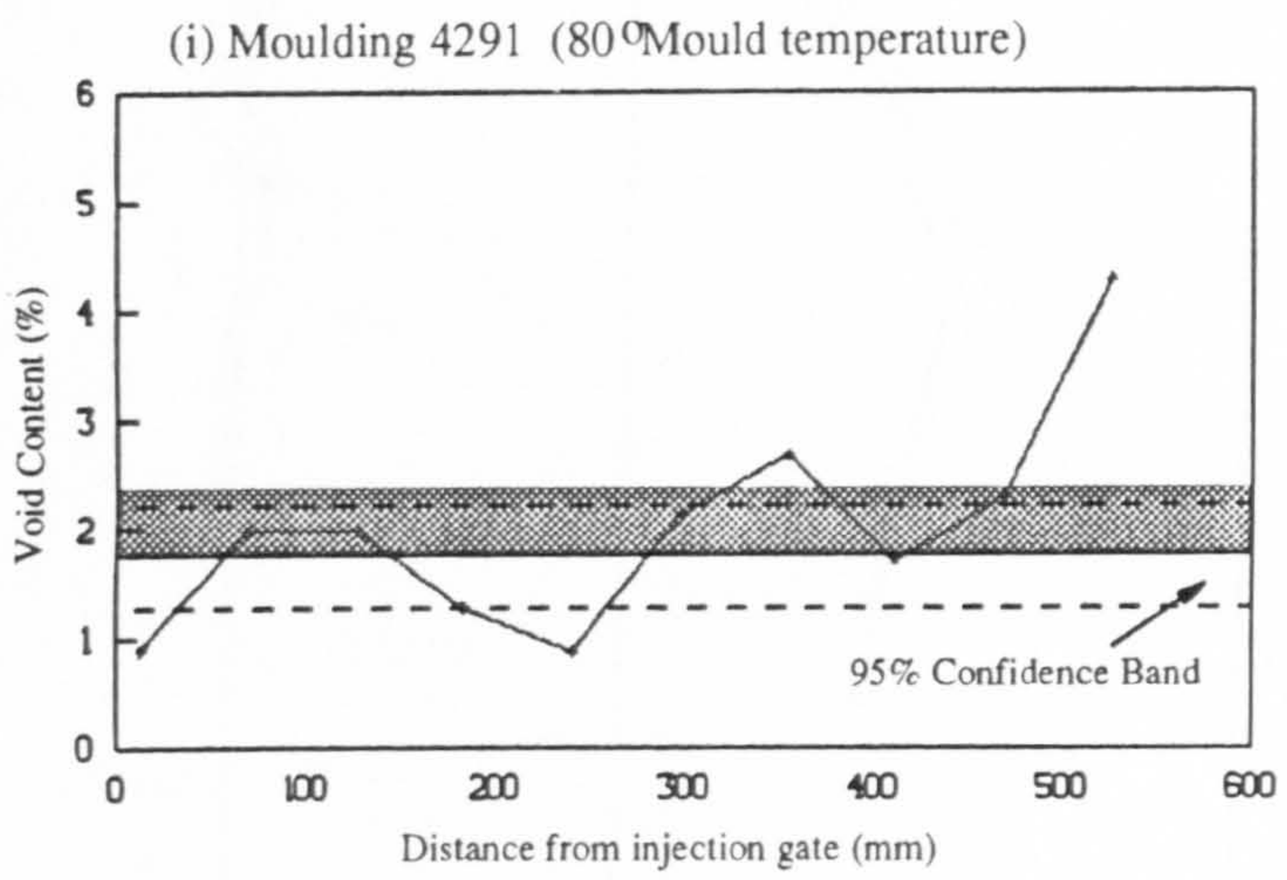

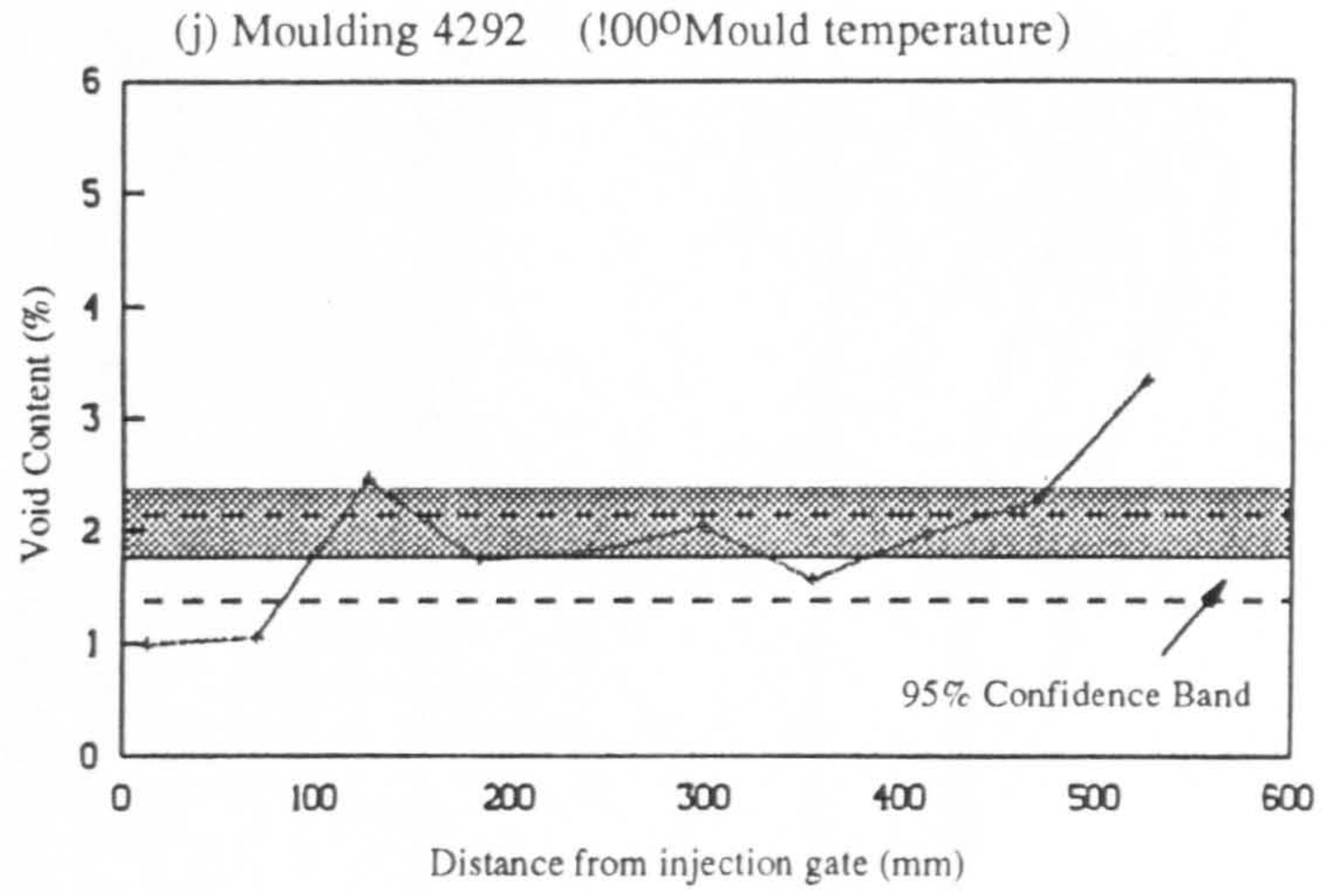

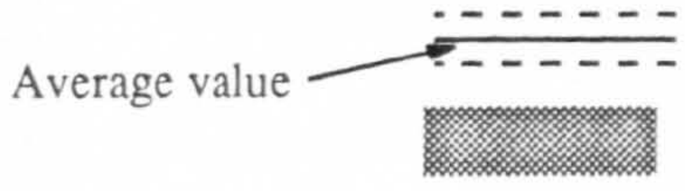

95% Confidence limit band

Shaded region shows the 95% confidence bands for the mid-range moulding conditions of 2 bar injection pressure and 90 C mould temperature

Figure 5.4(a,b) Thermal and Pressure Histories

(a)Moulding 4285 (Mid-range moulding conditions)

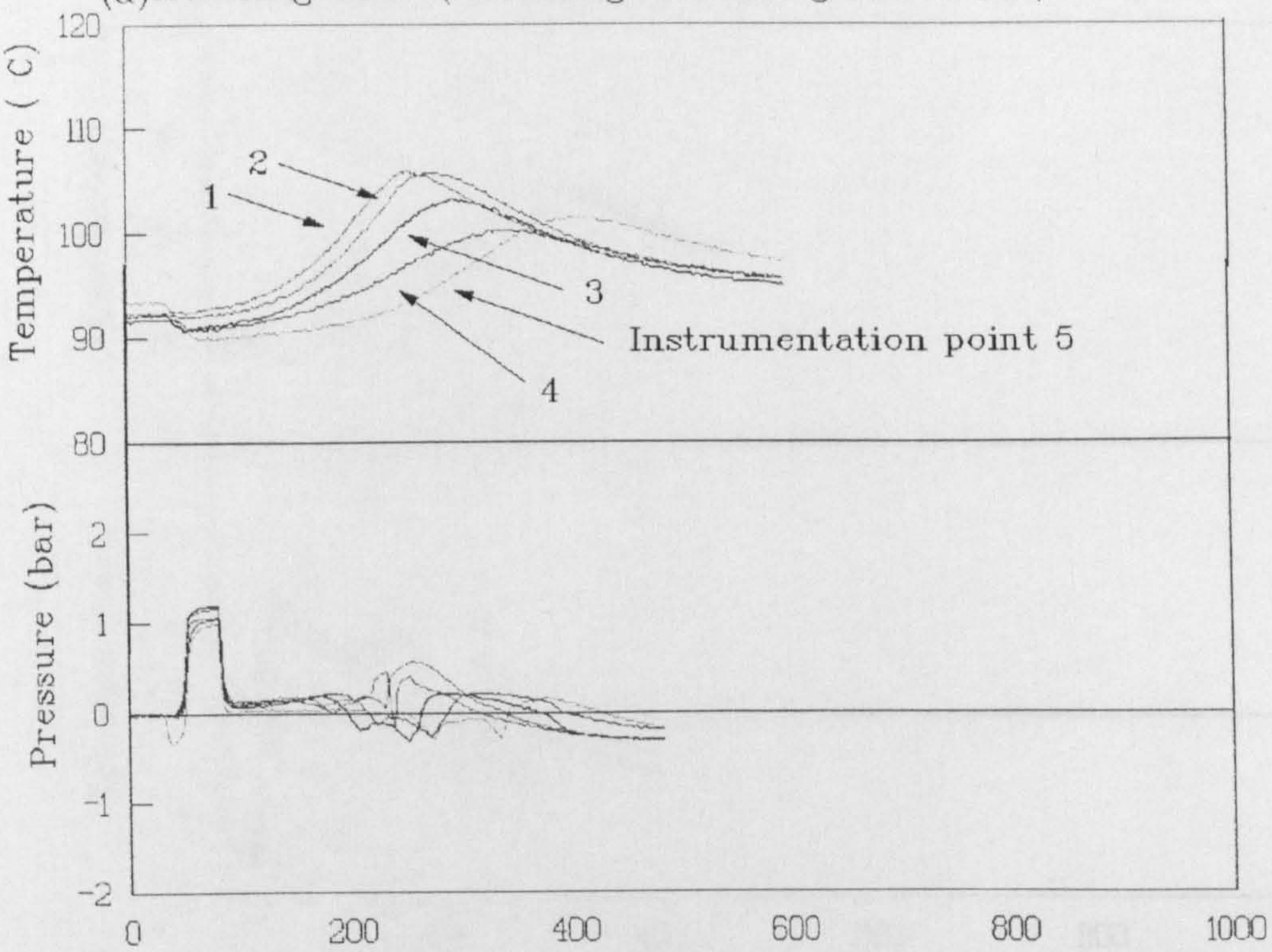

(b) Moulding 4286 (Resin pre-heating)

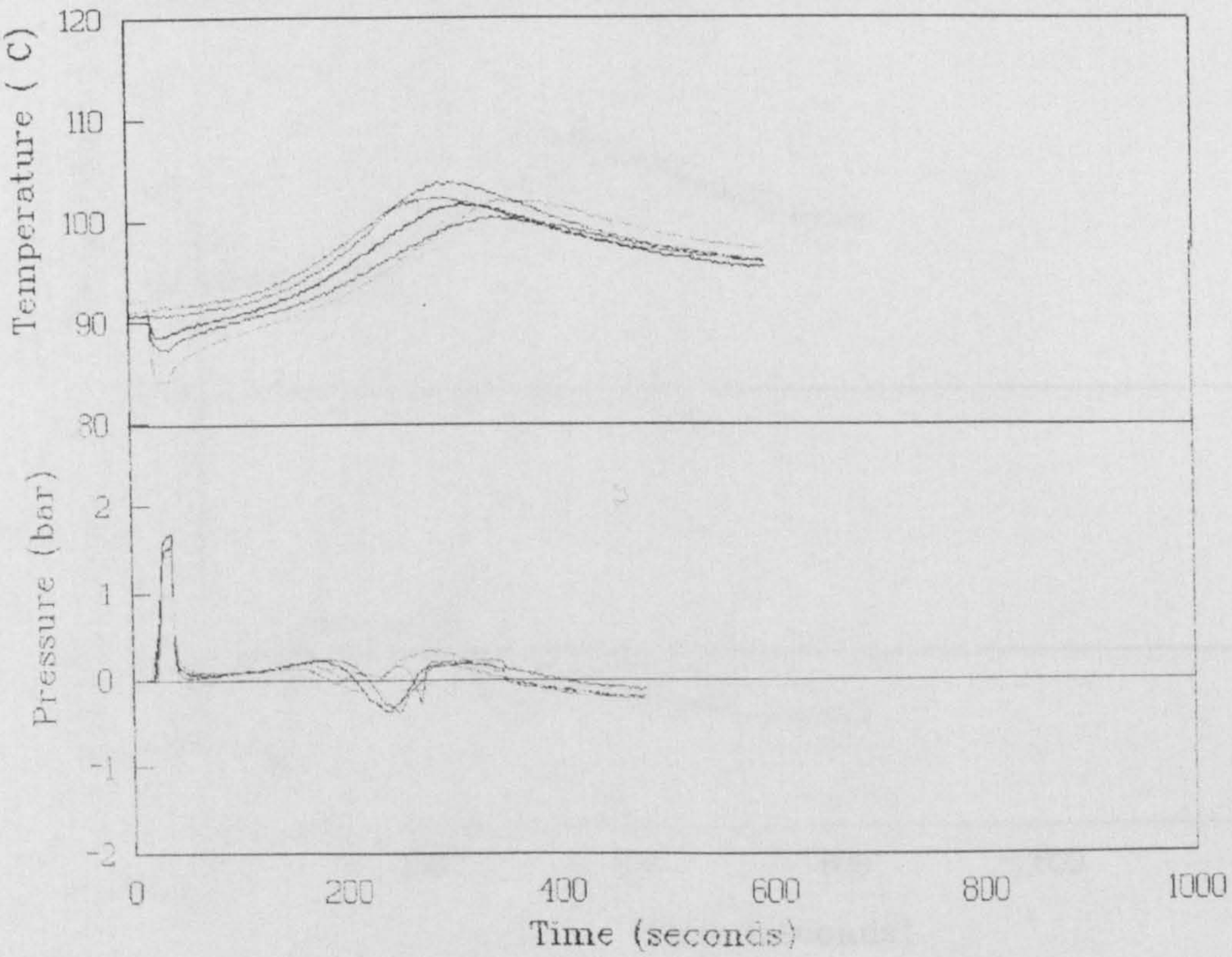

Figure 5.4(c,d) Thermal and Pressure Histories

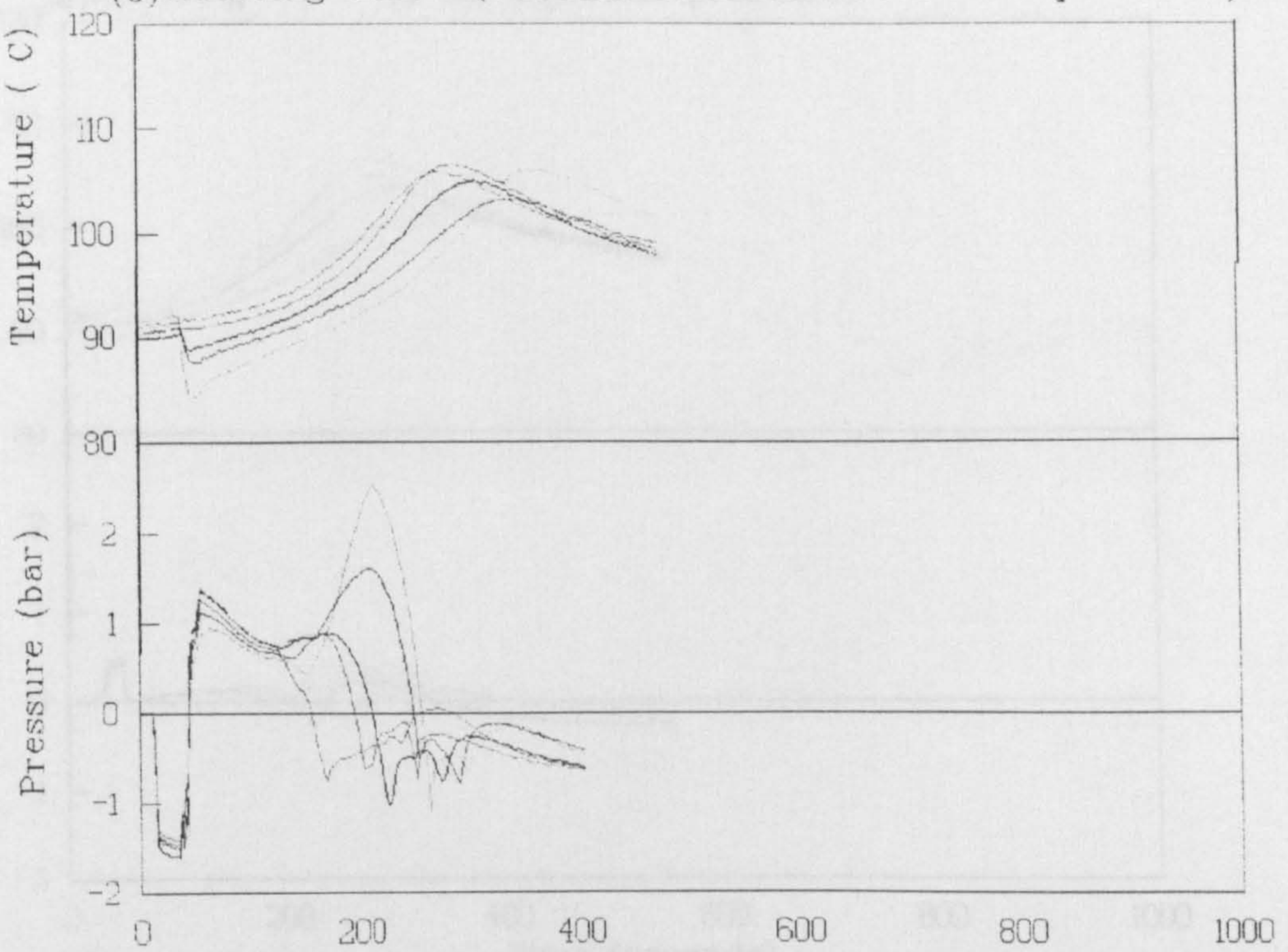

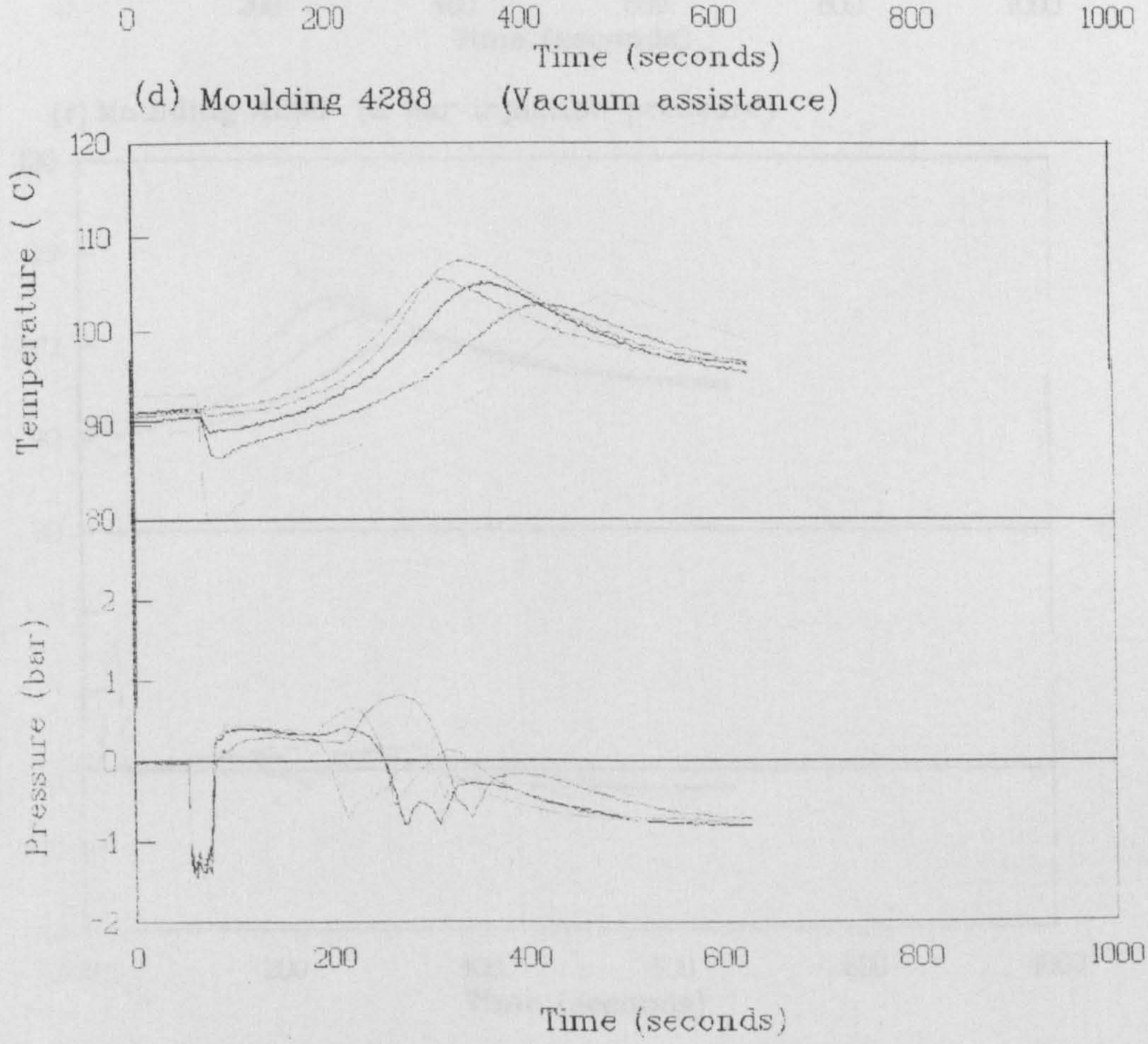

Figure 5.4(e,f) Thermal and Pressure Histories

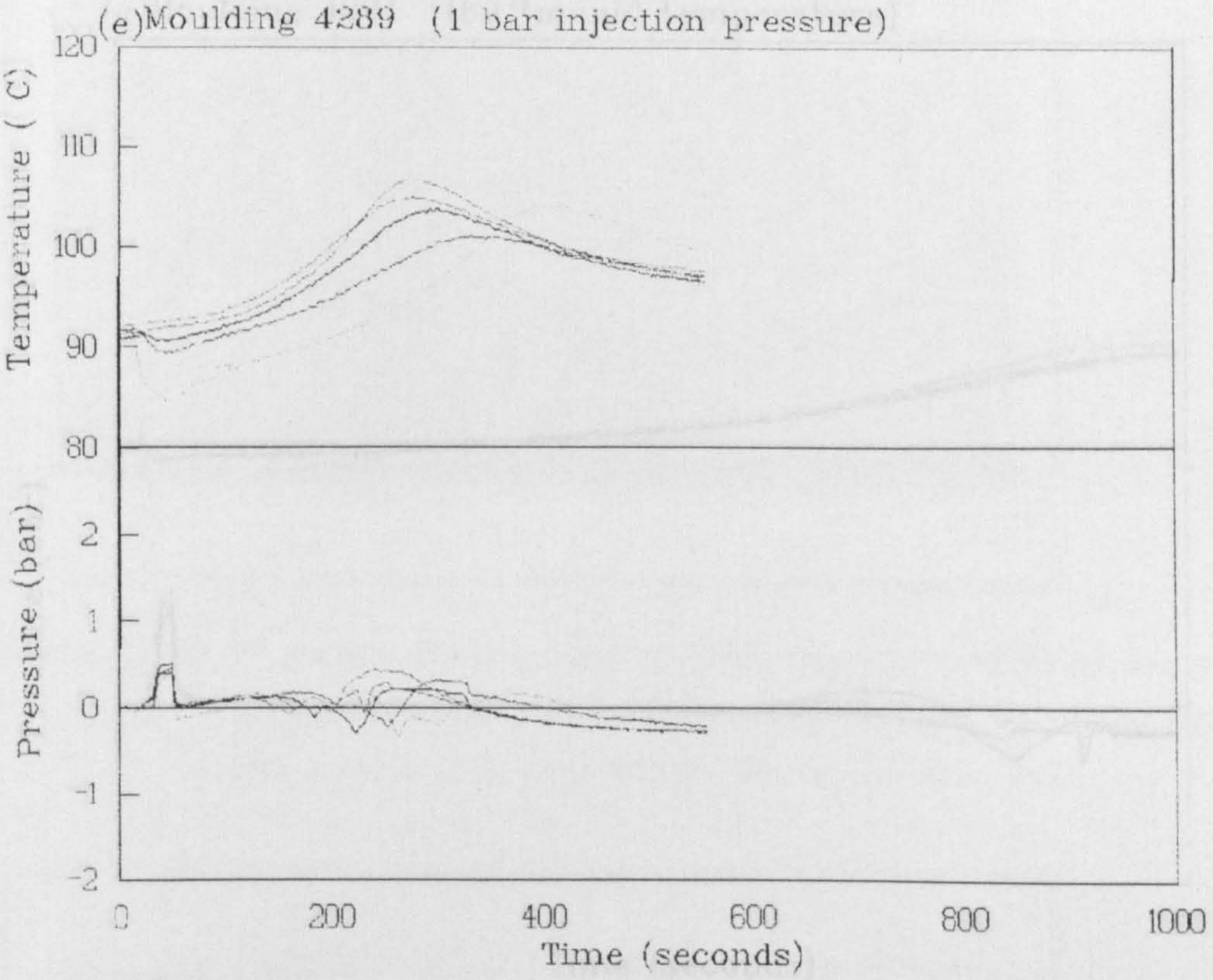

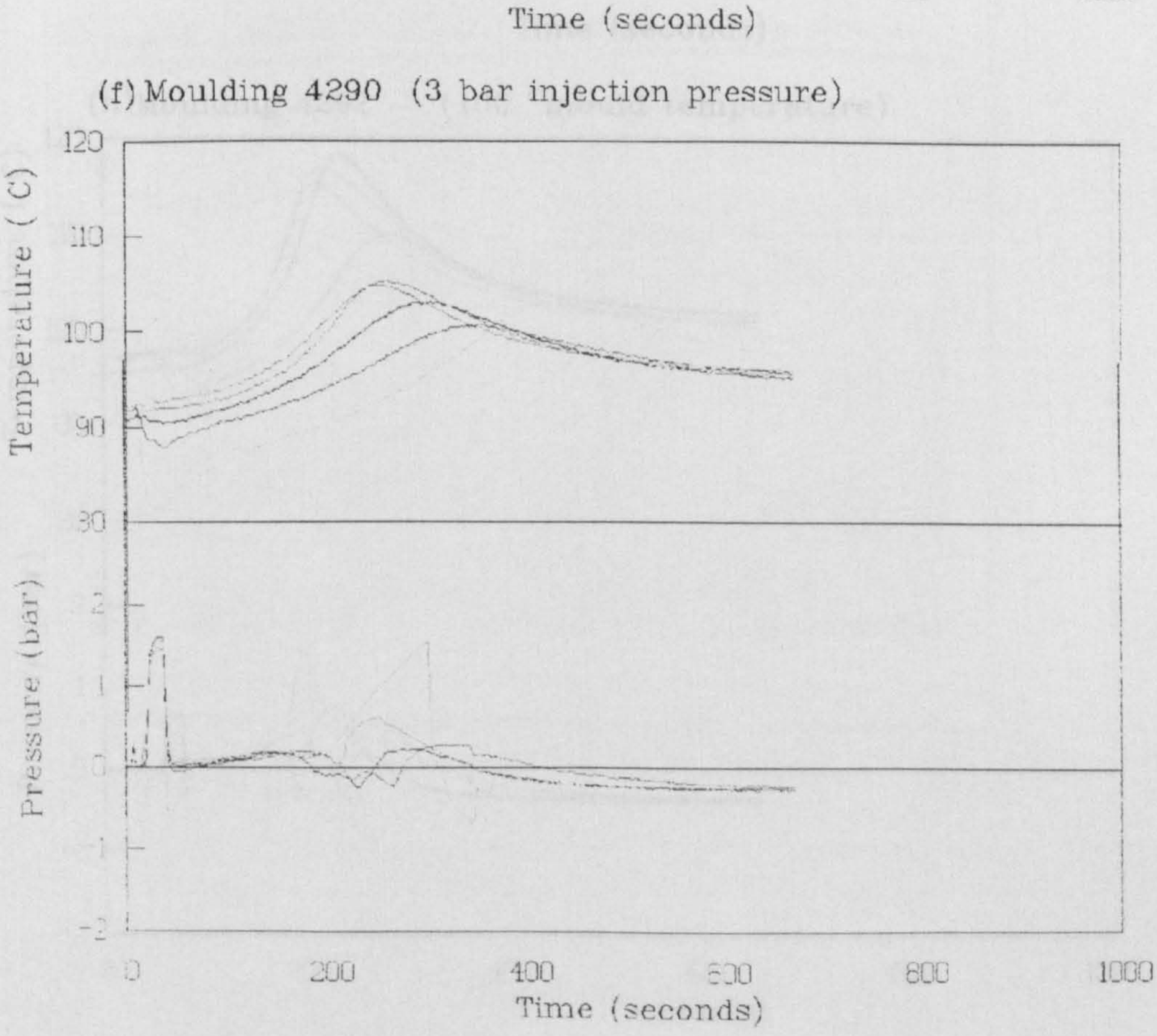

Figure 5.4(g,h) Thermal and Pressure Histories

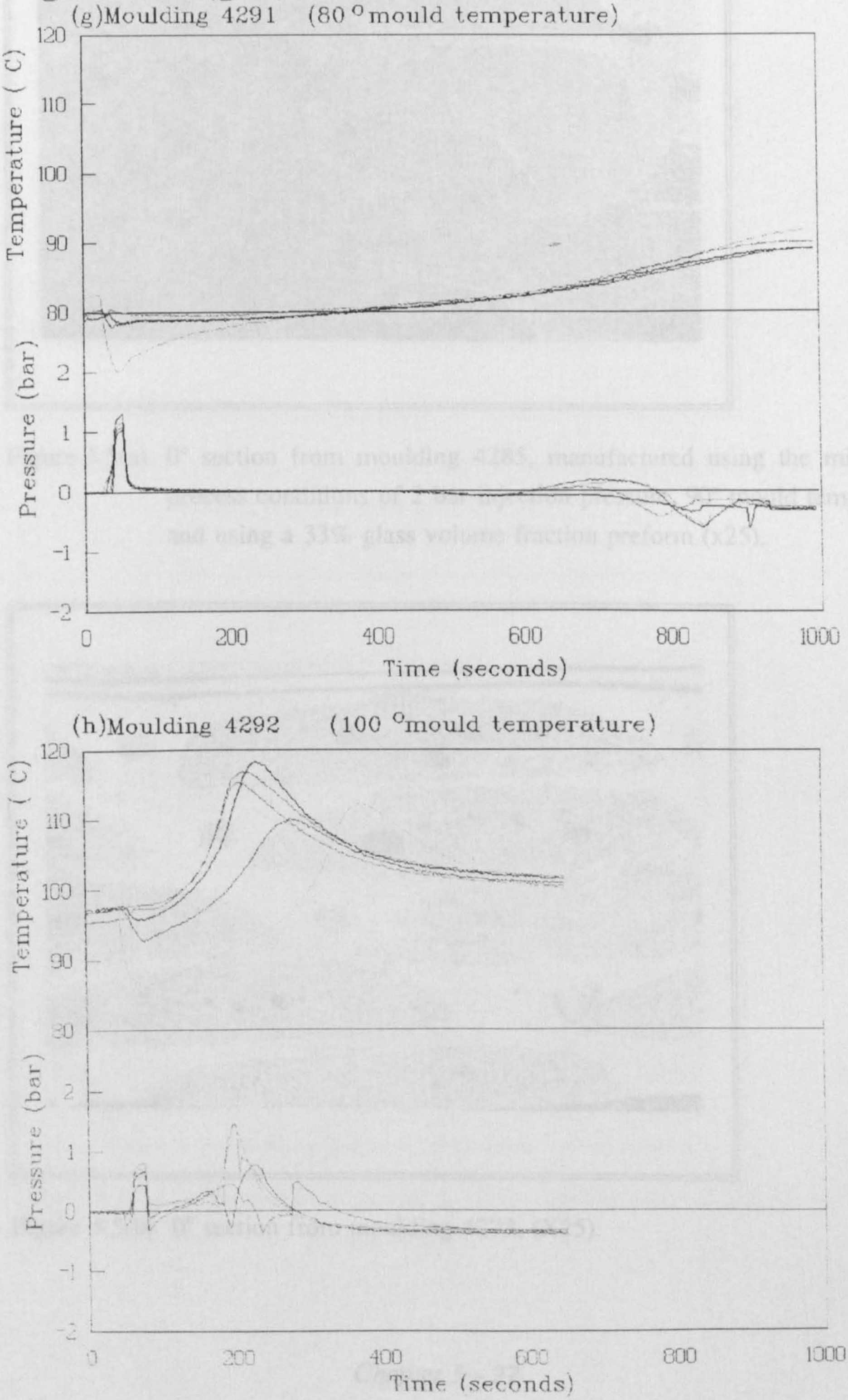

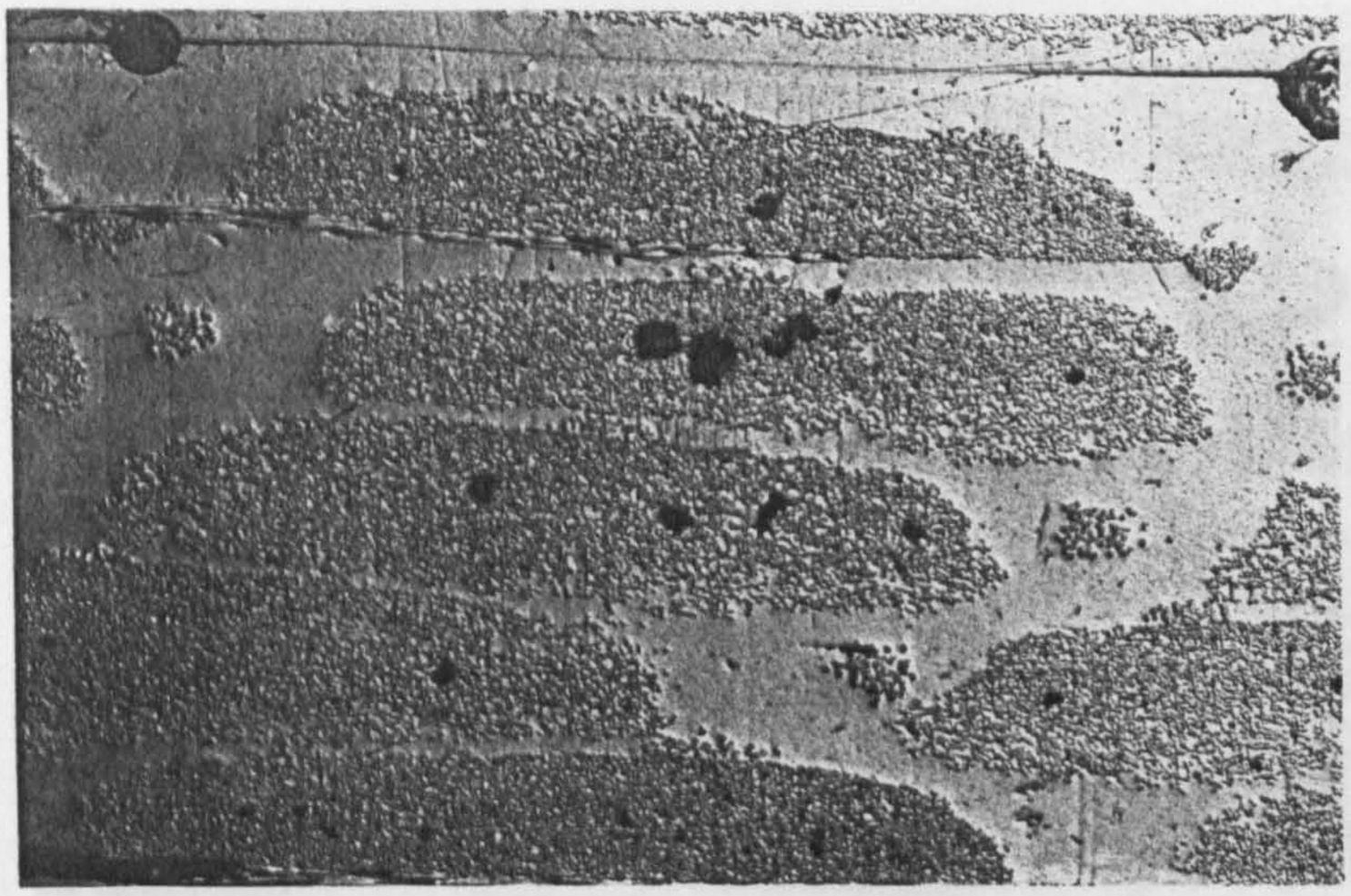

Figure 5.5(a) 0° section from moulding 4285, manufactured using the mid-range process conditions of 2 bar injection pressure, 90° mould temperature and using a 33% glass volume fraction preform (x25).

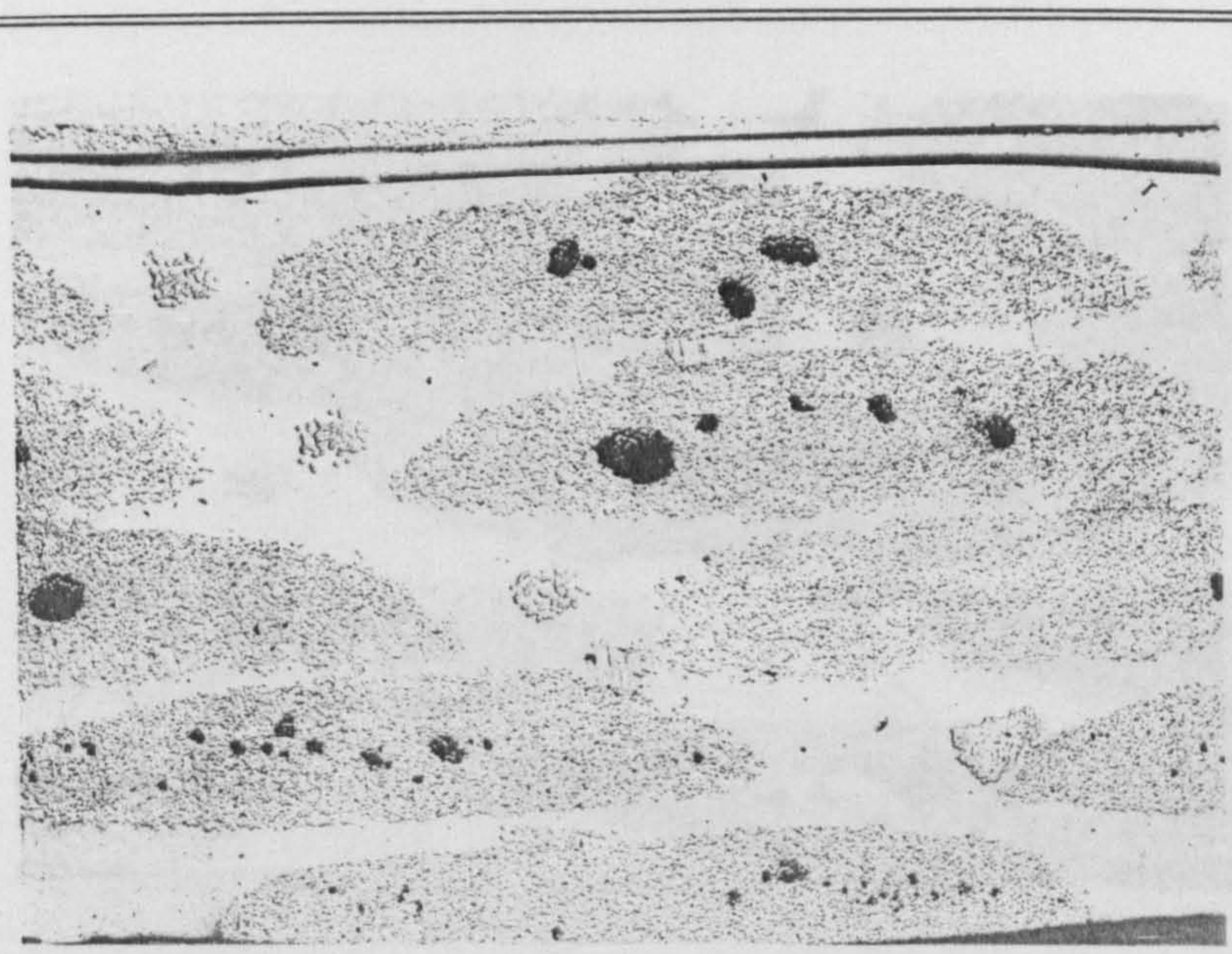

Figure 5.5(b) 0° section from moulding 4273, (X25).

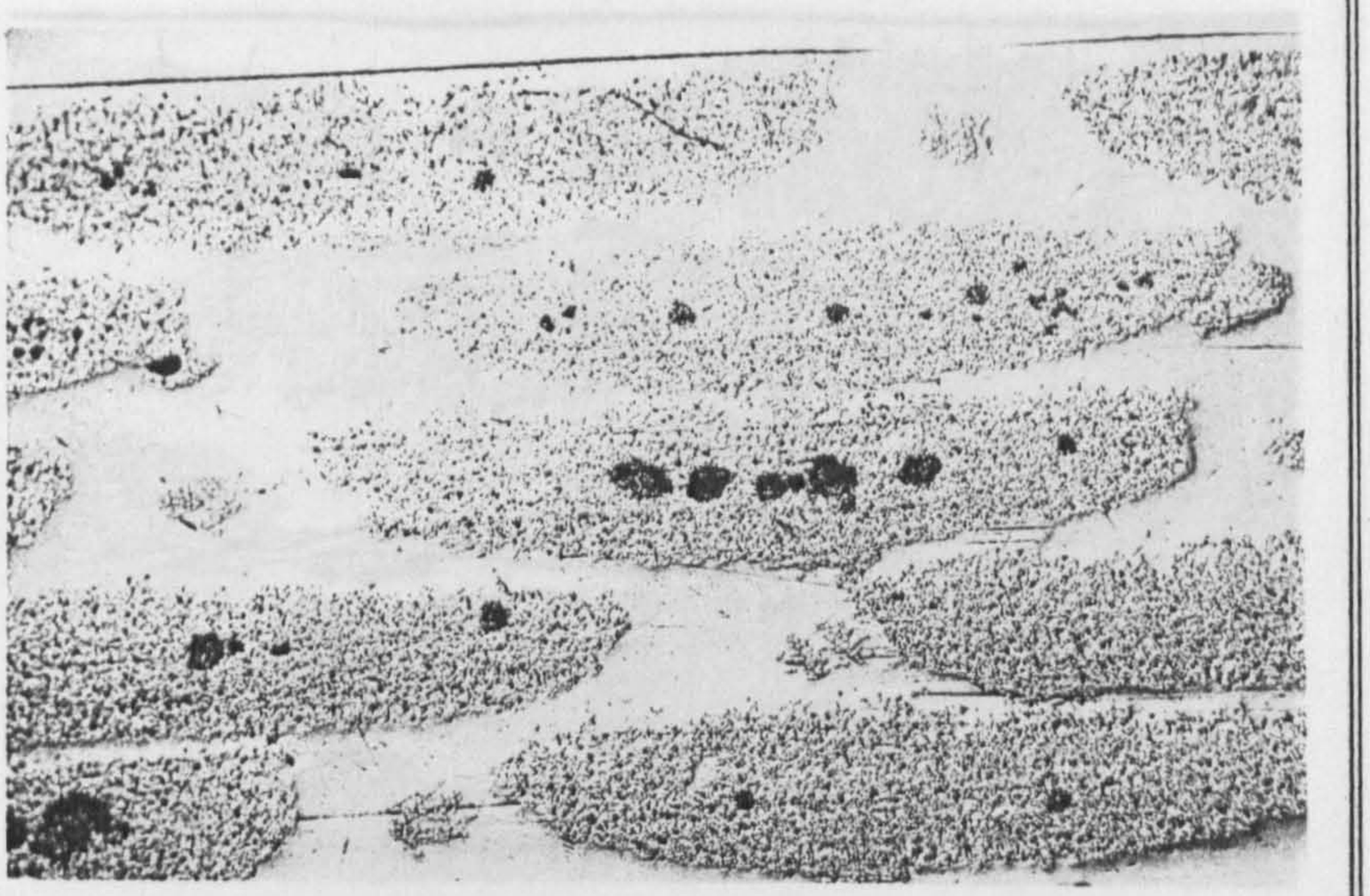

Figure 5.5(c) 0° section from moulding 4274, manufactured using a 25% glass volume fraction preform (x25).

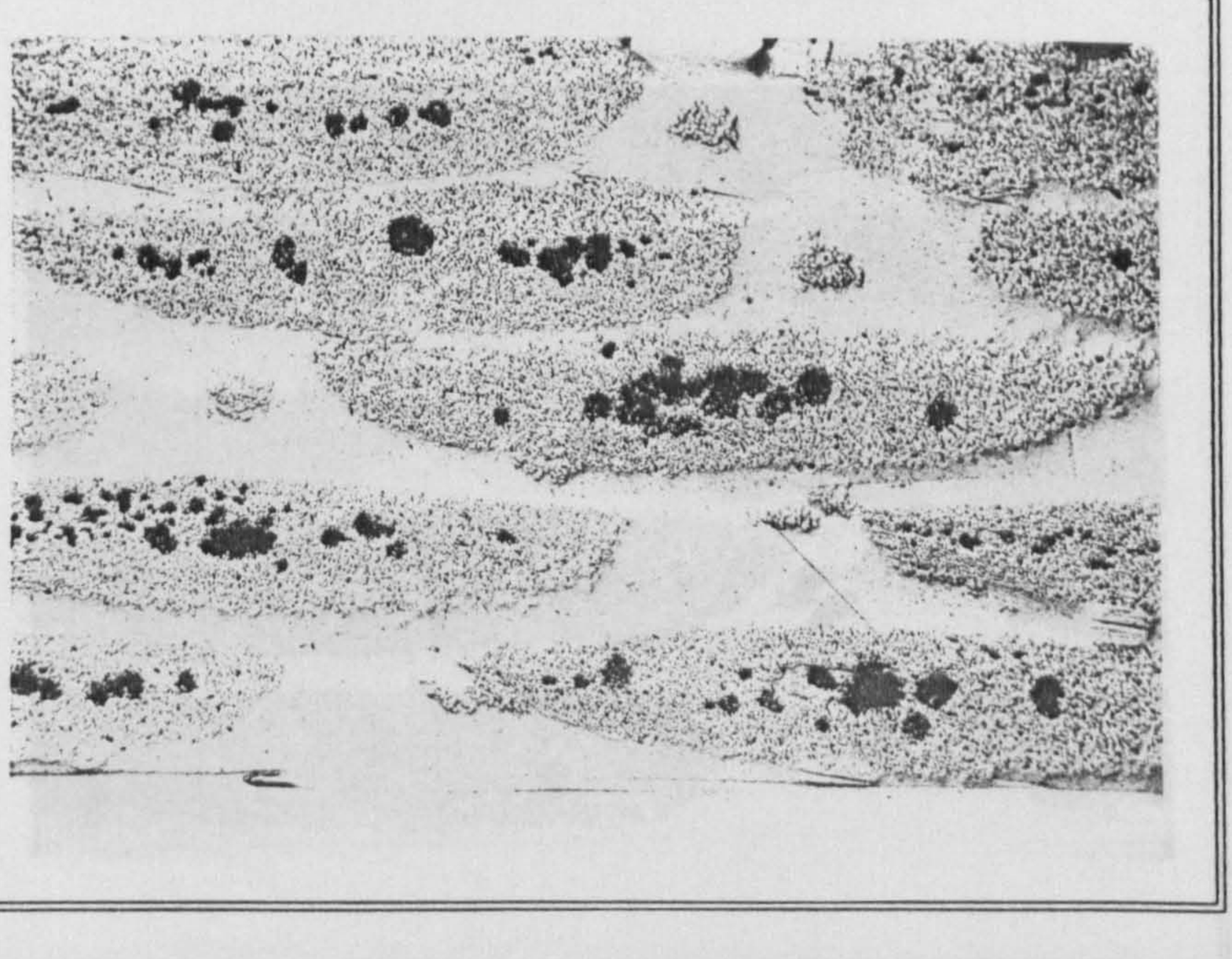

Figure 5.5(d) 0° section from moulding 4286, manufactured using resin pre-heated to 60°C prior to injection (x25).

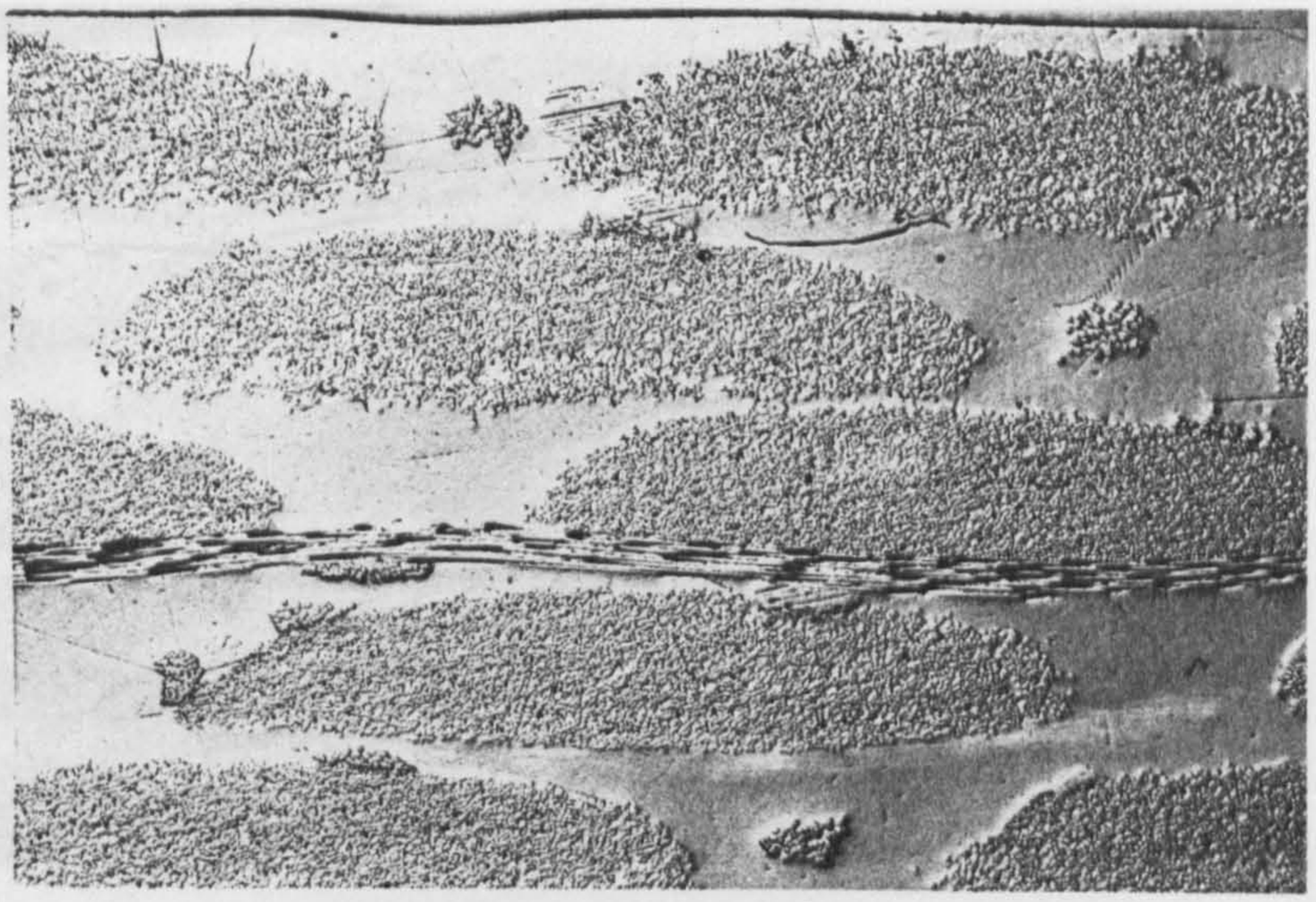

Figure 5.5(e) 0° section from moulding 4287, manufactured using vacuum assistance and resin pre-heated to 60°C prior to injection (x25).

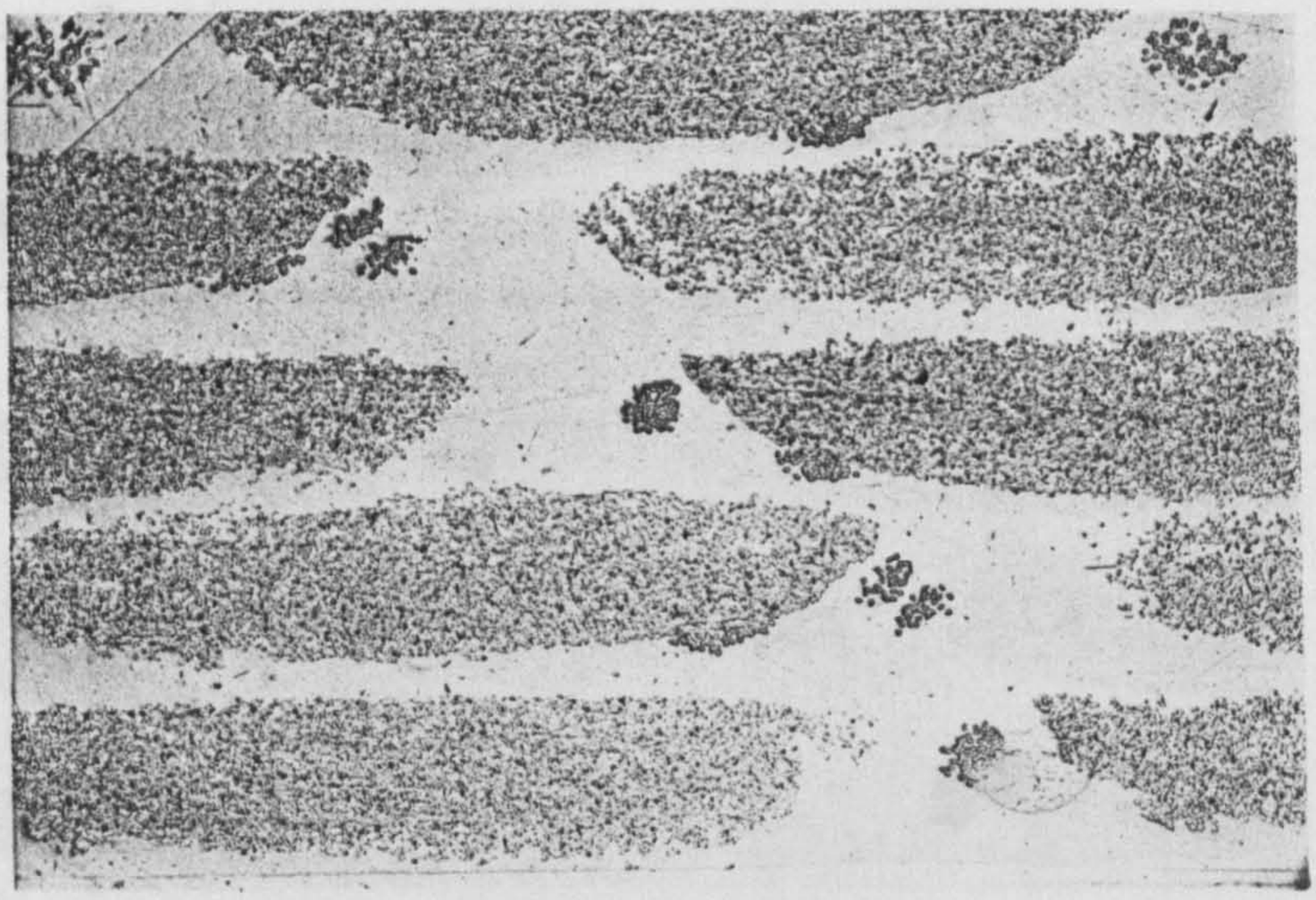

Figure 5.5(f) 0° section from moulding 4288, manufactured using vacuum assistance (x25).

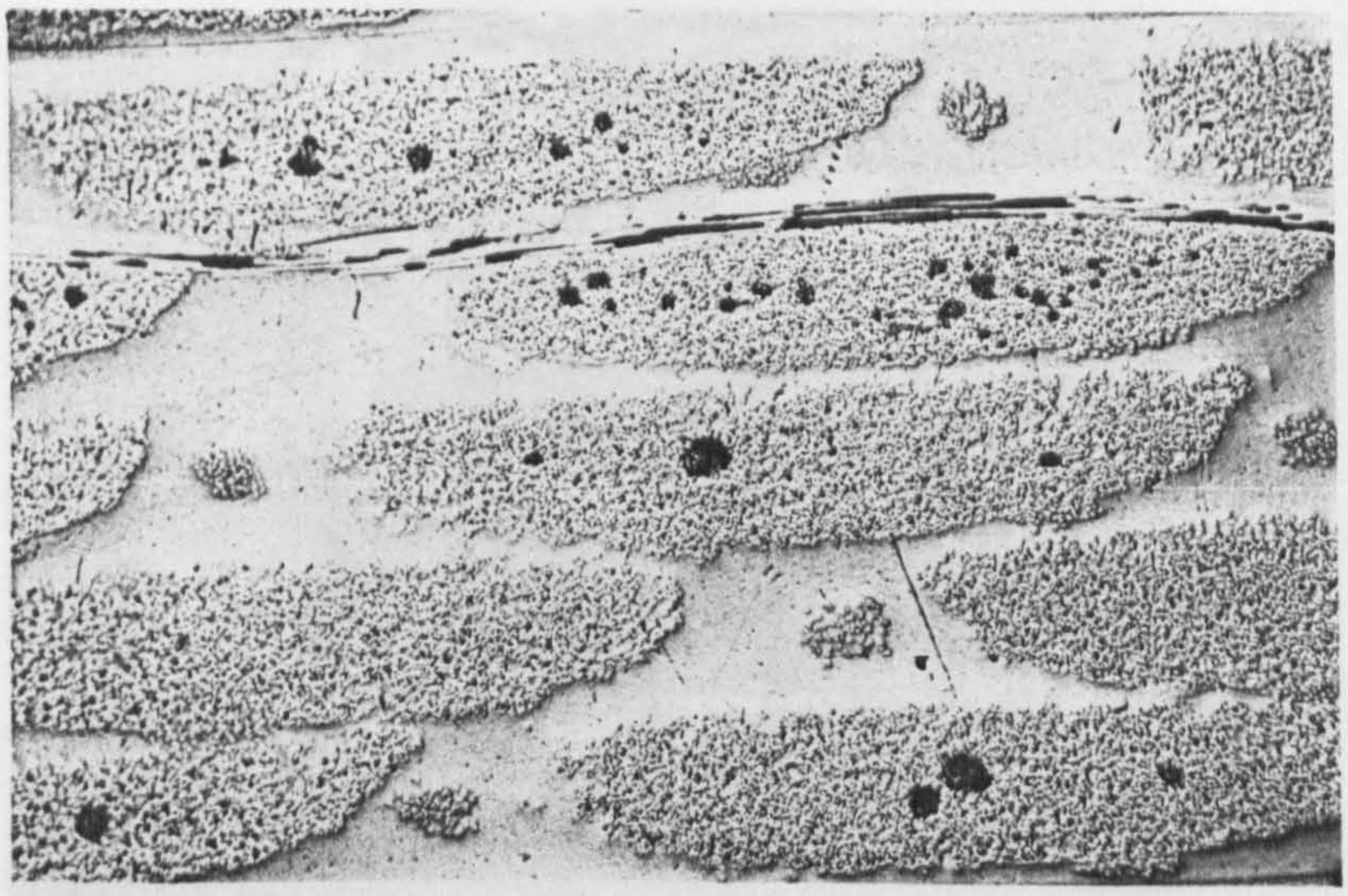

Figure 5.5(g) 0° section from moulding 4289, manufactured using a 1 bar injection pressure (x25).

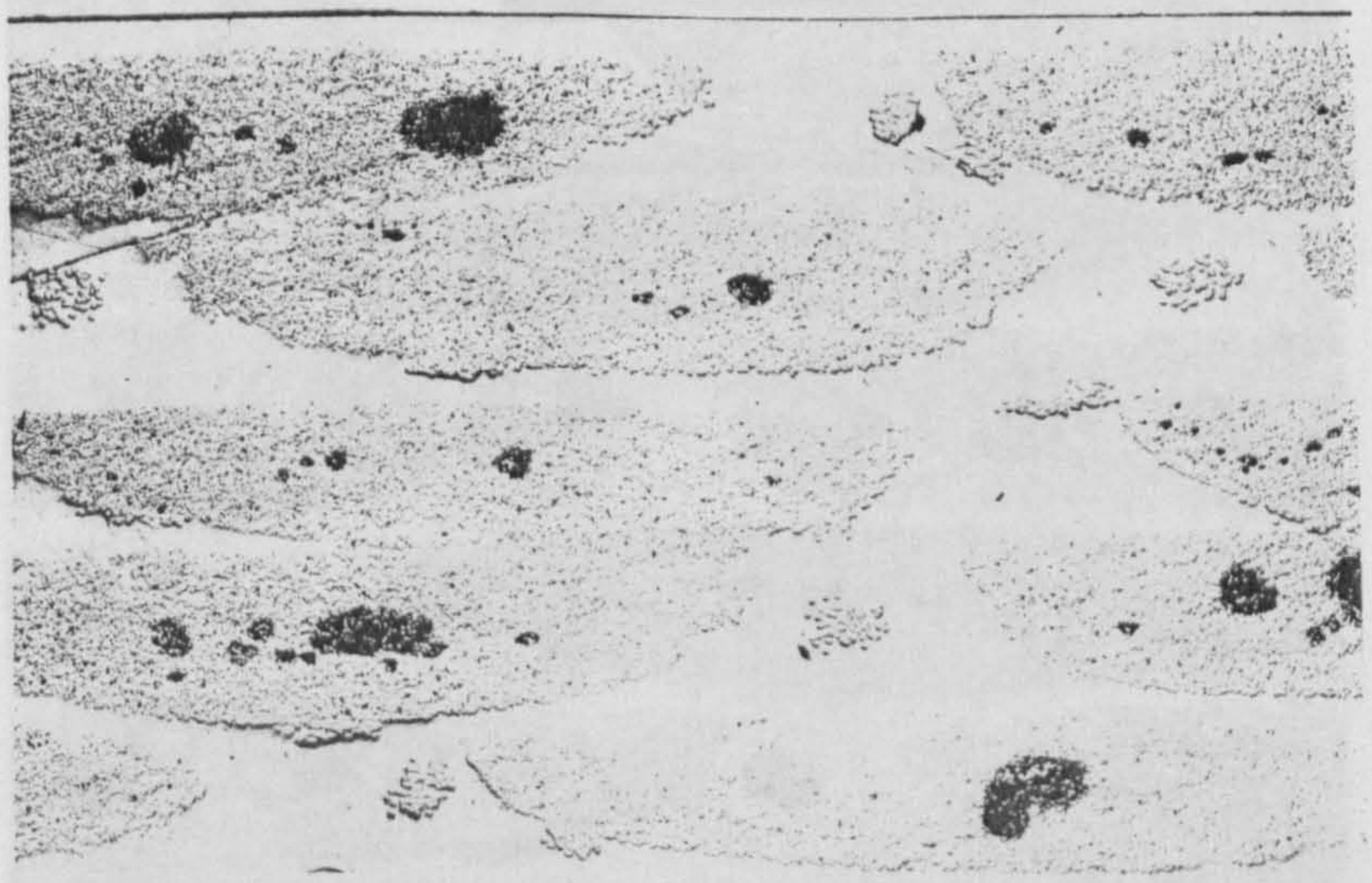

Figure 5.5(h) 0° section from moulding 4290, manufactured using a 3 bar injection pressure (x25).

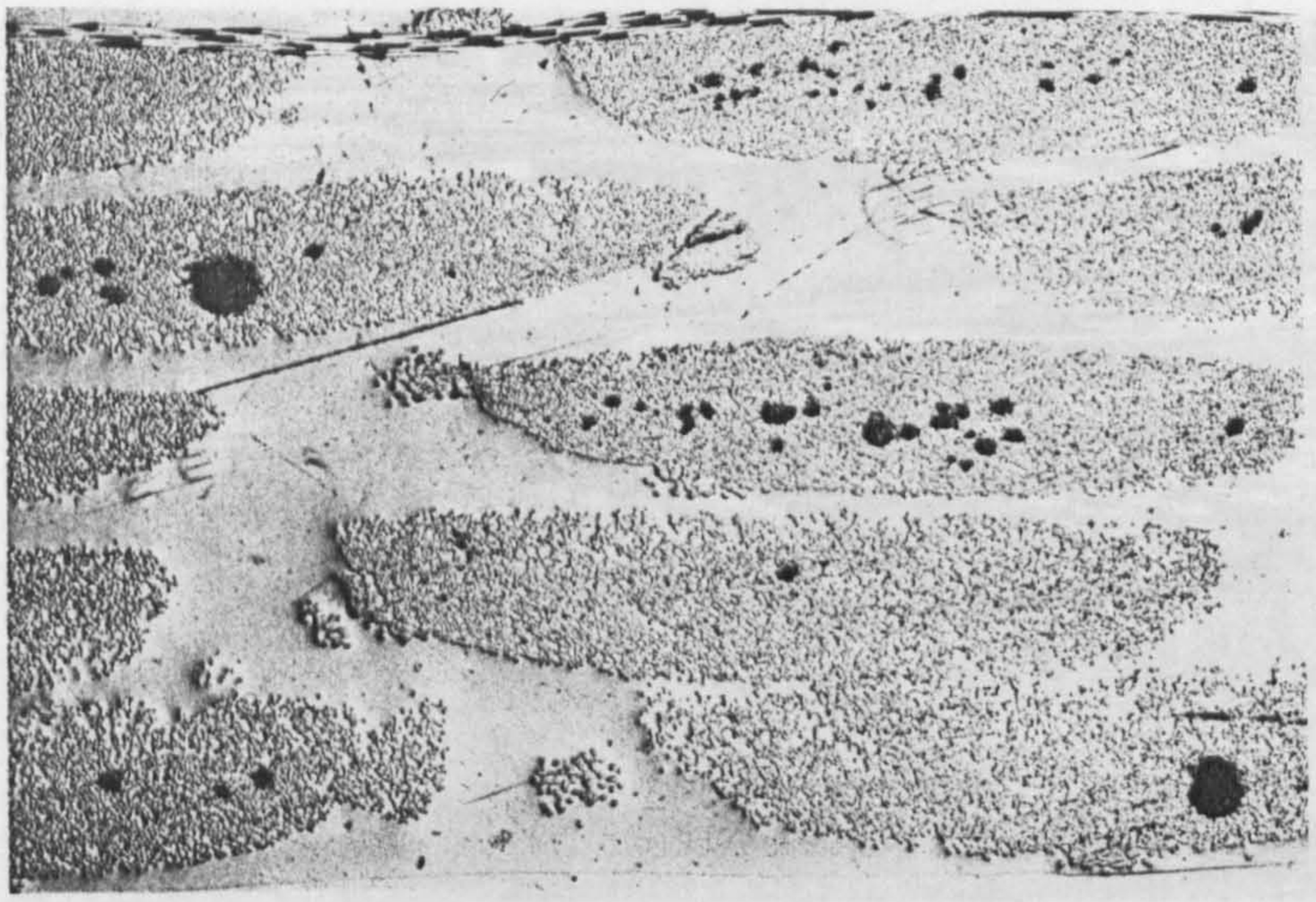

Figure 5.5(i) 0° section from moulding 4291, manufactured using a mould temperature of 80°C (x25).

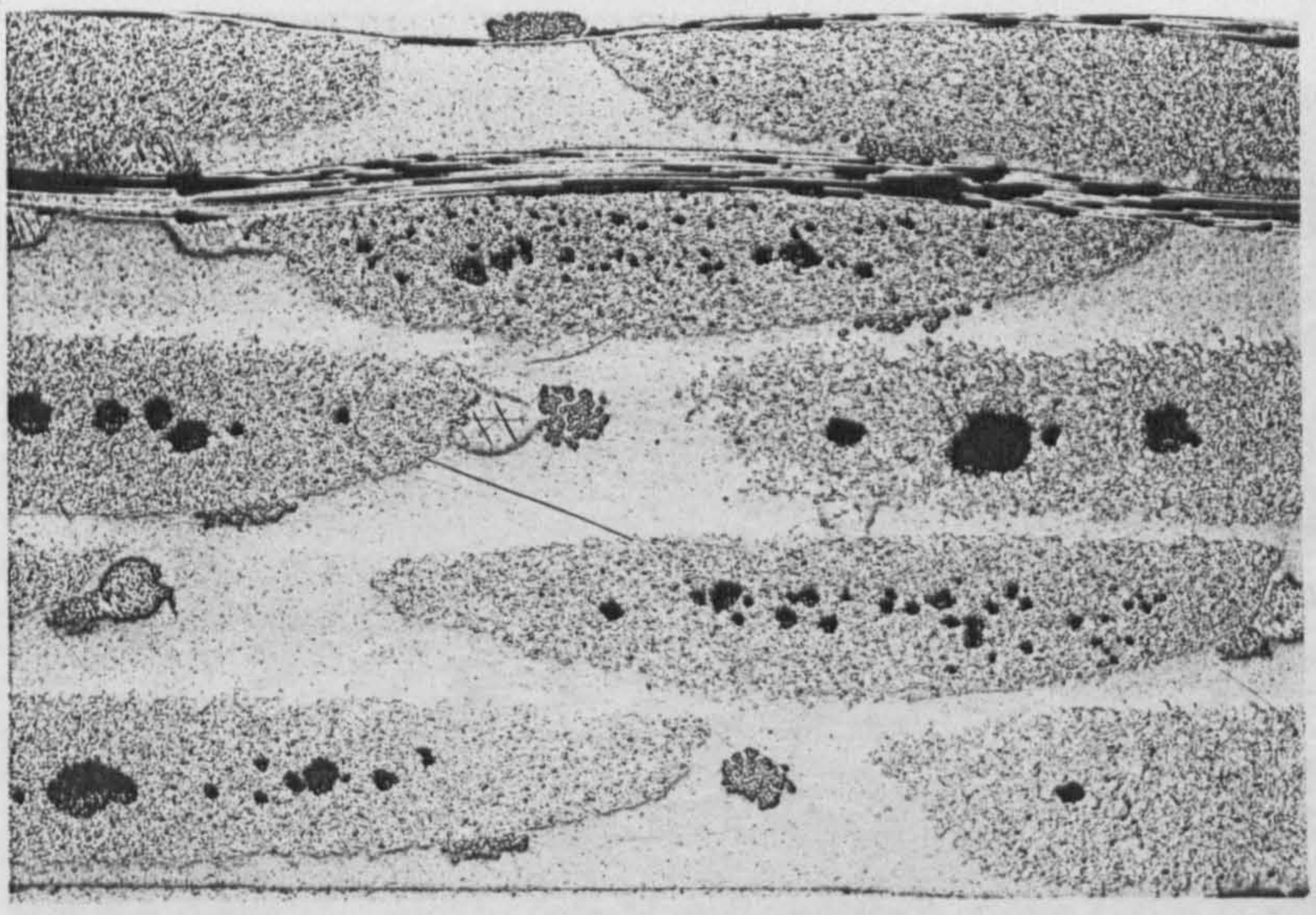

Figure 5.5(j) 0° section from moulding 4292, manufactured using a mould temperature of 100°C (x25).

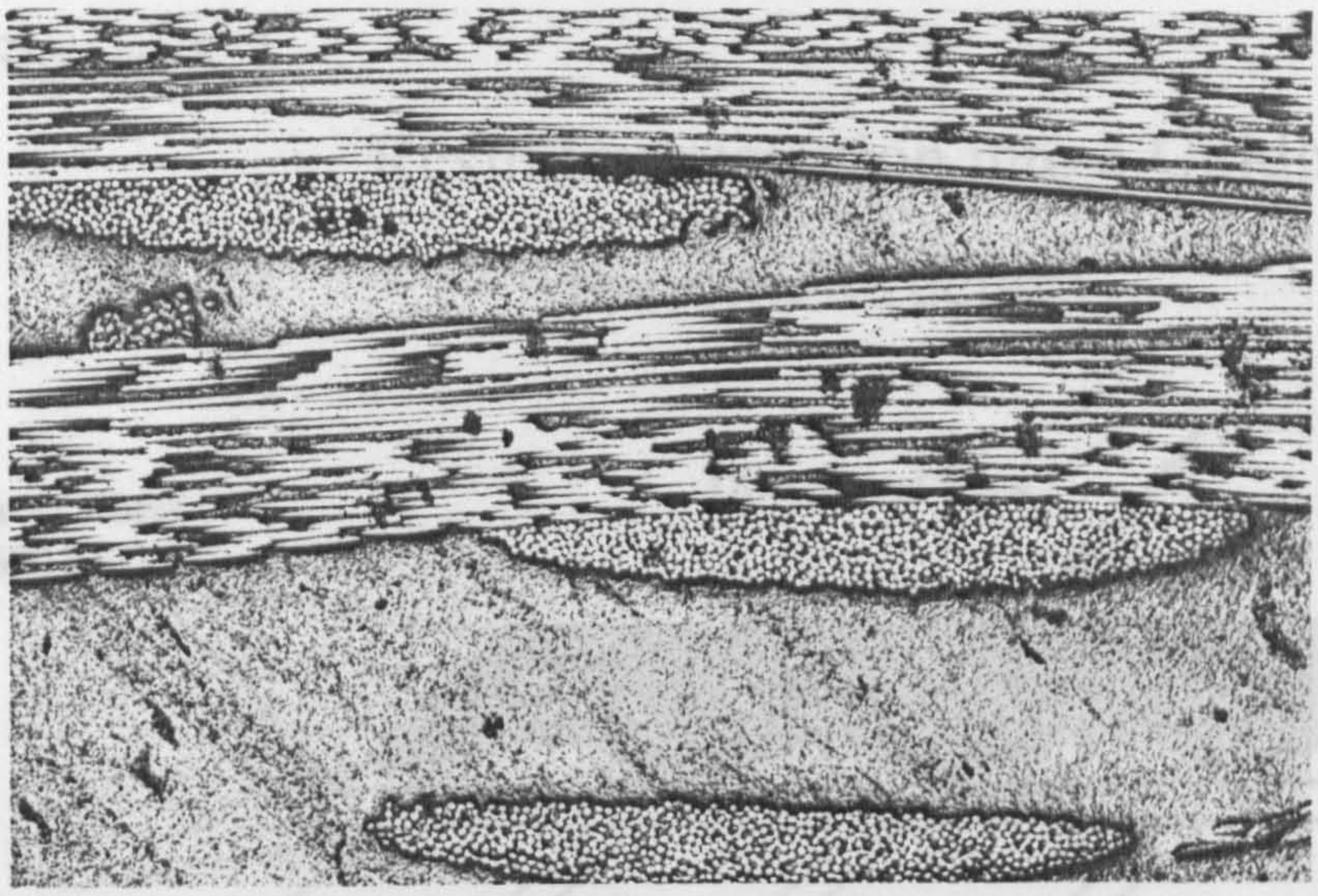

Figure 5.6(a) 90° section from moulding 4285, manufactured using the mid-range process conditions of 2 bar injection pressure, 90° mould temperature and using a 33% glass volume fraction preform (x25).

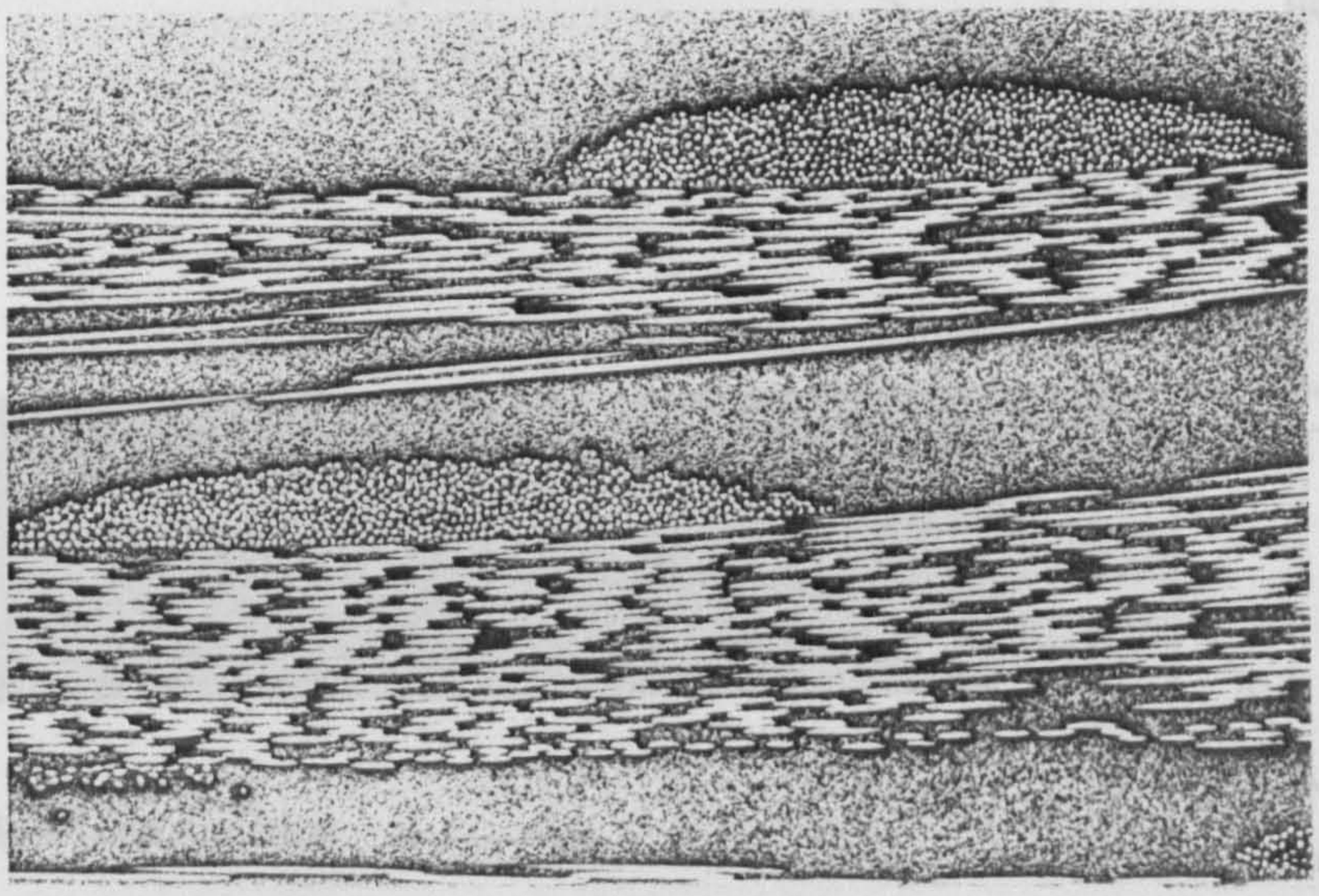

Figure 5.6(b) 90° section from moulding 4288, manufactured using vacuum assistance (x25).

Figure 5.7

Resin Impregnation into a Unidirectioal Preform Structure

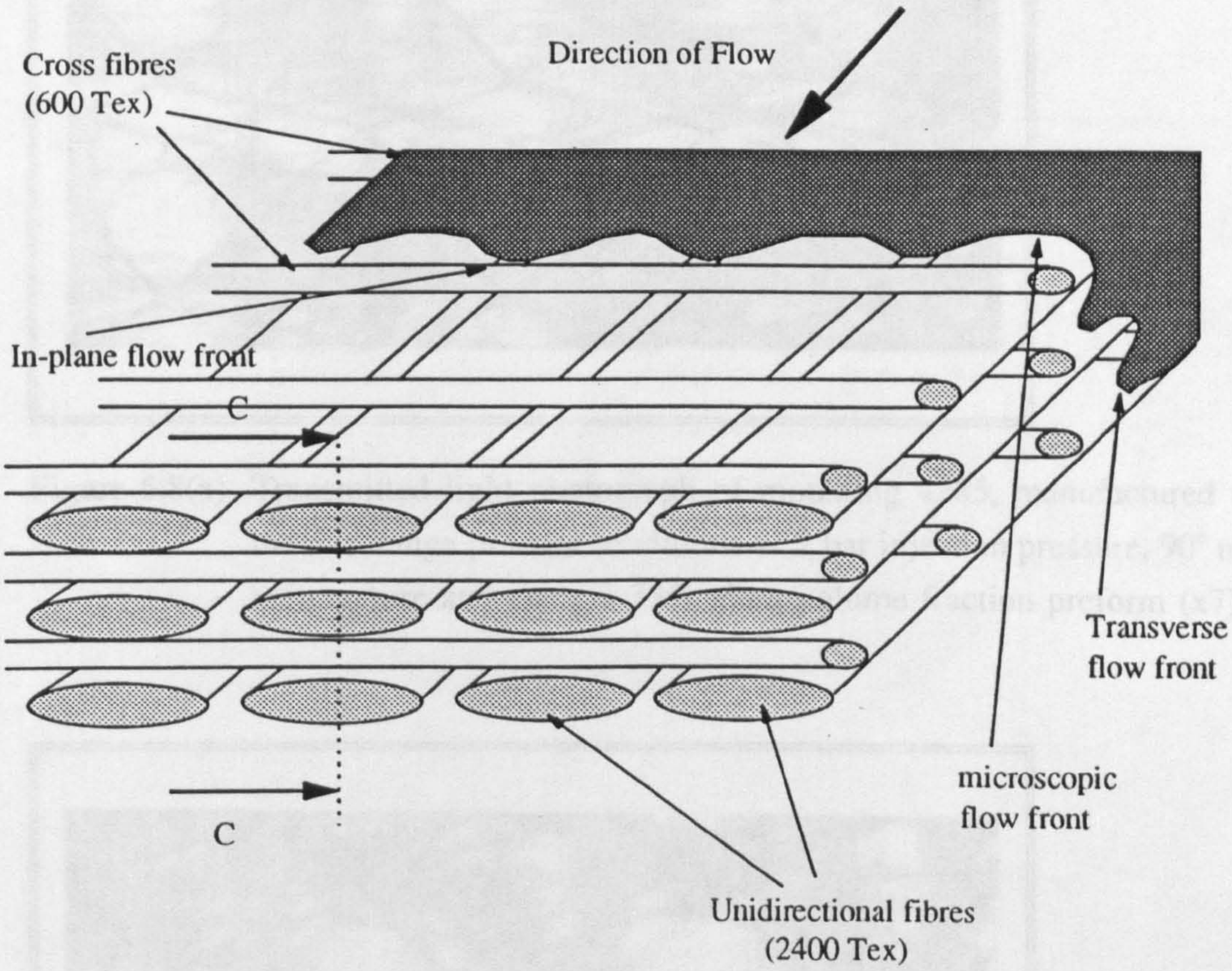

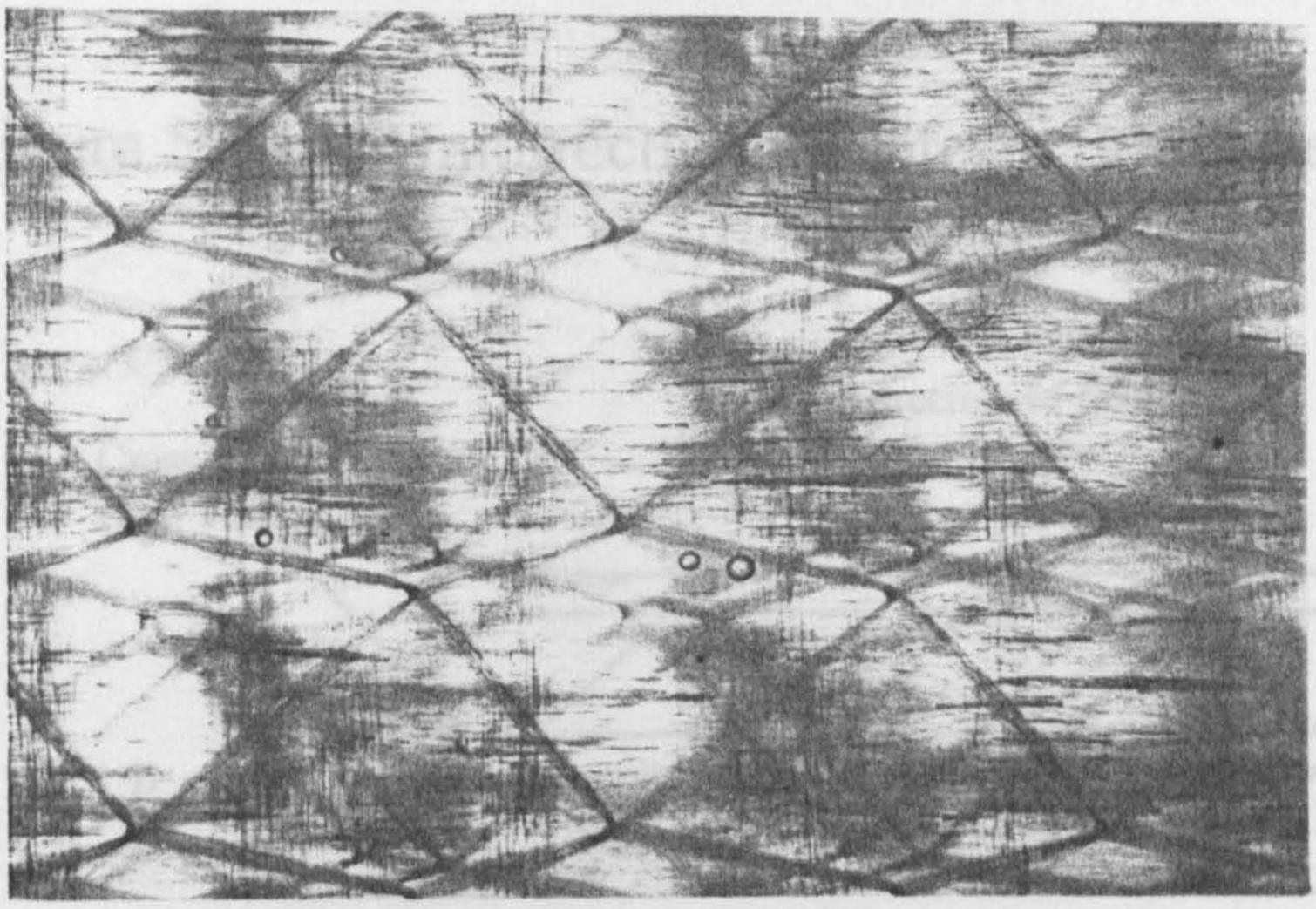

Figure 5.8(a) Transmitted light photograph of moulding 4285, manufactured using the mid-range process conditions of 2 bar injection pressure, 90° mould temperature and using a 33% glass volume fraction preform (x7).

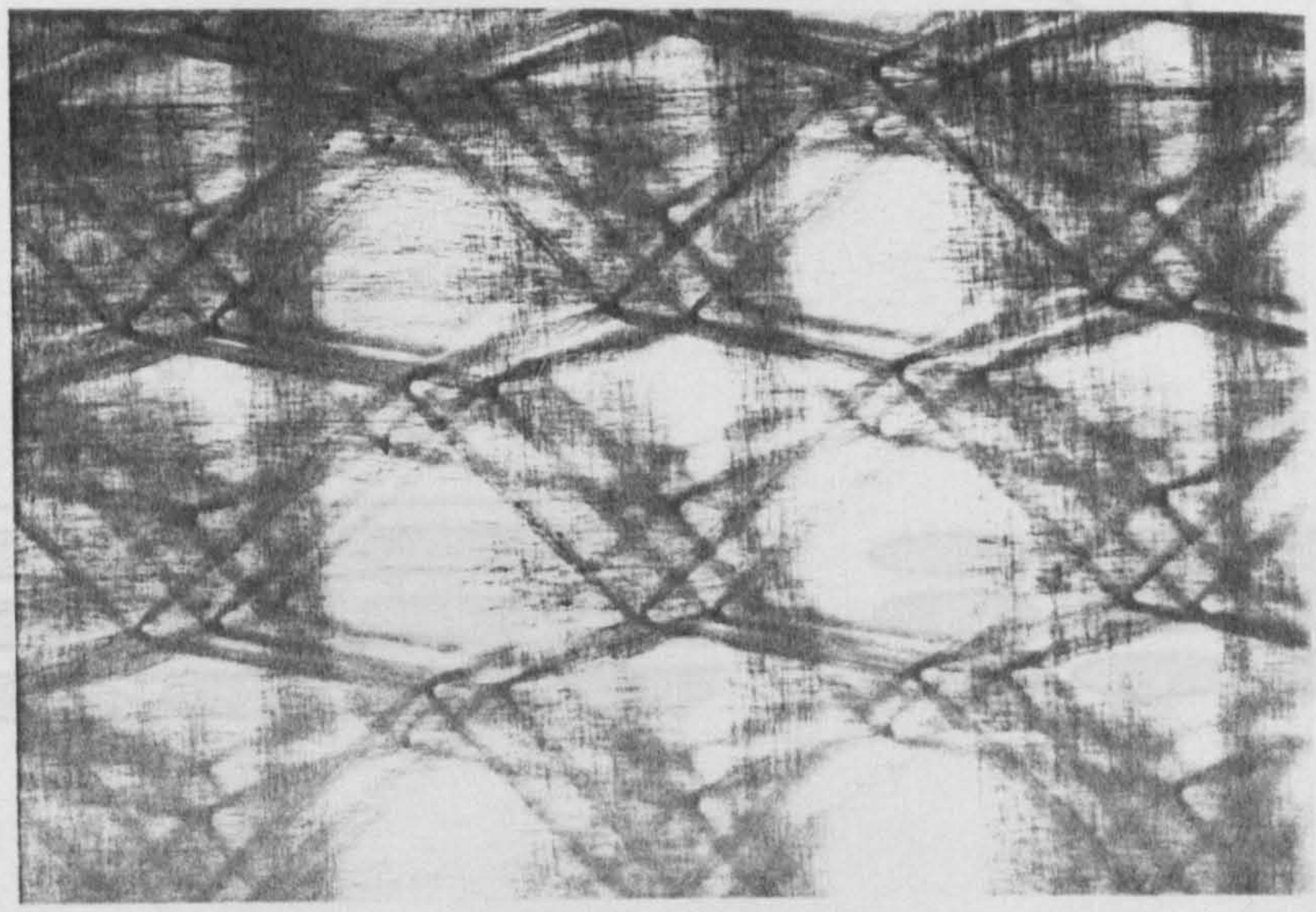

Figure 5.8(b) Transmitted light photograph of moulding 4288, manufactured using vacuum assistance (x7).

Figure 5.9 Unidirectional Preform Structure

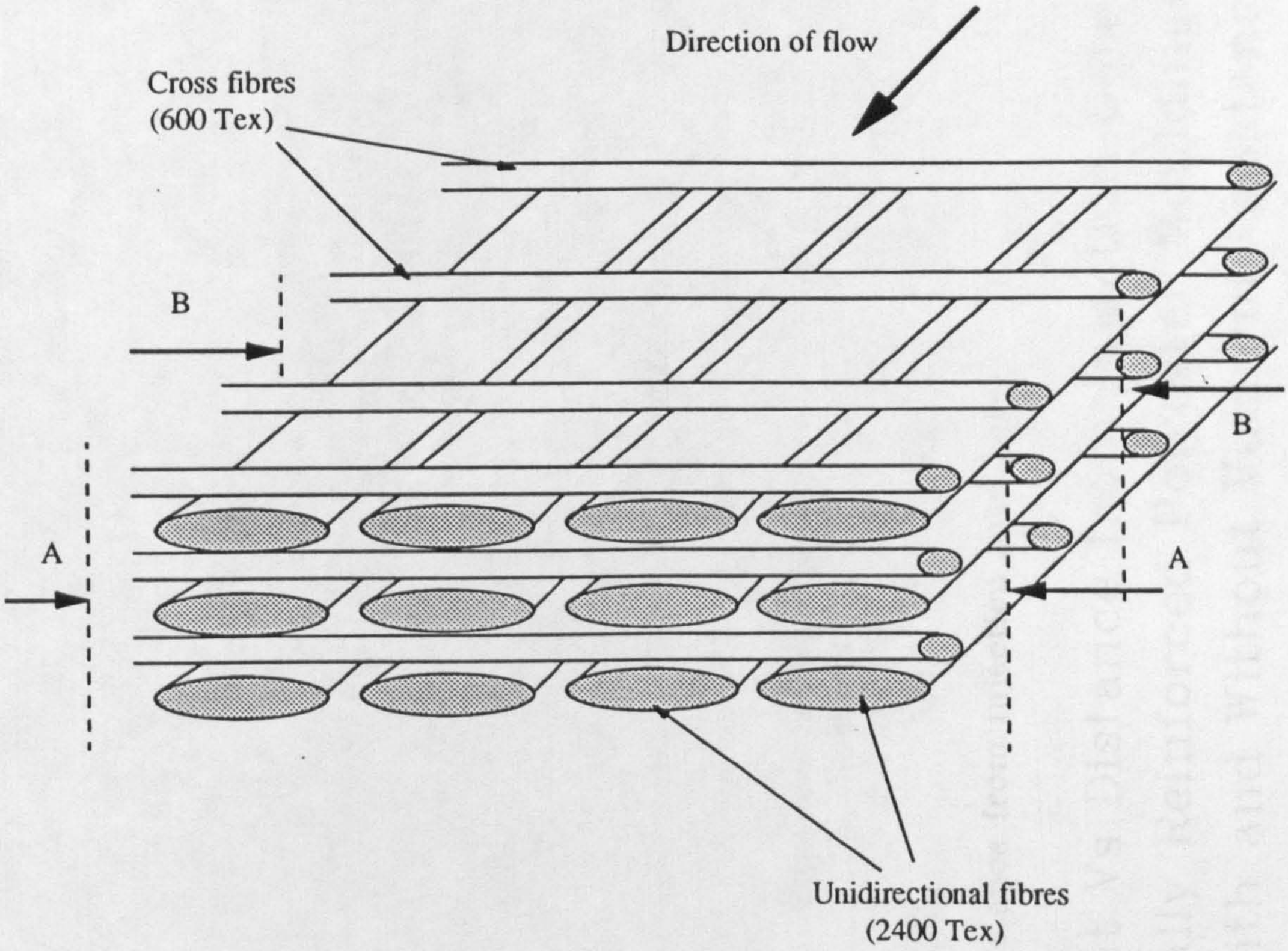

Section AA

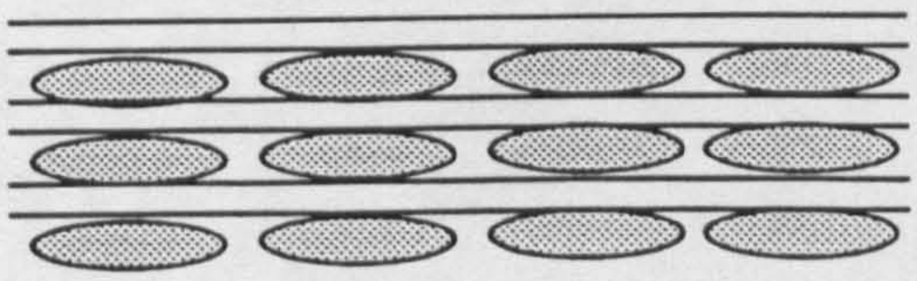

Section BB

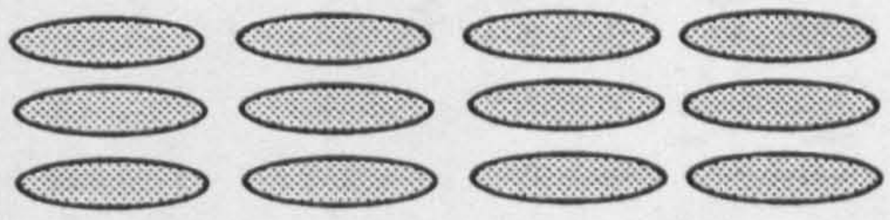

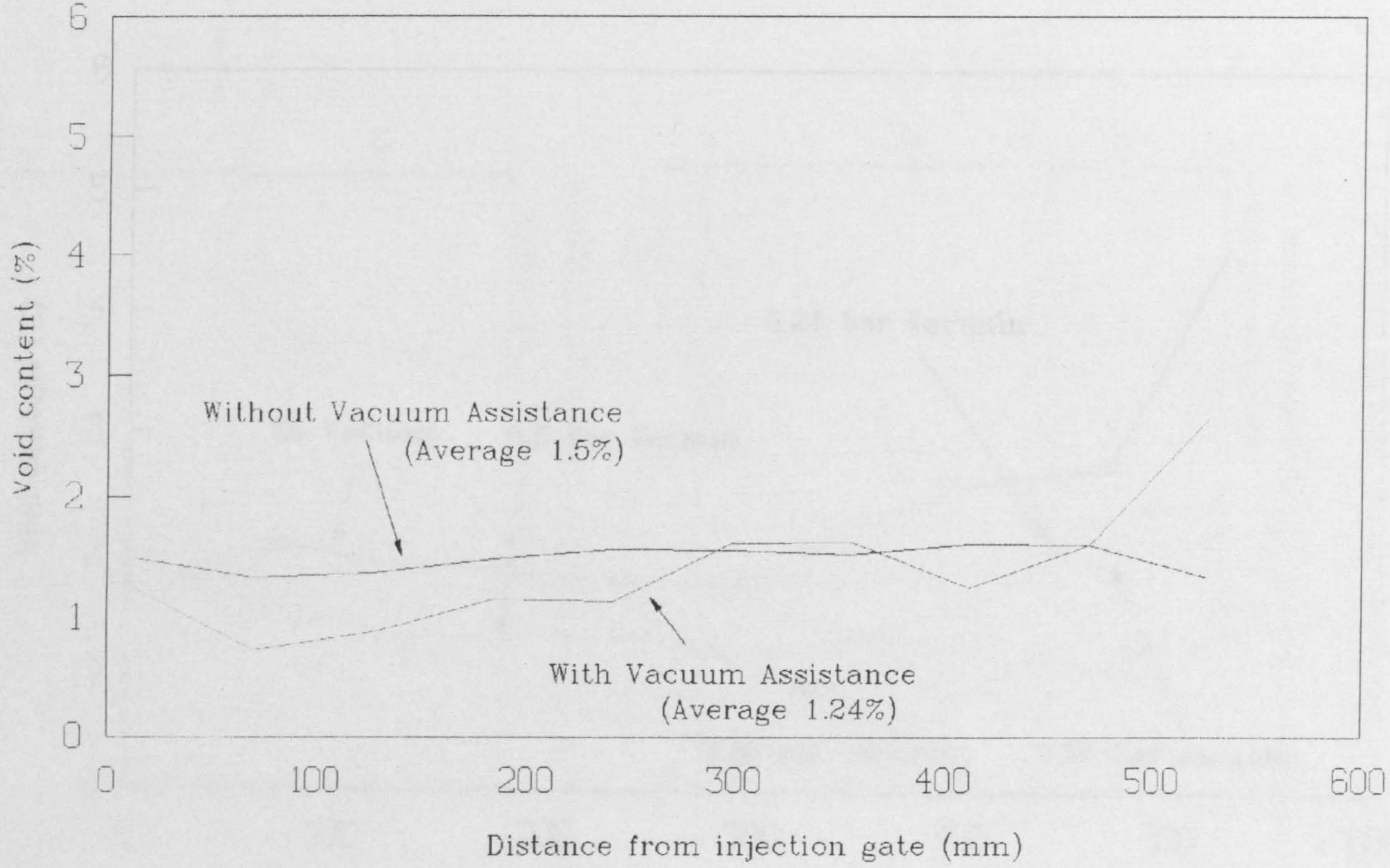

Figure 5.10 Void Content Vs Distance from Injection Gate for Bidirectionally Reinforced Polyester Mouldings Produced With and Without Vacuum Assistance

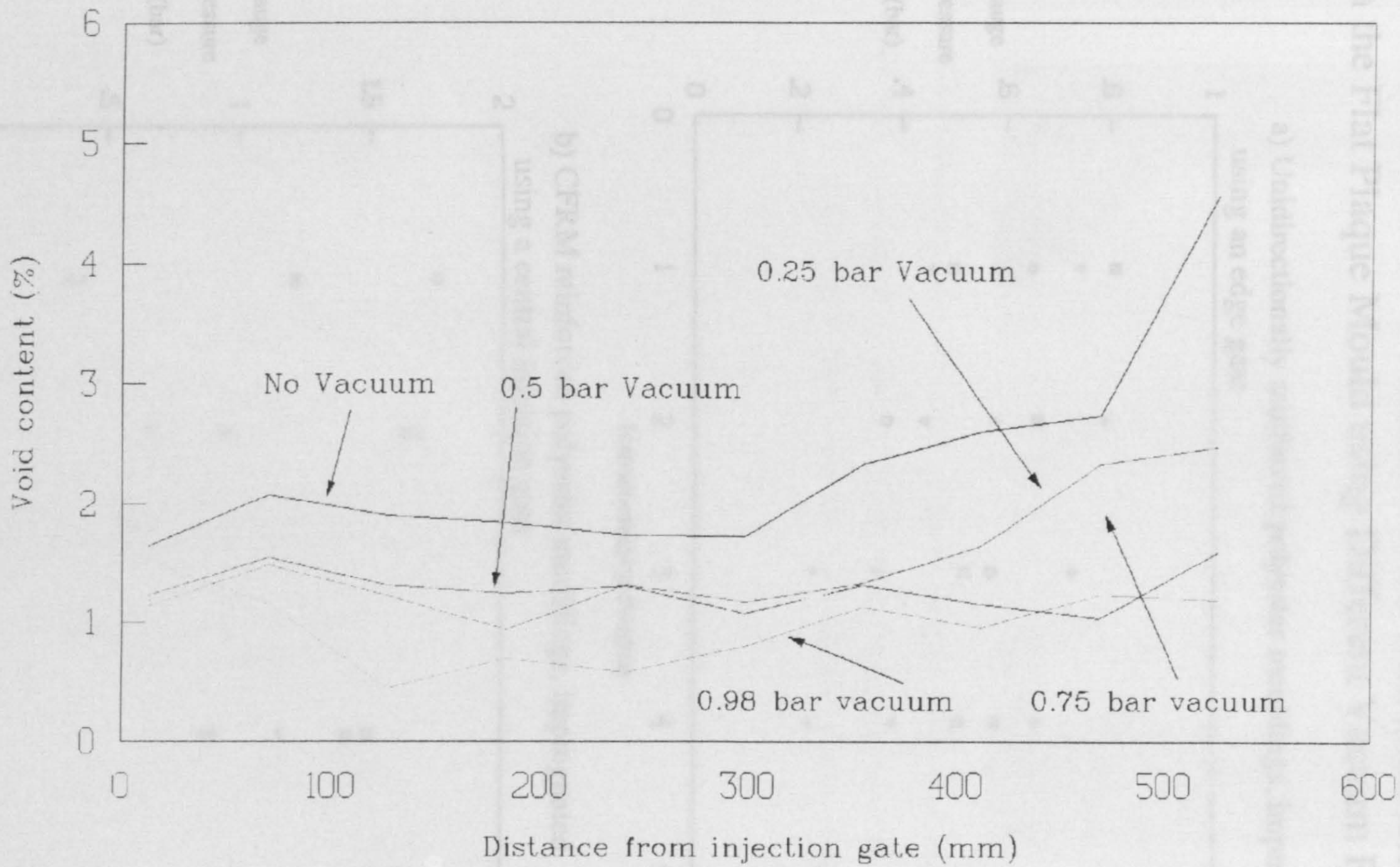

Figure 5.11 Void Content Vs Distance from Injection Gate, for End Gated Unidirectional Reinforced, Polyester Mouldings, with Increasing Amounts of Vacuum Assistance

Figure 5.12

Maximum Exotherm Pressures at the Instrumentation Positions in the Flat Plaque Mould using Different Vacuum Pressures

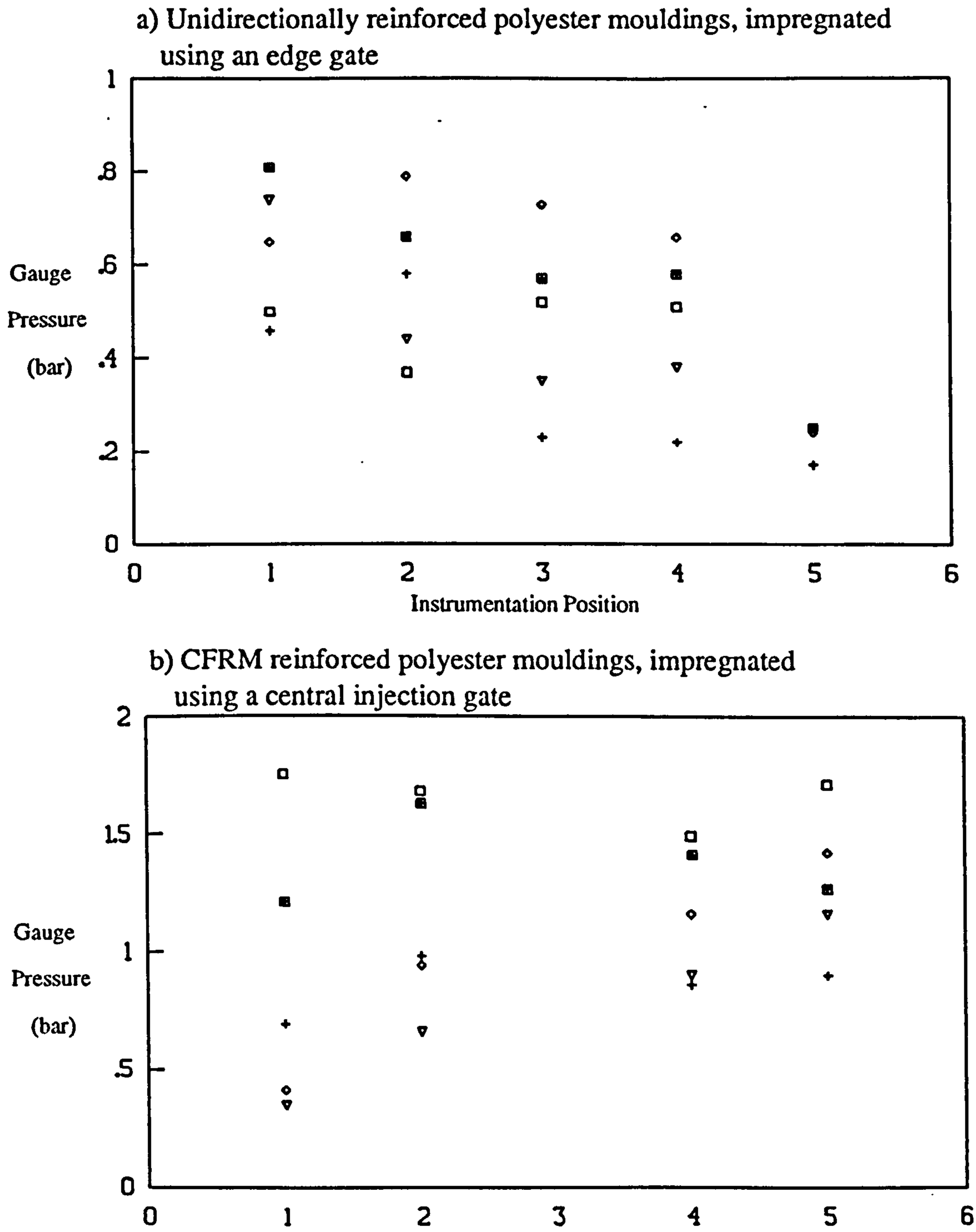

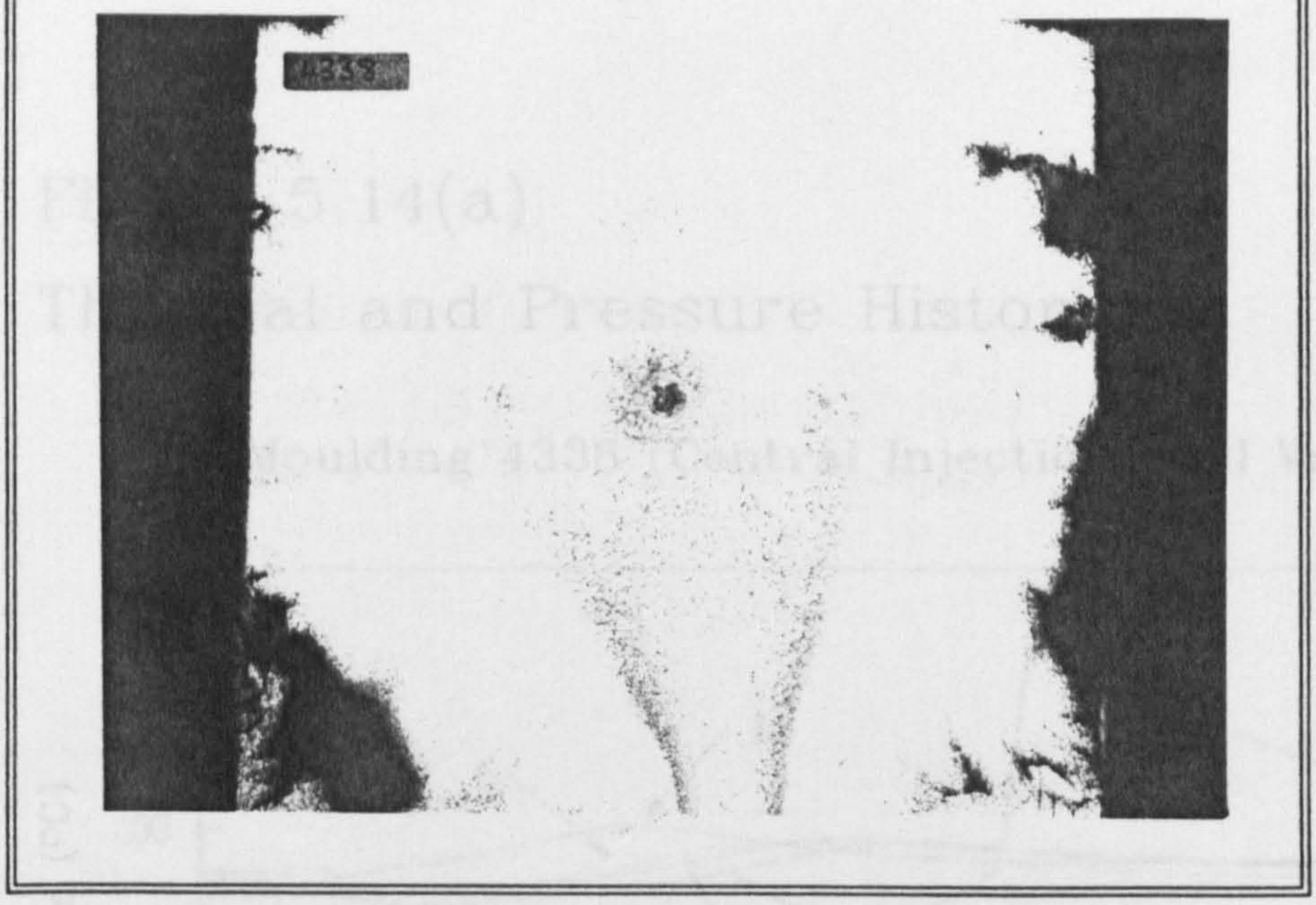

Figure 5.13 A centrally injected CFRM reinforced, polyester moulding, showing high void contents near the injection gate due to styrene boiling.

Figure 5.14(a)

Thermal and Pressure Histories

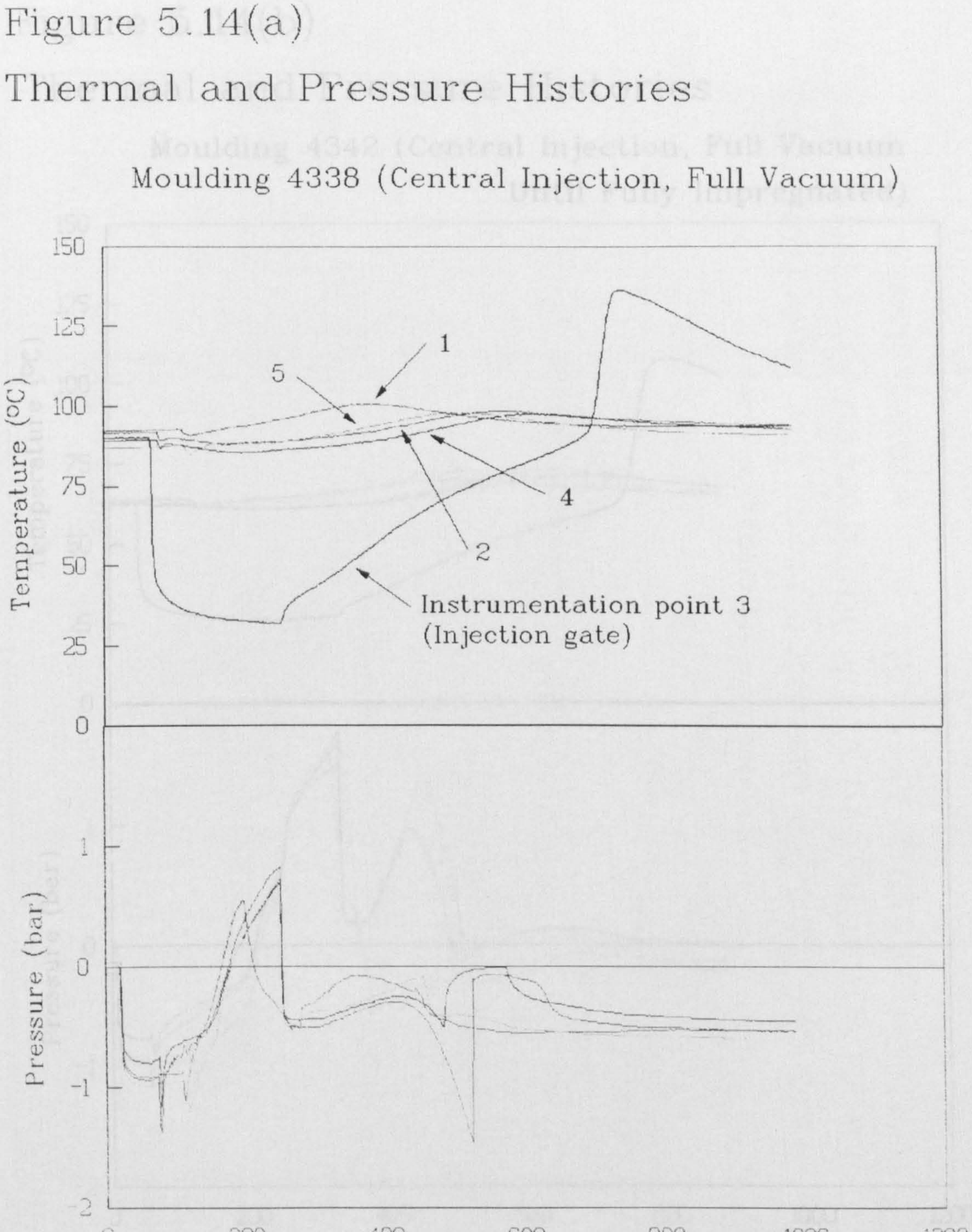

Figure 5.14(b)

Thermal and Pressure Histories

Moulding 4342 (Central Injection, Full Vacuum Until Fully Impregnated)

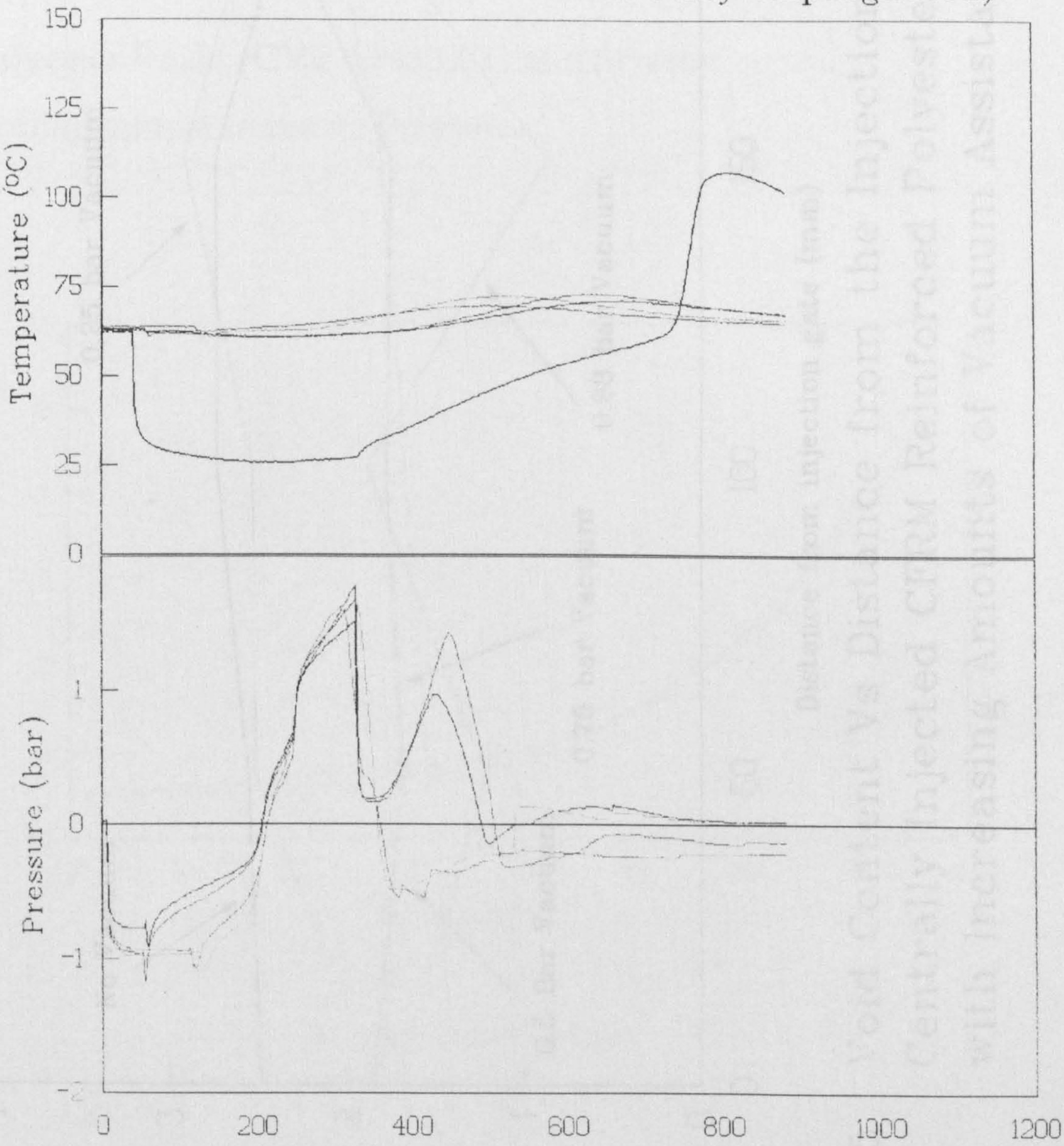

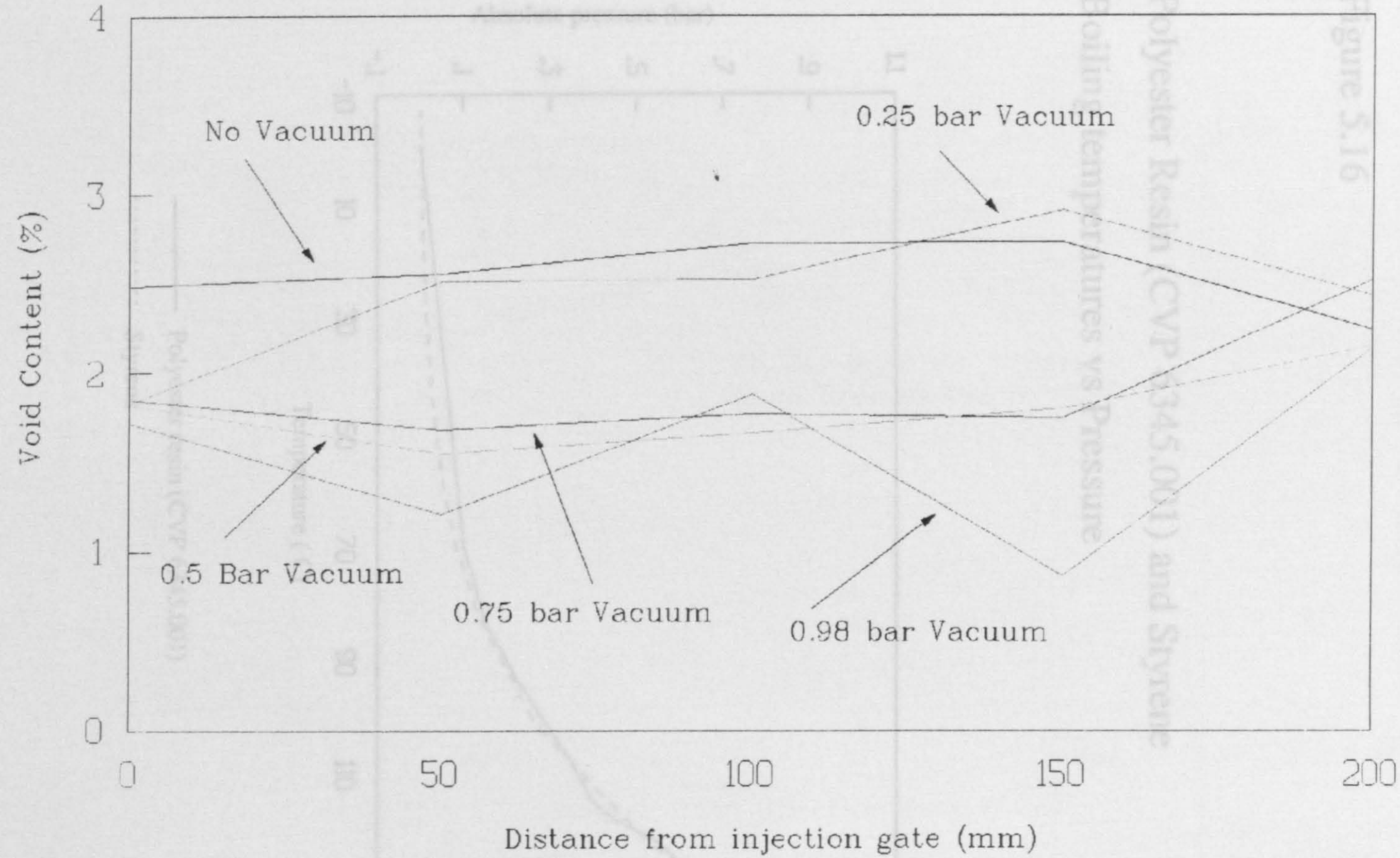

Figure 5.15 Void Content Vs Distance from the Injection gate for Centrally Injected CFRM Reinforced Polyester Mouldings with Increasing Amounts of Vacuum Assistance

Figure 5.16

Polyester Resin (CVP 6345.001) and Styrene

Boiling temperatures vs Pressure

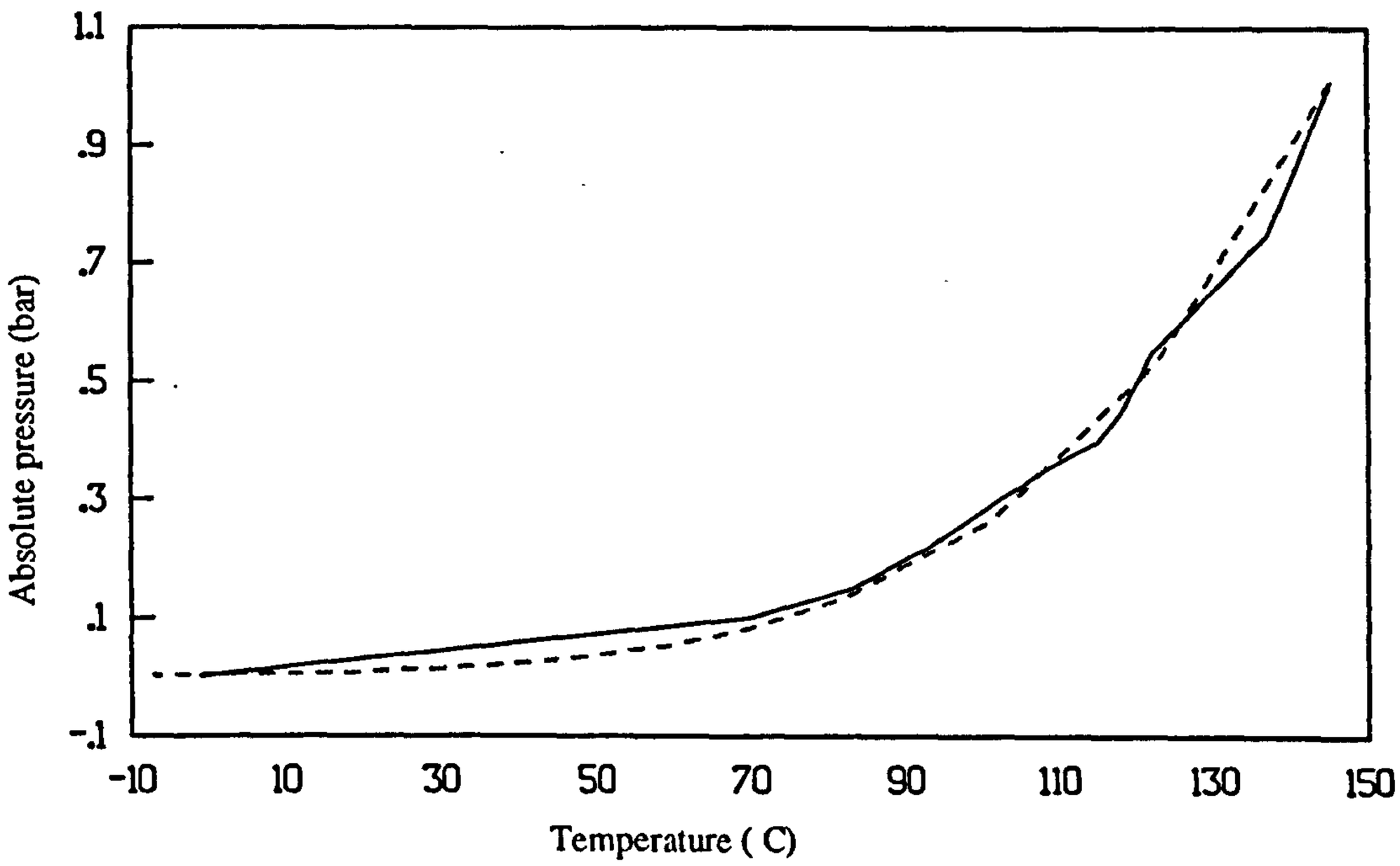

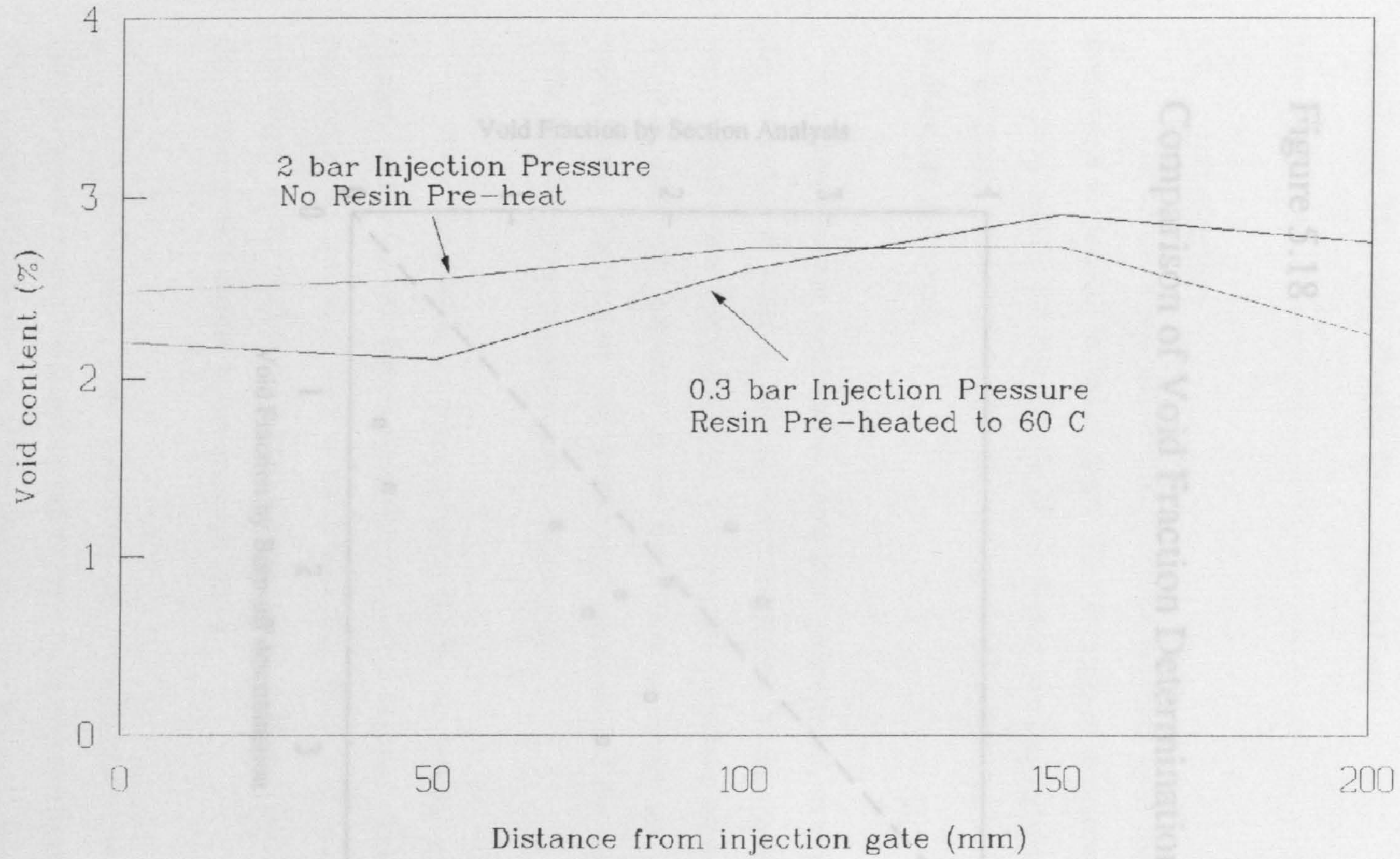

Figure 5.17 Void content Vs Distance from Injection Gate for Centrally Injected CFRM Reinforced, Polyester Mouldings, to Investigate the Effect of Resin Viscosity upon Void Content

Figure 5.18

Comparison of Void Fraction Determination Techniques

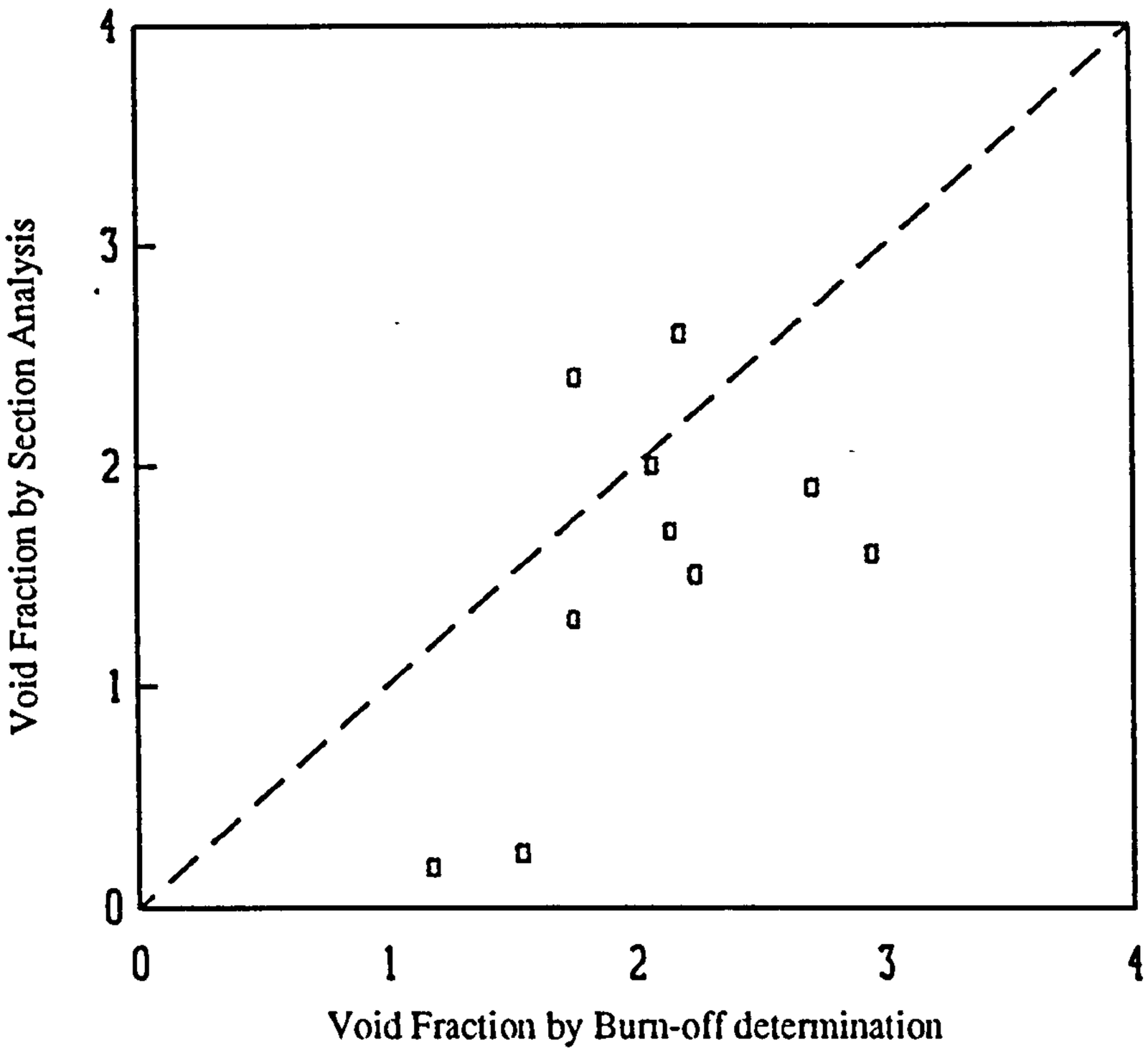

Chapter 6

Voidage During Resin Impregnation

6.1 Introduction

The effect of preform and fibre bundle structure upon the void content within mouldings is assessed in this chapter. The stacking of reinforcements and how their orientation affects the entrapment of air during the impregnation stage of RTM is investigated. Mechanisms for the formation of voids due to the structure of the preform are discussed.

Impregnation experiments, using high viscosity oil, were performed to observe the formation of voids in several reinforcements. These experiments showed that uneven flow fronts due to polyester stitching, thermoplastic binder and fibre direction allowed sufficient distortion of the flow front to entrap air. To understand the mechanisms which cause void entrapment, specimens of the reinforcements used in RTM mouldings were studied using microscopy.

The distribution of thermoplastic binder on fabrics and CRFM has been studied, as has the size distribution within the fibre bundles. The presence of the size and binder in laminates after a short moulding cycle (10 minutes) has also been examined. These studies have been undertaken to indicate whether the resin dissolves the binder or size before polymerisation occurs.

To understand void formation in multilayered preforms, permeability experiments were used to generate values for a finite element impregnation simulation. This simulation was used to predict the flow front shape during the impregnation of multilayered preforms. Several mouldings were produced to assess the effect of stacking low and high permeability reinforcements upon void formation, and to determine whether the flow front shape (predicted by the FE model) within the stack

affected the voidage within the moulding.

6.2 Flow Impregnation studies

Oil impregnation into the reinforcement which was described in section 3.4 was studied to assess the causes of air entrapment. This was undertaken using the apparatus described in section 3.7. The experiments were carried out to promote rectilinear flow in the plane of the fabric with a supply pressure of 0.1 bar gauge. The following reinforcements were studied:

i) Continuous filament random mat (Unifilo U750-450)

ii) Unidirectional mat (Tech Textiles ELPb-567 Non Crimp Fabric)

iii) Bidirectional ±45° mat (Tech Textiles EBX 936)

iv) Single rovings of Unidirectional fabric

CFRM (Unifilo U750-450)

Whilst penetrating a CFRM reinforcement with oil, the mechanical entrapment of air was observed in a series of photographs taken at 2 second intervals. The local flow front was seen to impregnate the mat unevenly, as regions of higher porosity, allowed the oil to travel quicker, entrapping air pockets in the regions which were bypassed (Figure 6.1).

Unidirectional material (Tech Textile ELPb-567)

Single strand

A single strand from 0° fabric was impregnated. The flow front in the tow was uneven and at points where the thermoplastic binder was in contact with the mould surface, liquid was prevented from flowing along the fibres causing voids to form (Figure 6.2).

0° fabric

A unidirectional non crimp fabric was impregnated with the side containing thermoplastic binder facing the glass top. The flow front progressed unevenly and could be seen to wick and follow the stitching. The distortion of the flow due to the

polyester stitching was seen to trap air within the preform (Figure 6.3).

The unidirectional fabric was impregnated with the cross stitching side facing the glass top. The oil travelled along the spaces between the fibre bundles and dry patches were formed (Figure 6.4). During the impregnation, small bubbles were seen to wash through the fibre becoming trapped in areas of high fibre volume fraction. At the intersections of the 0° fibres and the 90° fibres voids were formed as the resin flow front found a path between the fibre bundles (Figure 6.5).

Bidirectional material (EBX-936)

The impregnation of the ±45° fabric exhibited a local flow front at the surface which travelled preferentially in the direction of the fibres, but as a ±45° preform was being used the overall flow front was rectilinear (the lower layer filled at 90° to the upper layer). Small air bubbles were entrapped between the fibres which then wash behind the immediate flow front.

These impregnation studies have revealed the manner in which resin is able to impregnate a selection of fabrics used in RTM processing. The flow into the fibres was dictated by the orientation of the fabric, or more specifically the gaps between the fibre bundles. Polyester stitching or 90° rovings block the path of the advancing flow front, showing that the flow will find the easiest route past the obstruction and in many cases bypass the area, creating voids behind the flow front. The binder on the surface of 0° fabric also distorts the local flow front suggesting that voids may be created. The impregnation pressures, and thus the resin flow front speeds were much lower than the values used in RTM processing, but the oil has shown no tendency to wick along the fibre bundles due to capillary flow. The mechanisms of void formation shown by these experiments are thought to be valid although the speed at which they occur will be faster in practical moulding situations.

6.3 Thermoplastic Binder

The globules of thermoplastic binder present in many of the reinforcements used in RTM are thought to distort the resin flow front such that air entrapment occurs

(section 4.3 and 6.2). The dry reinforcements used during these studies were examined to determine how the structure of this binder is likely to affect void formation during impregnation.

Oil has been used to confirm that globules of binder allow the entrapment of air during impregnation trials. If resin was able to dissolve the thermoplastic binder during impregnation, this entrapment may not occur. Studies were undertaken to determine whether the thermoplastic binder is present in the composite after moulding and the dissolution times of binder in resin.

Mat structure

CFRM

The binder in CFRM mats is applied randomly to the fibres in a powder form during the fabrication of the mat to retain structure. Figure 6.6 shows thermoplastic binder coating and joining adjacent strands. The binder congeals on the strands and is able to penetrate into the bundle structure during its liquid stage, either during the manufacturing phase or during preforming (Figure 6.7). The amount of binder applied to the mat is dependant on the grade of reinforcement, which varies between 4%-10%.

NCF

Several of the NCF fabrics used in these studies have thermoplastic binder applied to one surface after manufacture. The majority of the binder adheres to the surface of the fabric in globule form, both on the glass rovings and the polyester stitch (Figure 6.8). During preforming the thermoplastic softens into a liquid and is able to penetrate the outer surface of the rovings.

Binder dissolving into the resin system during injection

Revill[19] identified two phases in CFRM polyester mouldings, which were assumed to be thermosetting resin and thermoplastic binder existing as a separate materials. To examine this assumption and to establish whether the binder dissolves into the resin system during an approximate 2-3 minute wet out period, several polyester, CFRM mouldings were sectioned and analysed.

These composite sections show three phases of material evident in the mouldings. The reinforcement fibres are clearly visible in the micrographs and two phases appear in the matrix. One of the phases is only present surrounding, or close to the fibre bundles, suggesting that it is the thermoplastic binder which was present in the original preform. To prove this assumption three methods were used to test the existence of the two phases.

i) Microhardness testing

Microhardness testing was carried out on three specimens of undershield mouldings. The hardness of the two phases in question was determined using a Vickers microhardness testing machine, in each case three values were taken for each area studied (Figure 6.9). The results of this testing are shown in table 6.1. A difference in hardness between the two phases occurred in each moulding, although the values varied between mouldings.

ii) Using an Electron Scanning Microscope

X-ray microanalysis using an scanning electron microscope was used to determine the elements present on the surface of the specimens. A sample of a calcium carbonate filled polyester, CFRM reinforced moulding was studied. Calcium carbonate filler was used in the resin system which might be used as a tracer. The two areas studied are shown in Figure 6.10. The elemental analysis graphs corresponding to these two areas are shown in Figures 6.11a and 6.11b. Area 1, the sample area which was considered to be the thermoplastic showed only an insignificant trace of calcium, which was probably due to debris from polishing. Area 2, the sample area which was considered to be polyester filled resin, showed a high level of calcium.

iii) Chemical etching

A specimen of moulding containing polyester resin with filler was placed in a hydrochloric acidic solution, to etch the calcium carbonate in preference to the surrounding areas (Figure 6.12). The sections showed pitting

in the areas of calcium carbonate removal. The areas surrounding the fibres which were assumed to be thermoplastic binder showed no signs of removal.

The results of these tests supported the existence of two resin phases in the mouldings studied.

Binder Solubility Tests

Tests were conducted by Bulmer[72] under ISO 2558[71] to determine the time taken for the dissolution of thermoplastic binder in a fluid. Two fluids were used in these tests, styrene and CVP 6345.001 polyester resin. A sample of reinforcement which was held together by thermoplastic binder was suspended in a container of liquid. The sample has a weight of 100g attached to its lower edge, 50mm above the bottom of the container. Failure of a specimen is defined as the time when the mat has stretched sufficiently to allow the lower weight to reach the bottom on the container. The results of the experiments carried out on Unifilo U750-450 are shown in Figure 6.13.

The U750-450 mat took over three hours to fail when the sample was placed in polyester resin at 20°C, and is not shown in the graph. The results in Figure 6.13 show that for a preformed mat in a resin solution at 60°C, the binder dissolves sufficiently to allow the mat to fail after 90 seconds. By this time in the RTM cycles in consideration for high volume production, the preform would be fully impregnated and the matrix would have begun to polymerise.

6.4 Fibre structure, Film formers and Size

The study of microvoids in section 4.3 indicated rough surfaces inside the voids between fibres, unlike the macrovoids between bundles where the surface was smooth. This rough surface was thought to be size deposition between fibres which is believed to restrict resin impregnation, creating voids.

Size structure

Size is applied on to fibres to protect the filaments from abrasion as has been

described in section 2.4. It is applied to the fibre as an aqueous emulsion, once the fibre has been drawn. The liquid is dried leaving a film coating. The solution collects both on the surface of the fibres and between fibres, leaving a dry size meniscus. This holds the fibres together in a tape like structure. Dry reinforcements have been examined to assess the magnitude of this size deposition and the structure of the fibre bundles. The meniscus is usually broken after the fibres have been mounted and cleaned prior to their study in the SEM, but the characteristic fracture line can usually be seen along many of the fibres (Figure 6.14). Fibres were analysed using X-ray analysis and the results for fibre and what is assumed to be size are shown in Figure 6.15a and 6.15b. The elemental analysis shows much higher levels of silicon in 8.9b which is the area of the fibre with a lower deposition of size, showing that this is an area of deposition and not part of the glass fibre.

CFRM

Study of fibres from CFRM have shown the size deposition varies between samples. The meniscus and size deposition can be limited, as shown in Figure 6.16, or extensive covering the whole fibre bundle as shown in Figure 6.17.

NCF

Rovings used in NCF fabrics were produced by Silenka b.v.. The amount of size deposition on the fibres studied was lower than that observed on the CRFM fibres, but globules of size and the distinctive menisci were evident, as shown in Figure 6.18.

Rovings

A range of rovings supplied from PPG, Silenka b.v. and Vetrotex were studied to examine for the same phenomena. All showed size deposition in similar quantities to the fabrics studied, a micrograph of PPG 1062 fibres is shown in Figure 6.19.

The effect of size during moulding

The size menisci and deposits may block the microscopic flow front in the fibre bundles. In this way the flow front may bypass regions of the fibre bundle,

entrapping air and creating voids. This would influence the transverse filling of the fibre bundles, where the menisci could restrict the flow between adjacent filaments. Axial impregnation of the fibres would be affected where the menisci or deposits could restrict the access of resin between the fibre capillaries.

Size dissolving into the resin system

For fast wetting systems size is designed to exhibit high solubility in styrene. Fibres subsequent to moulding were studied to determine if the size dissolved during a fast moulding cycle (3 minutes wet out period). Several polyester, unidirectional mouldings were fractured and the fibres which were pulled out examined. The fibres show size deposition (Figure 6.20a) and characteristic menisci fracture lines (Figure 6.20b). This suggests that the wet out times have not allowed the size to dissolve into the resin system. This indicates that interfacial bonding would be affected since there has been little time available for wet out (as suggested by Revill[19]). The presence of this size from these examinations suggests that since the menisci are unlikely to dissolve during impregnation the resin flow front will be retarded, which will aid the formation of microvoids.

6.5 Permeability

The permeability of two of the reinforcements used in these studies were measured to give an indication of their impregnation characteristics. The values obtained were used in the multilayer modelling studies described in section 6.6. As was discussed in Chapter 2 there are several methods for measuring both in-plane and transverse permeability. The methods previously discussed in section 3.7 were used to make permeability measurements for Unifilo U750-450 CFRM and Tech Textiles ELPb-567 unidirectional NCF.

Comparison of the principal permeabilities

The graph in Figure 6.21 shows the results for the three principal permeabilities, k_1 and k_2 in the plane of the fabric and k_3 through the thickness of the fabric. The graphs show values of permeability with respect to the fibre volume fraction in the mould. The value of the transverse permeability (k_3) is lower than the

other principal permeabilities k_1 and k_2. This is caused by the fluid having to penetrate fibres perpendicular (transverse) to their axes. In the case for the unidirectional fabric however, the values of k_2 and k_3 are similar since the flow is in both cases is perpendicular to the axes of the fibres.

6.6 Multilayer Flow

Visualisation

The object of this study was to consider the flow within multilayered stacks of different permeabilites. This was undertaken by simulating the impregnation of a multilayered preform using the apparatus described in section 3.3. Several flow visualisation experiments were carried out to examine the effect of different permeability conditions. Glass beads with diameters ranging from 1mm to 6mm were used to produce uniform layers of different permeabilities.

The results of these simple experiments are shown schematically in Figure 6.22(a) and 6.22(b). When a layer of lower permeability (2mm diameter beads) was sandwiched between layers of higher permeabilities (6mm diameter beads) the flow front of the impregnating oil was seen to travel along the central layer creating a non-uniform flow front (Figure 6.22(a)). With a layer of higher permeability sandwiched between layers of lower permeability the flow front was seen to distort in preference of the higher permeability layer.

These simple experiments have shown that there is a variation in the flow in layers of similar materials, the extent of variation being determined by the variation in the permeability of the layers. These trials have indicated that during the impregnation of materials of different permeabilities the flow front shape is non-uniform, and cannot be considered as a one dimensional flow through the thickness of the stack. These trials are relevant to the impregnation of multilayered preforms since the permeabilities between layers of reinforcement are likely to be distinct enough to permit the flow front shapes depicted by this visualisation experiment.

Finite Element Flow Simulation

As was discussed in section 4.4 air entrapment is thought to be caused by resin channelling along layers of high permeability in multilayer preforms trapping air in layers of lower permeability. To assess this effect of stacking reinforcement layers of different permeabilities a finite element model was used to predict the flow front in multilayered preforms. This model was developed in PAFEC finite element code by Rice[81] using the permeability data described in section 6.5. The mould filling simulation method is described in Appendix 16. Five preforms consisting of a combination of CFRM and unidirectional NCF were chosen. These preform stacks are shown in Table 6.2. The first four preforms consisted of three layered stacks, where layers of high permeability were sandwiched between layers of low permeability, or visa versa. These stacks were chosen to determine the effects of a central high permeability layer and outer high permeability layers upon the flow front shape. All were selected as realistic preforms which could be moulded in the flat plaque mould.

The first preform stack incorporated CFRM sandwiched between unidirectional fibres (stack A) with the second stack using unidirectional fabric sandwiched between CFRM (stack C). These were assessed in both 0° and 90° directions (stack B and D) for the unidirectional material. The fifth preform (stack E, 0°/90°) comprised four layers of unidirectional fabric. This preform was chosen to predict the flow front shape when unidirectional fibres were impregnated parallel and transverse to the flow front.

The thicknesses of each layer were calculated using a model described by Bulmer[79], these are shown in Table 6.2. Using this information, the fibre volume fractions which can be derived from them and the permeability measurements described above, the in-plane and transverse permeabilities for each layer was calculated. The model, which assumes a constant pressure during the resin injection, was used to simulate the flow through the first 50mm in the plane of the mould cavity. Figures 6.23(a) to (d) show the flow predictions for the preforms stacks A to D. These plots only show one half of the mould cavity, since the preforms are

symmetrical about their centre line. Figure 6.23(e) shows the flow predictions for the bidirectional preform (stack E) for the full cavity since the laminate is unbalanced.

The shadings in each diagram show the flow positions for percentages of impregnation. The first shaded area shows the amount filled 5% of the time available to fill the section. The areas are then incremented into 10% time steps, until the section is 95% filled. The final shaded areas shows the amount filled in the last 5% of the time available.

In each case the flow front in the stack develops quickly into a steady shape. This flow front shape remains constant during the impregnation of the preform. The fronts show that the flow is dictated by the layer, or layers of higher permeability. The layers of lower permeability appears to be impregnated transversely, which may cause air entrapment, both in the matrix, and more likely in the fibre bundles. The flow fronts predicted in these studies have been used to discuss the void content in the individual layers from the multilayered laminates described in section 6.7.

6.7 Moulding Investigations

Multilayered preforms

To investigate whether the transverse filling effect predicted in multiaxial preforms affected the void content in different layers, four mouldings were produced using the preform stacks A to D described in section 6.6. The mouldings were produced according to the procedure described in section 3.3 and sectioned according to Figure 5.1. The sections taken at 50mm from the injection gate are shown in Figures 6.24(a) to (d).

Figures 6.24(a) and 6.24(b) show sections taken from stacks A and B. No voids are apparent in the CFRM layers but voids are distinct in the outer unidirectional layers. Stack B (Figure 6.24(b)) shows a higher void content than does stack A (Figure 6.24(a)). The same is also true when comparing the sections in Figures 6.24(c) and 6.24(d), from stacks C and D. Voids are discernable in both sections but the void content is higher in the 90° layers of stack D.

The voidage trends shown in these sections suggest that the preform was impregnated as predicted by the finite element simulation. The 90° layers exhibit extensive voidage, suggesting that these layers have filled transversely, and air has been entrapped by doing so. The voids in the fibre bundles of the 0° layers could have been caused by the rapid impregnation of the preform, where the resin travelled between the fibre bundles causing fewer microvoids in the centre of the bundles.

Unidirectional NCF was used to create the fifth preform stack E described in section 6.6. Two mouldings were produced. These mouldings were used to study the influences of void formation on preform structure relative to the injection gate position. The areas of the mouldings which were examined are shown in Figure 6.25. Figures 6.26(a) to 6.26(c) show sections of the 0°/90° laminate. Figure 6.26(a) shows a section of the area C1. The previous experiments suggest that the preform filled along the 90° layers in the lower half of the preform whilst the 0° layers along the top of the moulding filled transversely from the lower layers. The cross section shows microvoids within the 90° fibre bundles. These bundles are assumed to have been impregnated due to axial filling. The voids at the centre of the fibre bundles suggest that the transverse flow has not completely filled the bundle. These studies indicate the same voidage trends as the three layered multilayered stacks (A to D).

Figure 6.26(b) shows a section of the area B1. The micrograph shows the fibres cut at 45° to the X axis. No voids are evident in this section. Figure 6.26(c) shows a section of the area D1. This area is likely to have filled along the 90° layers in the upper half of the preform and the 0° layers along the lower of the moulding were filled transversely from the upper layers. The cross section shows the 0° layers in the upper half of the picture and the 90° fibres in the lower half. Extensive voidage can be seen in the 90° fibres near the component surface.

The sections studied support the finite element prediction of the flow front, since the void content in the 90° layers is higher than the 0° layers, suggesting that the 90° layers were impregnated by transverse flow.

Unidirectional Preforms

The results from the multilayered laminates suggest the layers filling from transverse flow will contain higher void contents than those filled from axial flow. To confirm this observation a unidirectional moulding was produced using a central injection point, to allow transverse and axial penetration to occur in the same layer of layers. Sections were taken from the moulding as shown in Figure 6.27(b). Figures 6.27(a) and (b) show sections of the 0° laminate. Figure 6.27(a) shows a section of the area A. The fibre bundles which have been impregnated axially show very few voids. Figure 6.27(b) shows a section of the area R. These fibre bundles have been impregnated by a transverse flow showing widespread voidage.

6.8 Discussion

These investigations have shown that the preform structure affects impregnation, both on a microscopic and macroscopic scale. The impregnation trials have indicated that the direction of the fibres, stitching and thermoplastic binder has influenced the direction and speed of flow. If an uneven flow front was created, air became entrapped which would create macrovoids in the impregnated reinforcement.

The study of dry reinforcement indicates that the addition of binder and size onto freshly drawn fibres may create flow impeding regions which will distort the local flow front of the resin as impregnation proceeds. This distortion of the flow front is likely to entrap air as the flow surrounds and bypasses areas which have been obstructed. During a fast RTM cycle the binder and size constituents do not dissolve into the surrounding matrix, but remain as separate phases in the final composite.

Resin impregnation into multilayered preforms is likely to be uneven through the thickness of the stack. This uneven flow front may cause air entrapment, creating voids in the final composite. This flow front distortion was modelled using a finite element solution which estimated the flow front shape for each of the multiaxial laminates considered. The results suggested that the resin would flow preferentially along the layers of higher permeability, and the layers of lower permeability would fill due to a transverse impregnation mechanism. The layers of lower permeability in

this case were unidirectional fibres placed parallel to the rectilinear flow front. The void content in these layers, within the fibre bundles was higher than the lower permeability (CFRM) layers. The mouldings which used unidirectional fibres placed perpendicular to the rectilinear flow front direction, showed fewer voids within the fibre bundles than those placed parallel to the flow front. Microvoids were still evident in these sections. This was assumed to be caused by the rapid impregnation of the preform, where the fibre bundles could not completely fill before air was trapped.

The use of a high permeability layer within a preform stack may increase the permeability of the overall laminate, thus reducing injection times and improving overall wet-through. This layer is likely to distort the microscopic filling of the multilayered structure allowing voids to form in the high fibre volume fraction layers which are usually the load bearing fibres of the structure. In these areas the void volume fraction is likely to be much higher than a macroscopic void fraction analysis (such as the burn off method) will suggest.

The finite element model of the impregnation of a bidirectional preform using rectilinear flow showed a curved flow front, filling preferentially from the 0° layers. The resin flow front was thought to trap air in the 90° layer which filled due to a transverse flow. Study of a centrally injected 0° preform indicated that the fibre bundles which were filled due to a transverse impregnation mechanism exhibited more voids than those from axial filling.

Flow visualisation trials have been undertaken by several researchers[29,31,32] who have observed air entrapment due to stitching and resin travelling quicker in the spaces between fibre bundles. The effect of thermoplastic binder distorting the flow front has not been reported. The dry structure of glass reinforcements with both thermoplastic binder and size, has shown regions which are likely to impede resin impregnation.

Impregnation predictions using FE and finite difference models have been

studied and several methods have been described[51,52], using a Darcy's law to predict flow in a reinforcement. The majority of these models predict flow in the plane of the material. Little work has been covered in assessing the flow through the thickness of the fabric. Mechanisms for the flow through the thickness of multiaxial preforms and causes for air entrapment during resin impregnation have been proposed and will be examined in subsequent sections.

List of Tables

List of Figures

Table 6.1: Vickers Micro-Hardness Results for Polyester mouldings

Moulding No. Materials: (CFRM U750-450) (Resin CVP 6345.001)	Vickers Micro-Hardness Number	
	General Matrix	Assumed Thermoplastic region
5097	6.3	8.8
	5.4	7.4
	5.9	8.4
5107	23.7	10.9
	17.2	6.8
5133	12.7	13.4
	18.2	15.2

The Vickers Micro-Hardness values are an average of three measurements taken.

Table 6.2 **Details of Multiaxial Mouldings**

Moulding No.	Stack	Preform lay-up	Finite element Model Figure No.	Section Figure No.	Layer Thicknesses (mm)	Fibre Volume fractions (%)
4319	A	2 layers ELPb-567 (0°) 2 layers U750-450 2 layers ELPb-567 (0°)	7.8(a)	7.9(a)	1.025 1.55 1.025	43 23 43
4320	B	2 layers ELPb-567 (90°) 2 layers U750-450 2 layers ELPb-567 (90°)	7.8(b)	7.9(b)	1.025 1.55 1.025	43 23 43
4321	C	2 layers U750-450 2 layers ELPb-567 (0°) 2 layers U750-450	7.8(c)	7.9(c)	1.32 0.96 1.32	26.6 46 26.6
4322	D	2 layers U750-450 2 layers ELPb-567 (90°) 2 layers U750-450	7.8(d)	7.9(d)	1.32 0.96 1.32	26.6 46 26.6
4263	E	2 layers ELPb-567 (0°) 2 layers ELPb-567 (90°)	7.8(e)	7.11(a),(b),(c)	1.8 1.8	24.6 24.6

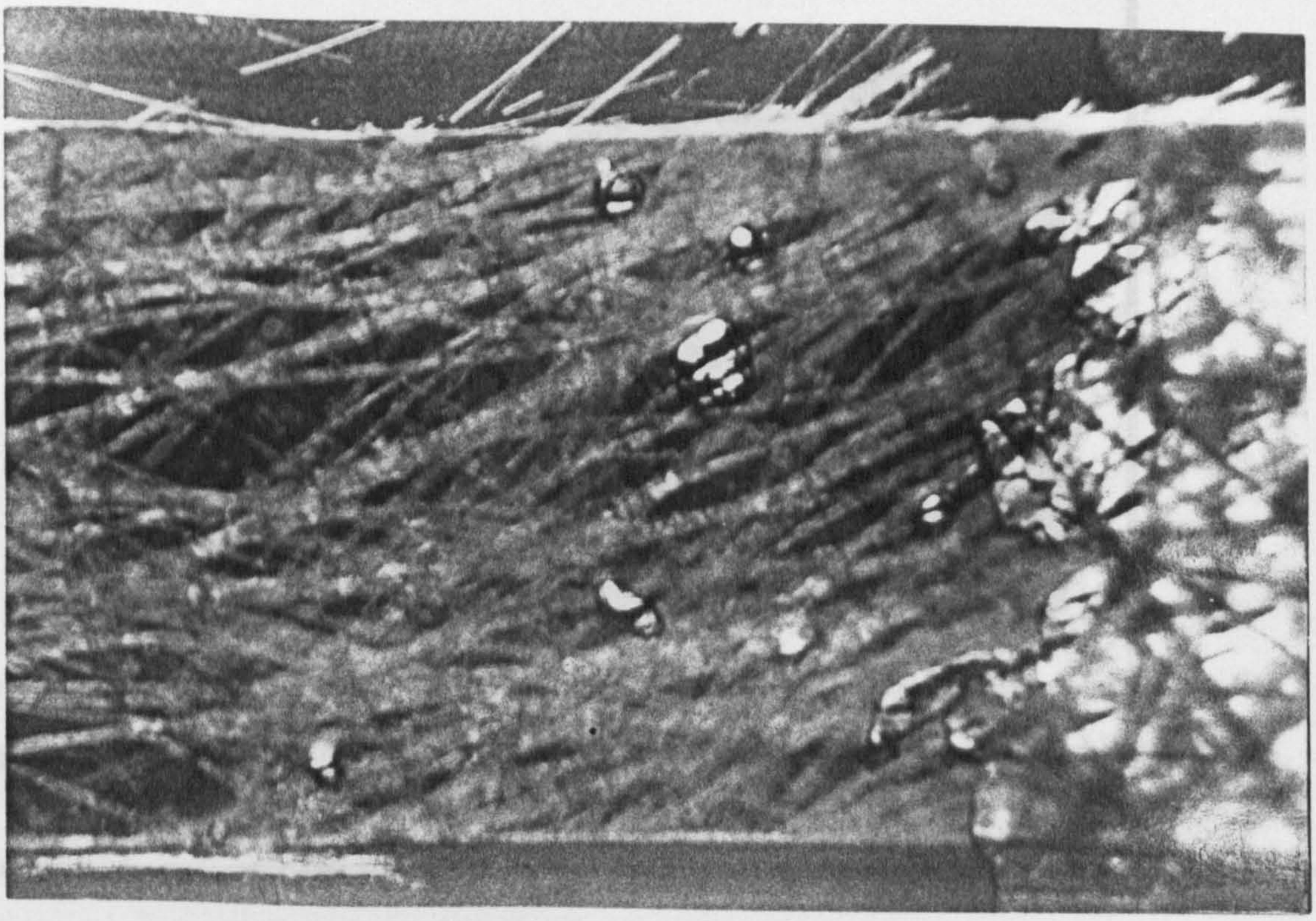

Figure 6.1 During oil impregnation trials of a U750-540 reinforcement air pockets were created during filling. An uneven flow front flowed around pockets of air entrapping them to create voids.

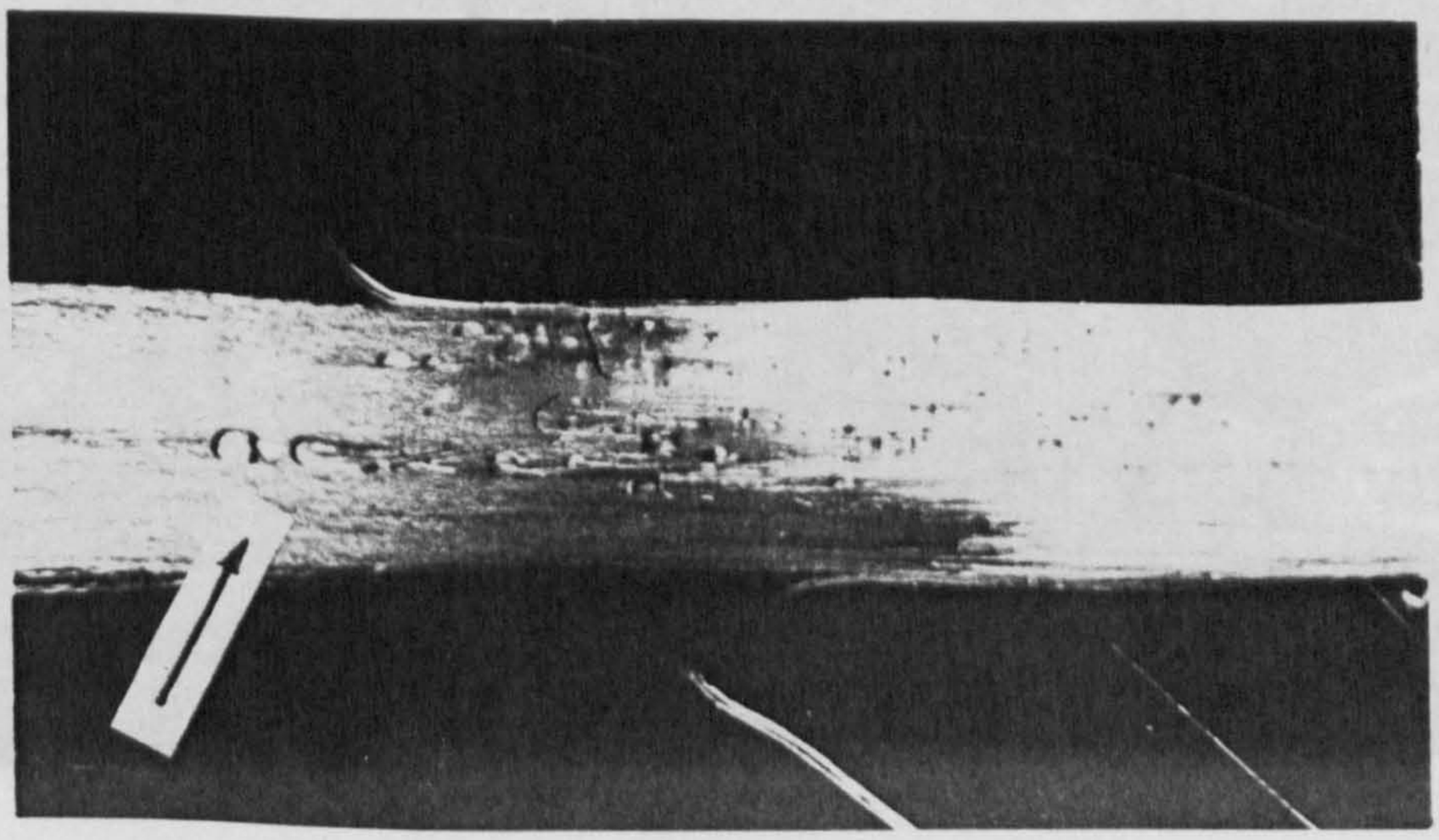

Figure 6.2 Voids which were created during the filling of a single tow of 0° fabric using high viscosity oil. Binder is visible as globules on the surface of the strand. Voids (marked by the arrow) were created were an uneven flow front entrapped air behind globules of thermoplastic binder.

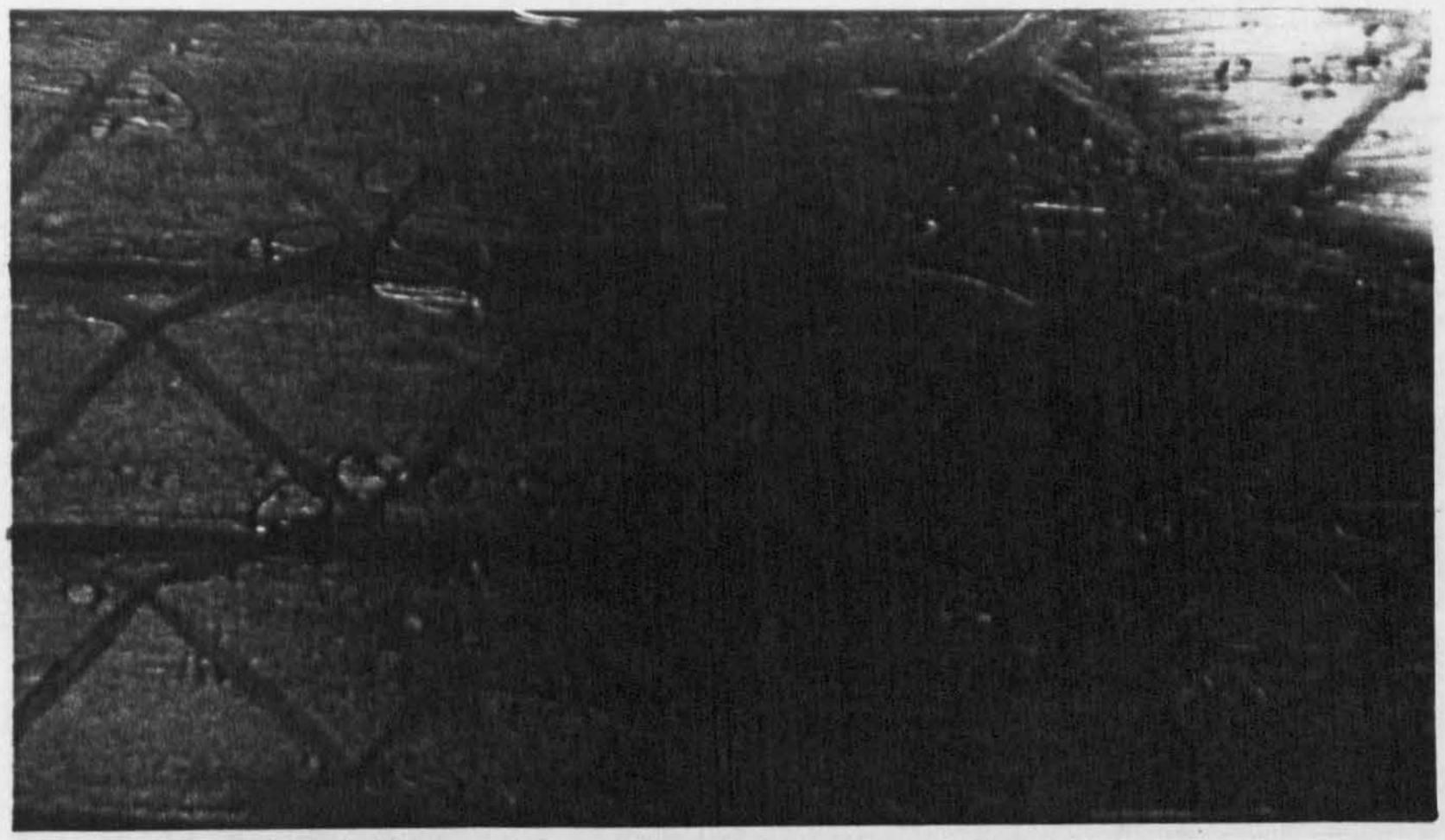

Figure 6.3 Air can be seen to have become entrapped between the stitching of this 0° fabric and the mould surface.

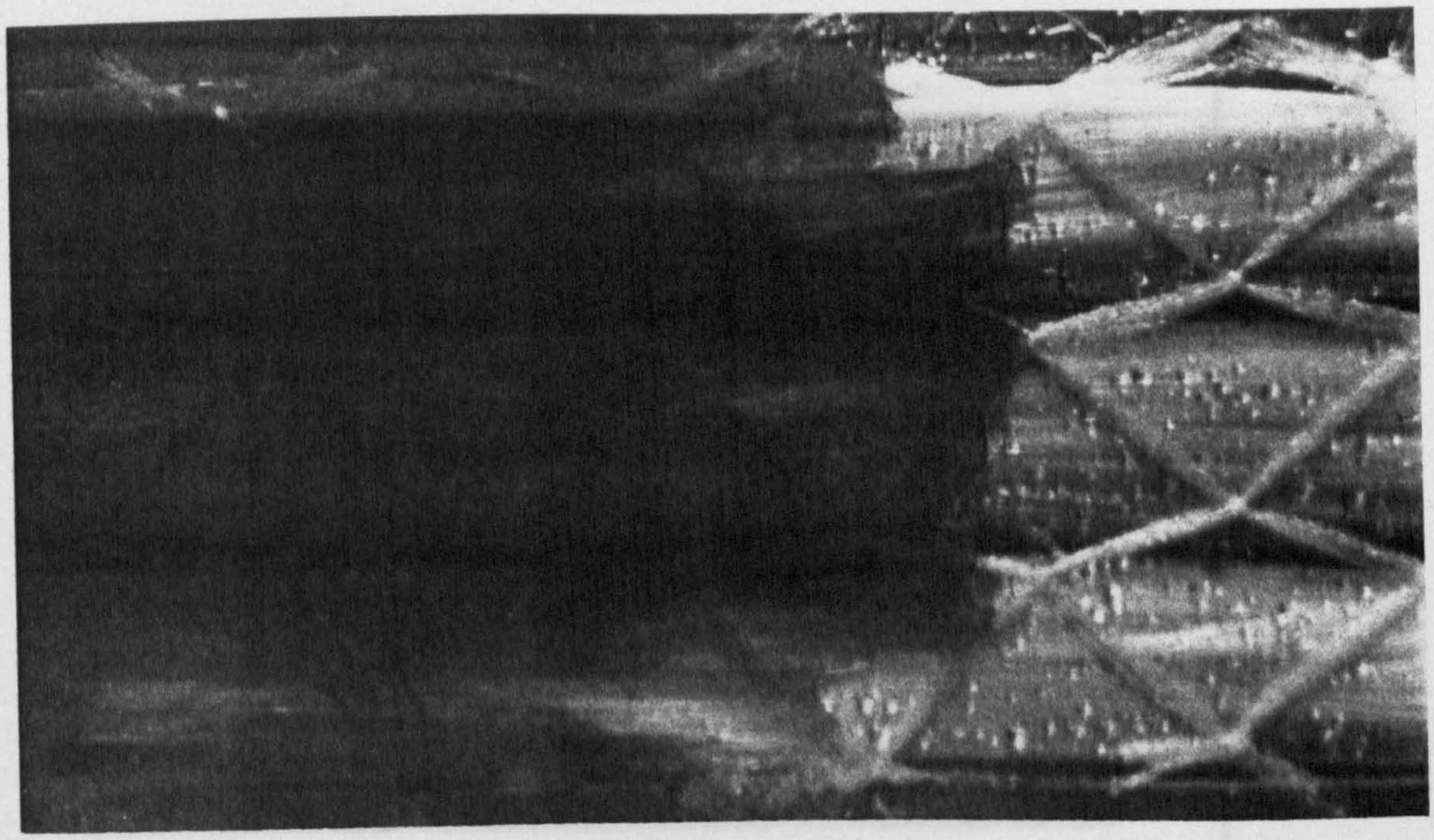

Figure 6.4 During the impregnation of a 0° fabric dry patches were created where the oil has flowed between the fibre bundles and entrapped air.

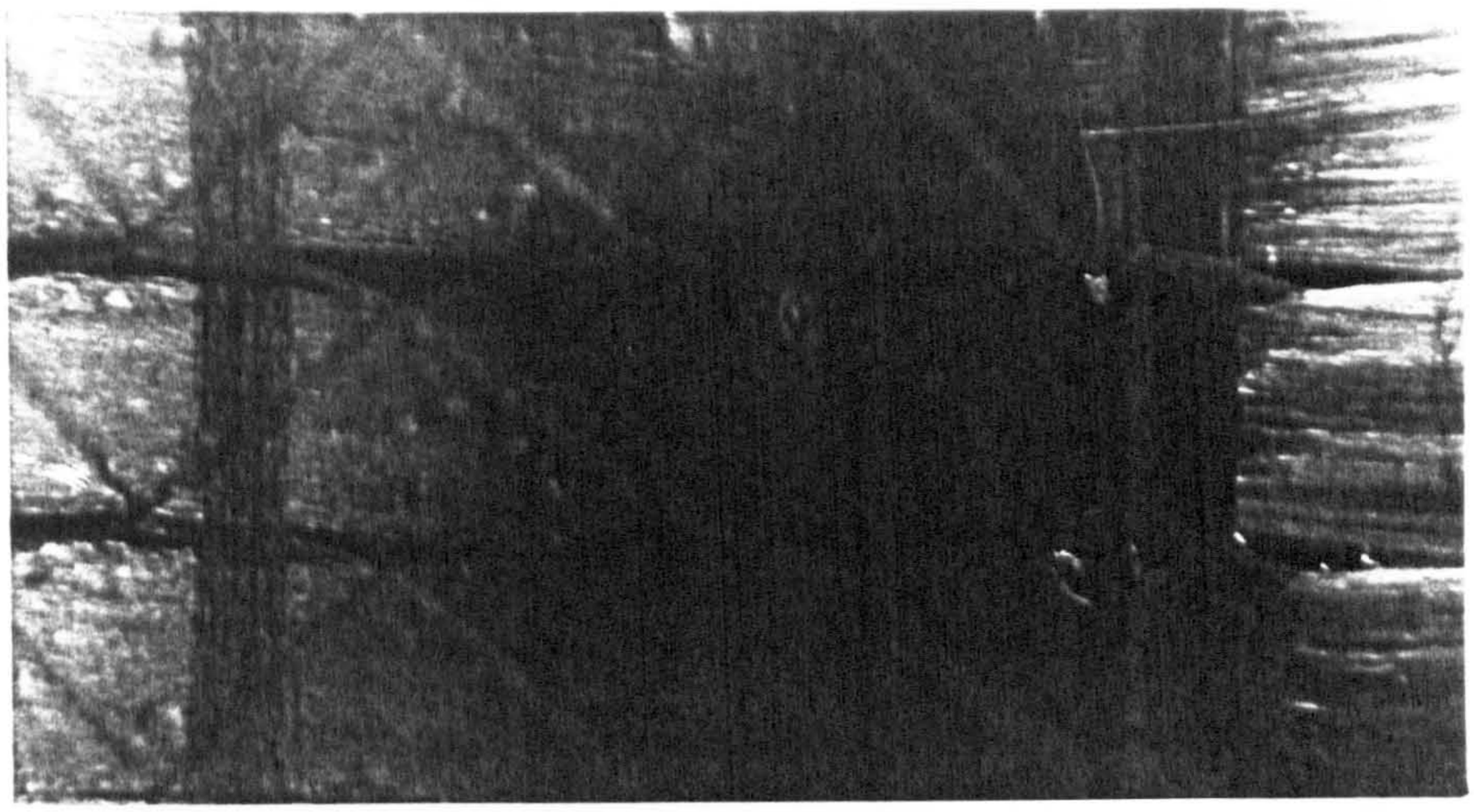

Figure 6.5 A void was created at the intersection between the 0° and the 90° rovings of fibres. The 90° roving has blocked the flow at the mould surface, allowing the resin to travel along the 0° bundles, creating a void at the mould surface.

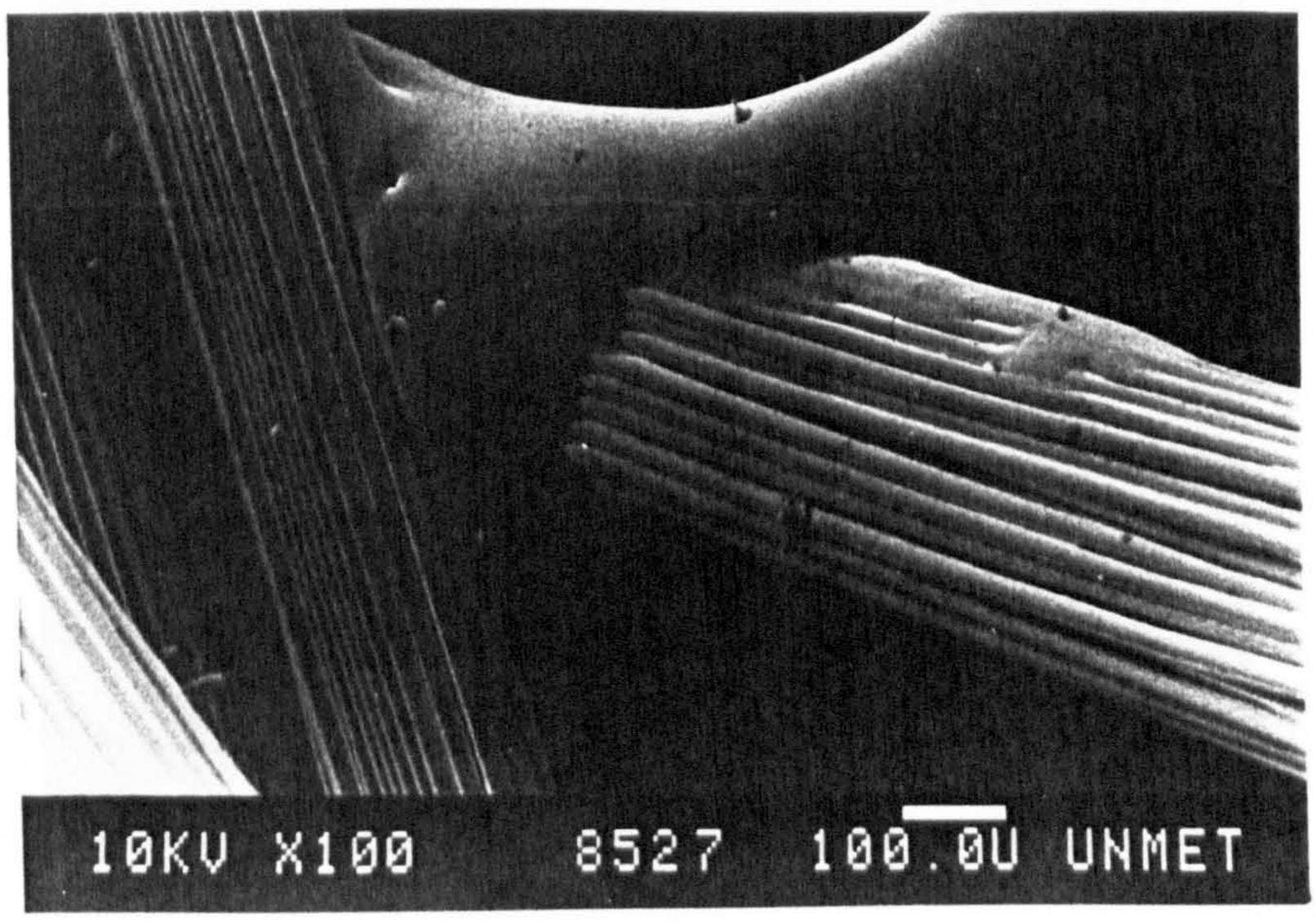

Figure 6.6 Thermoplastic binder joining strands in a U750-450 CFRM.

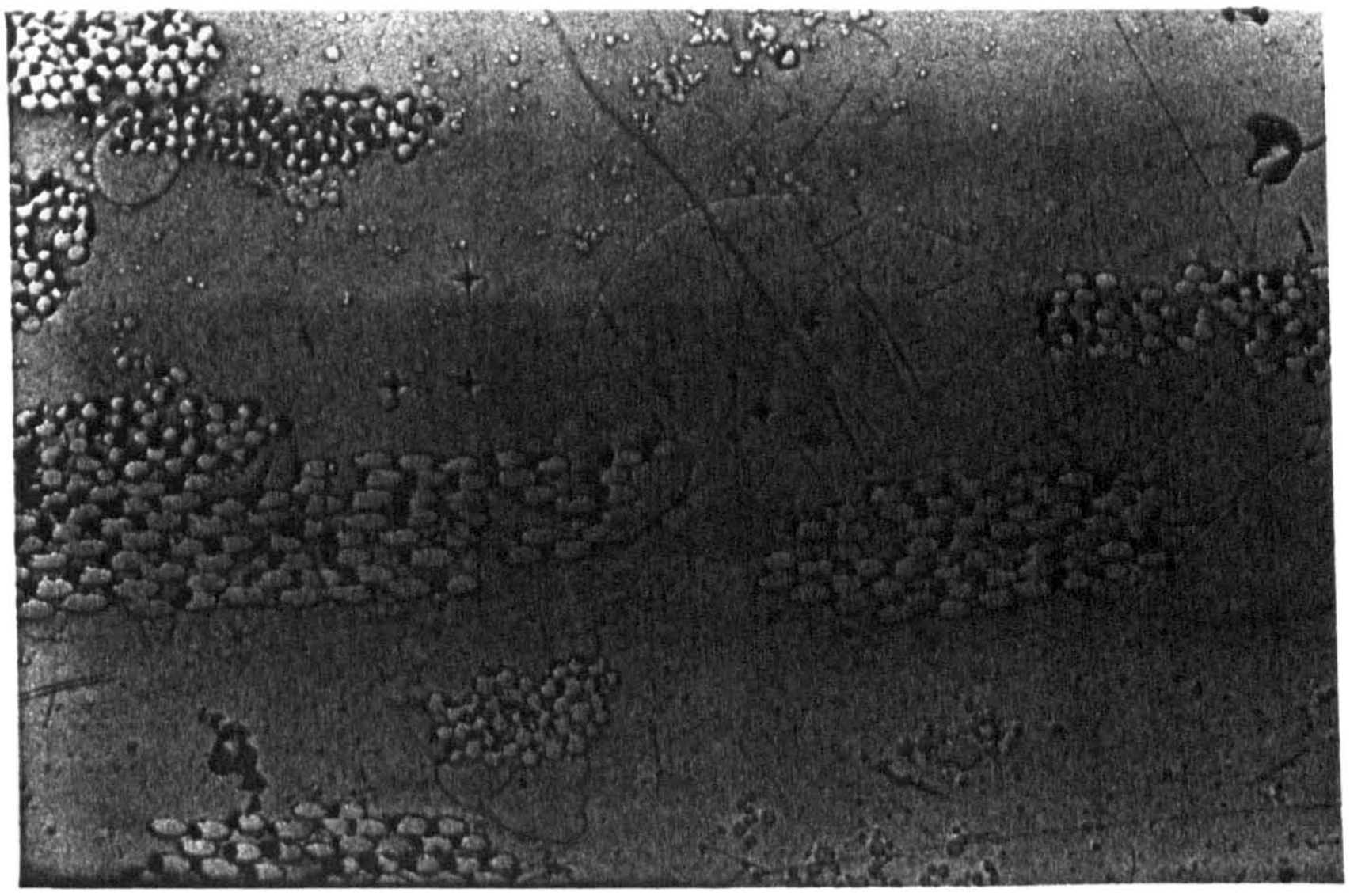

Figure 6.9 A polyester, CFRM moulding showing binder after Vickers Micro-Hardness testing (x50, Moulding 5097).

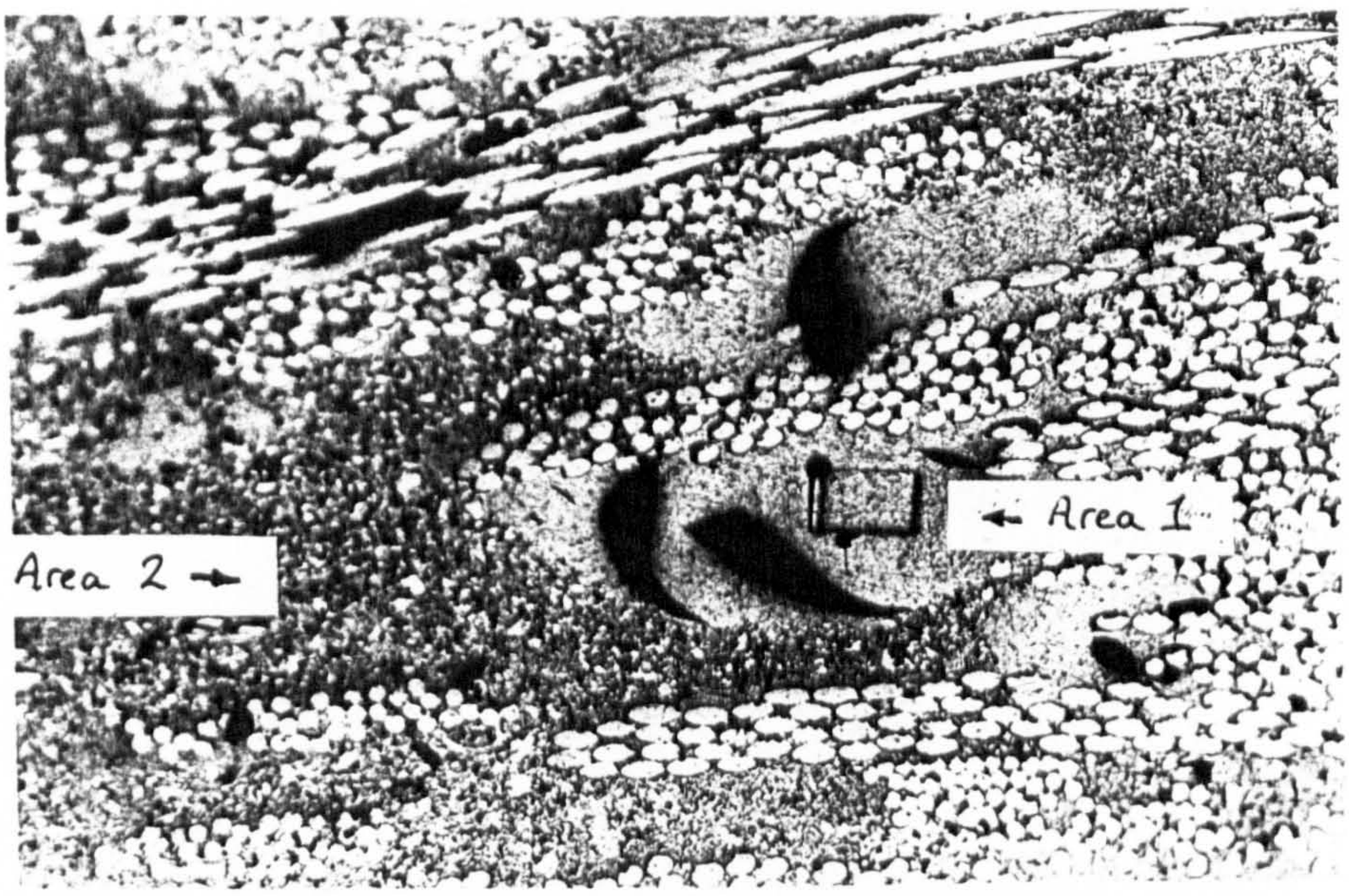

Figure 6.10 A section from a calcium carbonate filled, low profile polyester moulding. The areas from which elemental analyses were undertaken are shown (x50).

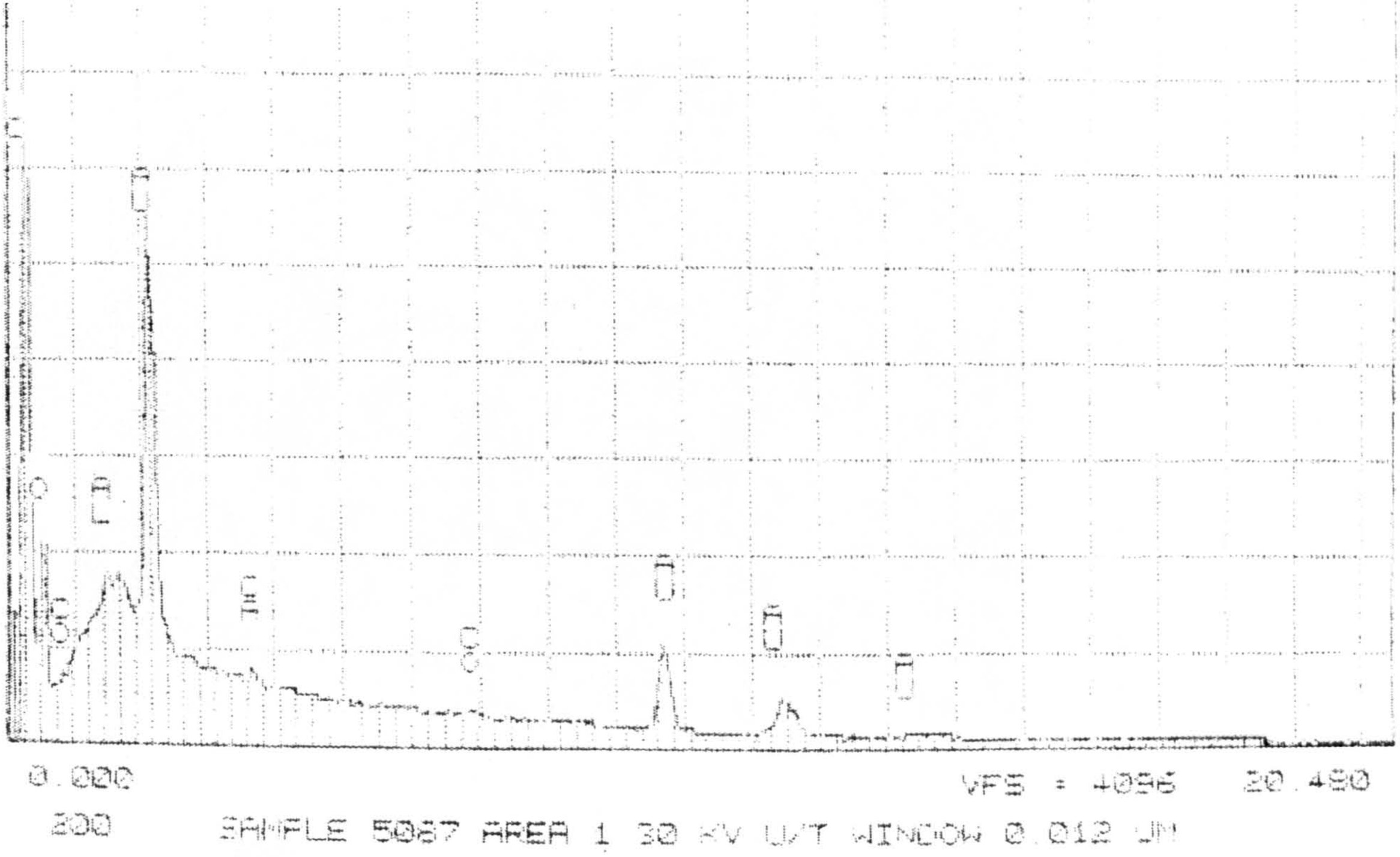

Figure 6.11a An elemental analysis of area 1, shown in Figure 8.5. Only a low trace of calcium is shown, indicating that the area is not the calcium carbonate filled thermosetting resin, but is the thermoplastic binder which was applied to the fibres prior to moulding.

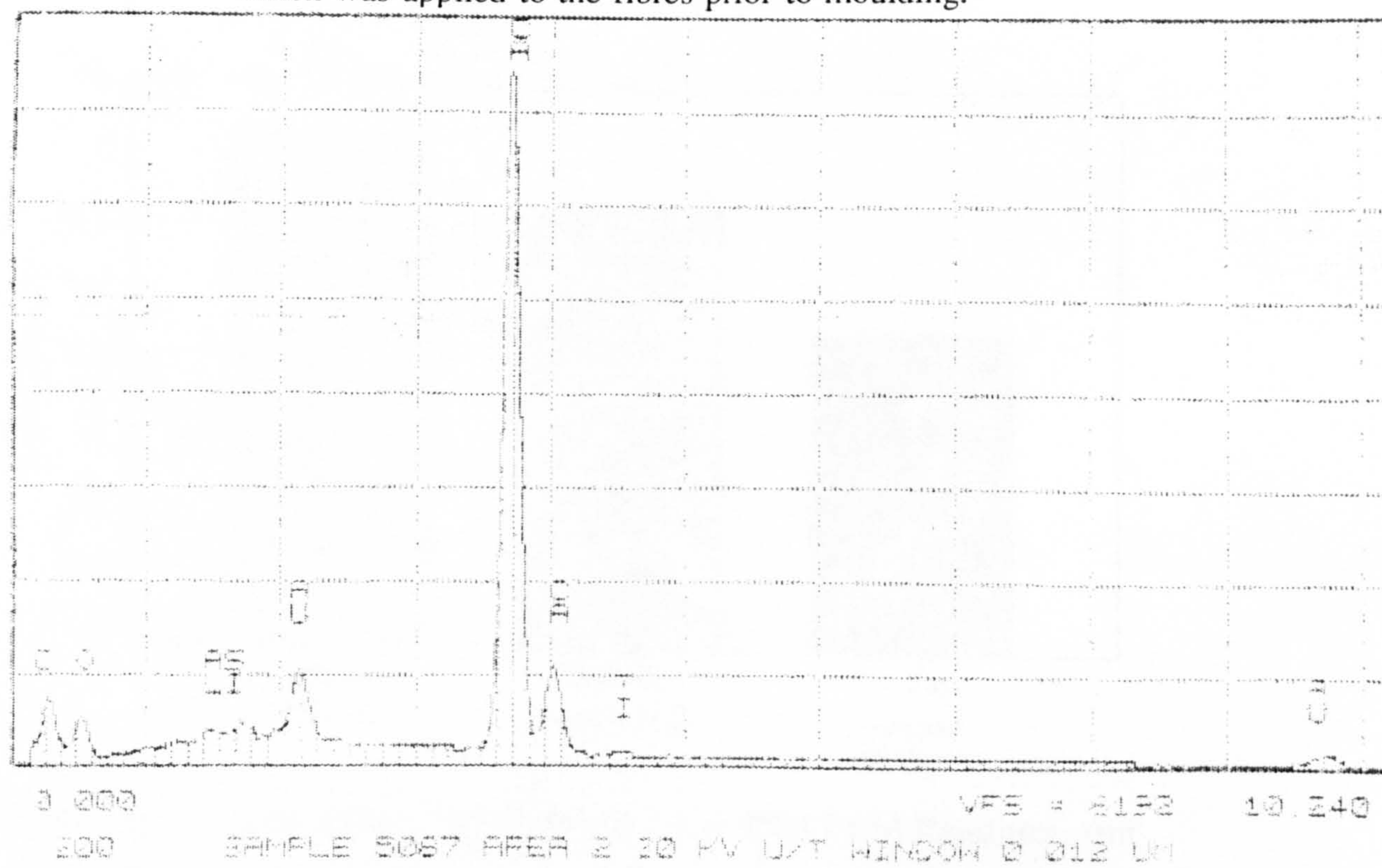

Figure 6.11b An elemental analysis of the area 2, shown in figure 8.5. This area consists of the thermosetting resin system, which is confirmed by the high calcium peak.

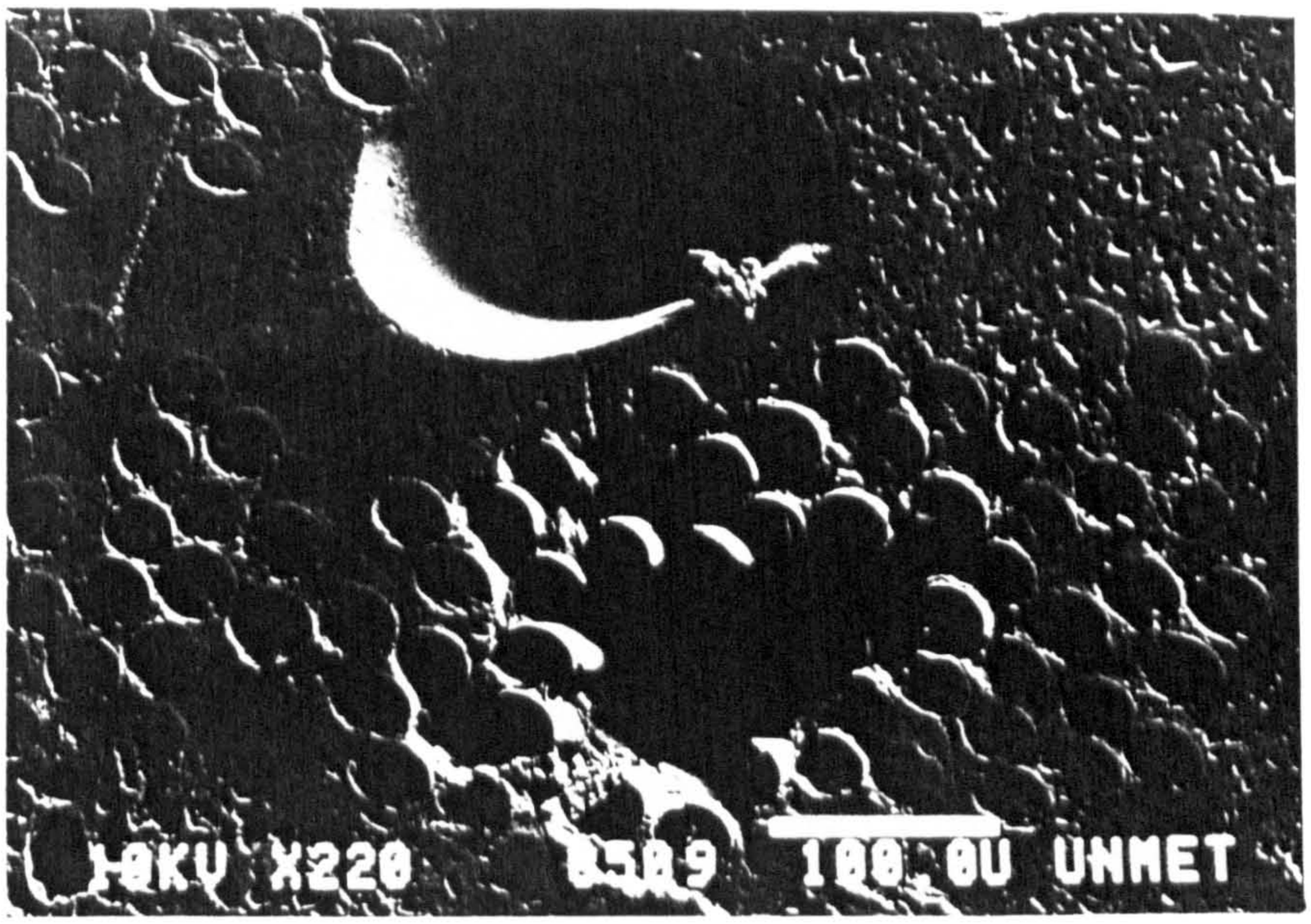

Figure 6.12 A SEM micrograph of a section from a calcium carbonate filed, low profile polyester moulding. The section was etched in a hydrochloric acid bath and pitting can be seen in the areas of calcium carbonate removal. The areas surrounding the voids and fibres show no pitting, suggesting no calcium carbonate was present in these areas, whilst in the corners of the figure many small craters are apparent.

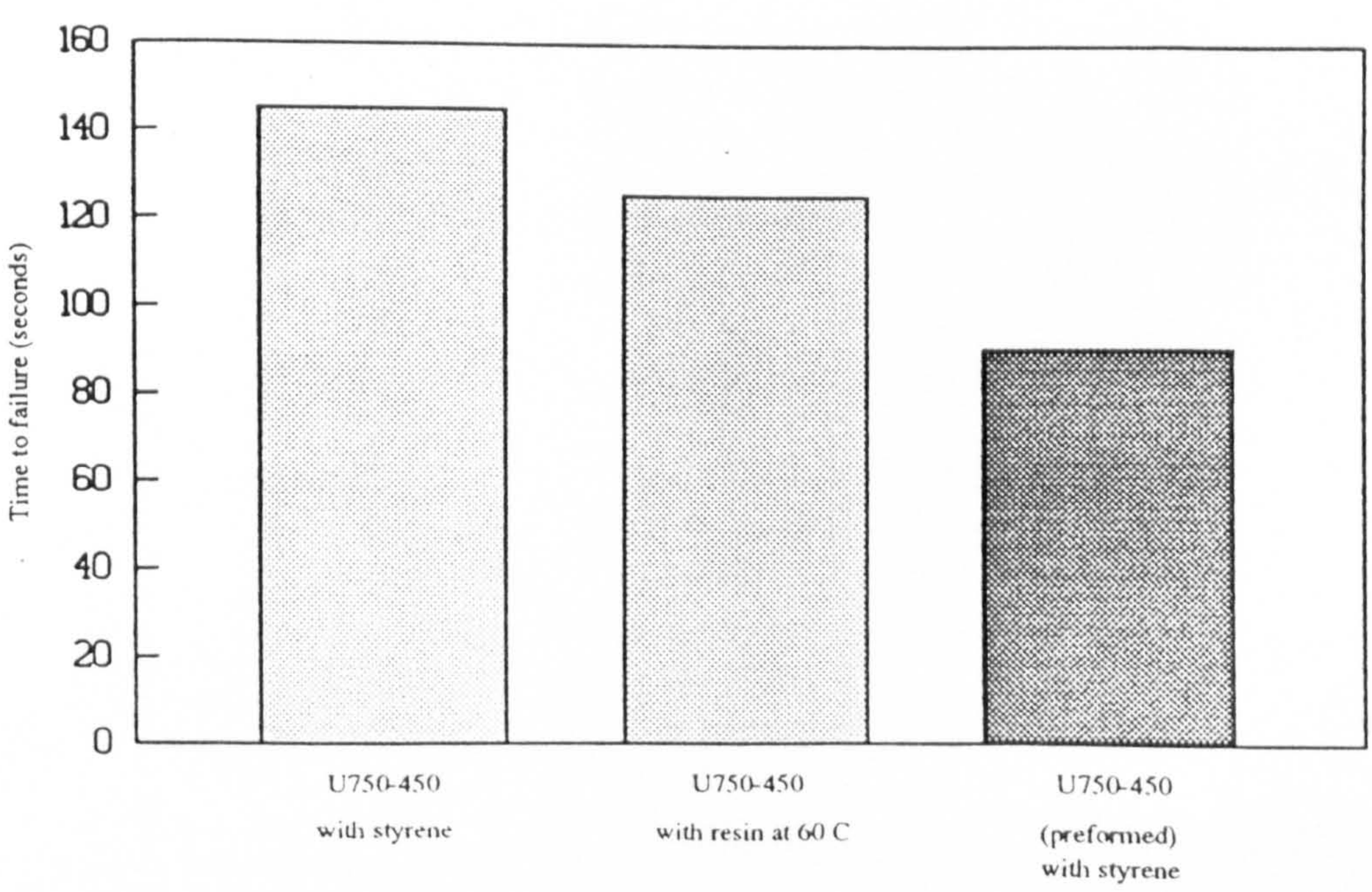

Figure 6.13 Binder Solubility of Unifilo U750-450 CFRM Reinforcement

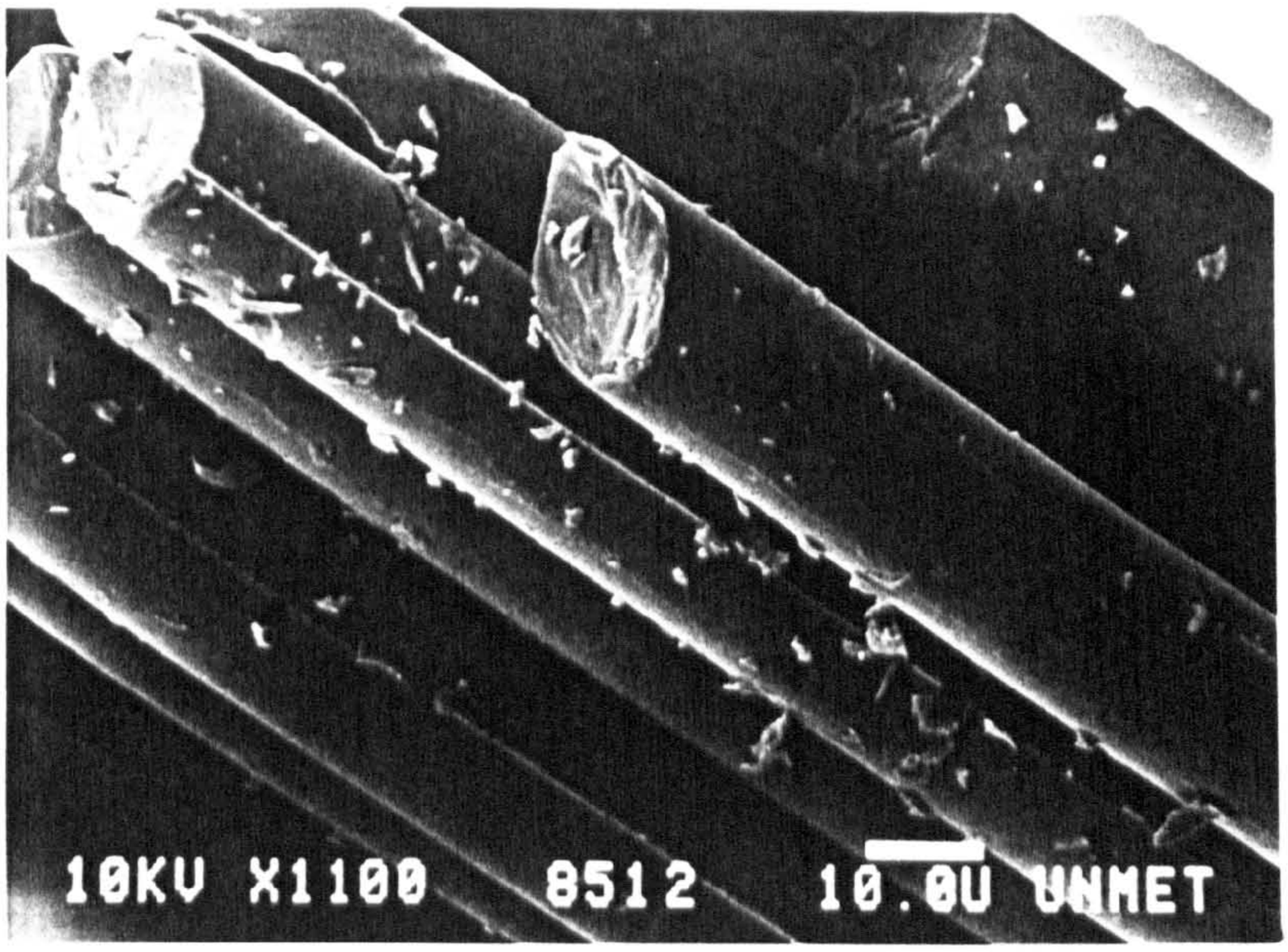

Figure 6.14 The end of a fibre bundle of a U750-450 CFRM reinforcement. The fibre bundle has been partially filamentised by a cutting action. The protruding lines along the fibres show the fracture surfaces of the size menisci which hold the fibre bundles together.

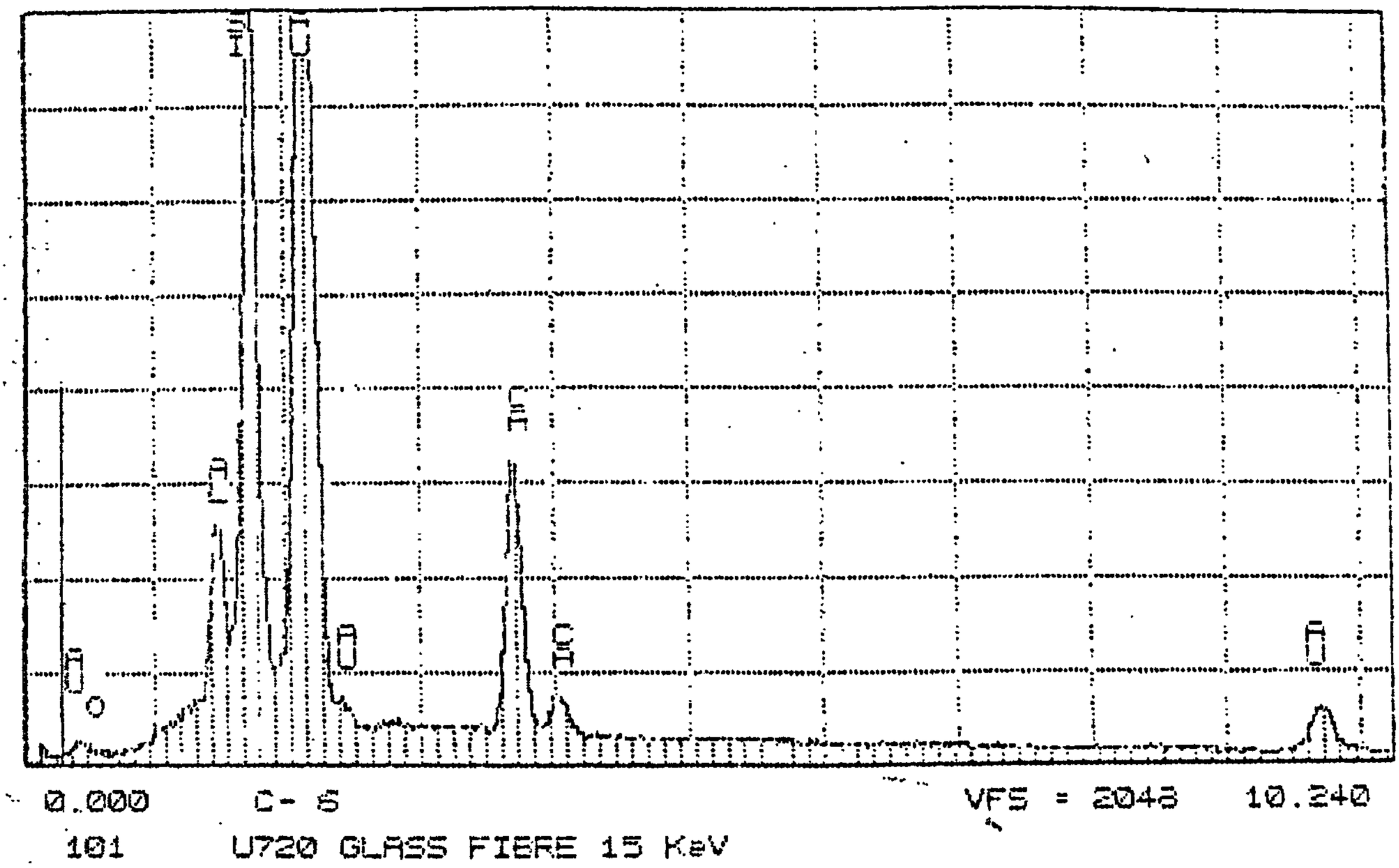

Figure 6.15(a) An elemental analysis of an area of a glass fibre, from a U720 CFRM.

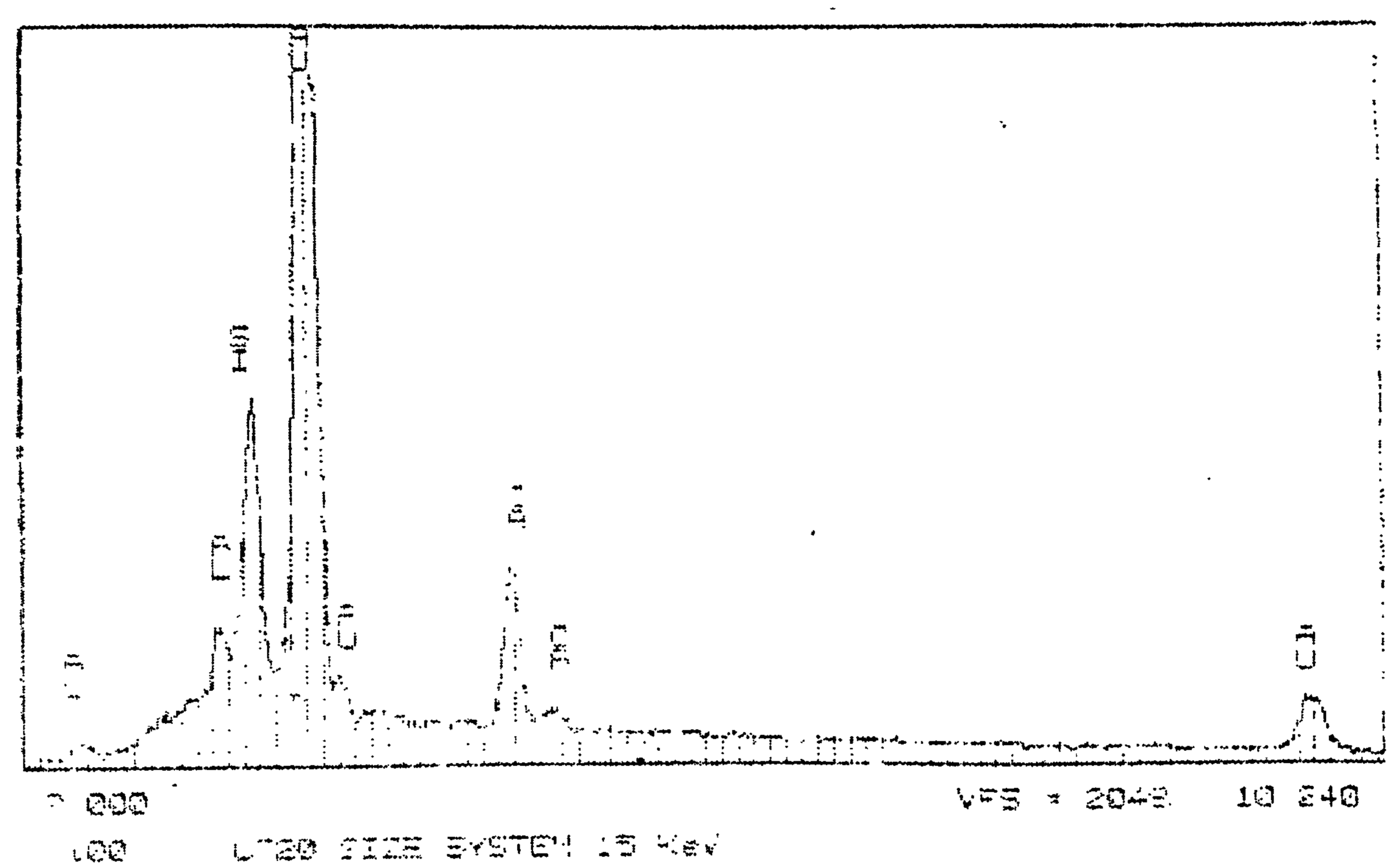

Figure 6.15(b) An element analysis of an area which is assumed to be size. The graph shows a much lower silicon peak than for the glass fibre sample.

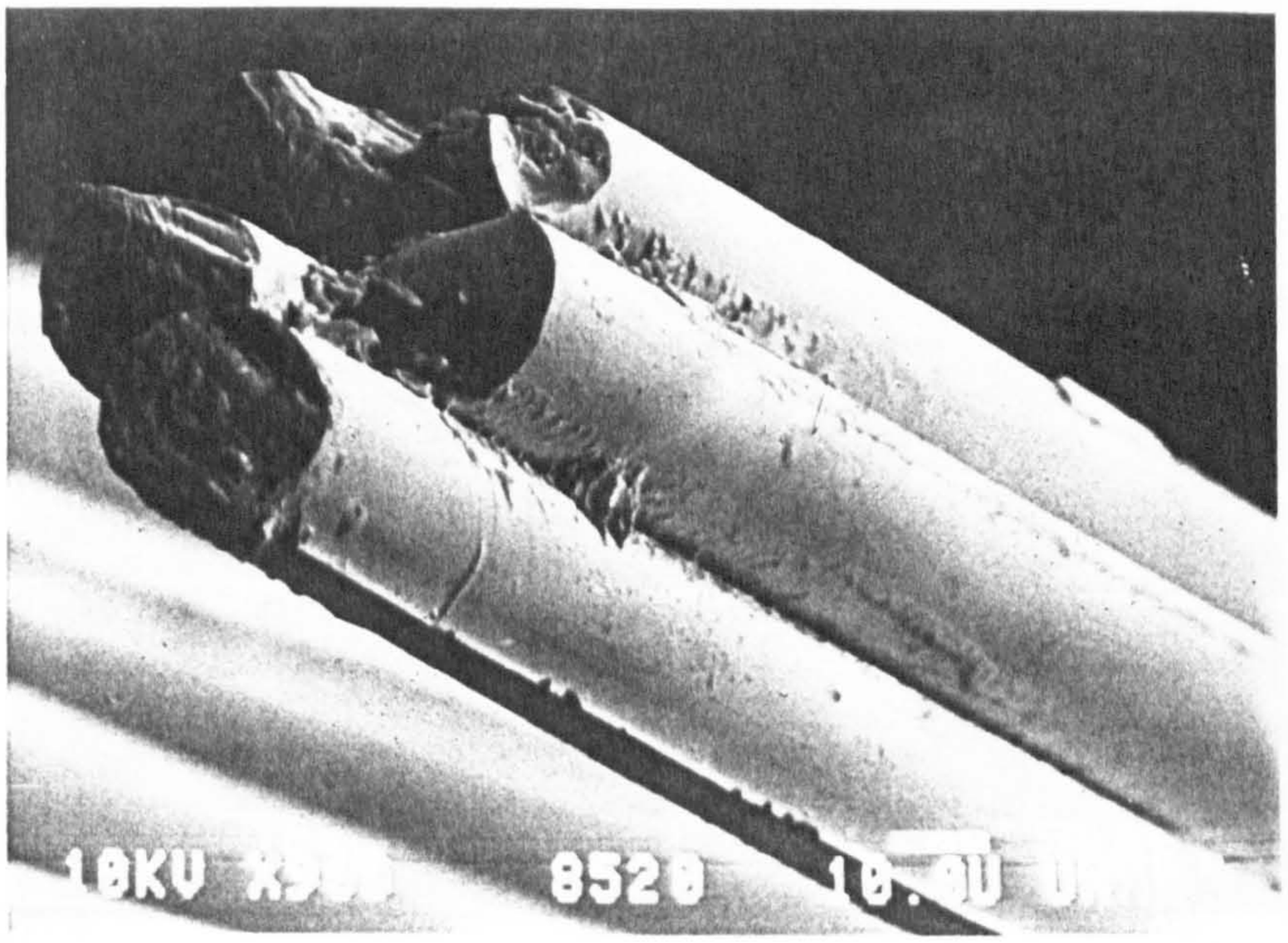

Figure 6.16 Size deposition between fibre in a U720 CFRM. The deposition and menisci are small. Note the fracture surface from a size meniscus along the lower fibre.

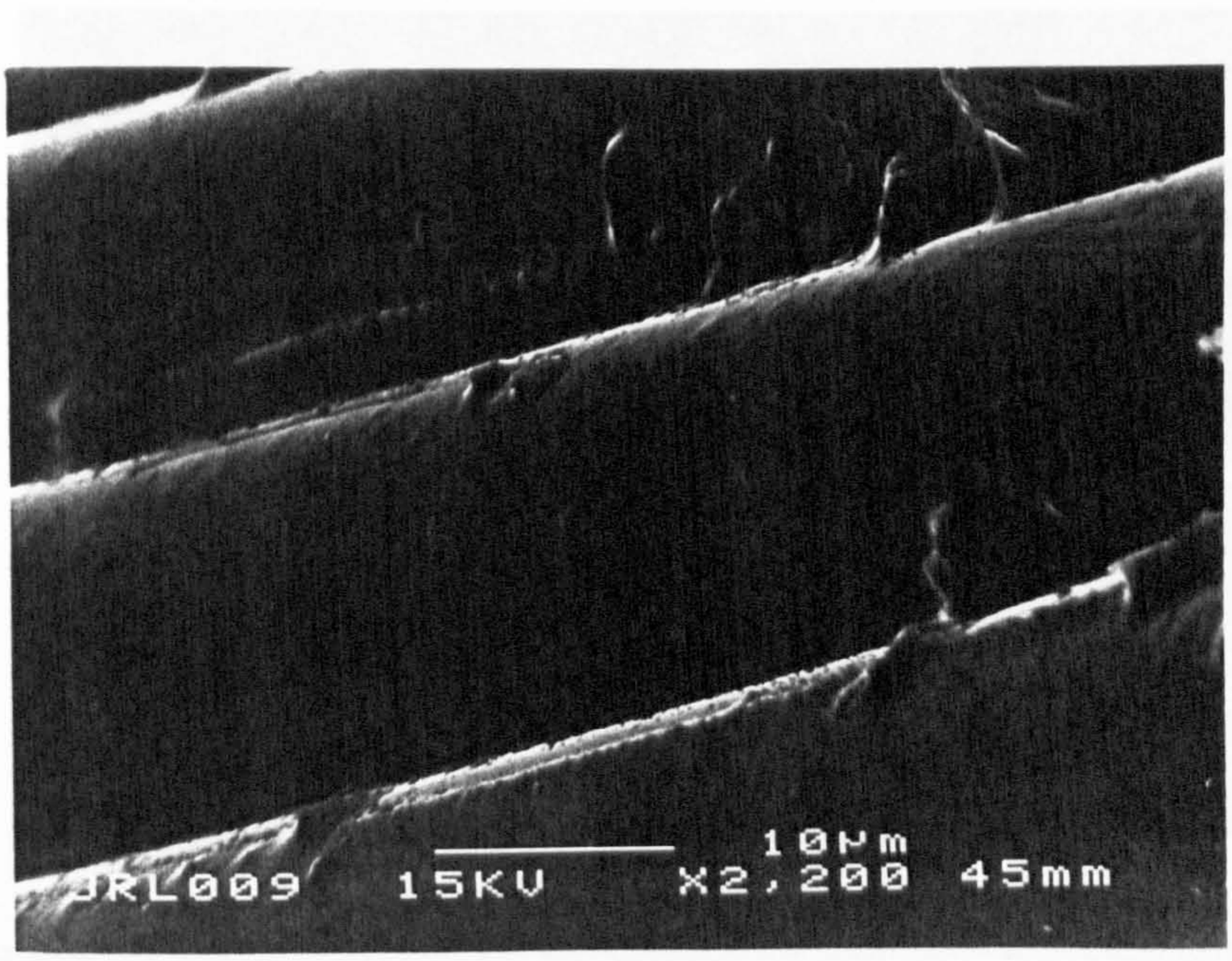

Figure 6.17 Extensive size coating with large menisci between fibres in this U720 CFRM.

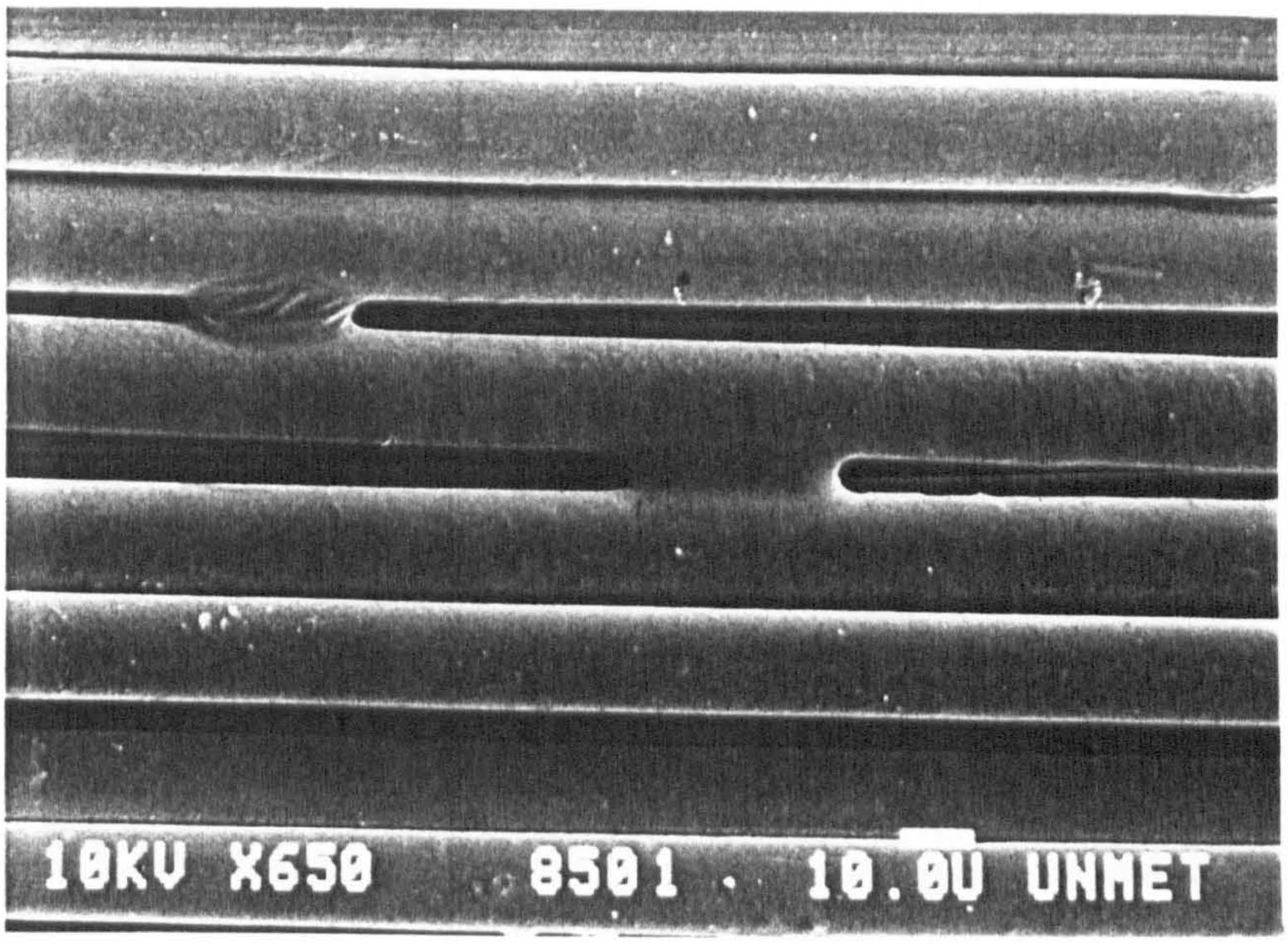

Figure 6.18 Size Globules Between Unidirectional fibres in this E-LPb 567 0° fabric.

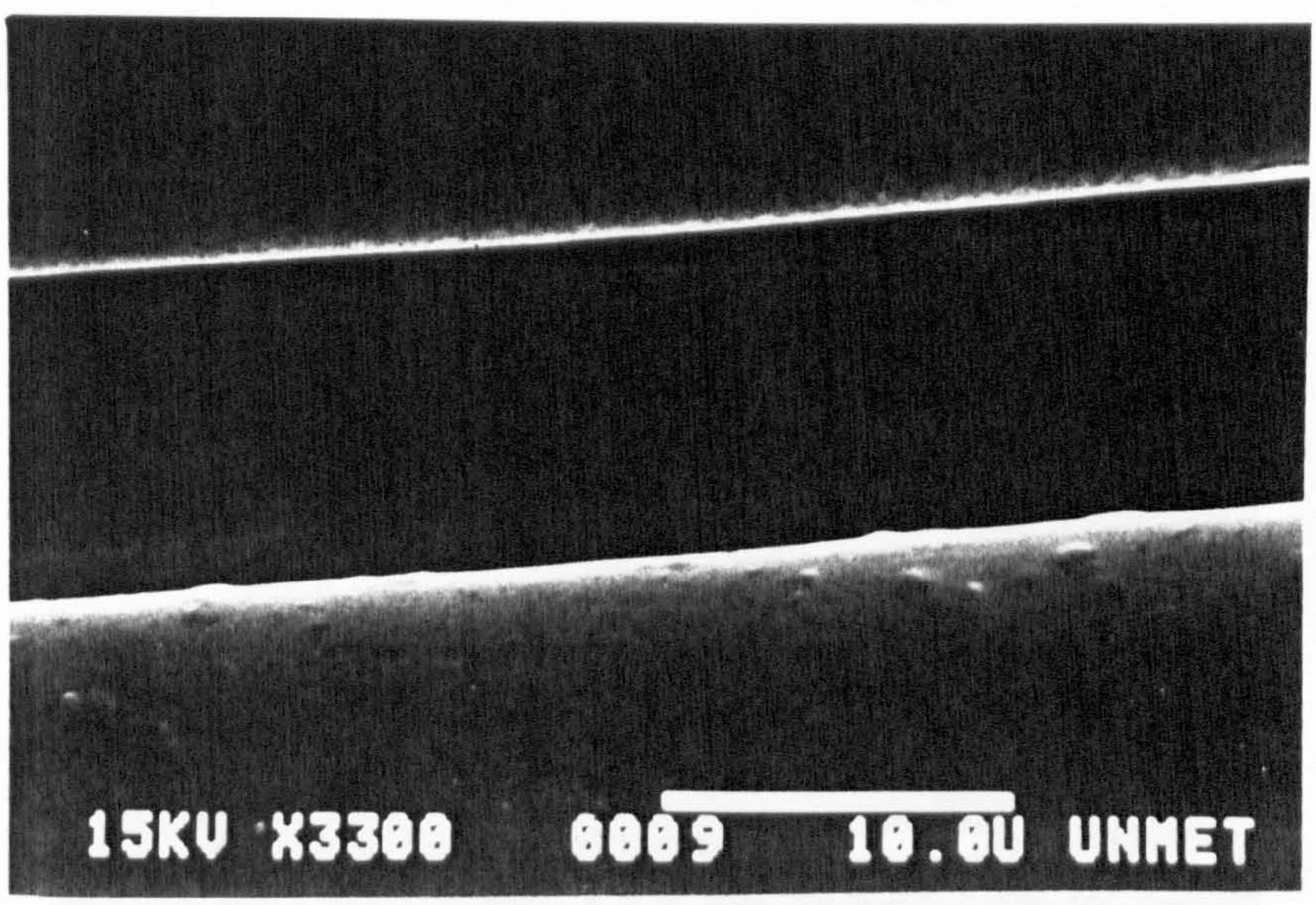

Figure 6.19 These PPG 1062 rovings exhibit size menisci and deposits between the fibres.

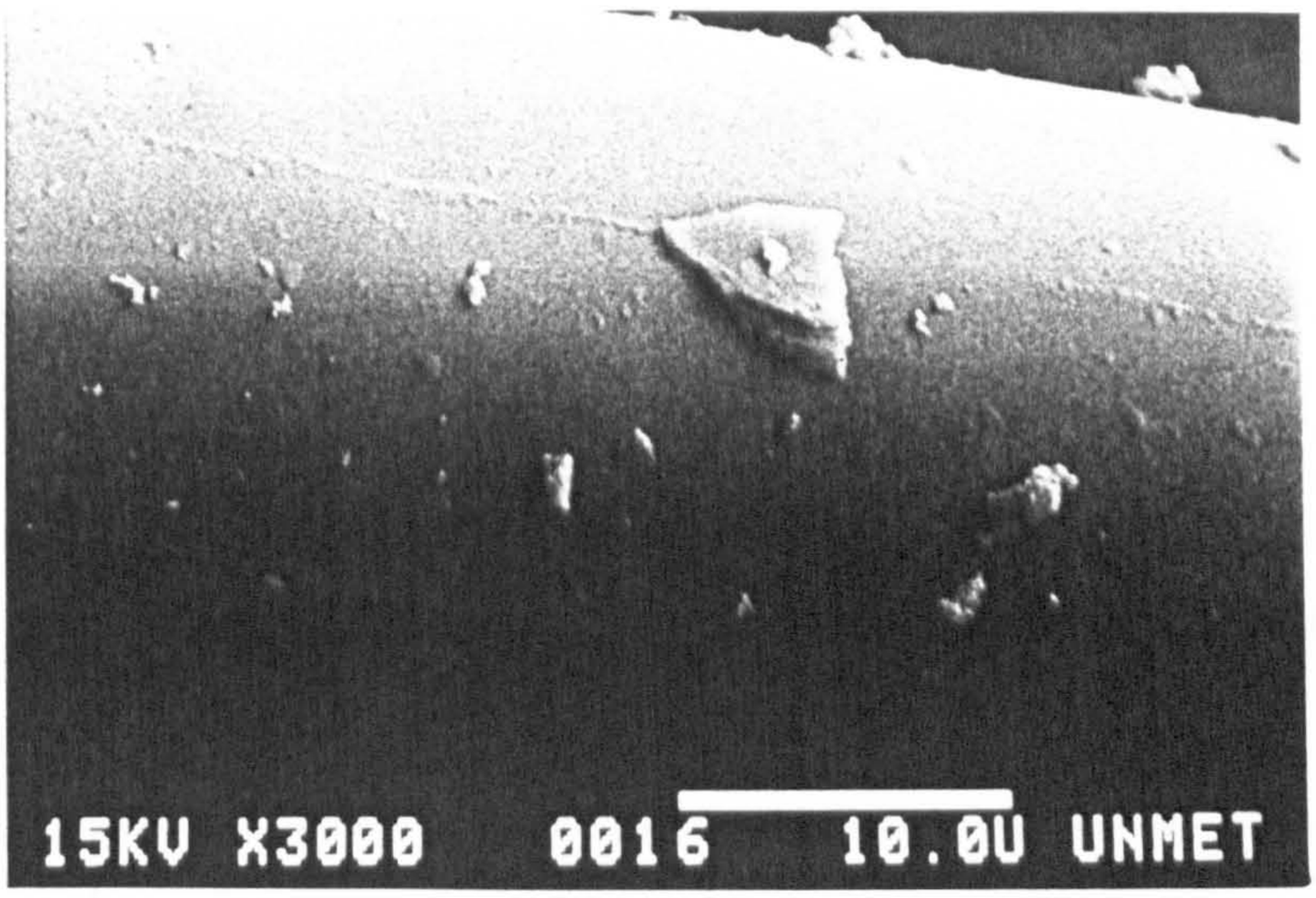

Figure 6.20a Fibre fracture surfaces from a unidirectionally reinforced, polyester moulding. The line along the fibre is thought to be size present on the fibres after an approximate 3 minute wet out period.

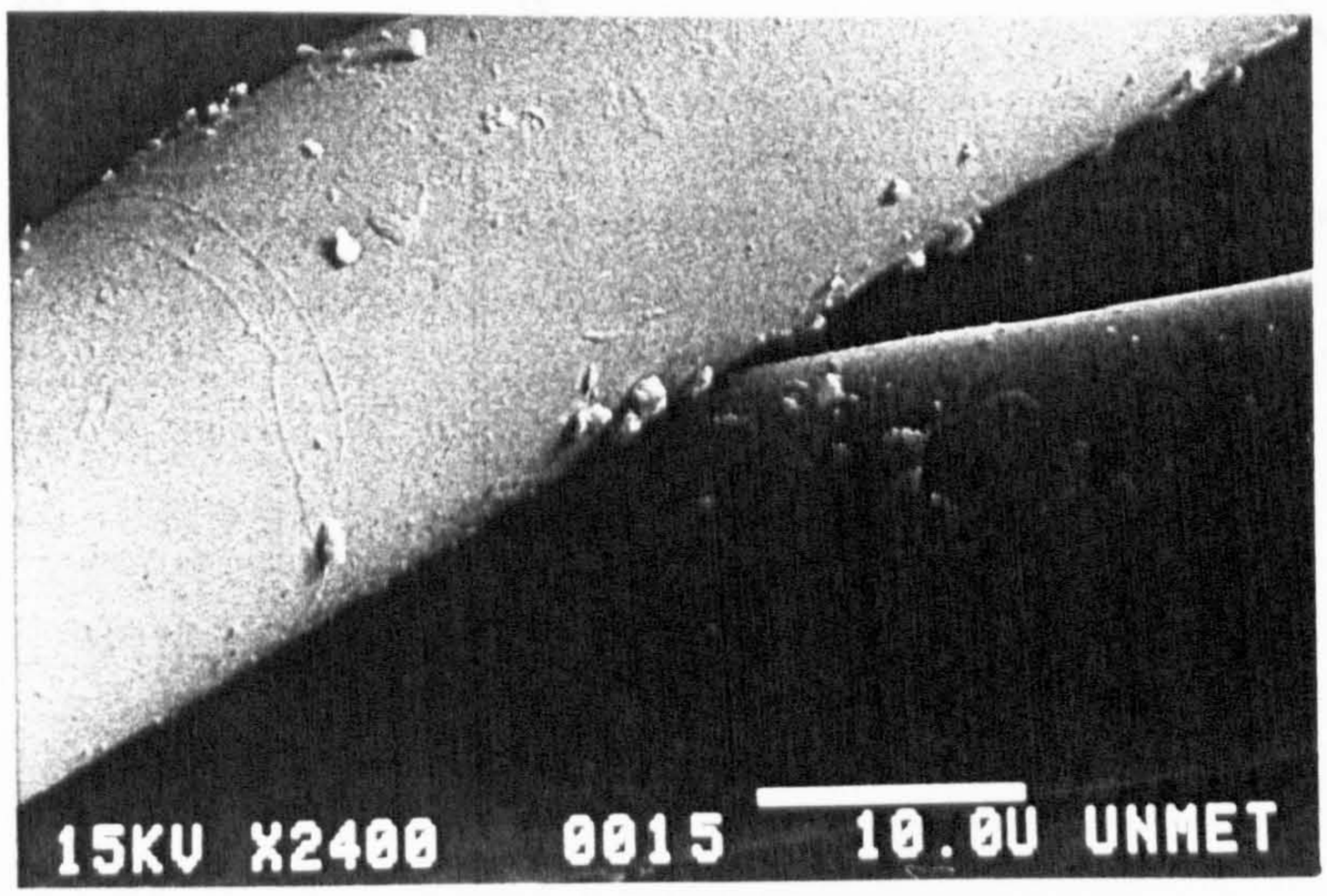

Figure 6.20b Deposition on fibre fracture surfaces from a unidirectionally reinforced, polyester moulding produced after a short wet out period.

Figure 6.21

Principal Permeability Vs Fibre Volume Fraction

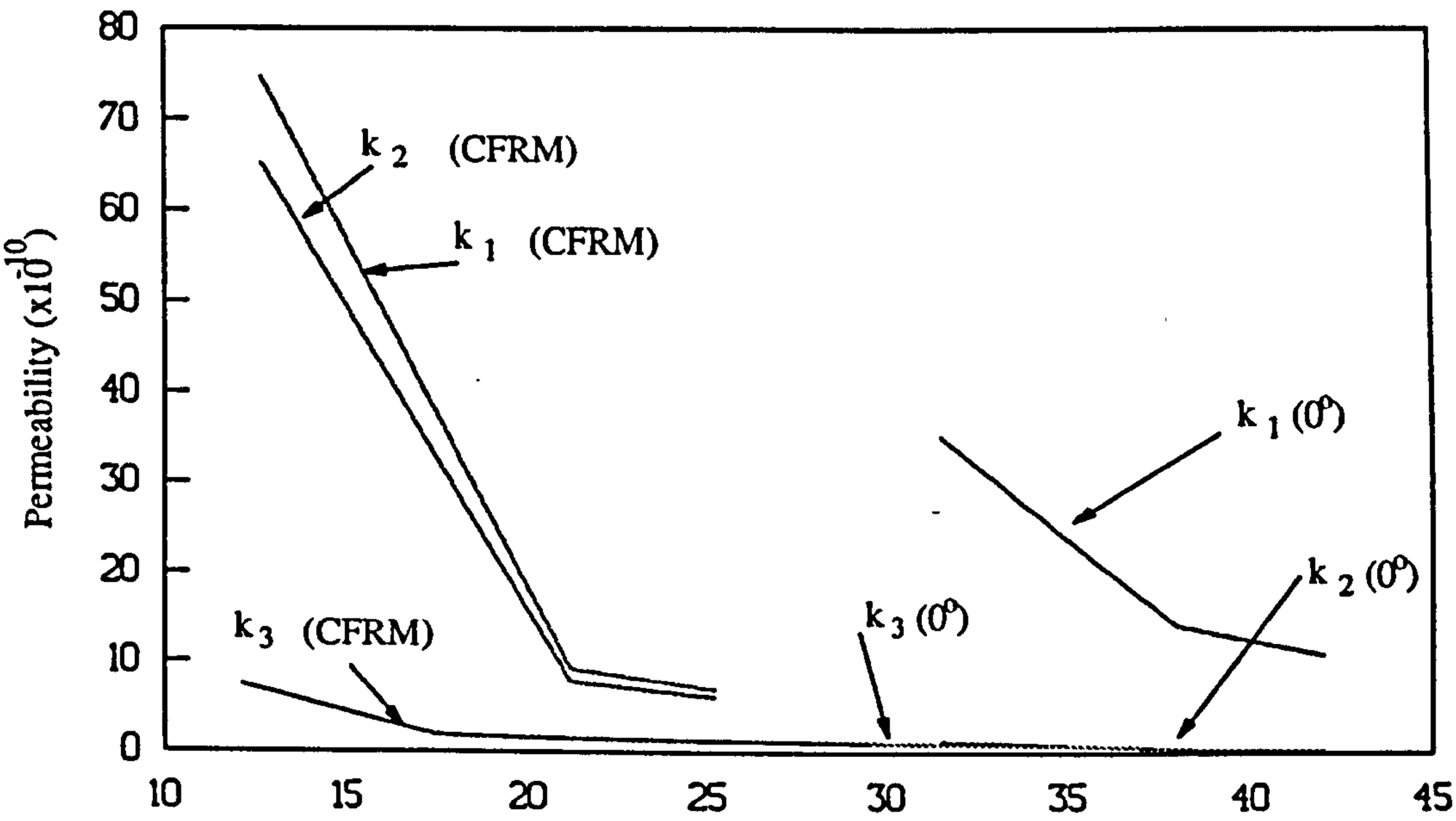

CFRM - Unifilo Continuous filament random mat (U750-450)

0°- Tech Textiles Non Crimp Fabric (ELPb-567)

Figure 6.22(a)

Multilayer Flow Simulation. A Low Permeability Layer Sandwiched by High Permeability Layers

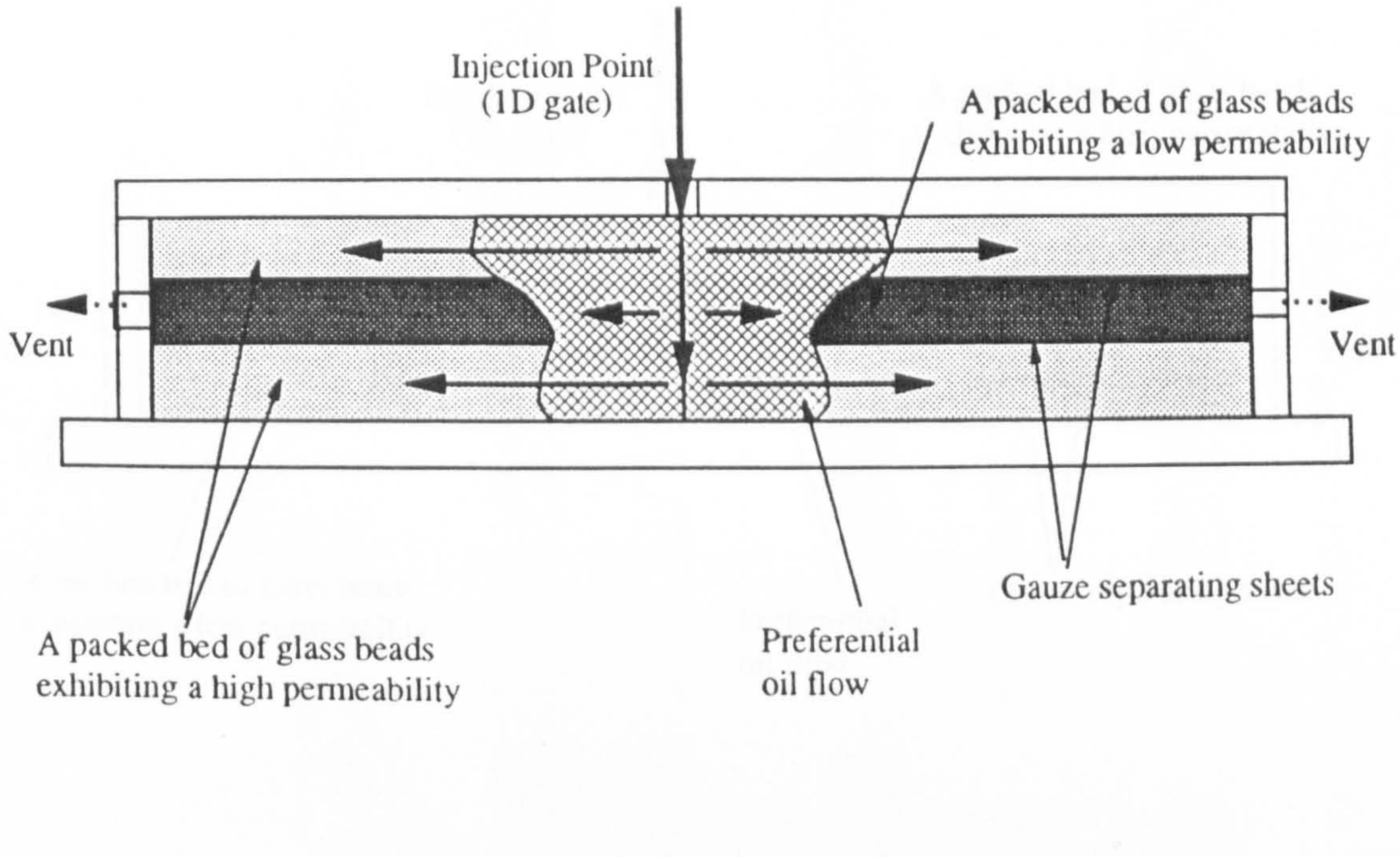

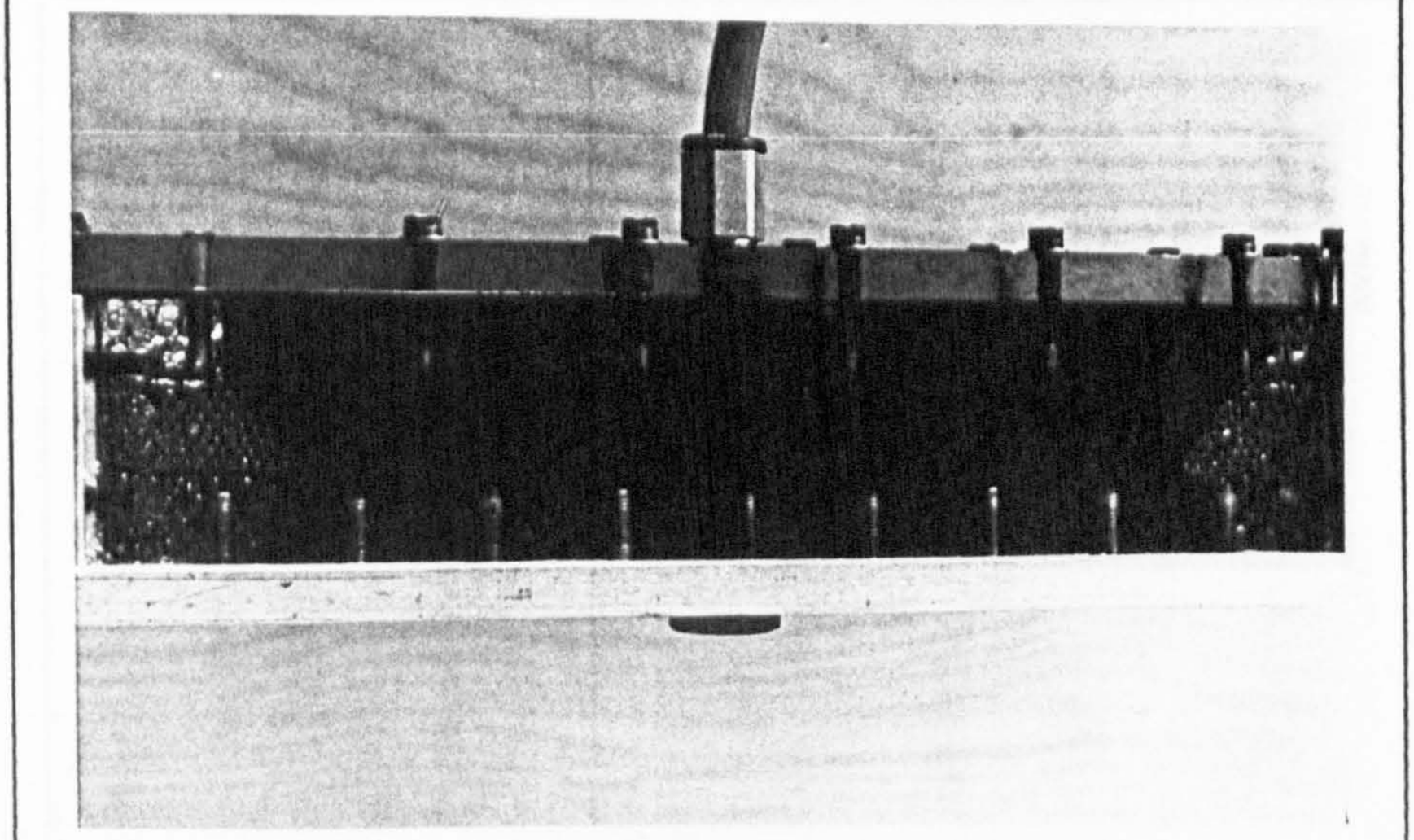

Figure 6.22(b)

Multilayer Flow Simulation. A High Permeability Layer Sandwiched by Low Permeability Layers

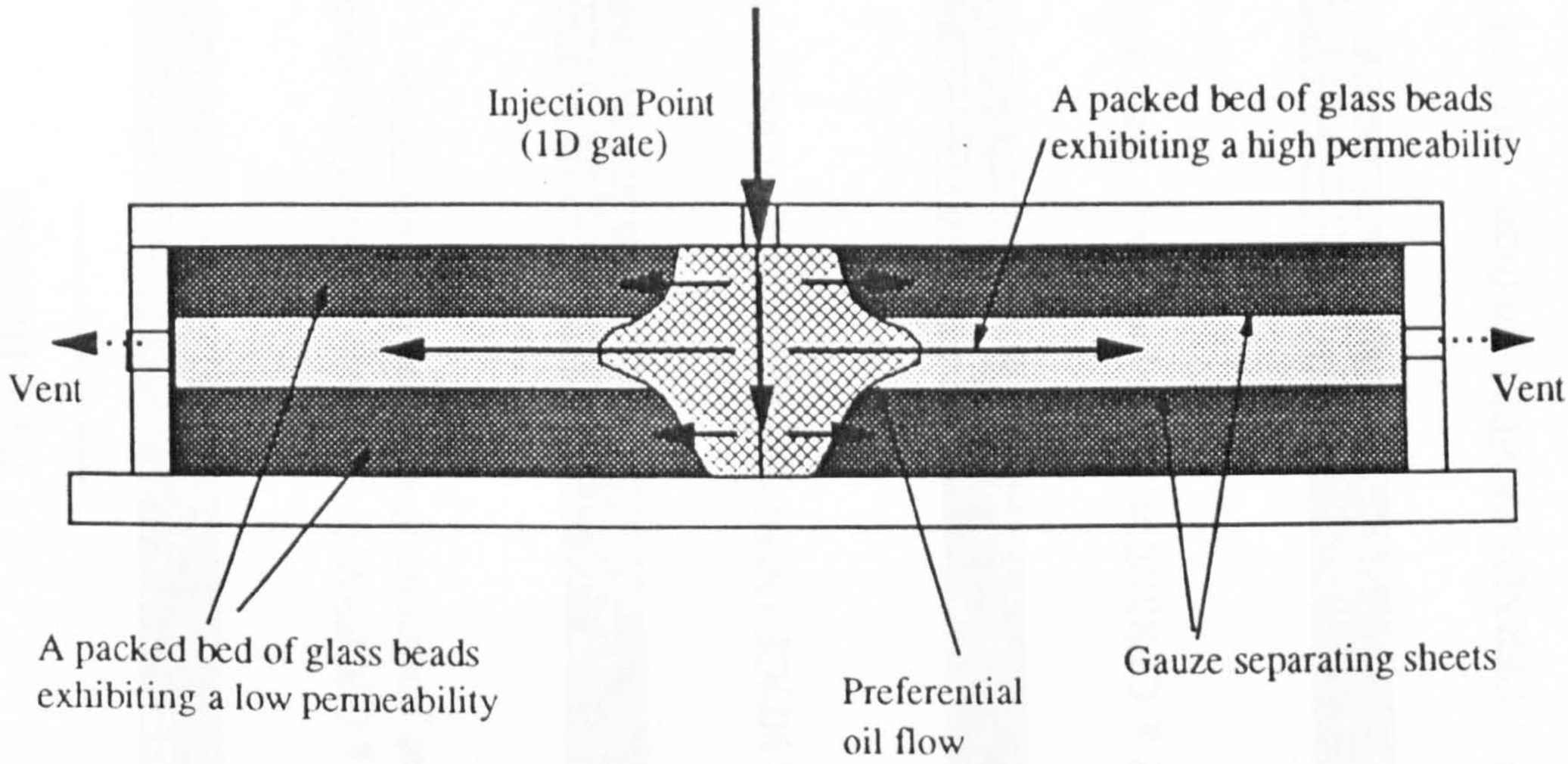

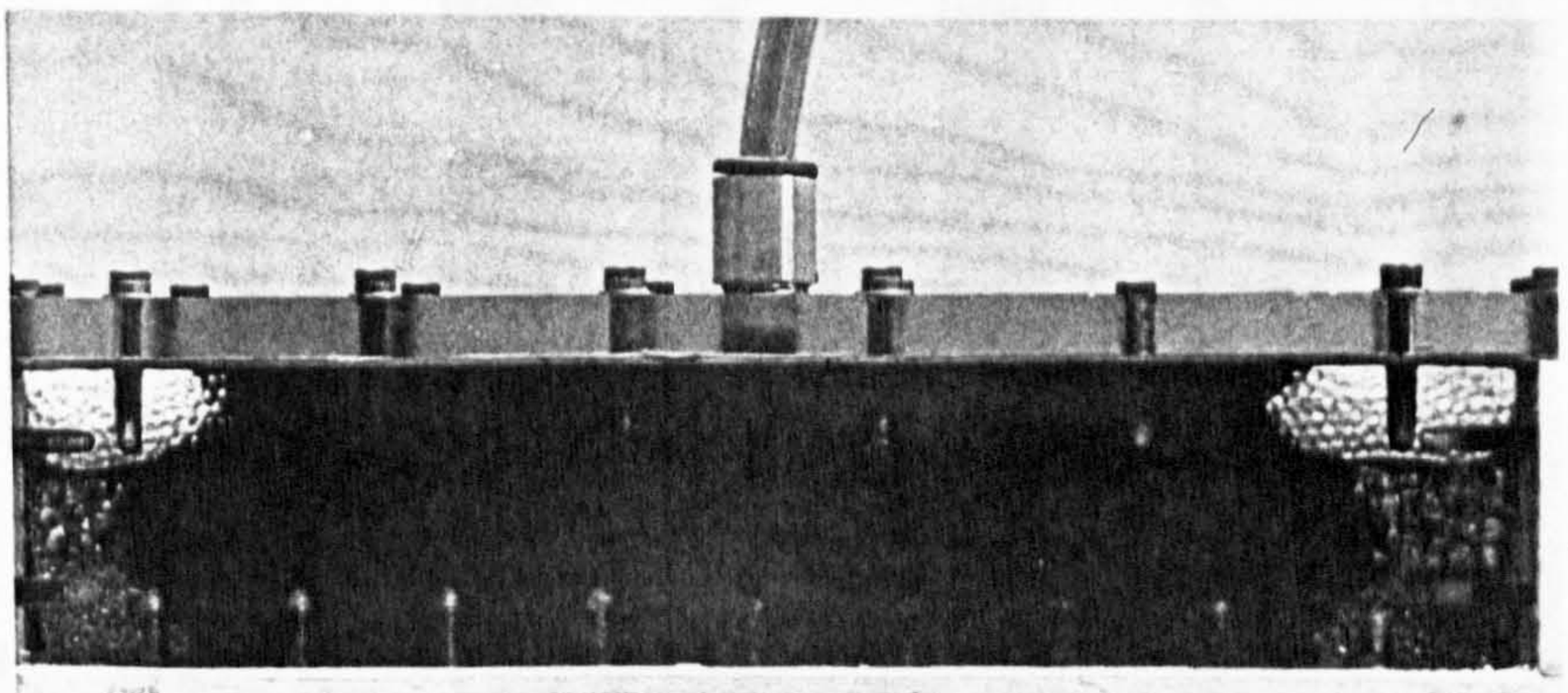

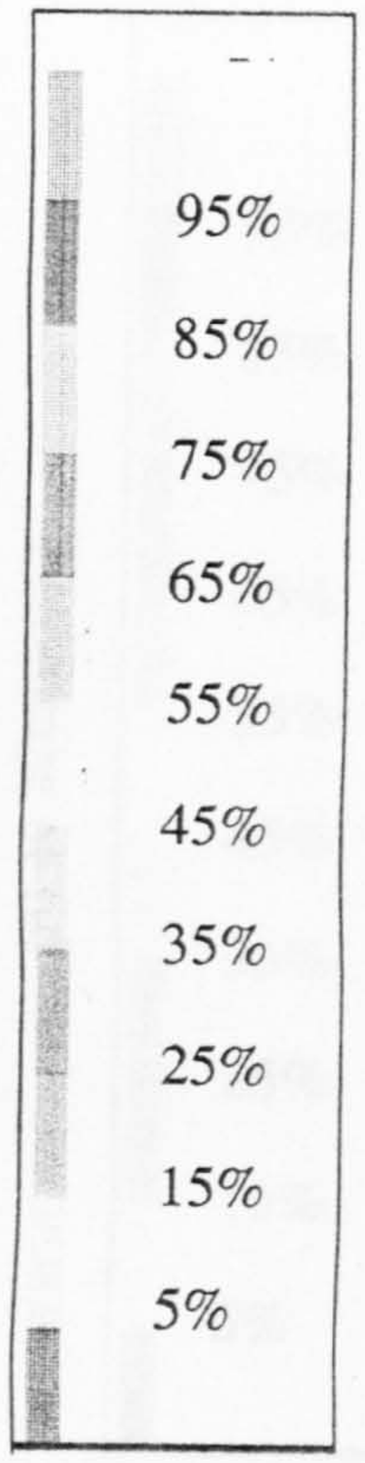

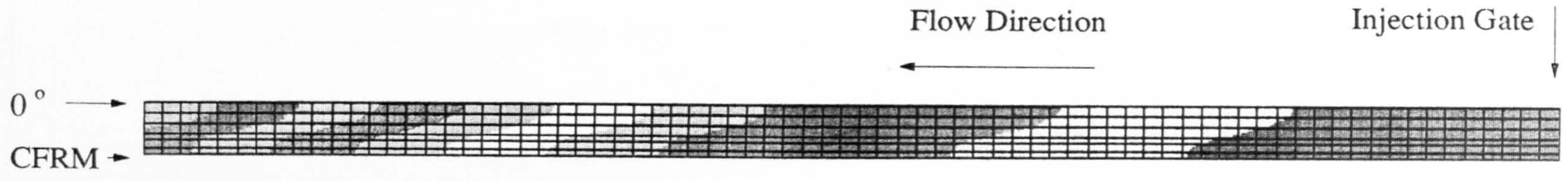

Figure 6.23(a) Resin impregnation into 50mm of a 0°/CFRM/0° preform. Half of the preform section is shown. The shaded areas indicate flow front positions at discrete time intervals.

Figure 6.23(b) Resin impregnation into 50mm of a 90°/CFRM/90° preform. Half of the preform section is shown.

Figure 6.23(c) Resin impregnation into 50mm of a CFRM/0°/CFRM preform. Half of the preform section is shown.

Figure 6.23(d) Resin impregnation into 50mm of a CFRM/90°/CFRM preform. Half of the preform section is shown.

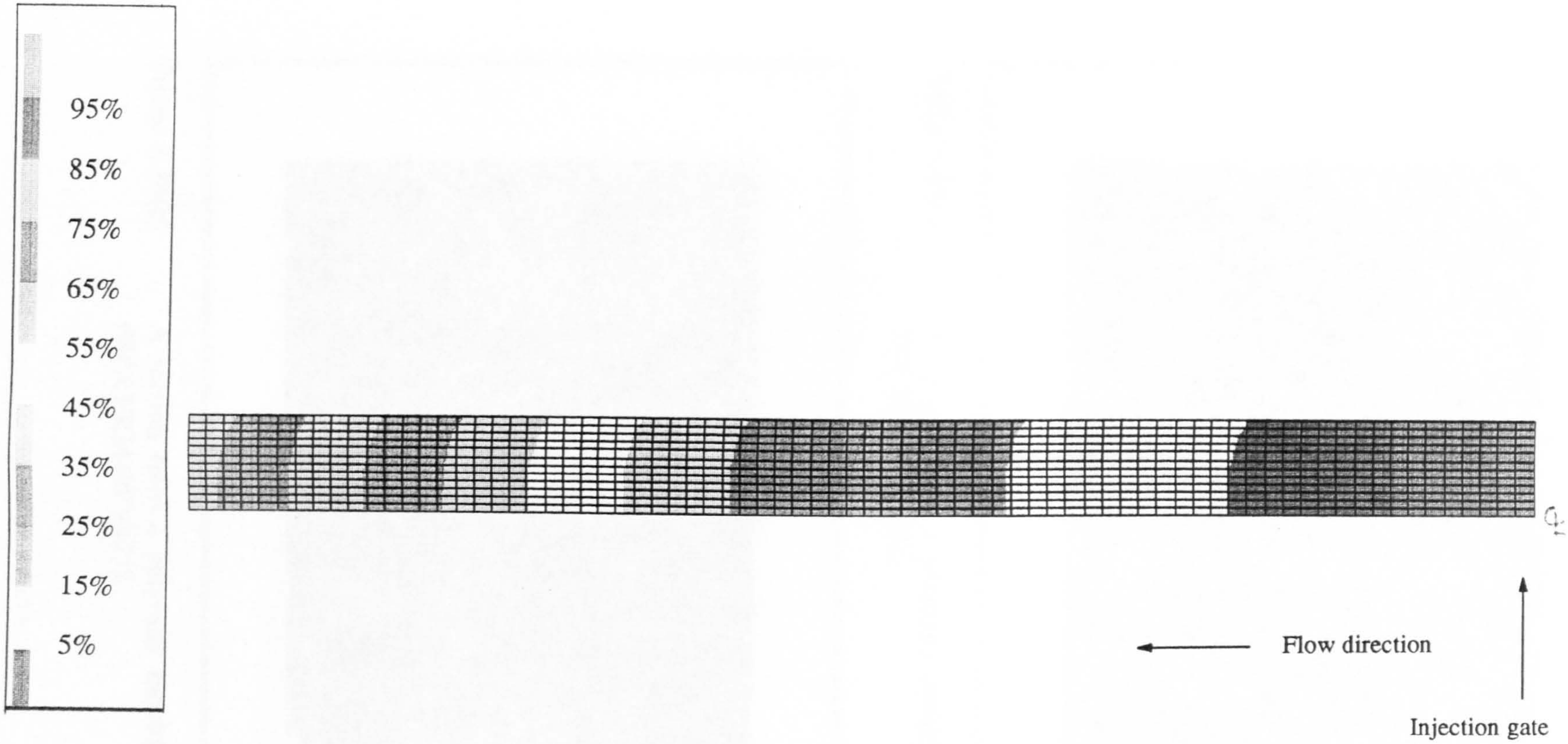

Figure 6.23(e) Resin impregnation into 50mm of a 0°/90° preform. The whole preform section is shown. The shaded areas indicate flow regimes at discrete time intervals.

Figure 6.24(a) A section from a polyester moulding using preform stack A (0°/CFRM/0°)(x25).

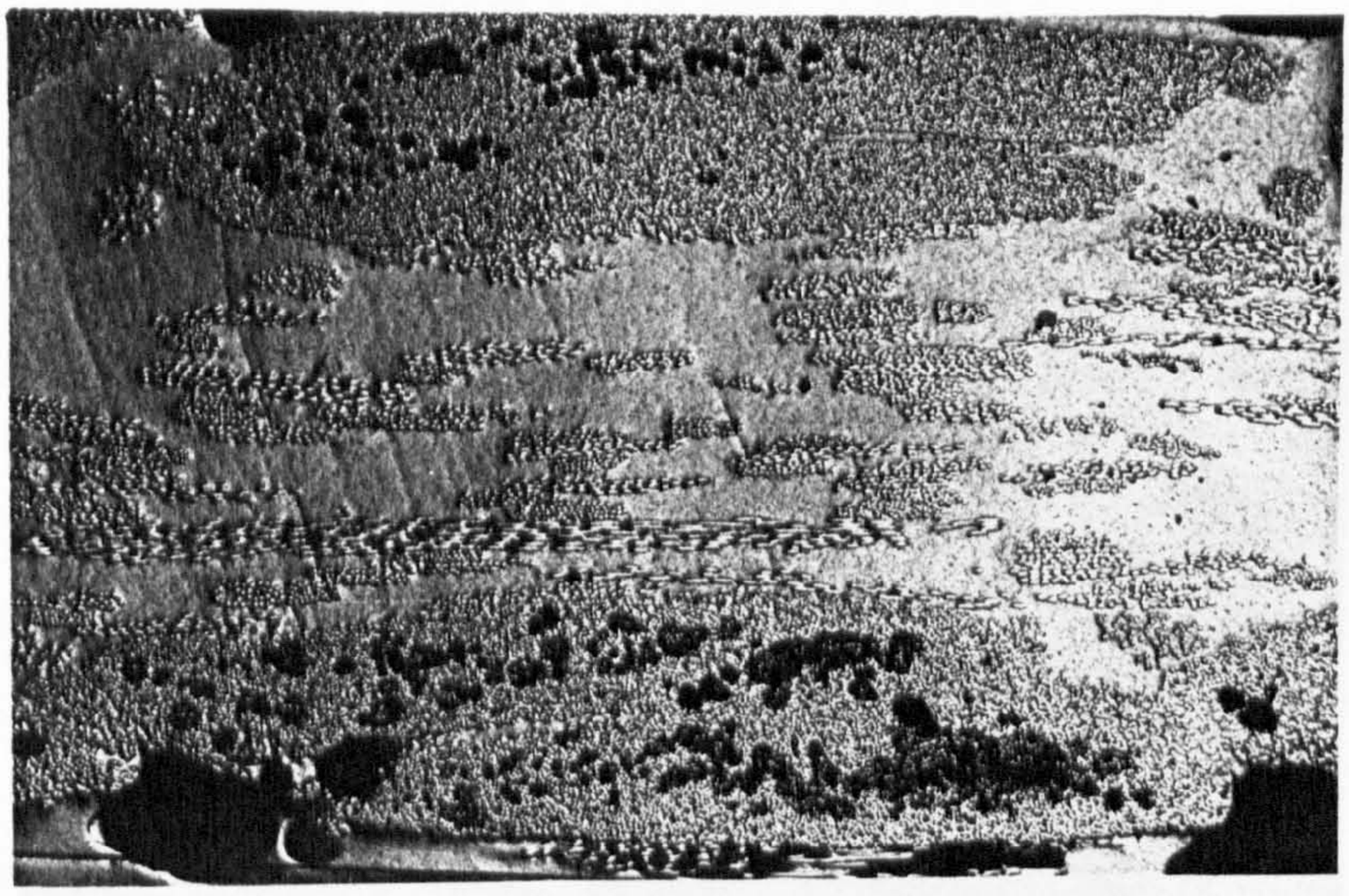

Figure 6.24(b) A section from a polyester moulding using preform stack B (90°/CFRM/90°)(x25).

Figure 6.24(c) A section from a polyester moulding using preform stack C (CFRM/0°/CFRM)(x25).

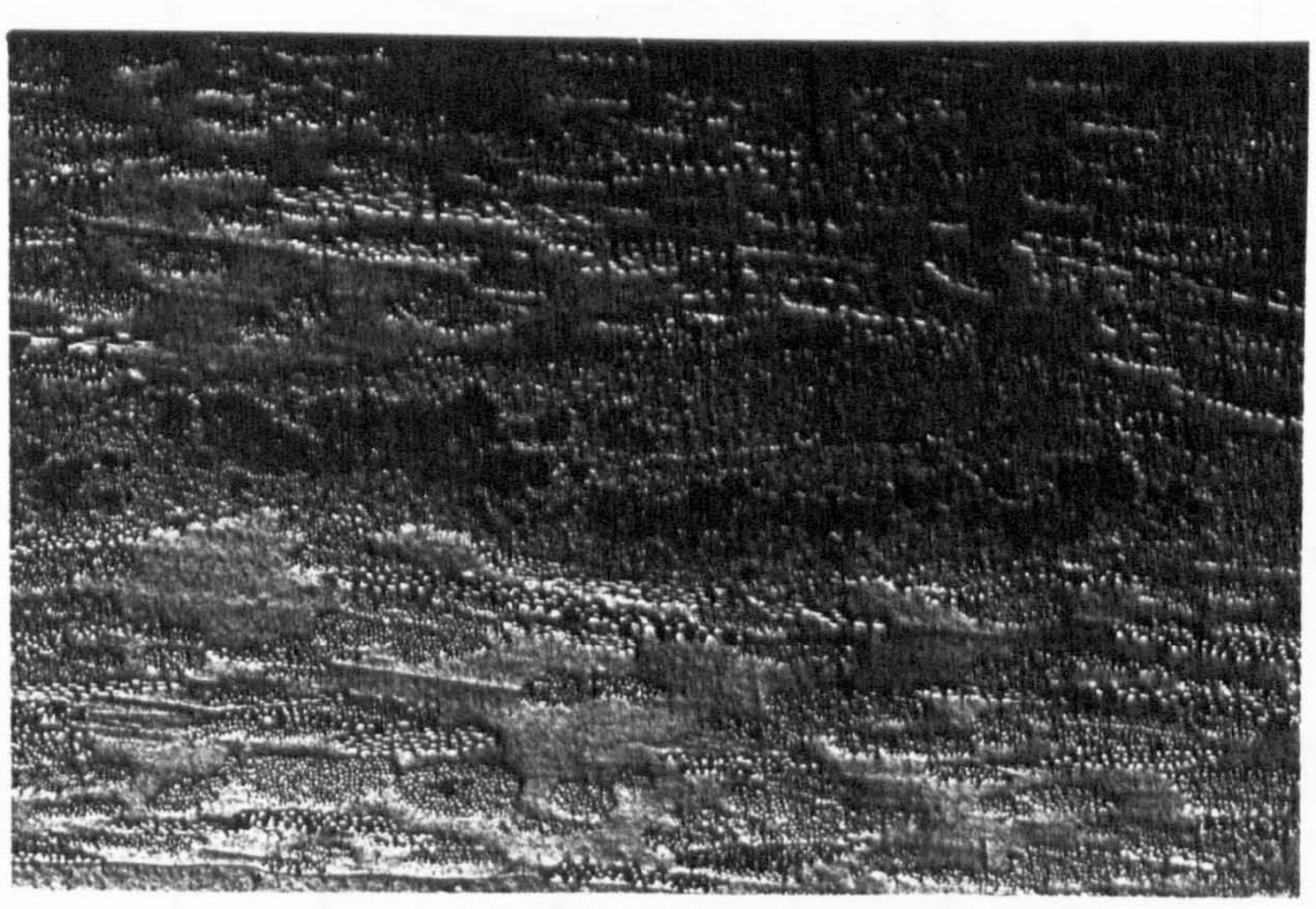

Figure 6.24(d) A section from a polyester moulding using preform stack D (CFRM/90°/CFRM)(x25).

Figure 6.25

Section Analysis Areas for Centrally Injected Bidirectional and Unidirectional Mouldings

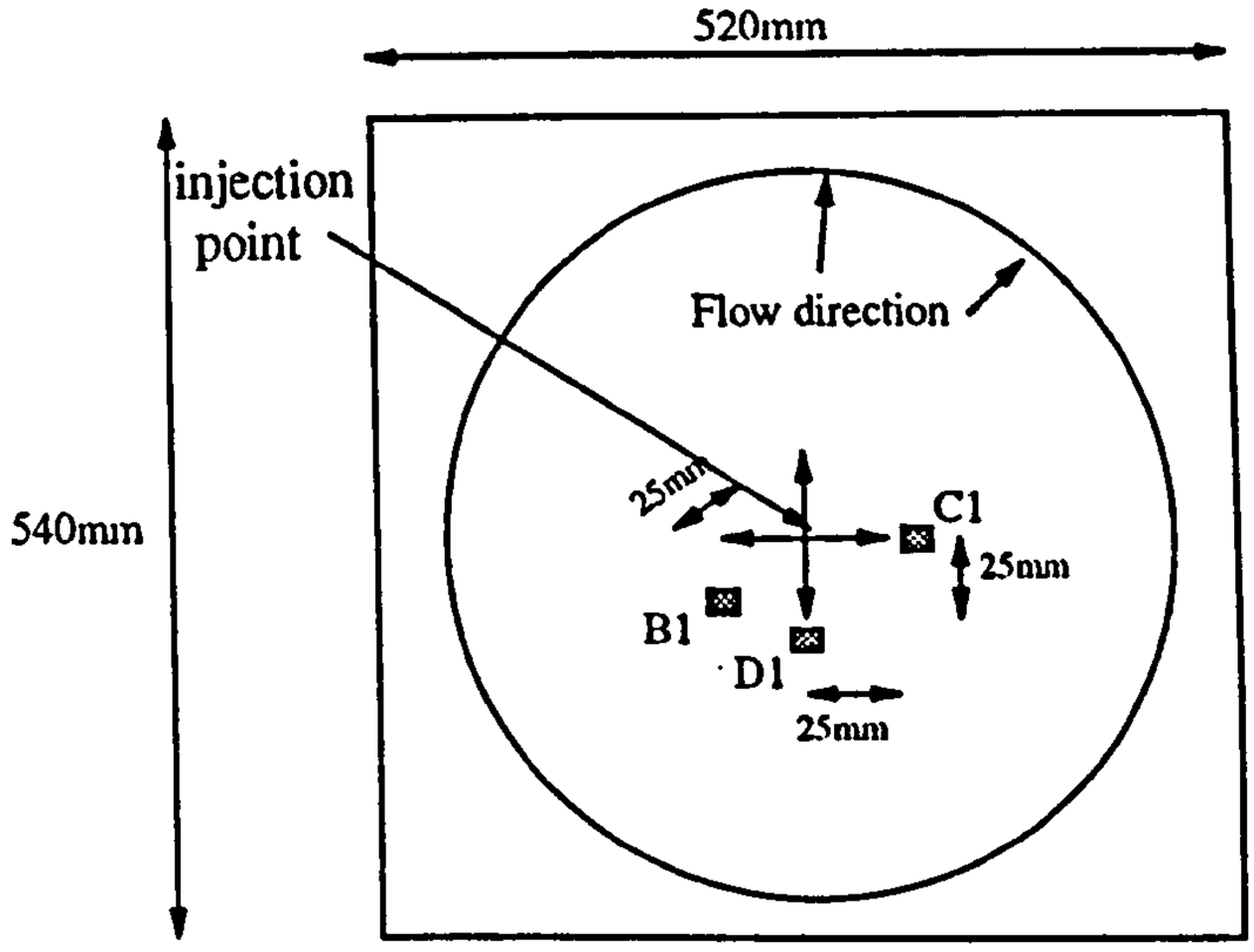

A) 0/90 Preform, Centre Injection

(moulding 4263)

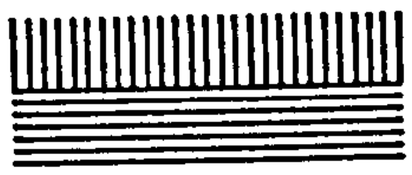

0 (2 layers)

90 (2 layers)

Fibre Orientation

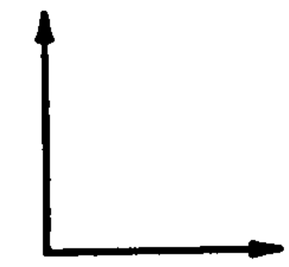

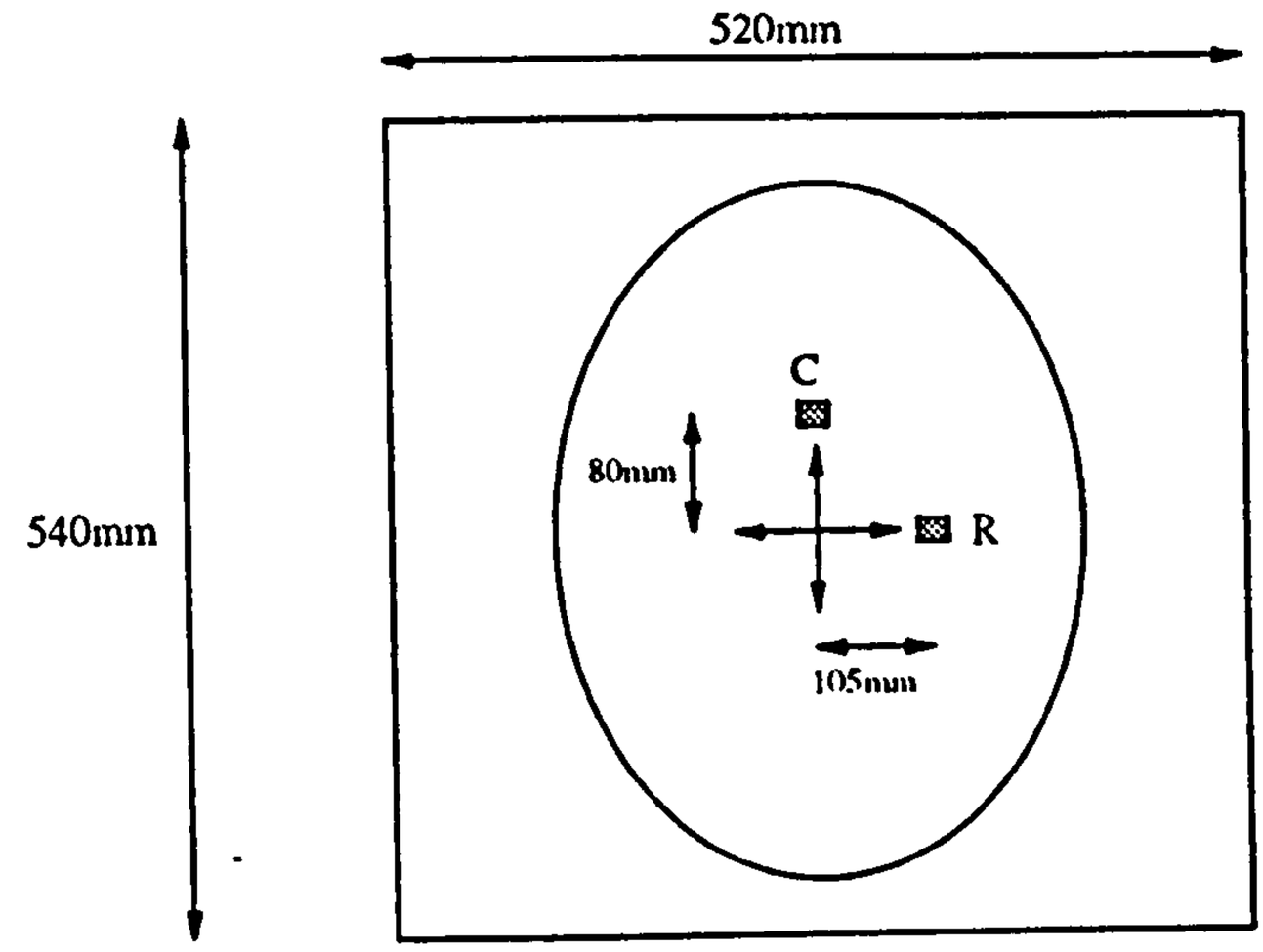

B) 0 Preform , Centre Injection

(moulding 4261)

0 (4 layers)

Fibre Orientation

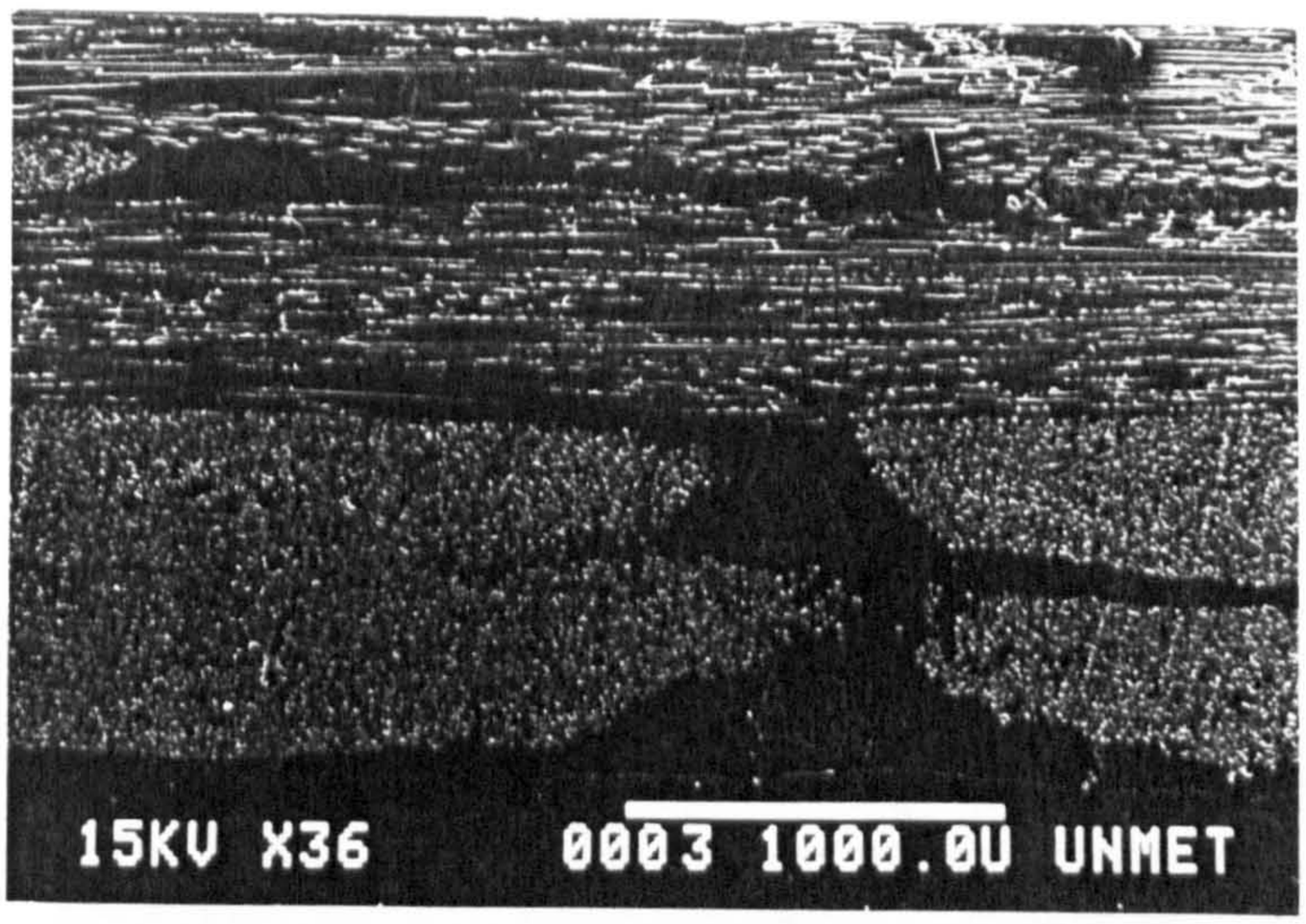

Figure 6.26a:
A section of the area C1 from Figure 6.25(a). The cross section shows the 0° fibres in the upper half of the picture and the 90° fibres in the lower half. Notice the microvoids within the fibre bundles of this 90°/0° laminate.

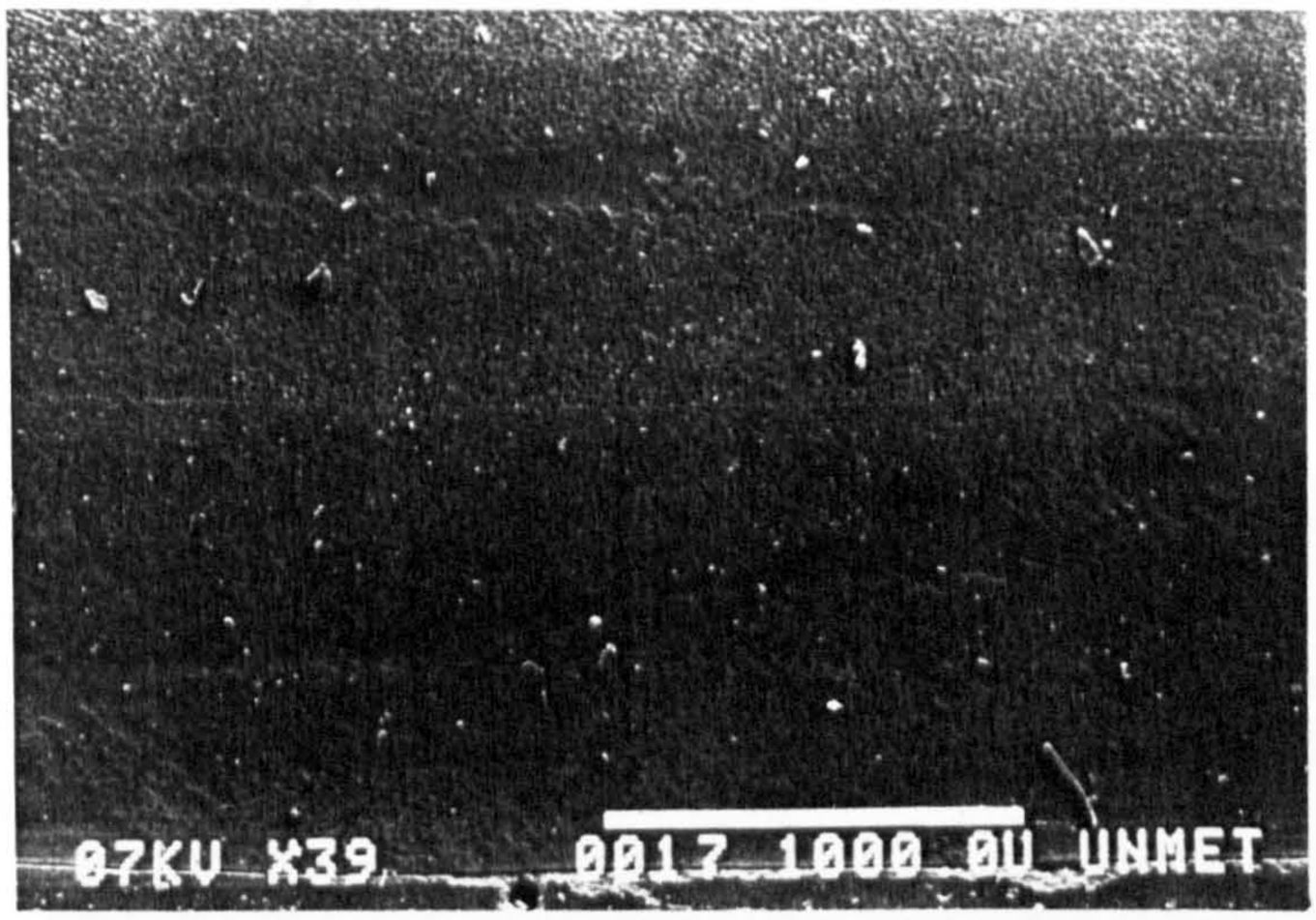

Figure 6.26b:
A section of the area B1 from Figure 6.25(a). The cross section shows the fibres cut at 45° to the x axis, no voids are evident in this section.

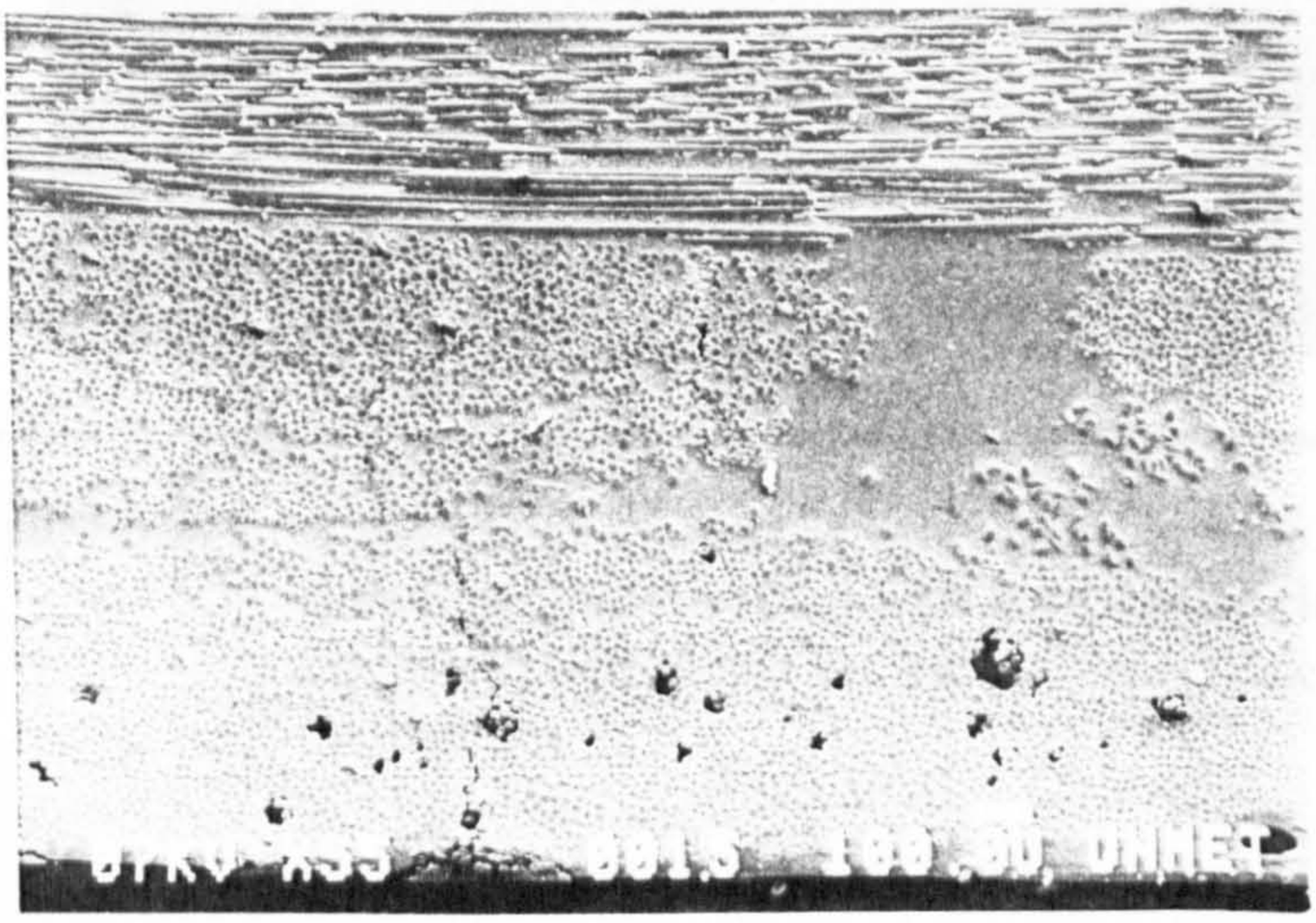

Figure 6.26c:
A section of the area D1 from Figure 6.25(a). The cross section shows the 0° layers in the upper half of the picture and the 90° fibres in the lower half. Extensive voidage can be seen in the 90° fibres near the component surface.

Figure 6.27a A section of the area C, shown in Figure 6.25(b). The fibre bundles of this 0° laminate which has filled during axial flow from the injection point are well wetted with few voids.

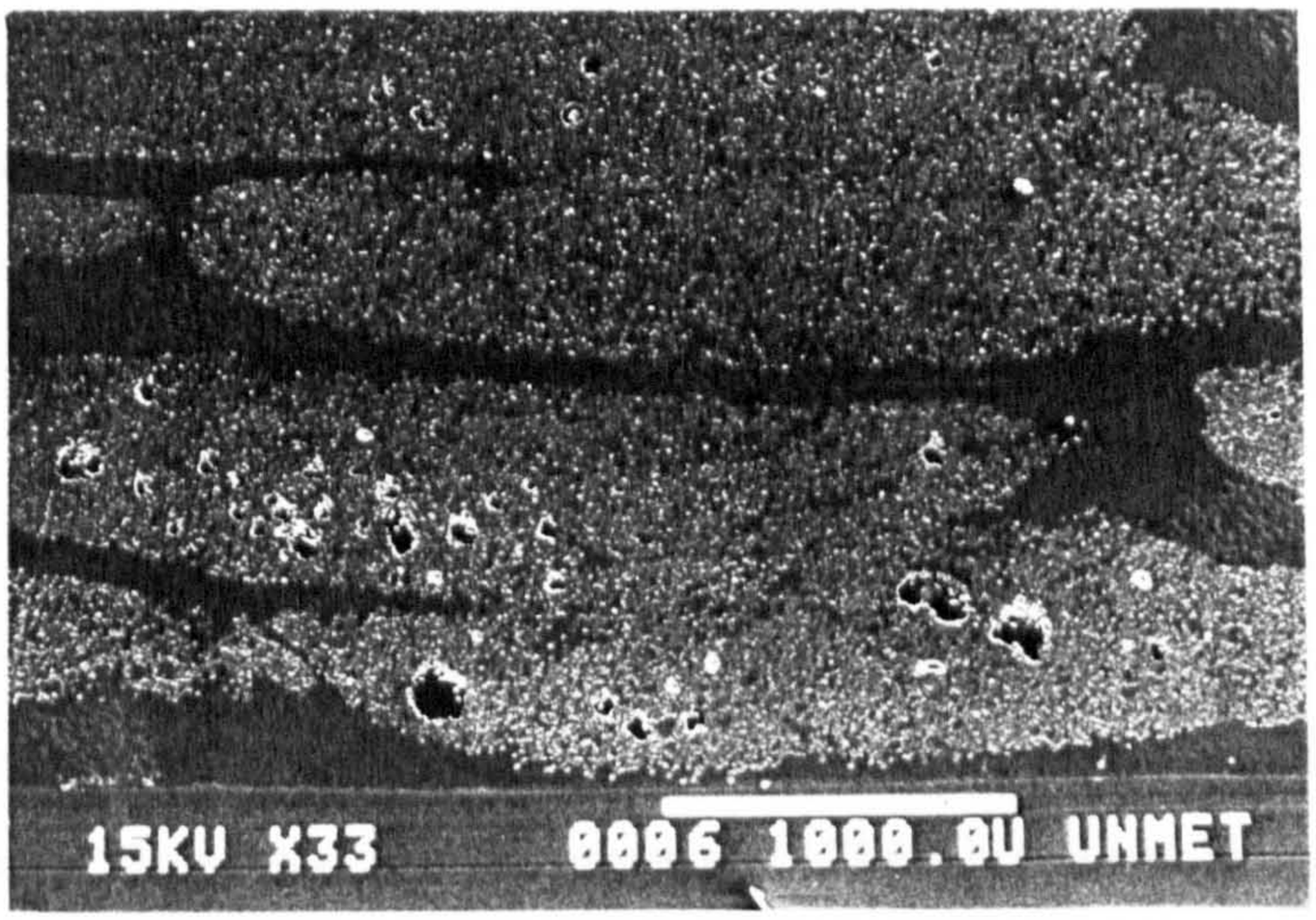

Figure 6.27b A section of the area R, shown in Figure 6.25(b). The fibre bundles have filled with a transverse flow from the injection point, voids are easily discernable throughout the bundles.

Chapter 7

Voidage During Filament Winding

7.1 Introduction

The filament winding process was investigated to study the penetration of resin into fibre bundles using similar impregnation speeds to those used in RTM. The filament winding process is a structural composite processing route which can produce components using similar materials with comparable fibre volume fractions to RTM. Filament wound components suffer the same internal defects as those produced by RTM[65]. A major factor affecting the quality of filament wound components is voidage, others being poorly distributed fibre and filamentisation[65]. Filament winding is mainly used as a manufacturing route for load bearing cylinders and pressure vessels. High void contents in these components will cause a reduction in their mechanical properties, as has been discussed in section 2.5. This work was directed at identifying the mechanisms causing void formation during the filament winding process and comparing these mechanisms to those previously discussed in Chapter 6.

RTM and filament winding use similar axial impregnation speeds (generally between 10mm and 150mm per second). The transverse impregnation of the fibre bundles is also a problem which links the two processes. E-glass is the predominant type of fibre used in both processes. The fibres used in filament winding are coated with the same size systems as those examined in Chapter 6, such that the size deposition on and between the fibres is likely to affect impregnation.

A Pultrex 5 axis filament winding machine was used to produce five filament wound cylinders. These cylinders have been used to study the formation and location of voids in filament wound components. The first four cylinders were manufactured using the standard fibre impregnation system described in section 3.5, with variations in the rotational speed of the mandrel and the amount of resin available to wet the

fibres. The final winding was made using an impregnation system with a partial vacuum to help the resin to penetrate the fibre bundle (Figure 3.7). The standard winding mechanism allowed three major variations in the process once the programme to position the fibres had been set; these being the position of the doctor blade, the tension on the fibre, and the speed of the fibre passing through the resin bath. Table 7.1 describes the conditions for each winding. The void content for these windings was assessed by burn-off determination and section analysis in both the hoop and axial directions. A length of impregnated strand was cured and examined after each winding, to assess its internal voidage. Finally the filament winding apparatus was assessed to determine the stages of the process in which voids form both in the strand and in the component.

7.2 Void Analysis

Fibre structure

The glass fibres used in the filament winding programme were studied for deposits of size in an SEM. A dried meniscus of size was evident on the majority of the fibres studied. This meniscus is shown in Figure 7.1. Filamentised fibres exhibited size fracture surfaces along their length, which can be seen as a line along the fibres shown in Figure 7.2.

Impregnated strands studied under transmitted light

After each winding a length of impregnated fibre strand was removed from between the component and the impregnation mechanism, cured and sections cut from the length. Figures 7.3a - 7.3d show magnified images of these strands taken from windings 1 - 4 respectively. The strands were photographed using light transmitted through the translucent composite. The cylindrical, darker shapes are voids within the fibre bundle structure.

The strands in Figures 7.3a & b were impregnated at 158mm/s. Long cylindrical voids are evident between the fibres. Figures 7.3c & d show strands after a slow impregnation (29mm/s). Small spherical voids are visible between the fibres. These observations indicate that air is entrapped due to the transverse filling of the

fibre bundle. The length of these voids appears to be dependant on the speed of impregnation.

Sections of impregnated strands

The strands impregnated with a fast impregnation speed (from windings 1 and 2), show large macrovoids (Figures 7.4a & b) when compared to those impregnated at slower speeds (Figures 7.4c & d). The two strands impregnated with the doctor blade set to 0.2mm (allowing a relatively thin film of resin on to the impregnation drum) shown in Figures 7.4b & c, exhibit higher void contents, especially microvoids, indicating that inadequate resin was available for impregnation.

Surfaces of impregnated strands

The surfaces of several of these impregnated strands were studied, to determine whether the strands were fully wetted. In several sections the outer layers of the roving were dry, as shown in Figure 7.5. This could be due to filamentisation, where broken fibres had fractured splitting from the bundle, or merely due to inadequate resin to completely wet the strand. There was little variation of this effect between windings.

Void content analysis

The filament wound cylinders were sectioned and polished as described in section 3.5. A schematic denoting the axial and hoop directions is shown in Figure 7.6. Void contents from samples of each cylinder were also determined by the burn-off method described in Appendix 4. Table 7.2 shows the void contents for each cylinder.

Cylinder 1 was wound using a high winding speed and with the resin layer available to impregnate the fibre set to 0.3mm (doctor blade setting). The void content of the composite was estimated at 2% by image analysis and 2.6% by burn-off. The sections shown in Figures 7.7a and 7.8b show this voidage to consist mainly of macrovoids both between the fibre bundles and within them, verifying the findings from the strand analysis.

The void content for the second cylinder, produced using a high winding speed and low doctor blade setting (0.2mm), was estimated at 3.4% by image analysis and 5.6% by burn-off. Hoop and axial sections from this winding are shown in Figures 7.7b and 7.8b. Numerous microvoids are evident within the fibre bundles, with macrovoids present between these bundles.

The third cylinder was wound using a slow winding speed, and low doctor blade setting (0.2mm). The void content in the composite was estimated at 2.3% by image analysis and 4.5% by burn-off. Microvoids are evident in the fibre bundles with macrovoids between them in Figures 7.7c and 7.8c.

Cylinder 4 was produced using a slow winding speed and a higher doctor blade setting (0.3mm). Void contents of 2.2% and 4.5% were determined from image analysis and burn-off respectively. Figure 7.7d and 7.8d show hoop and axial sections from the cylinder. The majority of voids evident are macrovoids between layers of strands.

The burn-off determinations indicate similar trends as from the section estimations, although the values are always higher (Table 7.2). The highest void contents were determined from the two cylinders produced using a low doctor blade setting (0.2mm). This setting permitted the impregnation drum to be coated with a thin layer of resin which was inadequate to fully wet the strand. The lowest void content was determined from the cylinder produced with a high winding speed and a thick layer of resin available to wet the strand. This low void content concurs with the strand analysis, where macrovoids were evident in both strand and component sections.

These studies have indicated that the voids formed within the strands during impregnation are wound on to the component. No further wetting seems to occur, as the voids appear to remain within the fibre bundles and form in the final composite.

7.3 Quality Issues

The most common defect encountered in the filament wound components studied was the presence of voids. The voids in the filament windings analysed were of two types, macrovoids between layers of rovings and in resin rich areas of the winding (Figures 7.9,7.10), or microvoids between individual fibres within the fibre bundle structure (Figure 7.11). Study of Figures 7.9 and 7.11 shows smooth resin faces within the void, whereas the internal surface of the void shown in Figure 7.10 shows a rougher surface which resembles the size deposition and menisci already examined in Figures 7.1, 7.2 and in section 6.2.

7.4 Void Formation Mechanisms

From visual inspection of the process there are several main stages in which air was trapped in the composite structure:

i) The resin bath and impregnation drum.

As the impregnation wheel rotated in the resin bath, air was mixed into the resin and a foam produced at the surface. This foam on the resin was transferred onto the impregnation drum as it rotated through the bath (Figure 7.12). Most of the larger bubbles in the resin were removed from the face of the wheel by the doctor blade, but some were able to pass under it.

ii) Resin impregnation into the fibre.

The resin had only a limited period to penetrate the fibre bundle (between 1 and 3 seconds depending on mandrel speed). Nearly all of this penetration was through transverse resin flow into the fibre strand. The overhead resin wheel helped to force the resin into the fibre as it passed over the impregnation drum, but the tape like roving exhibited dry areas as it passed over the drum.

iii) After the impregnation drum between overhead wheel and resin combs.

The roving changed shape several times between the resin impregnation drum and the first of the location guides. A schematic diagram of the cross

section of the tow as it passed from the impregnation drum towards the mandrel is shown in Figure 7.12. As the roving changed shape, the fibres slipped over each other, causing air to be entrapped in the section.

iv) Location guides and Payout eye.

As the strand was passed through the several location guides and finally the payout eye, resin was scraped from the strand and collected on the guides or eye. This resin foamed as the strand passed through it, allowing the foam to collect on the strand surface.

v) Fibre laydown on the mandrel.

As the strand was wound on to the mandrel, air entrapment took place between opposing layers of fibre. This occurred as the taut fibre was laid down onto an uneven surface. Macrovoids formed where fibre bridging occurred.

7.5 Vacuum Assisted Impregnation of the Fibre Bundles

In order to reduce the voidage in the strand prior to winding, it was postulated that if the strand was placed in a vacuum and passed into a resin bath, a reduction in the void content of the strand would ensue (described in section 3.5). This system worked effectively until the rubber seals began to wear and resin leaked into the vacuum tube. Resin was eventually drawn into the vacuum line and at this point the winding operation ceased. The system could be improved with the use of better seals and a method of controlling the amount of resin on the strand.

Impregnated strands

A transmitted light photograph of an impregnated strand produced by this process is shown in Figure 7.13. Voids are still apparent between fibres, but are smaller and less numerous than those observed in Figures 7.3a - d. A section of one of these strands is shown in Figure 7.14. Several macrovoids are evident but the void content appears to be lower than the sections already discussed in section 7.3.

Composite sections

A hoop section of the winding produced is shown in Figure 7.15. This section shows lower voidage (estimated at 2%, with the burn-off determination at 2.6%) compared with the sections shown in Figures 7.7a to 7.7d. The composite was however, resin rich (48% fibre volume fraction) in comparison to the other windings considered where the fibre volume fractions ranged between 50.7% and 60.1%. This lower fibre volume fraction was due to the impregnation mechanism having no control over the amount of resin applied to the fibres.

7.6 Discussion

Other researchers have studied the impregnation mechanisms used in filament winding[45,62]. Voids in the strands after the impregnation process were noted by these researchers but not examined. The effects of voids upon the mechanical properties were researched although the conditions which produced the voids were not investigated. Windings have been produced in a vacuum environment[62], but no mention of a vacuum impregnation mechanism for the strand as it passes through a resin bath has been made.

Study of the glass fibres used in these filament winding experiments has shown that the fibre bundles exhibit a meniscus of film former or size between individual filaments. If this meniscus is intact during the impregnation phase the resin may be restricted from completely wetting the fibres and microvoids between individual filaments will form in the final winding.

The examination of voids within the impregnated fibre strands revealed that under high impregnation speeds the rovings produced a few long cylindrical voids, whilst under low speeds, numerous small spherical voids were generated. Study of the cross sections of the impregnated strands verified these findings, with those produced using high speed impregnation exhibiting large voids in the cross sections, and those produced at slow speeds demonstrating smaller microvoids in the cross section. Reducing of the doctor blade setting showed an increase in voids in the strands, since less resin was available to wet the fibres.

The void fraction analyses confirmed that the void content increased with reduction in the doctor blade setting. Fibre volume fractions were lower with a high winding speed compared to the slower cases. This fraction is also likely to be affected by the tension applied to the fibres. The cylinder with the lowest void volume fraction also had the lowest fibre volume fraction in the studies. The hoop sections examined under the SEM showed that the cylinders produced with the smaller doctor blade settings generally produced microvoids in the composite, whilst sections produced using the higher blade settings exhibited larger voids. Axial sections confirmed these observations. The results from the cylinder produced using vacuum assisted impregnation indicated that the void content in both the strand and the sections were reduced. A vacuum impregnation mechanism, if fully developed could help reduce the voids in the strands during impregnation. The results from burn-off determination and section estimation concur.

This study has shown that composite sections from components produced by filament winding exhibit voids in similar volumes and sizes to those observed in mouldings produced by RTM. Void contents in the filament wound sections determined by the burn-off method were high (between 2.6.% and 5.6.%) when compared with void fractions from unidirectional mouldings produced by RTM (between 1.2% and 2.9%)(Chapter 6).

These studies have assisted the understanding of resin impregnation into fibre bundles. The impregnation of bundles at different speeds has indicated how voids form and how the length of these voids are affected. Once the voids were formed in the strands, no further wet out occurred. These voids were wound on to the cylinders, indicating that the impregnation phase is the most important stage to void formation. This investigation has reemphasised the problem of fully impregnating fibre bundles. Resin impregnation into a tightly packed bundle of fibres held together by size, coupled with air removal from the spaces between the fibres is the main similarity between the voidage problem of RTM and filament winding. On the whole voidage in filament wound components seems to be more apparent than in RTM, although many of the mechanisms which cause the problem are inherent in both processes.

List of Tables

List of Figures

Table 7.1: Process details.

Component No.	Mandrel Rotational speed (rpm)	Fibre laydown speed (mm/s)	Doctor blade position (mm)	Fibre tensioning system (bar)
1	27	158	0.3	1
2	27	158	0.2	1
3	5	29.3	0.2	1
4	5	29.3	0.3	1
5	27	158	-	-

Table 7.2: The void determination results for the windings analysed.

Component No.	Fibre volume content (%)	Void content (Burn-off %)	Void content by scanning analysis (%)
1	50.7	2.59	2.0
2	56.5	5.61	3.4
3	60.1	4.53	2.3
4	60.1	4.45	2.2
5	48.7	2.56	2.0

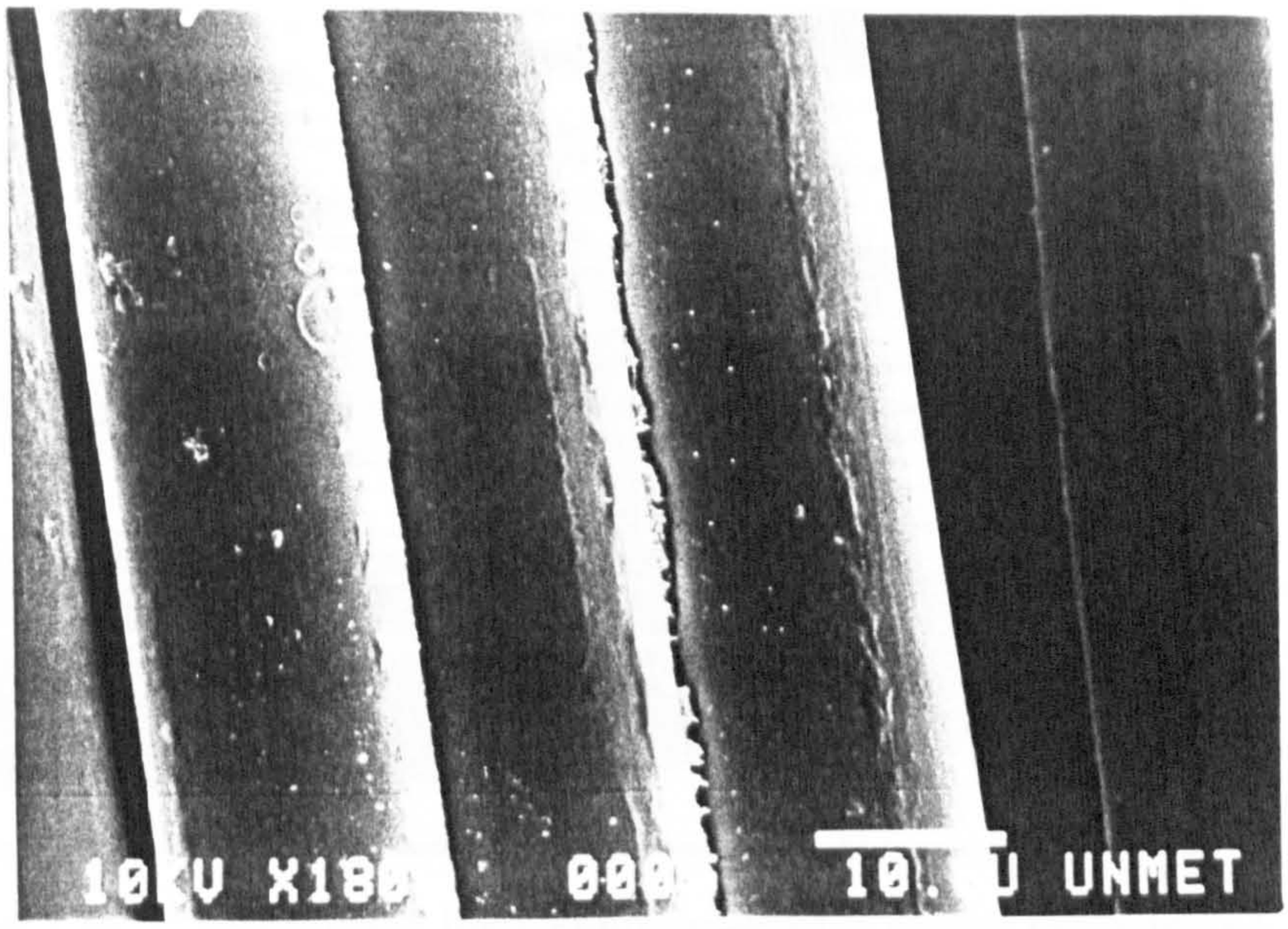

Figure 7.1 Silenka 2400 tex fibres used in the filament winding trials. Showing a meniscus between filaments, and the areas of poorly distributed film former and size.

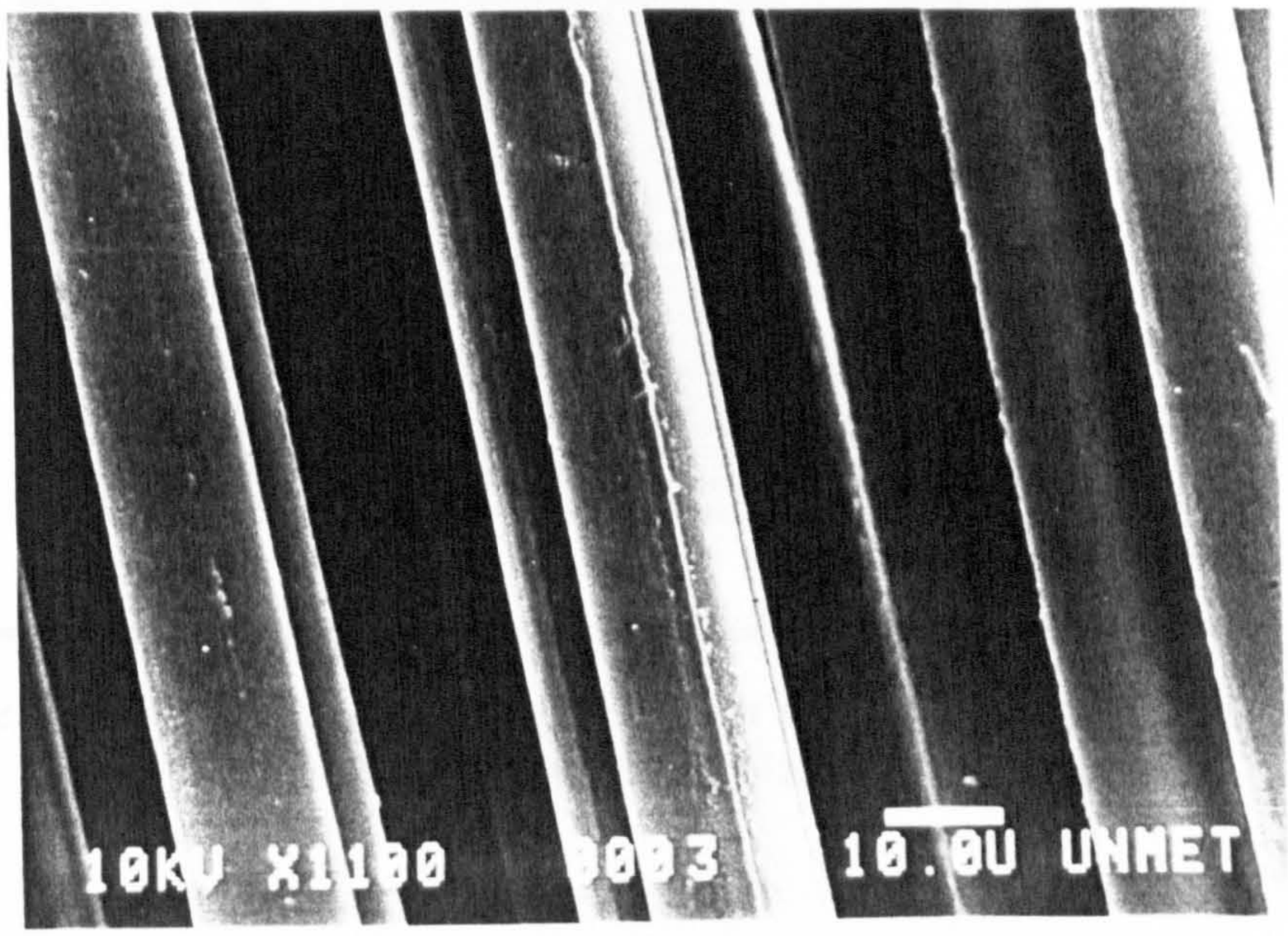

Figure 7.2 Silenka 2400 Tex fibres used in the filament winding trials. These filamentised fibres show the fractured remains of size menisci.

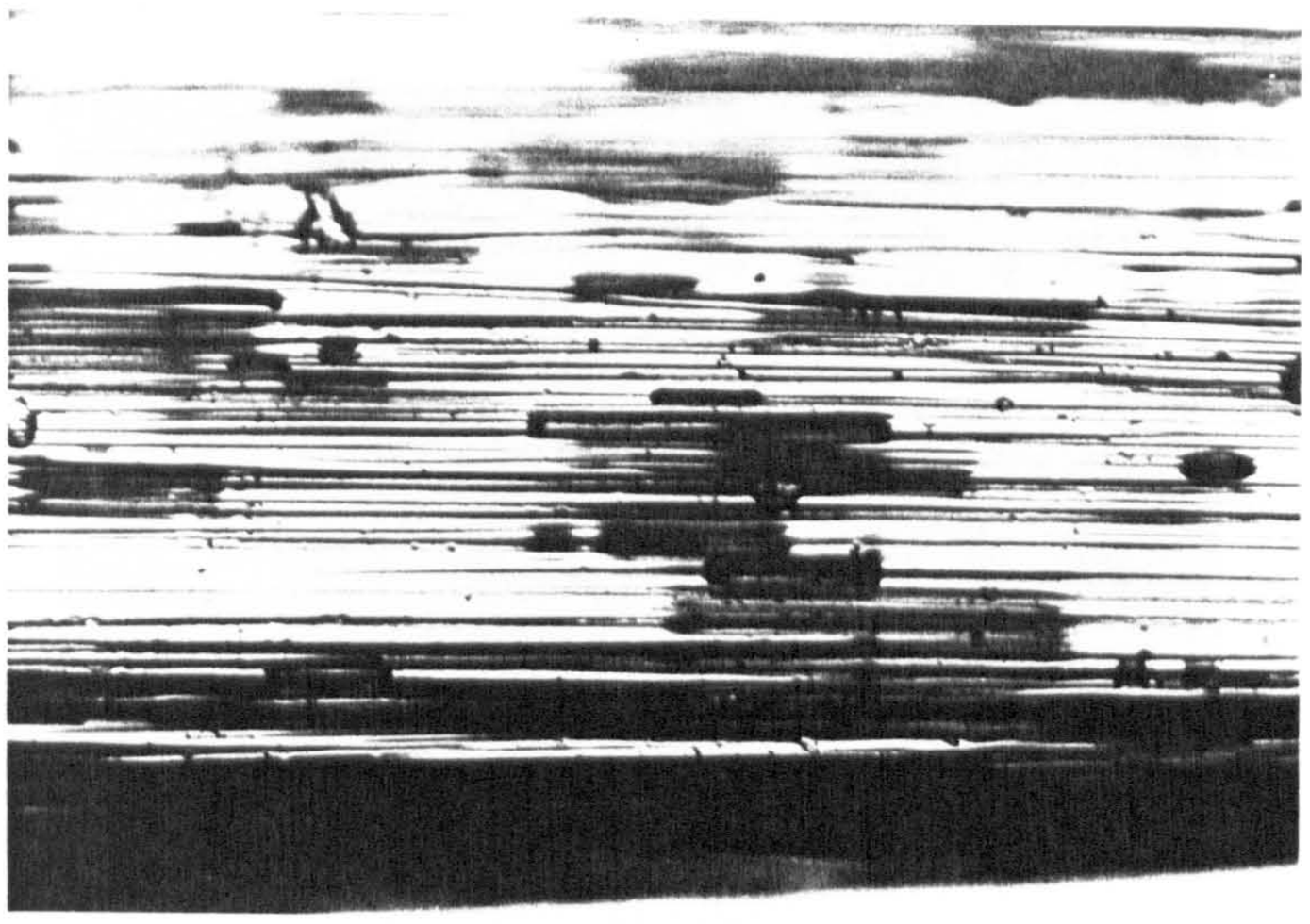

Figure 7.3a Translucent light photograph of a strand impregnated at a high speed (158mm/s) with the doctor blade set at 0.3mm.

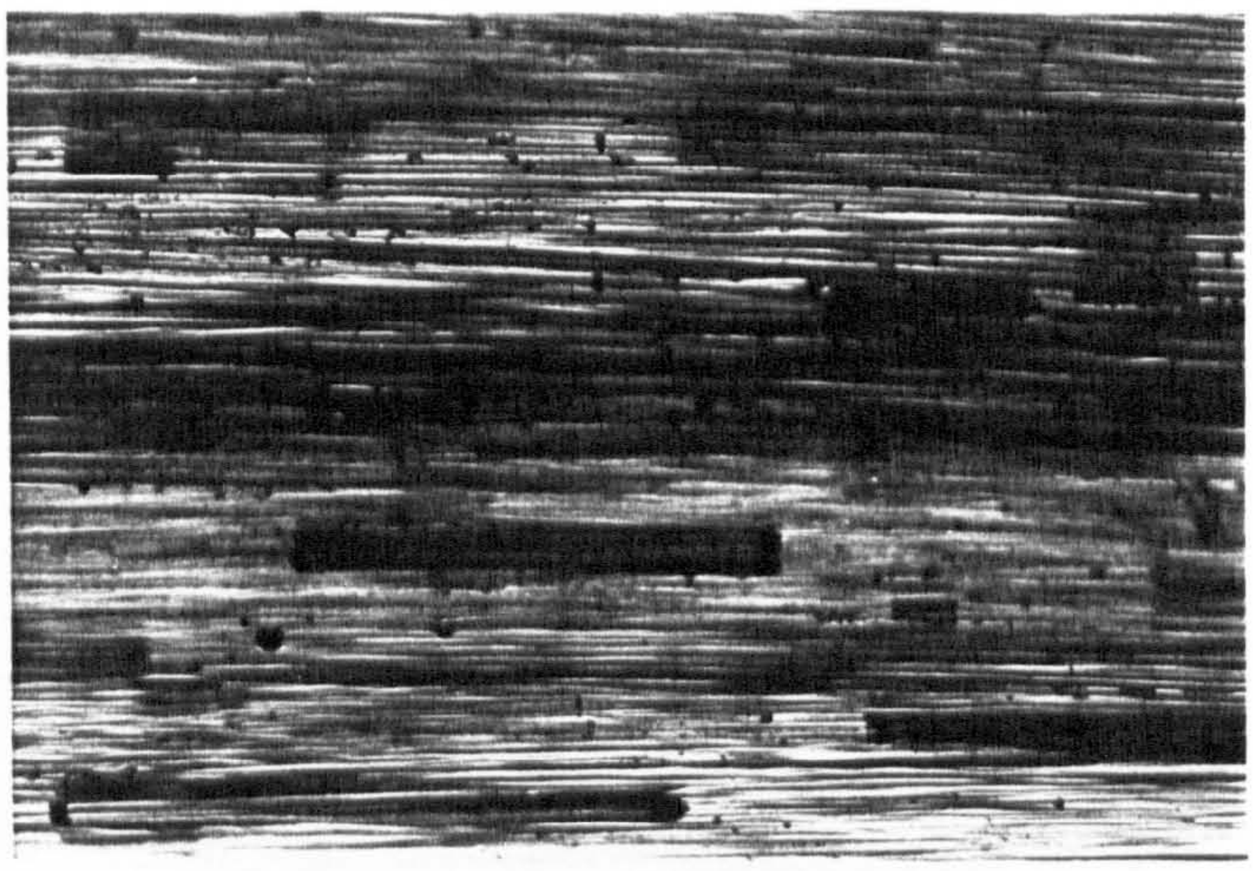

Figure 7.3b Translucent light photograph of a strand impregnated at a high speed (158mm/s) with the doctor blade set at 0.2mm.

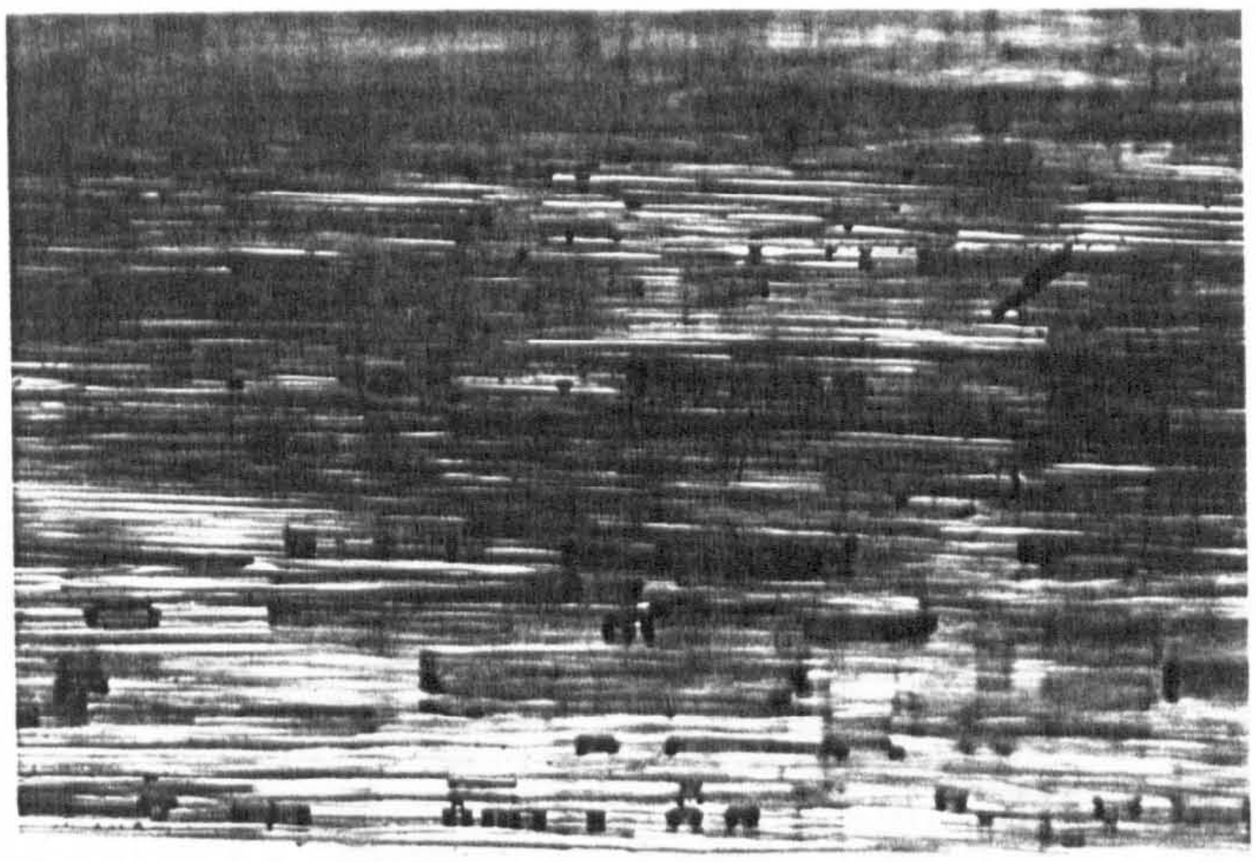

Figure 7.3c Translucent light photograph of a strand impregnated at a low winding speed (29 mm/s) with the doctor blade set to 0.2mm.

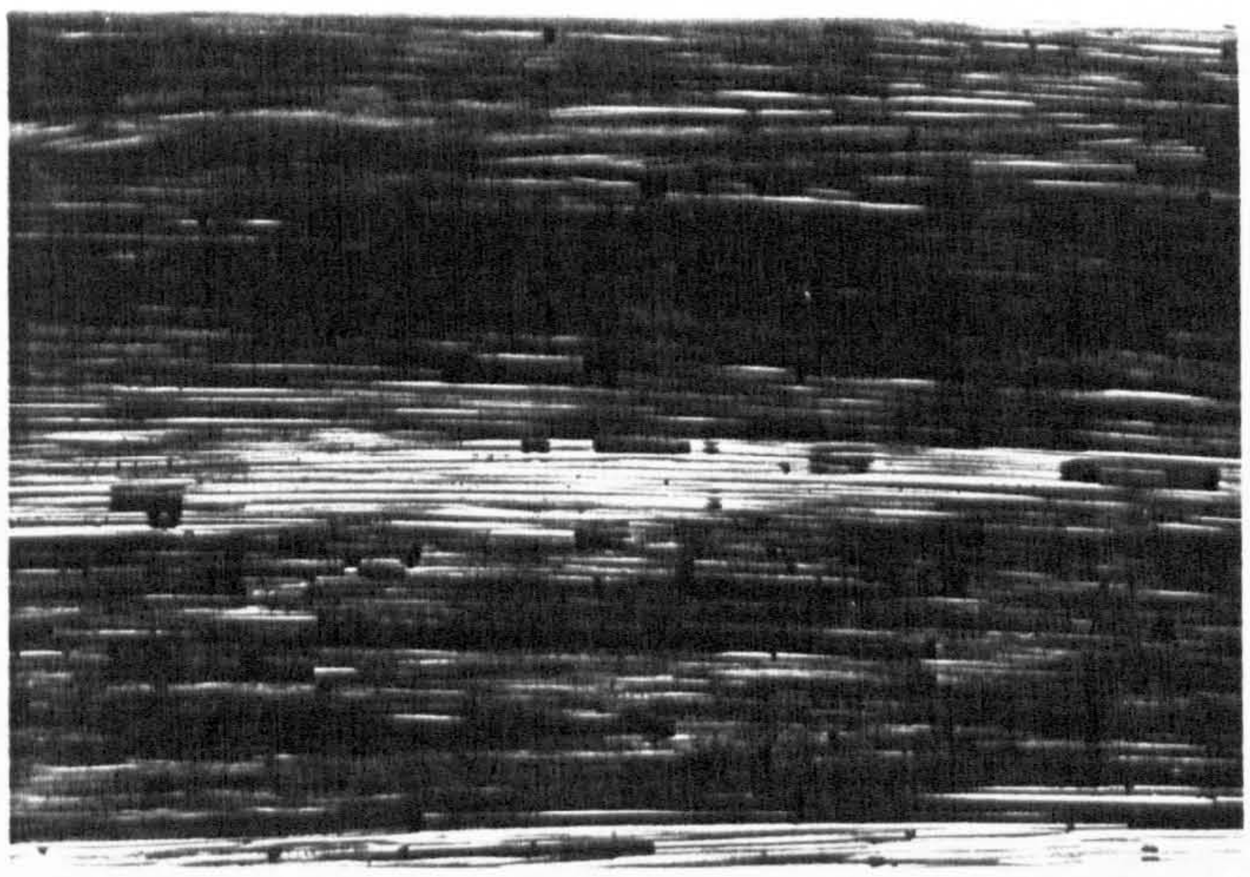

Figure 7.3d Translucent light photograph of a strand impregnated at a low winding speed (29mm/s) with the doctor blade set at 0.3mm.

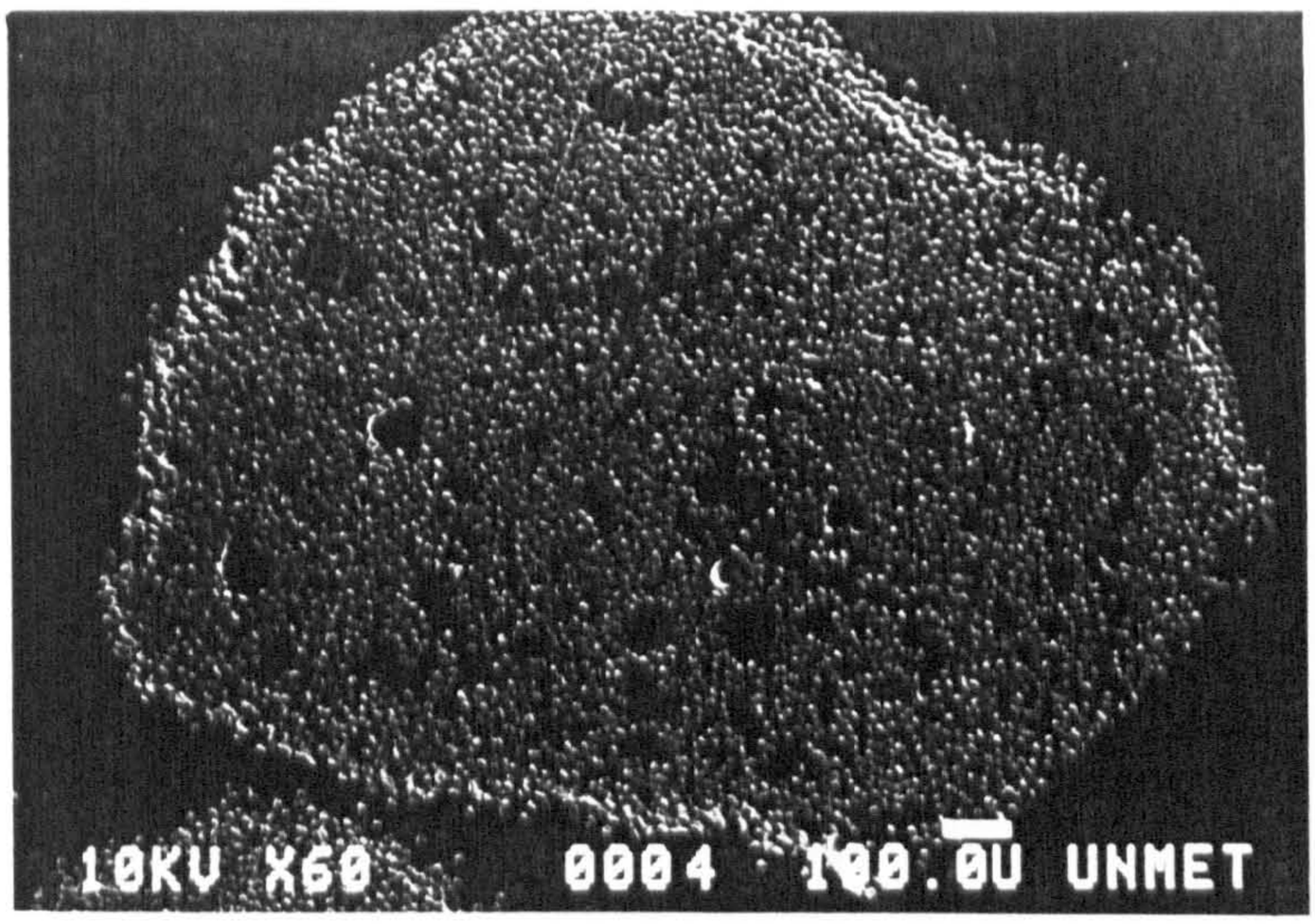

Figure 7.4a A cross section of an impregnated strand produced with a high impregnation speed of 158mm/s with the doctor blade setting at 0.3mm.

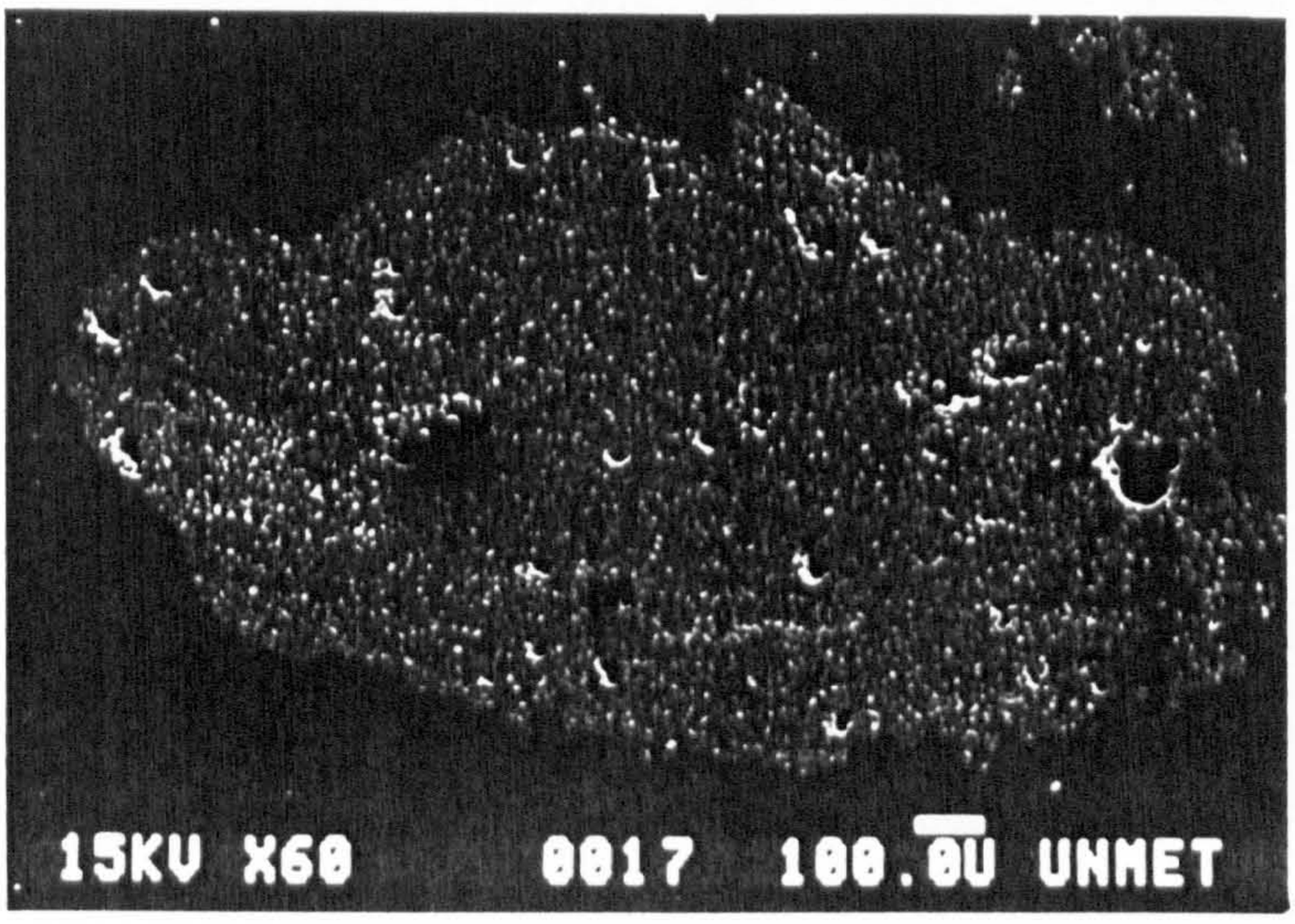

Figure 7.4b An impregnated strand produced with a high impregnation speed 158mm/s with the doctor blade setting at 0.2mm.

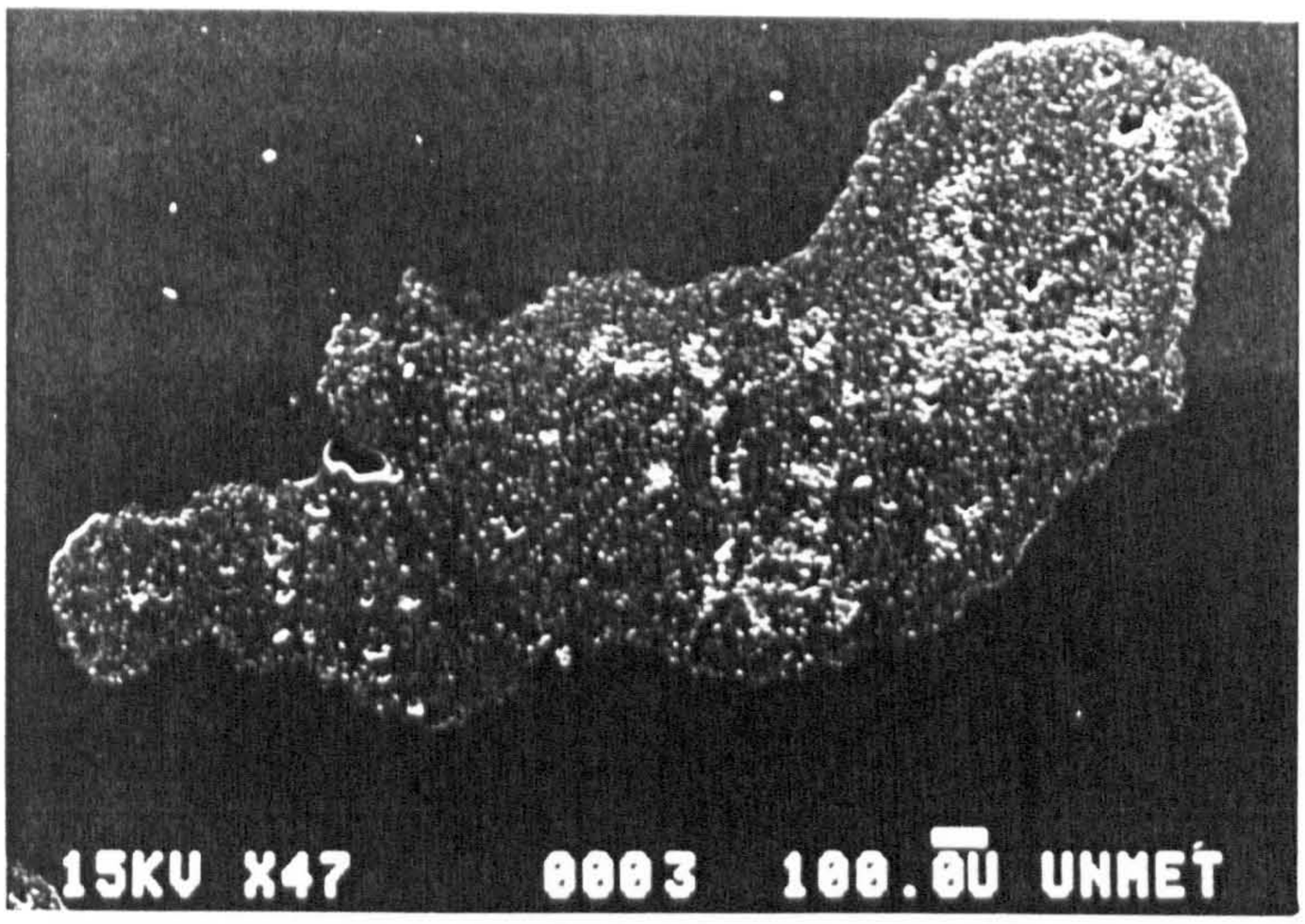

Figure 7.4c An impregnated strand produced with a low impregnation speed of 29mm/s with the doctor blade setting at 0.2mm.

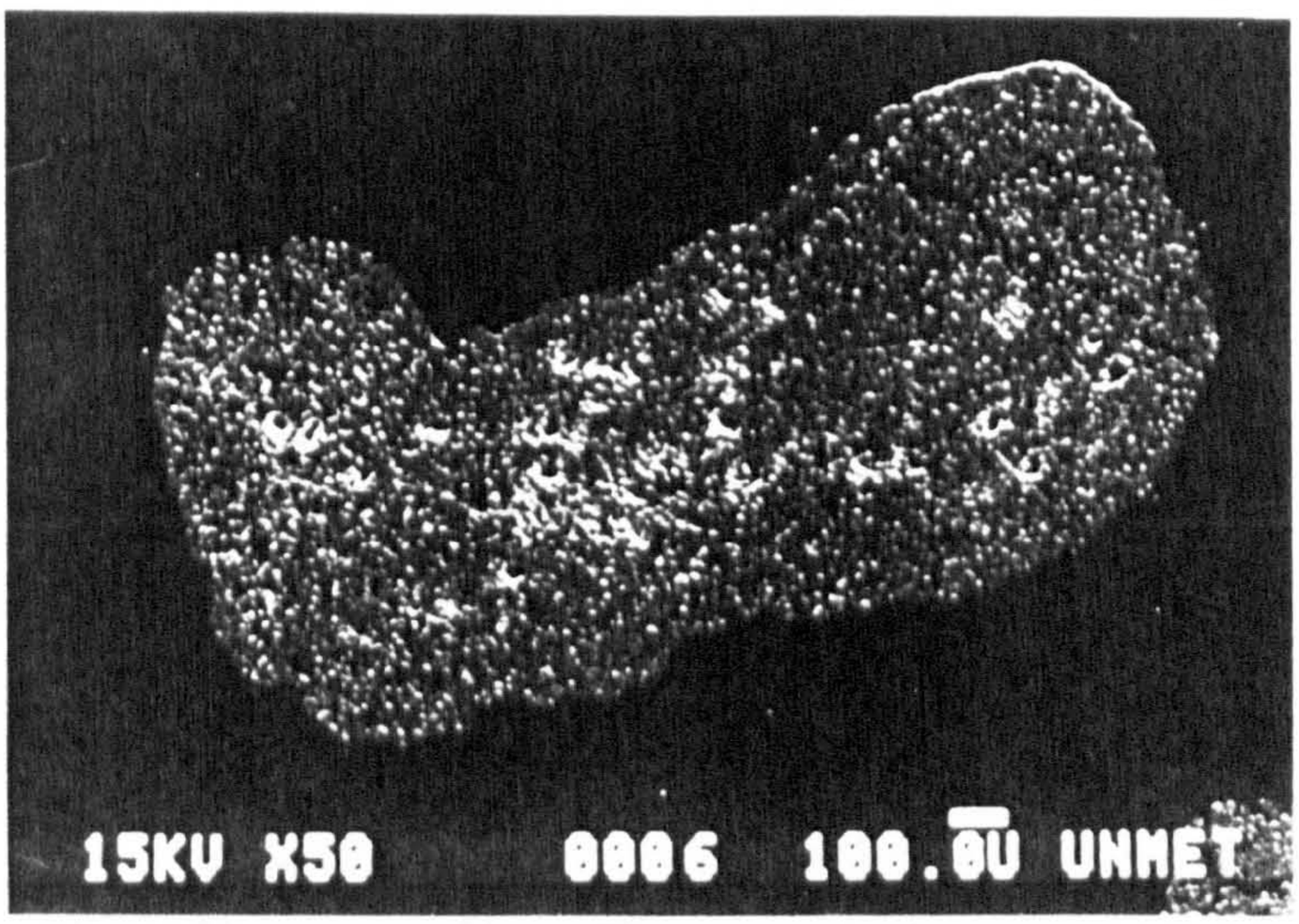

Figure 7.4d An impregnated strand produced with a low impregnation speed of 29mm/s with the doctor blade setting at 0.3mm.

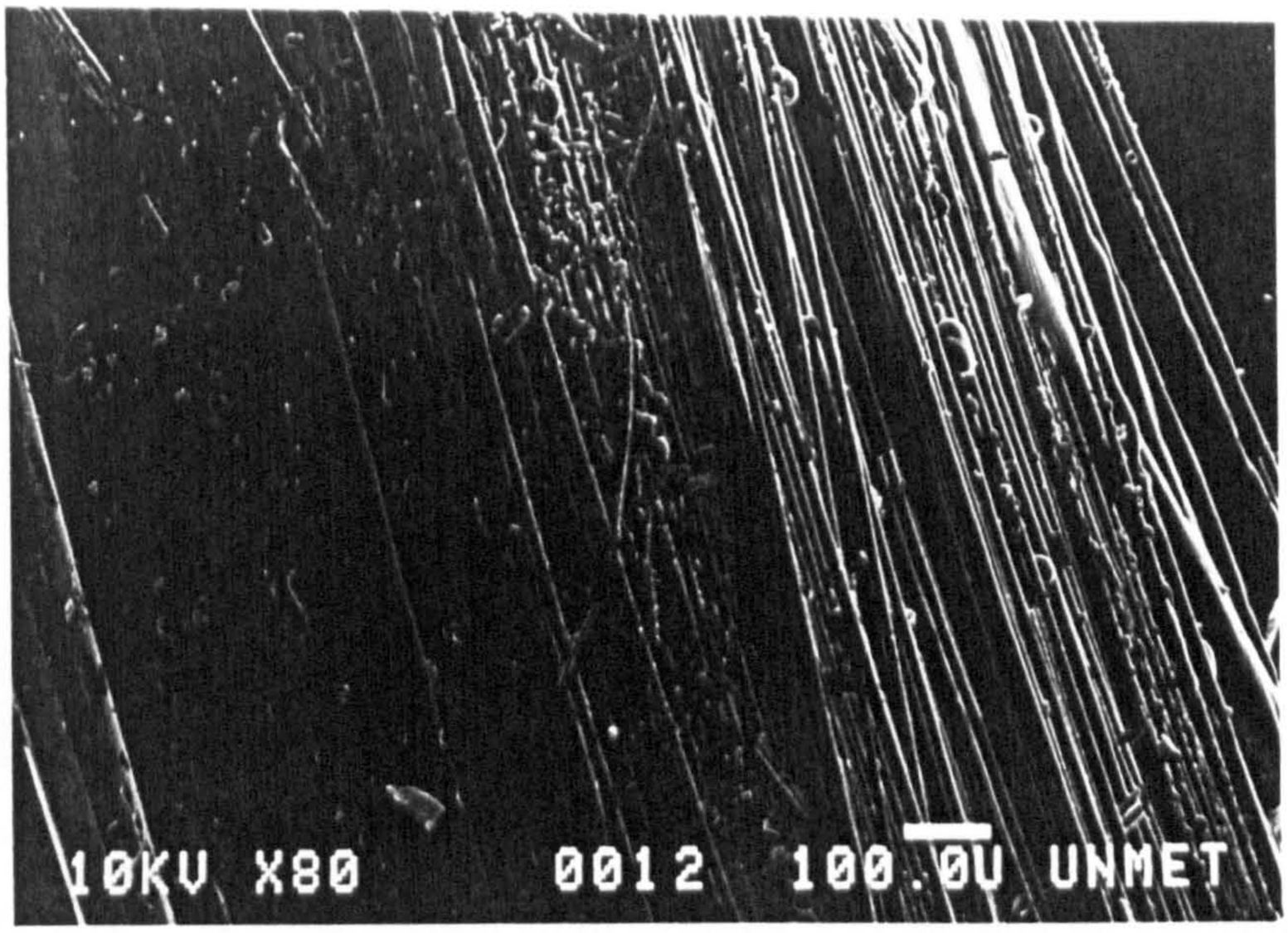

Figure 7.5 The outer surface of an impregnated roving showing dry fibres.

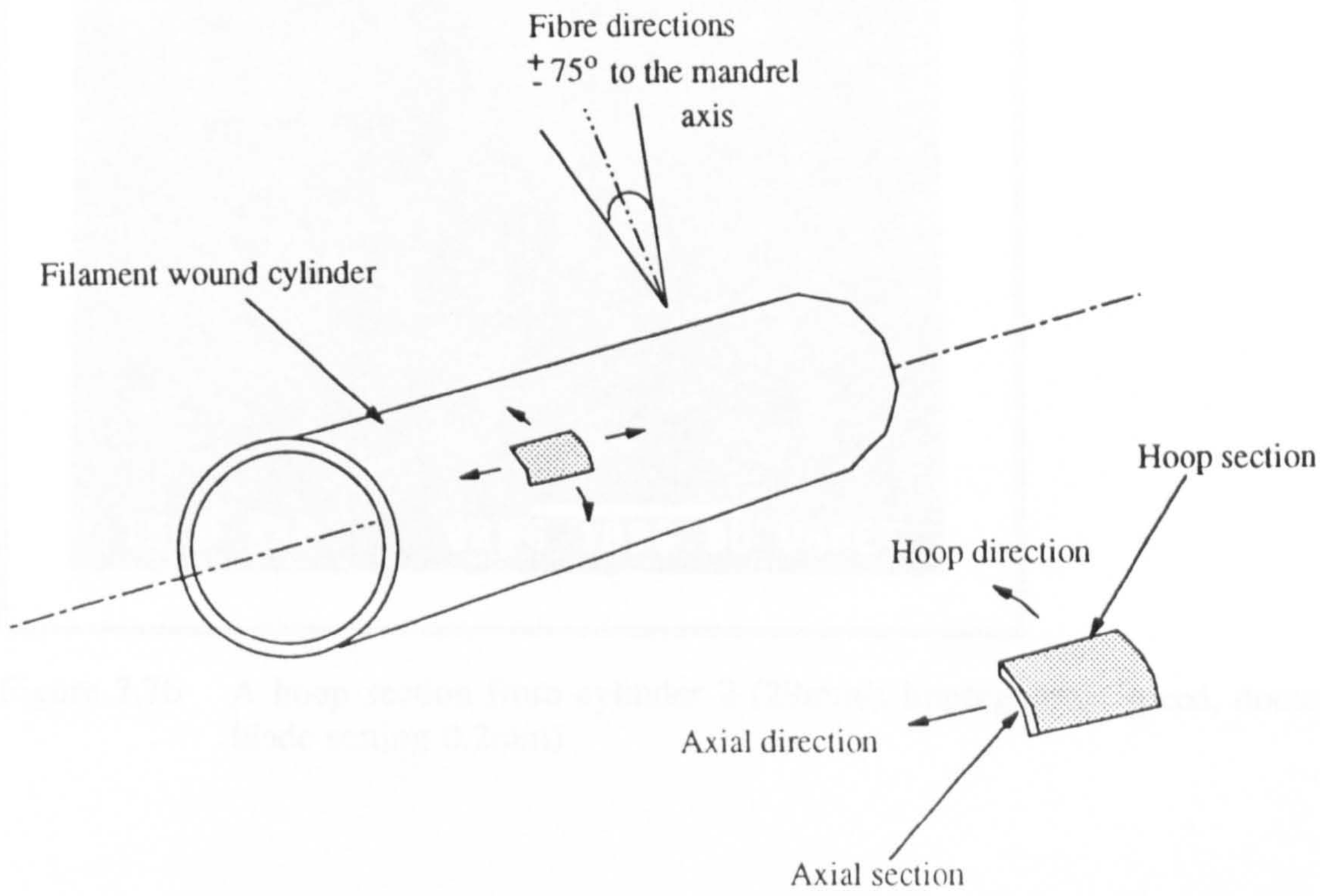

Figure 7.6 Axial and hoop sections taken from a ±75°C filament wound cylinder.

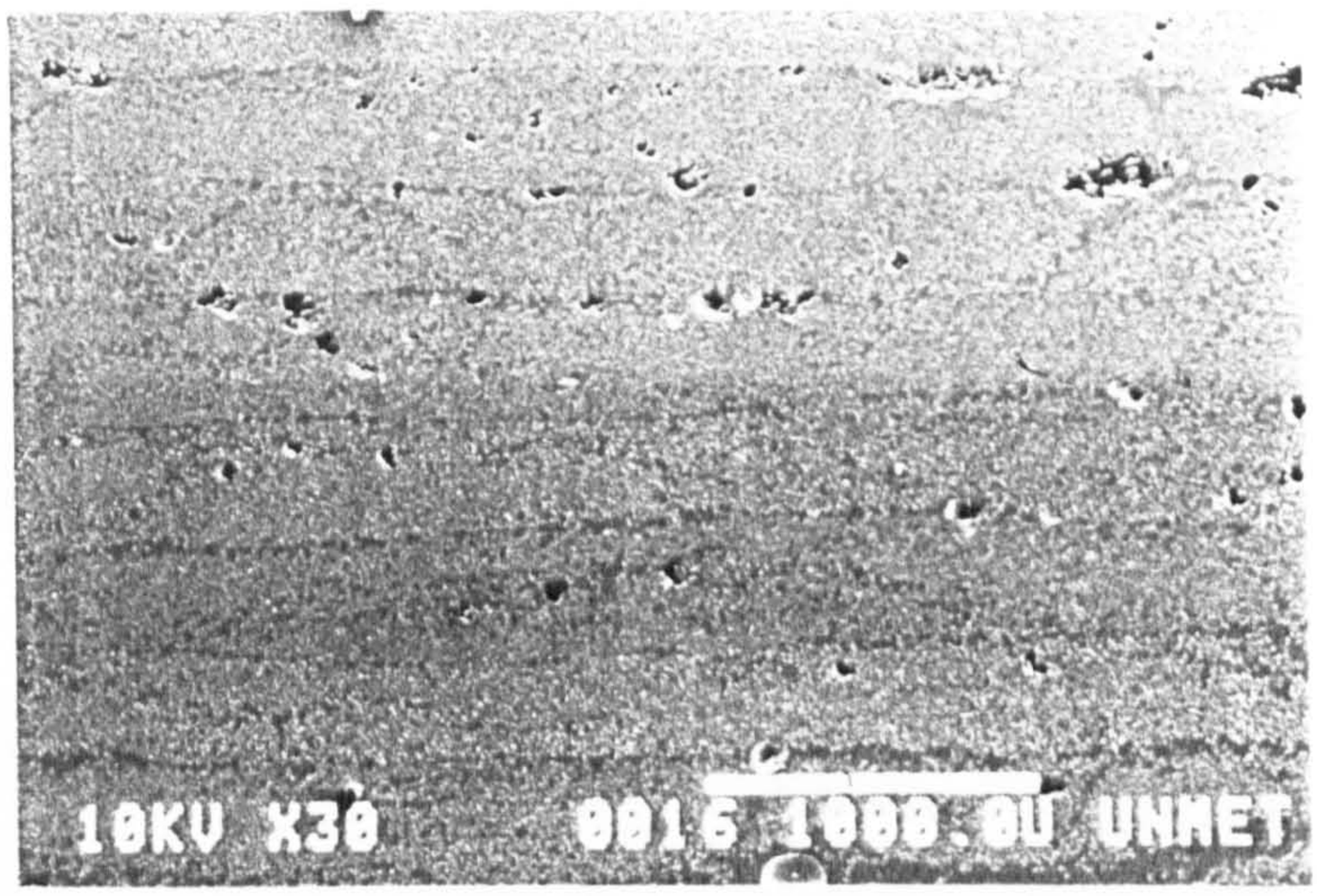

Figure 7.7a A hoop section from cylinder 1 (158mm/s impregnation speed, doctor blade setting 0.3mm)

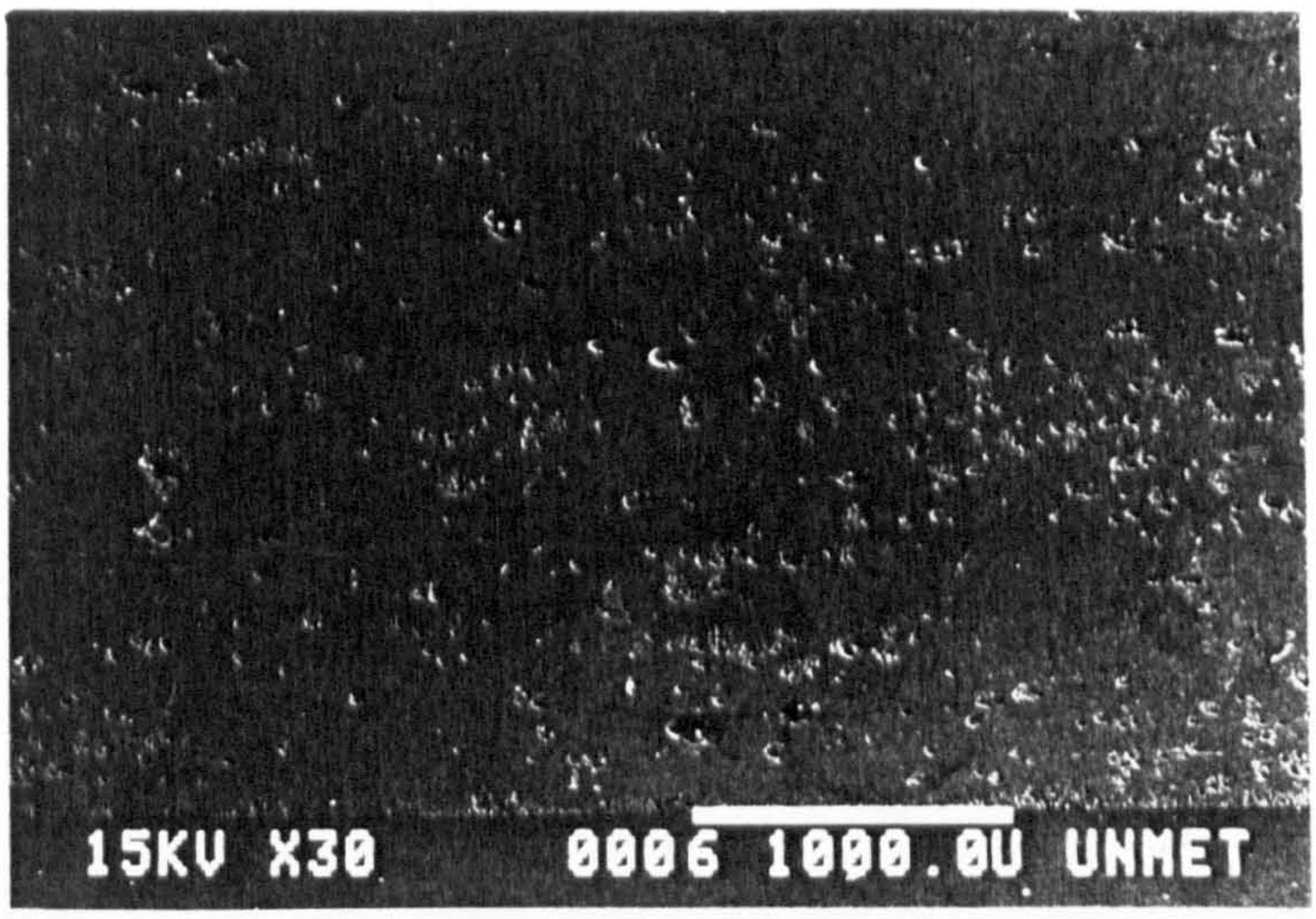

Figure 7.7b A hoop section from cylinder 2 (29mm/s impregnation speed, doctor blade setting 0.2mm)

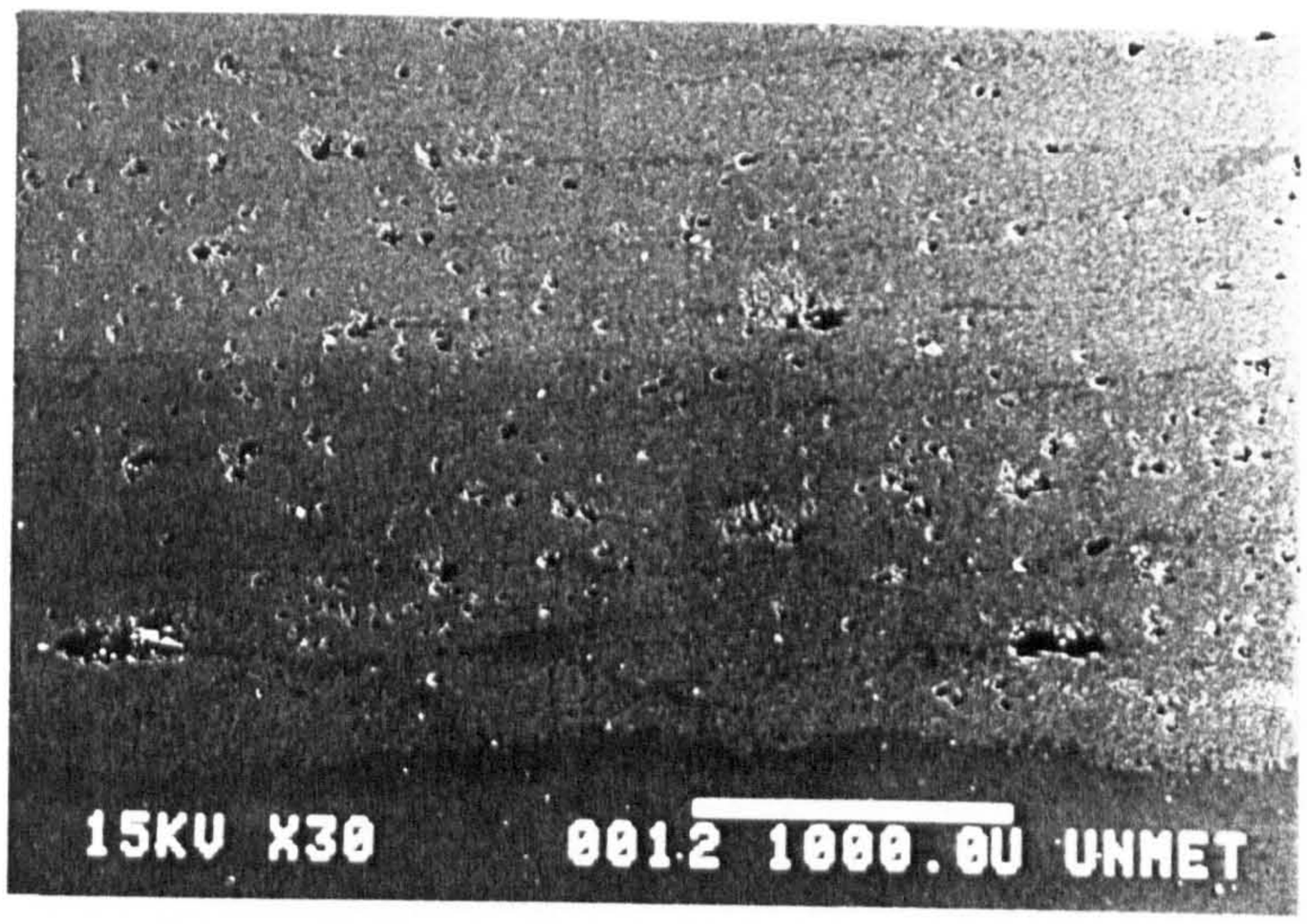

Figure 7.7c A hoop section from cylinder 3 (29mm/s impregnation speed, doctor blade setting 0.2mm)

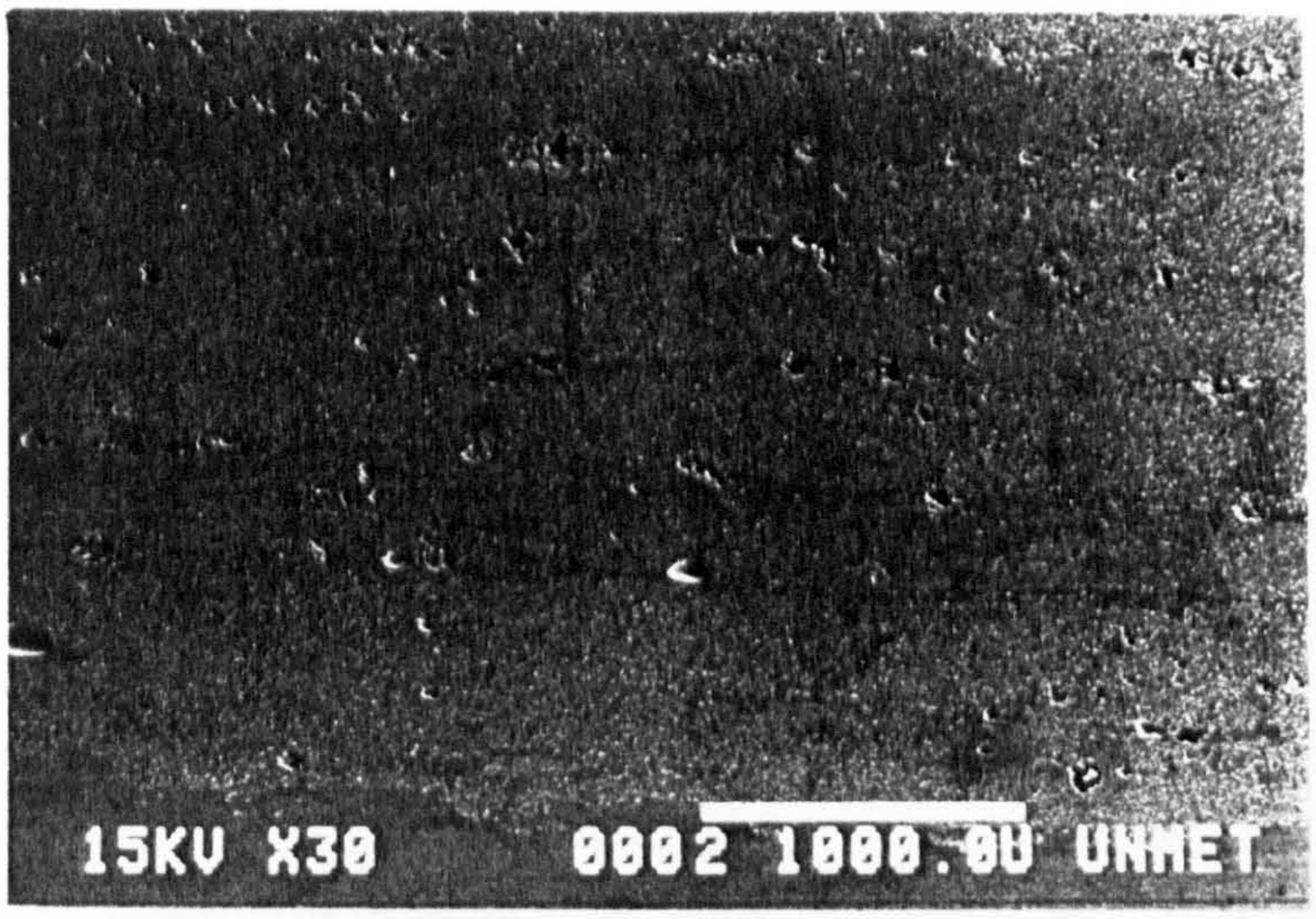

Figure 7.7d A hoop section from cylinder 4 (29mm/s impregnation speed, doctor blade setting 0.3mm)

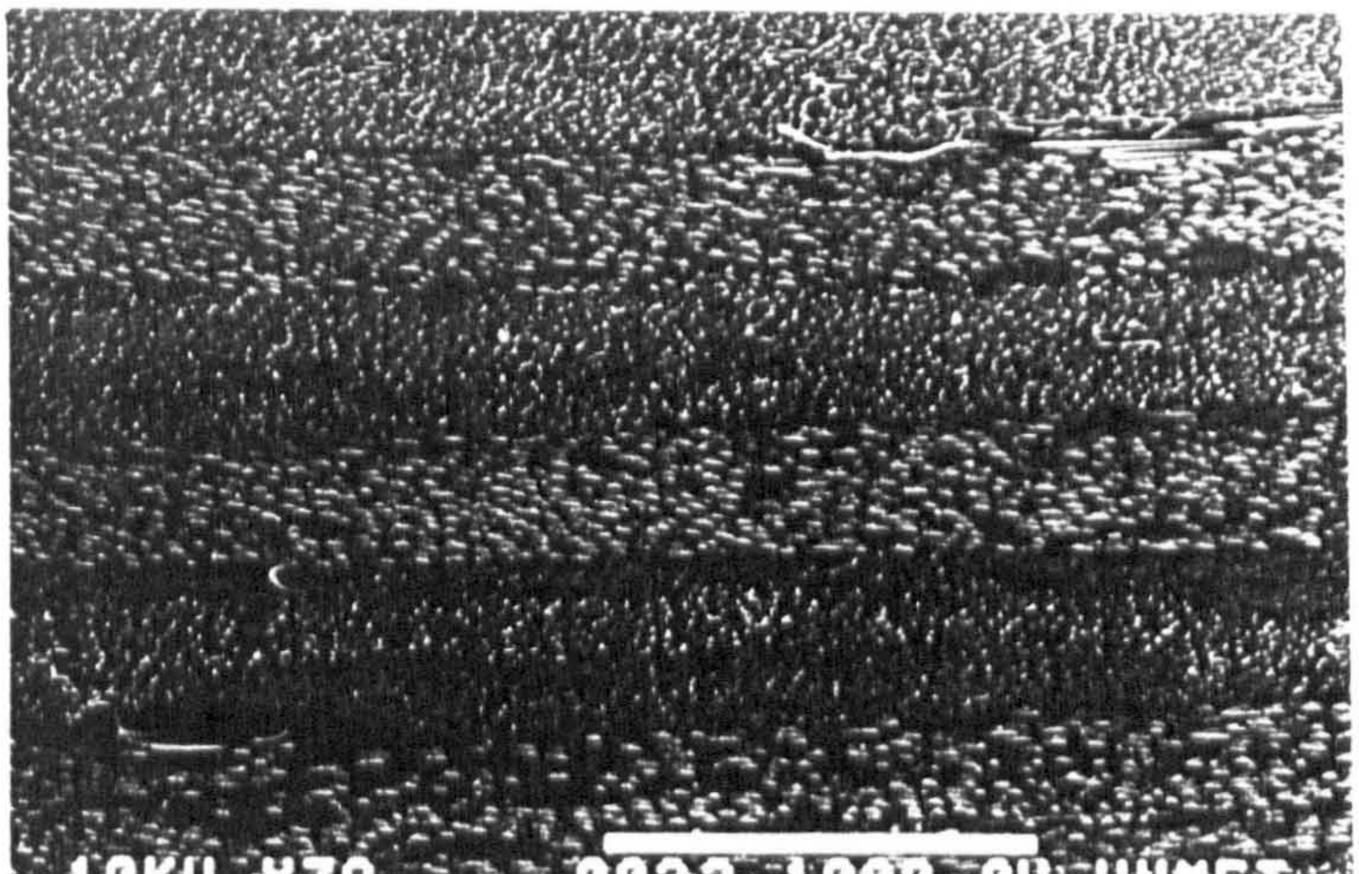

Figure 7.8a An axial section from cylinder 1 (158mm/s impregnation speed, doctor blade setting 0.3mm)

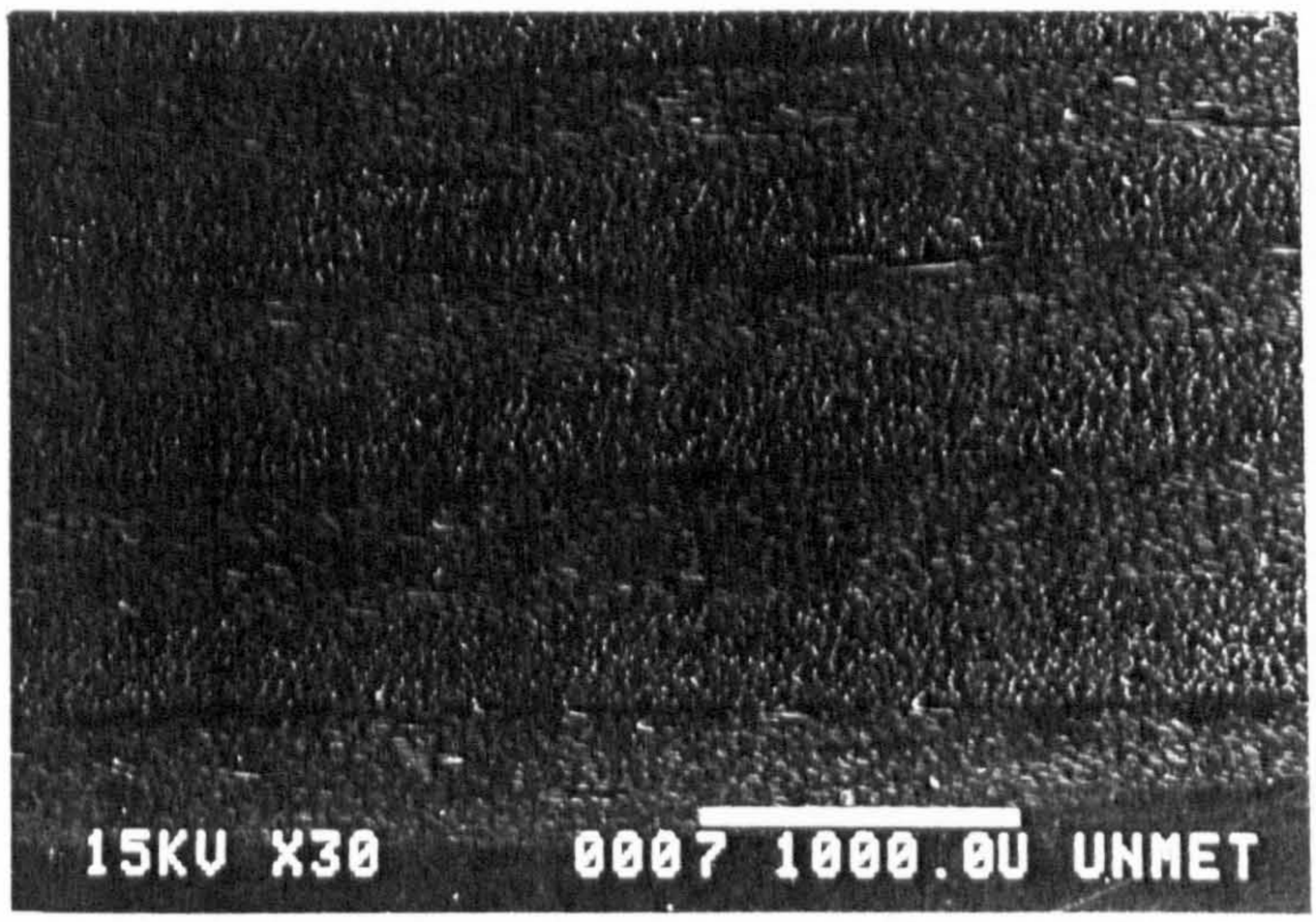

Figure 7.8b An axial section from cylinder 2 (158mm/s impregnation speed, doctor blade setting 0.3mm)

Figure 7.8c An axial section from cylinder 3 (29mm/s impregnation speed, doctor blade setting 0.2mm)

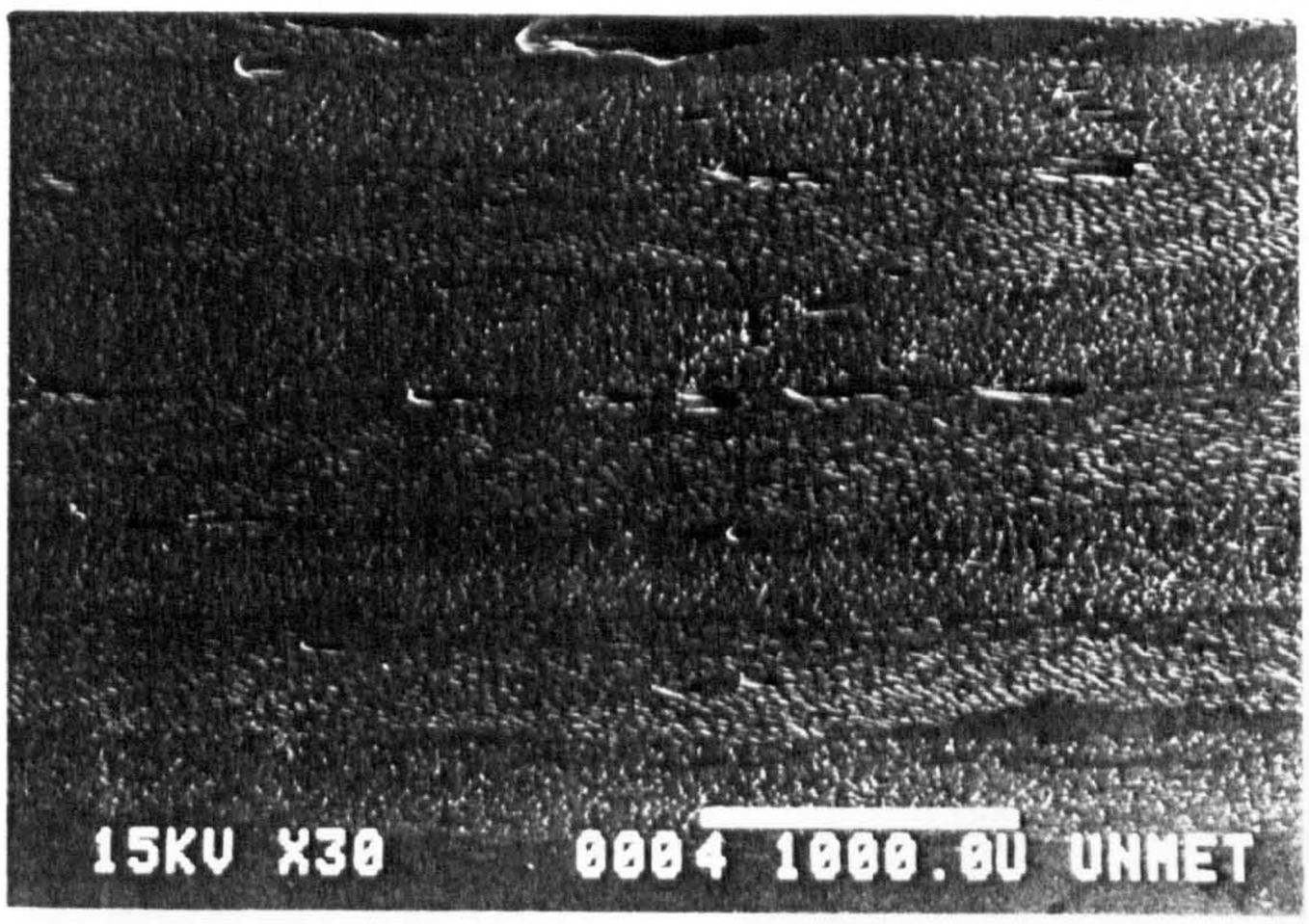

Figure 7.8d An axial section from cylinder 4 (29mm/s impregnation speed, doctor blade setting 0.3mm)

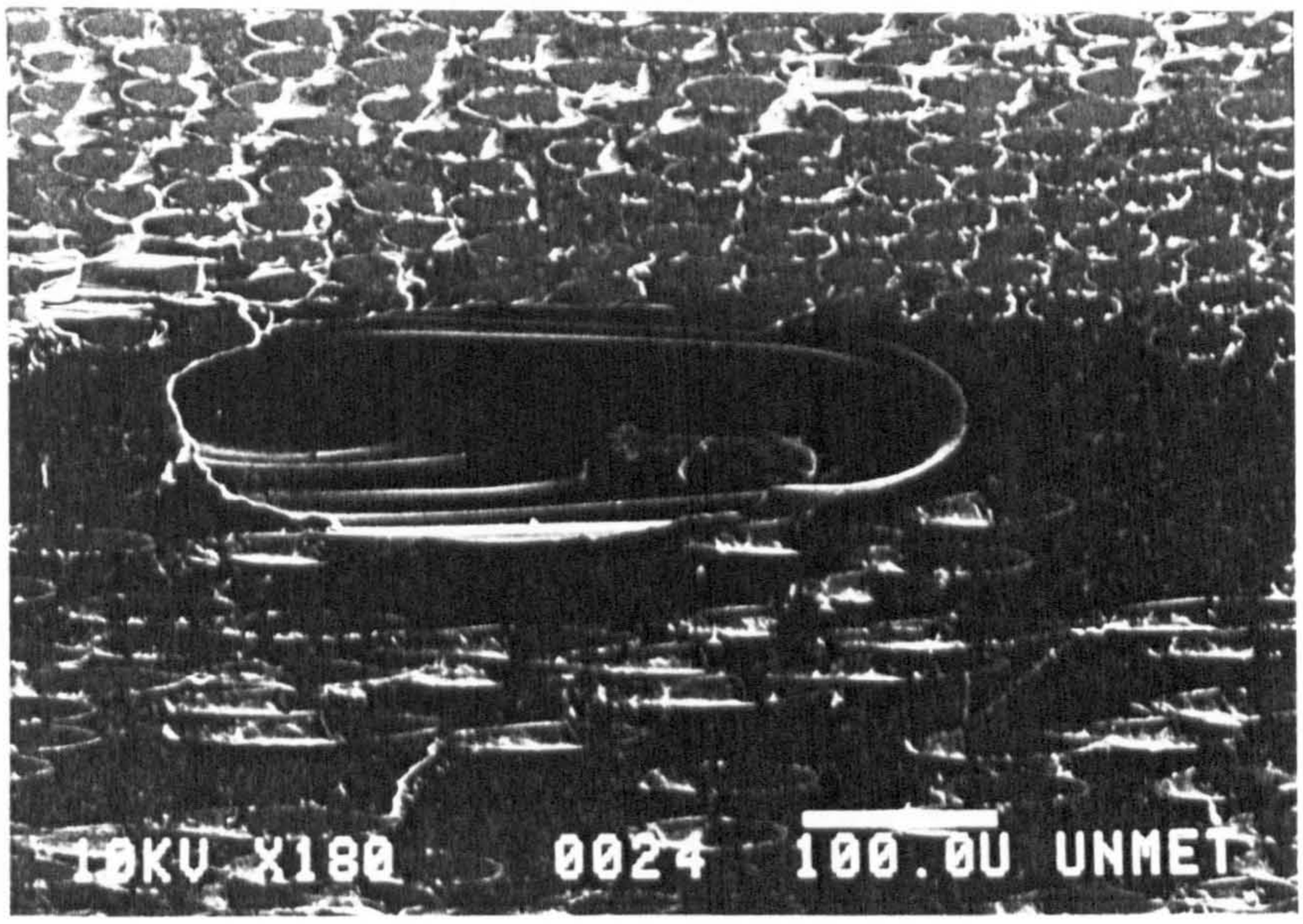

Figure 7.9 A cylindrical void between fibre bundles, thought to have been formed during fibre laydown, exhibiting the smooth surface within the void, from cylinder 1.

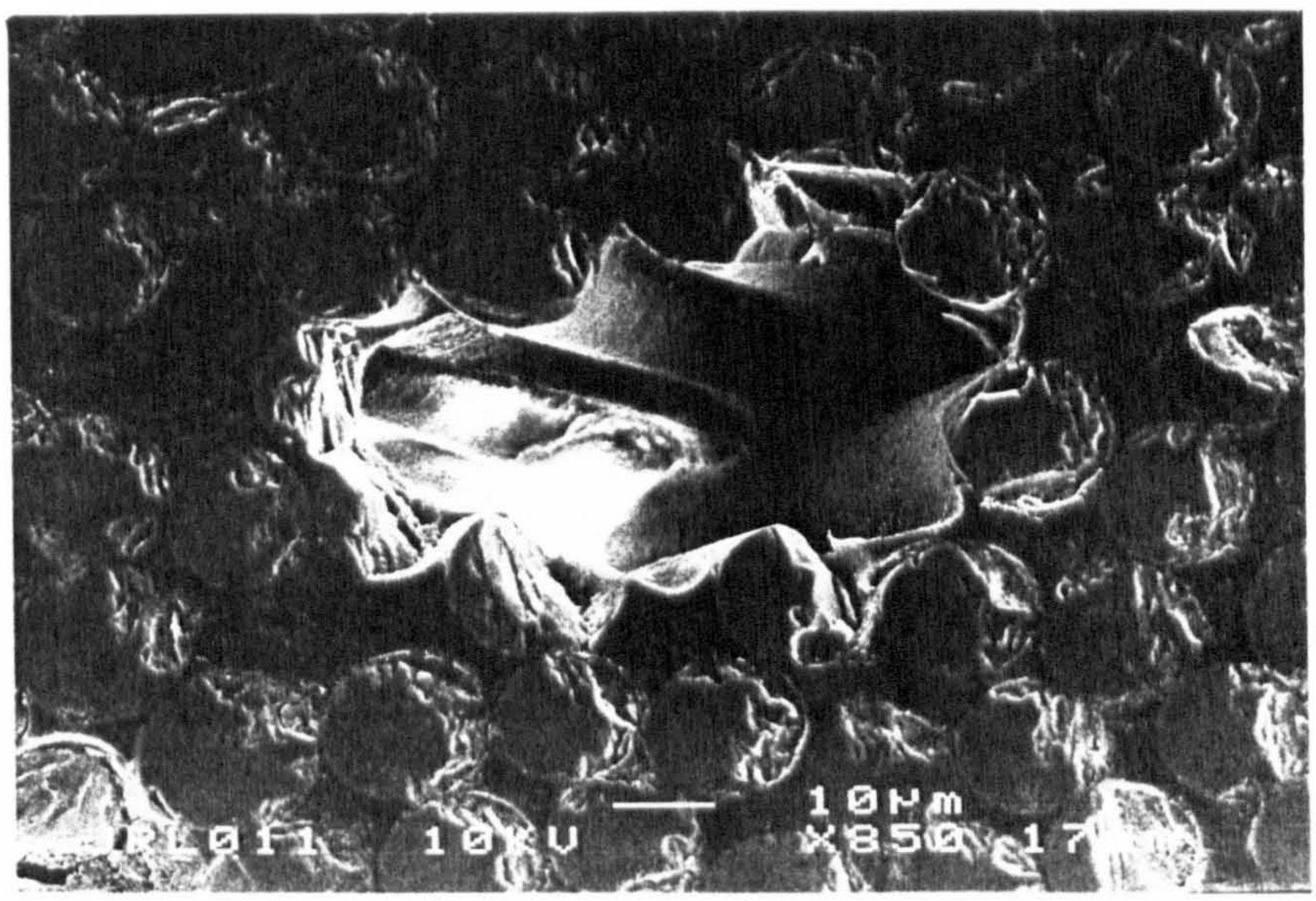

Figure 7.10 A void between fibre bundles, taken from cylinder 2. The dry fibres and what seems to be size deposition and menisci between the fibres.

Figure 7.11 The profile of this void follows the impregnated fibres surrounding the void within a fibre bundle (cylinder 2).

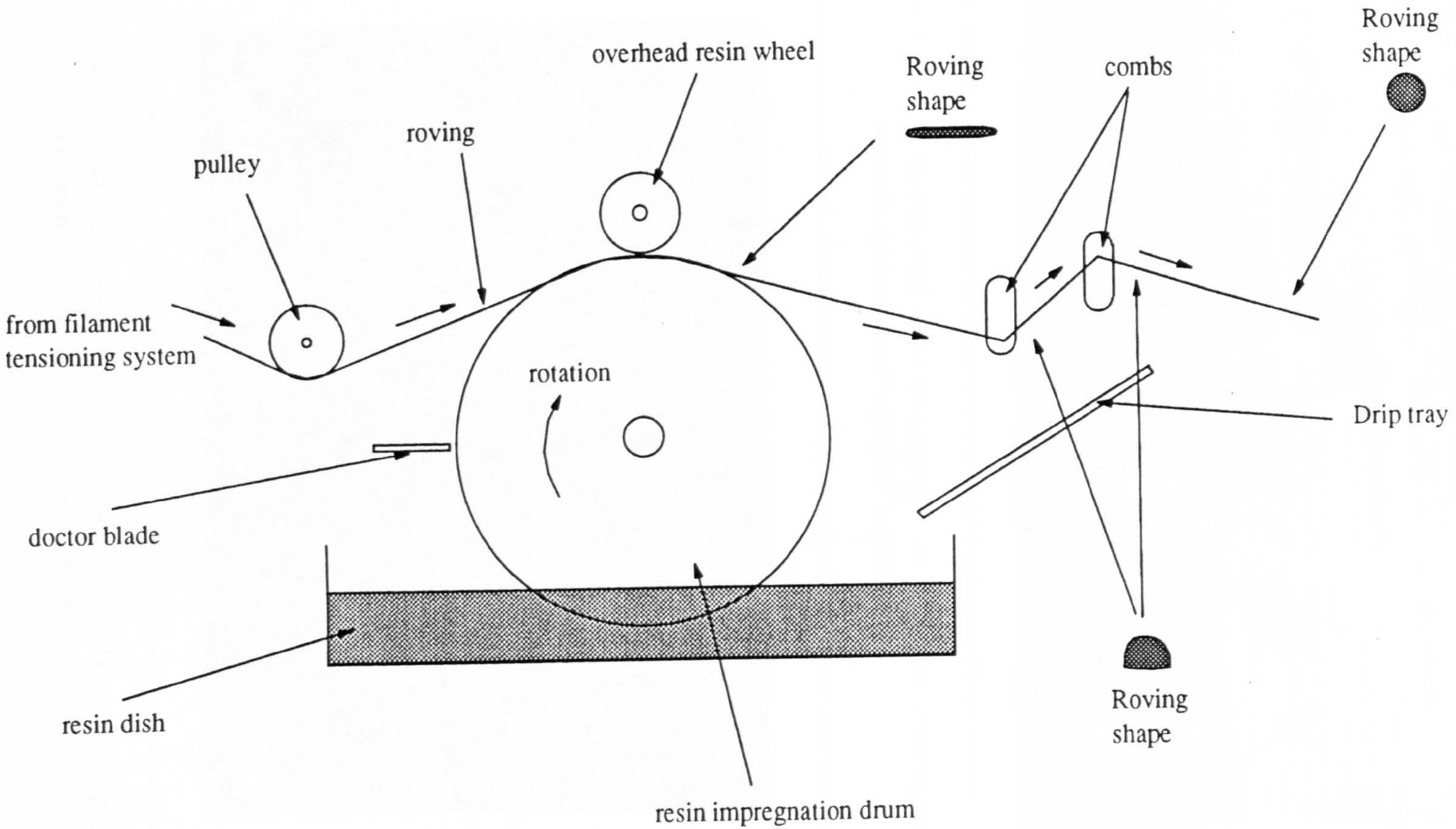

Figure 7.12 Filament Winding Fibre Impregnation System

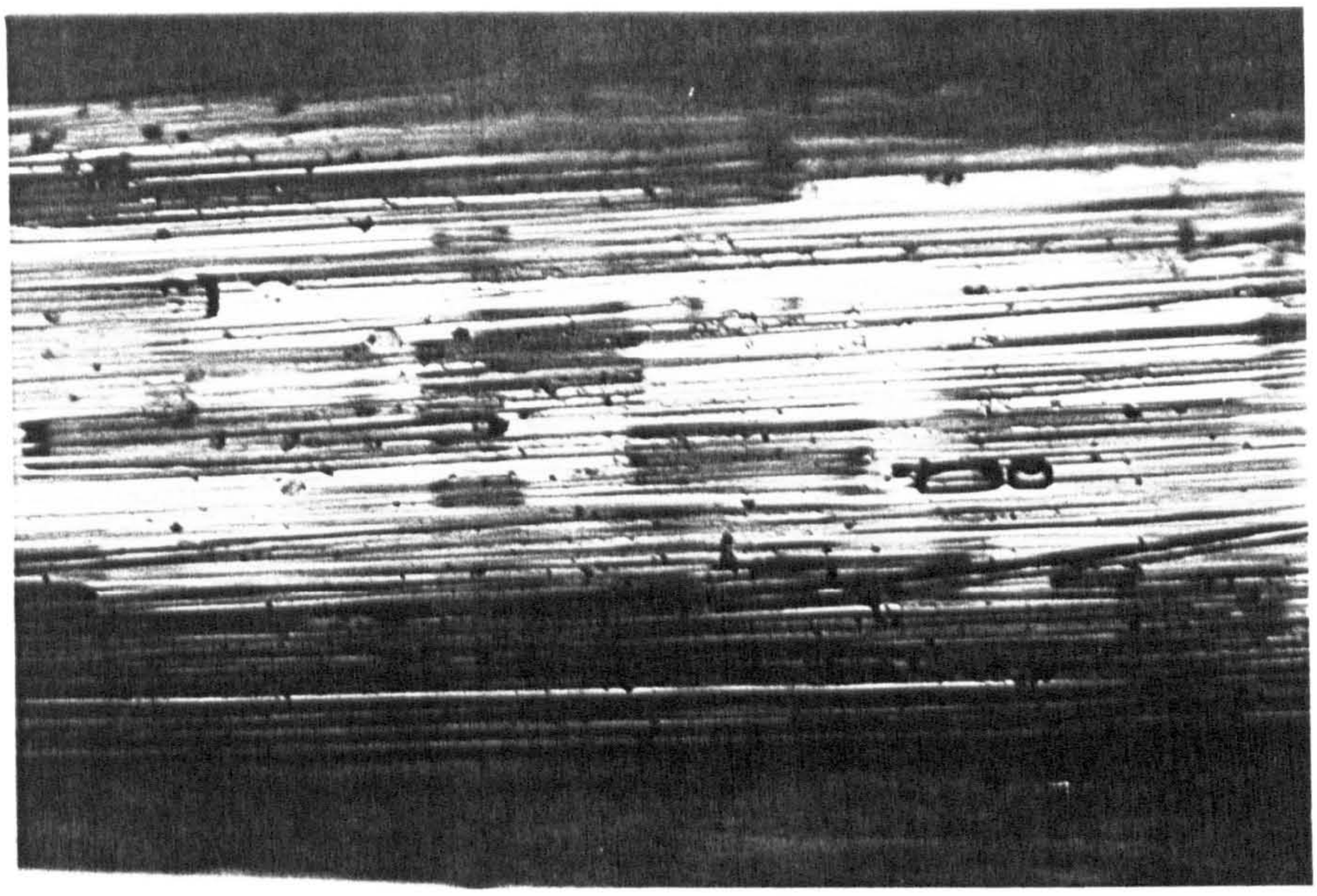

Figure 7.13 A transmitted light photograph of a strand impregnated using the vacuum assisted impregnation mechanism.

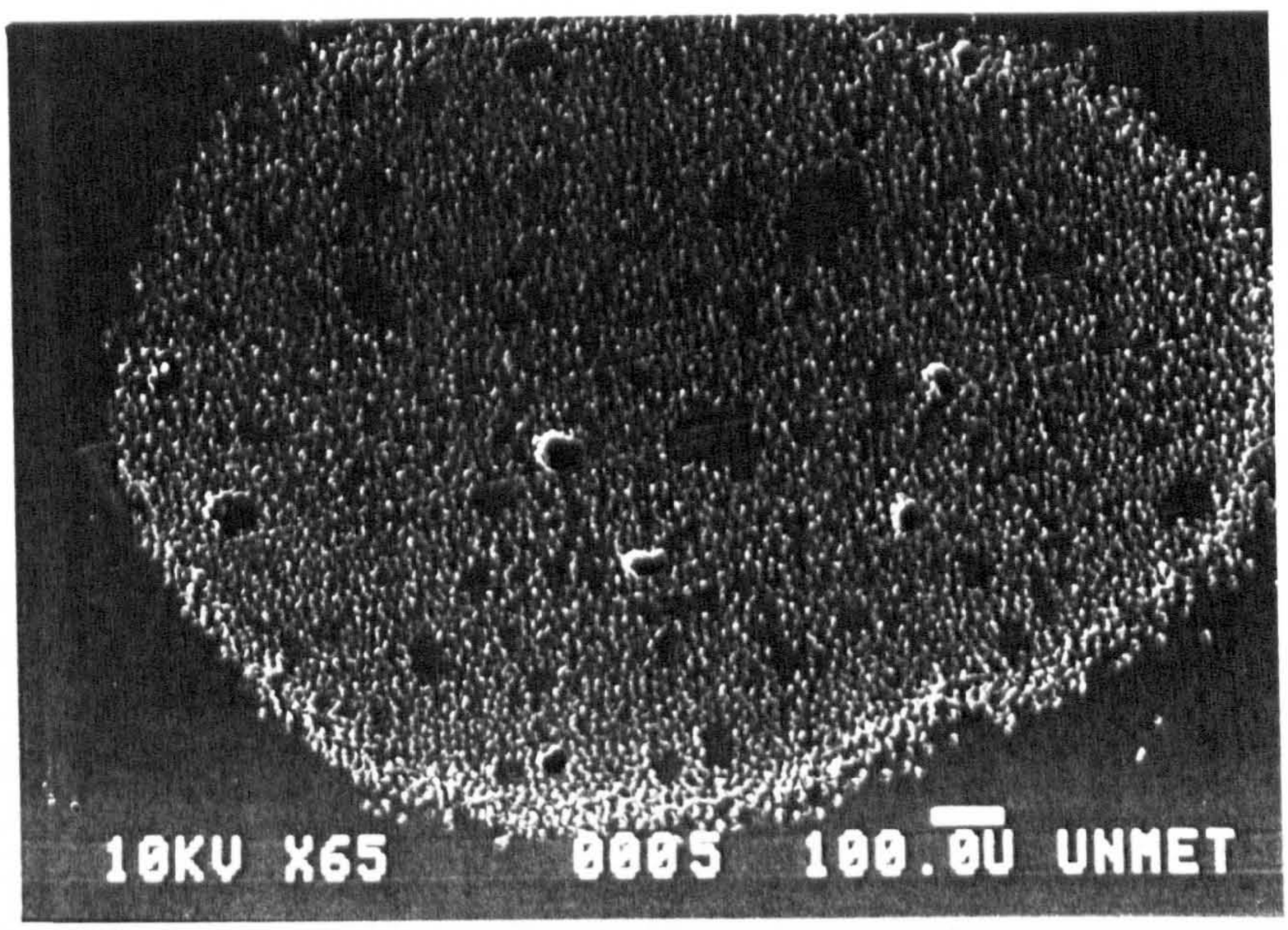

Figure 7.14 A cross section of a strand which has been impregnated using the vacuum assisted impregnation mechanism.

Figure 7.15 A hoop section from winding 5, which was produced using the vacuum assisted impregnation mechanism. Fewer voids are evident in this section in comparison to the sections considered in Figures 7.7a to 7.7d.

Chapter 8

A Model for Void formation in fibre bundles during the impregnation phase of RTM

8.1 Introduction

This chapter describes a mathematical simulation of the impregnation of a unidirectional preform, taking into account heat transfer, temperature dependant viscosity and gelation of the resin. Previous work in Chapters 6 and 7 has shown that a strand of fibres will become impregnated with resin due to a combination of two flows, that of axial flow in the capillaries between the filaments and that of transverse flow normal to the fibre axis. Revill[19] and others have considered axial penetration into small capillaries, whilst Bayramli et al[47] have studied flow transverse to ideally packed cylinders. This model proposes an approach to consider both situations, adapting them to predict flow into an idealised preform. Material data was first determined experimentally for resin viscosity and gelation times. The relative impregnation speeds between the flow regimes were then used to gain an insight into void formation within the fibre bundles.

In this study a model for both the axial and transverse impregnation of hexagonally packed fibres is proposed. Gravitational forces were neglected, with the impregnation being driven by injection and capillary pressures and retarded by viscous forces.

The model was split into three independent flow regimes:

i) Axial flow in the capillary between filaments within a fibre bundle (Figure 8.1).

ii) Transverse flow in the channels between filaments into a fibre bundle (Figure 8.1).

iii) Axial flow in the tricorn between fibre bundles (Figure 8.2).

The problem was considered in three dimensional space, using cylindrical polar co-ordinates (r and z), where z is the direction parallel to the fibre axis, and r is the direction the resin flows into the fibre bundles. The three flow regimes were assumed not to interact and were considered in isolation. The time step value used in the axial impregnation regimes was chosen by evaluating the effect of a range of time steps upon impregnation distance. A suitable time step was chosen where the impregnation distance was seen to converge. A mass conservation method was used to dictate the transverse flow regime. The area used in each time step was chosen using a similar method. The time steps to be used for heat transfer calculations were also assessed, and it was established that the resin and fibre reach an equilibrium temperature in less than one second.

The flow predictions in the capillaries between circular fibre bundles were perceived to be inaccurate. Sections of unidirectional mouldings were studied and the preform model was refined using elliptical fibre bundles.

This chapter compares the predictions made using each flow model with the fill times from the manufacture of mouldings with quasi-unidirectional reinforcement discussed in Chapter 5. The discussion (section 8.6) considers the validity of the impregnation model and the reasons for departures from experimental data.

8.2 Assumptions

Preform geometric model

The preform structure was modelled as an ideal packing of glass fibres within bundles (Figure 8.2), with a spacing of 2d between each fibre (Figure 8.3), packed in a regular hexagonal order (for an approximate volume fraction of 35%). The fibre bundles were assumed to be circular in cross section and close packed in a regular hexagonal array (Figure 8.2).

The fibre bundle radius R_b was calculated, by considering the area of a unit cell for each fibre (Figure 8.3(a)):

$$R_b=\sqrt{\frac{2\sqrt{3}N_f}{\pi}(R_f+d)^2} \tag{8.1}$$

Where N_f is the number of fibres in the bundle. The overall volume fraction of the glass fibres in the preform was calculated, by considering the unit cell for fibre bundle spacing (Figure 8.3(b)):

$$V_f=\frac{\pi R_f^2 N_f}{2\sqrt{3}R_b^2} \tag{8.2}$$

Number of layers in each fibre bundle

In any radial direction, from the circumference of the bundle to the centre, the number of fibres which may be wetted is finite. Using 2400 Tex fibre bundles, the density of the glass and the assumption that all of the fibres were 15μm in diameter the number of filaments within each bundle was calculated at approximately 5000. Using this information and assuming the hexagonally packed structure previously discussed, the number of fibres required to be wetted through to the centre of the circular bundle was calculated to be 38. This number is independent of the fibre volume fraction.

Angle of Contact

The contact angle between resin and fibre is required to calculate the capillary force in the spaces between the fibres. Revill[19] showed that the angle of contact between resin and fibre varied with the rate of resin flow. During these investigations the surface tension was determined to be 35 dynes/cm ($35x10^{-3}$ N/m). The results of Revills experiments are shown in Appendix 5. An equation relating contact angle (θ) and resin velocity was derived from these results:

$$\theta=a_{co}+b_{co}\ln\left(\frac{dx}{dt}\right) \tag{8.3}$$

Where a_{co}=2.846 and b_{co}=0.223.

Heat transfer between fibre and resin

During RTM cold resin is often injected into a mould and preform which have been preheated. The resin will be heated by the mould surface and the fibres, which in turn will cause a reduction in viscosity. The heating of the resin will initiate a reaction causing polymerisation. In this model only the microscopic heat transfer effects between the fibres and the resin were considered. The heat transfer from the mould surface was assumed to have no influence.

Before considering the transient problem of heat transfer through conduction and convection, a steady state temperature was calculated, to give an indication of the temperature at which the two materials might stabilise. From an energy balance, assuming that the resin and fibres are quenched to an equilibrium temperature:

$$Q_{resin}=Q_{fibre} \tag{8.4}$$

$$T_{ss}=\frac{(V_f C_{pf})T_f+((1-V_f)C_{pr})T_r}{(V_f C_{pf}+(1-V_f)C_{pr})} \tag{8.5}$$

Where T_{ss} is the temperature the resin and fibre reach in a steady state condition.

Resin viscosity

The resin was assumed to be a Newtonian fluid and the viscosity dependant on temperature. The viscosity of a resin (μ) can be shown in an Arrhenius equation[76]:

$$\mu=A_\mu \exp(\frac{E_\mu}{R_R T_r}) \tag{8.6}$$

Which can be rewritten in the form

$$\mu=\exp(a_\mu+\frac{B_\mu}{T_r}) \tag{8.7}$$

An oil bath was used to warm the CVP 6345.001 resin (Appendix 10), and a Brookfield viscometer used to measure the viscosity of the resin at temperatures ranging from 20°C to 100°C. The results from this experiment (Appendix 6) were fitted to equation (8.7), and the constants obtained (a_μ=-17.87 and B_μ=5092).

Resin gelation time

The resin gelation time can be expressed as a function of temperature using an empirical formula, derived from that given by Kamal and Sourour[77].

$$t_g = \exp(\Lambda + \frac{\beta}{T_r}) \qquad (8.8)$$

Where t_g is the gel time for the resin at a temperature T. The resin gel times with 1% of the catalyst TBPEH added were measured experimentally, according to the SPI procedure for running polyester resin exotherm curves[66]. The results of these experiments are shown in Appendix 7. The relationship between temperature and gel time was fitted to the form given in equation (8.8) (Λ= -20.1, β=9385).

The gel time is the time to give α_g conversion. Since α_g is small (≈5%)[81] the conversion was assumed to be proportional to time. The time for gelation of the resin to occur was calculated using a summation method, where;

$$\frac{\delta t_i}{t_{g_i}} + \frac{\delta t_{i+1}}{t_{g_{i+1}}} + \frac{\delta t_{i+2}}{\delta t_{g_{i+2}}} + \ldots\ldots = 1 \qquad (8.9)$$

Where $\delta t_i, \delta t_{i+1}, \delta t_{i+2}, \ldots$ are the resin residence times at the resin temperatures $T_{r,i}$, $T_{r,i+1}$, $T_{r,i+2}, \ldots$ and $t_{g,i}$, $t_{g,i+1}$, $t_{g,i+2}, \ldots$ are the resin gelation times corresponding to these temperatures. The gelation of the resin was assumed to occur instantaneously, halting the flow.

Pressure difference causing resin flow

The flow in both the axial regimes was assumed to be laminar and driven by capillary and external injection pressure. The injection pressure assisting flow through the preform was accounted for by the addition of an incremental pressure difference at the flow front, which decreased with the distance from the injection gate (assuming rectilinear flow). A full explanation of this increment can be found in Appendix 8. Depending on the flow rate within the capillaries, the capillary force could either promote or restrict flow.

In the transverse flow model no external driving pressure was assumed, only a capillary pressure promoting flow. An infinite sink was assumed to remove any air within this enveloped bundle.

Fibre Properties

The glass fibre data used in the model for the fibres in the preform are contained in Appendix 9.

Resin Properties

The resin data used in the model for the CVP 6345.001 polyester resin are contained in Appendix 10.

8.3 Axial flow between Fibre Bundles

The following mathematical model of flow in a fibre preform was solved using a finite difference method. A computer program written using Borland Turbo Pascal software was written on an IBM compatible Personal Computer. The flow chart for this program is shown in Figure 8.4.

The Hagen-Poiseuille law for flow through a tube was used, where an effective hydraulic diameter was estimated for the tricorn between the fibre bundles. A schematic of the inter-bundle space is shown in Figure 8.2. The discharge of a fluid through a tube is given in Equation (2.6). This discharge (Q) can be related to the velocity of the flow by[46]:

$$v_z = \frac{Q}{A_b} = \frac{\delta z}{\delta t} \tag{8.10}$$

From Equation (2.6) and (8.10) the distance increment of flow (δz) during the time increment (δt) was obtained:

$$\delta z = \frac{d_b^2 \delta P_A}{32 \mu l} \delta t \tag{8.11}$$

The capillary area between the fibre bundles (A_b) was equal to;

$$A_b = R_b^2(\sqrt{3} - \frac{\pi}{2}) \tag{8.12}$$

and the wetted perimeter (p_b) was;

$$p_b = \pi R_b \tag{8.13}$$

The effective hydraulic radius can then be calculated from[73]:

$$r_b = \frac{2A_b}{P_b} \tag{8.14}$$

The capillary pressure due to the wetting force (δP_{cw}) is given in equation (2.4). The total pressure difference available δP_A was equal to:

$$\delta P_A = \delta P_{ca} + \delta P_{ip} \tag{8.15}$$

Time step choice

A range of time steps was evaluated to assess the effect of δt on the impregnation distance (δz). The distance impregnated in a time of 30 seconds was calculated for these time steps and the results shown in Figure 8.5(a). The impregnation distance was seen to converge to a steady value using time steps lower than 1×10^{-3} seconds.

Results

The conditions used in the model were 35% fibre volume fraction, 20°C resin injection temperature and a fibre temperature of 90°C. The model predicted the time to flow 0.5m in the inter-bundle spaces to be 1312 seconds (Table 8.1). Figure 8.6 shows a graph distance of impregnation along the inter-bundle spaces and fibre capillaries vs time. A moulding using the same process conditions was filled in 22.1 seconds. Mould filling predictions using the principal permeability of unidirectional NCF[79] (discussed in Chapter 6) are compared in Figure 8.6 to the inter-bundle fill times.

The fill times predicted for flow in these inter-bundle spaces were orders of

magnitude higher than the experimental results, or the predicted permeability fill time. The reason for this large discrepancy was thought to be caused by the assumptions made during the geometric model development. The geometric model, of hexagonally packed fibres forming circular fibre bundles, is unrealistic. The idealised bundles bear little resemblance to the elliptical tape like strands in the unidirectional fabric used in the moulding trials. The spaces between these strands are much larger than those depicted in the geometric model.

Elliptical Fibre Bundle Preform Geometry

Following the initial predictions using a circular fibre bundle structure, the model was refined to take into account an elliptical bundle structure. After a study of approximately twenty sections of unidirectional mouldings (Figure 8.7a) an approximate elliptical shape for the fibre bundles was chosen (Figure 8.8a) from average measurement of the fibre bundles. The major axis length of the ellipse (J) was set at 2.6mm and the minor axis length (j) was fixed at 0.8mm. Using standard formulae[84] the area and the circumference of the bundles was calculated. The spacing of the bundles was chosen from average measurements of the sections assessed, where the horizontal spacing was eight times the vertical spacing (Figure 8.8b). The spacing of the bundles was calculated to depict the fibre volume fraction for the preform, using the unit cell structure shown in Figure 8.8c;

$$\frac{\pi N_f R_f^2}{V_f} = (J+8c)(j+c) \qquad (8.16)$$

Solving this quadratic equation gives a value for c (the fibre bundle spacing).

The capillary area (A_{Be}) was calculated from the unit cell and fibre bundle areas (Figure 8.9), where;

$$A_{Be} = 2\left((J+8c)(j+c) - \frac{\pi}{4}Jj\right) \qquad (8.17)$$

and the wetted perimeter (P_{Be}),

$$P_{Be} = \frac{\pi(J+j)}{4} \qquad (8.18)$$

From these values a hydraulic diameter of 1.67×10^{-4}m was calculated using Equation (8.14).

Results

Using the methods previously described the impregnation rates were calculated for the 35% fibre volume fraction preform.

The graph in Figure 8.10 shows the resin impregnation rate into the capillaries formed between elliptical fibre bundles and in the capillaries between fibres. In this case the resin was predicted to travel 0.5m along the inter bundle spaces in 55 seconds compared with 1214 seconds for the circular fibre bundle case (Figure 8.11). The ratio of the hydraulic diameters for the elliptical structure compared with the circular structure is approximately 4:1. This factor is able to reduce the predicted impregnation time of the preform to a more realistic value of 55 seconds compared to 22 seconds determined experimentally in a unidirectional moulding (Table 8.1).

To compare the effect of the heat transfer calculation with a set isothermal resin and fibre temperature, impregnation rates were calculated using a temperature of 90°C (the mould temperature). The resulting filling time was 31 seconds. The resin in this case was approximately 30°C higher than the equilibrium temperature used in the model.

The filling times predicted using the principal permeability values for the reinforcement are compared with the predicted rates in Figure 8.11. The permeability prediction for mould fill is 26 seconds, which is a factor of two lower than the model prediction. Using the model under an isothermal of 90°C the predicted fill time was further reduced to a value closer to the predicted permeability value and the mould filling time of 22 seconds.

8.4 Axial Flow in the Capillary between Filaments

A similar case to that considered for the axial flow in the inter-bundle spaces was considered for the axial flow in the capillaries formed between filaments. The polycorn between the fibres was used to gain an effective hydraulic diameter, which allowed the Hagen-Poiseuille law for flow through a tube to be used. This relied upon the resin having impregnated the strand to gain access to the capillary.

Since the area between fibres is a non-circular section an equivalent area (Figure 8.12) can be obtained by considering the cross sectional area A_c and the wetted perimeter (p_c). An equivalent hydraulic radius (r_c) was obtained;

$$r_c=\frac{2A_c}{p_c} \tag{8.19}$$

The capillary area can be calculated from:

$$A_c=\sqrt{3}(R_f+d)^2-\frac{1}{2}\pi R_f^2 \tag{8.20}$$

and the wetted perimeter (not the whole perimeter of the section) equal to;

$$p_c=\pi R \tag{8.21}$$

The impregnation was modelled using equations (8.11) and (8.15).

Elliptical fibre bundles

Since the magnitude of the elliptical fibre bundles were assumed to be fixed the fibre volume fraction within the bundles was also fixed. The fibre spacing (d) within these bundles was calculated from the bundle area, and the number of fibres in the bundle:

$$A_{Be}=2\sqrt{3}\,N_f(R_b+d)^2 \tag{8.22}$$

d was found from solving the above quadratic equation.

Heat transfer, axial flow case

Heat transfer was assumed to occur between the fibres and the resin only in

the radial direction. The axial heat transfer between the hot fibres and the colder resin can be described as forced convection in a non-circular section. Using the hydraulic radius calculated in equation (8.19), the Nusselt number for this section was estimated[74] to lie between 2.5 and 3. The surface heat transfer coefficient h_a can be calculated from:

$$Nu_c=\frac{h_A D_c}{K_r} \tag{8.23}$$

The rate of heat transferred in the axial case can now be determined.

$$\delta q=h_A(C_A\delta z)(T_f-T_r) \tag{8.24}$$

Where C is the peripheral contact surface area between resin and fibre.

The rate of change of heat stored in both the fibre and resin is:

$$\frac{\delta q}{\delta t}=\dot{m}C_p\frac{\delta T}{\delta z} \tag{8.25}$$

Where $\dot{m}_r$ is the mass flow rate of the resin:

$$\dot{m}_r=A_c\rho_r\delta z \tag{8.26}$$

and $\dot{m}_f$ is the corresponding mass of the fibre:

$$\dot{m}_f=\frac{\pi}{2}R_f^2\delta z\rho_f \tag{8.27}$$

An approach using resistance elements can be used[74] to calculate the heat conduction through the fibre to the resin, where the fibre and resin capillary are divided into regions (Figure 8.13)(Appendix 11). The heat transfer occurs between nodes which are assigned to each region. An electrical resistive network analogy may be used to consider the thermal resistances between resin and the fibre.

Temperature effects

A Fourier number, which is a dimensionless constant was used to determine

the time step δt such that stability criteria, which are established analytically for linear problems, are met[82]. For the solution in question the Fourier number was set at ¼, since a 2-D solution was required[82] and the time step solved from:

$$\delta t = \frac{\rho C_p (\Delta x)^2}{4k} \qquad (8.28)$$

The capillary diameter and specific heat capacity values were inserted into this equation and the time step obtained was found to be in the order of $1x10^{-4}$ seconds. This time step showed that equilibrium temperature in the sections considered was reached in less than one second. The heat transfer in the model was assumed to occur instantaneously and a steady state temperature (using equation 8.5) was used for the resin and fibres.

Time Step Choice

The method of calculating a time step was described in section 8.3. The value of $1x10^{-3}$ seconds chosen (Figure 8.5) was used in all axial flow models.

Results

Impregnation predictions were generated using the values for injection pressure and resin and fibre temperatures previously described (section 8.3). Although the circular fibre bundle preform was considered to be inaccurate, it was used to provide initial impregnation distances which could be compared to those generated for the elliptical structure. Since the size of the elliptical fibre bundles were assumed to be fixed, the filament spacing was predetermined. For the 35% fibre volume fraction preform considered, the local fibre volume fraction within these fibre bundles was approximately 54%, less than the local volume fraction when the circular fibre bundle geometry was considered. This increased fibre volume fraction reduced the fibre spacing.

Impregnation was predicted at 0.065m along the fibre capillaries during the time taken (1312 seconds) for the resin to fill 0.5m along the inter-bundle spaces, for the circular bundle geometry. Using the elliptical bundle geometry the capillary

impregnation distance was 0.01m in the 55 seconds taken for the inter-bundle spaces to fill. The rate of impregnation is shown compared to the inter-bundle flow in Figure 8.6. The flow rates within these capillaries may be 50 times lower than the axial flow rates in the inter-bundle spaces. The discrepancy between these two flow rates was expected since the impregnation is dependant on the square of the hydraulic diameter of the inter-bundle space or capillary. In experimental trials the difference between these two flow was noticeable.

8.5 Transverse Flow Model between Fibres

Transverse flow was assumed into the fibre bundle (Figure 8.14). The fibre surface in the transverse direction was divided into a number of finite parallel plates. Continuity of volume was assumed. A similar approach to that employed by Bayramli et al[47] was used, which assumed steady laminar flow between parallel plates. This method used a different method of calculating the time step for flow between the plates than was used for the axial flow models and an alternative method of determining bifurcation than was used by Bayramli et al[47]. Flow between plates can be determined from[46].

$$Q=\frac{b(2w)^3}{12\mu}\frac{\delta P_t}{r} \tag{8.29}$$

From this equation the time step δt was derived:

$$\delta t=\frac{12\mu}{(2w)^2}\frac{\delta r.r}{\delta P_T} \tag{8.30}$$

The capillary pressure between two parallel plates (δP_{cv}) is given in Equation (2.7). In the absence of gravity the radius of curvature of the meniscus was assumed to be constant. The capillary pressure was dependant on the position of the contact line on the circular cross section of the fibre (Figure 8.15). Geometric considerations give r_{cc}, (Figure 8.16), δP_{ct} became:

$$\delta P_{ct}=\frac{\gamma\cos^2(\theta-\phi)}{w_t} \tag{8.31}$$

The total pressure difference across distance δr was then,

$$\delta P_T = \delta P_\alpha + \delta P_\psi \tag{8.32}$$

The assumption that the radial spacing δr is changed during each incremental time step such that consecutive area elements were equal (conservation of volume), was made;

$$A = 2w_i \delta r_i \tag{8.33}$$

The meniscus contact angle to the fibre ϕ at any point was calculated from:

$$\phi_i = \sin^{-1}\left(1 - \frac{r}{R_f}\right) \tag{8.34}$$

Where r is the total distance travelled along the channel ($r = \Sigma\delta_r$). From the position of the flow front on the fibre, the half plate separation w (Figure 8.16) was obtained from,

$$w_i = R_f(1 - \cos\phi_i) + d \tag{8.35}$$

The overall viscous resistance results from the viscous forces which retard the flow in the channels between the fibres. Figure 8.17 shows several layers of fibres, with the spaces between the fibres being divided into channels from $\phi = \pi/6$ to $\phi = -\pi/6$. The unit cell structure for the transverse flow is shown in Figure 8.3(a). Figure 8.17 shows a unit cell with three channels per layer per meniscus. The triangular areas between each channel had not been included in the channel calculations and to incorporate these excess areas into the calculation (Figure 8.19), the unit channel length was increased to compensate for this excess quantity ϕ_{ex} which is given by,

$$\phi_{ex} = f(d, R_f) \tag{8.36}$$

The complete solution for ϕ_{ex} can be found in Appendix 12.

The condition under which bifurcation occurs was specified as:

$$s > s_{max} = \sqrt{3}(R_f + d) - R_f \tag{8.37}$$

Where s is the position of the centre of the resin meniscus and s_{max} is the point at

which the meniscus touches the next fibre (Figure 8.20). The meniscus position s was determined as:

$$s=R_f\sin\phi_i+\frac{w_i}{\cos(\theta-\phi_i)}(1-\sin(\theta-\phi_i)) \qquad (8.38)$$

The derivation of s and s_{max} can be found in Appendix 13.

Once bifurcation occurred, the resin meniscus was assumed to start in a new channel and ϕ_i was initialised as;

$$\phi_{initial}=-(|\phi_{last}|-\frac{\pi}{3}) \qquad (8.39)$$

This new value of ϕ_i replaces the initial starting condition of $-\pi/6+\phi_{ex}/3$.

These equations describe the flow though a single channel between fibres. For each layer of fibres there were three channels, but the wetting of the second and third channels occurred concurrently. Once the resin had wetted all three channels, a second layer of fibres started to be wetted and ϕ_i was initialised as:

$$\phi_{initial}=\frac{\pi}{6} \qquad (8.40)$$

Transverse volume step

A time step was not used to dictate the flow in the transverse model, since the cross sectional areas in each step would be dissimilar. Instead a conservation of volume method was used, where the volume in each step was kept constant and the time step for each cycle varied. The constant volume step of each section was calculated from the geometrical area between the fibres to provide greater than 100 steps in each channel. A range of areas were evaluated using the model and the value of $3x10^{-13}m^2$ was chosen.

Elliptical fibre bundles

The elliptical shape of the fibre bundles means that fewer filaments are

required to become impregnated compared to a circular bundle structure. The minimum number of filaments along the minor axis to the centre of the bundle was 21 (Figure 8.7b). The transverse flow into these fibre bundles was only considered in a central circular core of fibres.

Heat transfer, transverse flow case

For the heat transfer in the transverse direction a flow over a cylinder approach was used to obtain the Nusselt number[73,75]. From this value the surface heat transfer coefficient h_{ct} was obtained.

$$Nu_{ct}=JRe_{ct}^{n} \tag{8.41}$$

The Reynolds number Re was calculated from:

$$Re_{ct}=\frac{U_{max}D_f}{\nu} \tag{8.42}$$

Where ν is the kinematic viscosity of the resin. U_{max}, the maximum resin velocity occurring during transverse flow was used, since an analogy between flow over banks of tubes is being used.

$$\nu=\frac{\mu}{\rho_r} \tag{8.43}$$

J and n can be obtained from[75]:

$$J=\sqrt{a_1+B_1\sqrt{Re_{ct}}} \tag{8.44}$$

$$n=a_2+B_2\sqrt{Re_{ct}} \tag{8.45}$$

where a_1=0.16989, B_1=0.640323, a_2=0.076739 and B_2=0.2752. The heat transfer coefficient h_{ct} can now be found from Equation (8.23). Equations (8.24) and (8.25) were used to calculate the convective heat transfer coefficient during transverse flow. The effects of heat conduction through the fibre to the resin are also included into the transverse heat transfer calculation. The same network approach described above was used, where the fibre and resin flow front were divided into regions (Figure 8.21).

After consideration of the heat transfer in the axial flow regime, the heat transfer during transverse flow was assumed to occur almost instantaneously, such that a steady state temperature could be used for resin and fibre temperatures.

Results

For the standard process conditions described in section 8.3, the transverse impregnation of the circular fibre bundle was estimated to take 28.9 seconds for the resin to fill the 38 layers. The local fibre volume fraction in the elliptical fibre bundles was approximately 54%, since the area of the fibre bundle was determined experimentally. This caused the idealised spaces between the fibres to be reduced, slowing the transverse filling process. The two transverse impregnation cases are compared in Figure 8.22, where the 21 layers of fibre were impregnated in 16 seconds. The impregnation of these bundles will also be affected by the presence of size bonding individual fibres. The spacing of randomly distributed fibres, unlike those depicted in the model will affect this impregnation.

8.6 Gelation Predictions

Using the gelation model with the circular fibre bundle geometry the resin gelled when the inter-bundle spaces had filled 0.549m and the fibre capillaries 0.0711m. Resin pre-heated to 60°C was predicted to cure when the resin had reached 0.389m along the inter-bundle spaces and 0.0504m along the fibre capillaries. Gel predictions were not obtained using the elliptical model since the time scales for the inter-bundle spaces to fill were much lower and cure would not occur.

8.7 Discussion

The work contained within this chapter describes a series of simple mathematical models which can be applied to predict the impregnation by resin of an idealised preform. Both fluid and thermal effects between the fibres and resin have been considered in the model, although the heating effects of the mould are ignored.

The three impregnation models have been used to predict the rates at which an idealised preform would be impregnated under typical process conditions. The

model has suggested that the spaces between fibre bundles would fill more quickly than the axial flow along the capillaries within the fibre bundles. The fibre bundles would be impregnated by transverse flow more quickly than by axial flow along the inter-fibre capillaries. If the bundles fill by this transverse action, with the impregnation being led by the flow through the inter-bundle spaces, this would create the conditions for air to become entrapped within the bundles.

The gelation model was used to predict whether the resin cures prior to full impregnation of the mould. If so, the fibre bundles will not be fully impregnated and the resin flow front in the inter-bundle spaces will be further advanced than the flow within the bundle. Experimental work showed that pre-heated resin impregnated the flat plaque mould (moulding 4286) without pre-cure, this model (in conjunction with a valid impregnation model) could suggest suitable temperatures, to which the resin could be pre-heated to, before the being cured without filling the mould.

The impregnation model, using circular closely packed fibre bundles, suggested that the inter-bundle spaces would become impregnated after 1312 seconds compared with 22 seconds in the experimental case. With the geometric model modified to represent elliptical fibre bundles, the axial flow model suggested that the inter-bundle spaces would become impregnated after 55 seconds. The major reason for this discrepancy was the assumed size of the capillaries between fibre bundles. The ratio of capillary areas is 16:1 when the elliptical and circular bundle structures are compared.

The elliptical fibre bundle model was used to predict an isothermal impregnation with the resin and fibre temperatures at 90°C (approximately 30°C higher than that used previously). The inter-bundle spaces were predicted to fill in 31 seconds, which approached the experimental and permeability predicted values (22 & 26 seconds). The heat transfer model only considered the flow of heat between fibres and resin. The mould surface heat transfer has a significant effect on the heating of the preform and resin since it is the heating surface. Since microscopic flow around fibre bundles and into bundles has been considered, this important effect has had to

be ignored.

The preform structure described by the model has considered 0° fibre bundles and has assumed no stitching, or cross strands which hold the preform in shape. The quasi-unidirectional material which has been used in the moulding trials has both of these features plus a layer of thermoplastic binder between layers of the fabric. The fibre bundles are present in elliptical tape-like sections but the packing of layers does not conform to the hexagonal spacing depicted in the model. The spacing between the fibres is not uniform and may vary between tricorns to polycorns of different sizes. The effects of the cross bundles, the stitching and the thermoplastic binder have also been neglected in the model. The impregnation of the fibre bundles due to a transverse mechanism has been assumed although the presence of size bonding individual fibres impeding the flow has not been considered.

The modification of the preform model from closely packed circular fibre bundles to elliptical bundles affected the hydraulic radius value used in the inter-bundle flow model. The result of this modification was a significant reduction in the impregnation time for the inter-bundle spaces, indicating that the bundle shape and spacing are two of the most important factors affecting the model. It must be noted however that the use of a hydraulic radius for simple symmetrical sections, such as those considered, is only an approximate method[46] for determining flow within a section.

Another factor affecting the axial impregnation models is the driving pressure causing the resin flow in the preform. The models assume a capillary pressure and an additional injection pressure acting on the resin, which decreases with distance from the injection gate. In the axial inter-bundle model the driving pressure reduces during impregnation, until capillary flow is the major impregnation mechanism. Experiments have shown that the injection pressure is the major driving impregnation mechanism. Other factors which may influence the results are the assumed values of contact angles between glass and resin and surface tension data. The effects of viscosity and temperature on the contact angle between resin and glass have been

ignored. The contact angle data used was collected over a very low velocity range and the values interpolated to gain the expression used in the program. The surface tension value is from the same source and the effects of temperature, viscosity or velocity effects on this value are unknown. The effect of viscosity increasing with resin polymerisation has been ignored, since no data for this polyester resin was available.

Experimental impregnation studies (section 6.2) suggested the axial flow along the fibre capillaries would be slow in comparison to the inter-bundle flow. This is supported by the model predictions. The geometric model which assumes the capillaries are formed from a tricorn, do not represent reality since the fibre packing will be random and the capillaries will be formed from a selection of polycorns (Figure 8.7b). The model also assumes that the resin is able to reach the capillaries. As has been demonstrated in Chapter 6, the presence of size menisci may restrict the resin gaining access to the capillary, prohibiting impregnation.

The quasi-unidirectional mouldings sectioned in Chapter 5 were shown to have voids scattered within the bundle cross sections. The results from this model indicate that a central core of voidage is likely in the fibre bundle. The scattered voids within the bundles examined suggest that the voids are due to a transverse filling mechanism and an area of voidage close to the fibre bundle core has developed. However, during the final impregnation stages of the preform where the resin has reached a hydrostatic pressure, the air within the voids has become compressed and the area of voidage reduced.

The model described in this chapter can only address flow within unidirectional fibres. Its application is therefore limited to preforms with simple geometries and not more complex reinforcements. The model predicts flow into unidirectional preforms in time scales which are in excess of experimental values. The model can however only predict the filling of fibre bundles and does not face the issue of whether voids will become entrapped within the preform or the extent of voidage in the final moulding. Future work which could improve these models is discussed in section 9.3.

List of Tables

List of Figures

Table 8.1 **Model results using a 35% volume fraction preform**

Fibre Bundle Geometry	Injection Pressure (bar)	Resin inlet temperature	Predicted Time to impregnate 0.5m between fibre bundles (seconds)	Predicted Distance impregnated in fibre capillaries (m)	Predicted Time to fill the fibre bundle transversely (seconds)	Corres-ponding moulding No.	Impreg-nation Time (seconds)	Predicted Preform Fill Time from Permeability Values (seconds)
Circular	2	20	1312	0.0648	28.9 (38 layers)	4285	22.1	26
Circular	2	60	758	0.065	23.4 (38 layers)	4286	12	15.6
Elliptical	2	20	55	0.0095	20.5 (21 Layers)	4285	22.1	26

Figure 8.1

Co-ordinate System for Flow into a Unidirectional Preform

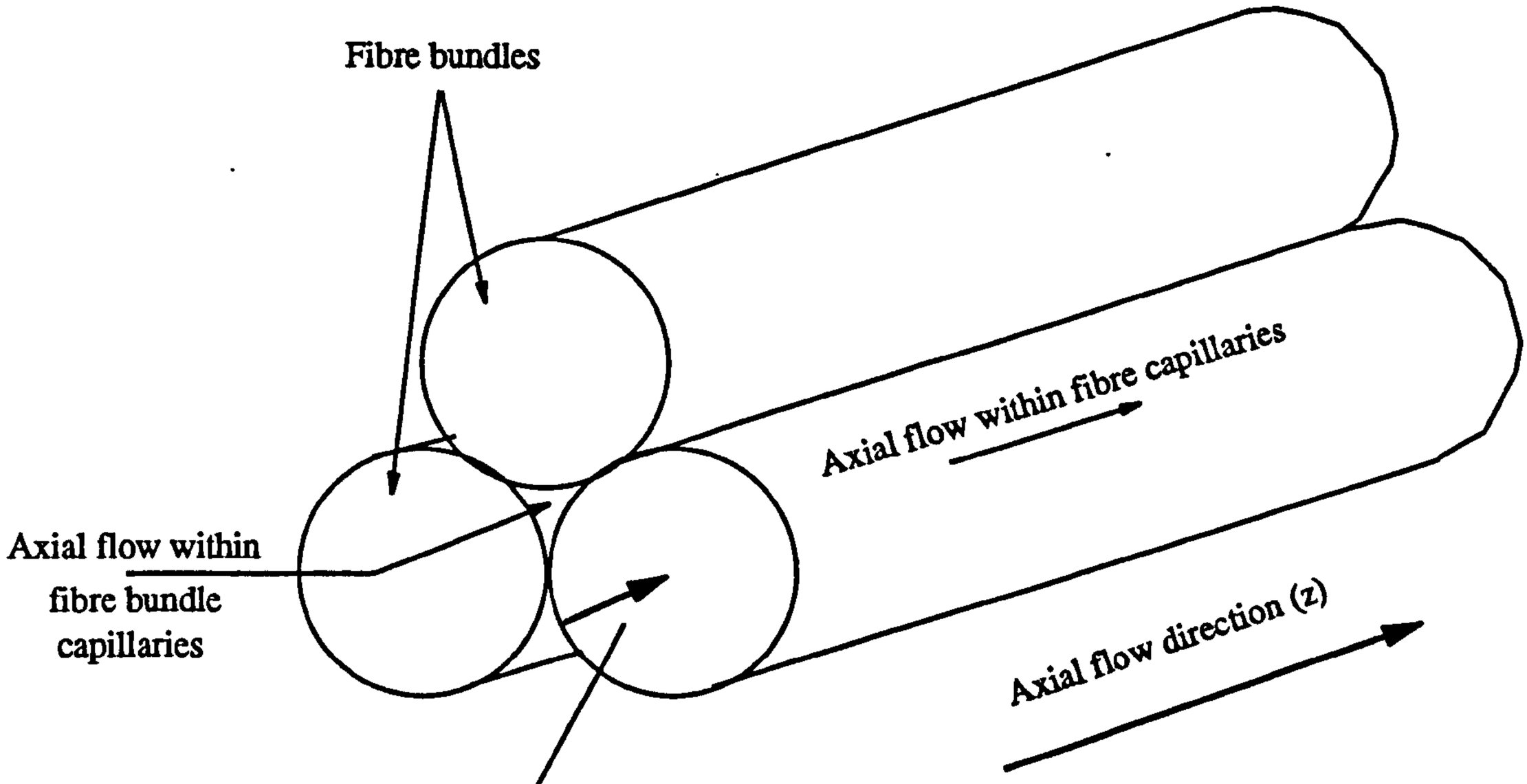

Figure 8.2 Preform Structure

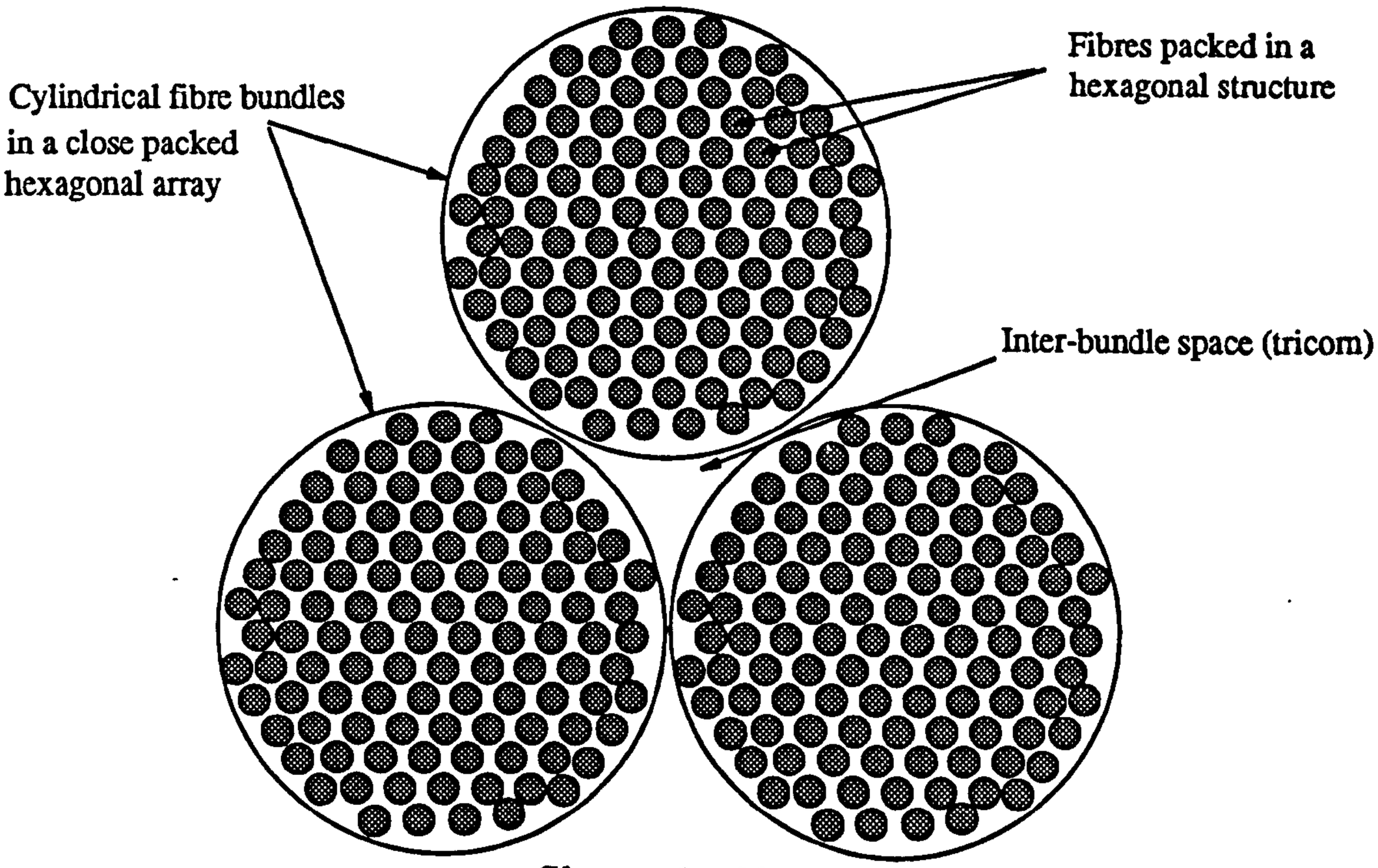

Figure 8.3 Preform Geometry

a) Fibre spacing

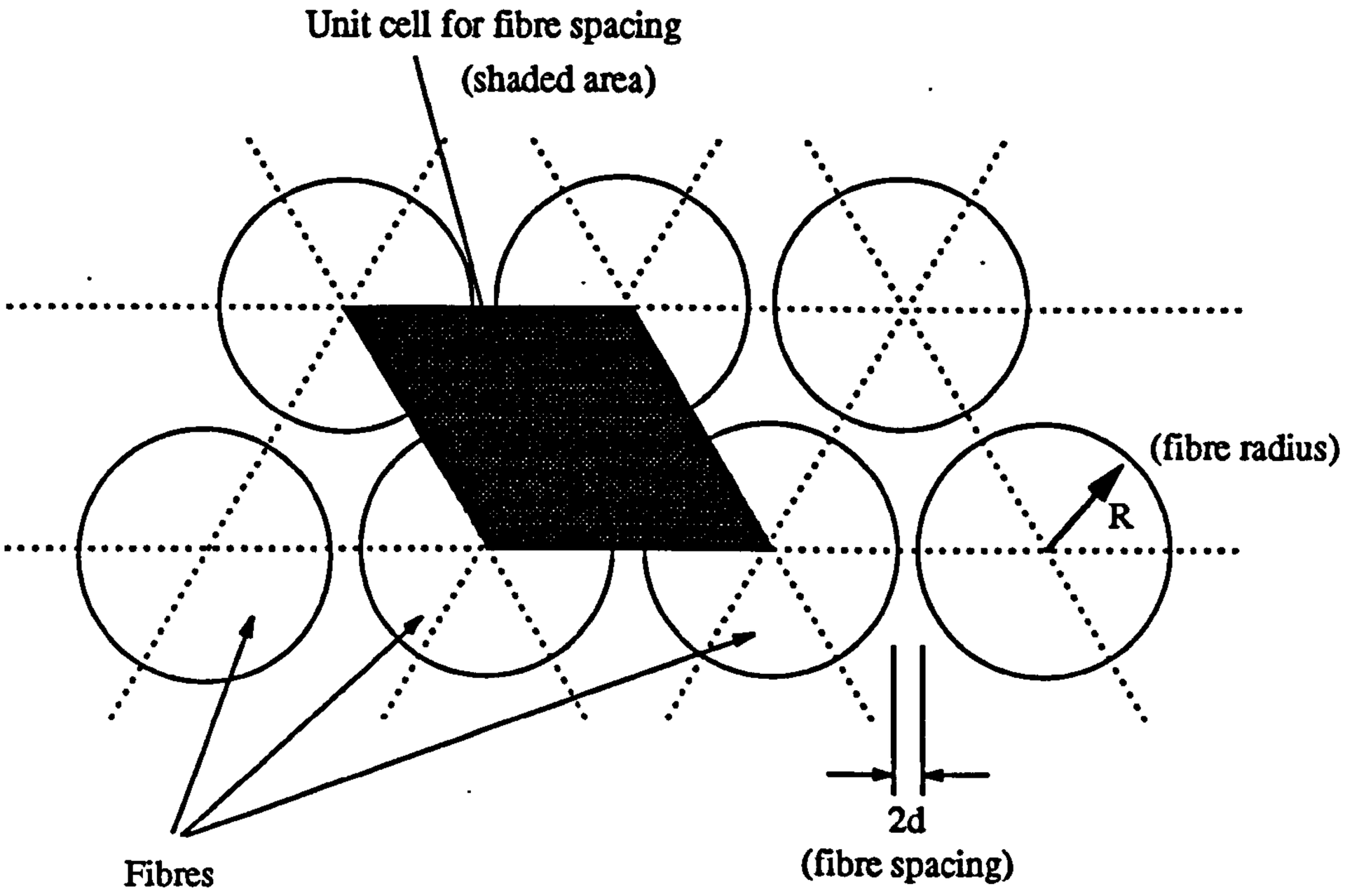

b) Fibre bundle spacing

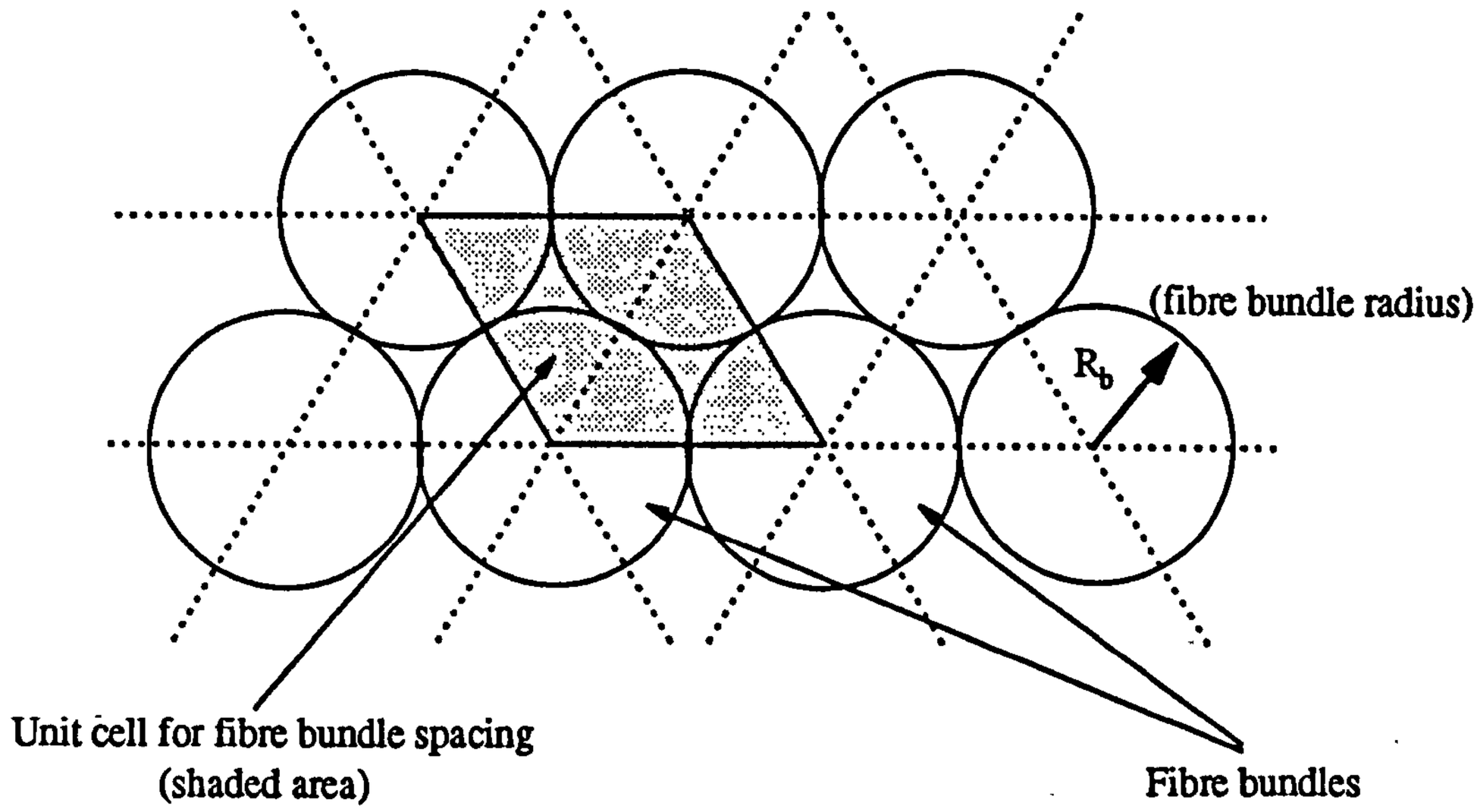

Figure 8.4 Flow Diagram for the Impregnation Model in a Unidirectional Preform

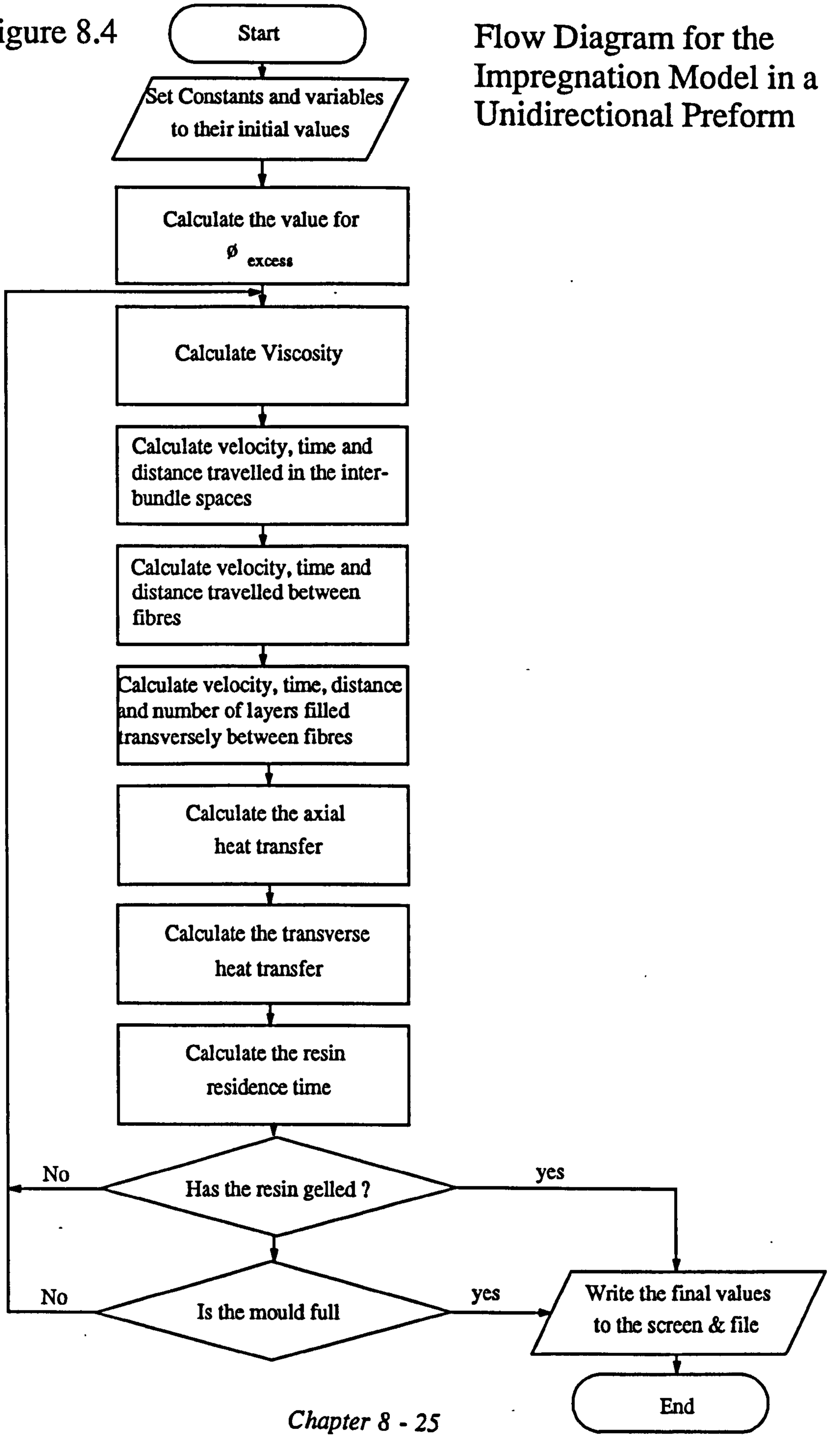

Figure 8.5 The Effect of Time Step upon Distance Impregnated (First 30 seconds)

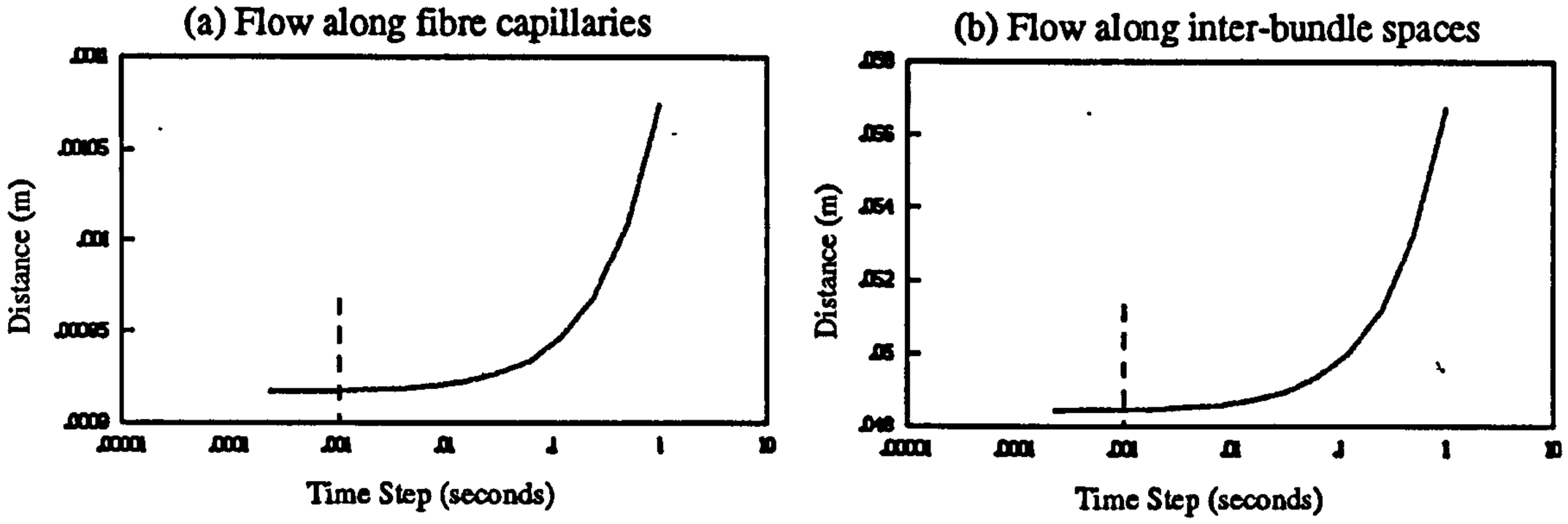

Figure 8.6 Resin Impregnation Distance Vs Time For The Standard Moulding Conditions

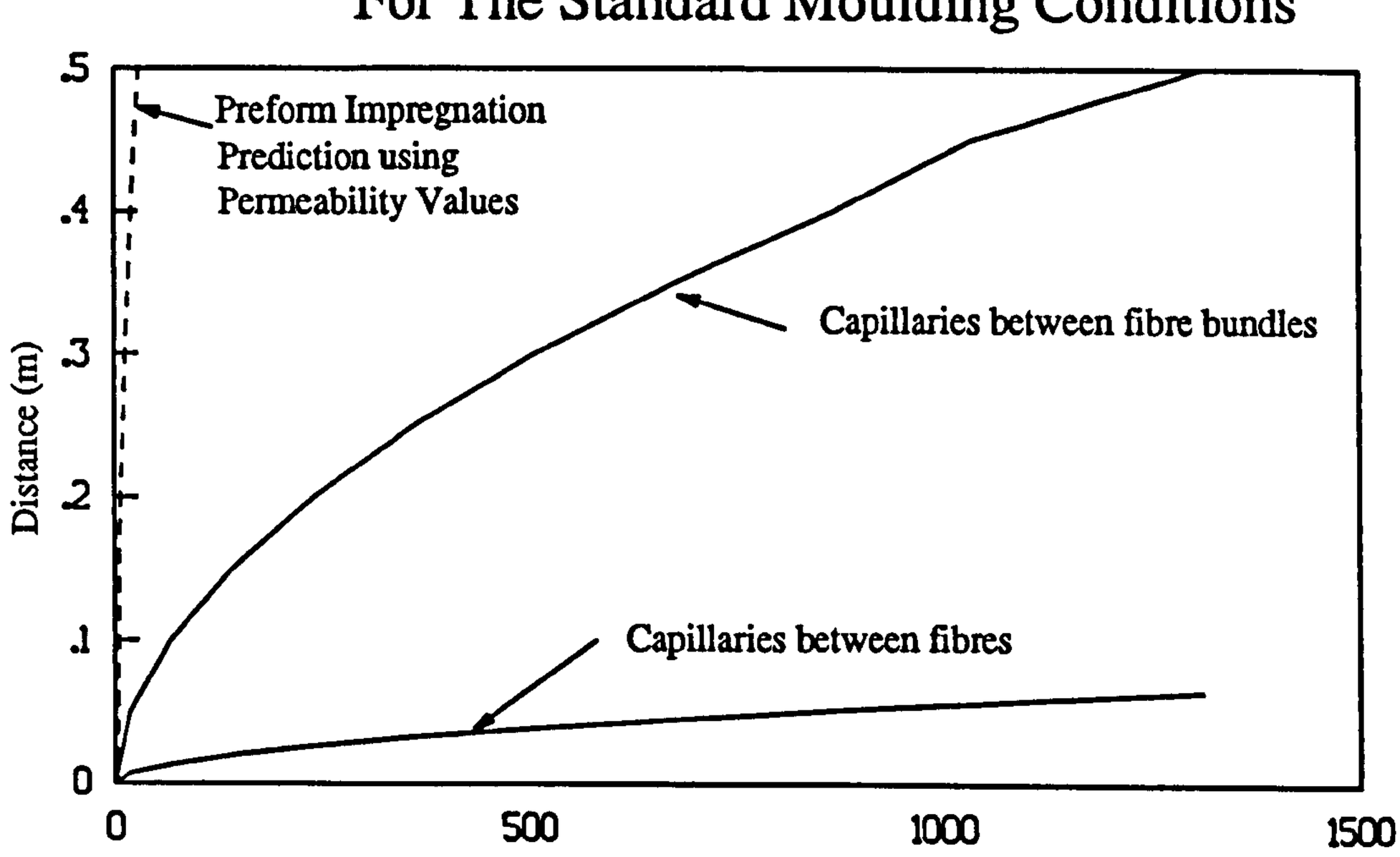

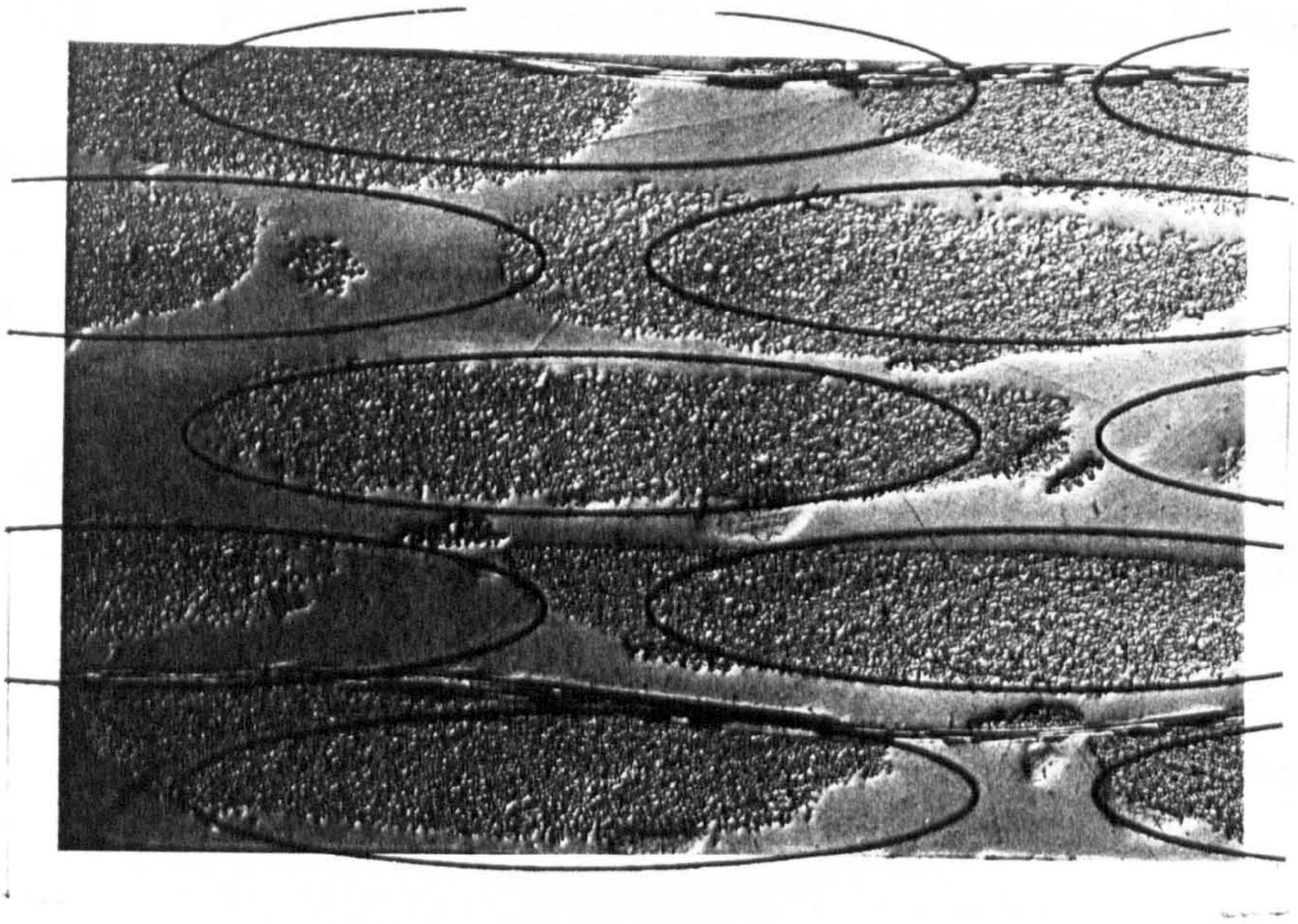

Figure 8.7(a) Elliptical Fibre Bundle Geometry Compared with a Unidirectional Laminate Section

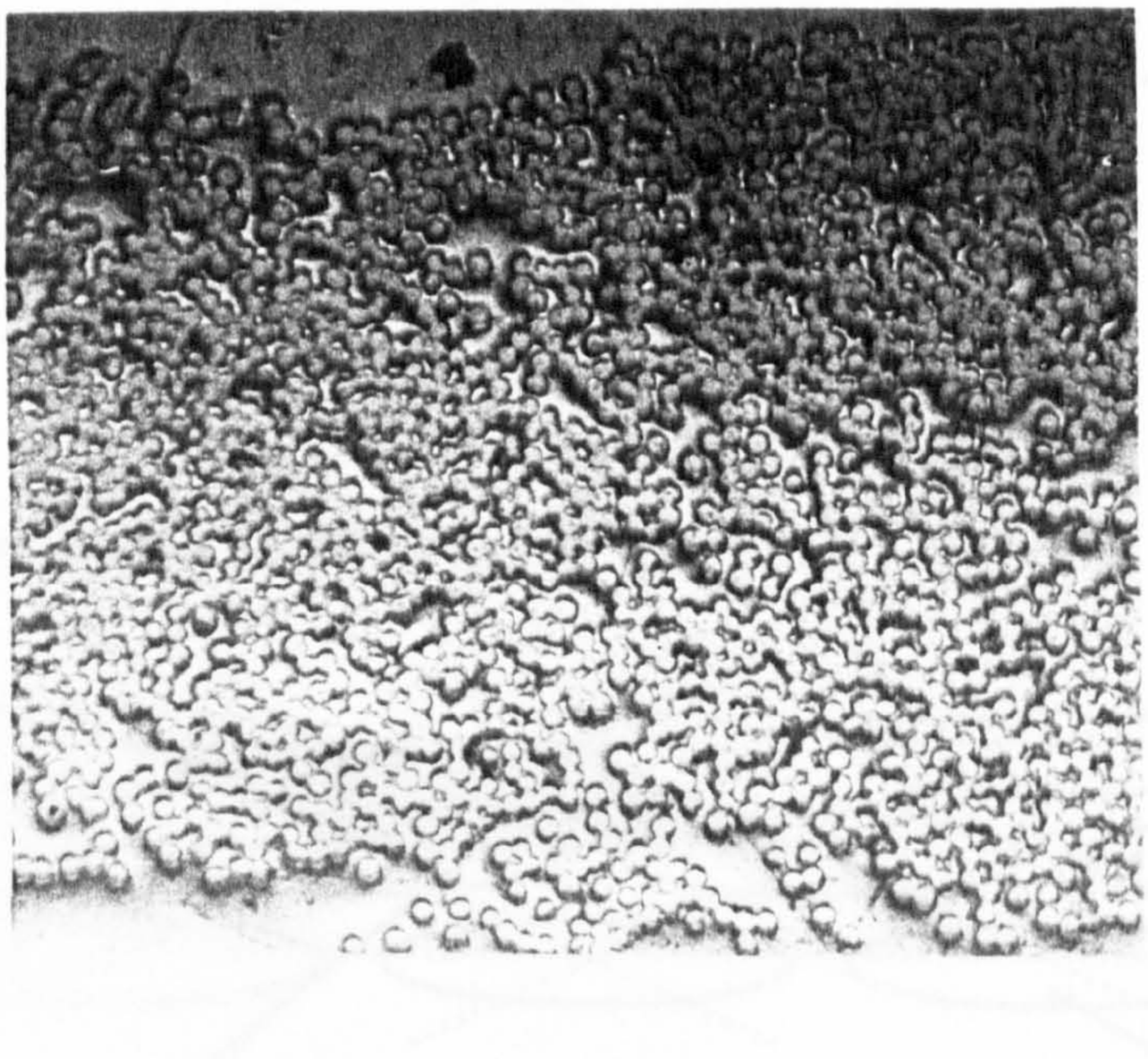

Figure 8.7(b) A 2400 Tex Fibre Bundle From a Unidirectional Moulding (x100)

Figure 8.8 Preform Geometry using Elliptical Fibre Bundles

a) Elliptical Fibre Bundle Geometry

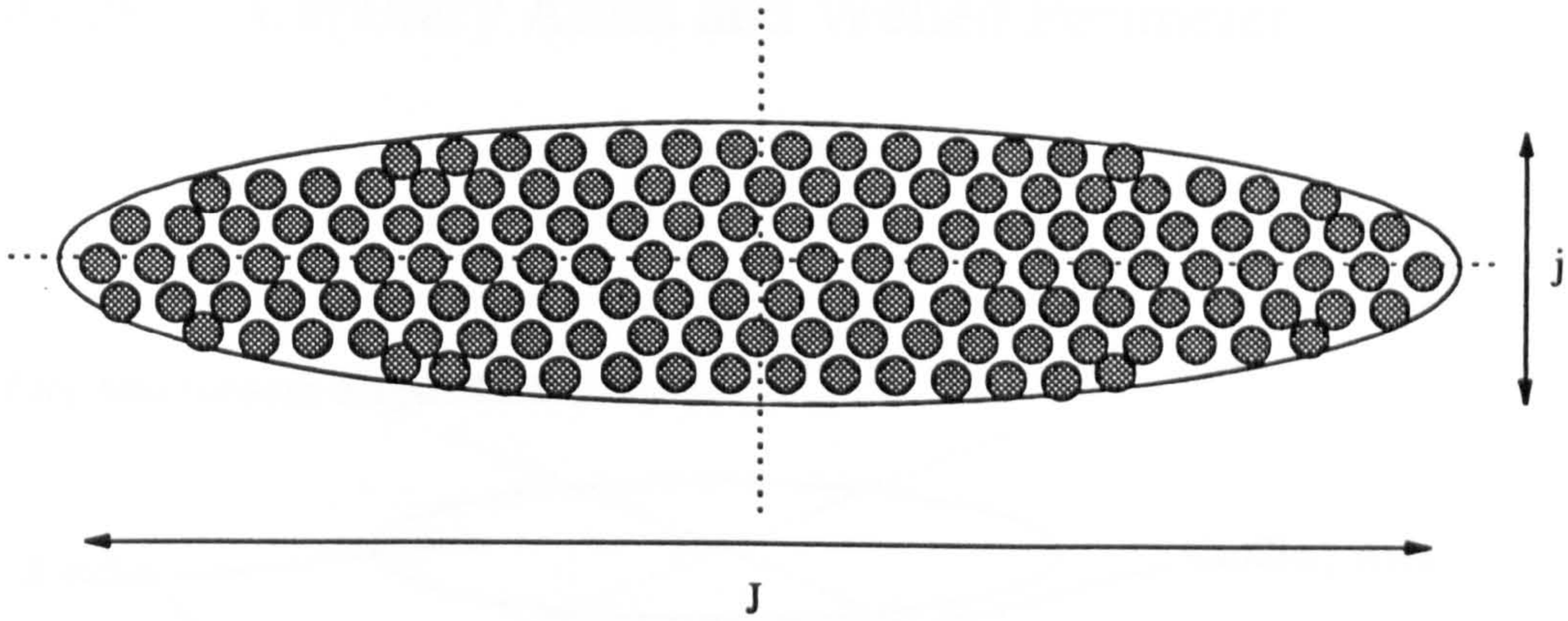

b) Elliptical bundle spacing

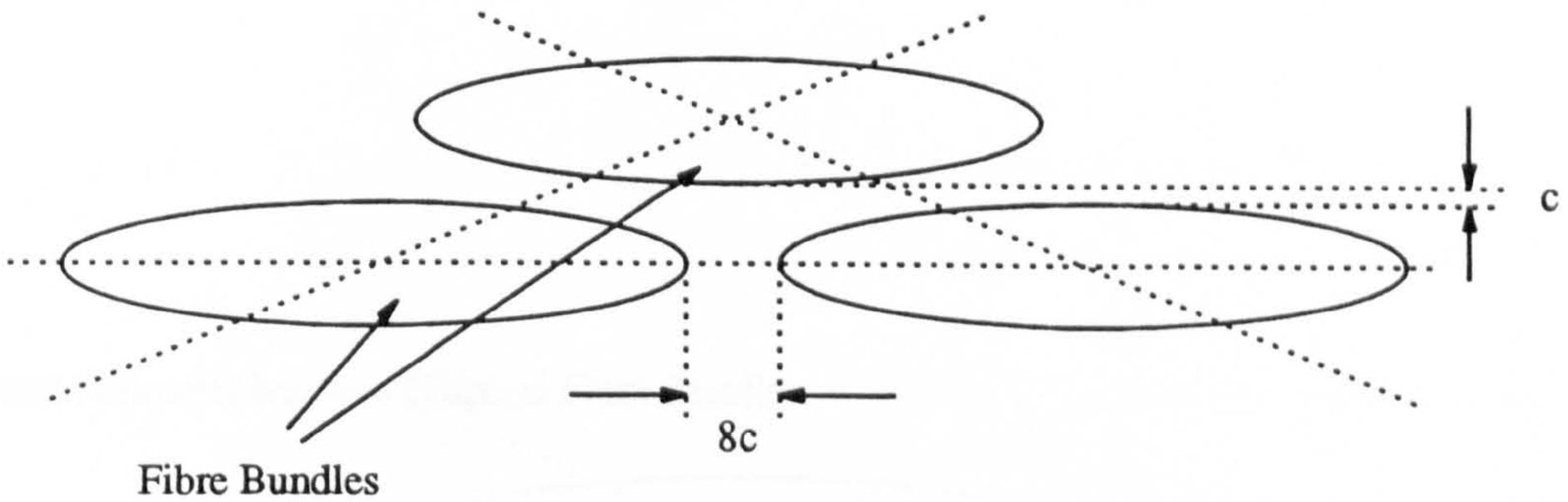

c) Elliptical Spacing for Unit Cell

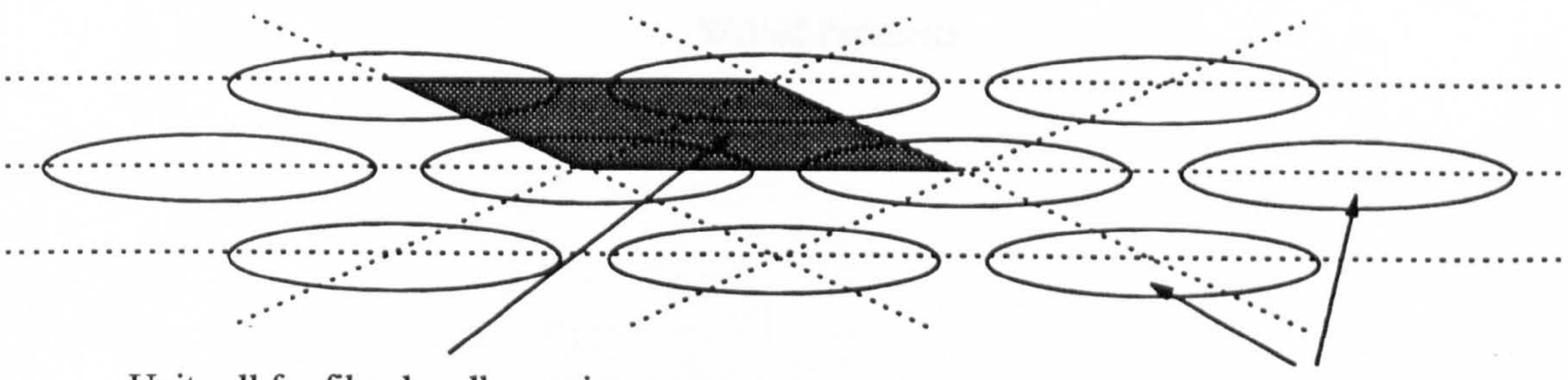

Figure 8.9 Capillary Areas and Wetted Perimeter

a) Capillary Area between Elliptical Fibre Bundles

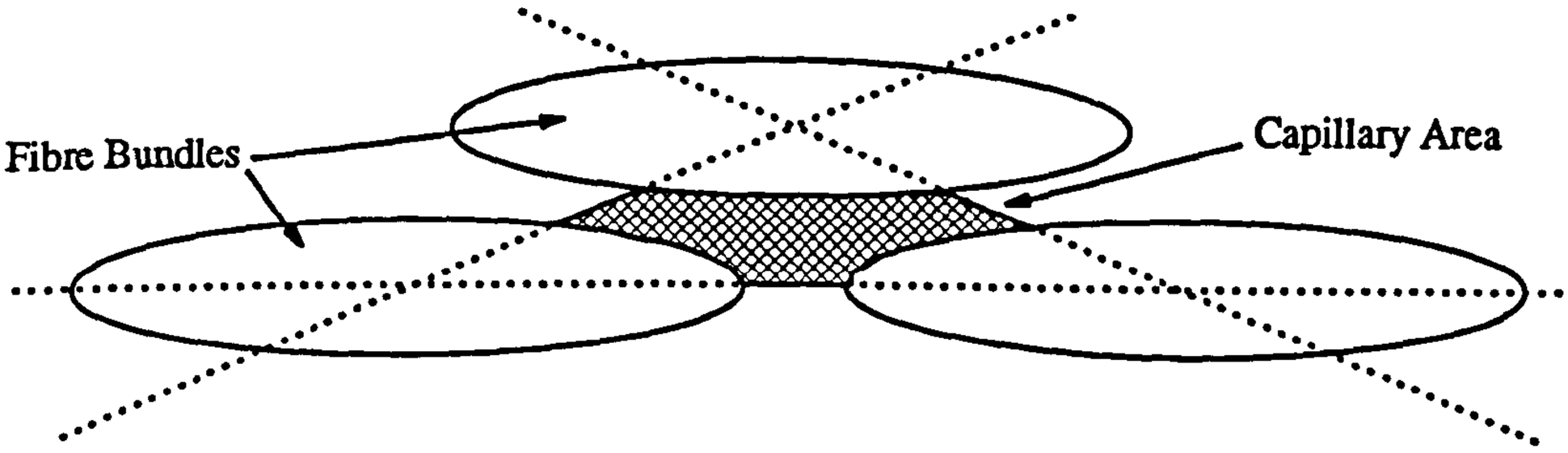

b) Wetted Perimeter between Ellipical Fibre Bundles

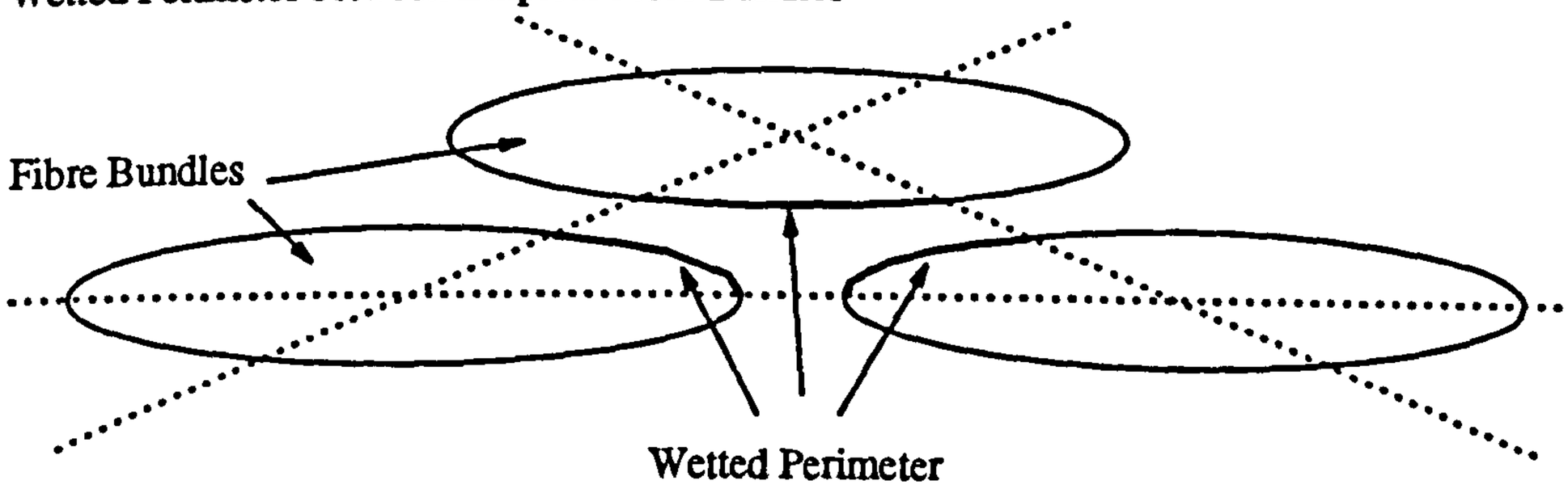

Figure 8.10 Resin Impregnation Distance Vs Time For The Standard Moulding Conditions Using Elliptical Fibre Bundles

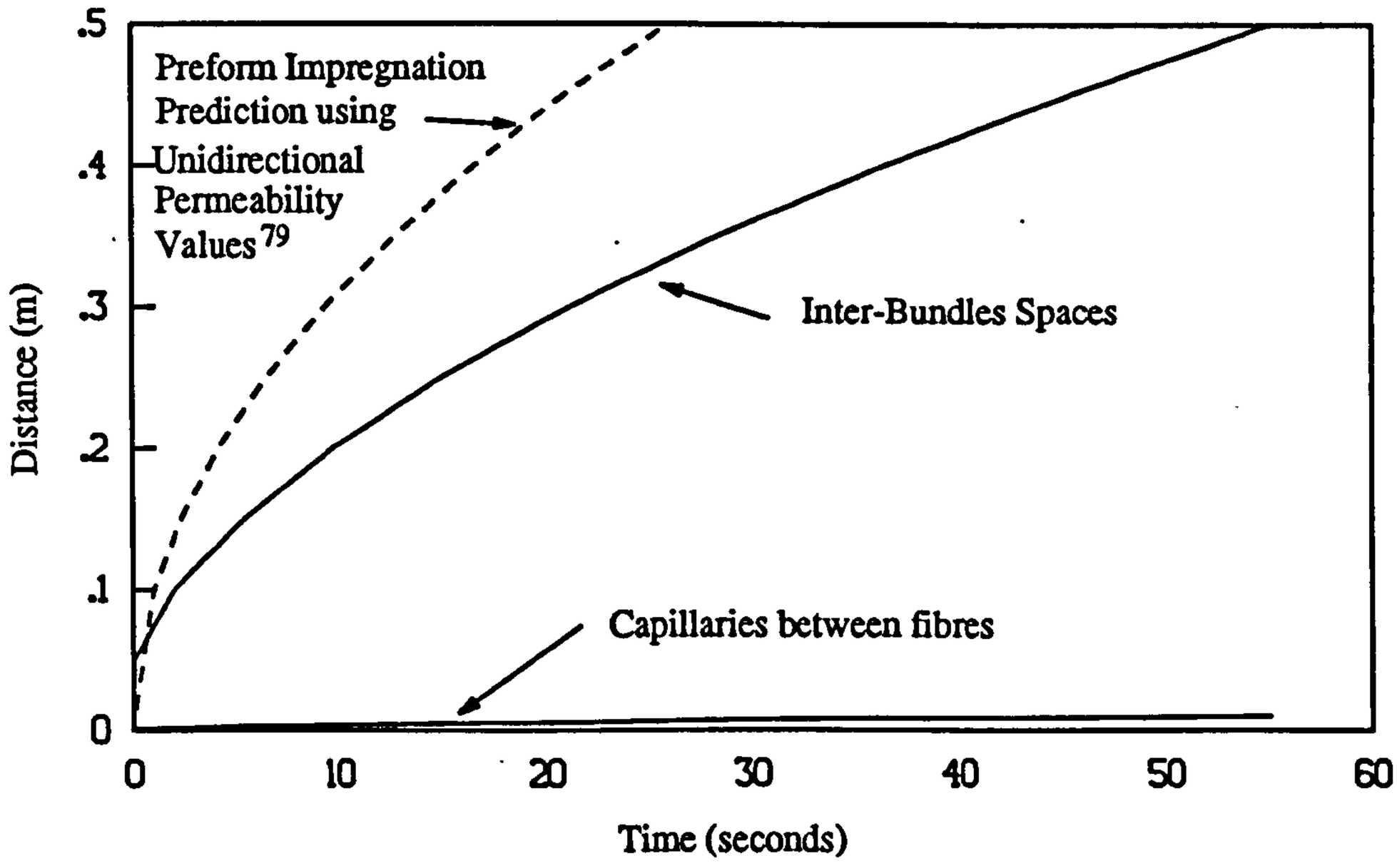

Figure 8.11 Comparison of Resin Impregnation Distance Vs Time using Circular and Elliptical Fibre Bundles

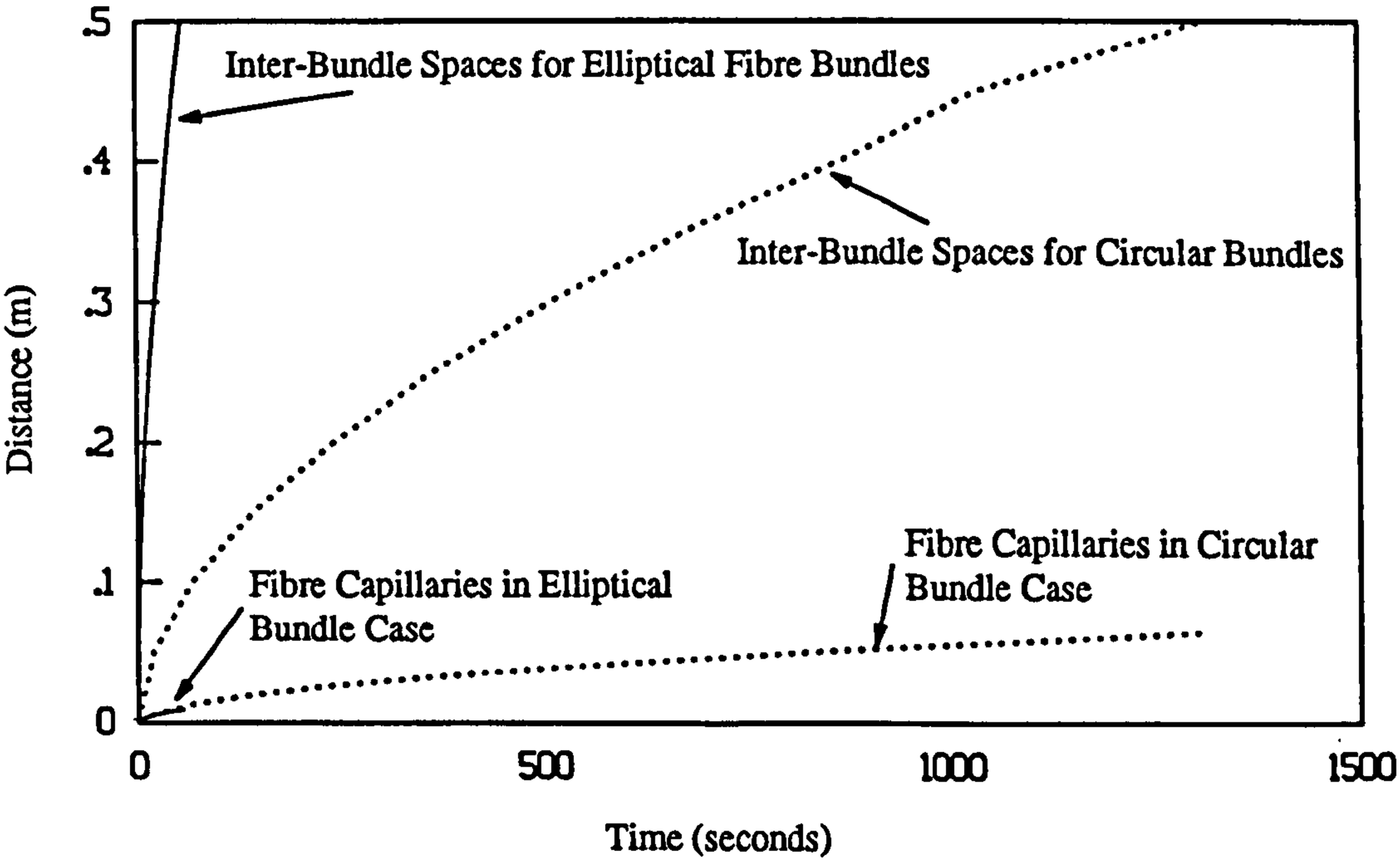

Figure 8.12
Axial Flow and Fibre Capillary
Formed by a Hexagonal
Packing Structure

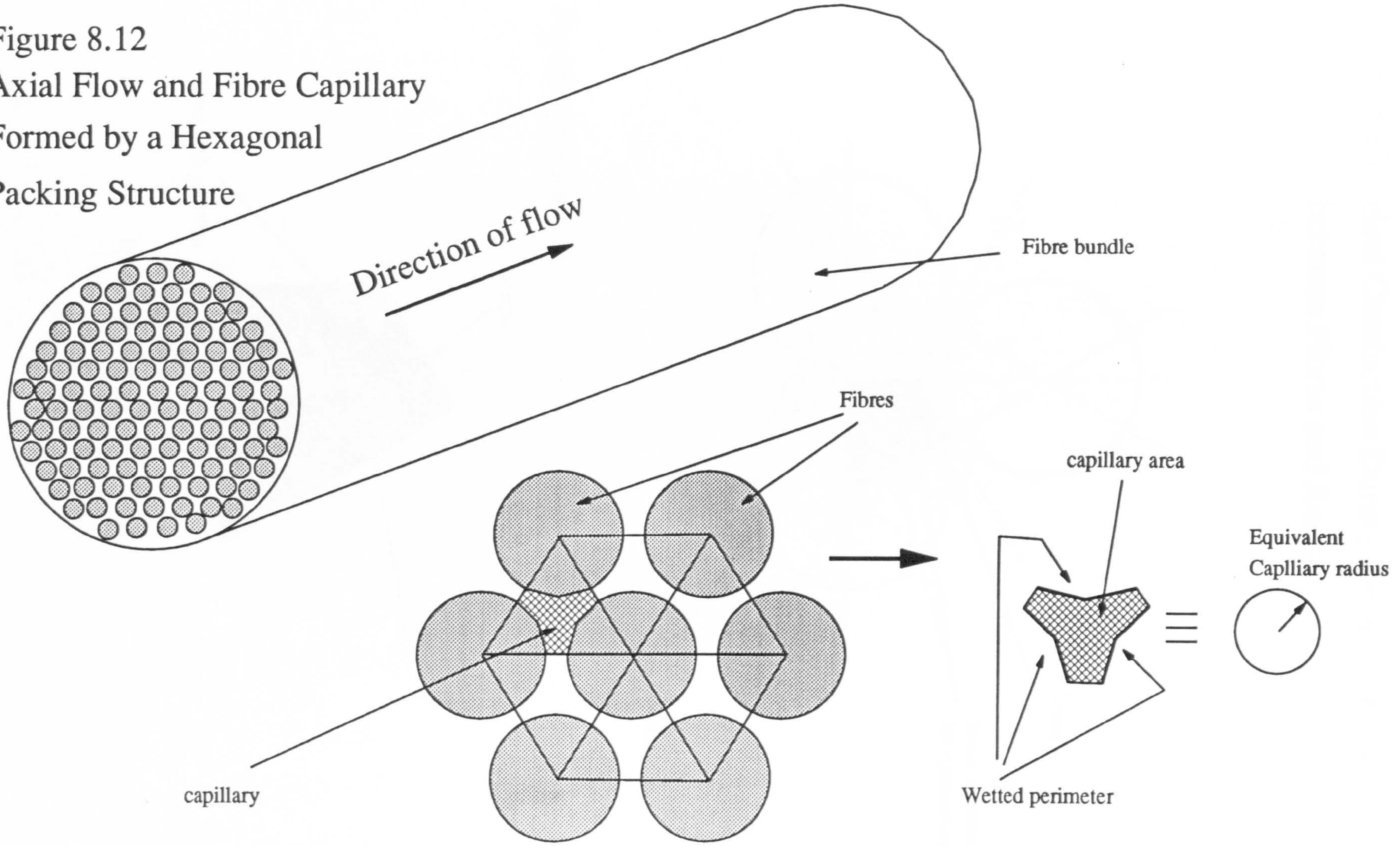

Figure 8.13 Heat Conduction During the Axial Flow between Fibres and Resin

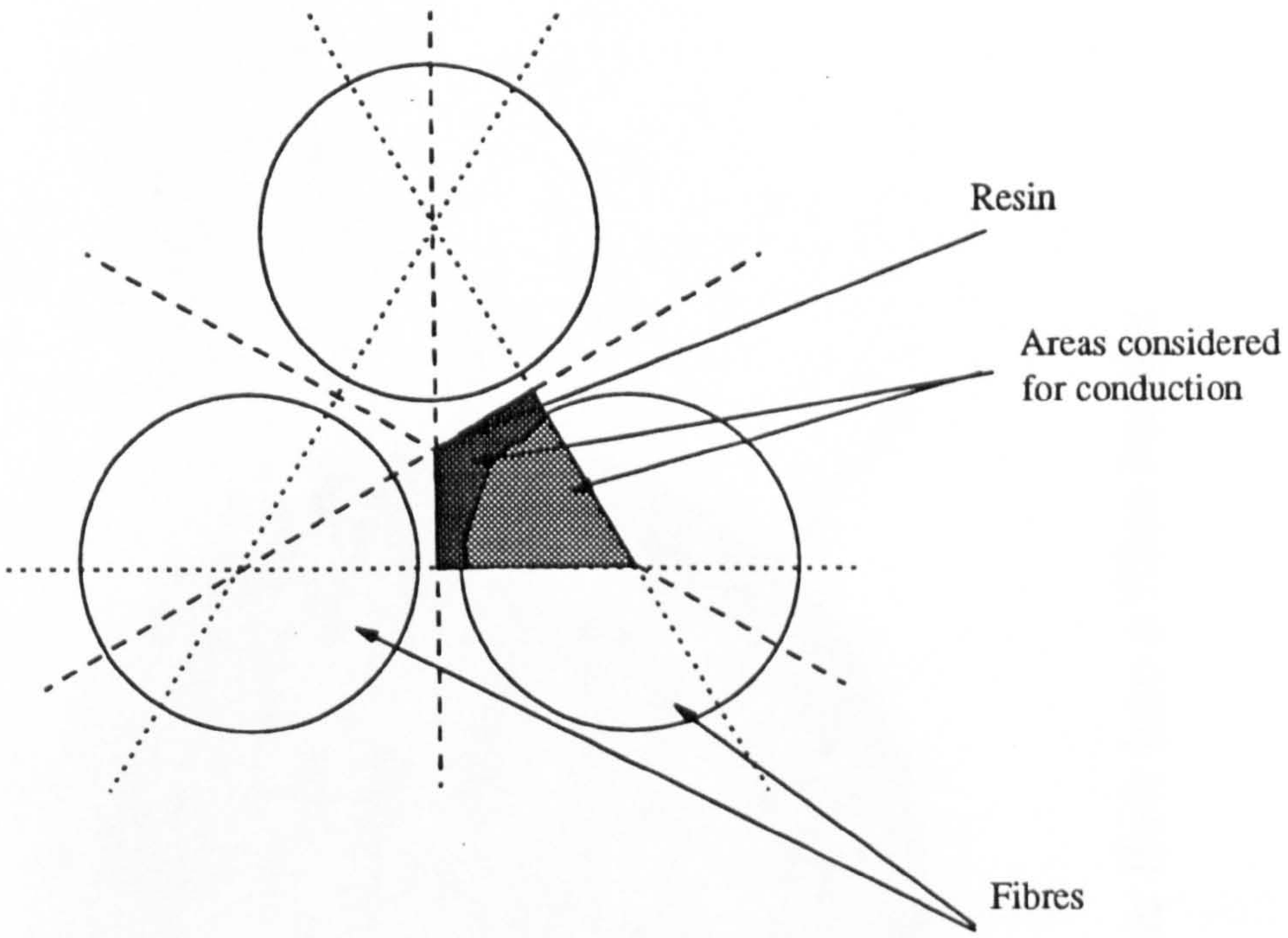

Nodal positions

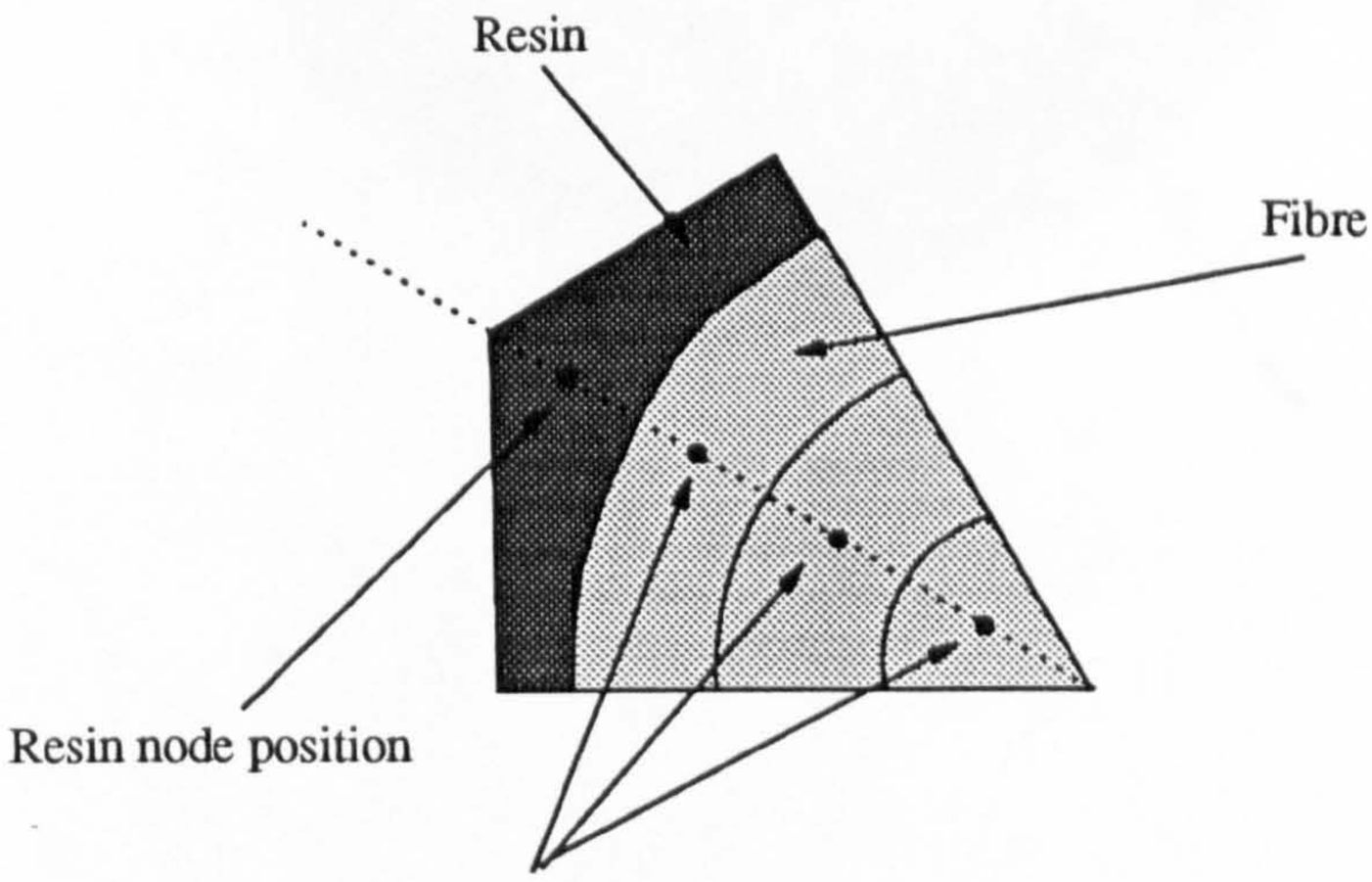

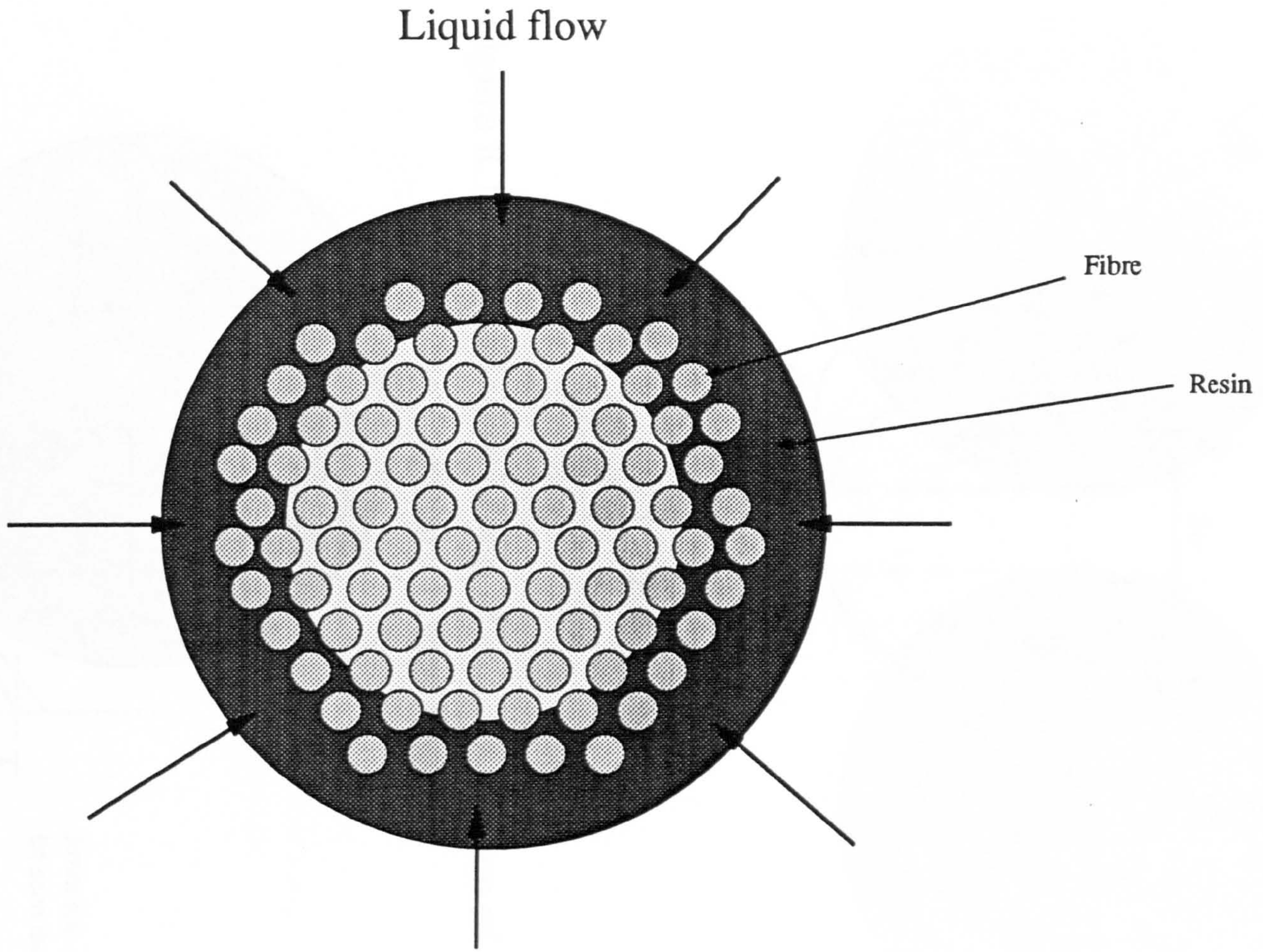

Figure 8.14 Transverse flow into a fibre bundle

Figure 8.15 Parallel Plate Approximation of the Circular Fibre Surface

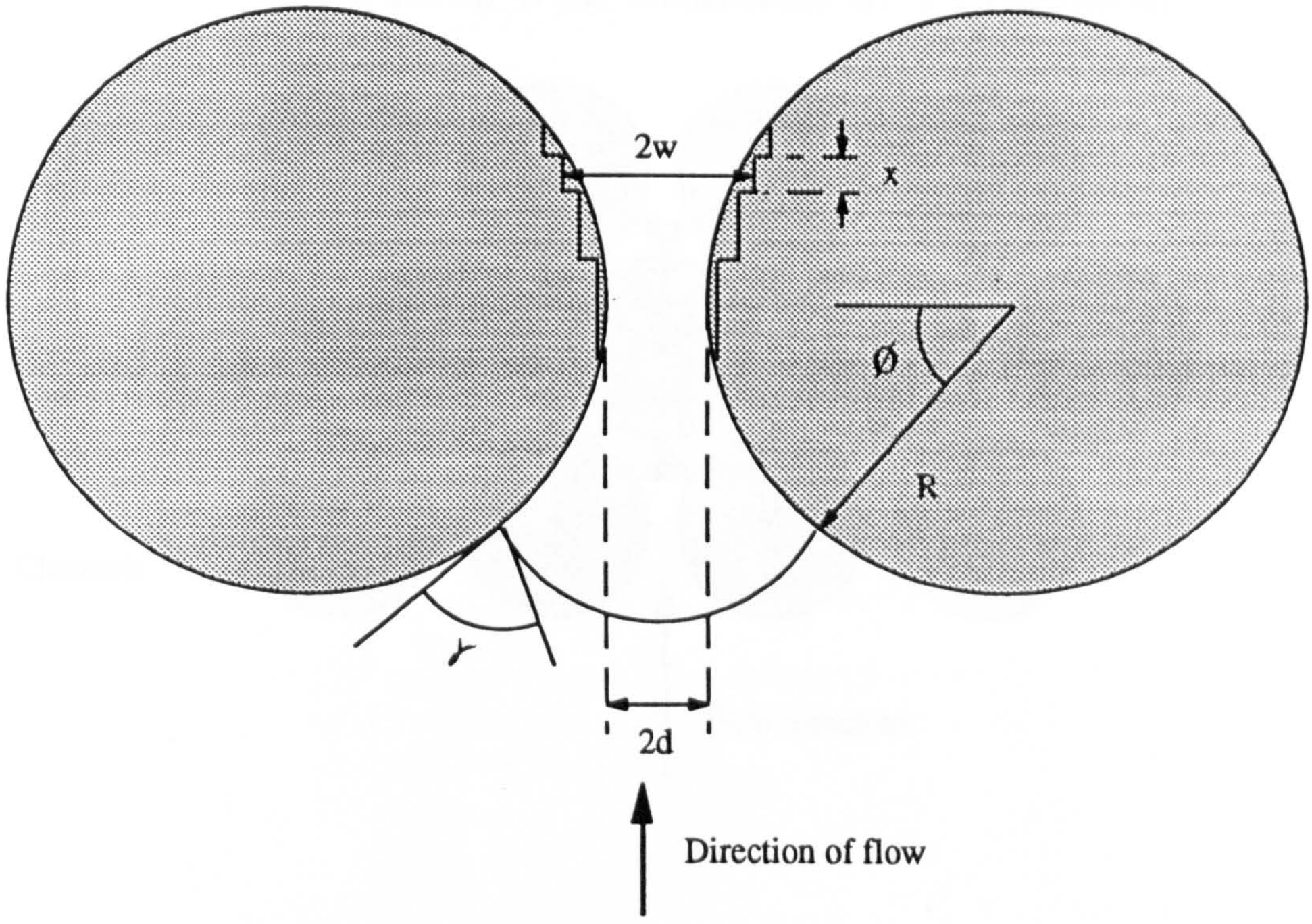

Figure 8.16 Calculation of the Meniscus Radius of Curvature and the Capillary Force Angle

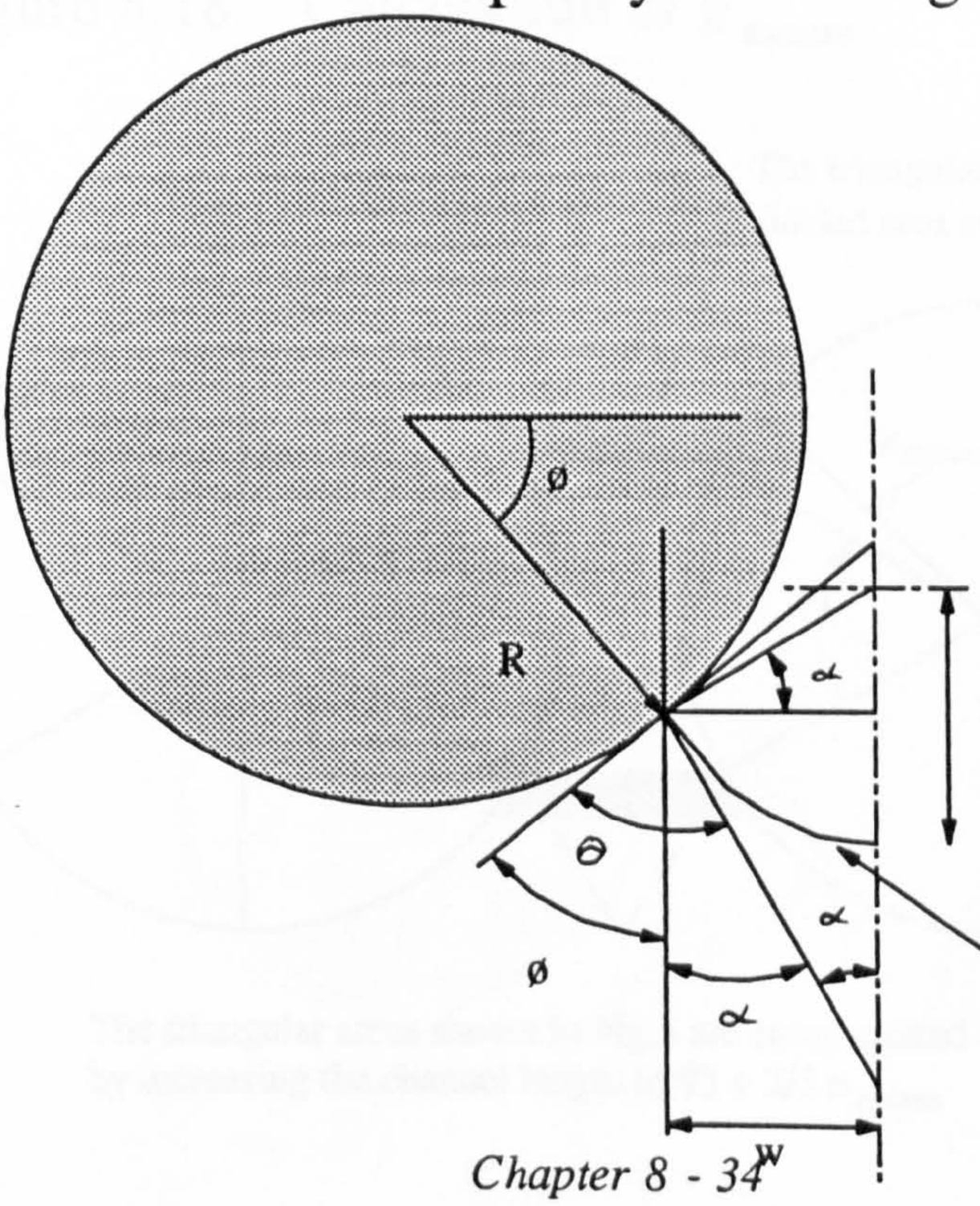

Figure 8.17 Schematic Diagram of Hexagonal Packing of Fibres with Channels of /3 Radians.

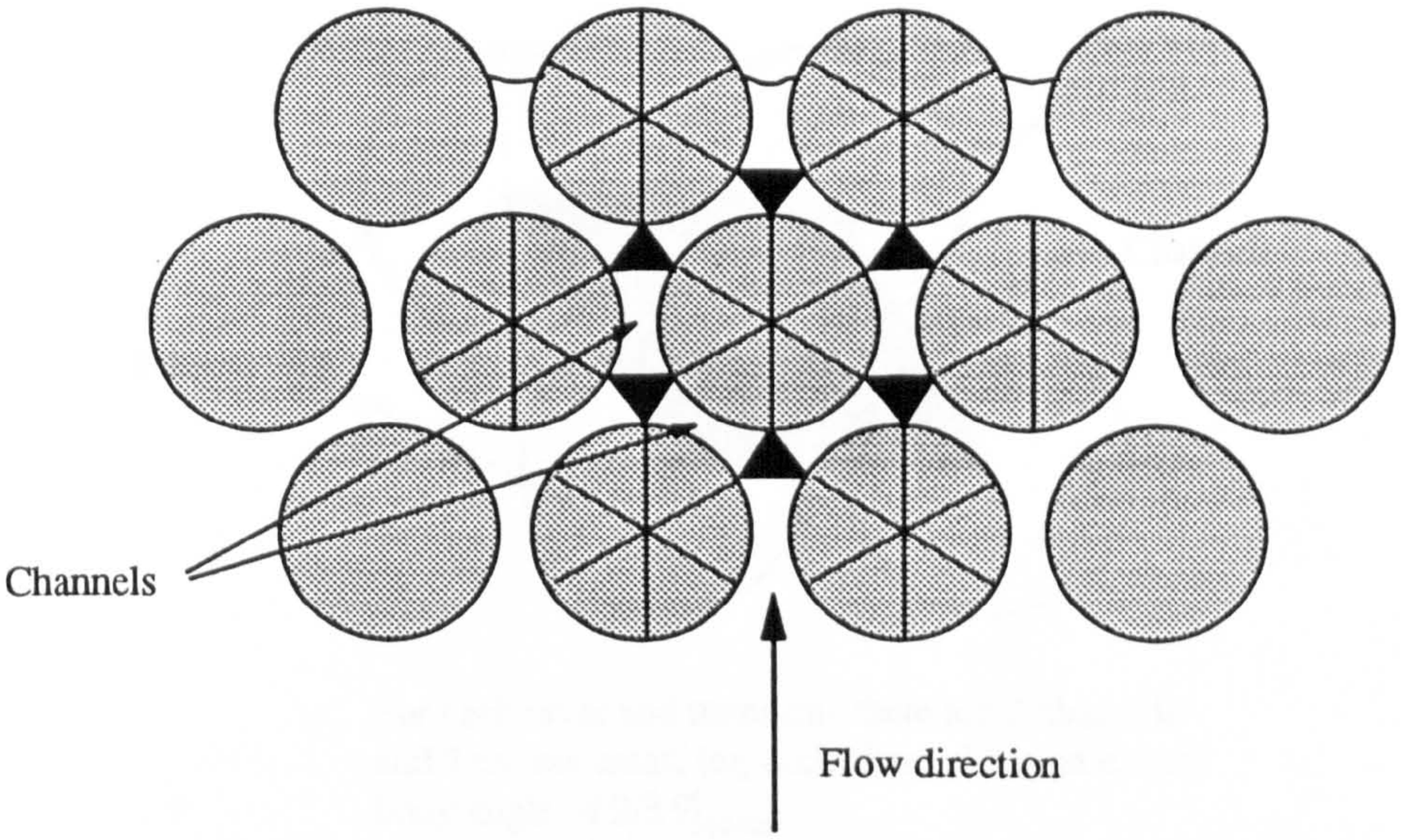

Figure 8.18 Calculation of ϕ_{excess}

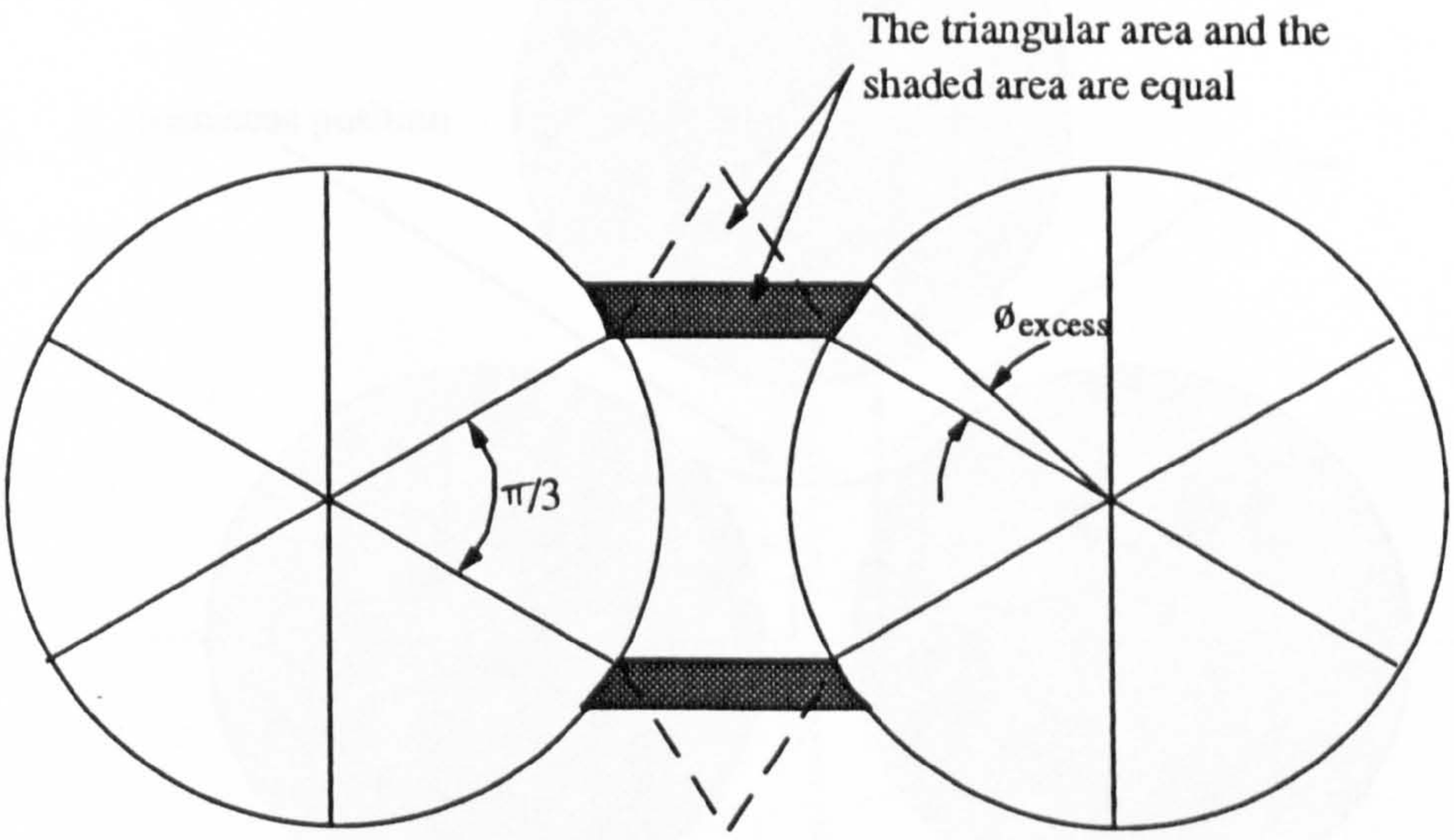

The triangular areas shown in Fig.5 are compensated for in area by increasing the channel length to $\pi/3 + 2/3\ \phi_{excess}$

Figure 8.19 Channels and Excess Areas for Flow in the Transverse Direction

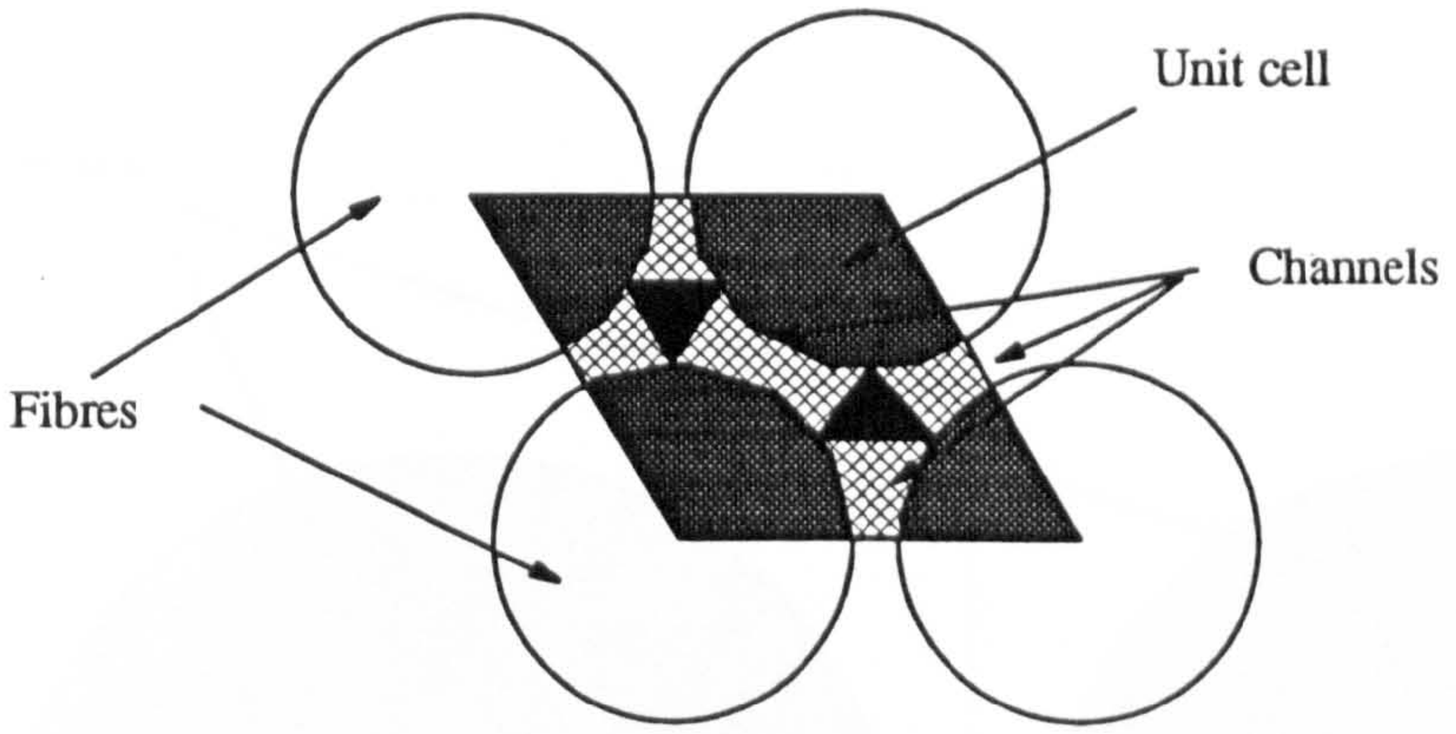

For each layer and meniscus there are 3 channels and 2 excess areas. (eg.each channel has an excess body angle of 2/3 $\emptyset_{excess}$)

Figure 8.20 The Positions of s and s_{max}

(where s is the resin meniscus distance from the centre line of the fibre)

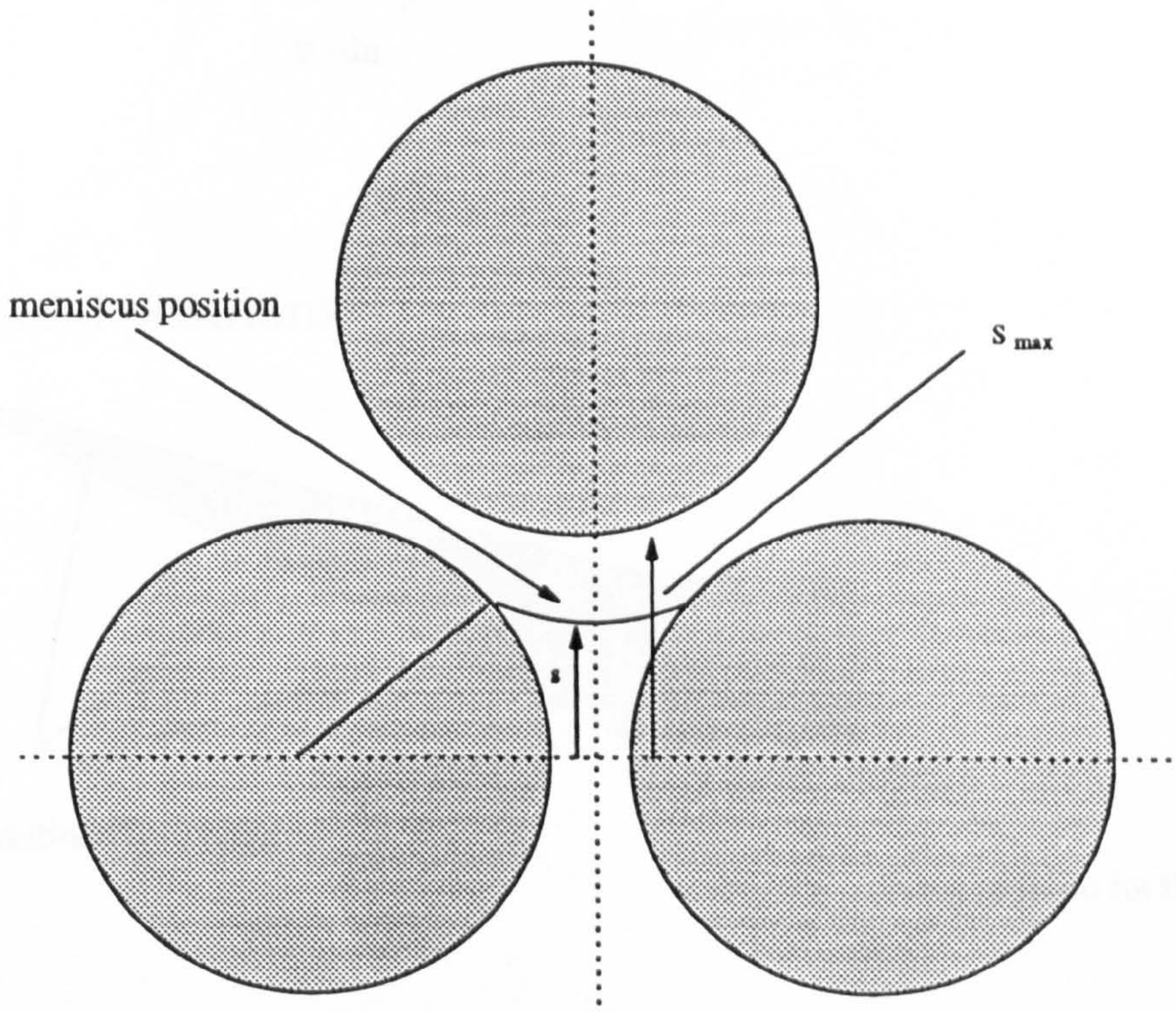

Figure 8.21 Conductive Heat Transfer Transverse to the Fibre Axis

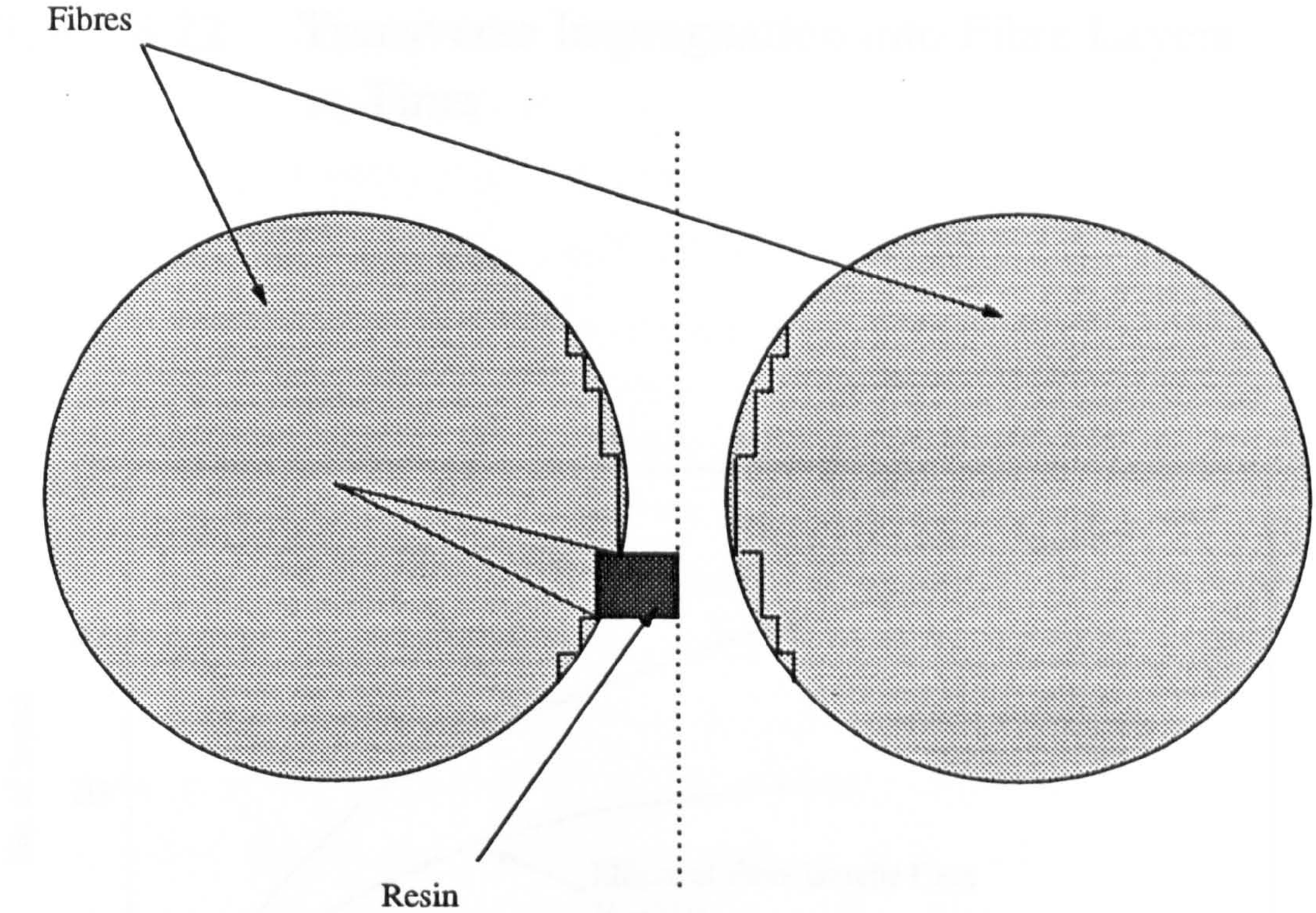

Nodal positions

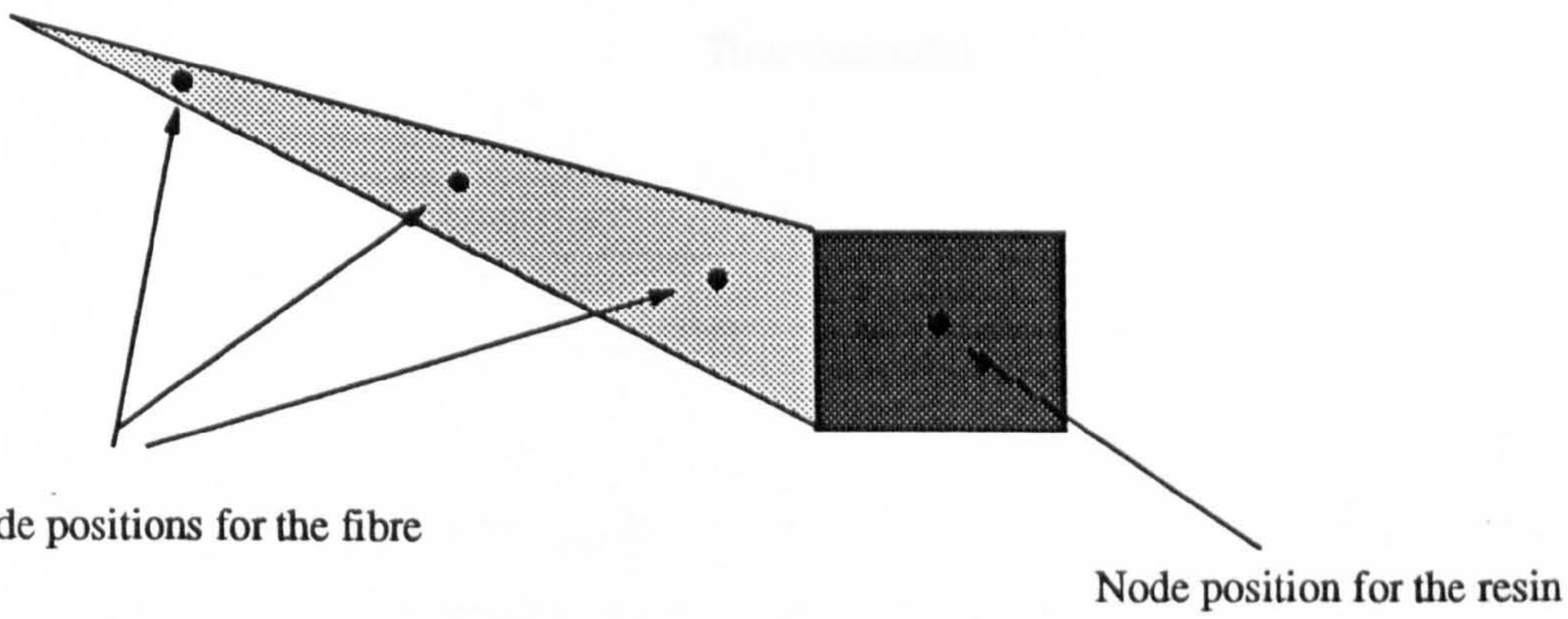

Figure 8.22 Transverse Impregnation into Fibre Layers vs Time

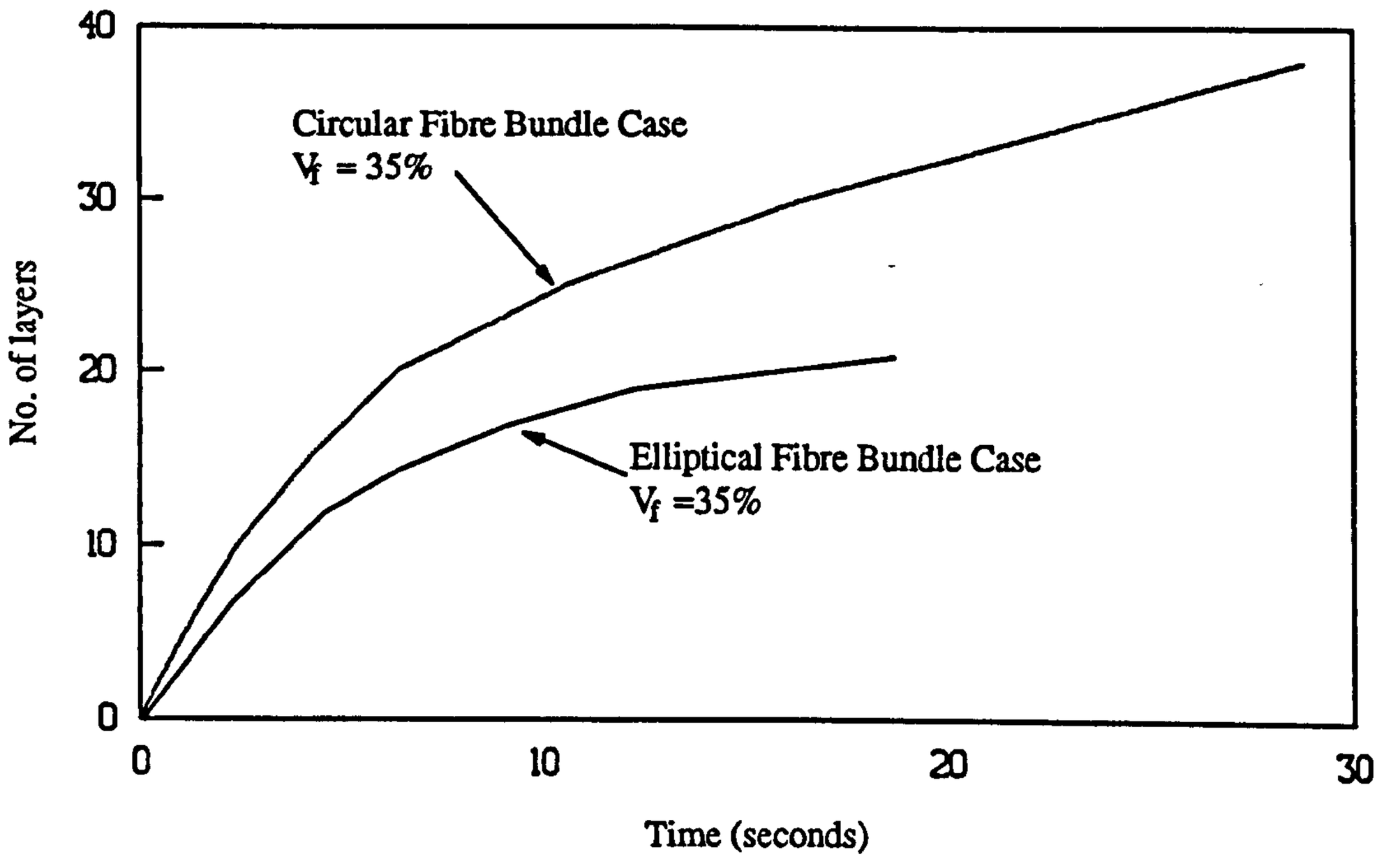

Chapter 9

Discussion

9.1 General Discussion

This chapter reviews findings presented in this thesis in the light of the original objectives. The phenomena which cause internal defects (voids) have been identified and mechanisms which generate these voids during the impregnation and cure stages of manufacture have been recognised.

Voids are formed during the impregnation and cure stages of RTM. The majority of voids appear to form from air entrapment during the impregnation phase. This entrapment is caused by uneven flow within the reinforcement. The uneven flow causes entrapment between fibre bundles creating macrovoids and entrapment within fibre bundles creating microvoids. Study of the impregnation phase of RTM has been carried out by several researchers[28,30,31], mainly relating to permeability measurement. No methodical flow studies have been carried out in the literature surveyed to determine the reasons for air entrapment at the resin flow front.

The results of the impregnation investigations have shown that resin flow into a fibre preform can be restricted by obstacles, such as globules of thermoplastic binder, film former or size menisci between fibres. Flow can also be hindered by the stitching, or fibres lying across the flow path. Fibre orientation within a preform directs flow. This orientation within multilayered preforms affects in-plane impregnation rates within layers. Transverse flow between these layers due to the differing in-plane flow is able to trap air.

Transverse impregnation into large fibre bundles (2400 Tex) has been highlighted during these studies as the major cause of microvoid formation. The impregnation of single strands of fibre was also studied during the manufacture of

filament wound cylinders to investigate the problem of fully wetting high Tex fibre bundles. High impregnation speeds indicated long cylindrical voids would be trapped in the strand, whilst slower impregnation speeds demonstrated entrapment of more numerous spherical voids. These experiments have shown that resin is likely to impregnate fibre bundles during the impregnation phase of RTM by rapid flow along the inter-bundle spaces, followed by transverse flow into the bundle.

Flow modelling has been tackled by researchers intent on predicting macroscopic in-plane flow into components[27,29,34], but little work has been undertaken to model microscopic flow[45,19]. In this research resin impregnation into ideally packed fibre bundles was modelled using three different flow regimes. Resin was assumed to fill an ideal unidirectional preform in three ways: axially in the spaces between fibre bundles, axially between the fibres, and transversely into the fibre bundles. Initial inter-bundle flow predictions using circular fibre bundles was of a magnitude different than results from experimental moulding trials, due to the idealistic preform geometry. This fibre bundle structure was modified to resemble the elliptical bundles observed in moulding sections. The results of these predictions matched actual moulding events more closely. Using isothermal conditions, with resin and fibre temperatures at 90°C, fill times in the inter-bundle spaces resembled permeability predictions and experimental results. The predictions from the model indicated the fibre bundles would become impregnated from transverse flow far quicker than from axial flow between the fibres, suggesting that voidage is more likely to be concentrated in a central core of the fibre bundles.

Process conditions used during the moulding operation influenced void formation and final void size. Several process conditions such as vacuum assistance and injection pressure have been studied by previous researchers to determine their effect on void content within mouldings[35,36,37]. In this study vacuum assisted impregnation was observed to influence void formation most significantly. The use of a vacuum however can create voids by permitting the monomer within the liquid polyester resin to boil at low pressures. The exothermic pressures experienced within the mould cavity were higher with the use of vacuum assistance. This was thought

to be caused by the reduction in void content within the composite, where the compression of the air within the voids reduces peak pressures. This may influence mould stiffness design. Lowering the viscosity of the resin by pre-heating was seen to increase the number of microvoids within the fibre bundles. Other process conditions including injection pressure, mould temperature and fibre volume fraction did not influence void formation.

Void content has been shown to increase with distance from the injection gate. This is thought to be caused by the rate of transverse impregnation into the fibre bundles, since the impregnation pressure decays from the injection point.

Voids can form during the cure stage of processing due to monomer boil. This has however only been observed during vacuum assisted moulding trials. The temperature versus pressure boiling curve for polyester resin indicates that boiling may occur if exotherm pressures exceed 140°C at atmospheric pressure.

The findings of this thesis may be relevant to other composite manufacturing processes, in addition to RTM. The effect of size between filaments affects resin impregnation in filament winding (as has been discussed in Chapter 7), SRIM, pultrusion and hand lamination. The reinforcement fabrics and mats discussed are limited to LMP's and hand lamination techniques, where the problems associated with binding and multilayered structures will have an effect.

9.2 Reduction of Void Formation During RTM

Several findings of this thesis can be used to assist the reduction of voids within components. The void content within mouldings can be reduced using vacuum assisted impregnation. The process conditions of temperatures, and pressures used with vacuum assistance require careful consideration to reduce the likelihood of monomer boiling. However, the automotive industry requires components to be manufactured at high volumes, which would require cycle times approximating 3 minutes or less[4]. In conditions such as these, impregnation times would be in the order of seconds and the wet out period prior to cure would be short. The process

conditions would have to be optimised for both processing speed and part quality. Drawing a vacuum within a mould will require a significant time within an already short moulding cycle. This along with the associated problems of monomer boiling (reduced moulding temperatures and processing speeds), higher exotherm pressures and mould sealing arrangements to maintain a vacuum, may detract from its use.

Air entrapment during impregnation could be reduced with the use of different binding methods, eg. lower thermoplastic binder contents, where regions within the preform which are likely to impede flow, are reduced or eliminated. The use of similar permeability layers within multilayered stacks will reduce the likelihood of uneven flow fronts between layers, and reduce air entrapment due to transverse flow.

Microvoid formation could be reduced with the use of lower Tex strands, which would allow the bundles to become impregnated quicker, reducing the possibility of air entrapment. Mechanical working of the fibres prior to fabric manufacture would break the size menisci between filaments decreasing any obstacles to resin impregnation.

The preform design should minimise possible void formation mechanisms, by consideration of preform stacking, fibre direction and reinforcement binder (stitching or thermoplastic). Finally a compromise may be necessary between component quality and processing speed.

9.3 Recommendations for Further Work

Following the discussions in this chapter several recommendations for further work can be made:

Reducing Air Entrapment

i) Thermoplastic globules and stitching can distort the flow front of impregnating resin. Alternatives for binding preforms require investigation. The use of thermoplastic threads laid in conjunction with fibres may reduce the problem of impeding flow. Once preformed, the softened thermoplastic thread may

cause problems during the transverse impregnation of the fibre bundles.

ii) Thermoplastic binders which quickly dissolve into the resin system during impregnation are required. These would reduce flow impedance.

iii) Size and film former solutions which do not produce extensive deposits or menisci when added to the fibres require investigation. If developed these sizes would permit unhindered impregnation into fibre bundles. The dissolution of this size at the resin flow front would also reduce the possibility of entrapment.

Processing

i) Several of the moulding trials contained within this thesis were inconclusive, or require further investigation. The influence of impregnation speed and partial vacuums during impregnation are not fully understood and require additional study.

ii) The effects of the cure phase during RTM upon the void creation and size, have not been studied within this thesis. The variation of resin exotherm pressures and temperatures need to be examined to determine their effects on the final void content of the component.

ii) Further investigation is required of the limitations of vacuum assisted impregnation due to monomer boiling and cavity pressures during moulding.

Modelling

i) The inter-bundle axial flow is dependant on the preform geometry and to a lesser extent the heat transfer to the resin. These variables require appraisal to determine the optimum and most realistic values.

ii) The material values used within a mathematical model determine the accuracy of the results. Properties such as contact angle and surface tension information

for a variety of realistic impregnation speeds and resin temperatures require characterisation.

iii) The preform model could be made more realistic to combine stitching and regions of thermoplastic binder.

iv) The model could be taken a stage further, to be used as a tool to determine optimum bundle Tex and to predict the likelihood of void formation within the fibre bundles.

v) Viscosity versus gel time information, along with a gelation model in a valid impregnation model, could provide useful predictions for moulding process conditions.

References

1. Ruhsert, C., *"Resins For Reasons"*, Automotive Materials, Volume 2, 1991, pp. 24-27.

2. Folonari, C.V., Bruno, A., *"New Applications for Plastics in Fiat Motor Cars"*, New Materials for Automotive Applications, RAPRA, 1990, Paper 1.

3. Anon, *"Worldwide Automotive Trends and Forecasts"*, EIU (The Economist Intelligence Unit) International Motor Business, April 1992.

4. Hutcheon, K.F., *"The Application of RTM to the Motor Industry"*, MPhil Thesis, University of Nottingham, 1989.

5. Rudd, C.D., *"Preform Design for High Volume Resin Transfer Moulding"*, Ph.D Thesis, University of Nottingham, 1989.

6. Chavka, N.G., Johnson, C.F., *"The Taming of Liquid Composite Molding for Automotive Applications"*, Advanced Composite Materials: New Developments and Applications Conference, 1991.

7. Pendrous, R., *"Making Light of car efficiency"*, The Engineer, January 1991, pp. 35-39.

8. Mayer, R., *"Design with Reinforced Plastics"*, The Design Council, London, 1993.

9. Gulino, J., Berthet, G., Harrison, A.R., *"A Composite Tailgate for the P100 Sierra Pickup Resin Transfer Moulding with class 'A' surface finish"*, The Institution of Mechanical Engineers, Autotech, 1989.

10. Kendall, K.N., Hill, D.J., Revill, I.D., & Rice, E.V., *"Structural Composites by Resin Transfer Moulding (RTM), Summary Report 1988-1991"*, Confidential report for Ford Motor Company, University of Nottingham 1991.

11. Jacobs, K.A., *"Primary processing equipment for RTM"*, Reinforced Plastics, June 1991, pp. 38-41.

12. Miller, B., *"Resin Transfer Molding now a big-league process"*, Plastics World, May 1990, pp. 60-64.

13. Toensmeier, P.A., *"Electric cars stage a comeback; Lightweighting makes them practical"*, Modern Plastics, September 1989, pp. 44-45.

14. Glaskin, M., *"The Clean Machine"*, Engineering, November 1991, pp. 26.27.

15. Dunbar, S.G., *"Preformable Continuous Strand Mat for Structural Applications"*, 44th Annual Conference, Composites Institute, The Society of the Plastics Industry, Feburary 6-9, 1989.

16. Kendall, K.N., *"Mould Design for High Volume Resin Transfer Moulding"*, Ph.D Thesis, University of Nottingham 1991.

17. Woolstencroft, D.H., Hogg, P.J., *"Non Crimp Material Forms, Performance Technology and Mass Manufacturing"*, Plastics and Rubber Institute, 3rd Annual Conference on Automated Composites, The Hague, The Netherlands, October 1991.

18. Anon, *"Vetrotex Glass Fibre"*, Vetrotex Commercial Brochure, Vetrotex (UK) Ltd., Wallingford, Oxon. 1990.

19. Revill, I.D., *"Interfacial Bond Formation During Resin Transfer Moulding Of Polymer Composites"*, Ph.D Thesis, The University of Nottingham, 1993.

20. Drzal, L.T., Iyer, S.R., *"A Formable, Flexible Composite Preform from Powder-Impregnated Fiber Tows"*, 6th Annual Advanced Composites Conference, Detroit, 1990.

21. Neoxil 940 product information sheet, Savid, S.p.A. Como, Italy.

22. Voeks, S.L., Kenneth, A.S., Kallaur, M., *"Advances in the Art of Preforming"*, 43rd Annual Conference, Composites Institute, The Society of the Plastics Industry, Feburary 1-5, 1988.

23. Judd N.C.W., Wright, W.W., *"Voids and their effects on the mechanical properties of composites- an appraisal"*. SAMPE Journal Jan/Feb 1978, pp. 10-14.

24. Bowles, K.J., Frimpong, S., *"Relationship between voids and interlaminar shear strength of polymer matrix composites"*, 36th International SAMPE Symposition and exhibition, San Diego, California, April 15-18, 1991.

25. Rowychowdhury, S., Gillespie, J.W., Advani, S.G., *"Void formation and growth in thermoplastic processing"*, Composite Materials Technology III, 1992, pp. 89-107.

26. Hull, D., *"An introduction to composite materials"*, Cambridge University Press, London, 1990, pp. 75-77.

27. Parnas, R.S., Phelan, F.R., *"The effect of heterogeneous porous media on mold filling in resin transfer molding"*, SAMPE Quarterly, Jan 1991, pp. 53-60.

28. Williams, J.G., Morris, C.E.M., Ennis, B.C., *"Liquid flow through aligned fibre*

beds", Polymer Engineering and Science, June 1974, Vol.14, No.6, pp. 413-419.

29. Peterson, R.C., Robertson, R.E., *"Flow characteristics of polymer resin through glass fibre preforms in resin transfer molding"*, Advanced Composite Materials: New Developments and Applications Conference Proceedings, Detroit, Michigan USA, September, 1991.

30. Peterson, R.C., Robertson, R.E., *"Mechanisms affecting void distribution and elimination in resin transfer molding"*, Proceedings of the 8th Advanced Composites Conference, Chicago, Illinois, 2-5 November 1992, pp. 63-67.

31. Molnar, J.A., Trevino, L., Lee, L.J., *"Liquid flow in moulds with prelocated fibre mats"*, Polymer Composites, December 1989, Vol.10, No.6., 414-423.

32. Wang, T.J., Perry, M.J., Lee, L.J., *"Analysis of permeability and void formation in resin transfer moulding"*, ANTEC'92, Detroit, Michigan, May 1992, pp. 756-760.

33. Wang, T., Wu, C.H., Patel, N., Lee, L.J., *"Fibre wetting and Permeability Analysis in liquid composite molding"*, Proceedings of the 8th Advanced Composites Conference, Chicago, Illinois, 2-5 November 1992, pp. 47-55.

34. Dave, R., Houle, S., *"The role of permeability during resin transfer molding"*, Proceedings of the American Society for Composites, 5th Technical Conference, June 1990.

35. Hayward, J.S., Harris, B., *"Processing factors affecting the quality of resin transfer moulded composites"*, Plastics and Rubber Processing and applications, Vol.11, No.4, 1989, pp. 191-198.

36. Hayward, J.S., Harris, B., *"Effect of process variables on the quality of RTM mouldings"*, SAMPE Journal, Vol.26, No.3, May/June 1990, pp. 39-46.

37. Hayward, J.S., Harris, B., *"The effect of vacuum assistance in resin transfer moulding"*, Composites Manufacturing, Vol.1, No.3, September 1990, 161-166.

38. Stabler, R.S., Tatterson, G.B., *"Void minimization in the manufacture of carbon fiber composites by resin transfer molding"*, Sampe Quarterly, January 1992, pp. 38-42.

39. Ghiorse S.R., Jurta, R.M., *"Effects of low frequency vibration processing on carbon/epoxy laminates"*, Composites, Vol. 22, No.1, January 1991, pp. 3-8.

40. Rudd, C.D, Harrison, A., Rice, E.V., Kendall, K.N., Bulmer, L.J., Longbottom, A.C., Owen, M.J., *"Integrated design for RTM components"*, ASM/ESM Advanced Composites Conference, Chicago, 21-24 October 1992.

41. Adams, K.L., Miller, B., Rebenfeld, L., *"Forced in-plane flow of an epoxy resin in fibrous networks"*, Polymer Engineering and Science, November 1986, Vol.26, No.20, pp. 1434-1441.

42. Ahn, K.J., Seferis, J.C., *"Simultaneous measurements of permeability and capillary pressure of thermosetting matrices in woven fabric reinforcements"*, Polymer Composites, June 1991, Vol.12, No.3, pp. 146-152.

43. Kardos, J.L., Dave, R., Dudukovic, M.P., *"Voids in composites"*, Proceedings of the ASME manufacturing international 88, Atlanta, Georgia, pp. 41-48.

44. Chan, A.W., Morgan, R.J., *"Resin impregnation and void formation in enhanced resin transfer molding"*, Proceedings of the 8th Advanced Composites Conference, Chicago, Illinois, 2-5 November 1992, pp. 69-73.

45. Bascom, W.D., Romans, J.B., "*Microvoids in glass-resin composites*", I&EC Product Research and Development, Vol.7, No.3, September 1968, pp. 172-178.

46. Massey, B.S., *"Mechanics of Fluids"*, Van Nostrand Reinhold (UK), 5th Edition, Great Britain, 1987.

47. Bayramli, E., Powell, R.L., *"The Normal (Transverse) Impregnation of Liquids into Axially Oriented Fibre Bundles"*, Journal of Colloid and Interface Science, Vol.138, No.2, September 1990, pp. 346-353.

48. Tang, J., Lee, W.I., Springer, G.S., *"The effects of cure pressure on resin flow, voids, and mechanical properties"*, Journal of Composite Materials, Vol.21, May 1987, pp. 421-440.

49. Loos, A.C., Springer, G.S., *"Curing of Epoxy Matrix Composites"*, Journal of Composite Materials, Vol.17, March 1983, pp. 135-169.

50. Baijal, S.K., *"Flow of Fluids Through Porous Media"*, Penn Well Publishing Company, Tulsa 1982.

51. Rice, E.V., *"A model for moulding"*, Advanced Composites Engineering, April 1992, pp. 11-12.

52. Bruno, A., Molina, G., Bertacchi, G. & Moroni, A., *"Flow Behaviour in Resin Transfer Moulding: Numerical simulation"*, Advanced Composites Materials: New Developments and Applications Conference Proceedings, Detroit, Michigan, September 30th - October 3rd, 1991, pp. 149-164.

53. Hirt, D.E., Adams, R.K., Prud'Homme, R.K. & Rebenfeld, L., *"In-Plane Characterization of Fibrous Materials"*, Journal of Thermal Insulation, Volume 10, January 1987.

54. British Standard, *"Resistance of clothing materials to permeation by liquids, Part 1. Method for the assessment of breakthrough time"*, BS 4724: Part 1: British Standards Institution, Milton Keynes, England, 1986.

55. British Standard, *"Resistance of clothing materials to permeation by liquids, Part 2. Method for the determination of liquid permeating after breakthrough*, BS 4724: Part 2: British Standards Institution, Milton Keynes, England, 1988.

56. British Standard, *"Determination of permeability of fabrics to air"*, BS 5636: British Standards Institution, Milton Keynes, England, 1990.

57. Gulino, J., Blanc, A., Berthet, G., *"Comparison of permeability between preformable Unifilo U720 and U750"*, Vetrotex International Chambery, 1988.

58. Adams, K.L., *"Permeability characterisation of engineering fabrics"*, Ph.D Thesis, Princeton University, 1989.

59. Greve, B.N., Sung, K.S., *"Directional Permeability Measurement of Fibreglass Reinforcements"*, Polymer Composites for Structural Automotive Applications, SAE, International Congress & Exposition, 1990, pp. 101-113.

60. Miller, B., Clark, D.B., *"Liquid Transport Through Fabrics; Wetting and Steady-State Flow, Part I: A New Experimental Approach"*, Textile Research Journal, March 1978, pp. 150-155.

61. Zisman, W.A., *"Improving the Performance of Reinforced Plastics"*, Industrial Engineering Chemistry, Vol.57, No.1, January 1965.

62. Paul, J.T., Thomson, J.B., *"The Importance of Voids in the Filament-Wound Structure"*, Proceedings of 20th Technical Conference, SPI Reinforced Plastics Division, Section 12-C, Feburary 1965.

63. Chandler, H.W., Devlin, B.J., Gibson, A.G., *"A model for the continuous impregnation of fibre tows in resin baths with pins"*, Plastics, Rubber and Composites Processing and Applications 18, 1992, pp. 215-220.

64. Kohn, E.J., Sands, A.G., Clark, R.C., *"Qualitative Measurement of Void Content in Glass Filament Wound Composites and Correlation of Interlaminar Shear Strength with Void Content"*, I&EC Product Research and Development, Vol.7, No.3, September 1968, pp. 179-182.

65. Weatherby, N.L., *"Strength of Filament Wound Glass Reinforced Polyester Resin"*, Ph.D Thesis, The University of Nottingham, 1987.

66. Oleesky, S.S., Mohr, J.G., *"SPI Procedure For Running Exotherm Curves - Polyester Resins"*, Appendix II-1.1, Handbook of Reinforced Plastics, SPI, 1964, New York, pp. 51-52.

67. Rudd, C.D., Rice, E.V., Kendall, K.N., Longbottom, A.C., "*Process Modelling and Design for Resin Transfer Moulding*", Plastics, Rubber and Composites Processing and Applications, 20, 1993, pp. 67-76.

68. Rudd, C.D., Middleton, V., Owen, M.J., Long, A.C., McGeehin, P., "*Design, Processing and Performance of Structural Preforms*", CANCOM 93, 2nd International Conference on Composite Structures and Materials, 27-29th September 1993.

69. Scott, F.N., "*Processing Characteristics of Polymer Resins for the Resin Transfer Moulding Process*", Ph.D Thesis, The University of Nottingham, 1988.

70. Lindsey, K.A., Rudd, C.D., Fraser, I.M., "*Effects of Postcure on the Interfacial Properties of Urethane Methacrelate Composites*", Journal of Material Science, Letters, accepted for publication, 1993.

71. ISO 2558, "*Determination of the time taken for the Dissolution of a Binder in a Fluid*".

72. Owen, M.J., Middleton, V., Pickering, S.J., Rudd, C.D., Hill, D.J., Lowe, J.R., Bulmer, L.J., Blanchard, P.J., Kingham, A.K., "*Progress Report No.79, Stressed Components By Resin Transfer Moulding (RTM)*", Confidential Report to Ford Motor Company, The University of Nottingham, 29th November 1991.

73. Chapman, A.J., "*Fundamentals of Heat Transfer*", Macmillan Publishing Company, London, 1987.

74. Holman, J.P., "*Heat Transfer*", McGraw-Hill, New York, 7th Edition, 1990.

75. Anon, "*Handbook of Heat Transfer Fundamentals*", 2nd Edition, McGraw-Hill, New York, 1985, pp. 8-19.

76. Seymour, R.B., Carraher, C.E., "*Polymer Chemistry An Introduction*", Marcel Dekker Inc., 1981.

77. Kamal, M.R., Sourour, S., "*Kinetics and Thermal Characterization of Thermoset Cure*", Polymer Engineering and Science, January, 1973, Vol.13, No.1.

78. Miner, M.A., Journal of Applied Mechanics, Vol.12, No.3, 1945, pp. A159-A164.

79. Bulmer, L.J., "*In-Plane Permeability of Reinforcements for Liquid Moulding Processes*", Ph.D Thesis, University of Nottingham, 1993 (To be submitted).

80. Klunder, J., *An Introduction to Glass Fibre Composites*, Silenka bv, Hoogezand, The Netherlands.

81. Hsu, C.P., Lee, L.J.,"*An Integrated Analysis of Free Radical Cross-Linking Co-Polymerizations*", ANTEC 1992 (SPI), Detroit MI, USA, May 1992, pp. 715-719.

82. Croft, D.R., Stone, J.A.R., *Heat Transfer Calculations using Finite Difference Equations*, Applied Science Publishers Ltd, 1977. pp. 99-110.

83. Rice, E.V.,"*Computer Aided Engineering Techniques for Resin Transfer Moulding*", Ph.D Thesis, The University of Nottingham, 1993.

Appendix 1

Personnel on the RTM Project

Supervisors

Ford Motor Company

1985 - 1991 E.M. Rowbothan

1985 - 1990 R. Murchie

1985 - 1993 A. Harrison

1991 - 1993 S. Scarborough

The University of Nottingham

1985 - 1993 M.J. Owen

1985 - 1993 V. Middleton

1988 - 1993 S.J. Pickering

1989 - 1993 C.D. Rudd

Research Staff

1985 - 1988 K.F. Hutcheon
MPhil Thesis 1989
"The Application of RTM to the Motor Industry"

1985 - 1988 F.N. Scott
PhD Thesis 1988
"Processing Characteristics of Polyester Resins for the RTM Process"

1986 - 1989 C.D. Rudd
PhD Thesis 1989
"Preform Processing for High Volume Resin Transfer Moulding"

1988 - 1991	K.N. Kendall PhD Thesis 1991 "Mould Design for High Volume Resin Transfer Moulding"
1988 - 1991	I.D. Revill PhD Thesis 1993 "Interfacial bond formation during RTM"
1989 -	A.K. Kingham Technician in control of the RTM facility Experimental officer (from September 1991)
1989 - 1992	D.J. Hill PhD Thesis 1993 "Preheating of Thermosetting resin for RTM"
1990 - 1993	E.V. Rice (Crescent Consultants) PhD Thesis 1993 "Computer Aided Engineering Techniques for Resin Transfer Moulding"
1990 - 1993	L.J. Bulmer "In-Plane Permeability of Reinforcements for Liquid Moulding Processes"
1990 - 1993	J.R. Lowe "Void Formation in RTM"
1991 - 1994	P.J. Blanchard "Release Problems associated with the RTM process"

Personnel on the Preforms for Liquid Moulding Processes (PLMP) Project

1990 - 1993	A.C. Longbottom "Preform Design for Liquid Moulding Processes"
1991 - 1994	P. McGeehin "Analysis of Fibre Structures and Assembly for Pressurised

Injection"

1991 - G.P. Tomlinson - Technician

Appendix - 3

Appendix 2

Moulding Procedure in the RTM Facility

Moulding Sequence

The moulding sequence in the RTM facility is as follows (Figure 1.1):

Preform

Place preform into the mould cavity

Clamping

Close mould

Lower clamping pins and clamp

Resin injection

Draw the pre-mixed resin into the homogeniser

Pressurise the homogeniser and open thermal break valve

Monitor the resin injection in the mould cavity

Close vent and injection thermal break valves

Polymerisation

Monitor the instrumentation to ensure the component is fully cured

Component removal

Open mould

Remove component

Deflash Component

Remove excess resin from the periphery of the component

Mould cleaning

Remove flash from the mould with the use of an airline.

Appendix 3

Moulding Program

This appendix contains a list and description of the moulding work which has been carried out in the undershield facility.

1 **Mould Commissioning**

Purpose : Initial mouldings, to determine approximate moulding temperatures and injection pressures. The short shots were produced to visualise the flow front positions.

Materials : Dow vinyl ester & CFRM.

Moulding No.s :	5001-5003	Initial moulding shots
	5004-5007	Short shots of 5,10,15,20 seconds

2 **Glass reinforced undershields**

Purpose : The first attempts at processing using higher volume fractions, and mulitiaxial reinforcement.

Materials : Dow vinyl ester resin, CFRM & NCF.

Moulding No.s :	5008-5009	NCF / CFRM
	5010-5015	Attempts to increase wet-out of surface fibres. Part fills 80% - 90%.
	5016-5021	NCF / CFRM poor release, injection-cure times approx. 26 mins
	5022-5025	New lay-up, difficult to clean flash. No.23 processed with a cross cut in an attempt to increase permeability, glass washed and choked resin flow.
	5026-5030	Undershields for Motorsport problems with warpage.

3 **Carbon / Glass reinforced undershields**

Purpose : Attempt at producing the first batch of undershields for motorsport using the high cost carbon reinforcement.

Materials : Dow vinyl ester resin, Carbon & Glass NCF, CFRM.

Moulding No.s :	5031-5035	Undershield mouldings for Motorsport,

		veil washing (9.5kg).
	5035-5050	Undershield mouldings for Motorsport, swage material moved 1 layer in.
	5055-5062	Variation in reinforcement, attempts to reduce moulding weight.

4 **Batch preheating**

Purpose : Proving out the process of batch preheating on the undershield mould. Also using the band heaters which were installed around the homogeniser.

Materials : CVP polyester, CFRM.

Moulding No.s :	5050-5054	Unifilo, CVP 6345.001 polyester mouldings

5 **Batch preheating undershield production for Motorsport**

Purpose : Production of undershields for Motorsport, batch preheating had to be seen to reduce cycle times and improve wet-through.

Materials : Dow vinyl ester, Carbon & Glass NCF, CFRM.

Moulding No.s :	5063-5065	Preheating Derakane (8.1 Kg)
	5066-5075	Some with preheat, some without, warpage problem solved by exactly balancing reinforcement.
	5078-5080	Undershield production with university logo

6 **Low Profile mouldings**

Purpose : Investigation of producing high quality components. Fast sequential moulding and consecutive moulding work. Batch preheating used to reduce cycle times.

Materials : DSM low profile polyester, Calcium carbonate filler, CFRM.

Moulding No.s :	5076-5077	DSM 40-7428 low profile resin (6 months old)
	5081-5095	Low profile work using DSM 40-7417 low profile resin, fast cycling work, with sequential mouldings maximum 6 made in 14 minutes per moulding.

7 **Sequential mouldings**

Purpose : Investigations of batch processing and fast sequential moulding
Materials : DSM low profile polyester, CFRM.
Moulding No.s : 5085-5088 Sequence 1
5090-5095 Sequence 2

8 **Mould Commissioning (After rework)**

Purpose : The first mouldings after the mould refurbishment, polyester mouldings produced in an attempt to condition the mould
Materials : CVP polyester, CFRM.

Moulding No.s :	5096-5104	A large amount of surface residue were seen to build up on the mould surfaces, this material has been discovered to be polystyrene.

9 **Modar moulding**

Purpose : One modar undershield produced for ICI to prove out their resin system on the undershield mould.
Materials : ICI modar (Acrylic), CFRM.
Moulding No. : 5105 1 modar undershield produced

10 **Sequential mouldings**

Purpose : In an attempt to condition the mould surface, filled polyester mouldings were produced. With these mouldings were combined the next set of fast sequential mouldings, this time using polyester not low profile resin.
Materials : CVP polyester, Calcium carbonate filler, CFRM.
Moulding No.s : 5106-5112 5 made in one batch until vacuum pump stopped working.

11 **Glass / lightweight core reinforcement**

Purpose : Production of lightweight undershields for Motorsport.
Materials : Dow vinyl ester, NCF, CFRM and various lightweight core materials.

Moulding No.s :	5113-5128	1st moulding refused to release good surface condition except for outer laminate left on the mould surface. Problems with air removal, bubbling and delamination.

12 **Low profile moulding**

Purpose: Production of high quality low profile undershields for painting trials at Ford.

Materials : DSM low profile resin, Calcium carbonate filler, CFRM.

Moulding No.s : 5129-5138

13 **Transit High roof mouldings**

Purpose : Production of components with a gel coat on the lower surface to emulate the moulding conditions and materials to be used in the Transit high roof moulding programme.

Materials : Scott Bader Crystic Polyester Resin and gel coat, Choromat Chopped strand mat.

Moulding No.s : 5164-5173

Gel coated surface exhibited fibre strike through, exotherm temperature were much higher than expected. Mould surface build-up was evident after two mouldings.

14 **Lightweight undershield moulding with low temperature catalyst**

Purpose : Lightweight undershields were moulded at lower temperatures in an attempt to reduce the bubbling seen in the lightweight core material.

Materials : Dow vinyl-ester, NCF glass, CFRM, Coremat.

Moulding No.s : 5153-5163

The bubbling in the core material was reduced, moulding average weight 5.1 kg.

Appendix 4

Determination of Fibre Volume Fraction and Estimation of Void Volume Fraction by the Burn Off Method

---

The fibre volume fraction of a composite can be estimated from the fibre mass faction, determined by a burn-off experment, and the density of the constituents.

$$V_f = \frac{\frac{M_f}{\rho_f}}{\frac{M_f}{\rho_f} + \frac{M_r}{\rho_r} + \frac{M_{bi}}{\rho_{bi}}} \qquad \textbf{(A4.1)}$$

Where:

M_b = The mass fraction of the binder on the reinforcement.

and

$$M_r = 1 - (M_f + M_b)$$

The void volume fraction is estimated from the actual density of the sample compared with the theoretical densities of the composites constituents. The density of the composite is determined by using Archimedes' principle to determine the density of a solid body. The sample is first weighed in air then while immersed in distilled water. This is accomplished by suspending the sample from a wire of known mass. The density of the composite can then be determined from:

$$\rho_{composite} = \frac{m_{air}}{m_{air} - (m_{immersed} - m_{wire})} \rho_{water} \qquad \textbf{(A4.2)}$$

The void volume fraction can then be approximated by:

$$V_v = 1 - (V_f + V_{bi} + V_r) \qquad \text{(A4.3)}$$

Where for any species (fibre, resin or binder):

$$V = M \frac{\rho_{composite}}{\rho} \qquad \text{(A4.4)}$$

Appendix - 10

Appendix 5

Contact Angle Data

The data was obtained by Revill[19].

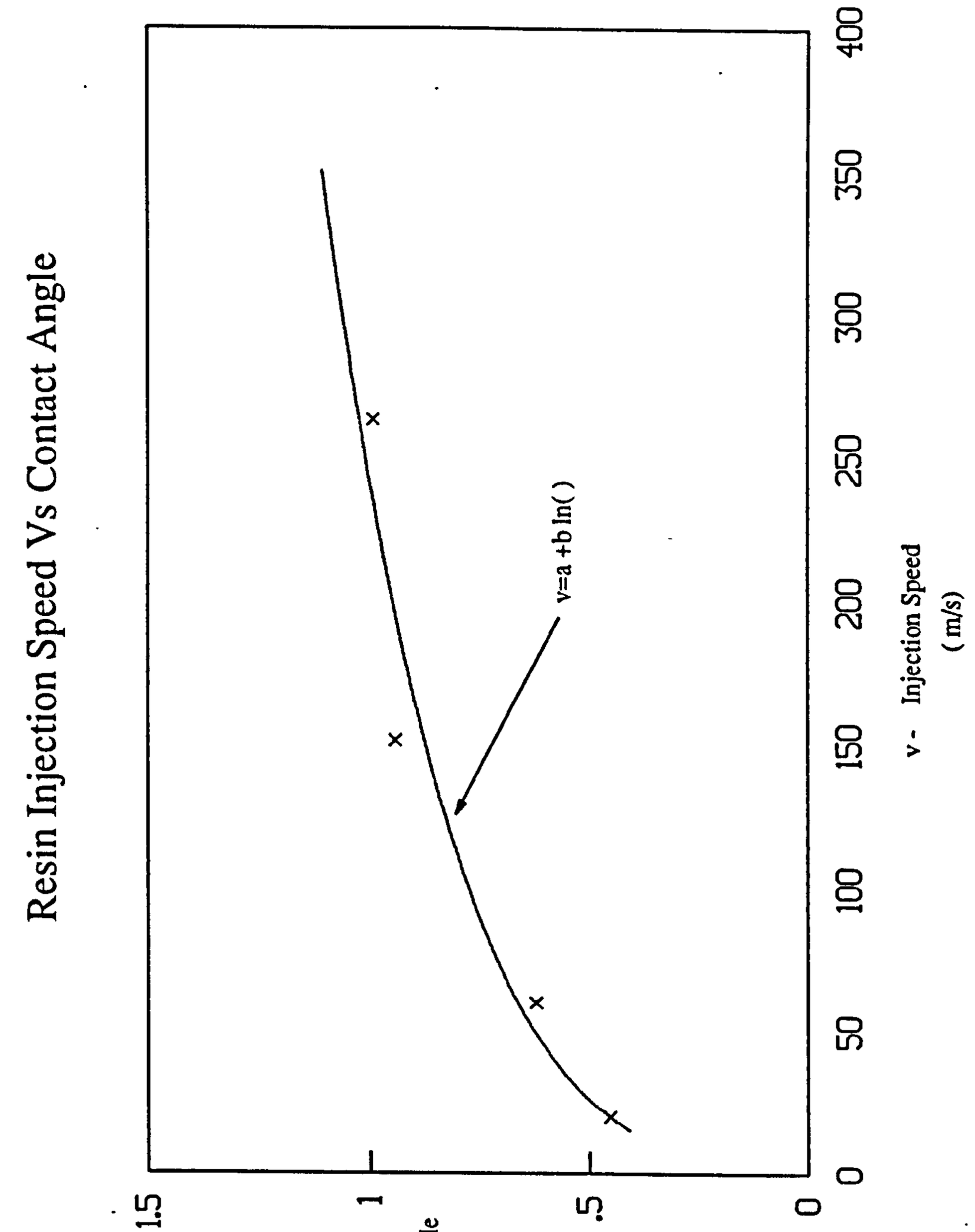

Appendix 6

Viscosity Measurements

The measurements were carried out on a Brookfield viscometer.

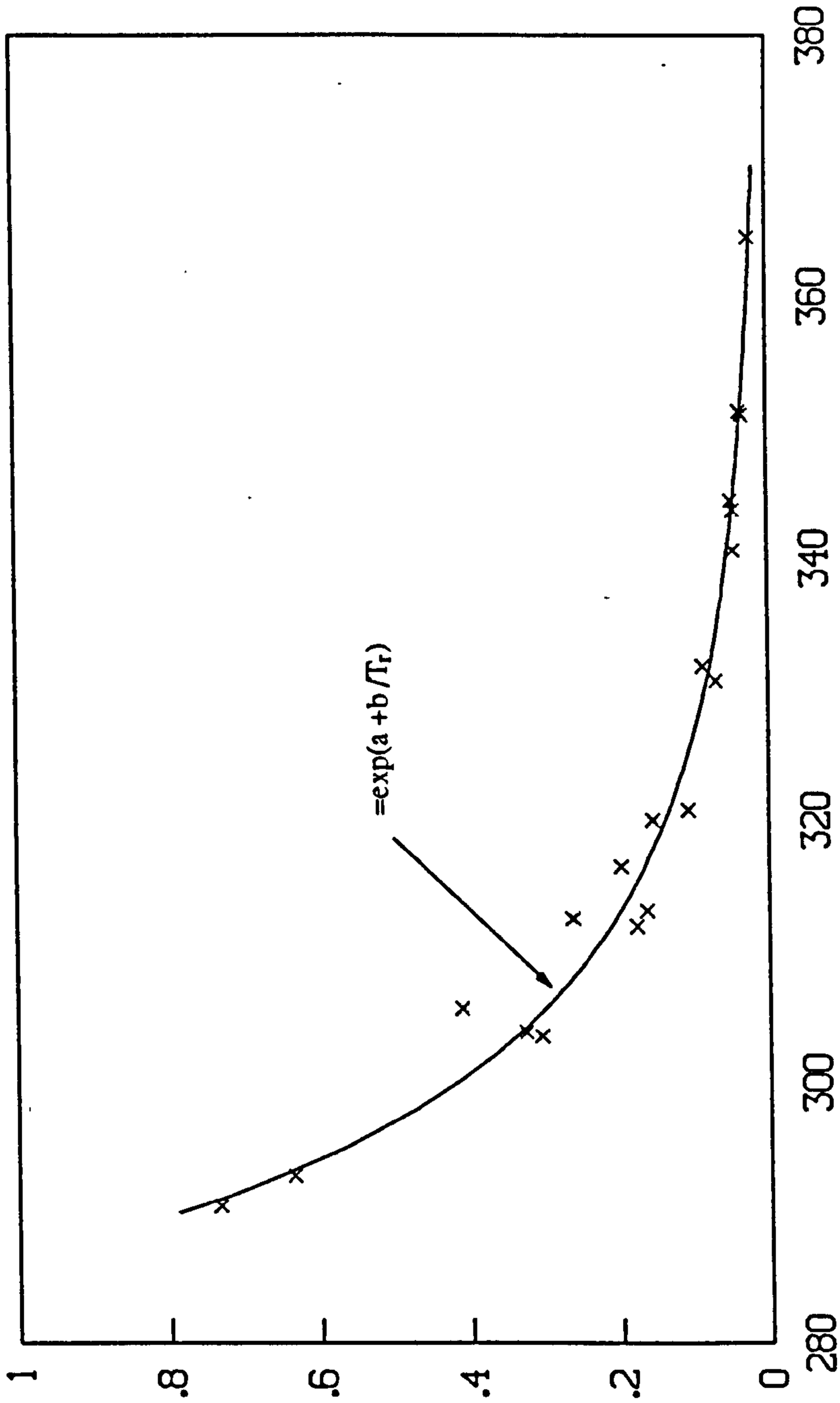

Appendix 7

Gel Time Measurements

These readings were carried according to the SPI procedure for running exotherm curves for polyester resins[66].

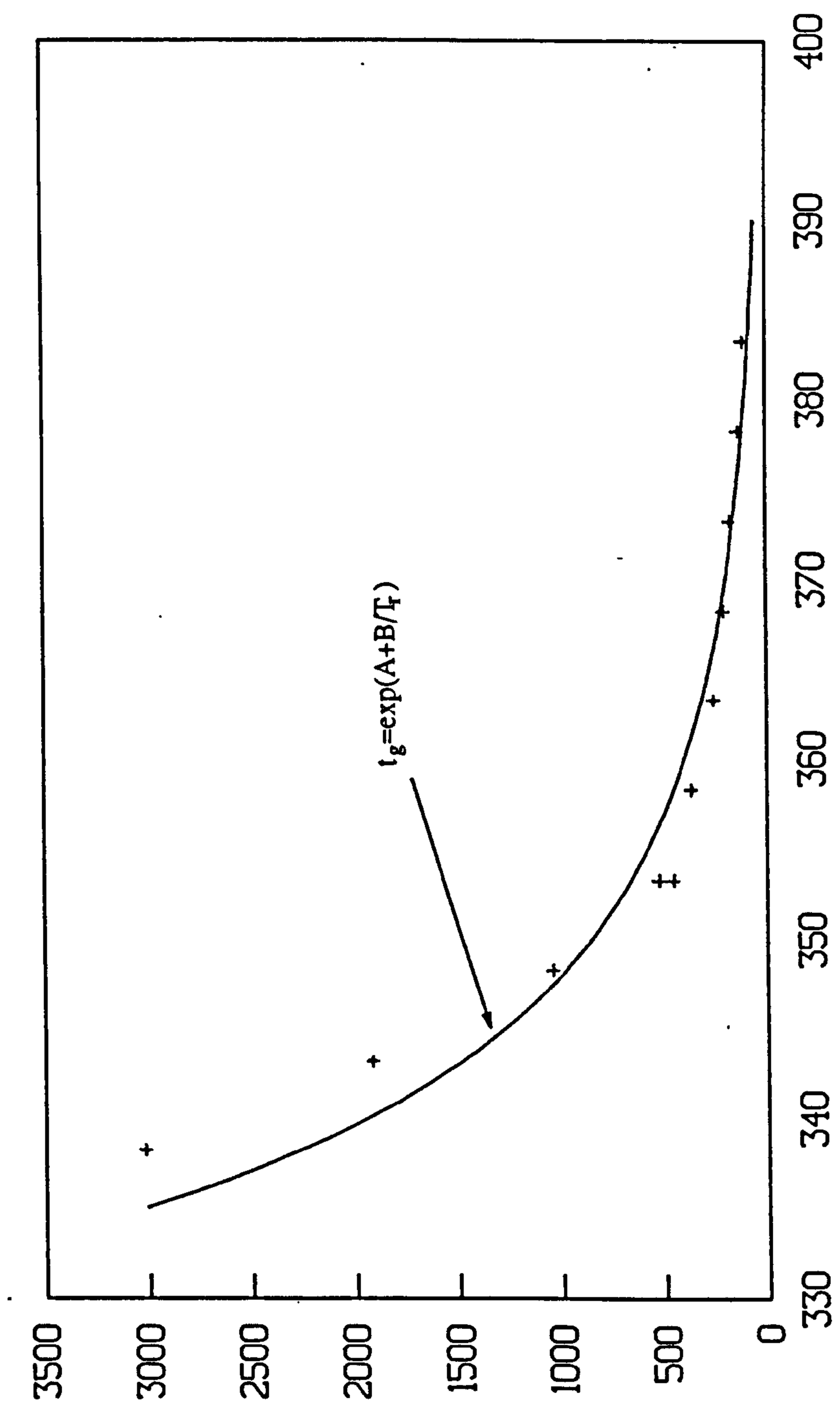

Appendix 8

Injection Pressure

During rectilinear flow, the flow advances in a single dimension from a one-dimensional origin. The pressure at the flow front is assumed to be zero. At any position of the flow front the pressure difference between the flow front and a distance δx behind the it is given by:

$$\delta P_{ip} = P_{ip} - \frac{P_{ip}}{l}(l - \delta x)$$

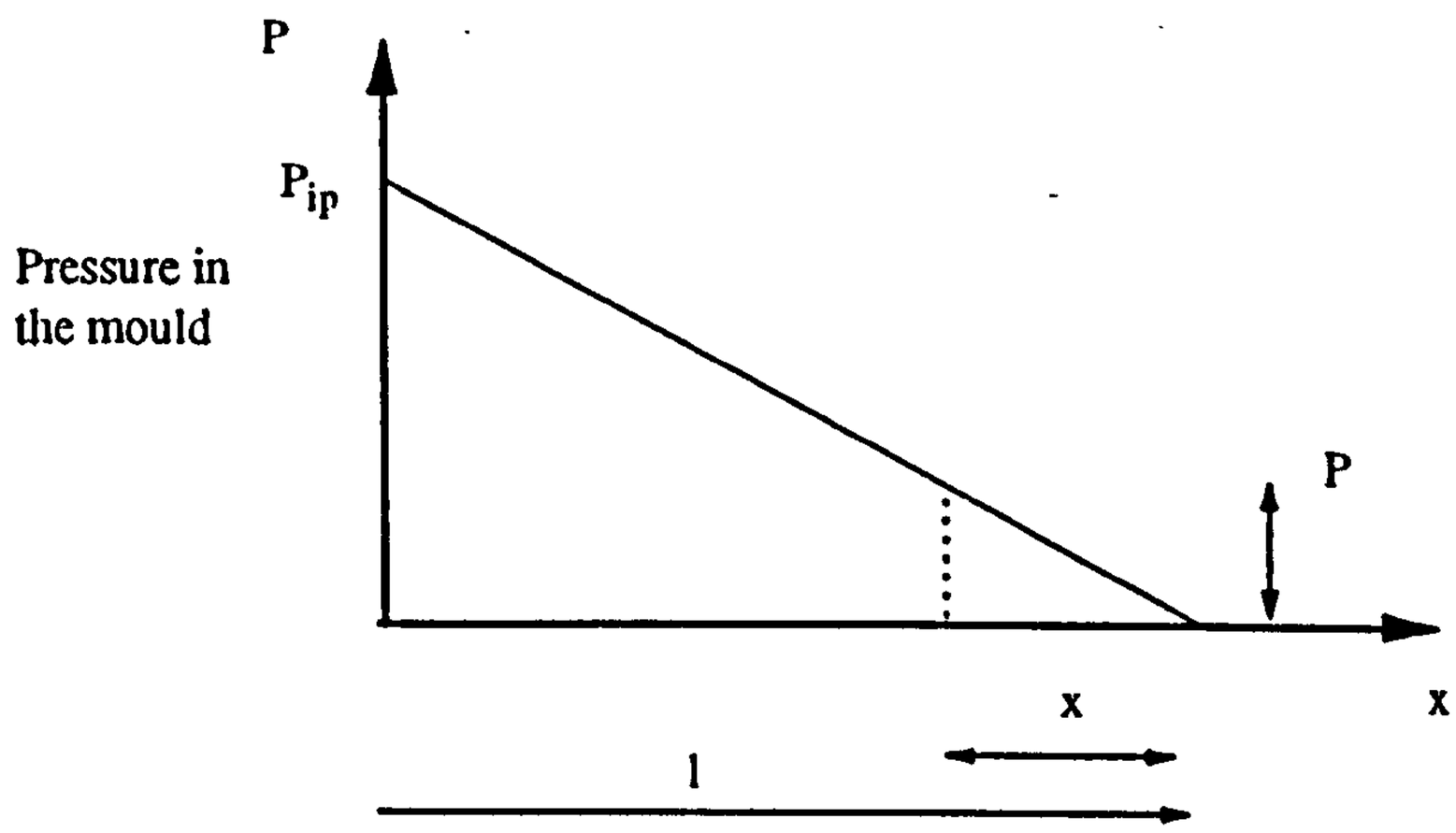

Distance from injection gate

Appendix 9

Reinforcement Details - Tech Textiles ELPb 567 - 0° Glass

ELpb 567 Unidirectional reinforcement[80]	
Description	Unidirectional glass fabric, consisting of rovings, stitched to form a Non Crimp Fabric (NCF).
Surface density	567 g/m^2
Rovings (fibre bundles)	2400 Tex (g/100m)
Approximate number of fibres per roving	5000
Fibre diameter	15µm (fibre radius = 7.5µm)
Glass type	E-glass
E-glass constituents	S_iO_2 = 54.1% Al_2O_3 = 15.2% CaO = 17.3% MgO = 4.7% Na_2O = 0.6% B_2O_3 = 8.0%
Size type	Pe/Epoxy
Specific heat capacity (C_f)	800
Thermal conductivity (k_f)	0.963 W/mK
Fibre density (ρ_f)	2605 kg/m^3

Appendix 10

Resin Details - CVP 6345.001 Orthophthalic Polyester Resin

CVP 6345.001 Polyester Resin[81]	
Description	Orthophthalic, medium reactivity, non-thixotropic.
Monomer	Styrene
Monomer Content	37%
Density (ρ_r)	1120 kg/m^3
Specific Heat capacity (C_r)	1900
Thermal conductivity (k_r)	0.218 W/mK
Interfacial tension (γ) (between glass and polyester resins)	0.35

Appendix 11

Heat Transfer Networks

---

1. Axial Flow

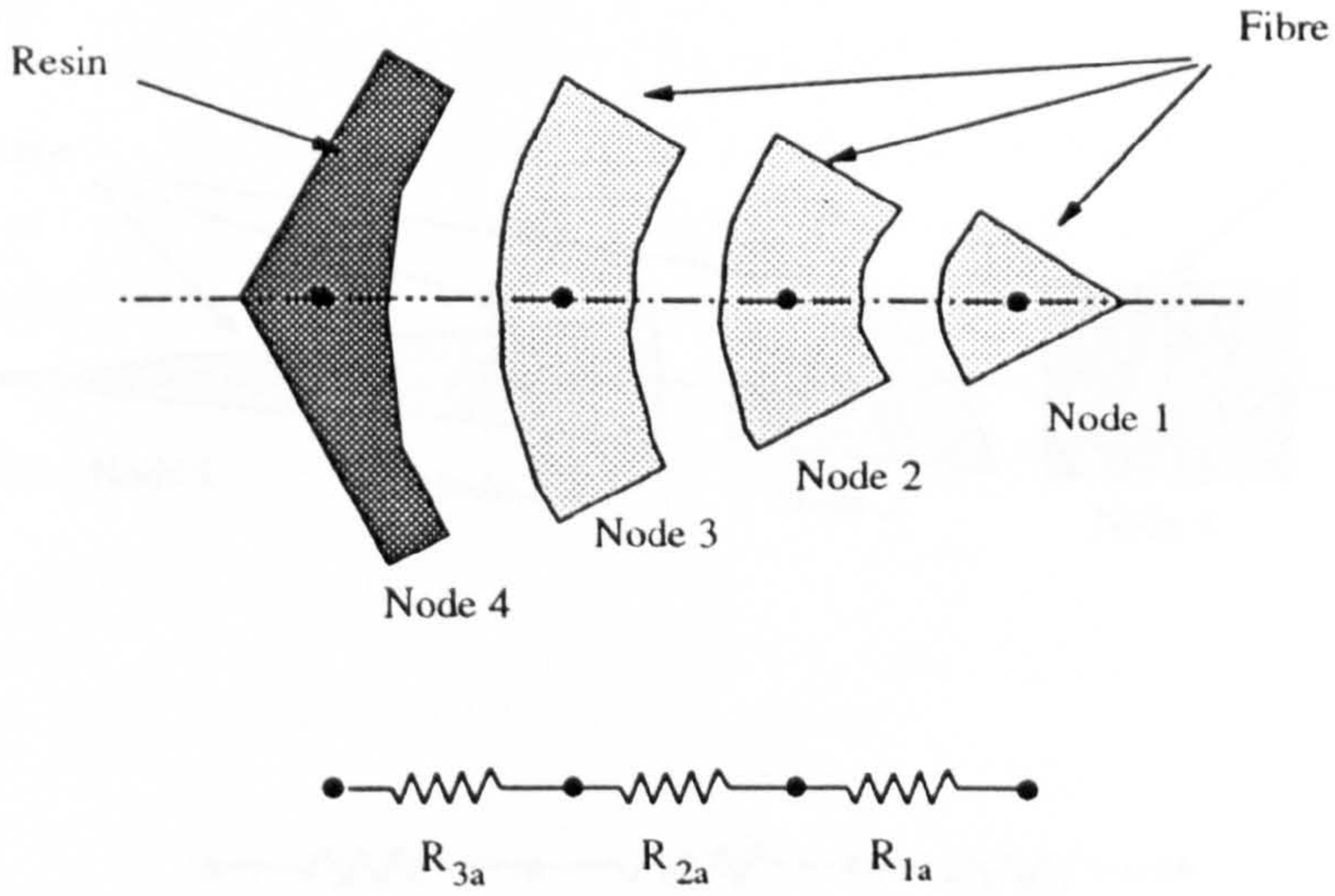

The thermal resistance for each element can be calculated from the following equation:

$$R_i = \frac{\Delta x}{kA} \qquad \textbf{(A11.1)}$$

From use of this equation the thermal resistances of the network shown can be calculated:

$$R_{1a} = \frac{\frac{R}{3}}{k_f \frac{\pi}{6} \frac{R}{3} \delta z} \qquad \textbf{(A11.2)}$$

$$R_{2a} = \frac{\frac{R}{3}}{k_f \frac{\pi}{6} \frac{2R}{3} \delta z} \qquad \textbf{(A11.3)}$$

$$R_{3a}=\frac{1}{h\pi\frac{R}{3}\delta z}+\frac{\frac{R}{6}}{k_f\frac{\pi}{6}\frac{5R}{6}}+\frac{\frac{\sqrt{3}}{4}(R+d)-\frac{R}{2}}{k_r\frac{\pi}{6}(\frac{\sqrt{3}}{4}(R+d)+R)} \qquad \textbf{(A11.4)}$$

2. Transverse Flow

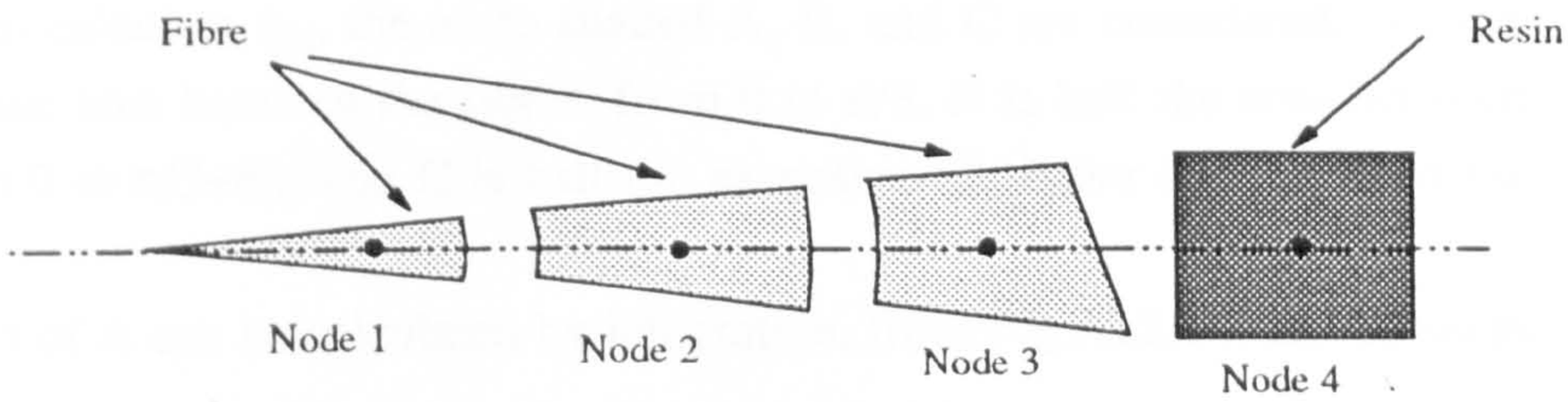

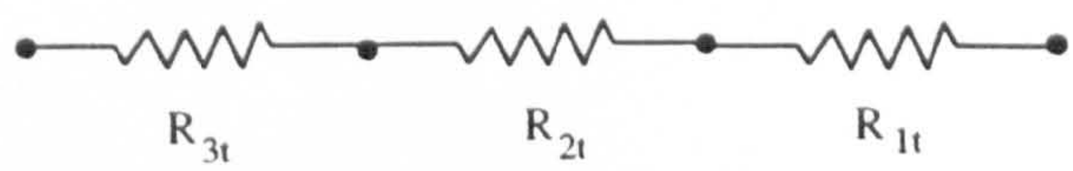

The thermal resistance for the heat transfer during transverse flow can be calculated in the same way:

$$R_{1t}=\frac{\frac{R}{3}}{k_f\delta\theta\frac{R}{3}\delta z} \qquad \textbf{(A11.5)}$$

$$R_{2t}=\frac{\frac{R}{3}}{k_f\delta\theta\frac{2R}{3}\delta z} \qquad \textbf{(A11.6)}$$

$$R_3t=\frac{i}{h\delta\theta R\delta z}+\frac{\frac{R}{6}}{k_f\delta\theta 5}+\frac{\frac{w}{2}}{k_r\delta\theta R} \qquad \textbf{(A11.7)}$$

Appendix 12

Calculation of the Excess Body Angle (ϕ_{excess})

The excess body angle is shown in Figure A12.1. Figure A12.2 shows the angle in greater detail, to calculate ϕ_{ex}, the areas shaded A, B, and C are considered. Where area A is half the area between the fibres, from 0 to $\pi/3$, B is half the area between the fibres, from 0 to $\pi/3+\phi_{ex}$, and C is half the excessive triangular area between the channels.

The area of A can be calculated by integration, from Fig.A12.1 it can be seem that:

$$y=R+d-\sqrt{(R^2-X^2)} \qquad \textbf{(A12.1)}$$

Therefore the area A is equal to:

$$A=\int_0^{RSin\frac{\pi}{6}} (R+d-\sqrt{(R^2-X^2)})dx \qquad \textbf{(A12.2)}$$

Since:

$$x=RSin\phi \qquad \textbf{(A12.3)}$$

$$\frac{dx}{d\phi}=RCos\phi \qquad \textbf{(A12.4)}$$

The Area A can now be calculated:

$$A=\frac{1}{2}R(R+d)-\int_0^{\frac{\pi}{6}} RCos^2\phi d\phi \qquad \textbf{(A12.5)}$$

Which gives:

$$A=\frac{1}{2}R(R+d)-R^2(\frac{\pi}{12}+\frac{\sqrt{3}}{8}) \qquad \textbf{(A12.6)}$$

For Area B the calculation is the same except that the integration is performed between 0 and $\pi/6+\phi_{ex}$.

$$B=RSin(\frac{\pi}{6}+\phi_{ex})-R^2\int_0^{\frac{\pi}{6}+\phi_{ex}} Cos^2\phi d\phi \qquad \textbf{(A12.7)}$$

Which gives:

$$B=R(R+d)Sin(\frac{\pi}{6}+\phi_{ex})-\frac{R^2}{2}(\frac{\pi}{6}+\phi_{ex})+\frac{1}{2}Sin(\frac{\pi}{3}+2\phi_{ex}) \qquad \textbf{(A12.8)}$$

The triangular area C can be calculated since the two sides, and the angle between them are known, which is:

$$C=\frac{1}{2}((1-\frac{\sqrt{3}}{2})R+d)^2 \qquad \textbf{(A12.9)}$$

To solve for ϕ_{ex} we know:

$$B=A+C \qquad \textbf{(A12.10)}$$

By rearranging the equation becomes:

$$f(\phi_{ex})=0=R^2[0.2925+\frac{\phi_{ex}}{2}+\frac{1}{4}Sin(\frac{\pi}{3}+2\phi_{ex})-Sin(\frac{\pi}{6}+\phi_{ex})]+Rd[0.634-Sin(\frac{\pi}{6}+\phi_{ex})]+$$

(A12.11)

The differential f'(ϕ_{ex}) is:

$$f'(\phi_{ex})=R^2[\frac{1}{2}+\frac{1}{2}Cos(\frac{\pi}{3}+\phi_{ex})-Cos(\frac{\pi}{6}+\phi_{ex})]-RdCos(\frac{\pi}{6}+\phi_{ex}) \qquad \textbf{(A12.12)}$$

A solution for ϕ_{ex} can now be obtained if values of R and d are inserted and the equation solved iteratively, by the Newton-Raphson approximation:

$$\phi_{ex(n+1)}=\phi_{ex(n)}-\frac{f(\phi_{ex(n)})}{f'(\phi_{ex(n)})} \qquad \textbf{(A12.13)}$$

Figure A12.1 Calculation of ϕ_{excess}

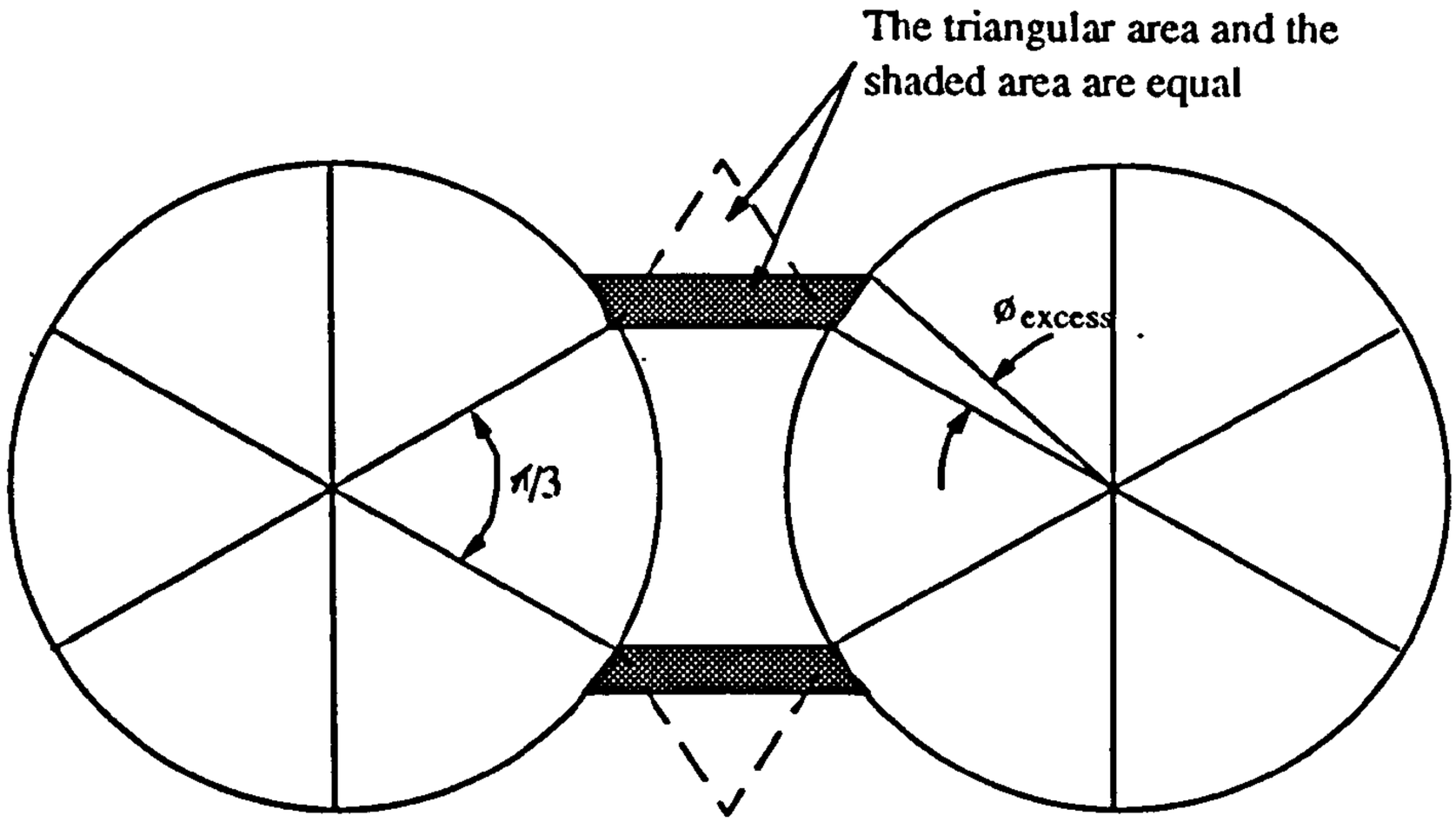

The triangular areas shown in Fig.5 are compensated for in area
by increasing the channel length to $\pi/3 + 2/3\ \phi_{excess}$

Figure A12.2 Solving ϕ_{excess} by Comparison of Areas

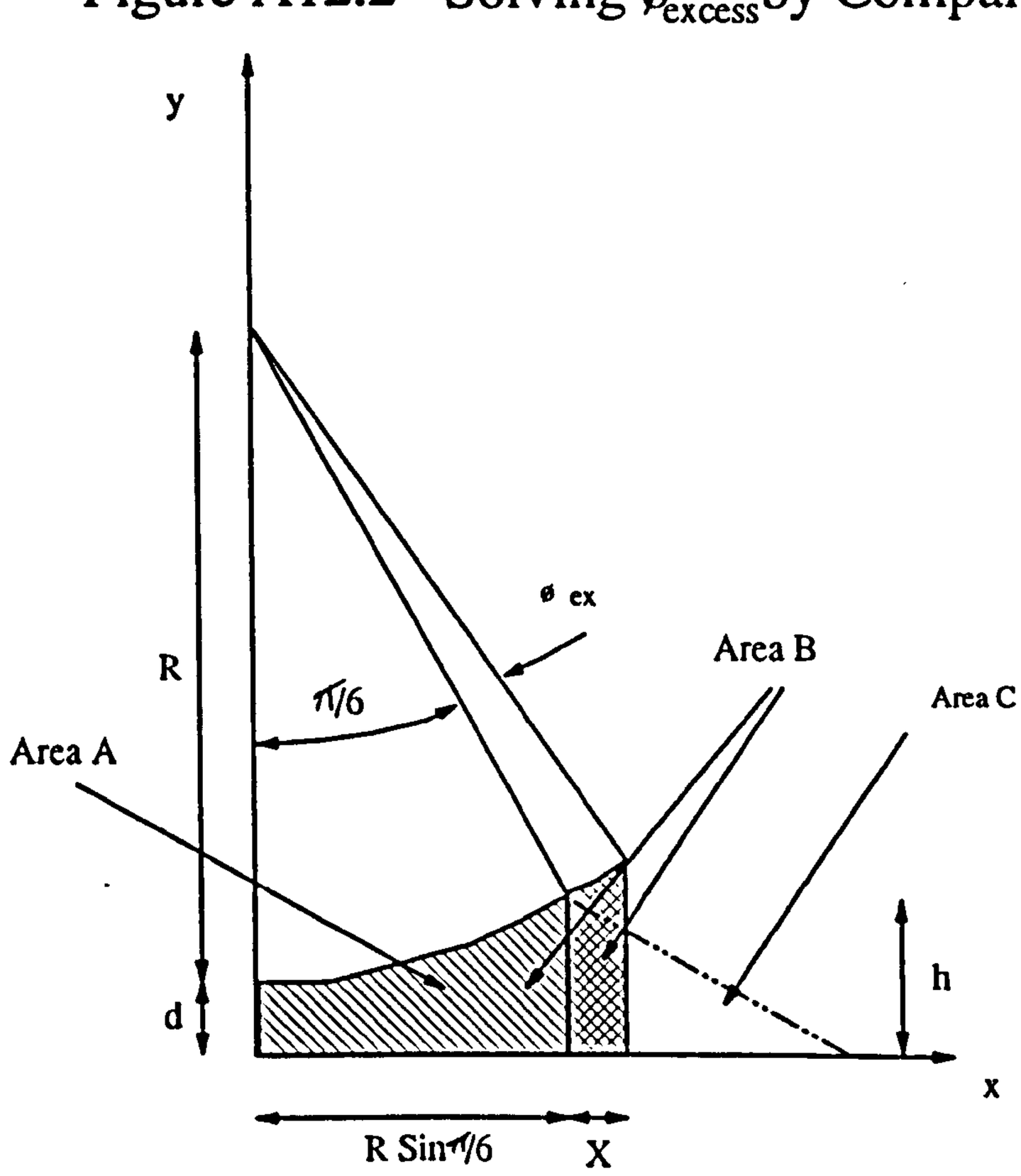

Appendix 13

Calculation of the Meniscus Position S

In order to predict the point at which bifircation will occur, the position of the meniscus from the centre of the flow channel is required.

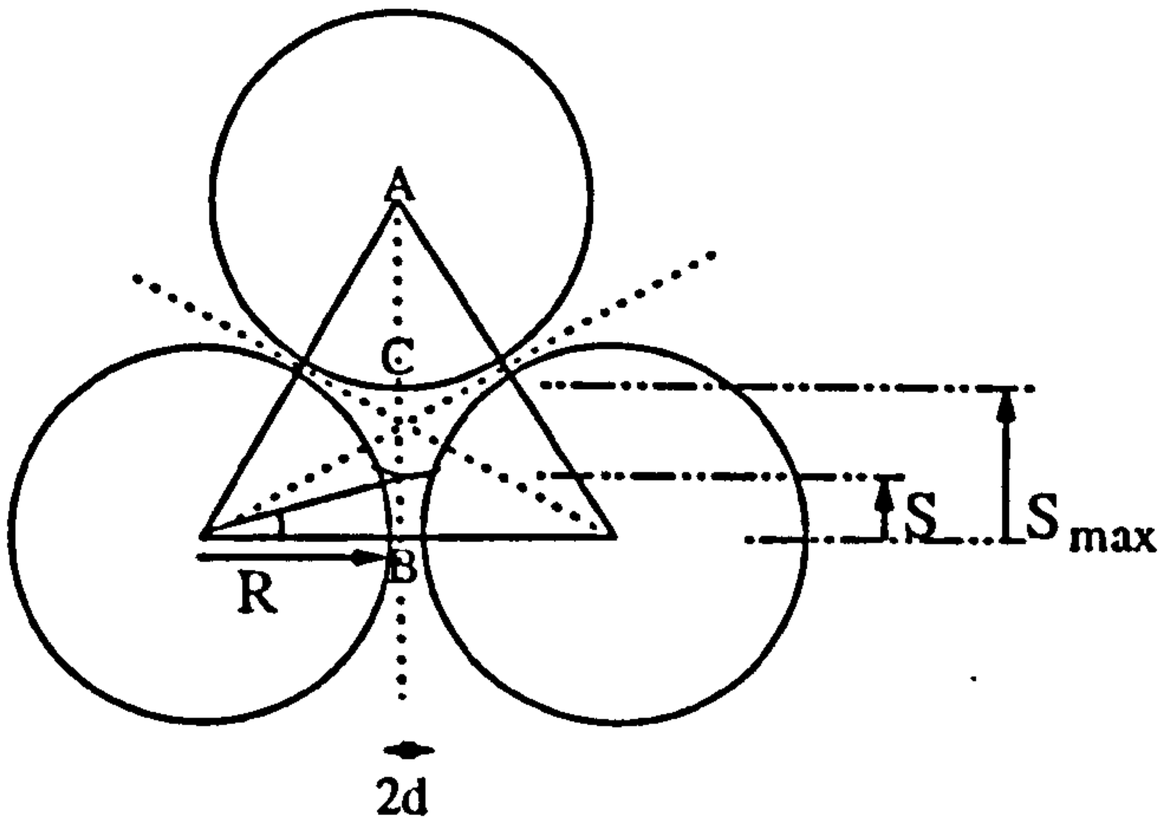

The position of s_{max} the position of the meniscus when bifircation occurs.

$$AB=2(R+d)\cos 30° \tag{A13.1}$$

$$CB=s_{max}=2(R+d)cos30° -R \tag{A13.2}$$

The position s at any value of ϕ can be determined by trigonometry:

$$s=R\sin\phi+r-w\tan\alpha \tag{A13.3}$$

$$s=r\sin\phi+w(\frac{1}{\cos(\alpha)}-\tan\alpha) \tag{A13.4}$$

$$s=Rsin\phi+(R(1-\cos\phi)+d)(\frac{1}{\cos(\theta-\phi)}-\tan(\theta-\phi)) \tag{A13.5}$$

$$s = R\sin\phi + \frac{(R(1-\cos\phi)+d)}{\cos(\theta-\phi)}(1-\sin(\theta-\phi)) \qquad \textbf{(A13.6)}$$

Appendix 14

In-Plane Permeability Measurement

Several techniques have been used to measure in-plane permeability[53,41]. It is of the key properties required for any RTM process simulation. At present no standard method of determining permeability, nor do any calibration materials exist for any test method.

In order to simulate the filling process as closely as possible, a transient wetting rather than steady state wetted permeability is desired, since the data is required in transient impregnation models. Edge effects should be minimised. Test equipment that allows flow parallel to mould walls should be avoided because the 'race track' effect of resin quickly passing through any gap between fibre preform and mould edge is well known. The advancing resin flow front at mould edges effectively pulls the resin through the fibre more quickly than would otherwise be the case. The cavity should be dimensionally stable since mould deflection allows flow fronts and rates to vary, making analytical methods impossible to apply. Test methods must be capable of measuring the permeability of anisotropic materials. An anisotropic test is required to obtain the two principal in-plane permeabilities and their orientation compared to the fabric direction. Permeability varies with the fibre volume fraction[40] and test equipment must allow for a sensible variation in this quantity.

The in-plane permeability measurement rig used at the University of Nottingham has been designed with the above considerations in mind[79]. The rig is based on radial impregnation (Figure A14.1). A central inlet introduces an isothermal Newtonian motor oil of known viscosity into a cavity at a constant pressure. This cavity is formed between a thick aluminium base and a clear Perspex top. The top is thick enough to resist bending and as an additional precaution an aluminium stiffener further minimises deflections. Six pressure transducers are placed on two perpendicular lines and another pressure transducer is located at the gate. The pressure readings from these sensors are recorded using a PC with data acquisition hardware and software. The cavity thickness can be varied from 3mm to 6mm to allow for different material thicknesses and to obtain a reasonable range of fibre volume fractions. Concentric circles centred at the central gate are inscribed on the Perspex. These are used to follow the filling of the cavity. The radius of the cavity

is 200mm. At the outer radius a gallery is used to collect any oil that overspills into a collection container via a vent line. A small circular hole is cut at the centre of the preform prior to injection to distribute the oil evenly through the thickness and to promote a two dimensional pressure gradient. The fill patterns are recorded using either a camera or a video camera and are stored for later interpretation. Figure A14.1 shows a schematic of the radial impregnation rig and Figure A14.2 shows an in-plane permeability test in progress.

For isotropic materials it can be shown that the time to fill to a radius r_m, from a source of radius r_{inj} is,

$$t_{fill} = \frac{\varepsilon \mu}{2KP_{inj}} \left\{ r_m^2 \ln\left(\frac{r_m}{r_{inj}}\right) - \frac{r_m^2 - r_{inj}^2}{2} \right\} \qquad \text{(A14.1)}$$

with the driving pressure at the source radius equal to P_{inj}. An isothermal, Newtonian fluid of viscosity μ passes through an isotropic porous medium of voidage ε, of Darcy permeability K[83]. All the values are known before the experiment or as a result of the experiment, apart from the voidage (the volume fraction not occupied by fibre), that is calculated directly from the preform areal mass and cavity thickness. The isotropic permeability can then be found.

For anisotropic materials a different controlling expression must be used. Adams et al[41] describe a method based upon radial magnitudes in the 0° (ξ_{f1}) and 90° (ξ_{f2}) directions (parallel to the principal directions), defined as:

$$\xi_{f1} = \sinh^{-1}\left(\frac{r_{f1}}{r_{inj}}\sqrt{\left\{\frac{1}{\alpha} - 1\right\}}\right) \qquad \text{(A14.2)}$$

$$\xi_{f2} = \cosh^{-1}\left(\frac{r_{f2}}{r_{inj}}\sqrt{1-\alpha}\right) \qquad \text{(A14.3)}$$

Flow in these two directions can then be calculated by using,

$$\frac{d\xi_{f1}}{dt} = \frac{K_1 P_{inj}}{\varepsilon \mu r_{inj}^2}\left(\frac{\alpha}{\alpha - 1}\right)\frac{1}{(\xi_{f1} - \xi_{inj})(\cosh^2 \xi_{f1})} \qquad \text{(A14.4)}$$

$$\frac{d\xi_{f2}}{dt} = \frac{K_2 P_{inj}}{\varepsilon \mu r_{inj}^2} \left(\frac{\alpha}{\alpha - 1}\right) \frac{1}{(\xi_{f2} - \xi_{inj})(\cosh^2 \xi_{f2} - 1)} \qquad \text{(A14.5)}$$

In the above expressions α is the ratio of principal permeabilities K_1/K_2 the radius travelled by the front along direction 1 is r_{f1} and the elliptical extent at the injection point is given by:

$$\xi_{inj} = \ln\left(\frac{1+\sqrt{\alpha}}{\sqrt{1-\alpha}}\right) \qquad \text{(A14.6)}$$

The equations A14.4 and A14.5 have to be solved iteratively to find values for the principal permeabilities. It is, however known that by use of an elliptical transformation of the governing partial differential equation for pressure in anisotropic porous media under the same conditions of the experiment,

$$\frac{\partial^2 P}{\partial x^2} + \frac{K_2}{K_1} \frac{\partial^2 P}{\partial y^2} = 0 \qquad \text{(A14.7)}$$

that at any time,

$$\alpha = \frac{K_1}{K_2} = \left(\frac{r_{f1}}{r_{f2}}\right)^2 \qquad \text{(A14.8)}$$

gives a good first approximation for α.

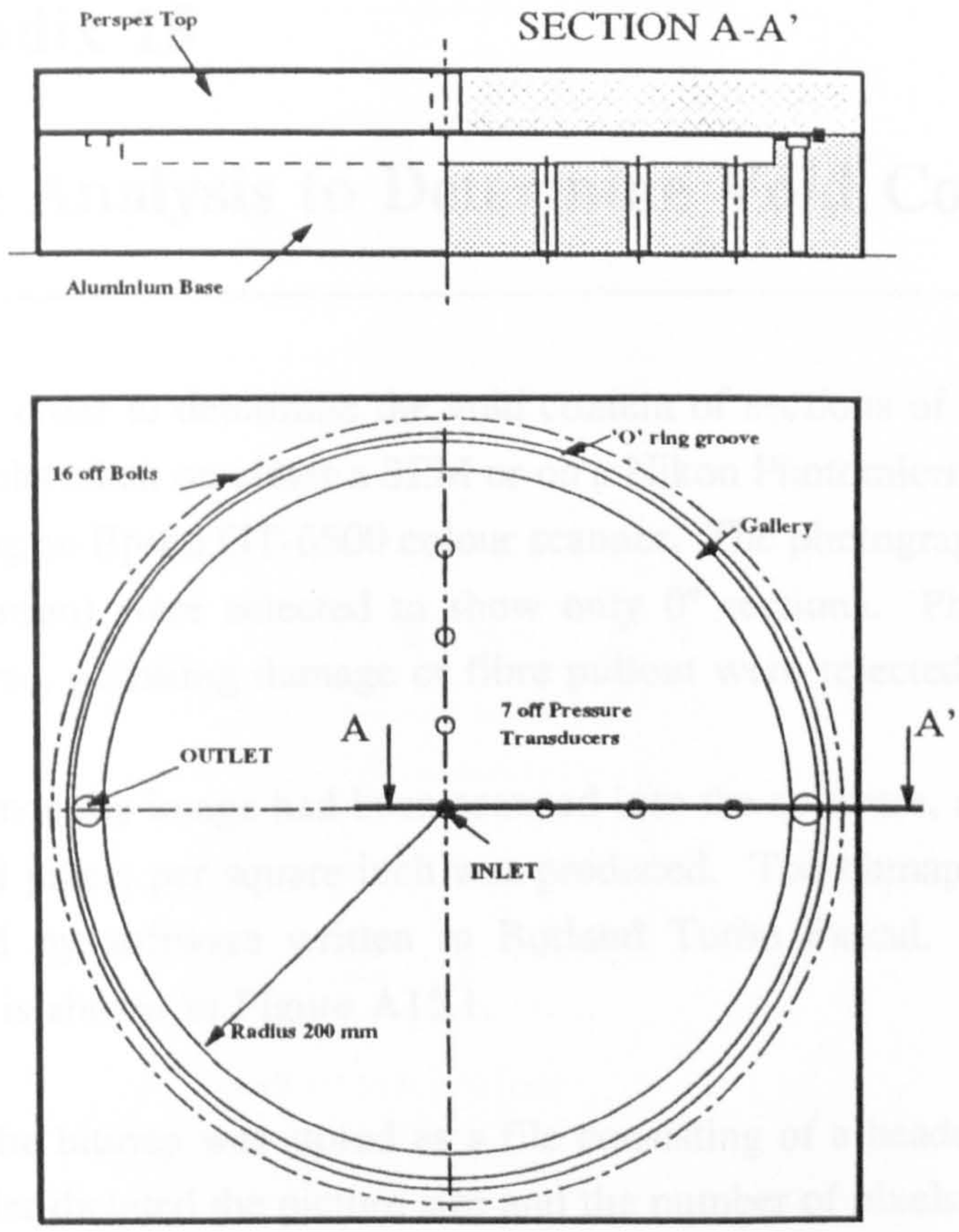

Figure A14.1 Schematic of Circular Permeability Rig
(Courtesy Dr. E.V. Rice)

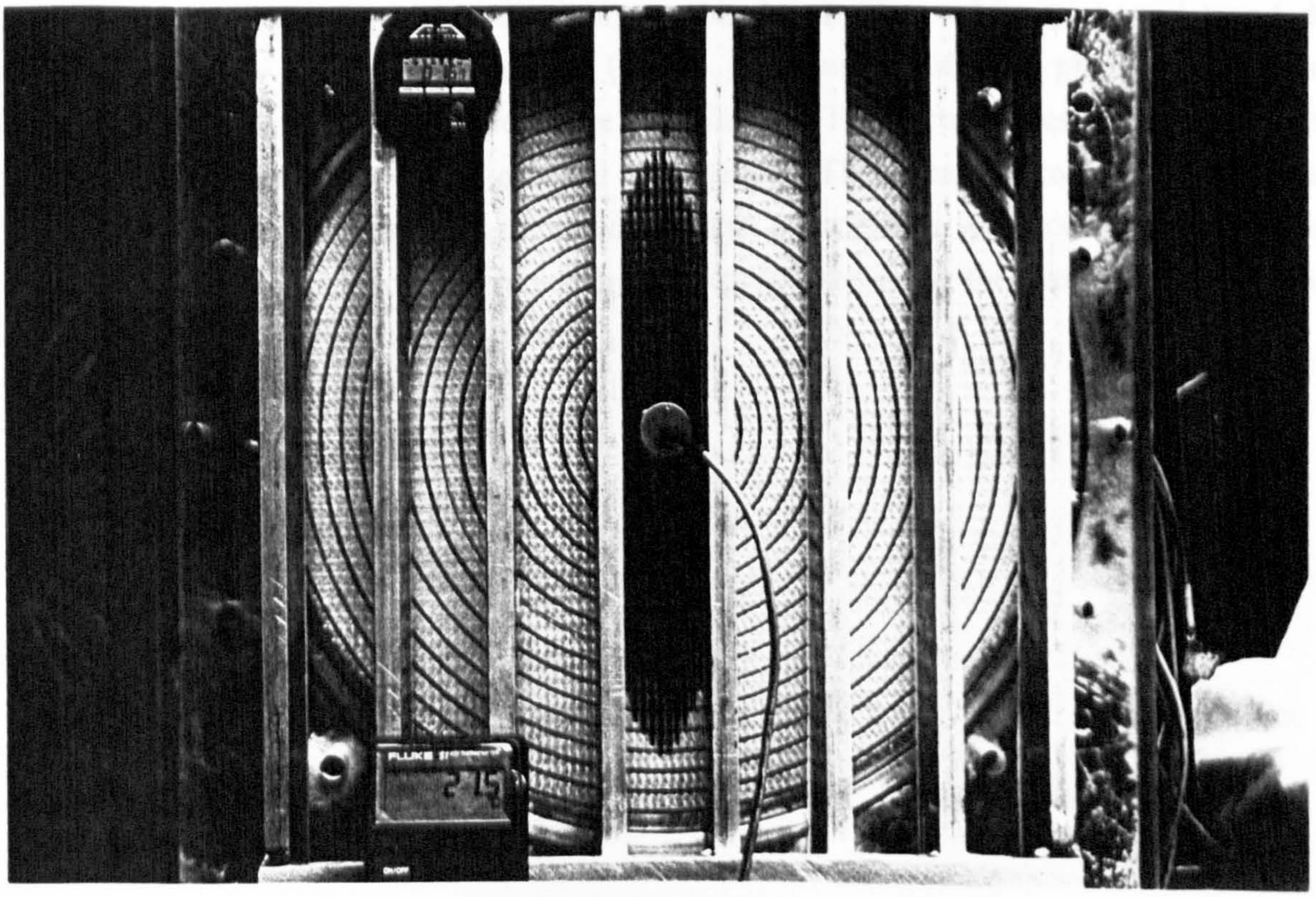

Figure A14.2 Permeability Test of Unidirectional Fabric

Appendix 15

Image Analysis to Determine Void Content

In order to determine the void content of sections of 0° FRP, black and white photographs taken on either a SEM or on a Nikon Photomicroscope were scanned into a PC using an Epson GT-6500 colour scanner. The photographs (all taken at 25 times magnification) were selected to show only 0° sections. Photographs with any 90° cross fibres, polishing damage or fibre pullout were rejected.

Once the image had been scanned into the software, a high definition bit map of 90,000 pixels per square inch was produced. The bitmap was saved as a file and processed by software written in Borland Turbo Pascal. The flowchart for this program is shown in Figure A15.1.

The bitmap was stored as a file consisting of a header and pixel information. The header dictated the picture size and the number of pixels in each line. Each pixel was stored as a single shade from 256 shades ranging between black and white. A threshold value was chosen objectively (at approximately 50) and the file was processed, converting the values above the threshold to white (not voids) and the values below the threshold to black (voids). The number of black pixels was summed and a percentage of void coverage calculated. The picture was displayed on the screen and compared to the original photograph. The threshold could then be altered depending on whether all the voids in the photograph were correctly identified. Batches of images from the moulding were processed using the same threshold values to gain an average void content.

Figure A15.1

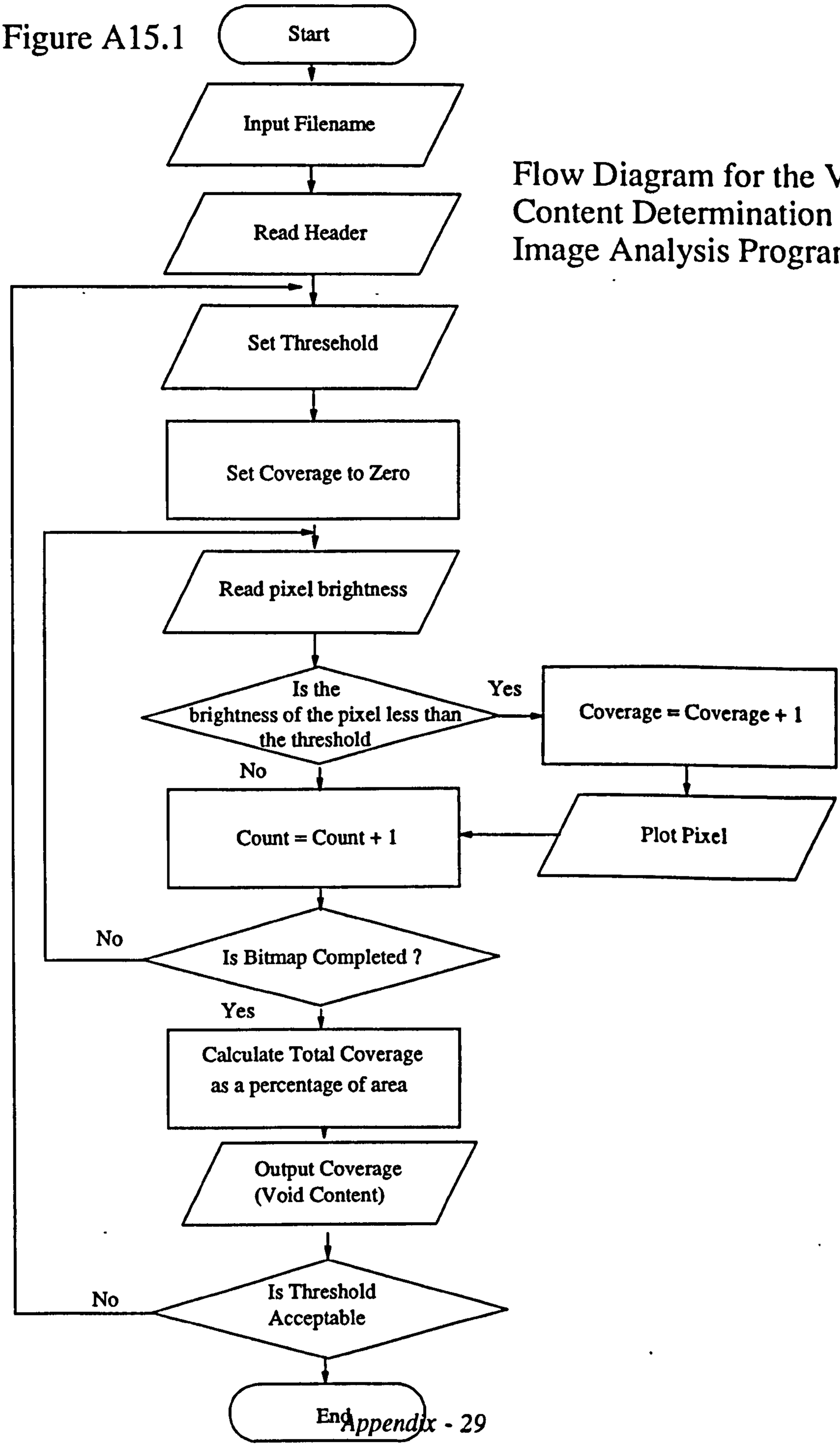

Flow Diagram for the Void Content Determination by Image Analysis Program

Appendix 16

Mould Filling Simulation Using Finite Element Techniques

A mould filling simulation has been achieved by modification of a commercially available finite-element (FE) program called PAFEC-FE[83]. The equations that govern the RTM process can be cast simply into an FE form. The basic physics of the fill phase of RTM is based on in-plane incompressible mass conservation and uses Darcy's law as a statement of the momentum balance. When proper initial and boundary conditions are imposed upon the model, the program calculates a pressure field over any impregnated preform. Once the pressure distribution is known, it may then be numerically differentiated to obtain pressure gradients. Control volume boundary segments are internally defined from the basic finite element geometry. The segments divide the finite elements into sub-elements. (Figure A16.1) The numerical calculation of the pressure field is based on the conservation of mass in each control volume, which can either be empty (ff=0), partially full (0<ff<1) or completely full (ff=1). The parameter ff (fill factor) defines the filled fraction of the control volume, ie. the ratio between the amount of fluid inside the control volume at any given time and the amount that the control volume is able to hold. The flow front location is defined by the partially filled control volumes which are allowed to advance in the calculation during each filling time step. Once the pressure is calculated at any given time step, the mass that flows into each control volume can be evaluated from a line integral along its boundaries. The fill factor is then updated according to the newly updated mass balance for a given time interval. A flow chart shoeing the mould filling algorithm is shown in Figure A16.2.

Initial conditions are defined such that the fill factor for each element in the mould cavity is set to zero. Boundary conditions permit a constant pressure, pressure function or a constant flux at the node(s) representing the injection point. Flow front node pressures are set to the vent pressure which is typically atmospheric. While concentrating on generally thin and curved components, the methods can be extended to full three-dimensional flow.

Figure A16.3 shows a short injection shot into the undershield mould where approximately 33% of the CFRM preform has become impregnated. To demonstrate

the potential of the model, the geometry of the undershield mould was obtained from the mould manufacturer and an FE mesh produced. Additional data required for the FE flow analysis was added and the analysis performed. Figure A16.4 shows the fill front locations for an analysis based on isothermal impregnation of CVP polyester resin injected at 6.5 bar into 6 layers of Unifilo U750-450 CFRM, by a central pin gate.

With this model it is possible to investigate moving the location and type of gate. The FE model can be used to perform a stress or deflection analysis on the part in service. During the flow analysis the fluid pressure may be integrated over the mould surface to determine clamping loads.

To assess the effect of stacking reinforcement layers of different permeabilities this program was used to predict the resin flow front as impregnation proceeded in multilayer preforms. The mould cavity was based on the 3.6mm deep flat plaque mould described in section 3.3. Five preforms were modelled, consisting of a combination of CFRM and unidirectional NCF. The permeability data for these materials were collected according to the methods described in section 3.7 and Appendix 14. The simple rectangular mould depicted in Figure A16.5 was assumed to contain a multilayered preform with layers of different permeability. One end of the mould was assumed to be held at a constant isobaric injection pressure, whilst the flow front was assumed to have a pressure of zero. The filling patterns obtained from these simulations are discussed in section 6.6.

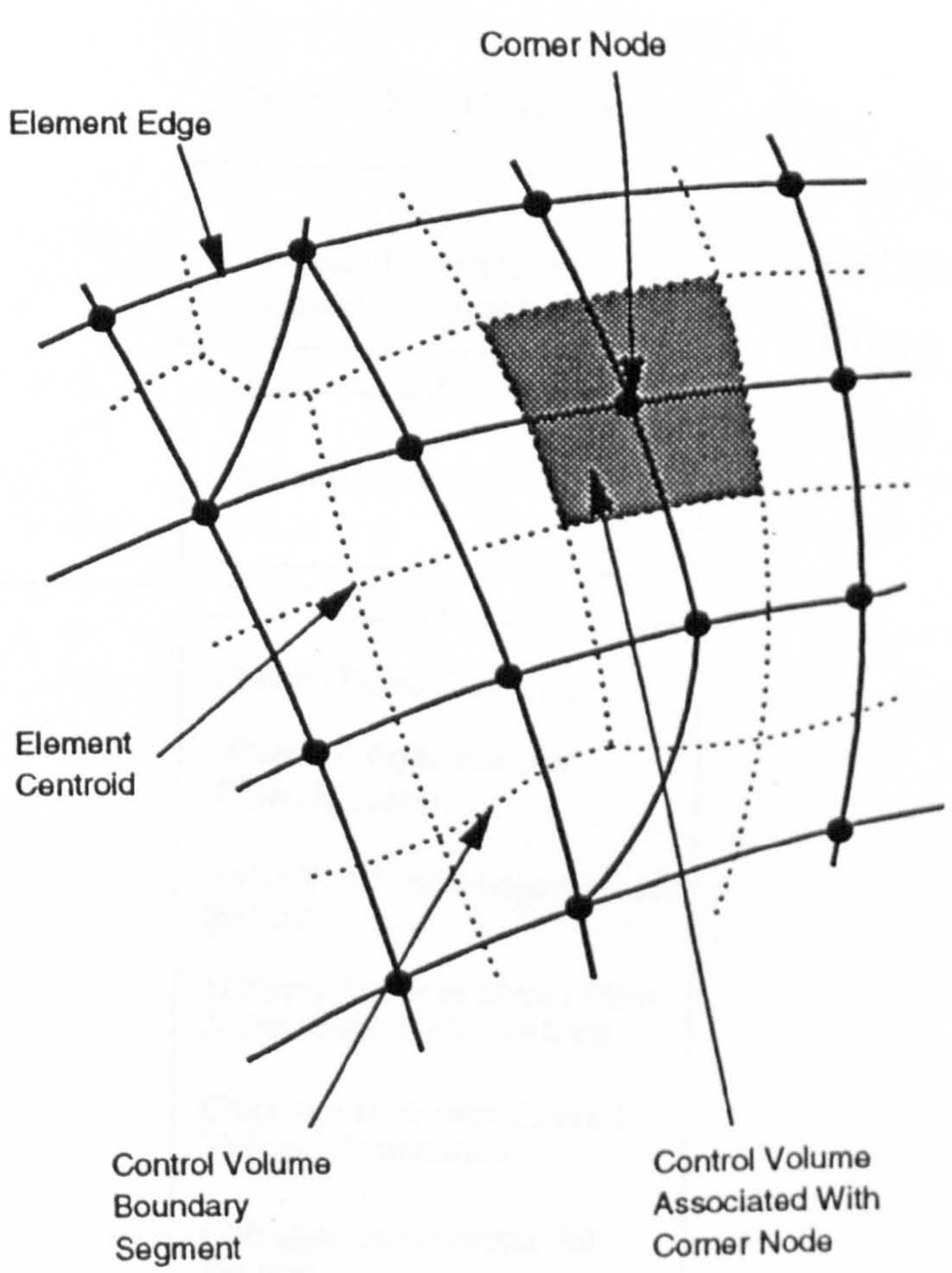

Figure A16.1 Sub-Division of FE Model into Control Volumes

(Courtesy Dr.E.V.Rice)

Figure A16.2

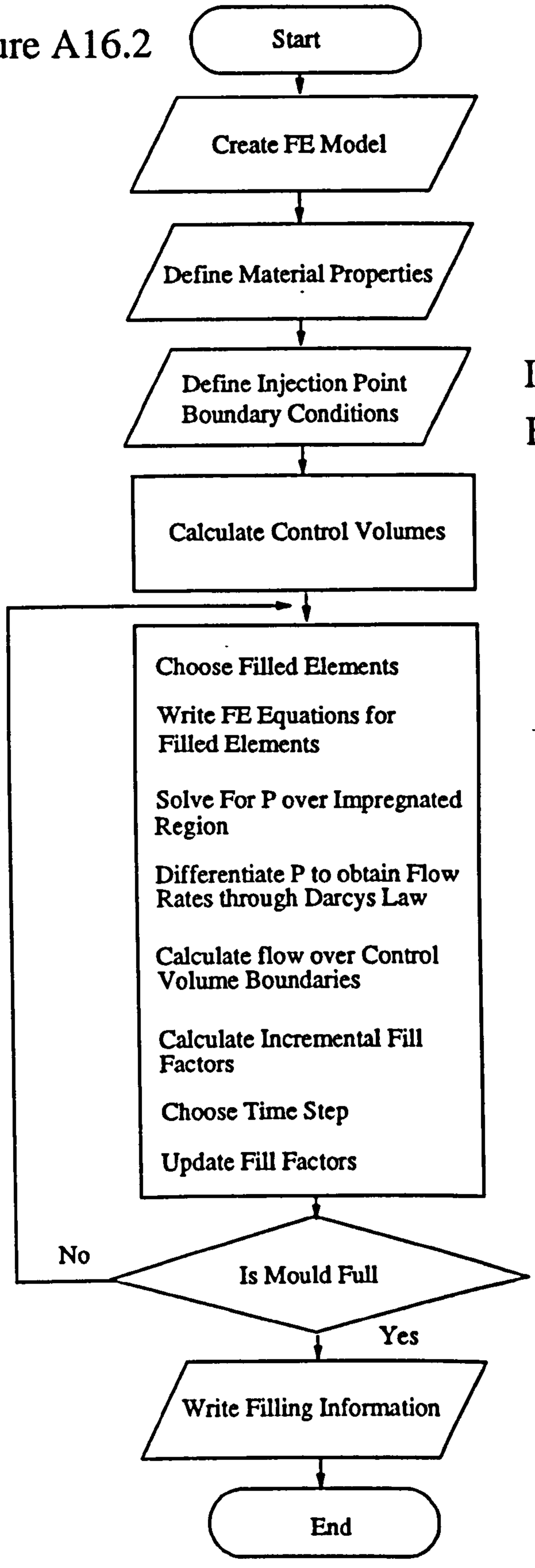

Isothermal Mould Filling Algorithm

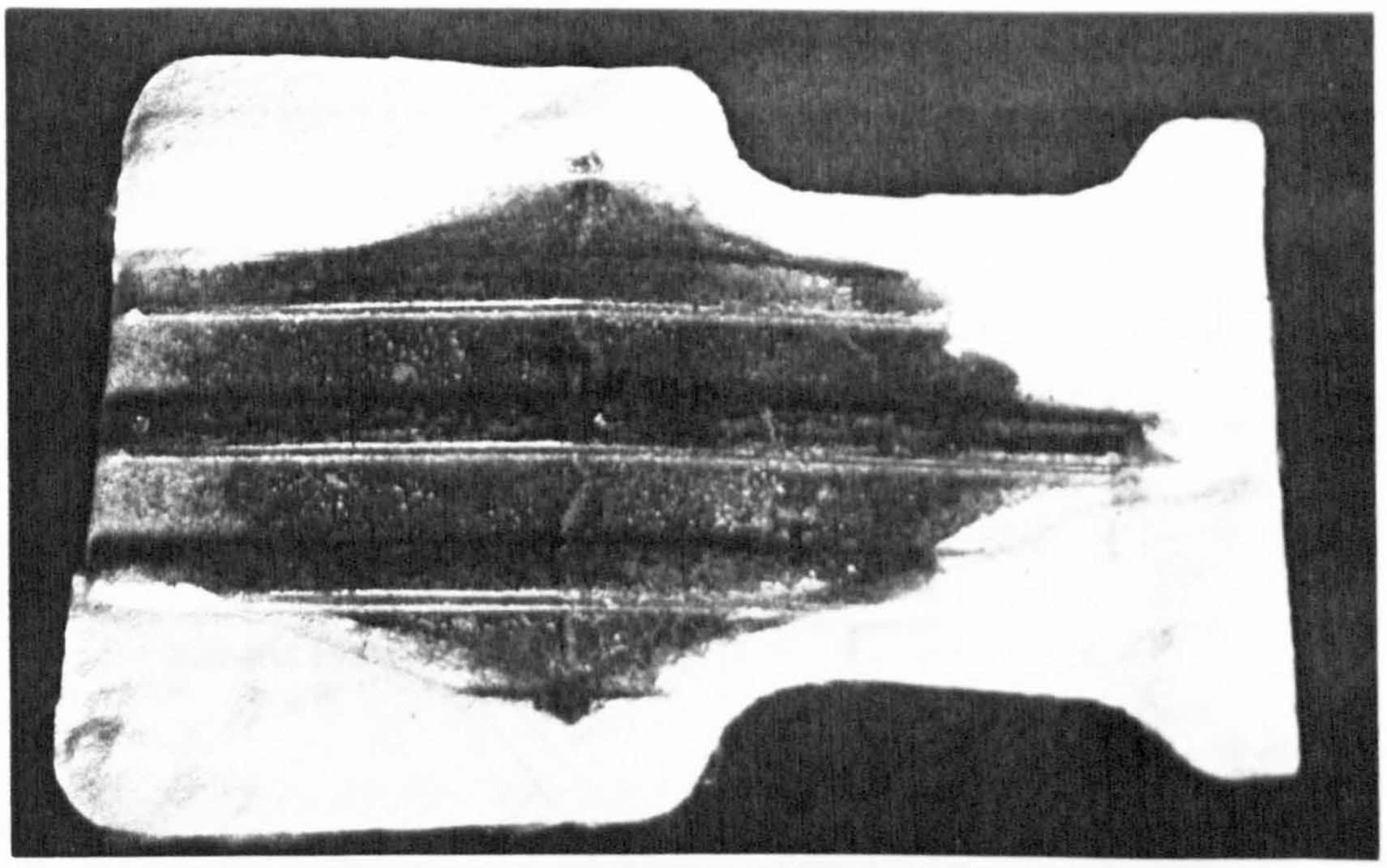

Figure A16.3 Short Injection Shot (33% Full) into Undershield Component

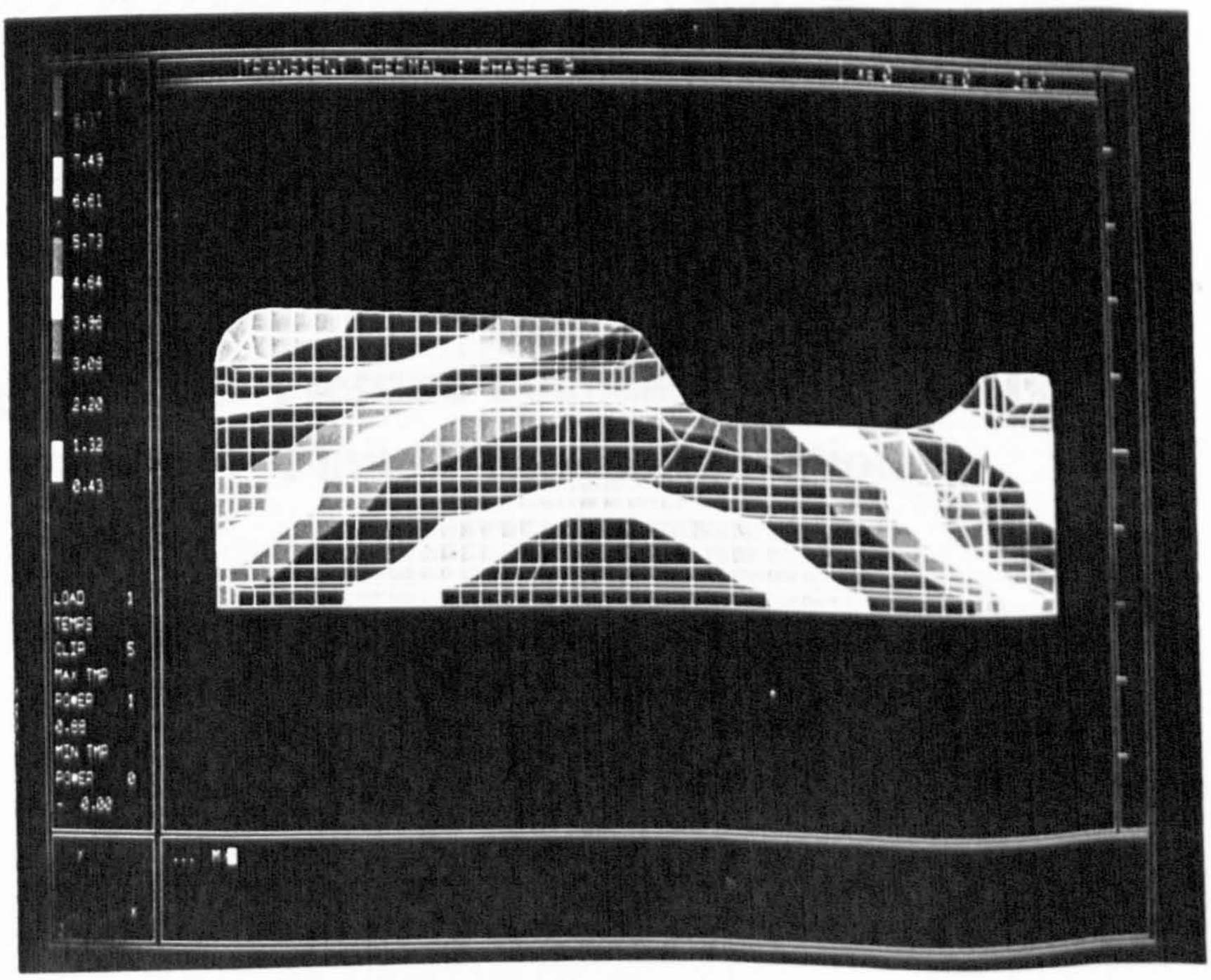

Figure A16.4 Finite Element Simulation of Fill Patterns into the Undershield Mould
(Courtesy Dr. E.V. Rice)

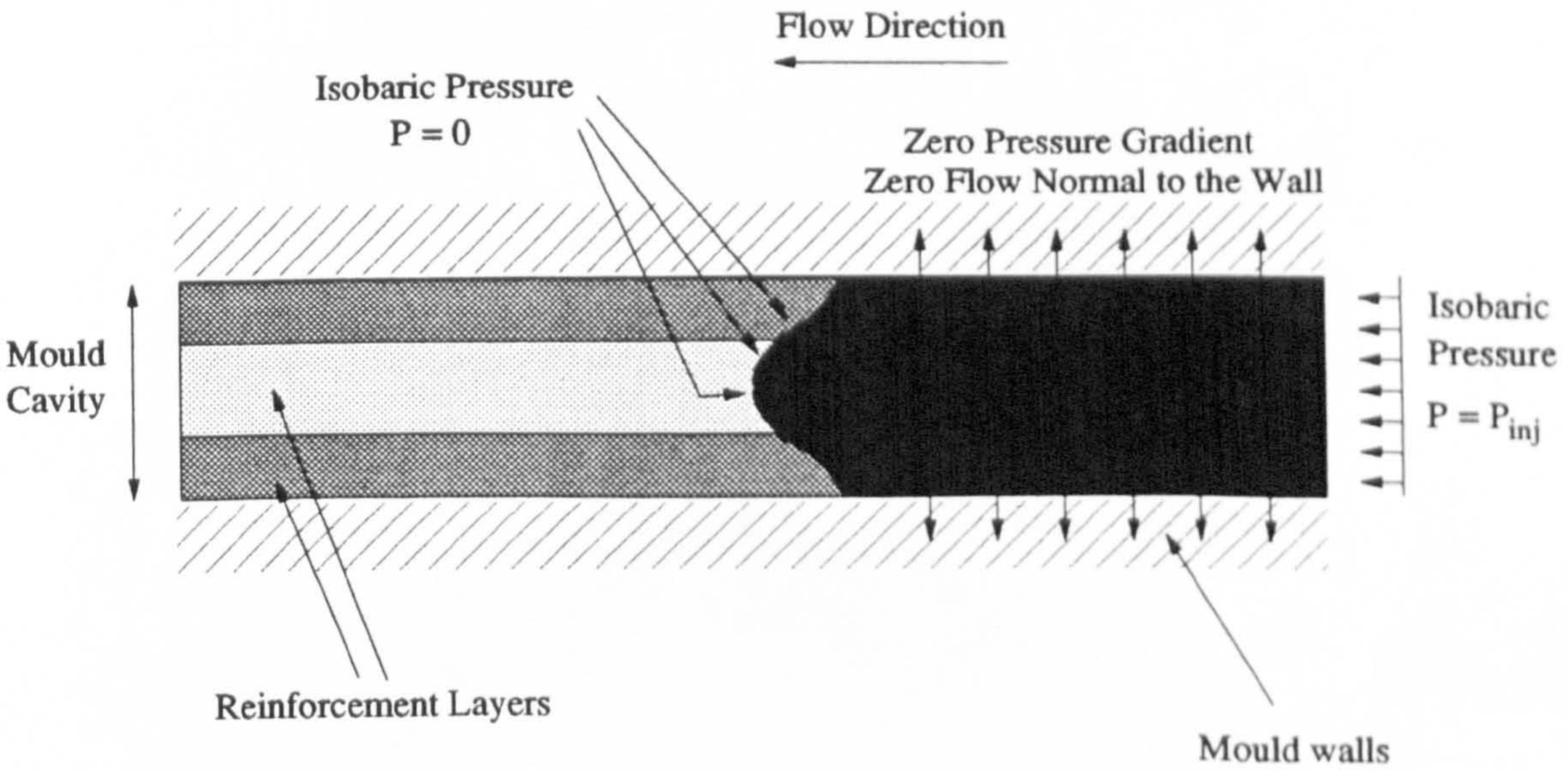

Figure A16.5 Pressure Boundary Conditions For Finite Element Simulation